

**Ongoing Face Recognition  
Vendor Test (FRVT)**  
**Part 1: Verification**

Patrick Grother  
Mei Ngan  
Kayee Hanaoka  
*Information Access Division  
Information Technology Laboratory*

This publication is available free of charge from:  
<https://www.nist.gov/programs-projects/face-recognition-vendor-test-frvt-ongoing>

2021/09/10

## ACKNOWLEDGMENTS

The authors are grateful to staff in the NIST Biometrics Research Laboratory for infrastructure supporting rapid evaluation of algorithms.

## DISCLAIMER

Specific hardware and software products identified in this report were used in order to perform the evaluations described in this document. In no case does identification of any commercial product, trade name, or vendor, imply recommendation or endorsement by the National Institute of Standards and Technology, nor does it imply that the products and equipment identified are necessarily the best available for the purpose.

## INSTITUTIONAL REVIEW BOARD

The National Institute of Standards and Technology's Research Protections Office reviewed the protocol for this project and determined it is not human subjects research as defined in Department of Commerce Regulations, 15 CFR 27, also known as the Common Rule for the Protection of Human Subjects (45 CFR 46, Subpart A).

## FRVT STATUS

**This report** is a draft NIST Interagency Report, and is open for comment. It is the twenty first edition of the report since the first was published in June 2017. Prior editions of this report are maintained on the FRVT [website](#), and may contain useful information about older algorithms and datasets no longer used in FRVT.

**FRVT remains open:** All [four tracks](#) of the FRVT are open to new algorithm submissions.

**2021-09-08** changes since 2021-08-02:

- ▷ We have added results for first algorithms from seven new developers: Griaule, SQISoft, Qnap Security, Techsign, Smart Engines, Verihubs, and Wuhan Tianyu Information Industry.
- ▷ We have added results for new algorithms from sixteen returning developers: ADVANCE.AI, AuthenMetric, CloudSmart Consulting, Code Everest Pvt, Cognitec Systems, Thales Gemalto Cogent, Intel Research Group, Omnidarde, Oz Forensics, Rank One Computing, Samsung S1 Corp, Securif AI, Tevian, TigerIT Americas, Universidade de Coimbra, and Vigilant Solutions
- ▷ We have retired results for eleven algorithms per our policy to only list results for two algorithms per developer. Results for retired algorithms appear in prior versions of this report in the [archive](#).

**2021-08-02** changes since 2021-06-25:

- ▷ We have added results for first algorithms from eight new developers: Bee the Data, Closeli Inc, Coretech Knowledge Inc, DeepSense (France), ioNetworks Inc, Kakao Pay Corp, Seventh Sense Artificial Intelligence, and SK Telecom.
- ▷ We have added results for new algorithms from fifteen returning developers: Alchera Inc, Adera Global PTE, Aware, Bresee Technology, Cyberlink Corp, Expasoft LLC, Fujitsu Research and Development Center, Gorilla Technology, Idemia, Neurotechnology, NEO Systems, NHN Corp, Paravision, Panasonic R+D Center Singapore, and Shenzhen University-Macau University of Science and Technology.
- ▷ We have retired results for twelve algorithms per our policy to only list results for two algorithms per developer. Results for retired algorithms appear in prior versions of this report in the [archive](#).

**2021-06-25** changes since 2021-05-21:

- ▷ We have added results for first algorithms from six new developers: Alice Biometrics, BOE Technology Group, Fincore, Neosecu, Sodec App, and Yuntu Data and Technology.
- ▷ We have added results for new algorithms from seven returning developers: Incode Technologies, HyperVerge, Mobbeel Solutions, Guangzhou Pixel Solutions, Remark Holdings, Sensetime, and Vietnam Posts and Telecommunications Group.
- ▷ We have retired results for four algorithms per our policy to only list results for two algorithms per developer. Results for retired algorithms appear in prior versions of this report in the [archive](#).

**2021-05-21** changes since 2021-04-26:

- ▷ We have added results for first algorithms from five new developers: Ekin Smart City Technologies, Suprema ID, Tripleize, Taiwan-Certificate Authority, and Vision Intelligence Center of Meituan.

- ▷ We have added results for new algorithms from eight returning developers: ID3 Technology, Imagus Technology, Momentum Digital, N-Tech Lab, NSENSE, Shanghai Jiao Tong University, Vision-Box, and Yuan High-Tech Development
- ▷ We have retired results for seven algorithms per our policy to only list results for two algorithms per developer. Results for retired algorithms appear in prior versions of this report in the [archive](#).

**2021-04-26 changes since 2021-04-16:**

- ▷ We have added results for first algorithms from three new developers: Quantasoft, Rendip, and NEO Systems.
- ▷ We have added results for new algorithms from four returning developers: 3Divi, Realnetworks, Veridas Digital Authentication Solutions, and Universidade de Coimbra.
- ▷ We have retired results for three algorithms per our policy to only list results for two algorithms per developer. Results for retired algorithms appear in prior versions of this report in the [archive](#).

**2021-04-16 changes since 2021-03-19:**

- ▷ We have added results for first algorithms from six new developers: 20Face, Beijing DeepSense Technologies, BitCenter UK, Enface, FaceTag, InsightFace AI, Line Corporation, Lema Labs, Nanjing Kiwi Network Technology, Omnidarde, Regula Forensics, and Suprema.
- ▷ We have added results for new algorithms from ten returning developers: CloudSmart Consulting, Dermalog, GeoVision, Neurotechnology, Panasonic R+D Center Singapore, Samsung S1, Securif AI, Trueface.ai, Vigilant Solutions, and Visidon.
- ▷ We have retired results for ten algorithms per our policy to only list results for two algorithms per developer. Results for retired algorithms appear in prior versions of this report in the [archive](#).

**2021-03-19 changes since 2021-03-05:**

- ▷ We have added results for first algorithms from six new developers: Ajou University, AuthenMetric, Code Everest, Corsight, Papilon Savunma, and NHN Corp
- ▷ We have added results for new algorithms from seven returning developers: Alchera, Deepglint, Fiber-home Telecommunication Technologies, Kakao Enterprise, Kookmin University, Megvii/Face++, and NotionTag Technologies.
- ▷ We have updated many of the hyperlinked HTML report-cards to include seven figures on demographic dependence. Figures of this kind first appeared, and are documented in, the December 2019 document, [NIST Interagency Report 8280](#) on demographic differentials in face recognition. The figures quantify false negative dependence on demographics using “visa-border” comparisons, and false positive dependence using comparisons of “application” photos that uniformly of quality and similar to visa photos.

**2021-03-05 changes since 2021-01-19:**

- ▷ We have added results for first algorithms from three new developers: IVA Cognitive, Mobbeel, and MoreDian Technology.

- ▷ We have added results for new algorithms from returning developers: Ability Enterprise - Andro Video, ACI Software, Adera Global, AnyVision, BioID Technologies, China Electronics Import-Export, Cognitec Systems, Fujitsu Research and Development Center, Glory, Guangzhou Pixel Solutions, Hengrui AI Technology, Incode Technologies, Intel Research, iQIYI, Mobai, Oz Forensics, Paravision, VisionLabs, and Xforward AI Technology.
- ▷ We have added a new “resources” tab to the main [webpage](#). It includes sortable columns for data related to speed, model size, storage, and memory consumption.
- ▷ We have retired results for 13 algorithms per our policy to only list results for two algorithms per developer. Results for retired algorithms appear in prior versions of this report in the [archive](#).

**2021-01-19 changes since 2020-12-18:**

- ▷ This report adds results for first algorithms from four developers: Herta Security, Irax AI, Shenzhen University-Macau University of Science and Technology, and Vietnam Posts and Telecommunications Group. See Table 5 for more information.
- ▷ The report also includes results for thirteen developers who have previously submitted algorithms: Bresee Technology, Canon (previously Canon Information Technology (Beijing)), Cyberlink, CSA IntelliCloud Technology, Dahua Technology, ID3 Technology, Imagus Technology (Vixvization), Moontime Smart Technology, N-Tech Lab, Thales Cogent, Veridas Digital Authentication Solutions, Vocord, and Yuan High-Tech Development.
- ▷ We have retired results for ten algorithms per our policy to only list results for two algorithms per developer. Results for retired algorithms appear in prior versions of this report in the [archive](#).

**2020-12-18 changes since 2020-10-09:**

- ▷ This report adds results for first algorithms from ten developers: BitCenter UK, CloudSmart Consulting, Cubox, Institute of Computing Technology, Naver Corp, Minivision, NSENSE Corp, Viettel Group, Visage Technologies, and Xiamen University. See Table 5 for more information.
- ▷ The report also includes results for eighteen developers who have previously submitted algorithms: ADVANCE.AI, Awudit Systems, Chosun University, Dermalog, GeoVision, ICM Airport Technics, Idemia, Institute of Information Technologies, Kakao Enterprise, Neurotechnology, Panasonic R+D Center Singapore, Rank One Computing, Sensetime Group, Shanghai Jiao Tong University, TigerIT Americas LLC, Vigilant Solutions, Winsense, and YooniK
- ▷ We have retired results for twelve algorithms per our policy to only list results for two algorithms per developer. Results for retired algorithms appear in prior versions of this report in the [archive](#).

**Changes since September 18, 2020:**

- ▷ This report adds results for first algorithms from five developers: Aigen, Cortica, Kookmin University, Securif AI and Vinai.
- ▷ The report also includes results for three developers who have previously submitted algorithms: Fujitsu Laboratories, Hengrui AI, and X-Forward AI.
- ▷ In the per-algorithm report-cards linked from tables and the main webpage, we have added a chart to showing reduction in error rates over the course of FRVT i.e. from 2017 onwards for all algorithms supplied by that developer. Similarly we have added a chart showing error rate reductions for our test of protective face mask verification.

- ▷ We plan to continue evaluating algorithms on various mask datasets. We hold that algorithms should be capable of detecting masks and verifying identity of all combinations of masked and unmasked faces. We have accordingly increased the amount of time allowed to extract those features from 1.0 to 1.5 seconds.

#### **Changes since August 25, 2020:**

- ▷ This report adds results for first algorithms from eight new developers. Akurat Satu Indonesia, Cybercore, Decatur Industries, Innef Labs, Satellite Innovation/Eocortex, Expasoft, and Mobai.
- ▷ The report includes results for seven developers who have previously submitted algorithms: 3Divi, BioID Technologies, Incode Technologies, Innovatrics, iSAP Solution, Synology, and Tevian.
- ▷ We have retired results for five algorithms per our policy to only list results for two algorithms per developer. Results for retired algorithms appear in prior versions of this report in the [archive](#).

#### **Changes since July 27, 2020:**

- ▷ We have introduced per-algorithm report sheets. These are HTML documents linked from the accuracy tables in this report (i.e. Table 21) and on the FRVT 1:1 [homepage](#). The sheets contain interactive graphics allowing, for example, mouseover exploration of FNMR(T) and FMR(T). Some of their content had previously appeared in this document.
- ▷ This report adds results for algorithms from six new developers. ACI Software, Bresee Technology, Fiberhome Telecommunication Technologies, Imageware Systems, Oz Forensics, and Pensees.
- ▷ The report includes results for thirteen developers who have previously submitted algorithms: Canon Information Technology (Beijing), Cyberlink, Dahua Technology, Gorilla Technology, ID3 Technology, Intel Research Group, iQIYI Inc, Momentum Digital, Netbridge Technology, Tech5 SA, Shenzhen AiMall Tech, Vigilant Solutions, and VisionLabs.
- ▷ We have retired results for nine algorithms per our policy to only list results for two algorithms per developer. Results for retired algorithms appear in prior versions of this report in the [archive](#).

#### **Changes since May 18, 2020:**

- ▷ The report is the first FRVT update since the pandemic closed it from March to June 2020.
- ▷ This report includes results for algorithms from nine new developers: GeoVision Inc, Su Zhou NaZhi-TianDi Intelligent Technology, YooniK, AYF Technology, PXL Vision AG, Yuan High-Tech Development, Beihang University-ERCACAT, ICM Airport Technics, and Staqu Technologies
- ▷ This report includes results for algorithms from 15 returning developers Acer Incorporated, Antheus Technologia, Chosun University, Chunghwa Telecom, Idemia, Moontime Smart Technology, Neurotechnology, Guangzhou Pixel Solutions, Panasonic R+D Center Singapore, Rank One Computing, Scanovate, Shanghai Universiy - Shanghai Film Academy, Synesis, Trueface.ai, and Veridas Digital Authentication Solutions
- ▷ We have retired results for ten algorithms per our policy to only list results for two algorithms per developer. Results for retired algorithms appear in prior versions of this report in the [archive](#).
- ▷ We separated timing and other resource consumption from the main participation table. The new Table 13 includes template generation durations for four kinds of images, not just mugshots.

- ▷ We have published a separate report, [NIST Interagency Report 8311](#) on accuracy of pre-pandemic algorithms on subjects wearing face masks. We plan to track improvements in accuracy on masked images going forward. In particular, we invite submission of algorithms that can detect whether a person is wearing a mask, extract features from the full face or the exposed periocular region, and do appropriate comparison. We do not intend to evaluate algorithms that assume 100% of images will be of masked individuals.

#### **Changes since March 25, 2020:**

- ▷ The report is a maintenance release - it does not add any new algorithms, and FRVT has been closed to new algorithms since mid March 2020.
- ▷ We modified the primary accuracy summary, Table 21, as follows:
  - ▷▷ For visa images, the column for FNMR at FMR = 0.0001 has been removed. The visa images are so highly controlled that the error rates for the most accurate algorithms are dominated by false rejection of very young children and by the presence of a few noisy greyscale images. For now, two visa columns remain: FNMR at FMR=  $10^{-6}$  and, for matched covariates, FNMR at FMR=  $10^{-4}$ .
  - ▷▷ We have inserted a new column labelled “BORDER” giving accuracy for comparison of moderately poor webcam border-crossing photos that exhibit pose variations, poor compression, and low contrast due to strong background illumination. The accuracies are the worst from all cooperative image datasets used in FRVT.
- ▷ Accordingly, we updated the failure-to-template rates in Table 27.
- ▷ We withdrew a figure showing how false matches are concentrated in certain visa images used in cross-comparison, because it didn't attempt to include demographic information.

#### **Changes since February 27, 2020:**

- ▷ The report adds results algorithms from two new developers: Beijing Alleyes Technology, and the Chinese University of Hong Kong. Results for newly submitted algorithms from two other developers will appear in the next report.
- ▷ The report adds results for algorithms from thirteen returning developers: ASUSTek Computer, Aware, Cyberlink Corp, Gorilla Technology, Innovative Technology, Kakao Enterprise, Lomonosov Moscow State University, Panasonic R+D Center Singapore, Shenzhen AiMall Technology, Shenzhen Intellifusion Technologies, Synology, Tech5 SA, and Via Technologies.
- ▷ Per policy to only list results for two algorithms per developer, we have dropped results for algorithms from Aware, Cyberlink, Gorilla Technology, Kakao Enterprise, Lomonosov Moscow State University, Panasonic R+D Center Singapore, and Tech5 SA.

#### **Changes since January 20, 2020:**

- ▷ The report adds results for five new developers: Ability Enterprise (Andro Video), Chosun University, Fujitsu Research and Development Center, University of Coimbra, and Xforward AI Technology.
- ▷ The report adds results for algorithms from six returning developers: AlphaSSTG, Incode Technologies, Kneron, Shanghai Jiao Tong University, Vocord, and X-Laboratory.
- ▷ We have corrected template comparison timing numbers for algorithms submitted September 2019 to January 2020. The values reported previously were slower due to a software bug.

- ▷ We have dropped results for algorithms from Vocord and Incode per policy to only list results for two algorithms per developer.
- ▷ The [FRVT 1:1 homepage](#) has been updated with latest accuracy results.
- ▷ The [FRVT 1:N homepage](#) now includes an update to the September 2019 NIST Interagency Report 8271. The new report adds results for one-to-many search algorithms submitted to NIST from June 2019 to January 2020.

### **Changes since January 6, 2020:**

- ▷ Section 2 has been updated to better describe the Visa and Border images. The caption for Table 21 has been updated to better relate the accuracy values to particular image comparisons.
- ▷ The report adds results for five new developers: Acer, Advance.AI, Expasoft, Netbridge Technology, and Videmo Intelligent Videoanalyse.
- ▷ The report adds results for algorithms from 7 returning developers: China Electronics Import-Export Corp, Intel Research Group, ITMO University, Neurotechnology, N-Tech Lab, Rokid, and VisionLabs.
- ▷ We have dropped results from this edition of the report per policy to only list results for two algorithms per developer: N-Tech Lab, Neurotechnology, ITMO, Visionlabs, and CEIEC.
- ▷ The [FRVT homepage](#) has been updated with latest accuracy results.

### **Changes since November 11, 2019:**

- ▷ Table 13 has been updated to include runtime memory usage. This is the first time such a quantity has been reported. The value is the peak size of the resident set size logged during enrollment of single images.
- ▷ We have migrated summary results table to a new platform that supports sortable tables:  
<https://pages.nist.gov/frvt/html/frvt11.html>
- ▷ The report adds results for four new developers: Antheus Technologia, BioID Technologies SA, Canon Information Tech. (Beijing), Samsung S1 (listed in the tables as S1), and Taiwan AI Labs.
- ▷ The report adds results for algorithms from 13 returning developers: Anke Investments, Chunghwa Telecom, Deepglint, Institute of Information Technologies, iQIYI, Kneron, Ping An Technology, Paravision, KanKan Ai, Rokid Corporation, Shanghai Universiy - Shanghai Film Academy, Veridas Digital Authentication Solutions, and Videonetics Technology.
- ▷ We have dropped results from this edition of the report per policy to only list results for two algorithms per developer: remarkai-000, veridas-001, sensetime-001, iit-000, anke-003, and everai-002. Results for these are available in prior editions of this report linked from the FRVT page.
- ▷ We issued [NIST Interagency Report 8280: FRVT Part 3: Demographics](#) on 2019-12-19. It includes results for many of the algorithms covered by this report.

### **Changes since October 16, 2019:**

- ▷ The report adds results for ten new developers: Ai-Union Technology, ASUSTek Computer, DiDi ChuXing Technology, Innovative Technology, Luxand, MVision, Pyramid Cyber Security + Forensic, Scanovate, Shenzhen AiMall Tech, and TUPU Technology.

- ▷ The report adds results for 12 returning developers: CTBC Bank Glory Gorilla Technology Guangzhou Pixel Solutions Imagus Technology Incode Technologies Lomonosov Moscow State University Rank One Computing Samtech InfoNet Shanghai Ulucu Electronics Technology Synesis, and Winsense.
- ▷ We have dropped results from this edition of the report per policy to only list results for two algorithms per developer: glory-000, gorilla-002, incode-003, rankone-006, and synesis-004.
- ▷ Results for five recently submitted algorithms will appear in the next report.

#### **Changes since September 11, 2019:**

- ▷ The report adds results for five new participants: Awidit Systems (Awiros), Momenmtum Digital (Sertis), Trueface AI, Shanghai Jiao Tong University, and X-Laboratory.
- ▷ The reports adds results for five new algorithms from returning developers: Cyberlink, Hengrui AI Technology, Idemia, Panasonic R+D Singapore, and Tevian. This causes three algorithm, to be de-listed from the report per policy to list results for two algorithms per developer.

#### **Changes since July 31 2019:**

- ▷ The HTML table on the [FRVT 1:1 homepage](#) has been updated to include a column for cross-domain Visa-Border verification. Results for this new dataset appeared in the July 29 report under the name "CrossEV" - these are now renamed "Visa-Border".
- ▷ The [FRVT 1:1 homepage](#) lists algorithms according to lowest mean rank accuracy:
 
$$\begin{aligned} &\text{Rank(FNMR}_{\text{VISA}} \text{ at FMR = 0.000001}) + \\ &\text{Rank(FNMR}_{\text{VISA-BORDER}} \text{ at FMR = 0.000001}) + \\ &\text{Rank(FNMR}_{\text{MUGSHOT}} \text{ at FMR = 0.00001 after 14 years}) + \\ &\text{Rank(FNMR}_{\text{WILD}} \text{ at FMR = 0.00001}) \end{aligned}$$

This ordering rewards high accuracy across all datasets.
- ▷ The main results in Table 21 is now in landscape format to accomodate extra columns for the Visa-Border set, and mugshot comparisons after at least 12 years.
- ▷ The report adds results for nine new participants: Alpha SSTG, Intel Research, ULSee, Chungwa Telecon, iSAP Solution, Rokid, Shenzhen EI Networks, CSA Intellicloud, Shenzhen Intellifusion Technologies.
- ▷ The reports adds results for six new algorithms from returning developers: Innovatrics, Dahua Technology, Tech5 SA, Intellivision, Nodeflux and Imperial College, London. One algorithm, from Imperial has been retired, per policy to list results for two algorithms per developer.
- ▷ The cross-country false match rate heatmaps have been replotted to reveal more structure by listing countries by region instead of alphabetically.
- ▷ The next version of this report will be posted around October 18, 2019.

#### **Changes since July 3 2019:**

- ▷ The HTML table on the [FRVT 1:1 homepage](#) has been updated to list the 20 most accurate developers rather than algorithms, choosing the most accurate algorithm from each developer based on visa and mugshot results. Also, the algorithms are ordered in terms of lowest mean rank across mugshot, visa and wild datasets, rewarding broad accuracy over a good result on one particular dataset.
- ▷ This report includes results for a new dataset - see the column labelled "visa-border" in Table 5. It compares a new set of high quality visa-like portraits with a set webcam border-crossing photos that exhibit moderately poor pose variations and background illumination. The two new sets are described in sections 2.3 and 2.4. The comparisons are "cross-domain" in that the algorithm must compare "visa" and "wild" images. Results for other algorithms will be added in future reports as they become available.

- ▷ This report adds results for algorithms from 9 developers submitted in early July 2019. These are from 3DiVi, Camvi, EverAI-Paravision, Facesoft, Farbar (F8), Institute of Information Technologies, Shanghai U. Film Academy, Via Technologies, and Ulucu Electronics Tech. Six of these are new participants.
- ▷ Several other algorithms have been submitted and are being evaluated. Results will be released in the next report, scheduled for September 5. That report will include results for new datasets.
- ▷ Older algorithms from Everai, Camvi and 3DiVi, have been retired, per the policy to list only two algorithms per developer.

#### **Changes since June 2019:**

- ▷ This report adds results for algorithms from 18 developers submitted in early June 2019. These are from CTBC Bank, Deep Glint, Thales Cogent, Ever AI Paravision, Gorilla Technology, Imagus, Incode, Kneron, N-Tech Lab, Neurotechnology, Notiontag Technologies, Star Hybrid, Videonetics, Vigilant Solutions, Winsense, Anke Investments, CEIEC, and DSK. Nine of these are new participants.
- ▷ Several other algorithms have been submitted and are being evaluated. Results will be released in the next report, scheduled for August 1.
- ▷ Older algorithms from Everai, Thales Cogent, Gorilla Technology, Incode, Neurotechnology, N-Tech Lab and Vigilant Solutions have been retired, per the policy to list only two algorithms per developer.

#### **Changes since April 2019:**

- ▷ This report adds results for nine algorithms from nine developers submitted in early June 2019. These are from Tencent Deepsea, Hengrui, Kedacom, Moontime, Guangzhou Pixel, Rank One Computing, Synesis, Sensetime and Vocord.
- ▷ Another 23 algorithms have been submitted and are being evaluated. Results will be released in the next report, scheduled for July 3.
- ▷ Older algorithms for Rank One, Synesis, and Vocord have been retired, per the policy to list only two algorithms per developer.

#### **Changes since February 2019:**

- ▷ This report adds results for 49 algorithms from 42 developers submitted in early March 2019.
- ▷ This report omits results for algorithms that we retired. We retired for three reasons: 1. The developer submitted a new algorithm, and we only list two. 2. The algorithm needs a GPU, and we no longer allow GPU-based algorithms. 3. Inoperable algorithms.
- ▷ Previous results for retired algorithms are available in older editions of this report linked [here](#).
- ▷ The mugshot database used from February 2017 to January 2019 has been replaced with an extract of the mugshot database documented in NIST Interagency Report 8238, November 2018. The new mugshot set is described in section [2.5](#) and is adopted because:
  - ▷▷ It has much better identity label integrity, so that false non-match rates are substantially lower than those reported in FRVT 1:1 reports to date - see Figure [70](#).
  - ▷▷ It includes images collected over a 17 year period such that ageing can be much better characterized - - see Figure [258](#).
- ▷ Using the new mugshot database, Figure [258](#) shows accuracy for four demographic groups identified in the biographic metadata that accompanies the data: black females, black males, white females and white males.
- ▷ The report adds Figure [18](#) with results for the twenty human-difficult pairs used in the May 2018 paper [Face recognition accuracy of forensic examiners, superrecognition, and face recognition algorithms](#) by Phillips et al. [[1](#)].

- ▷ The report uses an update to the wild image database that corrects some ground truth labels.
- ▷ Some results for the child exploitation database are not complete. They are typically updated less frequently than for other image sets.

## Contents

<b>ACKNOWLEDGMENTS</b>	<b>1</b>
<b>DISCLAIMER</b>	<b>1</b>
<b>INSTITUTIONAL REVIEW BOARD</b>	<b>1</b>
<b>1 METRICS</b>	<b>41</b>
1.1 CORE ACCURACY . . . . .	41
<b>2 DATASETS</b>	<b>42</b>
2.1 CHILD EXPLOITATION IMAGES . . . . .	42
2.2 VISA IMAGES . . . . .	42
2.3 APPLICATION IMAGES . . . . .	42
2.4 BORDER CROSSING IMAGES . . . . .	43
2.5 MUGSHOT IMAGES . . . . .	43
2.6 WILD IMAGES . . . . .	43
<b>3 RESULTS</b>	<b>44</b>
3.1 TEST GOALS . . . . .	44
3.2 TEST DESIGN . . . . .	44
3.3 FAILURE TO ENROLL . . . . .	47
3.4 RECOGNITION ACCURACY . . . . .	53
3.5 GENUINE DISTRIBUTION STABILITY . . . . .	259
3.5.1 EFFECT OF BIRTH PLACE ON THE GENUINE DISTRIBUTION . . . . .	259
3.5.2 EFFECT OF AGEING . . . . .	289
3.5.3 EFFECT OF AGE ON GENUINE SUBJECTS . . . . .	311
3.6 IMPOSTOR DISTRIBUTION STABILITY . . . . .	342
3.6.1 EFFECT OF BIRTH PLACE ON THE IMPOSTOR DISTRIBUTION . . . . .	342
3.6.2 EFFECT OF AGE ON IMPOSTORS . . . . .	346

## List of Tables

1 PARTICIPANT INFORMATION . . . . .	18
2 PARTICIPANT INFORMATION . . . . .	19
3 PARTICIPANT INFORMATION . . . . .	20
4 PARTICIPANT INFORMATION . . . . .	21
5 PARTICIPANT INFORMATION . . . . .	22
6 ALGORITHM SUMMARY . . . . .	23
7 ALGORITHM SUMMARY . . . . .	24
8 ALGORITHM SUMMARY . . . . .	25
9 ALGORITHM SUMMARY . . . . .	26
10 ALGORITHM SUMMARY . . . . .	27
11 ALGORITHM SUMMARY . . . . .	28
12 ALGORITHM SUMMARY . . . . .	29
13 ALGORITHM SUMMARY . . . . .	30
14 FALSE NON-MATCH RATE . . . . .	31
15 FALSE NON-MATCH RATE . . . . .	32
16 FALSE NON-MATCH RATE . . . . .	33
17 FALSE NON-MATCH RATE . . . . .	34
18 FALSE NON-MATCH RATE . . . . .	35
19 FALSE NON-MATCH RATE . . . . .	36
20 FALSE NON-MATCH RATE . . . . .	37

21	FALSE NON-MATCH RATE . . . . .	38
22	FAILURE TO ENROL RATES . . . . .	47
23	FAILURE TO ENROL RATES . . . . .	48
24	FAILURE TO ENROL RATES . . . . .	49
25	FAILURE TO ENROL RATES . . . . .	50
26	FAILURE TO ENROL RATES . . . . .	51
27	FAILURE TO ENROL RATES . . . . .	52

## List of Figures

1	PERFORMANCE SUMMARY: FNMR VS. TEMPLATE SIZE TRADEOFF . . . . .	39
2	PERFORMANCE SUMMARY: FNMR VS. TEMPLATE TIME TRADEOFF . . . . .	40
3	EXAMPLE IMAGES . . . . .	44
(A)	VISA . . . . .	44
(B)	MUGSHOT . . . . .	44
(C)	WILD . . . . .	44
(D)	BORDER . . . . .	44
4	PERFORMANCE ON 20 HUMAN-DIFFICULT PAIRS . . . . .	54
5	PERFORMANCE ON 20 HUMAN-DIFFICULT PAIRS . . . . .	55
6	PERFORMANCE ON 20 HUMAN-DIFFICULT PAIRS . . . . .	56
7	PERFORMANCE ON 20 HUMAN-DIFFICULT PAIRS . . . . .	57
8	PERFORMANCE ON 20 HUMAN-DIFFICULT PAIRS . . . . .	58
9	PERFORMANCE ON 20 HUMAN-DIFFICULT PAIRS . . . . .	59
10	PERFORMANCE ON 20 HUMAN-DIFFICULT PAIRS . . . . .	60
11	PERFORMANCE ON 20 HUMAN-DIFFICULT PAIRS . . . . .	61
12	PERFORMANCE ON 20 HUMAN-DIFFICULT PAIRS . . . . .	62
13	PERFORMANCE ON 20 HUMAN-DIFFICULT PAIRS . . . . .	63
14	PERFORMANCE ON 20 HUMAN-DIFFICULT PAIRS . . . . .	64
15	PERFORMANCE ON 20 HUMAN-DIFFICULT PAIRS . . . . .	65
16	PERFORMANCE ON 20 HUMAN-DIFFICULT PAIRS . . . . .	66
17	PERFORMANCE ON 20 HUMAN-DIFFICULT PAIRS . . . . .	67
18	PERFORMANCE ON 20 HUMAN-DIFFICULT PAIRS . . . . .	68
19	ERROR TRADEOFF CHARACTERISTIC: VISA IMAGES . . . . .	69
20	ERROR TRADEOFF CHARACTERISTIC: VISA IMAGES . . . . .	70
21	ERROR TRADEOFF CHARACTERISTIC: VISA IMAGES . . . . .	71
22	ERROR TRADEOFF CHARACTERISTIC: VISA IMAGES . . . . .	72
23	ERROR TRADEOFF CHARACTERISTIC: VISA IMAGES . . . . .	73
24	ERROR TRADEOFF CHARACTERISTIC: VISA IMAGES . . . . .	74
25	ERROR TRADEOFF CHARACTERISTIC: VISA IMAGES . . . . .	75
26	ERROR TRADEOFF CHARACTERISTIC: VISA IMAGES . . . . .	76
27	ERROR TRADEOFF CHARACTERISTIC: VISA IMAGES . . . . .	77
28	ERROR TRADEOFF CHARACTERISTIC: VISA IMAGES . . . . .	78
29	ERROR TRADEOFF CHARACTERISTIC: VISA IMAGES . . . . .	79
30	ERROR TRADEOFF CHARACTERISTIC: VISA IMAGES . . . . .	80
31	ERROR TRADEOFF CHARACTERISTIC: VISA IMAGES . . . . .	81
32	ERROR TRADEOFF CHARACTERISTIC: VISA IMAGES . . . . .	82
33	ERROR TRADEOFF CHARACTERISTIC: VISA IMAGES . . . . .	83
34	ERROR TRADEOFF CHARACTERISTIC: VISA IMAGES . . . . .	84
35	ERROR TRADEOFF CHARACTERISTIC: VISA IMAGES . . . . .	85
36	ERROR TRADEOFF CHARACTERISTIC: VISA IMAGES . . . . .	86
37	ERROR TRADEOFF CHARACTERISTIC: VISA IMAGES . . . . .	87
38	ERROR TRADEOFF CHARACTERISTIC: VISA IMAGES . . . . .	88
39	ERROR TRADEOFF CHARACTERISTIC: VISA IMAGES . . . . .	89
40	ERROR TRADEOFF CHARACTERISTIC: VISA IMAGES . . . . .	90
41	ERROR TRADEOFF CHARACTERISTIC: VISA IMAGES . . . . .	91

42	ERROR TRADEOFF CHARACTERISTIC: VISA IMAGES	92
43	ERROR TRADEOFF CHARACTERISTIC: VISA IMAGES	93
44	ERROR TRADEOFF CHARACTERISTIC: VISA IMAGES	94
45	ERROR TRADEOFF CHARACTERISTIC: VISA IMAGES	95
46	ERROR TRADEOFF CHARACTERISTIC: VISA IMAGES	96
47	ERROR TRADEOFF CHARACTERISTIC: VISA IMAGES	97
48	ERROR TRADEOFF CHARACTERISTIC: VISA IMAGES	98
49	ERROR TRADEOFF CHARACTERISTIC: VISA IMAGES	99
50	ERROR TRADEOFF CHARACTERISTIC: VISA IMAGES	100
51	ERROR TRADEOFF CHARACTERISTIC: VISA IMAGES	101
52	ERROR TRADEOFF CHARACTERISTIC: VISA IMAGES	102
53	ERROR TRADEOFF CHARACTERISTIC: VISA IMAGES	103
54	ERROR TRADEOFF CHARACTERISTIC: MUGSHOT IMAGES	104
55	ERROR TRADEOFF CHARACTERISTIC: MUGSHOT IMAGES	105
56	ERROR TRADEOFF CHARACTERISTIC: MUGSHOT IMAGES	106
57	ERROR TRADEOFF CHARACTERISTIC: MUGSHOT IMAGES	107
58	ERROR TRADEOFF CHARACTERISTIC: MUGSHOT IMAGES	108
59	ERROR TRADEOFF CHARACTERISTIC: MUGSHOT IMAGES	109
60	ERROR TRADEOFF CHARACTERISTIC: MUGSHOT IMAGES	110
61	ERROR TRADEOFF CHARACTERISTIC: MUGSHOT IMAGES	111
62	ERROR TRADEOFF CHARACTERISTIC: MUGSHOT IMAGES	112
63	ERROR TRADEOFF CHARACTERISTIC: MUGSHOT IMAGES	113
64	ERROR TRADEOFF CHARACTERISTIC: MUGSHOT IMAGES	114
65	ERROR TRADEOFF CHARACTERISTIC: MUGSHOT IMAGES	115
66	ERROR TRADEOFF CHARACTERISTIC: MUGSHOT IMAGES	116
67	ERROR TRADEOFF CHARACTERISTIC: MUGSHOT IMAGES	117
68	ERROR TRADEOFF CHARACTERISTIC: MUGSHOT IMAGES	118
69	ERROR TRADEOFF CHARACTERISTIC: MUGSHOT IMAGES	119
70	ERROR TRADEOFF CHARACTERISTIC: MUGSHOT IMAGES	120
71	ERROR TRADEOFF CHARACTERISTIC: WILD IMAGES	121
72	ERROR TRADEOFF CHARACTERISTIC: WILD IMAGES	122
73	ERROR TRADEOFF CHARACTERISTIC: WILD IMAGES	123
74	ERROR TRADEOFF CHARACTERISTIC: WILD IMAGES	124
75	ERROR TRADEOFF CHARACTERISTIC: WILD IMAGES	125
76	ERROR TRADEOFF CHARACTERISTIC: WILD IMAGES	126
77	ERROR TRADEOFF CHARACTERISTIC: WILD IMAGES	127
78	ERROR TRADEOFF CHARACTERISTIC: WILD IMAGES	128
79	ERROR TRADEOFF CHARACTERISTIC: WILD IMAGES	129
80	ERROR TRADEOFF CHARACTERISTIC: WILD IMAGES	130
81	ERROR TRADEOFF CHARACTERISTIC: WILD IMAGES	131
82	ERROR TRADEOFF CHARACTERISTIC: WILD IMAGES	132
83	ERROR TRADEOFF CHARACTERISTIC: WILD IMAGES	133
84	ERROR TRADEOFF CHARACTERISTIC: WILD IMAGES	134
85	ERROR TRADEOFF CHARACTERISTIC: WILD IMAGES	135
86	ERROR TRADEOFF CHARACTERISTICS: CHILD EXPLOITATION IMAGES	136
87	ERROR TRADEOFF CHARACTERISTICS: CHILD EXPLOITATION IMAGES	137
88	ERROR TRADEOFF CHARACTERISTICS: CHILD EXPLOITATION IMAGES	138
89	CMC CHARACTERISTICS: CHILD EXPLOITATION IMAGES	139
90	CMC CHARACTERISTICS: CHILD EXPLOITATION IMAGES	140
91	CMC CHARACTERISTICS: CHILD EXPLOITATION IMAGES	141
92	CMC CHARACTERISTICS: CHILD EXPLOITATION IMAGES	142
93	CMC CHARACTERISTICS: CHILD EXPLOITATION IMAGES	143
94	FALSE MATCH RATES WITHIN AND ACROSS DEMOGRAPHIC GROUPS	144
95	FALSE MATCH RATES WITHIN AND ACROSS DEMOGRAPHIC GROUPS	145
96	FALSE MATCH RATES WITHIN AND ACROSS DEMOGRAPHIC GROUPS	146
97	FALSE MATCH RATES WITHIN AND ACROSS DEMOGRAPHIC GROUPS	147
98	FALSE MATCH RATES WITHIN AND ACROSS DEMOGRAPHIC GROUPS	148

99	FALSE MATCH RATES WITHIN AND ACROSS DEMOGRAPHIC GROUPS	149
100	FALSE MATCH RATES WITHIN AND ACROSS DEMOGRAPHIC GROUPS	150
101	FALSE MATCH RATES WITHIN AND ACROSS DEMOGRAPHIC GROUPS	151
102	FALSE MATCH RATES WITHIN AND ACROSS DEMOGRAPHIC GROUPS	152
103	FALSE MATCH RATES WITHIN AND ACROSS DEMOGRAPHIC GROUPS	153
104	FALSE MATCH RATES WITHIN AND ACROSS DEMOGRAPHIC GROUPS	154
105	FALSE MATCH RATES WITHIN AND ACROSS DEMOGRAPHIC GROUPS	155
106	FALSE MATCH RATES WITHIN AND ACROSS DEMOGRAPHIC GROUPS	156
107	FALSE MATCH RATES WITHIN AND ACROSS DEMOGRAPHIC GROUPS	157
108	FALSE MATCH RATES WITHIN AND ACROSS DEMOGRAPHIC GROUPS	158
109	FALSE MATCH RATES WITHIN AND ACROSS DEMOGRAPHIC GROUPS	159
110	FALSE MATCH RATES WITHIN AND ACROSS DEMOGRAPHIC GROUPS	160
111	SEX AND RACE EFFECTS: MUGSHOT IMAGES	161
112	SEX AND RACE EFFECTS: MUGSHOT IMAGES	162
113	SEX AND RACE EFFECTS: MUGSHOT IMAGES	163
114	SEX AND RACE EFFECTS: MUGSHOT IMAGES	164
115	SEX AND RACE EFFECTS: MUGSHOT IMAGES	165
116	SEX AND RACE EFFECTS: MUGSHOT IMAGES	166
117	SEX AND RACE EFFECTS: MUGSHOT IMAGES	167
118	SEX AND RACE EFFECTS: MUGSHOT IMAGES	168
119	SEX AND RACE EFFECTS: MUGSHOT IMAGES	169
120	SEX AND RACE EFFECTS: MUGSHOT IMAGES	170
121	SEX AND RACE EFFECTS: MUGSHOT IMAGES	171
122	SEX AND RACE EFFECTS: MUGSHOT IMAGES	172
123	SEX AND RACE EFFECTS: MUGSHOT IMAGES	173
124	SEX AND RACE EFFECTS: MUGSHOT IMAGES	174
125	SEX AND RACE EFFECTS: MUGSHOT IMAGES	175
126	SEX AND RACE EFFECTS: MUGSHOT IMAGES	176
127	SEX AND RACE EFFECTS: MUGSHOT IMAGES	177
128	SEX EFFECTS: VISA IMAGES	178
129	SEX EFFECTS: VISA IMAGES	179
130	SEX EFFECTS: VISA IMAGES	180
131	SEX EFFECTS: VISA IMAGES	181
132	SEX EFFECTS: VISA IMAGES	182
133	SEX EFFECTS: VISA IMAGES	183
134	SEX EFFECTS: VISA IMAGES	184
135	SEX EFFECTS: VISA IMAGES	185
136	SEX EFFECTS: VISA IMAGES	186
137	SEX EFFECTS: VISA IMAGES	187
138	SEX EFFECTS: VISA IMAGES	188
139	SEX EFFECTS: VISA IMAGES	189
140	SEX EFFECTS: VISA IMAGES	190
141	SEX EFFECTS: VISA IMAGES	191
142	SEX EFFECTS: VISA IMAGES	192
143	SEX EFFECTS: VISA IMAGES	193
144	SEX EFFECTS: VISA IMAGES	194
145	SEX EFFECTS: VISA IMAGES	195
146	SEX EFFECTS: VISA IMAGES	196
147	SEX EFFECTS: VISA IMAGES	197
148	SEX EFFECTS: VISA IMAGES	198
149	SEX EFFECTS: VISA IMAGES	199
150	SEX EFFECTS: VISA IMAGES	200
151	SEX EFFECTS: VISA IMAGES	201
152	SEX EFFECTS: VISA IMAGES	202
153	SEX EFFECTS: VISA IMAGES	203
154	SEX EFFECTS: VISA IMAGES	204
155	SEX EFFECTS: VISA IMAGES	205

156	SEX EFFECTS: VISA IMAGES . . . . .	206
157	FALSE MATCH RATE CALIBRATION: MUGSHOT IMAGES . . . . .	207
158	FALSE MATCH RATE CALIBRATION: MUGSHOT IMAGES . . . . .	208
159	FALSE MATCH RATE CALIBRATION: MUGSHOT IMAGES . . . . .	209
160	FALSE MATCH RATE CALIBRATION: MUGSHOT IMAGES . . . . .	210
161	FALSE MATCH RATE CALIBRATION: MUGSHOT IMAGES . . . . .	211
162	FALSE MATCH RATE CALIBRATION: MUGSHOT IMAGES . . . . .	212
163	FALSE MATCH RATE CALIBRATION: MUGSHOT IMAGES . . . . .	213
164	FALSE MATCH RATE CALIBRATION: MUGSHOT IMAGES . . . . .	214
165	FALSE MATCH RATE CALIBRATION: MUGSHOT IMAGES . . . . .	215
166	FALSE MATCH RATE CALIBRATION: MUGSHOT IMAGES . . . . .	216
167	FALSE MATCH RATE CALIBRATION: MUGSHOT IMAGES . . . . .	217
168	FALSE MATCH RATE CALIBRATION: MUGSHOT IMAGES . . . . .	218
169	FALSE MATCH RATE CALIBRATION: MUGSHOT IMAGES . . . . .	219
170	FALSE MATCH RATE CALIBRATION: MUGSHOT IMAGES . . . . .	220
171	FALSE MATCH RATE CALIBRATION: MUGSHOT IMAGES . . . . .	221
172	FALSE MATCH RATE CALIBRATION: MUGSHOT IMAGES . . . . .	222
173	FALSE MATCH RATE CALIBRATION: MUGSHOT IMAGES . . . . .	223
174	FALSE MATCH RATE CALIBRATION: VISA IMAGES . . . . .	224
175	FALSE MATCH RATE CALIBRATION: VISA IMAGES . . . . .	225
176	FALSE MATCH RATE CALIBRATION: VISA IMAGES . . . . .	226
177	FALSE MATCH RATE CALIBRATION: VISA IMAGES . . . . .	227
178	FALSE MATCH RATE CALIBRATION: VISA IMAGES . . . . .	228
179	FALSE MATCH RATE CALIBRATION: VISA IMAGES . . . . .	229
180	FALSE MATCH RATE CALIBRATION: VISA IMAGES . . . . .	230
181	FALSE MATCH RATE CALIBRATION: VISA IMAGES . . . . .	231
182	FALSE MATCH RATE CALIBRATION: VISA IMAGES . . . . .	232
183	FALSE MATCH RATE CALIBRATION: VISA IMAGES . . . . .	233
184	FALSE MATCH RATE CALIBRATION: VISA IMAGES . . . . .	234
185	FALSE MATCH RATE CALIBRATION: VISA IMAGES . . . . .	235
186	FALSE MATCH RATE CALIBRATION: VISA IMAGES . . . . .	236
187	FALSE MATCH RATE CALIBRATION: VISA IMAGES . . . . .	237
188	FALSE MATCH RATE CALIBRATION: VISA IMAGES . . . . .	238
189	FALSE MATCH RATE CALIBRATION: VISA IMAGES . . . . .	239
190	FALSE MATCH RATE CALIBRATION: VISA IMAGES . . . . .	240
191	FALSE MATCH RATE CALIBRATION: VISA IMAGES . . . . .	241
192	FALSE MATCH RATE CALIBRATION: VISA IMAGES . . . . .	242
193	FALSE MATCH RATE CALIBRATION: VISA IMAGES . . . . .	243
194	FALSE MATCH RATE CALIBRATION: VISA IMAGES . . . . .	244
195	FALSE MATCH RATE CALIBRATION: VISA IMAGES . . . . .	245
196	FALSE MATCH RATE CALIBRATION: VISA IMAGES . . . . .	246
197	FALSE MATCH RATE CALIBRATION: VISA IMAGES . . . . .	247
198	FALSE MATCH RATE CALIBRATION: VISA IMAGES . . . . .	248
199	FALSE MATCH RATE CALIBRATION: VISA IMAGES . . . . .	249
200	FALSE MATCH RATE CALIBRATION: VISA IMAGES . . . . .	250
201	FALSE MATCH RATE CALIBRATION: VISA IMAGES . . . . .	251
202	FALSE MATCH RATE CALIBRATION: VISA IMAGES . . . . .	252
203	FALSE MATCH RATE CALIBRATION: VISA IMAGES . . . . .	253
204	FALSE MATCH RATE CALIBRATION: VISA IMAGES . . . . .	254
205	FALSE MATCH RATE CALIBRATION: VISA IMAGES . . . . .	255
206	FALSE MATCH RATE CALIBRATION: VISA IMAGES . . . . .	256
207	FALSE MATCH RATE CALIBRATION: VISA IMAGES . . . . .	257
208	FALSE MATCH RATE CALIBRATION: VISA IMAGES . . . . .	258
209	EFFECT OF COUNTRY OF BIRTH ON FNMR . . . . .	260
210	EFFECT OF COUNTRY OF BIRTH ON FNMR . . . . .	261
211	EFFECT OF COUNTRY OF BIRTH ON FNMR . . . . .	262
212	EFFECT OF COUNTRY OF BIRTH ON FNMR . . . . .	263

213	EFFECT OF COUNTRY OF BIRTH ON FNMR . . . . .	264
214	EFFECT OF COUNTRY OF BIRTH ON FNMR . . . . .	265
215	EFFECT OF COUNTRY OF BIRTH ON FNMR . . . . .	266
216	EFFECT OF COUNTRY OF BIRTH ON FNMR . . . . .	267
217	EFFECT OF COUNTRY OF BIRTH ON FNMR . . . . .	268
218	EFFECT OF COUNTRY OF BIRTH ON FNMR . . . . .	269
219	EFFECT OF COUNTRY OF BIRTH ON FNMR . . . . .	270
220	EFFECT OF COUNTRY OF BIRTH ON FNMR . . . . .	271
221	EFFECT OF COUNTRY OF BIRTH ON FNMR . . . . .	272
222	EFFECT OF COUNTRY OF BIRTH ON FNMR . . . . .	273
223	EFFECT OF COUNTRY OF BIRTH ON FNMR . . . . .	274
224	EFFECT OF COUNTRY OF BIRTH ON FNMR . . . . .	275
225	EFFECT OF COUNTRY OF BIRTH ON FNMR . . . . .	276
226	EFFECT OF COUNTRY OF BIRTH ON FNMR . . . . .	277
227	EFFECT OF COUNTRY OF BIRTH ON FNMR . . . . .	278
228	EFFECT OF COUNTRY OF BIRTH ON FNMR . . . . .	279
229	EFFECT OF COUNTRY OF BIRTH ON FNMR . . . . .	280
230	EFFECT OF COUNTRY OF BIRTH ON FNMR . . . . .	281
231	EFFECT OF COUNTRY OF BIRTH ON FNMR . . . . .	282
232	EFFECT OF COUNTRY OF BIRTH ON FNMR . . . . .	283
233	EFFECT OF COUNTRY OF BIRTH ON FNMR . . . . .	284
234	EFFECT OF COUNTRY OF BIRTH ON FNMR . . . . .	285
235	EFFECT OF COUNTRY OF BIRTH ON FNMR . . . . .	286
236	EFFECT OF COUNTRY OF BIRTH ON FNMR . . . . .	287
237	EFFECT OF COUNTRY OF BIRTH ON FNMR . . . . .	288
238	ERROR TRADEOFF CHARACTERISTIC: MUGSHOT IMAGES . . . . .	290
239	ERROR TRADEOFF CHARACTERISTIC: MUGSHOT IMAGES . . . . .	291
240	ERROR TRADEOFF CHARACTERISTIC: MUGSHOT IMAGES . . . . .	292
241	ERROR TRADEOFF CHARACTERISTIC: MUGSHOT IMAGES . . . . .	293
242	ERROR TRADEOFF CHARACTERISTIC: MUGSHOT IMAGES . . . . .	294
243	ERROR TRADEOFF CHARACTERISTIC: MUGSHOT IMAGES . . . . .	295
244	ERROR TRADEOFF CHARACTERISTIC: MUGSHOT IMAGES . . . . .	296
245	ERROR TRADEOFF CHARACTERISTIC: MUGSHOT IMAGES . . . . .	297
246	ERROR TRADEOFF CHARACTERISTIC: MUGSHOT IMAGES . . . . .	298
247	ERROR TRADEOFF CHARACTERISTIC: MUGSHOT IMAGES . . . . .	299
248	ERROR TRADEOFF CHARACTERISTIC: MUGSHOT IMAGES . . . . .	300
249	ERROR TRADEOFF CHARACTERISTIC: MUGSHOT IMAGES . . . . .	301
250	ERROR TRADEOFF CHARACTERISTIC: MUGSHOT IMAGES . . . . .	302
251	ERROR TRADEOFF CHARACTERISTIC: MUGSHOT IMAGES . . . . .	303
252	ERROR TRADEOFF CHARACTERISTIC: MUGSHOT IMAGES . . . . .	304
253	ERROR TRADEOFF CHARACTERISTIC: MUGSHOT IMAGES . . . . .	305
254	ERROR TRADEOFF CHARACTERISTIC: MUGSHOT IMAGES . . . . .	306
255	ERROR TRADEOFF CHARACTERISTIC: MUGSHOT IMAGES . . . . .	307
256	ERROR TRADEOFF CHARACTERISTIC: MUGSHOT IMAGES . . . . .	308
257	ERROR TRADEOFF CHARACTERISTIC: MUGSHOT IMAGES . . . . .	309
258	ERROR TRADEOFF CHARACTERISTIC: MUGSHOT IMAGES . . . . .	310
259	EFFECT OF SUBJECT AGE ON FNMR . . . . .	312
260	EFFECT OF SUBJECT AGE ON FNMR . . . . .	313
261	EFFECT OF SUBJECT AGE ON FNMR . . . . .	314
262	EFFECT OF SUBJECT AGE ON FNMR . . . . .	315
263	EFFECT OF SUBJECT AGE ON FNMR . . . . .	316
264	EFFECT OF SUBJECT AGE ON FNMR . . . . .	317
265	EFFECT OF SUBJECT AGE ON FNMR . . . . .	318
266	EFFECT OF SUBJECT AGE ON FNMR . . . . .	319
267	EFFECT OF SUBJECT AGE ON FNMR . . . . .	320
268	EFFECT OF SUBJECT AGE ON FNMR . . . . .	321

269	EFFECT OF SUBJECT AGE ON FNMR	322
270	EFFECT OF SUBJECT AGE ON FNMR	323
271	EFFECT OF SUBJECT AGE ON FNMR	324
272	EFFECT OF SUBJECT AGE ON FNMR	325
273	EFFECT OF SUBJECT AGE ON FNMR	326
274	EFFECT OF SUBJECT AGE ON FNMR	327
275	EFFECT OF SUBJECT AGE ON FNMR	328
276	EFFECT OF SUBJECT AGE ON FNMR	329
277	EFFECT OF SUBJECT AGE ON FNMR	330
278	EFFECT OF SUBJECT AGE ON FNMR	331
279	EFFECT OF SUBJECT AGE ON FNMR	332
280	EFFECT OF SUBJECT AGE ON FNMR	333
281	EFFECT OF SUBJECT AGE ON FNMR	334
282	EFFECT OF SUBJECT AGE ON FNMR	335
283	EFFECT OF SUBJECT AGE ON FNMR	336
284	EFFECT OF SUBJECT AGE ON FNMR	337
285	EFFECT OF SUBJECT AGE ON FNMR	338
286	EFFECT OF SUBJECT AGE ON FNMR	339
287	EFFECT OF SUBJECT AGE ON FNMR	340
288	WORST CASE REGIONAL EFFECT FNMR	343
289	IMPOSTOR DISTRIBUTION SHIFTS FOR SELECT COUNTRY PAIRS	345

	Location	Developer Name	Short Name	Seq. Num.	Validation Date
1	NL	20Face	20face-000	000	2021-04-12
2	US	3Divi	3divi-005	005	2020-08-28
3	US	3Divi	3divi-006	006	2021-04-14
4	TH	ACI Software	acisw-003	003	2020-08-03
5	TH	ACI Software	acisw-006	006	2021-02-25
6	SG	ADVANCE.AI	advance-002	002	2019-12-19
7	SG	ADVANCE.AI	advance-003	003	2021-08-05
8	TW	ASUSTek Computer Inc	asusaics-000	000	2019-10-24
9	TW	ASUSTek Computer Inc	asusaics-001	001	2020-02-25
10	CN	AYF Technology	ayftech-001	001	2020-07-06
11	TW	Ability Enterprise - Andro Video	androvideo-000	000	2021-01-25
12	TW	Acer Incorporated	acer-000	000	2020-01-08
13	TW	Acer Incorporated	acer-001	001	2020-06-30
14	SG	Adera Global PTE	adera-002	002	2021-02-16
15	SG	Adera Global PTE	adera-003	003	2021-07-12
16	TH	Ai First	aifirst-001	001	2019-11-21
17	TW	AiUnion Technology	aiunionface-000	000	2019-10-22
18	TH	Aigen	aigen-001	001	2020-10-06
19	TH	Aigen	aigen-002	002	2021-03-15
20	KR	Ajou University	ajou-001	001	2021-03-08
21	ID	Akurat Satu Indonesia	ptakuratsatu-000	000	2020-09-11
22	KR	Alchera Inc	alchera-002	002	2021-03-05
23	KR	Alchera Inc	alchera-003	003	2021-07-13
24	ES	Alice Biometrics	alice-000	000	2021-06-15
25	RU	Alivia / Innovation Sys	isystems-001	001	2018-06-12
26	RU	Alivia / Innovation Sys	isystems-002	002	2018-10-18
27	IN	AllGoVision	allgovision-000	000	2019-03-01
28	CN	AlphaSSTG	alphaface-001	001	2019-09-03
29	CN	AlphaSSTG	alphaface-002	002	2020-02-20
30	GB	Amplified Group	amplifiedgroup-001	001	2019-03-01
31	CN	Anke Investments	anke-004	004	2019-06-27
32	CN	Anke Investments	anke-005	005	2019-11-21
33	BR	Antheus Technologia	antheus-000	000	2019-12-05
34	BR	Antheus Technologia	antheus-001	001	2020-06-25
35	GB	AnyVision	anyvision-004	004	2018-06-15
36	GB	AnyVision	anyvision-005	005	2021-02-03
37	CN	AuthenMetric	authenmetric-002	002	2021-03-10
38	CN	AuthenMetric	authenmetric-003	003	2021-08-09
39	US	Aware	aware-005	005	2020-02-27
40	US	Aware	aware-006	006	2021-07-03
41	IN	Awidit Systems	awiros-001	001	2019-09-23
42	IN	Awidit Systems	awiros-002	002	2020-10-28
43	JP	Ayonix	ayonix-000	000	2017-06-22
44	CN	BOE Technology Group	boetech-001	001	2021-06-22
45	ES	Bee the Data	beethedata-000	000	2021-07-26
46	CN	Beihang University-ERCACAT	ercacat-001	001	2020-07-06
47	CN	Beijing Alleyes Technology	alleyes-000	000	2020-03-09
48	CN	Beijing DeepSense Technologies	deepsense-000	000	2021-03-19
49	CN	Beijing Vion Technology Inc	vion-000	000	2018-10-19
50	CH	BioID Technologies SA	bioidtechswiss-001	001	2020-08-28
51	CH	BioID Technologies SA	bioidtechswiss-002	002	2021-02-17
52	UK	BitCenter UK	farfaces-001	001	2021-04-09
53	CN	Bitmain	bm-001	001	2018-10-17
54	CN	Bresee Technology	bresee-001	001	2020-12-30
55	CN	Bresee Technology	bresee-002	002	2021-06-30
56	CN	CSA IntelliCloud Technology	intellicloudai-001	001	2019-08-13
57	CN	CSA IntelliCloud Technology	intellicloudai-002	002	2020-12-17
58	TW	CTBC Bank	ctbcbank-000	000	2019-06-28
59	TW	CTBC Bank	ctbcbank-001	001	2019-10-28
60	US	Camvi Technologies	camvi-002	002	2018-10-19
61	US	Camvi Technologies	camvi-004	004	2019-07-12
62	CN	Canon Inc	canon-002	002	2020-12-29
63	CN	Canon Inc	cib-001	001	2020-08-05
64	CN	China Electronics Import-Export Corp	ceiec-003	003	2020-01-06
65	CN	China Electronics Import-Export Corp	ceiec-004	004	2021-01-18
66	CN	China University of Petroleum	upc-001	001	2019-06-05
67	CN	Chinese University of Hong Kong	cuhknee-001	001	2020-03-18
68	KR	Chosun University	chosun-001	001	2020-07-01
69	KR	Chosun University	chosun-002	002	2020-11-25
70	TW	Chungwha Telecom	chtface-002	002	2019-12-07

Table 1: Summary of participant information included in this report.

	Location	Developer Name	Short Name	Seq. Num.	Validation Date
71	TW	Chunghwa Telecom	chtface-003	003	2020-06-24
72	CN	Closeli Inc	closeli-001	001	2021-07-15
73	US	CloudSmart Consulting LLC	csc-002	002	2021-03-24
74	US	CloudSmart Consulting LLC	csc-003	003	2021-08-26
75	CN	Cloudwalk - Hengrui AI Technology	cloudwalk-hr-003	003	2020-09-25
76	CN	Cloudwalk - Hengrui AI Technology	cloudwalk-hr-004	004	2021-02-10
77	CN	Cloudwalk - Moontime Smart Technology	cloudwalk-mt-002	002	2020-07-02
78	CN	Cloudwalk - Moontime Smart Technology	cloudwalk-mt-003	003	2020-12-22
79	IN	Code Everest Pvt	facex-001	001	2021-03-08
80	IN	Code Everest Pvt	facex-002	002	2021-08-24
81	DE	Cognitec Systems GmbH	cognitec-002	002	2021-02-24
82	DE	Cognitec Systems GmbH	cognitec-003	003	2021-07-30
83	TW	Coretech Knowledge Inc	coretech-000	000	2021-07-12
84	IL	Corsight	corsight-001	001	2021-03-11
85	IL	Cortica	cor-001	001	2020-09-24
86	KR	Cubox	cubox-001	001	2020-12-07
87	KR	Cubox	cubox-002	002	2021-08-24
88	JP	Cybercore	cybercore-000	000	2020-08-26
89	US	Cyberextruder	cyberextruder-001	001	2017-08-02
90	US	Cyberextruder	cyberextruder-002	002	2018-01-30
91	TW	Cyberlink Corp	cyberlink-006	006	2021-01-08
92	TW	Cyberlink Corp	cyberlink-007	007	2021-07-16
93	CN	DSK	dsk-000	000	2019-06-28
94	CN	Dahua Technology	dahua-005	005	2020-08-13
95	CN	Dahua Technology	dahua-006	006	2020-12-30
96	US	Decatur Industries Inc	decatur-000	000	2020-08-18
97	CN	Deepglint	deepglint-002	002	2019-11-15
98	CN	Deepglint	deepglint-003	003	2021-03-03
99	FR	Deepsense	dps-000	000	2021-07-16
100	DE	Dermalog	dermalog-006	006	2018-10-18
101	DE	Dermalog	dermalog-008	008	2021-03-25
102	CN	DiDi ChuXing Technology	didiglobalface-001	001	2019-10-23
103	GB	Digital Barriers	digitalbarriers-002	002	2019-03-01
104	TR	Ekin Smart City Technologies	ekin-002	002	2021-05-04
105	RU	Enface	enface-000	000	2021-04-09
106	RU	Expasoft LLC	expasoft-001	001	2020-09-03
107	RU	Expasoft LLC	expasoft-002	002	2021-07-26
108	GB	FaceSoft	facesoft-000	000	2019-07-10
109	KR	FaceTag Co	facetag-000	000	2021-03-22
110	TW	FarBar Inc	f8-001	001	2019-07-11
111	UK	Fincore Ltd	fincore-000	000	2021-06-07
112	CN	Fujitsu Research and Development Center	fujitsulab-002	002	2021-02-24
113	CN	Fujitsu Research and Development Center	fujitsulab-003	003	2021-07-12
114	US	Gemalto Cogent	cogent-005	005	2020-12-29
115	US	Gemalto Cogent	cogent-006	006	2021-07-28
116	TW	GeoVision Inc	geo-001	001	2020-10-30
117	TW	GeoVision Inc	geo-002	002	2021-04-01
118	JP	Glory	glory-002	002	2019-11-12
119	JP	Glory	glory-003	003	2021-01-15
120	TW	Gorilla Technology	gorilla-006	006	2020-07-31
121	TW	Gorilla Technology	gorilla-007	007	2021-06-28
122	US	Griaule	griaule-000	000	2021-08-20
123	CN	Guangzhou Pixel Solutions	pixelall-005	005	2021-02-05
124	CN	Guangzhou Pixel Solutions	pixelall-006	006	2021-06-17
125	ES	Herta Security	hertasecurity-000	000	2021-01-05
126	CN	Hikvision Research Institute	hik-001	001	2019-03-01
127	IN	HyperVerge Inc	hyperverge-001	001	2020-12-13
128	IN	HyperVerge Inc	hyperverge-002	002	2021-05-27
129	AU	ICM Airport Technics	icm-002	002	2020-11-13
130	FR	ID3 Technology	id3-006	006	2020-12-17
131	FR	ID3 Technology	id3-007	007	2021-05-17
132	RU	ITMO University	itmo-006	006	2019-03-01
133	RU	ITMO University	itmo-007	007	2020-01-06
134	RU	IVA Cognitive	ivacognitive-001	001	2021-01-29
135	FR	Idemia	idemia-007	007	2020-12-04
136	FR	Idemia	idemia-008	008	2021-07-07
137	US	Imageware Systems	iws-000	000	2020-08-12
138	AU	Imagus Technology Pty	imagus-002	002	2020-12-31
139	AU	Imagus Technology Pty	imagus-003	003	2021-05-18
140	GB	Imperial College London	imperial-000	000	2019-03-01

Table 2: Summary of participant information included in this report.

	Location	Developer Name	Short Name	Seq. Num.	Validation Date
141	GB	Imperial College London	imperial-002	002	2019-08-28
142	US	Incode Technologies Inc	incode-008	008	2021-01-19
143	US	Incode Technologies Inc	incode-009	009	2021-06-22
144	IN	Innef Labs	inneflabs-000	000	2020-09-04
145	GB	Innovative Technology	innovativetechnologyltd-001	001	2019-10-22
146	GB	Innovative Technology	innovativetechnologyltd-002	002	2020-02-26
147	SK	Innovatrics	innovatrics-006	006	2019-08-13
148	SK	Innovatrics	innovatrics-007	007	2020-08-19
149	CN	InsightFace AI	insightface-000	000	2021-03-17
150	CN	Institute of Computing Technology	icthtc-000	000	2020-11-29
151	RU	Institute of Information Technologies	iit-002	002	2019-12-04
152	RU	Institute of Information Technologies	iit-003	003	2020-12-01
153	IS	Intel Research Group	intelresearch-003	003	2021-01-18
154	IS	Intel Research Group	intelresearch-004	004	2021-08-24
155	US	Intellivision	intellivision-001	001	2017-10-10
156	US	Intellivision	intellivision-002	002	2019-08-23
157	US	IrexAI	irex-000	000	2020-12-17
158	IL	Is It You	isityou-000	000	2017-06-26
159	KR	Kakao Enterprise	kakao-004	004	2020-10-28
160	KR	Kakao Enterprise	kakao-005	005	2021-03-09
161	KR	Kakao Pay Corp	kakaopay-001	001	2021-07-06
162	SG	Kedacom International Pte	kedacom-000	000	2019-06-03
163	US	Kneron Inc	kneron-003	003	2019-07-01
164	US	Kneron Inc	kneron-005	005	2020-02-21
165	KR	Kookmin University	kookmin-001	001	2020-09-28
166	KR	Kookmin University	kookmin-002	002	2021-03-05
167	IN	Lema Labs	lemalabs-001	001	2021-04-13
168	JP	Line Corporation	line-000	000	2021-03-31
169	RU	Lomonosov Moscow State University	intsyssmu-001	001	2019-10-22
170	RU	Lomonosov Moscow State University	intsyssmu-002	002	2020-03-12
171	IN	Lookman Electroplast Industries	lookman-002	002	2018-06-13
172	IN	Lookman Electroplast Industries	lookman-004	004	2019-06-03
173	US	Luxand Inc	luxand-000	000	2019-11-07
174	RU	MVision	mvision-001	001	2019-11-12
175	CN	Megvii/Face++	megvii-002	002	2018-10-19
176	CN	Megvii/Face++	megvii-003	003	2021-03-08
177	GB	MicroFocus	microfocus-001	001	2018-06-13
178	GB	MicroFocus	microfocus-002	002	2018-10-17
179	CN	Minivision	minivision-000	000	2020-10-28
180	NO	Mobai	mobai-000	000	2020-08-26
181	NO	Mobai	mobai-001	001	2021-02-17
182	ES	Mobbel Solutions	mobbl-000	000	2021-01-28
183	ES	Mobbel Solutions	mobbl-001	001	2021-06-16
184	TH	Momentum Digital	sertis-000	000	2019-10-07
185	TH	Momentum Digital	sertis-002	002	2021-05-13
186	CN	MoreDian Technology	moreedian-000	000	2021-02-24
187	RU	N-Tech Lab	ntechlab-009	009	2020-12-30
188	RU	N-Tech Lab	ntechlab-010	010	2021-04-30
189	CA	NEO Systems	neosystems-001	001	2021-03-02
190	CA	NEO Systems	neosystems-002	002	2021-07-03
191	KR	NHN Corp	nhn-001	001	2021-03-15
192	KR	NHN Corp	nhn-002	002	2021-07-15
193	KR	NSENSE Corp	nsensecorp-001	001	2020-10-20
194	KR	NSENSE Corp	nsensecorp-002	002	2021-05-06
195	CN	Nanjing Kiwi Network Technology	kiwitech-000	000	2021-03-19
196	KR	Naver Corp	clova-000	000	2020-10-21
197	KR	Neosecu Co	openface-001	001	2021-06-15
198	TW	Netbridge Technology Incoporation	netbridgetech-001	001	2020-01-08
199	TW	Netbridge Technology Incoporation	netbridgetech-002	002	2020-08-11
200	LT	Neurotechnology	neurotechnology-011	011	2021-03-26
201	LT	Neurotechnology	neurotechnology-012	012	2021-07-26
202	ID	Nodeflux	nodeflux-002	002	2019-08-13
203	IN	NotionTag Technologies Private Limited	notiontag-000	000	2019-06-12
204	IN	NotionTag Technologies Private Limited	notiontag-001	001	2021-03-04
205	US	Omnigarde Ltd	omnigarde-000	000	2021-04-05
206	US	Omnigarde Ltd	omnigarde-001	001	2021-08-23
207	RU	Oz Forensics LLC	oz-002	002	2021-01-18
208	RU	Oz Forensics LLC	oz-003	003	2021-08-09
209	CH	PXL Vision AG	pxl-001	001	2020-06-30
210	SG	Panasonic R+D Center Singapore	psl-007	007	2021-03-19

Table 3: Summary of participant information included in this report.

	Location	Developer Name	Short Name	Seq. Num.	Validation Date
211	SG	Panasonic R+D Center Singapore	psl-008	008	2021-07-21
212	TR	Papilon Savunma	papsav1923-001	001	2021-03-10
213	US	Paravision (EverAI)	paravision-004	004	2019-12-11
214	US	Paravision (EverAI)	paravision-008	008	2021-06-30
215	SG	Pensees Pte	pensees-001	001	2020-08-17
216	IN	Pyramid Cyber Security + Forensic (P)	pyramid-000	000	2019-11-04
217	TW	Qnap Security	qnap-000	000	2021-08-09
218	CZ	Quantasoft	quantasoft-003	003	2021-04-19
219	US	Rank One Computing	rankone-010	010	2020-11-05
220	US	Rank One Computing	rankone-011	011	2021-08-27
221	US	Realnetworks Inc	realnetworks-002	002	2019-02-28
222	US	Realnetworks Inc	realnetworks-004	004	2021-04-15
223	US	Regula Forensics	regula-000	000	2021-04-13
224	CN	Remark Holdings	remarkai-001	001	2019-03-01
225	CN	Remark Holdings	remarkai-003	003	2021-06-22
226	SG	Rendip	rendip-000	000	2021-04-19
227	CN	Rokid Corporation	rokid-000	000	2019-08-01
228	CN	Rokid Corporation	rokid-001	001	2019-12-13
229	KR	SK Telecom	sktelecom-000	000	2021-07-09
230	KR	SQIsoft	sqisoft-001	001	2021-07-27
231	DE	Saffe	saffe-001	001	2018-10-19
232	DE	Saffe	saffe-002	002	2019-03-01
233	KR	Samsung SI Corp	s1-002	002	2021-03-24
234	KR	Samsung SI Corp	s1-003	003	2021-08-24
235	IN	Samtech InfoNet Limited	samtech-001	001	2019-10-15
236	RU	Satellite Innovation/Eocortex	eocortex-000	000	2020-08-26
237	IL	Scanovate	scanovate-001	001	2019-11-12
238	IL	Scanovate	scanovate-002	002	2020-06-26
239	RO	Securif AI	securifai-001	001	2020-10-06
240	RO	Securif AI	securifai-003	003	2021-08-03
241	CN	Sensetime Group	sensetime-004	004	2020-11-20
242	CN	Sensetime Group	sensetime-005	005	2021-05-24
243	SG	Seventh Sense Artificial Intelligence	seventhsense-000	000	2021-06-29
244	US	Shaman Software	shaman-000	000	2017-12-05
245	US	Shaman Software	shaman-001	001	2018-01-13
246	CN	Shanghai Jiao Tong University	situ-003	003	2020-11-02
247	CN	Shanghai Jiao Tong University	situ-004	004	2021-05-13
248	CN	Shanghai Ulucu Electronics Technology	uluface-002	002	2019-07-10
249	CN	Shanghai Ulucu Electronics Technology	uluface-003	003	2019-11-12
250	CN	Shanghai University - Shanghai Film Academy	shu-002	002	2019-12-10
251	CN	Shanghai University - Shanghai Film Academy	shu-003	003	2020-06-24
252	CN	Shanghai Yitu Technology	yitu-003	003	2019-03-01
253	CN	Shenzhen AiMall Tech	aimall-002	002	2020-03-12
254	CN	Shenzhen AiMall Tech	aimall-003	003	2020-08-12
255	CN	Shenzhen EI Networks	einetworks-000	000	2019-08-13
256	CN	Shenzhen Inst Adv Integrated Tech CAS	siat-002	002	2018-06-13
257	CN	Shenzhen Inst Adv Integrated Tech CAS	siat-004	004	2019-03-01
258	CN	Shenzhen Intellifusion Technologies	intellifusion-001	001	2019-08-22
259	CN	Shenzhen Intellifusion Technologies	intellifusion-002	002	2020-03-18
260	CN	Shenzhen University-Macau University of Science and Technology	sztu-000	000	2020-12-17
261	CN	Shenzhen University-Macau University of Science and Technology	sztu-001	001	2021-07-13
262	RU	Smart Engines	smartengines-000	000	2021-08-25
263	DE	Smilart	smilart-002	002	2018-02-06
264	DE	Smilart	smilart-003	003	2018-06-18
265	TR	Sodec App Inc	sodec-000	000	2021-06-02
266	IN	Staqu Technologies	st aqu-000	000	2020-07-15
267	CN	Star Hybrid Limited	starhybrid-001	001	2019-06-19
268	CN	Su Zhou NaZhiTianDi intelligent technology	nazhiai-000	000	2020-06-25
269	KR	Suprema	suprema-000	000	2021-03-31
270	KR	Suprema ID Inc	supremai d-001	001	2021-05-04
271	RU	Synesis	synesis-006	006	2019-10-10
272	RU	Synesis	synesis-007	007	2020-06-24
273	TW	Synology Inc	synology-000	000	2019-10-23
274	TW	Synology Inc	synology-002	002	2020-08-20
275	CN	TUPU Technology	tuputech-000	000	2019-10-11
276	TW	Taiwan AI Labs	ailabs-001	001	2019-12-18
277	TW	Taiwan-Certificate Authority Incorporatio	twface-000	000	2021-05-14
278	CH	Tech5 SA	tech5-004	004	2020-03-09
279	CH	Tech5 SA	tech5-005	005	2020-07-24
280	TR	Techsign	techsign-000	000	2021-08-25

Table 4: Summary of participant information included in this report.

	Location	Developer Name	Short Name	Seq. Num.	Validation Date
281	CN	Tencent Deepsea Lab	deepsea-001	001	2019-06-03
282	RU	Tevian	tevian-006	006	2020-09-11
283	RU	Tevian	tevian-007	007	2021-08-06
284	US	TigerIT Americas LLC	tiger-003	003	2018-10-16
285	US	TigerIT Americas LLC	tiger-005	005	2021-07-29
286	RU	Tinkoff Bank	tinkoff-001	001	2021-05-13
287	CN	TongYi Transportation Technology	tongyi-005	005	2019-06-12
288	JP	Toshiba	toshiba-002	002	2018-10-19
289	JP	Toshiba	toshiba-003	003	2019-03-01
290	JP	Tripleize	aize-001	001	2021-04-23
291	US	Trueface.ai	trueface-001	001	2020-07-20
292	US	Trueface.ai	trueface-002	002	2021-03-29
293	CN	ULSee Inc	ulsee-001	001	2019-07-31
294	PT	Universidade de Coimbra	visteam-001	001	2021-03-16
295	PT	Universidade de Coimbra	visteam-002	002	2021-08-20
296	US	VCognition	vcog-002	002	2017-06-12
297	ES	Veridas Digital Authentication Solutions S.L.	veridas-004	004	2020-07-21
298	ES	Veridas Digital Authentication Solutions S.L.	veridas-006	006	2021-04-15
299	TW	Via Technologies Inc	via-000	000	2019-07-08
300	TW	Via Technologies Inc	via-001	001	2020-01-08
301	DE	Videmo Intelligente Videoanalyse	videmo-000	000	2019-12-19
302	IN	Videonetech Technology Pvt	videonetechs-001	001	2019-06-19
303	IN	Videonetech Technology Pvt	videonetechs-002	002	2019-11-21
304	VN	Vietnam Posts and Telecommunications Group	vnpt-001	001	2021-01-08
305	VN	Vietnam Posts and Telecommunications Group	vnpt-002	002	2021-06-08
306	VN	Viettel Group	vts-000	000	2020-11-04
307	US	Vigilant Solutions	vigilantsolutions-010	010	2021-04-07
308	US	Vigilant Solutions	vigilantsolutions-011	011	2021-08-07
309	VN	VinAI Research VietNam	vinai-000	000	2020-09-24
310	SE	Visage Technologies	visage-000	000	2020-12-09
311	FI	Visidon	vd-001	001	2019-02-26
312	FI	Visidon	vd-002	002	2021-04-12
313	CN	Vision Intelligence Center of Meituan	meituan-000	000	2021-05-14
314	PT	Vision-Box	visionbox-001	001	2019-03-01
315	PT	Vision-Box	visionbox-002	002	2021-04-29
316	RU	VisionLabs	visionlabs-009	009	2020-07-27
317	RU	VisionLabs	visionlabs-010	010	2021-01-25
318	RU	Vocord	vocord-008	008	2020-01-31
319	RU	Vocord	vocord-009	009	2020-12-28
320	CN	Winsense	winsense-001	001	2019-10-16
321	CN	Winsense	winsense-002	002	2020-11-20
322	CN	Wuhan Tianyu Information Industry	wuhantianyu-001	001	2021-08-05
323	CN	Xforward AI Technology	xforwardai-001	001	2020-09-25
324	CN	Xforward AI Technology	xforwardai-002	002	2021-02-10
325	CN	Xiamen Meiya Pico Information	meiya-001	001	2019-03-01
326	CN	Xiamen University	xm-000	000	2020-10-19
327	PT	Yoonik	yoonik-000	000	2020-06-24
328	PT	Yoonik	yoonik-001	001	2020-10-26
329	TW	Yuan High-Tech Development	yuan-001	001	2021-01-08
330	TW	Yuan High-Tech Development	yuan-002	002	2021-05-17
331	CN	Yuntu Data and Technology	ytu-000	000	2021-06-16
332	CN	Zhuhai Yisheng Electronics Technology	yisheng-004	004	2018-06-12
333	CN	iQIYI Inc	iqface-000	000	2019-06-04
334	CN	iQIYI Inc	iqface-003	003	2021-02-23
335	TW	iSAP Solution Corporation	isap-001	001	2019-08-07
336	TW	iSAP Solution Corporation	isap-002	002	2020-09-01
337	TW	ioNetworks Inc	ionetworks-000	000	2021-07-20

Table 5: Summary of participant information included in this report.



				TEMPLATE								COMPARISON <sup>4</sup>	
ALGORITHM		CONFIG	LIBRARY	GENERATION TIME (ms) <sup>4</sup>								TIME (ns) <sup>5</sup>	
NAME		DATA	DATA	MEMORY	SIZE	MUGSHOT	480x720	960x1440	1600x2400	3000x4500	GENUINE	IMPOSTOR	
(KB) <sup>1</sup>	(KB) <sup>2</sup>	(MB) <sup>3</sup>	(B)										
45	ayonix-000	59909936	5252	5 <sup>69</sup>	67 <sup>1036 ± 0</sup>	2 <sup>18 ± 2</sup>	-	-	-	-	49 <sup>621 ± 23</sup>	53 <sup>620 ± 26</sup>	
46	beethedata-000	233318297	1087592	105 <sup>555</sup>	198 <sup>2048 ± 0</sup>	89 <sup>465 ± 0</sup>	65 <sup>467 ± 0</sup>	51 <sup>468 ± 0</sup>	38 <sup>467 ± 0</sup>	24 <sup>467 ± 0</sup>	179 <sup>2121 ± 34</sup>	179 <sup>2110 ± 38</sup>	
47	bioittechswiss-001	1207059515	120811	251 <sup>1455</sup>	27 <sup>512 ± 0</sup>	271 <sup>966 ± 4</sup>	275 <sup>1270 ± 270</sup>	261 <sup>1294 ± 96</sup>	251 <sup>1409 ± 157</sup>	234 <sup>1793 ± 79</sup>	201 <sup>2610 ± 25</sup>	203 <sup>2624 ± 32</sup>	
48	bioittechswiss-002	762660868	114842	198 <sup>993</sup>	25 <sup>512 ± 0</sup>	254 <sup>917 ± 2</sup>	207 <sup>930 ± 2</sup>	190 <sup>952 ± 2</sup>	167 <sup>947 ± 3</sup>	156 <sup>1058 ± 11</sup>	183 <sup>2177 ± 29</sup>	184 <sup>2170 ± 31</sup>	
49	bm-001	294640228	38076	21 <sup>148</sup>	7 <sup>64 ± 0</sup>	83 <sup>444 ± 88</sup>	-	-	-	-	166 <sup>1887 ± 31</sup>	166 <sup>1877 ± 26</sup>	
50	boetech-001	267649084	88710	241 <sup>1384</sup>	110 <sup>2048 ± 0</sup>	40 <sup>271 ± 1</sup>	27 <sup>268 ± 1</sup>	18 <sup>273 ± 0</sup>	17 <sup>286 ± 1</sup>	15 <sup>318 ± 1</sup>	326 <sup>68519 ± 1921</sup>	326 <sup>67648 ± 822</sup>	
51	bresee-001	294790077	23227	221 <sup>1214</sup>	231 <sup>2048 ± 0</sup>	317 <sup>1223 ± 3</sup>	266 <sup>1216 ± 1</sup>	268 <sup>1331 ± 1</sup>	225 <sup>1227 ± 1</sup>	202 <sup>1360 ± 1</sup>	314 <sup>37240 ± 655</sup>	315 <sup>37167 ± 384</sup>	
52	bresee-002	321154814	30902	285 <sup>1956</sup>	140 <sup>2048 ± 0</sup>	200 <sup>743 ± 4</sup>	255 <sup>1143 ± 2</sup>	238 <sup>1146 ± 2</sup>	209 <sup>1148 ± 2</sup>	178 <sup>1176 ± 2</sup>	154 <sup>1778 ± 22</sup>	155 <sup>1775 ± 23</sup>	
53	camvi-002	241949538	225285	141 <sup>737</sup>	57 <sup>1024 ± 0</sup>	181 <sup>677 ± 7</sup>	147 <sup>726 ± 36</sup>	161 <sup>869 ± 28</sup>	204 <sup>1129 ± 43</sup>	257 <sup>2785 ± 113</sup>	44 <sup>612 ± 26</sup>	46 <sup>603 ± 20</sup>	
54	camvi-004	287471548	615819	179 <sup>919</sup>	149 <sup>2048 ± 0</sup>	203 <sup>759 ± 10</sup>	186 <sup>861 ± 17</sup>	199 <sup>986 ± 34</sup>	234 <sup>1279 ± 51</sup>	258 <sup>2891 ± 158</sup>	91 <sup>948 ± 40</sup>	93 <sup>963 ± 31</sup>	
55	canon-002	457207046	130232	173 <sup>891</sup>	300 <sup>4096 ± 0</sup>	327 <sup>1308 ± 2</sup>	280 <sup>1315 ± 1</sup>	266 <sup>1326 ± 2</sup>	242 <sup>1345 ± 1</sup>	213 <sup>1452 ± 1</sup>	264 <sup>6211 ± 25</sup>	262 <sup>6194 ± 25</sup>	
56	ceiec-003	266620201	88707	61 <sup>430</sup>	174 <sup>2048 ± 0</sup>	222 <sup>817 ± 4</sup>	196 <sup>883 ± 57</sup>	171 <sup>897 ± 60</sup>	156 <sup>899 ± 72</sup>	130 <sup>944 ± 72</sup>	187 <sup>2256 ± 38</sup>	188 <sup>2241 ± 54</sup>	
57	ceiec-004	269799940	67011	55 <sup>408</sup>	145 <sup>2048 ± 0</sup>	282 <sup>1024 ± 1</sup>	227 <sup>1027 ± 1</sup>	209 <sup>1027 ± 1</sup>	186 <sup>1030 ± 1</sup>	154 <sup>1055 ± 1</sup>	163 <sup>1844 ± 26</sup>	163 <sup>1836 ± 28</sup>	
58	chosun-001	783990750	707	82 <sup>491</sup>	111 <sup>2048 ± 0</sup>	211 <sup>783 ± 2</sup>	173 <sup>826 ± 4</sup>	288 <sup>1662 ± 13</sup>	291 <sup>3679 ± 67</sup>	289 <sup>11694 ± 243</sup>	98 <sup>998 ± 25</sup>	104 <sup>1035 ± 14</sup>	
59	chosun-002	239617968	31875	67 <sup>450</sup>	98 <sup>2048 ± 0</sup>	34 <sup>248 ± 3</sup>	28 <sup>273 ± 3</sup>	283 <sup>1495 ± 14</sup>	294 <sup>7920 ± 90</sup>	297 <sup>80302 ± 1349</sup>	50 <sup>623 ± 17</sup>	60 <sup>634 ± 13</sup>	
60	chtface-002	371869498	369529	210 <sup>1100</sup>	171 <sup>2048 ± 0</sup>	136 <sup>584 ± 14</sup>	141 <sup>712 ± 41</sup>	216 <sup>1038 ± 42</sup>	271 <sup>1861 ± 75</sup>	270 <sup>4661 ± 232</sup>	188 <sup>2264 ± 26</sup>	187 <sup>2234 ± 103</sup>	
61	chtface-003	371869498	369529	217 <sup>1178</sup>	159 <sup>2048 ± 0</sup>	147 <sup>594 ± 16</sup>	145 <sup>720 ± 33</sup>	218 <sup>1050 ± 41</sup>	274 <sup>1884 ± 90</sup>	274 <sup>5606 ± 334</sup>	178 <sup>2110 ± 37</sup>	186 <sup>2219 ± 65</sup>	
62	cib-001	446723681	133766	160 <sup>836</sup>	119 <sup>2048 ± 0</sup>	166 <sup>651 ± 2</sup>	139 <sup>707 ± 13</sup>	128 <sup>716 ± 15</sup>	107 <sup>728 ± 3</sup>	104 <sup>820 ± 5</sup>	235 <sup>3783 ± 38</sup>	234 <sup>3765 ± 32</sup>	
63	closeti-001	430430427	9851	143 <sup>773</sup>	292 <sup>4096 ± 0</sup>	232 <sup>839 ± 1</sup>	180 <sup>843 ± 1</sup>	154 <sup>841 ± 1</sup>	138 <sup>845 ± 1</sup>	115 <sup>865 ± 1</sup>	250 <sup>5404 ± 17</sup>	250 <sup>5400 ± 26</sup>	
64	cloudwalk-hr-003	392949139	144263	196 <sup>984</sup>	267 <sup>2057 ± 0</sup>	149 <sup>606 ± 0</sup>	106 <sup>588 ± 0</sup>	88 <sup>594 ± 0</sup>	75 <sup>612 ± 1</sup>	-	270 <sup>6982 ± 80</sup>	268 <sup>6972 ± 38</sup>	
65	cloudwalk-hr-004	514986414	520169	243 <sup>1394</sup>	236 <sup>2049 ± 0</sup>	244 <sup>873 ± 1</sup>	193 <sup>877 ± 1</sup>	166 <sup>876 ± 1</sup>	149 <sup>879 ± 1</sup>	123 <sup>902 ± 3</sup>	284 <sup>11652 ± 127</sup>	283 <sup>11608 ± 128</sup>	
66	cloudwalk-mt-002	297731560	145340	162 <sup>844</sup>	234 <sup>2049 ± 0</sup>	131 <sup>573 ± 1</sup>	143 <sup>717 ± 78</sup>	124 <sup>700 ± 66</sup>	115 <sup>749 ± 96</sup>	96 <sup>770 ± 80</sup>	275 <sup>7205 ± 204</sup>	273 <sup>7211 ± 44</sup>	
67	cloudwalk-mt-003	502133796	494959	235 <sup>1342</sup>	235 <sup>2049 ± 0</sup>	256 <sup>923 ± 1</sup>	204 <sup>918 ± 1</sup>	181 <sup>926 ± 1</sup>	159 <sup>925 ± 1</sup>	129 <sup>936 ± 1</sup>	283 <sup>11620 ± 179</sup>	284 <sup>11661 ± 28</sup>	
68	clova-000	203182777	6824	71 <sup>464</sup>	100 <sup>2048 ± 0</sup>	81 <sup>437 ± 0</sup>	54 <sup>431 ± 0</sup>	41 <sup>435 ± 0</sup>	34 <sup>452 ± 2</sup>	28 <sup>508 ± 7</sup>	155 <sup>1794 ± 16</sup>	160 <sup>1795 ± 19</sup>	
69	cogent-005	1921839276	75276	307 <sup>2806</sup>	277 <sup>2523 ± 0</sup>	316 <sup>1221 ± 2</sup>	269 <sup>1236 ± 1</sup>	257 <sup>1289 ± 2</sup>	254 <sup>1420 ± 4</sup>	221 <sup>1602 ± 5</sup>	307 <sup>24854 ± 69</sup>	306 <sup>24858 ± 71</sup>	
70	cogent-006	1104043825	58108	258 <sup>1547</sup>	70 <sup>1062 ± 0</sup>	207 <sup>768 ± 0</sup>	164 <sup>789 ± 1</sup>	149 <sup>831 ± 2</sup>	160 <sup>930 ± 1</sup>	136 <sup>971 ± 1</sup>	158 <sup>1802 ± 17</sup>	161 <sup>1797 ± 20</sup>	
71	cognitec-002	403546749	62354	121 <sup>624</sup>	247 <sup>2052 ± 0</sup>	25 <sup>192 ± 6</sup>	17 <sup>219 ± 6</sup>	16 <sup>233 ± 8</sup>	14 <sup>241 ± 6</sup>	14 <sup>314 ± 10</sup>	220 <sup>3250 ± 41</sup>	221 <sup>3241 ± 48</sup>	
72	cognitec-003	482773320	62502	153 <sup>817</sup>	238 <sup>2052 ± 0</sup>	63 <sup>366 ± 9</sup>	48 <sup>403 ± 9</sup>	33 <sup>408 ± 9</sup>	29 <sup>424 ± 9</sup>	29 <sup>509 ± 13</sup>	223 <sup>3417 ± 51</sup>	227 <sup>3433 ± 53</sup>	
73	cor-001	1223627342	11240	225 <sup>1249</sup>	269 <sup>2060 ± 0</sup>	191 <sup>699 ± 3</sup>	188 <sup>863 ± 76</sup>	160 <sup>865 ± 80</sup>	145 <sup>872 ± 89</sup>	133 <sup>952 ± 39</sup>	336 <sup>270145 ± 2259</sup>	336 <sup>282686 ± 1178</sup>	
74	coretech-000	190897979	43964	52 <sup>393</sup>	35 <sup>512 ± 0</sup>	148 <sup>602 ± 15</sup>	124 <sup>659 ± 12</sup>	235 <sup>1139 ± 24</sup>	211 <sup>1149 ± 25</sup>	173 <sup>1165 ± 23</sup>	17 <sup>333 ± 14</sup>	17 <sup>321 ± 13</sup>	
75	corsight-001	1472269967	31525	290 <sup>2040</sup>	271 <sup>2064 ± 0</sup>	325 <sup>1291 ± 3</sup>	276 <sup>1285 ± 1</sup>	259 <sup>1293 ± 1</sup>	236 <sup>1303 ± 2</sup>	203 <sup>1379 ± 3</sup>	335 <sup>249340 ± 1713</sup>	335 <sup>248929 ± 1908</sup>	
76	csc-002		0	519768	240 <sup>1376</sup>	46 <sup>544 ± 0</sup>	91 <sup>473 ± 0</sup>	75 <sup>494 ± 0</sup>	55 <sup>481 ± 1</sup>	44 <sup>490 ± 1</sup>	33 <sup>514 ± 5</sup>	21 <sup>367 ± 11</sup>	
77	csc-003		0	400435	264 <sup>1609</sup>	45 <sup>544 ± 0</sup>	102 <sup>499 ± 0</sup>	80 <sup>500 ± 1</sup>	64 <sup>502 ± 0</sup>	51 <sup>508 ± 1</sup>	38 <sup>535 ± 4</sup>	23 <sup>393 ± 8</sup>	
78	ctbcbank-000	263381717	599238	109 <sup>570</sup>	156 <sup>2048 ± 0</sup>	129 <sup>568 ± 3</sup>	111 <sup>606 ± 38</sup>	118 <sup>690 ± 53</sup>	102 <sup>711 ± 50</sup>	108 <sup>831 ± 51</sup>	229 <sup>3551 ± 87</sup>	244 <sup>4805 ± 109</sup>	
79	ctbcbank-001	282123885	599238	116 <sup>603</sup>	197 <sup>2048 ± 0</sup>	168 <sup>652 ± 35</sup>	163 <sup>781 ± 30</sup>	165 <sup>875 ± 43</sup>	155 <sup>898 ± 51</sup>	148 <sup>1030 ± 47</sup>	236 <sup>3926 ± 45</sup>	236 <sup>3924 ± 56</sup>	
80	cubox-001	378498689	75427	124 <sup>649</sup>	133 <sup>2048 ± 0</sup>	252 <sup>907 ± 1</sup>	203 <sup>902 ± 1</sup>	173 <sup>903 ± 0</sup>	158 <sup>917 ± 0</sup>	127 <sup>931 ± 0</sup>	128 <sup>1379 ± 37</sup>	133 <sup>1417 ± 38</sup>	
81	cubox-002	555268218	90975	286 <sup>1964</sup>	206 <sup>2048 ± 0</sup>	255 <sup>921 ± 1</sup>	205 <sup>921 ± 1</sup>	179 <sup>922 ± 1</sup>	161 <sup>933 ± 1</sup>	144 <sup>1003 ± 1</sup>	173 <sup>2008 ± 72</sup>	174 <sup>1969 ± 57</sup>	
82	cuhkee-001	806762318	74917	301 <sup>2515</sup>	239 <sup>2052 ± 0</sup>	273 <sup>977 ± 31</sup>	-	-	-	-	203 <sup>2719 ± 60</sup>	205 <sup>2783 ± 56</sup>	
83	cybercore-000	88073082	55441	31 <sup>200</sup>	31 <sup>512 ± 0</sup>	172 <sup>655 ± 3</sup>	132 <sup>689 ± 71</sup>	108 <sup>649 ± 6</sup>	84 <sup>648 ± 8</sup>	71 <sup>680 ± 6</sup>	292 <sup>14800 ± 75</sup>	294 <sup>15757 ± 82</sup>	
84	cyberextruder-001	124120800	13629	26 <sup>178</sup>	4 <sup>256 ± 0</sup>	251 <sup>893 ± 25</sup>	-	-	-	-	108 <sup>1083 ± 16</sup>	109 <sup>1079 ± 19</sup>	
85	cyberextruder-002	172963574	13924	30 <sup>194</sup>	226 <sup>2048 ± 0</sup>	116 <sup>532 ± 6</sup>	-	-	-	-	159 <sup>1803 ± 14</sup>	156 <sup>1779 ± 22</sup>	
86	cyberlink-006	349866738	102456	244 <sup>1400</sup>	335 <sup>6212 ± 0</sup>	187 <sup>690 ± 1</sup>	137 <sup>702 ± 0</sup>	126 <sup>703 ± 0</sup>	103 <sup>712 ± 0</sup>	87 <sup>741 ± 0</sup>	11 <sup>270 ± 13</sup>	14 <sup>271 ± 13</sup>	
87	cyberlink-007	389168020	102446	272 <sup>1743</sup>	336 <sup>6212 ± 0</sup>	195 <sup>725 ± 1</sup>	149 <sup>732 ± 1</sup>	132 <sup>734 ± 1</sup>	110 <sup>736 ± 1</sup>	95 <sup>767 ± 1</sup>	15 <sup>304 ± 16</sup>	15 <sup>304 ± 16</sup>	
88	dahua-005	1624985571	169478	334 <sup>7360</sup>	302 <sup>4096 ± 0</sup>	337 <sup>1418 ± 34</sup>	-	-	-	-	93 <sup>957 ± 23</sup>	95 <sup>969 ± 19</sup>	

## Notes

- 1 The configuration size does not capture static data included in libraries.
- 2 The library size is the combined total of all files provided in the submission lib folder. These libraries e.g. OpenCV may or may not be installed on any end user's platform natively and would not need to be installed with the algorithm. Some developers put neural network models in their libraries.
- 3 The memory usage is the peak resident set size reported by the ps system call during template generation.
- 4 The median template creation times are measured on Intel® Xeon® CPU E5-2630 v4 @ 2.20GHz processors.
- 5 The comparison durations, in nanoseconds, are estimated using std::chrono::high\_resolution\_clock which on the machine in (2) counts 1ns clock ticks. Precision is somewhat worse than that however. The ± value is the median absolute deviation times 1.48 for Normal consistency.

Table 7: Summary of algorithms and properties included in this report. The red superscripts give ranking for the quantity in that column.











	ALGORITHM	CONFIG	LIBRARY	TEMPLATE								COMPARISON <sup>4</sup>									
				NAME	DATA	DATA	MEMORY	SIZE	GENERATION TIME (ms) <sup>4</sup>				TIME (ns) <sup>5</sup>								
									(KB) <sup>1</sup>	(KB) <sup>2</sup>	(MB) <sup>3</sup>	(B)	MUGSHOT	480x720	960x1440	1600x2400	3000x4500	GENUINE	IMPOSTOR		
309	videmo-000	142994889	39470	51	390	150	2048 ± 0	17	142 ± 5	10	150 ± 4	9	150 ± 6	7	151 ± 4	6	155 ± 8	32	513 ± 16	34	523 ± 38
310	videonetechs-001	31616555	5963	4	61	34	512 ± 0	38	262 ± 3	29	273 ± 1	44	439 ± 3	131	820 ± 3	248	2393 ± 43	116	1153 ± 38	118	1142 ± 65
311	videonetechs-002	124908941	6289	15	115	250	2052 ± 0	45	282 ± 5	33	295 ± 1	67	513 ± 4	185	1029 ± 3	263	3151 ± 46	119	1219 ± 57	127	1262 ± 56
312	vigilantsolutions-010	357169886	49973	161	840	78	1548 ± 0	155	615 ± 0	118	631 ± 0	102	632 ± 0	81	636 ± 0	66	659 ± 0	29	490 ± 13	32	488 ± 11
313	vigilantsolutions-011	261797614	49973	112	591	77	1548 ± 0	70	402 ± 0	51	418 ± 0	37	418 ± 0	27	422 ± 0	23	445 ± 0	20	339 ± 20	22	366 ± 37
314	vinal-000	412049069	866522	200	1032	205	2048 ± 0	295	1099 ± 1	243	1095 ± 1	226	1093 ± 1	199	1099 ± 1	166	1126 ± 1	210	2996 ± 20	211	2993 ± 26
315	vion-000	233696726	7533	83	498	249	2052 ± 0	55	333 ± 1	-	-	-	-	-	-	315	39839 ± 3561	310	26830 ± 2241		
316	visage-000	50400173	70150	6	73	20	512 ± 0	37	27 ± 0	1	27 ± 0	1	31 ± 0	2	38 ± 0	63	± 0	184	2220 ± 14	185	2218 ± 14
317	visionbox-001	263034670	190645	110	579	217	2048 ± 0	274	983 ± 7	242	1093 ± 46	271	1360 ± 68	279	2181 ± 105	276	5955 ± 281	117	1161 ± 22	120	1154 ± 20
318	visionbox-002	265280900	135281	120	612	268	2059 ± 0	96	482 ± 1	70	482 ± 0	57	484 ± 1	47	492 ± 1	35	517 ± 3	172	1969 ± 44	170	1931 ± 42
319	visionlabs-009	723046025	19862	66	444	36	513 ± 0	109	515 ± 41	66	472 ± 1	53	474 ± 1	40	476 ± 1	36	521 ± 1	92	957 ± 28	94	965 ± 32
320	visionlabs-010	1092895531	19357	174	902	37	513 ± 0	197	730 ± 0	144	717 ± 1	127	709 ± 0	104	713 ± 1	86	739 ± 0	41	600 ± 41	54	626 ± 35
321	visteam-001	190915457	30878	56	410	311	4096 ± 0	241	869 ± 7	191	872 ± 6	232	1121 ± 15	265	1719 ± 38	268	4375 ± 157	271	7054 ± 108	270	7025 ± 109
322	visteam-002	190915457	30888	101	547	305	4096 ± 0	229	829 ± 5	177	832 ± 6	153	839 ± 7	142	853 ± 6	145	1013 ± 14	269	6952 ± 118	267	6970 ± 120
323	vnpt-001	272895047	535529	51	384	108	2048 ± 0	101	499 ± 2	78	499 ± 2	59	494 ± 3	48	502 ± 3	30	512 ± 2	175	2049 ± 29	21	337 ± 121
324	vnpt-002	278169517	3203296	81	489	161	2048 ± 0	198	739 ± 2	148	731 ± 2	134	740 ± 1	114	742 ± 2	93	763 ± 2	77	766 ± 13	78	762 ± 13
325	vocord-008	618359916	345047	259	1559	279	2688 ± 0	268	962 ± 2	219	976 ± 2	220	1061 ± 3	226	1236 ± 23	235	1851 ± 9	211	3015 ± 50	210	2988 ± 62
326	vocord-009	1413255249	201560	327	4162	83	1920 ± 0	341	1472 ± 2	293	1472 ± 1	285	1549 ± 1	263	1667 ± 2	238	2064 ± 2	176	2052 ± 50	178	2056 ± 39
327	vts-000	262747358	169760	269	1704	103	2048 ± 0	98	486 ± 1	68	481 ± 0	56	484 ± 0	43	485 ± 1	34	517 ± 0	331	124209 ± 352	331	123652 ± 358
328	winsense-001	270774312	32035	181	922	73	1280 ± 0	206	766 ± 7	236	1058 ± 47	198	983 ± 97	193	1053 ± 119	195	1320 ± 84	141	1631 ± 28	173	1964 ± 171
329	winsense-002	288132712	25780	273	1781	96	2048 ± 0	100	494 ± 2	77	498 ± 1	69	519 ± 1	54	537 ± 1	60	634 ± 1	145	1683 ± 8	145	1685 ± 7
330	wuhantianyu-001	476280956	66457	168	866	167	2048 ± 0	163	642 ± 1	121	642 ± 1	107	644 ± 0	86	652 ± 0	75	697 ± 0	281	9502 ± 151	281	9202 ± 253
331	x-laboratory-000	532501437	197310	256	1524	266	2056 ± 0	216	808 ± 7	201	897 ± 113	175	907 ± 103	152	886 ± 103	70	673 ± 39	70	725 ± 19	76	749 ± 34
332	x-laboratory-001	640144084	398792	277	1844	256	2056 ± 0	138	586 ± 2	110	596 ± 5	93	603 ± 6	78	620 ± 7	98	793 ± 14	84	813 ± 28	88	872 ± 32
333	xforwardai-001	348262545	51163	293	2173	219	2048 ± 0	309	1180 ± 2	264	1182 ± 1	247	1194 ± 1	217	1186 ± 2	182	1203 ± 1	80	779 ± 17	83	797 ± 13
334	xforwardai-002	724700382	51163	288	1989	295	4096 ± 0	263	944 ± 1	212	942 ± 1	186	943 ± 4	162	935 ± 1	135	967 ± 1	133	1406 ± 8	132	1405 ± 13
335	xm-000	591914905	148920	131	688	246	2052 ± 0	247	878 ± 2	193	882 ± 1	200	988 ± 2	229	1258 ± 3	250	2434 ± 7	142	1634 ± 17	142	1632 ± 20
336	yisheng-004	498023846	38653	230	1279	286	3704 ± 0	65	378 ± 12	-	-	-	-	-	-	64	693 ± 137	35	526 ± 34		
337	yitu-003	1562336990	138919	319	3737	273	2082 ± 0	238	860 ± 0	-	-	-	-	-	-	297	18305 ± 71	297	18286 ± 62		
338	yooniik-000	297384719	206059	159	836	221	2048 ± 0	260	941 ± 3	215	965 ± 13	193	964 ± 10	172	964 ± 9	137	974 ± 23	114	1116 ± 34	115	1113 ± 54
339	yooniik-001	354948637	265353	294	2192	227	2048 ± 0	318	1223 ± 3	271	1238 ± 1	252	1238 ± 1	227	1240 ± 1	187	1240 ± 1	67	706 ± 29	70	690 ± 26
340	ytu-000	1512817409	44032	300	2484	210	2048 ± 0	112	530 ± 0	87	533 ± 0	105	640 ± 0	144	861 ± 2	236	1949 ± 8	312	31797 ± 131	313	31794 ± 133
341	yuan-001	379364823	189558	309	2829	173	2048 ± 0	332	1383 ± 3	286	1394 ± 3	276	1408 ± 3	257	1461 ± 4	222	1615 ± 4	191	2344 ± 25	191	2325 ± 42
342	yuan-002	379363758	165662	310	2838	190	2048 ± 0	338	1420 ± 3	290	1429 ± 4	284	1511 ± 4	264	1695 ± 4	249	2408 ± 5	190	2297 ± 23	190	2310 ± 31

## Notes

- 1 The configuration size does not capture static data included in libraries.
- 2 The library size is the combined total of all files provided in the submission lib folder. These libraries e.g. OpenCV may or may not be installed on any end user's platform natively and would not need to be installed with the algorithm. Some developers put neural network models in their libraries.
- 3 The memory usage is the peak resident set size reported by the ps system call during template generation.
- 4 The median template creation times are measured on Intel®Xeon®CPU E5-2630 v4 @ 2.20GHz processors.
- 5 The comparison durations, in nanoseconds, are estimated using std::chrono::high\_resolution\_clock which on the machine in (2) counts 1ns clock ticks. Precision is somewhat worse than that however. The ± value is the median absolute deviation times 1.48 for Normal consistency.

Table 13: Summary of algorithms and properties included in this report. The red superscripts give ranking for the quantity in that column.

	Algorithm	FALSE NON-MATCH RATE (FNMR)																	
		CONSTRAINED, COOPERATIVE												LESS CONSTRAINED, NON-COOP.					
		Name	VISAMC	VISA	MUGSHOT	MUGSHOT12+YRS	VISABORDER	BORDER	BORDER	WILD	CHILDEXP								
		FMR	0.0001	1E-06	1E-05	1E-05	1E-06	1E-06	1E-05	0.0001	0.01								
1	20face-000	0.1268	287	0.1828	284	0.1748	292	0.2768	292	0.1765	279	0.1864	234	0.0927	258	0.0405	197	-	
2	3divi-005	0.0094	157	0.0151	164	0.0078	145	0.0121	144	0.0135	142	0.0231	127	0.0156	144	0.0351	181	-	
3	3divi-006	0.0064	107	0.0094	102	0.0047	84	0.0066	84	0.0091	91	0.0191	105	0.0113	98	0.0289	94	-	
4	acer-000	0.1393	290	0.9075	334	0.9981	332	-		1.0000	329	1.0000	321	0.9998	326	0.9841	329	-	
5	acer-001	0.0294	253	0.0504	258	0.0240	248	0.0463	250	0.0436	247	0.0622	200	0.0360	221	0.0307	130	-	
6	acisw-003	0.9682	339	0.9971	339	0.7892	328	0.8738	326	0.8752	321	0.8275	295	0.6698	312	0.4470	311	-	
7	acisw-006	0.2945	305	0.9788	337	0.6044	315	-		0.9900	325	1.0000	322	0.9999	328	1.0000	338	-	
8	adera-002	0.0052	73	0.0071	68	0.0047	82	0.0064	79	0.0087	85	0.0159	83	0.0136	120	0.0990	255	-	
9	adera-003	0.0043	55	0.0059	53	0.0036	47	0.0043	34	0.0076	72	0.0151	77	0.0128	113	0.0989	254	-	
10	advance-002	0.0089	146	0.0137	148	0.0073	137	0.0115	140	0.0400	239	0.0722	207	0.0593	243	0.0498	220	-	
11	advance-003	0.0060	99	0.0087	96	0.0052	92	0.0067	85	0.0389	238	0.4914	263	0.1291	267	0.0508	222	-	
12	aifirst-001	0.0119	186	0.0170	178	0.0084	159	0.0127	154	0.0131	139	0.0212	115	0.0138	123	0.0432	204	0.4301	11
13	aigen-001	0.0124	190	0.0219	199	0.0143	216	0.0217	212	0.0236	209	0.8960	299	0.3255	287	0.0681	241	-	
14	aigen-002	0.0192	235	0.0343	236	0.0256	249	0.0402	245	0.0389	237	0.9196	302	0.3876	293	0.1096	263	-	
15	ailabs-001	0.0158	218	0.0276	230	0.0192	237	0.0317	236	0.0352	232	0.0608	196	0.0434	230	0.0338	167	-	
16	aimall-002	0.0119	184	0.0167	176	0.0224	244	0.0411	247	0.0233	205	0.0373	176	0.0235	195	0.0327	157	-	
17	aimall-003	0.0033	36	0.0041	29	0.0033	38	0.0035	22	0.0056	45	0.0109	48	0.0087	63	0.0312	140	-	
18	aiunionface-000	0.0104	169	0.0154	168	0.0082	157	0.0122	145	0.0141	149	0.0243	131	0.0169	152	0.0306	127	-	
19	aize-001	0.0223	242	0.0344	237	0.0199	238	0.0313	234	0.0367	233	0.0522	189	0.0359	220	0.0446	209	-	
20	ajou-001	0.0093	154	0.0147	160	0.0071	134	0.0126	149	0.0173	181	0.0274	143	0.0186	165	0.0348	174	-	
21	alchera-002	0.0107	174	0.0157	170	0.0104	186	0.0229	214	0.0144	154	0.0246	132	0.0198	178	0.0328	159	-	
22	alchera-003	0.0044	56	0.0055	51	0.0031	26	0.0039	29	0.0042	15	0.0077	13	0.0065	15	0.0339	169	-	
23	alice-000	0.0119	187	0.0192	188	0.0106	189	0.0170	189	0.0167	175	0.0265	140	0.0150	138	0.0288	86	-	
24	alleyes-000	0.0058	91	0.0090	99	0.0055	100	0.0087	116	0.0068	66	0.0105	45	0.0076	38	0.0282	60	-	
25	allgogvision-000	0.0346	260	0.0527	261	0.0232	246	0.0339	237	0.0372	236	0.0620	199	0.0443	231	0.0607	236	-	
26	alphaface-001	0.0065	109	0.0097	108	0.0039	57	0.0063	78	0.0083	80	-	-	-	0.0280	45	-		
27	alphaface-002	0.0052	75	0.0075	77	0.0030	19	0.0044	35	1.0000	332	0.0115	55	0.0084	58	0.0279	38	-	
28	amplifiedgroup-001	0.5034	326	0.5848	320	0.6973	322	0.8316	321	0.7807	313	0.7724	288	0.6354	308	0.4250	309	-	
29	androvideo-000	0.0243	246	0.0438	251	0.0239	247	0.0365	243	0.0483	250	0.1870	235	0.0635	245	0.1163	266	-	
30	anke-004	0.0080	137	0.0154	167	0.0073	136	0.0112	138	0.0102	113	0.0178	98	0.0118	105	0.0288	87	0.3577	6
31	anke-005	0.0070	116	0.0109	128	0.0059	110	0.0094	119	0.0105	116	0.0142	66	0.0102	83	0.0289	92	0.3337	4
32	antheus-000	0.2564	301	0.3776	303	0.7240	324	0.8699	324	0.8899	322	0.9872	306	0.9483	318	0.7668	323	0.9233	52
33	antheus-001	0.1311	288	0.2306	290	0.5113	308	0.6797	308	0.8748	320	0.9908	307	0.9649	322	0.7586	322	-	
34	anyvision-004	0.0267	251	0.0385	246	0.0258	250	0.0487	252	0.0234	208	0.0301	152	0.0191	170	0.0470	213	0.4633	12
35	anyvision-005	0.0023	18	0.0037	20	0.0027	17	0.0035	21	0.0049	29	0.0084	19	0.0069	22	0.0285	72	-	
36	asusaics-000	0.0125	195	0.0209	195	0.0085	160	0.0134	161	0.0143	152	0.7189	282	0.0285	210	0.0295	110	-	
37	asusaics-001	0.0125	196	0.0210	196	0.0085	162	0.0134	162	0.0143	153	0.7437	285	0.0289	211	0.0295	109	-	
38	authenmetric-002	0.0092	152	0.0134	147	0.0095	178	0.0177	192	0.0192	191	0.0463	184	0.0236	196	0.0306	129	-	
39	authenmetric-003	0.0036	41	0.0053	46	0.0039	59	0.0051	52	0.0095	104	0.9930	308	0.5932	306	0.0290	95	-	
40	aware-005	0.0457	267	0.0643	265	0.0603	274	0.1094	274	0.0613	257	0.1075	225	0.0491	233	0.0314	142	-	
41	aware-006	0.0487	269	0.0819	273	0.0529	270	0.1090	273	0.1011	272	0.1058	221	0.0502	235	0.0317	145	-	
42	awiros-001	0.4044	314	0.4622	310	0.5530	310	0.6518	307	0.2008	283	0.1994	239	0.1386	270	0.5584	320	-	
43	awiros-002	0.1990	296	0.2561	293	0.3319	300	0.4411	300	0.3821	298	0.9938	309	0.2634	281	0.0997	256	-	
44	ayftech-001	0.0946	283	0.1941	285	0.2438	296	0.3625	295	0.1558	277	0.1589	231	0.0936	259	0.0785	249	-	

Table 14: FNMR is the proportion of mated comparisons below a threshold set to achieve the FMR given in the header on the fourth row. FMR is the proportion of impostor comparisons at or above that threshold. The light grey values give rank over all algorithms in that column. The pink columns use only same-sex impostors; others are selected regardless of demographics. The exception, in the green column, uses “matched-covariates” i.e. impostors of the same sex, age group, and country of birth. The second pink column includes effects of extended ageing. Missing entries for border, visa, mugshot and wild images generally mean the algorithm did not run to completion. For child exploitation, missing entries arise because NIST executes those runs only infrequently. The VISA columns compare images described in section 2.2. The MUGSHOT columns compare images described in section 2.5. The VISA-BORDER column compare images described in section 2.3 with those of section 2.4. The BORDER column compares images described in section 2.4. The WILD columns compare images described in section 2.6. The CHILD-EXPLOITATION columns compare images described in section 2.1.

	Algorithm	FALSE NON-MATCH RATE (FNMR)																	
		CONSTRAINED, COOPERATIVE								LESS CONSTRAINED, NON-COOP.									
		Name	ViSAMC	VISA	MUGSHOT	MUGSHOT12+YRS	ViSABORDER	BORDER	BORDER	WILD	CHILDEXP								
	FMR	0.0001	1E-06	1E-05	1E-05	1E-05	1E-06	1E-06	1E-05	0.0001	0.01								
45	ayonix-000	0.4351	319	0.4872	311	0.6150	317	0.7510	315	0.6557	306	0.6361	274	0.4981	300	0.3635	306	0.8434	46
46	beethedata-000	0.0127	197	0.0195	189	0.0092	172	0.0157	182	0.0171	178	0.0306	154	0.0204	180	0.0285	74	-	
47	bioidtechswiss-001	0.0054	78	0.0072	69	0.0069	129	0.0124	148	0.0060	52	0.0094	29	0.0065	17	0.0313	141	-	
48	bioidtechswiss-002	0.0049	65	0.0067	65	0.0064	120	0.0116	141	0.0067	65	0.0117	56	0.0086	61	0.0279	31	-	
49	bm-001	0.7431	334	0.9494	335	0.9586	330	0.9843	328	0.9049	323	0.9021	301	0.8395	316	0.9935	331	0.8845	49
50	boetech-001	0.0662	277	0.0802	272	0.0493	266	0.0791	265	0.0682	261	0.1074	224	0.0758	253	0.1719	279	-	
51	bresee-001	0.0085	143	0.0143	154	0.0086	166	0.0153	179	0.0108	120	0.0168	90	0.0115	102	0.0355	185	-	
52	bresee-002	0.0079	136	0.0101	121	0.0065	123	0.0079	103	0.0129	136	0.0263	138	0.0224	189	0.0327	158	-	
53	camvi-002	0.0125	194	0.0221	203	0.0089	170	0.0145	173	0.0142	150	0.2650	249	0.0166	151	0.0288	83	0.5760	22
54	camvi-004	0.0171	225	0.0316	232	0.0042	66	0.0049	48	0.0097	109	0.6636	277	0.0141	127	0.0284	67	0.5788	23
55	canon-002	0.0034	40	0.0050	41	0.0026	12	0.0033	19	0.0043	18	0.0182	99	0.0065	16	0.0279	35	-	
56	ceiec-003	0.0071	121	0.0107	126	0.0061	116	0.0079	104	0.0160	167	0.0316	156	0.0260	204	0.0308	135	-	
57	ceiec-004	0.0038	46	0.0051	42	0.0045	80	0.0053	56	0.0062	58	0.3939	258	0.0104	88	0.0325	154	-	
58	chosun-001	0.0525	271	0.0936	275	0.0742	278	0.1263	278	0.0978	271	1.0000	328	0.9354	317	0.4446	310	-	
59	chosun-002	0.0390	263	0.0646	266	0.0339	259	0.0576	259	0.0455	248	0.6904	279	0.1746	275	0.0696	244	-	
60	chtface-002	0.0150	213	0.0268	226	0.0096	180	0.0140	166	0.0186	187	0.0320	158	0.0194	174	0.0306	128	-	
61	chtface-003	0.0091	148	0.0146	158	0.0083	158	0.0128	156	0.0132	140	0.0220	122	0.0149	136	0.0301	119	-	
62	canon-001	0.0041	53	0.0061	58	0.0030	24	0.0041	32	0.0048	28	0.0578	192	0.0069	23	0.0279	32	-	
63	closeli-001	0.0136	201	0.0163	172	0.0039	58	0.0054	58	0.0072	70	1.0000	323	0.0094	75	0.0318	146	-	
64	cloudwalk-hr-003	0.0026	25	0.0041	28	0.0040	62	0.0058	66	0.0060	56	0.9992	314	0.0094	72	0.7206	321	-	
65	cloudwalk-hr-004	0.0009	1	0.0018	2	0.0034	39	0.0028	10	0.0052	35	0.9992	315	0.0093	71	0.1625	278	-	
66	cloudwalk-mt-002	0.0064	108	0.0085	91	0.0054	97	0.0098	127	0.0070	68	0.0108	47	0.0076	37	0.0283	65	-	
67	cloudwalk-mt-003	0.0013	2	0.0022	3	0.0026	9	0.0027	6	0.0039	9	0.0076	9	0.0067	19	0.0347	172	-	
68	clova-000	0.0099	163	0.0150	161	0.0094	176	0.0147	175	0.0136	143	0.0213	117	0.0152	141	0.0307	131	-	
69	cogent-005	0.0060	96	0.0112	132	0.0064	122	0.0070	87	0.0095	103	0.0184	101	0.0135	116	0.0423	202	-	
70	cogent-006	0.0046	61	0.0059	55	0.0036	44	0.0047	40	0.0058	50	0.0113	52	0.0091	68	0.0343	171	-	
71	cognitec-002	0.0066	110	0.0101	118	0.0079	148	0.0108	135	0.0181	183	0.0317	157	0.0237	197	0.0372	190	-	
72	cognitec-003	0.0038	44	0.0052	43	0.0054	99	0.0057	64	0.0225	203	0.0416	182	0.0388	224	0.0348	175	-	
73	cor-001	0.0075	129	0.0113	136	0.0055	102	0.0084	110	0.0091	93	0.0148	72	0.0092	70	0.0277	26	-	
74	coretech-000	0.7699	336	1.0000	343	1.0000	341	-	1.0000	334	1.0000	330	1.0000	344	1.0000	340	-		
75	corsight-001	0.0040	51	0.0057	52	0.0033	37	0.0047	39	0.0045	20	0.0095	32	0.0063	13	0.0276	18	-	
76	csc-002	0.0099	164	0.0132	145	0.0077	142	0.0142	170	0.0126	134	0.0195	107	0.0146	132	0.1779	282	-	
77	csc-003	0.0053	76	0.0065	62	0.0037	51	0.0047	41	0.0074	71	0.0124	61	0.0112	97	0.1773	281	-	
78	ctbcbank-000	0.0168	221	0.0250	218	0.0146	219	0.0224	213	0.0211	199	0.8964	300	0.3779	292	1.0000	344	0.8803	48
79	ctbcbank-001	0.0155	216	0.0235	211	0.0148	224	0.0243	219	0.0207	196	0.9279	303	0.3469	289	1.0000	343	-	
80	cubox-001	0.0064	106	0.0080	86	0.0037	49	0.0055	61	0.0060	53	0.0111	49	0.0077	40	0.0300	117	-	
81	cubox-002	0.0034	39	0.0041	30	0.0025	7	0.0025	5	0.0033	3	0.0064	4	0.0058	8	0.0480	216	-	
82	cukee-001	0.0036	43	0.0045	36	0.0031	29	0.0046	37	0.0051	34	0.0095	33	0.0079	45	0.1492	275	-	
83	cybercore-000	0.0728	279	0.1110	278	0.1521	289	0.2375	287	0.1874	282	0.1907	236	0.1178	265	0.1191	269	-	
84	cyberextruder-001	0.1972	294	0.2547	292	0.4686	307	0.6387	306	0.3807	297	0.3806	257	0.2582	278	0.1747	280	0.7804	45
85	cyberextruder-002	0.0811	281	0.1336	280	0.1465	288	0.2266	286	0.2086	286	1.0000	337	1.0000	337	0.1000	257	0.6105	25
86	cyberlink-006	0.0042	54	0.0054	48	0.0043	69	0.0049	46	0.0052	39	0.0097	36	0.0077	41	0.0278	27	-	
87	cyberlink-007	0.0032	35	0.0053	45	0.0041	64	0.0043	33	0.0052	38	0.0243	130	0.0084	59	0.0280	43	-	
88	dahua-005	0.0031	33	0.0046	37	0.0035	43	0.0049	49	0.0046	22	0.0076	10	0.0062	12	0.0277	24	-	

Table 15: FNMR is the proportion of mated comparisons below a threshold set to achieve the FMR given in the header on the fourth row. FMR is the proportion of impostor comparisons at or above that threshold. The light grey values give rank over all algorithms in that column. The pink columns use only same-sex impostors; others are selected regardless of demographics. The exception, in the green column, uses “matched-covariates” i.e. impostors of the same sex, age group, and country of birth. The second pink column includes effects of extended ageing. Missing entries for border, visa, mugshot and wild images generally mean the algorithm did not run to completion. For child exploitation, missing entries arise because NIST executes those runs only infrequently. The VISA columns compare images described in section 2.2. The MUGSHOT columns compare images described in section 2.5. The ViSABORDER column compare images described in section 2.3 with those of section 2.4. The BORDER column compares images described in section 2.4. The WILD columns compare images described in section 2.6. The CHILD-EXPLOITATION columns compare images described in section 2.1.

Algorithm Name	FALSE NON-MATCH RATE (FNMR)									
	CONSTRAINED, COOPERATIVE								LESS CONSTRAINED, NON-COOP.	
	VISAMC	VISA	MUGSHOT	MUGSHOT12+YRS	VISABORDER	BORDER	BORDER	WILD	CHILDEXP	
FMR	0.0001	1E-06	1E-05	1E-05	1E-06	1E-06	1E-06	0.0001	0.01	
89 <b>dahua-006</b>	0.0027	26	0.0039	24	0.0031	28	0.0039	30	0.0039	10
90 <b>decatur-000</b>	0.0714	278	0.1115	279	0.0608	275	0.1106	275	0.0866	266
91 <b>deepglint-002</b>	0.0016	8	0.0027	13	0.0032	30	0.0033	20	0.0043	17
92 <b>deepglint-003</b>	0.0027	27	0.0038	21	0.0030	22	0.0032	18	0.0043	16
93 <b>deepsea-001</b>	0.0136	202	0.0215	198	0.0142	215	0.0214	211	0.0163	171
94 <b>deeplense-000</b>	0.0145	208	0.0265	225	0.0113	201	0.0196	204	0.0151	157
95 <b>dermalog-006</b>	0.0253	249	0.0369	243	0.0171	232	0.0283	230	0.0217	200
96 <b>dermalog-008</b>	0.0096	161	0.0166	175	0.0086	164	0.0133	160	0.0165	173
97 <b>didiglobalface-001</b>	0.0055	82	0.0092	100	0.0030	20	0.0045	36	0.0088	87
98 <b>digitalbarriers-002</b>	0.3360	310	0.3690	301	0.0877	281	0.1557	279	0.0971	270
99 <b>dps-000</b>	0.0115	180	0.0176	182	0.0149	226	0.0185	199	0.0173	180
100 <b>dsk-000</b>	0.1526	291	0.2169	288	0.3787	303	0.5426	304	0.3115	290
101 <b>einetworks-000</b>	0.0099	165	0.0180	184	0.0088	169	0.0140	168	0.0130	138
102 <b>ekin-002</b>	0.1168	285	0.2042	286	0.1530	290	0.2524	289	0.1777	281
103 <b>enface-000</b>	0.0028	29	0.0049	40	0.0043	73	0.0072	89	0.0058	51
104 <b>ecortex-000</b>	0.3485	311	0.6943	326	0.1122	284	0.1574	280	0.2155	288
105 <b>ercacat-001</b>	0.0036	42	0.0044	34	0.0033	35	0.0047	42	0.0106	117
106 <b>expasoft-001</b>	0.0328	259	0.0488	256	0.0211	242	0.0342	239	0.0629	259
107 <b>expasoft-002</b>	0.0170	223	0.0274	228	0.0787	279	0.0768	264	0.1629	278
108 <b>f8-001</b>	0.0249	248	0.0336	234	0.0178	234	0.0232	215	0.0303	227
109 <b>facesoft-000</b>	0.0085	144	0.0112	134	0.0064	121	0.0107	134	0.0091	92
110 <b>facetag-000</b>	0.2836	302	0.4081	307	0.2933	298	0.4303	298	0.3448	293
111 <b>facex-001</b>	1.0000	342	1.0000	341	1.0000	336	-	1.0000	340	1.0000
112 <b>facex-002</b>	0.0803	280	0.1404	281	0.1283	286	0.1979	284	0.1440	276
113 <b>farfaces-001</b>	0.4890	325	0.5860	321	0.5650	311	0.7268	312	0.8015	315
114 <b>fiberhome-nanjing-002</b>	0.0217	241	0.0381	245	0.0874	280	0.1770	282	0.0271	219
115 <b>fiberhome-nanjing-003</b>	0.0090	147	0.0139	151	0.0082	156	0.0144	171	0.0110	124
116 <b>fincore-000</b>	0.0309	256	0.0502	257	0.0281	253	0.0510	254	0.0521	252
117 <b>fujitsulab-002</b>	0.0091	149	0.0124	139	0.0105	187	0.0156	181	0.0169	177
118 <b>fujitsulab-003</b>	0.0045	59	0.0065	63	0.0057	107	0.0083	108	0.0080	76
119 <b>geo-001</b>	0.0180	230	0.0198	190	0.0037	50	0.0055	60	0.0070	67
120 <b>geo-002</b>	0.0171	226	0.0187	187	0.0035	42	0.0051	55	0.0064	60
121 <b>glory-002</b>	0.0241	244	0.0311	231	0.0116	205	0.0151	178	0.0157	164
122 <b>glory-003</b>	0.0076	132	0.0125	142	0.0077	144	0.0103	131	0.0130	137
123 <b>gorilla-006</b>	0.0105	173	0.0152	165	0.0106	188	0.0203	207	0.0155	160
124 <b>gorilla-007</b>	0.0074	127	0.0111	130	0.0065	124	0.0126	150	0.0100	112
125 <b>griaule-000</b>	0.0071	123	0.0099	112	0.0050	90	0.0072	88	0.0160	165
126 <b>hertasecurity-000</b>	0.0630	275	0.0780	271	0.0503	268	0.0898	268	0.0738	262
127 <b>hik-001</b>	0.0096	160	0.0125	141	0.0093	175	0.0164	187	0.0108	121
128 <b>hyperverge-001</b>	1.0000	341	1.0000	344	1.0000	342	-	1.0000	337	1.0000
129 <b>hyperverge-002</b>	0.0050	66	0.0066	64	0.0035	41	0.0051	51	0.0062	57
130 <b>icm-002</b>	0.0143	205	0.0249	217	0.0144	217	0.0256	221	0.0236	211
131 <b>ichthtc-000</b>	0.0260	250	0.0396	247	0.0207	241	0.0339	238	0.0291	224
132 <b>id3-006</b>	0.0072	125	0.0103	122	0.0049	88	0.0074	95	0.0095	102

FRVT - FACE RECOGNITION VENDOR TEST - VERIFICATION

Table 16: FNMR is the proportion of mated comparisons below a threshold set to achieve the FMR given in the header on the fourth row. FMR is the proportion of impostor comparisons at or above that threshold. The light grey values give rank over all algorithms in that column. The pink columns use only same-sex impostors; others are selected regardless of demographics. The exception, in the green column, uses “matched-covariates” i.e. impostors of the same sex, age group, and country of birth. The second pink column includes effects of extended ageing. Missing entries for border, visa, mugshot and wild images generally mean the algorithm did not run to completion. For child exploitation, missing entries arise because NIST executes those runs only infrequently. The VISA columns compare images described in section 2.2. The MUGSHOT columns compare images described in section 2.5. The VISA-BORDER column compare images described in section 2.3 with those of section 2.4. The BORDER column compares images described in section 2.4. The WILD columns compare images described in section 2.6. The CHILD-EXPLOITATION columns compare images described in section 2.1.

		FALSE NON-MATCH RATE (FNMR)																	
	Algorithm	CONSTRAINED, COOPERATIVE								LESS CONSTRAINED, NON-COOP.									
	Name	VISAMC	VISA	MUGSHOT	MUGSHOT12+YRS	VISABORDER	BORDER	BORDER	WILD	CHILDEXP									
	FMR	0.0001	1E-06	1E-05	1E-05	1E-06	1E-06	1E-06	0.0001	0.01									
133	id3-007	0.0056	84	0.0078	81	0.0060	114	0.0072	91	0.0275	221	0.1374	230	0.0519	236	0.0487	218	-	
134	idemia-007	0.0024	20	0.0039	25	0.0032	34	0.0038	27	0.0046	24	0.0092	27	0.0070	26	0.0288	89	-	
135	idemia-008	0.0023	19	0.0032	16	0.0023	3	0.0028	7	0.0034	5	0.0067	6	0.0056	6	0.0290	97	-	
136	iit-002	0.0111	178	0.0177	183	0.0085	161	0.0140	167	0.0193	192	0.0332	164	0.0260	203	0.1373	272	-	
137	iit-003	0.0082	142	0.0151	163	0.0053	93	0.0084	111	0.0122	132	0.0199	109	0.0137	122	0.0407	198	-	
138	imagus-002	0.0062	102	0.0086	92	0.0053	95	0.0075	96	0.0121	131	0.0207	113	0.0161	147	0.0735	245	-	
139	imagus-003	0.0059	95	0.0084	89	0.0059	109	0.0081	106	0.0119	128	0.0209	114	0.0162	148	0.1068	261	-	
140	imperial-000	0.0067	113	0.0108	127	0.0080	152	0.0134	163	0.0087	86	0.0581	193	0.0102	84	0.0281	49	-	
141	imperial-002	0.0058	90	0.0081	87	0.0055	101	0.0085	113	0.0083	81	0.0157	82	0.0103	85	0.0273	8	0.5151	15
142	incode-008	0.0063	103	0.0101	119	0.0046	81	0.0086	115	0.0057	46	0.0104	41	0.0074	31	0.0297	114	-	
143	incode-009	0.0044	57	0.0067	66	0.0034	40	0.0051	50	0.0049	30	0.0091	26	0.0067	20	0.0296	113	-	
144	innefulabs-000	0.0122	188	0.0199	191	0.0112	199	0.0197	205	0.0222	202	0.0372	175	0.0271	207	0.0348	176	-	
145	innovativetechnologyltd-001	0.0578	273	0.0938	276	0.0501	267	0.0981	269	0.0592	256	0.0779	209	0.0422	229	0.0449	211	-	
146	innovativetechnologyltd-002	0.0451	266	0.0716	268	0.0541	271	0.1009	271	0.0506	251	0.0682	203	0.0371	222	0.0804	251	-	
147	innovatrics-006	0.0058	89	0.0089	98	0.0061	117	0.0096	123	0.0096	107	0.0165	89	0.0103	86	0.0281	47	0.3056	3
148	innovatrics-007	0.0040	50	0.0054	50	0.0057	106	0.0078	101	0.0079	75	0.0123	60	0.0088	64	0.0282	59	-	
149	insightface-000	0.0018	13	0.0027	12	0.0029	18	0.0030	17	0.0038	8	0.0077	12	0.0068	21	0.0276	19	-	
150	intellicloudai-001	0.0142	204	0.0234	209	0.0092	174	0.0145	172	0.0162	169	0.0371	174	0.0171	155	0.0409	199	-	
151	intellicloudai-002	0.0059	94	0.0085	90	0.0060	113	0.0069	86	0.0108	119	0.2477	248	0.0171	154	0.0303	123	-	
152	intellifusion-001	0.0072	124	0.0094	104	0.0056	105	0.0085	114	0.0111	126	0.0212	116	0.0143	128	0.0289	91	0.5454	18
153	intellifusion-002	0.0059	93	0.0077	80	0.0040	61	0.0074	94	0.0085	84	0.5352	267	0.0104	89	0.0305	126	-	
154	intellivision-001	0.1335	289	0.2205	289	0.1090	282	0.1670	281	0.1385	274	0.1676	232	0.1170	264	0.2445	294	0.7766	44
155	intellivision-002	0.1000	284	0.1775	283	0.0610	276	0.1009	270	0.0805	265	0.1074	223	0.0682	246	0.0768	247	-	
156	intelresearch-003	0.0046	60	0.0062	60	0.0038	55	0.0060	70	0.0088	89	0.0168	91	0.0136	118	0.0304	125	-	
157	intelresearch-004	0.0025	21	0.0035	19	0.0032	32	0.0038	25	0.0049	31	0.0094	28	0.0072	27	0.0290	98	-	
158	intsysmsu-001	0.9543	338	0.9888	338	0.9923	331	-	-	0.9977	326	0.9955	310	0.9892	323	0.7871	324	-	
159	intsysmsu-002	0.0130	198	0.0254	220	0.0137	213	0.0267	228	0.0160	166	0.0267	142	0.0145	131	0.0289	93	-	
160	ionetworks-000	0.0060	100	0.0087	94	0.0044	74	0.0058	67	0.0080	78	0.0144	70	0.0112	95	0.0319	147	-	
161	iqface-000	0.0091	151	0.0143	153	0.0075	141	0.0110	136	0.0171	179	0.2234	243	0.0359	219	0.0381	192	0.6490	28
162	iqface-003	0.0058	88	0.0079	85	0.0051	91	0.0058	68	0.0104	115	0.0200	110	0.0193	172	0.0402	196	-	
163	irex-000	0.0052	74	0.0099	113	0.0056	104	0.0083	109	0.0137	146	0.0163	87	0.0078	43	0.0285	73	-	
164	isap-001	0.5092	327	0.6588	324	0.6899	321	0.7978	318	0.7200	309	0.7253	283	0.5373	302	0.1931	285	-	
165	isap-002	0.0114	179	0.0186	186	0.0087	167	0.0151	177	0.0156	163	0.5134	266	0.0333	214	0.0354	184	-	
166	isityou-000	0.5682	329	0.7033	327	1.0000	343	-	-	1.0000	338	1.0000	333	1.0000	341	1.0000	335	1.0000	86
167	isystems-001	0.0149	212	0.0245	215	0.0138	214	0.0210	209	0.0209	198	0.0332	163	0.0223	188	0.0524	226	0.5152	16
168	isystems-002	0.0118	182	0.0182	185	0.0111	196	0.0162	185	0.0166	174	0.0284	148	0.0195	175	0.0516	223	0.4876	13
169	itmo-006	0.0125	192	0.0220	202	0.0149	225	0.0266	226	0.0233	206	0.0383	177	0.0285	209	0.0329	160	-	
170	itmo-007	0.0080	138	0.0125	140	0.0107	190	0.0185	197	0.0167	176	0.0222	124	0.0144	130	0.0300	118	-	
171	ivacognitive-001	0.0189	233	0.0351	238	0.0123	208	0.0235	216	0.0198	194	0.0274	144	0.0155	142	0.0296	112	-	
172	iws-000	0.4824	324	0.5801	319	0.6859	320	0.8155	320	0.8251	316	0.7756	289	0.6400	310	0.3251	305	-	
173	kakao-004	0.0078	133	0.0103	123	0.0059	111	0.0102	129	0.0155	161	0.1182	227	0.0230	192	0.0277	25	-	
174	kakao-005	0.0040	49	0.0059	54	0.0036	48	0.0057	63	0.0085	83	0.0239	128	0.0125	110	0.0280	42	-	
175	kakaoopay-001	0.0152	215	0.0252	219	0.0145	218	0.0270	229	0.0232	204	0.0344	166	0.0194	173	0.0416	201	-	
176	kedacom-000	0.0055	81	0.0081	88	0.0111	198	0.0120	143	0.0415	241	0.0966	219	0.0686	247	0.2511	297	0.7650	42

Table 17: FNMR is the proportion of mated comparisons below a threshold set to achieve the FMR given in the header on the fourth row. FMR is the proportion of impostor comparisons at or above that threshold. The light grey values give rank over all algorithms in that column. The pink columns use only same-sex impostors; others are selected regardless of demographics. The exception, in the green column, uses “matched-covariates” i.e. impostors of the same sex, age group, and country of birth. The second pink column includes effects of extended ageing. Missing entries for border, visa, mugshot and wild images generally mean the algorithm did not run to completion. For child exploitation, missing entries arise because NIST executes those runs only infrequently. The VISA columns compare images described in section 2.2. The MUGSHOT columns compare images described in section 2.5. The VISA-BORDER column compare images described in section 2.3 with those of section 2.4. The BORDER column compares images described in section 2.4. The WILD columns compare images described in section 2.6. The CHILD-EXPLOITATION columns compare images described in section 2.1.

	Algorithm	FALSE NON-MATCH RATE (FNMR)																	
		CONSTRAINED, COOPERATIVE								LESS CONSTRAINED, NON-COOP.									
		Name	ViSAMC	VISA	MUGSHOT	MUGSHOT12+YRS	VisABORDER	BORDER	BORDER	WILD	CHILDEXP								
FMR		0.0001	1E-06	1E-05	1E-05	1E-06	1E-06	1E-06	1E-05	0.0001	0.01								
177	kiwitech-000	0.0076	131	0.0105	124	0.0081	154	0.0128	157	0.0096	105	0.0163	86	0.0101	81	0.0279	37	-	
178	kneron-003	0.0542	272	0.0902	274	0.0346	260	0.0562	257	0.0919	268	0.1251	229	0.0973	260	0.3053	304	0.6962	33
179	kneron-005	0.0157	217	0.0259	222	0.0126	211	0.0212	210	0.0406	240	0.0693	205	0.0542	240	0.0471	214	-	
180	kookmin-001	0.0462	268	0.0750	269	0.0489	265	0.0842	266	0.0659	260	0.8380	298	0.3212	286	0.0491	219	-	
181	kookmin-002	0.0054	80	0.0077	79	0.0043	70	0.0065	80	0.0123	133	0.7591	287	0.0198	177	0.0285	75	-	
182	lemalabs-001	0.0111	177	0.0175	180	0.0088	168	0.0142	169	0.0143	151	0.0228	126	0.0140	125	0.0281	46	-	
183	line-000	0.0172	227	0.0236	212	0.0109	194	0.0194	202	0.0183	184	0.0291	150	0.0204	181	0.0298	115	-	
184	lookman-002	0.0297	254	0.0547	262	0.0339	258	0.0562	256	0.0614	258	0.0960	218	0.0790	254	0.2640	301	-	
185	lookman-004	0.0074	128	0.0099	111	0.0124	210	0.0149	176	0.0430	246	0.0866	213	0.0694	248	0.2516	298	0.7664	43
186	luxand-000	0.2056	297	0.2814	295	0.4053	305	0.5365	303	0.3497	294	0.3743	255	0.2605	279	0.2222	292	-	
187	megvii-002	0.0104	170	0.0145	157	0.0225	245	0.0345	240	0.0099	111	0.0286	149	0.0240	199	0.0692	243	0.3013	2
188	megvii-003	0.0064	104	0.0094	103	0.0136	212	0.0260	223	0.0050	32	0.0080	15	0.0059	10	0.0288	81	-	
189	meituan-000	0.0197	236	0.0424	250	0.0078	146	0.0074	93	0.0103	114	0.0193	106	0.0164	149	0.1063	259	-	
190	meiya-001	0.0171	224	0.0275	229	0.0159	230	0.0261	225	0.0311	229	0.2250	244	0.0245	201	0.0363	189	-	
191	microfocus-001	0.4482	321	0.5524	318	0.7256	325	0.8416	322	0.7301	310	0.6926	280	0.5180	301	0.2567	300	0.6890	32
192	microfocus-002	0.3605	312	0.5057	313	0.5783	313	0.7223	311	0.5909	302	0.5963	272	0.4160	297	0.1582	277	0.6517	29
193	minivision-000	0.0033	37	0.0048	39	0.0038	56	0.0049	45	0.0055	44	0.0094	31	0.0079	47	0.0273	6	-	
194	mobai-000	0.0360	262	0.0439	253	0.0372	262	0.0700	262	0.0367	234	0.0939	216	0.0795	255	0.2640	302	-	
195	mobai-001	0.0199	238	0.0219	200	0.0047	83	0.0061	73	0.0093	100	0.0174	95	0.0138	124	0.1045	258	-	
196	mobbl-000	0.2938	304	0.3861	304	0.5391	309	0.6888	309	0.6545	305	0.8027	290	0.6207	307	0.5471	318	-	
197	mobbl-001	0.3208	307	0.4375	308	0.5680	312	0.7193	310	0.6282	303	0.5783	270	0.3984	294	0.1866	284	-	
198	moreedian-000	0.3874	313	0.4912	312	0.9988	334	-		0.9990	327	0.9999	318	0.9998	327	0.4788	313	-	
199	mvision-001	0.0191	234	0.0233	207	0.0204	240	0.0356	241	0.0198	195	0.0337	165	0.0242	200	0.0431	203	-	
200	nazhaiai-000	0.0040	52	0.0059	56	0.0036	45	0.0048	44	0.0057	47	0.0125	62	0.0083	55	0.0275	15	-	
201	neosystems-001	1.0000	344	1.0000	342	0.2987	299	0.4382	299	0.5173	301	0.6570	276	0.4043	296	0.5091	316	-	
202	neosystems-002	0.2905	303	0.4077	306	0.2028	294	0.3252	293	0.4088	299	0.5519	268	0.3331	288	0.4500	312	-	
203	netbridgeTech-001	0.4749	323	0.6599	325	0.4438	306	0.5676	305	0.4491	300	1.0000	320	0.9541	319	0.1098	264	-	
204	netbridgeTech-002	0.0101	167	0.0166	174	0.0077	143	0.0127	153	0.0133	141	0.8215	293	0.0523	238	0.0351	182	-	
205	neurotechnology-011	0.0050	67	0.0087	93	0.0061	118	0.0097	125	0.0077	74	0.0404	181	0.0092	69	0.0293	107	-	
206	neurotechnology-012	0.0051	72	0.0070	67	0.0038	53	0.0056	62	0.0066	64	0.0112	51	0.0075	34	0.0279	36	-	
207	rhn-001	0.0066	111	0.0098	109	0.0053	94	0.0079	105	0.0093	97	0.0156	81	0.0109	93	0.0308	137	-	
208	rhn-002	0.0068	115	0.0096	105	0.0057	108	0.0087	117	0.0136	145	0.0253	135	0.0186	166	0.0302	121	-	
209	nodeflux-002	0.0186	232	0.0340	235	0.0261	251	0.0451	249	0.0548	253	1.0000	326	1.0000	330	0.0299	116	-	
210	notiontag-000	0.6669	331	0.7885	330	0.3715	302	0.4978	301	0.8571	317	0.8102	292	0.6460	311	0.1807	283	0.6479	27
211	notiontag-001	0.6846	332	0.8006	331	0.3955	304	0.5247	302	0.8669	319	0.8313	296	0.6362	309	0.2221	291	-	
212	nsensecorp-001	0.9909	340	0.9994	340	0.9987	333	-		1.0000	331	1.0000	329	1.0000	331	0.9858	330	-	
213	nsensecorp-002	0.4277	317	0.5375	316	0.6734	319	0.7924	317	0.7194	308	0.6937	281	0.5617	303	0.5530	319	-	
214	ntechlab-009	0.0039	48	0.0054	49	0.0042	68	0.0063	76	0.0275	222	0.0674	202	0.0532	239	0.0537	228	-	
215	ntechlab-010	0.0013	3	0.0017	1	0.0024	6	0.0029	13	0.0031	2	0.0058	2	0.0050	2	0.0292	102	-	
216	omnigarde-000	0.0633	276	0.1002	277	0.1109	283	0.2042	285	0.1288	273	0.5113	265	0.1227	266	0.0357	186	-	
217	omnigarde-001	0.0168	222	0.0260	223	0.0203	239	0.0402	244	0.0243	214	0.0327	160	0.0177	158	0.0288	84	-	
218	openface-001	0.1804	293	0.2921	296	0.2878	297	0.3906	297	0.2054	285	0.2338	247	0.1549	273	0.2445	295	-	
219	oz-002	0.0071	122	0.0099	115	0.0099	182	0.0100	128	0.0139	147	0.0502	187	0.0202	179	0.5084	315	-	
220	oz-003	0.0095	159	0.0143	152	0.0054	98	0.0077	100	0.0096	106	0.0175	96	0.0118	106	0.0288	88	-	

Table 18: FNMR is the proportion of mated comparisons below a threshold set to achieve the FMR given in the header on the fourth row. FMR is the proportion of impostor comparisons at or above that threshold. The light grey values give rank over all algorithms in that column. The pink columns use only same-sex impostors; others are selected regardless of demographics. The exception, in the green column, uses “matched-covariates” i.e. impostors of the same sex, age group, and country of birth. The second pink column includes effects of extended ageing. Missing entries for border, visa, mugshot and wild images generally mean the algorithm did not run to completion. For child exploitation, missing entries arise because NIST executes those runs only infrequently. The VISA columns compare images described in section 2.2. The MUGSHOT columns compare images described in section 2.5. The VISA-BORDER column compare images described in section 2.3 with those of section 2.4. The BORDER column compares images described in section 2.4. The WILD columns compare images described in section 2.6. The CHILD-EXPLOITATION columns compare images described in section 2.1.

		FALSE NON-MATCH RATE (FNMR)																	
	Algorithm	CONSTRAINED, COOPERATIVE								LESS CONSTRAINED, NON-COOP.									
	Name	VISAMC	VISA	MUGSHOT	MUGSHOT12+YRS	VISABORDER	BORDER	BORDER	WILD	CHILDEXP									
	FMR	0.0001	1E-06	1E-05	1E-05	1E-06	1E-06	1E-05	0.0001	0.01									
221	papsav1923-001	0.0078	134	0.0130	144	0.0068	127	0.0105	133	0.0119	129	0.0221	123	0.0136	119	0.0293	104	-	
222	paravision-004	0.0030	31	0.0046	38	0.0030	21	0.0036	23	0.0091	95	0.0188	104	0.0173	156	0.0288	85	0.2467	1
223	paravision-008	0.0018	12	0.0025	7	0.0024	4	0.0025	4	0.0036	7	0.0070	8	0.0063	14	0.0279	34	-	
224	pensees-001	0.0087	145	0.0133	146	0.0071	132	0.0122	147	0.0145	155	0.0252	134	0.0195	176	0.0283	63	-	
225	pixelall-005	0.0038	45	0.0052	44	0.0043	71	0.0051	53	0.0077	73	0.0839	212	0.0136	121	0.0279	30	-	
226	pixelall-006	0.0032	34	0.0042	32	0.0032	31	0.0039	28	0.0063	59	0.9960	311	0.0723	251	0.0283	61	-	
227	psl-007	0.0026	24	0.0040	26	0.0027	14	0.0030	15	0.0054	40	0.0101	40	0.0081	51	0.0282	55	-	
228	psl-008	0.0026	22	0.0040	27	0.0024	5	0.0028	11	0.0041	12	0.0077	11	0.0055	5	0.0280	41	-	
229	ptakuratsatu-000	0.0060	98	0.0089	97	0.0070	130	0.0104	132	0.0096	108	0.0152	78	0.0100	78	0.0284	68	-	
230	pxl-001	0.0488	270	0.0752	270	0.0586	273	0.1087	272	0.0946	269	0.1065	222	0.0625	244	0.1088	262	-	
231	pyramid-000	0.0136	200	0.0233	208	0.0117	206	0.0192	201	0.0185	186	0.0322	159	0.0206	183	0.0304	124	-	
232	qnap-000	0.0149	209	0.0228	205	0.0155	228	0.0267	227	0.0238	213	0.8329	297	0.0396	226	0.0324	152	-	
233	quantasoft-003	0.0081	141	0.0113	135	0.0056	103	0.0076	98	0.0091	94	0.0161	85	0.0107	92	0.0414	200	-	
234	rankone-010	0.0079	135	0.0112	133	0.0061	115	0.0081	107	0.0088	88	0.0149	73	0.0117	104	0.0320	150	-	
235	rankone-011	0.0049	64	0.0075	76	0.0038	52	0.0048	43	0.0060	55	0.0143	69	0.0080	49	0.0359	187	-	
236	realnetworks-002	0.0248	247	0.0358	240	0.0513	269	0.1127	276	0.0371	235	0.0614	197	0.0316	213	0.0334	163	-	
237	realnetworks-004	0.0075	130	0.0101	120	0.0066	125	0.0097	126	0.0108	123	0.0187	103	0.0131	115	0.0285	77	-	
238	regula-000	0.0184	231	0.0376	244	0.0103	184	0.0185	196	0.0120	130	0.9983	313	0.0231	193	0.0273	9	-	
239	remarkai-001	0.0144	206	0.0256	221	0.0102	183	0.0159	183	0.0162	170	0.0582	194	0.0185	164	0.0308	134	-	
240	remarkai-003	0.0047	62	0.0063	61	0.0033	36	0.0049	47	0.0054	41	0.0100	39	0.0072	28	0.0275	17	-	
241	rendip-000	0.0055	83	0.0077	78	0.0048	86	0.0060	71	0.0080	77	0.0142	68	0.0110	94	0.0433	205	-	
242	rokid-000	0.0093	155	0.0145	156	0.0073	138	0.0102	130	0.0164	172	0.0280	147	0.0214	185	0.0857	252	-	
243	rokid-001	0.0105	172	0.0162	171	0.0094	177	0.0163	186	0.0181	182	0.0276	146	0.0165	150	0.0325	155	-	
244	s1-002	0.0095	158	0.0144	155	0.0112	200	0.0196	203	0.0234	207	0.0371	173	0.0282	208	0.1167	267	-	
245	s1-003	0.0051	70	0.0073	72	0.0044	75	0.0063	77	0.0052	37	0.0096	35	0.0070	24	0.1321	271	-	
246	saffe-001	0.4339	318	0.5261	314	0.7539	327	0.8736	325	0.7977	314	0.9810	305	0.7435	314	0.3887	307	0.8973	50
247	saffe-002	0.0119	185	0.0206	192	0.0107	193	0.0177	191	0.0244	215	0.9998	317	0.2785	282	0.0308	133	-	
248	samtech-001	0.0197	237	0.0365	241	0.0146	222	0.0241	218	0.0238	212	0.0394	179	0.0251	202	0.0337	164	-	
249	scanovate-001	0.0175	228	0.0331	233	0.0163	231	0.0248	220	0.2476	289	0.3801	256	0.3740	291	0.4060	308	-	
250	scanovate-002	0.0175	229	0.0355	239	0.0146	220	0.0286	231	0.0269	218	0.0301	151	0.0178	159	0.0301	120	-	
251	securifai-001	0.4538	322	0.6142	322	0.5844	314	0.7428	313	0.7051	307	0.9961	312	0.9558	320	0.1963	286	-	
252	securifai-003	0.4086	315	0.7577	329	0.7233	323	0.8070	319	0.7787	312	1.0000	327	0.9988	325	0.8326	326	-	
253	sensetime-004	0.0026	23	0.0038	22	0.0022	2	0.0023	2	0.0042	14	0.0082	17	0.0078	42	0.0293	103	-	
254	sensetime-005	0.0019	14	0.0029	14	0.0022	1	0.0021	1	0.0023	1	0.0044	1	0.0039	1	0.0273	7	-	
255	sertis-000	0.0118	183	0.0208	193	0.0080	150	0.0127	152	0.0110	125	0.0176	97	0.0114	100	0.0285	76	-	
256	sertis-002	0.0049	63	0.0061	57	0.0039	60	0.0061	75	0.0055	43	0.0099	38	0.0070	25	0.0281	48	-	
257	sevensense-000	0.0067	114	0.0099	117	0.0045	77	0.0065	81	0.0093	98	0.0169	92	0.0124	109	0.0275	16	-	
258	shaman-000	0.9297	337	0.9774	336	0.9990	335	-		0.9999	328	1.0000	324	0.9999	329	0.9575	328	0.9618	54
259	shaman-001	0.3346	309	0.4616	309	0.2368	295	0.3723	296	0.3574	295	0.3527	254	0.2304	277	0.1498	276	0.8990	51
260	shu-002	-	0.0079	84	0.0146	221	0.0308	233	1.0000	330	0.0183	100	0.0115	101	0.0284	69	-		
261	shu-003	0.0028	28	0.0041	31	0.0050	89	0.0088	118	0.0081	79	0.0133	65	0.0094	74	0.0283	66	-	
262	siat-002	0.0091	150	0.0126	143	0.0109	195	0.0190	200	0.0276	223	0.0516	188	0.0464	232	0.0520	225	0.4277	10
263	siat-004	0.0067	112	0.0099	114	0.0152	227	-		0.0275	220	0.4823	262	0.4823	298	1.0000	333	-	
264	sjtu-003	0.0017	9	0.0033	17	0.0030	23	0.0037	24	0.0058	48	0.0104	42	0.0081	52	0.0284	71	-	

Table 19: FNMR is the proportion of mated comparisons below a threshold set to achieve the FMR given in the header on the fourth row. FMR is the proportion of impostor comparisons at or above that threshold. The light grey values give rank over all algorithms in that column. The pink columns use only same-sex impostors; others are selected regardless of demographics. The exception, in the green column, uses “matched-covariates” i.e. impostors of the same sex, age group, and country of birth. The second pink column includes effects of extended ageing. Missing entries for border, visa, mugshot and wild images generally mean the algorithm did not run to completion. For child exploitation, missing entries arise because NIST executes those runs only infrequently. The VISA columns compare images described in section 2.2. The MUGSHOT columns compare images described in section 2.5. The VISA-BORDER column compare images described in section 2.3 with those of section 2.4. The BORDER column compares images described in section 2.4. The WILD columns compare images described in section 2.6. The CHILD-EXPLOITATION columns compare images described in section 2.1.

	Algorithm	FALSE NON-MATCH RATE (FNMR)										LESS CONSTRAINED, NON-COOP.								
		CONSTRAINED, COOPERATIVE								WILD										
		Name	VISAMC	VISA	MUGSHOT	MUGSHOT12+YRS	VISABORDER	BORDER	BORDER	CHILDEXP										
	FMR		0.0001	1E-06	1E-05	1E-05	1E-06	1E-06	1E-05		0.0001	0.01								
265	sjtu-004		0.0014	4	0.0025	6	0.0027	15	0.0028	12	0.0046	23	0.0086	22	0.0073	29	0.0272	4	-	
266	sktelecom-000		0.0038	47	0.0054	47	0.0031	25	0.0051	54	0.0042	13	0.3418	253	0.0061	11	0.0293	106	-	
267	smartengines-000		0.6240	330	0.7562	328	0.9552	329	0.9784	327	0.9515	324	0.9288	304	0.8200	315	0.8037	325	-	
268	smilart-002		0.2440	299	0.3532	300	-	-	-	0.3785	296	0.4145	260	0.2611	280	-	0.6999	34		
269	smilart-003		0.6944	333	0.8836	332	0.0695	277	0.1193	277	0.0894	267	0.1221	228	0.0737	252	0.1190	268	-	
270	sodec-000		0.0033	38	0.0044	35	0.0040	63	0.0053	57	0.0054	42	0.0096	34	0.0080	48	0.0274	11	-	
271	sqisoft-001		0.1220	286	0.2088	287	0.1978	293	0.3386	294	0.2111	287	0.2798	251	0.1474	272	0.0519	224	-	
272	st aqu-000		0.0139	203	0.0208	194	0.0104	185	0.0145	174	0.0156	162	0.8063	291	0.1408	271	0.0332	162	-	
273	starhybrid-001		0.0108	175	0.0138	149	0.0081	153	0.0113	139	0.0152	158	0.0265	141	0.0189	169	0.0350	180	0.5584	19
274	suprema-000		0.0064	105	0.0092	101	0.0081	155	0.0096	124	0.0139	148	0.0254	137	0.0220	186	0.1131	265	-	
275	supremaid-001		0.0053	77	0.0073	73	0.0045	78	0.0066	83	0.0099	110	0.0186	102	0.0148	135	0.0352	183	-	
276	synesis-006		0.0070	118	0.0096	107	0.0107	191	0.0166	188	-	0.0128	63	0.0089	65	0.0292	101	-		
277	synesis-007		0.0050	68	0.0073	75	0.0062	119	0.0076	97	-	0.0105	43	0.0080	50	0.0288	82	-		
278	synology-000		0.0149	211	0.0238	213	0.0148	223	0.0261	224	0.0221	201	0.0331	162	0.0209	184	0.0330	161	-	
279	synology-002		0.0104	171	0.0153	166	0.0107	192	0.0184	194	0.0189	189	0.2032	241	0.0180	160	0.0312	139	-	
280	sztu-000		0.0092	153	0.0139	150	0.0091	171	0.0201	206	0.0136	144	0.0685	204	0.0118	107	0.0270	2	-	
281	sztu-001		0.0031	32	0.0043	33	0.0025	8	0.0028	9	0.0051	33	0.0113	53	0.0089	66	0.0275	13	-	
282	tech5-004		0.0123	189	0.0234	210	0.0086	165	0.0162	184	0.0065	63	0.0112	50	0.0082	53	0.0281	51	-	
283	tech5-005		0.0054	79	0.0072	70	0.0069	128	0.0122	146	0.0060	54	0.0094	30	0.0066	18	0.0349	178	-	
284	techsign-000		0.0325	258	0.0511	259	0.0435	264	0.0710	263	0.0746	263	0.1104	226	0.0841	256	0.0639	239	-	
285	tevian-006		0.0045	58	0.0061	59	0.0045	79	0.0066	82	0.0046	26	0.0091	25	0.0075	35	0.0308	136	-	
286	tevian-007		0.0019	15	0.0027	11	0.0032	33	0.0041	31	0.0045	19	0.0086	21	0.0078	44	0.0310	138	-	
287	tiger-003		0.0313	257	0.0602	264	0.0188	236	0.0359	242	0.0344	231	-	-	-	0.0482	217	0.5610	21	
288	tiger-005		0.0624	274	0.2450	291	0.0292	256	0.0556	255	0.0430	245	1.0000	319	0.9964	324	0.0278	29	-	
289	tinkoff-001		0.0145	207	0.0244	214	0.0318	257	0.0636	260	0.0236	210	1.0000	339	0.0339	215	0.0563	232	-	
290	tongyi-005		0.0073	126	0.0146	159	0.0187	235	0.0421	248	0.0161	168	0.0215	118	0.0149	137	0.0399	194	0.6195	26
291	toshiba-002		0.0134	199	0.0222	204	0.0097	181	0.0154	180	-	0.0327	161	0.0158	145	0.0434	206	0.7103	35	
292	toshiba-003		0.0125	193	0.0214	197	0.0085	163	0.0131	159	-	0.0241	129	0.0151	140	0.0282	52	-		
293	trueface-001		0.0204	239	0.0438	252	0.0095	179	0.0138	165	0.0154	159	0.0253	136	0.0169	153	0.0772	248	-	
294	trueface-002		0.0060	97	0.0096	106	0.0048	85	0.0061	74	0.0112	127	0.0198	108	0.0155	143	0.0793	250	-	
295	tuputech-000		0.3218	308	0.3696	302	-	-	-	0.3237	291	0.4304	261	0.2973	285	0.9415	327	-		
296	twface-000		0.0051	71	0.0072	71	0.0041	65	0.0058	65	0.0071	69	0.0153	79	0.0100	77	0.0276	20	-	
297	ulsee-001		0.0151	214	0.0246	216	0.0113	202	0.0185	198	0.0187	188	0.6766	278	0.0181	162	0.0316	144	-	
298	ultinous-000		0.2343	298	0.3484	298	-	-	-	-	-	-	-	-	-	0.9447	53			
299	ultinous-001		0.2485	300	0.4003	305	-	-	-	-	-	-	-	-	-	0.6847	31			
300	uluface-002		0.0081	140	0.0123	137	0.0071	131	0.0095	122	0.0107	118	1.0000	340	0.0140	126	0.0444	208	0.6729	30
301	uluface-003		0.0100	166	0.0150	162	0.0079	147	0.0128	155	-	-	-	-	-	0.0635	238	-		
302	upc-001		0.0234	243	0.0519	260	0.0291	255	0.0490	253	0.0294	225	0.2316	246	0.0389	225	0.0314	143	0.4224	8
303	vcog-002		0.7522	335	0.9033	333	-	-	-	-	-	-	-	-	-	-	0.7523	40		
304	vd-001		0.0243	245	0.0452	254	0.0271	252	0.0402	246	0.0424	244	-	-	-	0.1389	273	-		
305	vd-002		0.0429	265	0.0704	267	0.0569	272	0.0844	267	0.0801	264	0.0937	214	0.0577	242	0.0556	231	-	
306	veridas-004		0.0281	252	0.0467	255	0.0353	261	0.0643	261	0.0424	243	0.0644	201	0.0342	216	0.0291	100	-	
307	veridas-006		0.0098	162	0.0167	177	0.0079	149	0.0127	151	0.0127	135	0.0217	120	0.0151	139	0.0286	80	-	
308	verihubs-inteligensia-000		0.0070	119	0.0098	110	0.0048	87	0.0076	99	0.0092	96	0.0160	84	0.0117	103	0.0283	64	-	

Table 20: FNMR is the proportion of mated comparisons below a threshold set to achieve the FMR given in the header on the fourth row. FMR is the proportion of impostor comparisons at or above that threshold. The light grey values give rank over all algorithms in that column. The pink columns use only same-sex impostors; others are selected regardless of demographics. The exception, in the green column, uses “matched-covariates” i.e. impostors of the same sex, age group, and country of birth. The second pink column includes effects of extended ageing. Missing entries for border, visa, mugshot and wild images generally mean the algorithm did not run to completion. For child exploitation, missing entries arise because NIST executes those runs only infrequently. The VISA columns compare images described in section 2.2. The MUGSHOT columns compare images described in section 2.5. The VISA-BORDER column compare images described in section 2.3 with those of section 2.4. The BORDER column compares images described in section 2.4. The WILD columns compare images described in section 2.6. The CHILD-EXPLOITATION columns compare images described in section 2.1.

	Algorithm	FALSE NON-MATCH RATE (FNMR)												LESS CONSTRAINED, NON-COOP.					
		CONSTRAINED, COOPERATIVE																	
		Name	VISAMC	VISA	MUGSHOT	MUGSHOT12+YRS	VISABORDER	BORDER	BORDER	WILD	CHILDEXP								
	FMR	0.0001	1E-06	1E-05	1E-05	1E-06	1E-06	1E-06	1E-05	0.0001	0.01								
309	via-000	0.0216	240	0.0365	242	0.0177	233	0.0287	232	0.0296	226	0.0572	190	0.0290	212	0.0349	177	0.7638	41
310	via-001	0.0149	210	0.0229	206	0.0114	204	0.0177	193	0.0183	185	0.4056	259	0.0176	157	0.0373	191	-	
311	videmo-000	0.0298	255	0.0423	248	0.0155	229	0.0260	222	0.0246	216	0.0397	180	0.0239	198	0.0541	229	-	
312	videonetics-001	0.5483	328	0.6446	323	0.7517	326	0.8607	323	0.8664	318	0.8255	294	0.6956	313	0.2986	303	0.7297	37
313	videonetics-002	0.4274	316	0.5329	315	0.6081	316	0.7438	314	0.7775	311	0.7297	284	0.5756	304	0.1976	288	0.7435	39
314	vigilantsolutions-010	0.0109	176	0.0164	173	0.0074	140	0.0095	121	0.0209	197	0.0365	172	0.0233	194	0.0277	22	-	
315	vigilantsolutions-011	0.0124	191	0.0176	181	0.0073	135	0.0095	120	0.0196	193	0.0360	171	0.0221	187	0.0274	10	-	
316	vinai-000	0.0081	139	0.0124	138	0.0045	76	0.0072	90	0.0089	90	0.1814	233	0.0112	96	0.0274	12	-	
317	vion-000	0.0419	264	0.0590	263	0.0422	263	0.0478	251	0.0581	255	0.0968	220	0.0847	257	0.2479	296	0.8765	47
318	visage-000	0.0933	282	0.1441	282	0.1316	287	0.2416	288	0.1395	275	0.1920	237	0.1001	261	0.0500	221	-	
319	visionbox-001	0.0159	219	0.0270	227	0.0111	197	0.0173	190	0.0190	190	0.0315	155	0.0205	182	0.0389	193	-	
320	visionbox-002	0.0058	87	0.0079	82	0.0060	112	0.0074	92	0.0084	82	0.0149	74	0.0113	99	0.0447	210	-	
321	visionlabs-009	0.0018	11	0.0025	8	0.0026	10	0.0029	14	0.0035	6	0.0064	5	0.0054	4	0.0283	62	-	
322	visionlabs-010	0.0017	10	0.0024	5	0.0026	11	0.0030	16	0.0033	4	0.0061	3	0.0052	3	0.0282	57	-	
323	visteam-001	0.4417	320	0.5385	317	0.6410	318	0.7788	316	0.6386	304	0.5904	271	0.4023	295	0.1413	274	-	
324	visteam-002	0.1564	292	0.2789	294	0.1581	291	0.2567	290	0.1776	280	0.2090	242	0.1021	262	0.0349	179	-	
325	vnpt-001	0.3117	306	0.3523	299	0.3474	301	0.2747	291	0.3405	292	0.5015	264	0.4827	299	0.5337	317	-	
326	vnpt-002	0.0351	261	0.0424	249	0.0220	243	0.0316	235	0.0471	249	0.0817	211	0.0698	249	0.0400	195	-	
327	vocord-008	0.0029	30	0.0038	23	0.0042	67	0.0055	59	0.0045	21	0.0086	23	0.0073	30	0.0286	78	-	
328	vocord-009	0.0022	17	0.0029	15	0.0036	46	0.0046	38	0.0052	36	0.0098	37	0.0086	62	0.0284	70	-	
329	vts-000	0.0103	168	0.0174	179	0.0080	151	0.0129	158	0.0250	217	0.0450	183	0.0372	223	0.0596	235	-	
330	winsense-001	0.0062	101	0.0099	116	0.0092	173	0.0210	208	0.0093	99	0.0144	71	0.0098	76	0.0320	149	0.4155	7
331	winsense-002	0.0050	69	0.0073	74	0.0038	54	0.0059	69	0.0064	61	0.0118	58	0.0084	57	0.0307	132	-	
332	wuhantianyu-001	0.0163	220	0.0262	224	0.0281	254	0.0569	258	0.0316	230	0.0486	186	0.0344	217	0.0324	153	-	
333	x-laboratory-000	0.0071	120	0.0106	125	0.0123	209	0.0138	164	0.0419	242	0.5629	269	0.2852	284	0.0295	111	0.9686	55
334	x-laboratory-001	0.0059	92	0.0110	129	0.0054	96	0.0078	102	0.0094	101	0.0142	67	0.0100	79	0.0294	108	-	
335	xforwardai-001	0.0021	16	0.0034	18	0.0027	16	0.0028	8	0.0046	25	0.0088	24	0.0079	46	0.0281	50	-	
336	xforwardai-002	0.0016	7	0.0023	4	0.0026	13	0.0025	3	0.0040	11	0.0081	16	0.0074	32	0.0282	53	-	
337	xm-000	0.0015	5	0.0026	10	0.0031	27	0.0038	26	0.0058	49	0.0105	44	0.0082	54	0.0282	56	-	
338	yisheng-004	0.1988	295	0.3329	297	0.1147	285	0.1849	283	0.2044	284	-	-	-	0.0908	253	0.7152	36	
339	yitu-003	0.0015	6	0.0026	9	0.0066	126	0.0085	112	0.0064	62	0.0114	54	0.0103	87	0.0325	156	-	
340	yoonik-000	0.0070	117	0.0112	131	0.0074	139	0.0118	142	0.0564	254	0.2013	240	0.1160	263	0.0590	234	-	
341	yoonik-001	0.0057	85	0.0079	83	0.0043	72	0.0061	72	0.0307	228	0.0762	208	0.0556	241	0.0526	227	-	
342	ytu-000	0.0057	86	0.0087	95	0.0121	207	0.0238	217	0.0047	27	0.0078	14	0.0059	9	0.0286	79	-	
343	yuan-001	0.0116	181	0.0220	201	0.0114	203	0.0184	195	0.0149	156	0.0574	191	0.0160	146	0.0321	151	-	
344	yuan-002	0.0094	156	0.0154	169	0.0071	133	0.0110	137	0.0108	122	0.0348	168	0.0127	112	0.0319	148	-	

Table 21: FNMR is the proportion of mated comparisons below a threshold set to achieve the FMR given in the header on the fourth row. FMR is the proportion of impostor comparisons at or above that threshold. The light grey values give rank over all algorithms in that column. The pink columns use only same-sex impostors; others are selected regardless of demographics. The exception, in the green column, uses “matched-covariates” i.e. impostors of the same sex, age group, and country of birth. The second pink column includes effects of extended ageing. Missing entries for border, visa, mugshot and wild images generally mean the algorithm did not run to completion. For child exploitation, missing entries arise because NIST executes those runs only infrequently. The VISA columns compare images described in section 2.2. The MUGSHOT columns compare images described in section 2.5. The VISA-BORDER column compare images described in section 2.3 with those of section 2.4. The BORDER column compares images described in section 2.4. The WILD columns compare images described in section 2.6. The CHILD-EXPLOITATION columns compare images described in section 2.1.

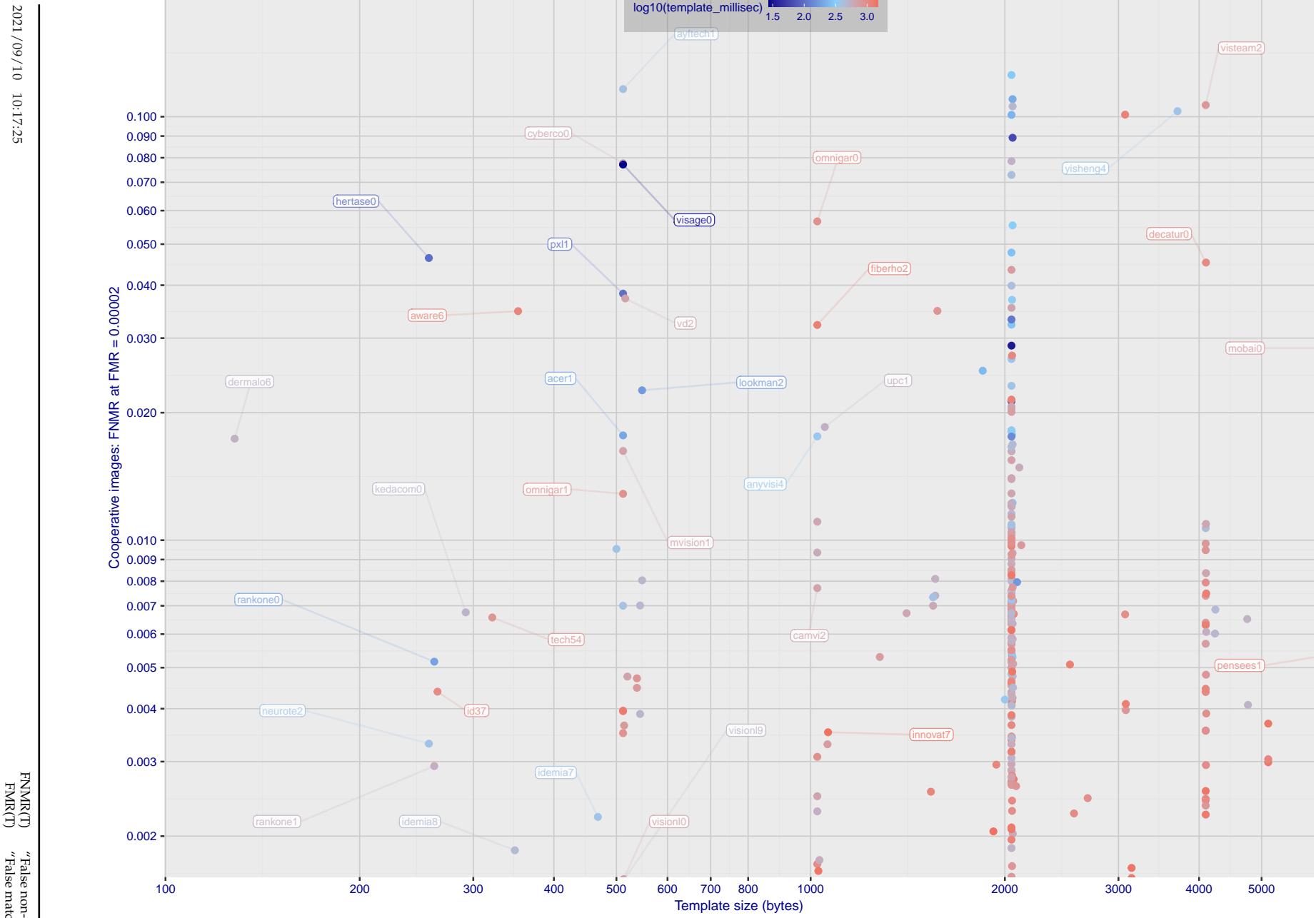


Figure 1: The points show false non-match rates (FNMR) versus the size of the encoded template. FNMR is the geometric mean of FNMR values for visa and mugshot images (from Figs. 53 and 70) at a false match rate (FMR) of 0.0001. The color of the points encodes template generation time - which spans at least one order of magnitude. Durations are measured on a single core of a c. 2016 Intel Xeon E5-2630 v4 running at 2.20GHz. Algorithms with poor FNMR are omitted.

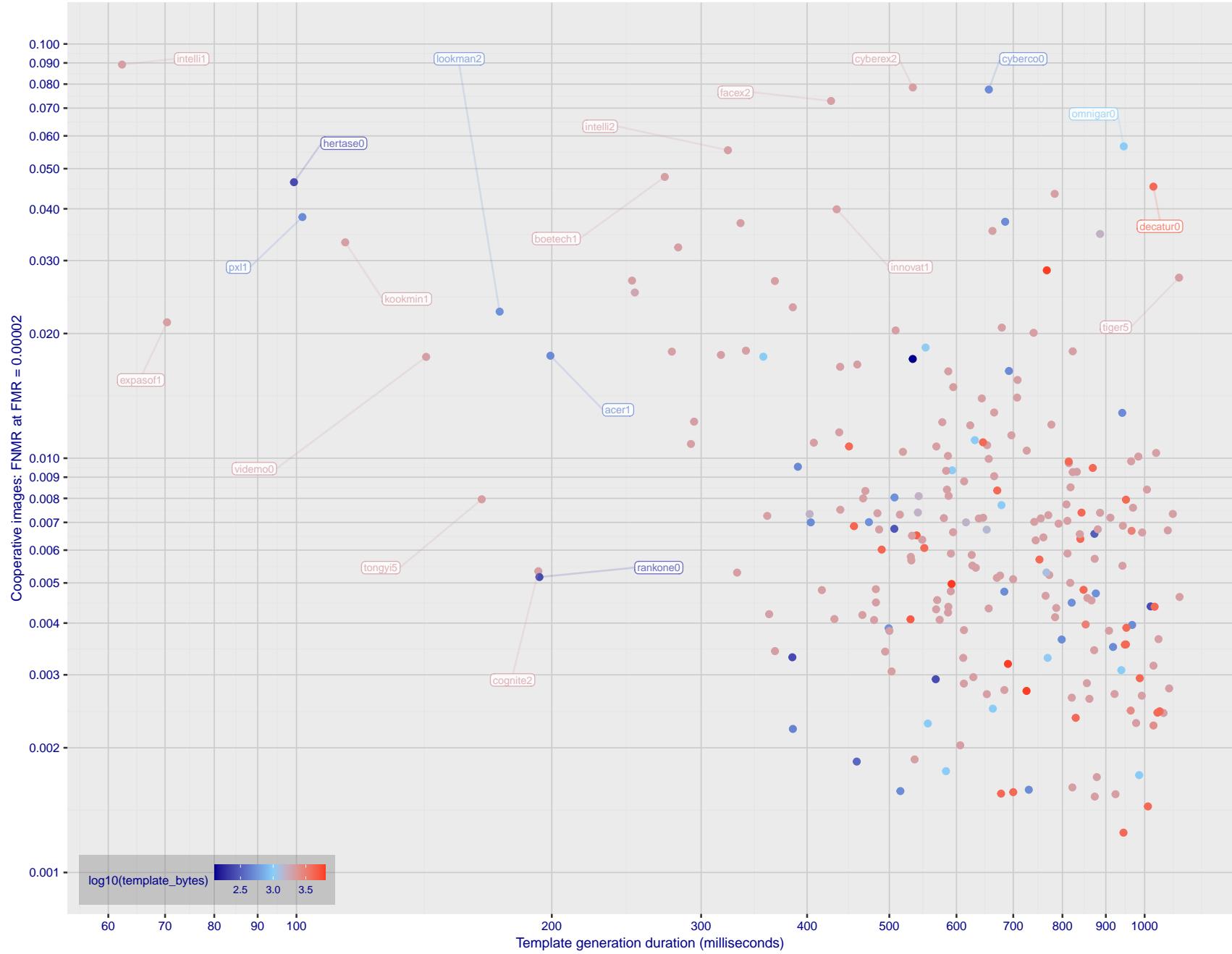


Figure 2: The points show false non-match rates (FNMR) versus the duration of the template generation operation. FNMR is the geometric mean of FNMR values for visa and mugshot images (from Figs. 53 and 70) at a false match rate (FMR) of 0.0001. Template generation time is a median estimated over 640 x 480 pixel portraits. It is measured on a single core of a c. 2016 Intel Xeon CPU E5-2630 v4 running at 2.20GHz. The color of the points encodes template size - which span two orders of magnitude. Algorithms with poor FNMR are omitted.

# 1 Metrics

## 1.1 Core accuracy

Given a vector of N genuine scores,  $u$ , the false non-match rate (FNMR) is computed as the proportion below some threshold, T:

$$\text{FNMR}(T) = 1 - \frac{1}{N} \sum_{i=1}^N H(u_i - T) \quad (1)$$

where  $H(x)$  is the unit step function, and  $H(0)$  taken to be 1.

Similarly, given a vector of N impostor scores,  $v$ , the false match rate (FMR) is computed as the proportion above T:

$$\text{FMR}(T) = \frac{1}{N} \sum_{i=1}^N H(v_i - T) \quad (2)$$

The threshold, T, can take on any value. We typically generate a set of thresholds from quantiles of the observed impostor scores,  $v$ , as follows. Given some interesting false match rate range,  $[\text{FMR}_L, \text{FMR}_U]$ , we form a vector of K thresholds corresponding to FMR measurements evenly spaced on a logarithmic scale

$$T_k = Q_v(1 - \text{FMR}_k) \quad (3)$$

where  $Q$  is the quantile function, and  $\text{FMR}_k$  comes from

$$\log_{10} \text{FMR}_k = \log_{10} \text{FMR}_L + \frac{k}{K} [\log_{10} \text{FMR}_U - \log_{10} \text{FMR}_L] \quad (4)$$

Error tradeoff characteristics are plots of FNMR(T) vs. FMR(T). These are plotted with  $\text{FMR}_U \rightarrow 1$  and  $\text{FMR}_L$  as low as is sustained by the number of impostor comparisons, N. This is somewhat higher than the “rule of three” limit  $3/N$  because samples are not independent, due to re-use of images.

## 2 Datasets

### 2.1 Child exploitation images

- ▷ The number of images is on the order of  $10^4$ .
- ▷ The number of subjects is on the order of  $10^3$ .
- ▷ The number of subjects with two images on the order of  $10^3$ .
- ▷ The images are operational. They are taken from ongoing investigations of child exploitation crimes. The images are arbitrarily unconstrained. Pose varies considerably around all three axes, including subject lying down. Resolution varies very widely. Faces can be occluded by other objects, including hair and hands. Lighting varies, although the images are intended for human viewing. Mis-focus is rare. Images are given to the algorithm without any cropping; faces may occupy widely varying areas.
- ▷ The images are usually large from contemporary cameras. The mean interocular distance (IOD) is 70 pixels.
- ▷ The images are of subjects from several countries, due to the global production of this imagery.
- ▷ The images are of children, from infancy to late adolescence.
- ▷ All of the images are live capture, none are scanned. Many have been cropped.
- ▷ When these images are input to the algorithm, they are labelled as being of type "EXPLOITATION" - see Table 4 of the FRVT API.

### 2.2 Visa images

- ▷ The number of images is on the order of  $10^5$ .
- ▷ The number of subjects is on the order of  $10^5$ .
- ▷ The number of subjects with two images is on the order of  $10^4$ .
- ▷ The images have geometry in reasonable conformance with the ISO/IEC 19794-5 Full Frontal image type. Pose is generally excellent.
- ▷ The images are of size 252x300 pixels. The mean interocular distance (IOD) is 69 pixels.
- ▷ The images are of subjects from greater than 100 countries, with significant imbalance due to visa issuance patterns.
- ▷ The images are of subjects of all ages, including children, again with imbalance due to visa issuance demand.
- ▷ Many of the images are live capture. A substantial number of the images are photographs of paper photographs.
- ▷ When these images are input to the algorithm, they are labelled as being of type "ISO" - see Table 4 of the FRVT API.

### 2.3 Application images

- ▷ The number of images is on the order of  $10^6$ .
- ▷ The number of subjects is on the order of  $10^6$ .
- ▷ The number of subjects with two images is on the order of  $10^6$ .
- ▷ The images have geometry in good conformance with the ISO/IEC 19794-5 Full Frontal image type. Pose is generally excellent.
- ▷ The images are of size 300x300 pixels. The mean interocular distance (IOD) is 61 pixels.
- ▷ The images are of subjects from greater than 100 countries, with significant imbalance due to population and immigration patterns.

- ▷ The images are of subjects of adults with imbalance due to population and immigration patterns and demand.
- ▷ All of the images are live capture.
- ▷ When these images are input to the algorithm, they are labelled as being of type "ISO" - see Table 4 of the FRVT API.

## 2.4 Border crossing images

- ▷ The number of images is on the order of  $10^6$ .
- ▷ The number of subjects is on the order of  $10^6$ .
- ▷ The number of subjects with two images is on the order of  $10^6$ .
- ▷ The images are taken with a camera oriented by an attendant toward a cooperating subject. This is done under time constraints so there are roll, pitch and yaw angle variations. Also background illumination is sometimes strong, so the face is under-exposed. There is some perspective distortion due to close range images. Some faces are partially cropped.
- ▷ The images are of subjects from greater than 100 countries, with significant imbalance due to population and immigration patterns.
- ▷ The images are of subjects of adults with imbalance due to population and immigration patterns and demand.
- ▷ The images have mean IOD of 38 pixels.
- ▷ The images are all live capture.
- ▷ When these images are input to the algorithm, they are labelled as being of type "WILD" - see Table 4 of the FRVT API.

## 2.5 Mugshot images

- ▷ The number of images is on the order of  $10^6$ .
- ▷ The number of subjects is on the order of  $10^6$ .
- ▷ The number of subjects with two images is on the order of  $10^6$ .
- ▷ The images have geometry in reasonable conformance with the ISO/IEC 19794-5 Full Frontal image type.
- ▷ The images are of variable sizes. The median IOD is 105 pixels. The mean IOD is 113 pixels. The 1-st, 5-th, 10-th, 25-th, 75-th, 90-th and 99-th percentiles are 34, 58, 70, 87, 121, 161 and 297 pixels.
- ▷ The images are of subjects from the United States.
- ▷ The images are of adults.
- ▷ The images are all live capture.
- ▷ When these images are input to the algorithm, they are labelled as being of type "mugshot" - see Table 4 of the FRVT API.

## 2.6 Wild images

- ▷ The number of images is on the order of  $10^5$ .
- ▷ The number of subjects is on the order of  $10^3$ .
- ▷ The number of subjects with two images on the order of  $10^3$ .
- ▷ The images include many photojournalism-style images. Images are given to the algorithm using a variable but generally tight crop of the head. Resolution varies very widely. The images are very unconstrained, with wide yaw and pitch pose variation. Faces can be occluded, including hair and hands.



*Figure 3: The figure gives simulated samples of image types used in this report.*

- ▷ The images are of adults.
- ▷ All of the images are live capture, none are scanned.
- ▷ When these images are input to the algorithm, they are labelled as being of type "WILD" - see Table 4 of the FRVT API.

## 3 Results

### 3.1 Test goals

- ▷ To state absolute accuracy for different kinds of images, including those with and without subject cooperation.
- ▷ To state comparative accuracy, across algorithms.

### 3.2 Test design

**Method:** For visa images:

- ▷ The comparisons are of visa photos against visa photos.
- ▷ The number of genuine comparisons is on the order of  $10^4$ .
- ▷ The number of impostor comparisons is on the order of  $10^{10}$ .
- ▷ The comparisons are fully zero-effort, meaning impostors are paired without attention to sex, age or other covariates. However, later analysis is conducted on subsets.
- ▷ The number of persons is on the order of  $10^5$ .
- ▷ The number of images used to make 1 template is 1.
- ▷ The number of templates used to make each comparison score is two corresponding to simple one-to-one verification.

**Method:** For mugshot images:

- ▷ The comparisons are of mugshot photos against mugshot photos.

- ▷ The number of genuine comparisons is on the order of  $10^6$ .
- ▷ The number of impostor comparisons is on the order of  $10^8$ .
- ▷ The impostors are paired by sex, but not by age or other covariates.
- ▷ The number of persons is on the order of  $10^6$ .
- ▷ The number of images used to make 1 template is 1.
- ▷ The number of templates used to make each comparison score is two corresponding to simple one-to-one verification.

**Method:** For visa-border comparisons:

- ▷ The comparisons are of visa-like frontals against border crossing webcam photos.
- ▷ The number of genuine comparisons is on the order of  $10^6$ .
- ▷ The number of impostor comparisons is on the order of  $10^8$ .
- ▷ The impostors are paired by sex, but not by age or other covariates.
- ▷ The number of persons is on the order of  $10^6$ .
- ▷ The number of images used to make 1 template is 1.
- ▷ The number of templates used to make each comparison score is two corresponding to simple one-to-one verification.

**Method:** For border-border comparisons:

- ▷ The comparisons are of border crossing webcam photos.
- ▷ The number of genuine comparisons is on the order of  $10^6$ .
- ▷ The number of impostor comparisons is on the order of  $10^8$ .
- ▷ The impostors are paired by sex, but not by age or other covariates.
- ▷ The number of persons is on the order of  $10^6$ .
- ▷ The number of images used to make 1 template is 1.
- ▷ The number of templates used to make each comparison score is two corresponding to simple one-to-one verification.

**Method:** For wild images:

- ▷ The comparisons are of wild photos against wild photos.
- ▷ The number of genuine comparisons is on the order of  $10^6$ .
- ▷ The number of impostor comparisons is on the order of  $10^7$ .
- ▷ The comparisons are fully zero-effort, meaning impostors are paired without attention to sex, age or other covariates.
- ▷ The number of persons is on the order of  $10^4$ .
- ▷ The number of images used to make 1 template is 1.
- ▷ The number of templates used to make each comparison score is two corresponding to simple one-to-one verification.

**Method:** For child exploitation images:

- ▷ The comparisons are of unconstrained child exploitation photos against others of the same type.

- ▷ The number of genuine comparisons is on the order of  $10^4$ .
- ▷ The number of impostor comparisons is on the order of  $10^7$ .
- ▷ The comparisons are fully zero-effort, meaning impostors are paired without attention to sex, age or other covariates.
- ▷ The number of persons is on the order of  $10^3$ .
- ▷ The number of images used to make 1 template is 1.
- ▷ The number of templates used to make each comparison score is two corresponding to simple one-to-one verification.
- ▷ We produce two performance statements. First, is a DET as used for visa and mugshot images. The second is a cumulative match characteristic (CMC) summarizing a simulated one-to-many search process. This is done as follows.
  - We regard  $M$  enrollment templates as items in a gallery.
  - These  $M$  templates come from  $M > N$  individuals, because multiple images of a subject are present in the gallery under separate identifiers.
  - We regard the verification templates as search templates.
  - For each search we compute the rank of the highest scoring mate.
  - This process should properly be conducted with a 1:N algorithm, such as those tested in NIST IR 8009. We use the 1:1 algorithms in a simulated 1:N mode here to a) better reflect what a child exploitation analyst does, and b) to show algorithm efficacy is better than that revealed in the verification DETs.

### 3.3 Failure to enroll

	Algorithm Name	Failure to Enrol Rate <sup>1</sup>							
		APPLICATION	BORDER	CHILD-EXPLOIT	MUGSHOT	VISA	WILD	SEC. 2.3	SEC. 2.4
	Name	SEC. 2.1	SEC. 2.5	SEC. 2.2	SEC. 2.6				
1	20face-000	0.0000	183	0.0008	168	-	304	0.0000	100
2	3divi-005	0.0000	238	0.0008	161	-	158	0.0000	123
3	3divi-006	0.0000	167	0.0007	149	-	260	0.0001	176
4	acer-000	0.0000	264	0.0024	257	-	137	0.0002	219
5	acer-001	0.0000	142	0.0011	204	-	219	0.0001	158
6	acisw-003	0.0000	70	0.0000	50	-	313	0.0000	46
7	acisw-006	0.0000	15	0.0000	65	-	199	0.0000	3
8	adera-002	0.0000	263	0.0034	274	-	102	0.0003	243
9	adera-003	0.0000	262	0.0034	275	-	202	0.0003	242
10	advance-002	0.0000	208	0.0013	225	-	121	0.0000	142
11	advance-003	0.0000	253	0.0012	215	-	308	0.0001	194
12	aifirst-001	0.0000	107	0.0000	34	0.0000	2	0.0000	66
13	aigen-001	0.0000	87	0.0000	26	-	60	0.0000	57
14	aigen-002	0.0000	40	0.0000	35	-	289	0.0000	43
15	ailabs-001	0.0000	146	0.0090	311	-	195	0.0007	288
16	aimall-002	0.0000	267	0.0043	287	-	287	0.0012	301
17	aimall-003	0.0000	244	0.0012	218	-	58	0.0004	256
18	aiunionface-000	0.0000	64	0.0000	49	-	346	0.0000	54
19	aize-001	0.0001	299	0.0040	283	-	153	0.0026	319
20	ajou-001	0.0000	162	0.0020	250	-	272	0.0001	179
21	alchera-002	0.0000	182	0.0008	172	-	306	0.0001	201
22	alchera-003	0.0001	310	0.0013	223	-	238	0.0002	226
23	alice-000	0.0000	71	0.0006	126	-	312	0.0000	109
24	alleyes-000	0.0000	188	0.0010	189	-	78	0.0002	207
25	allgovision-000	0.0007	322	0.0062	303	-	92	0.0026	318
26	alphaface-001	0.0000	147	0.0012	211	-	194	0.0000	143
27	alphaface-002	0.0000	193	0.0012	210	-	68	0.0000	146
28	amplifiedgroup-001	0.0114	335	0.1023	337	-	284	0.0189	337
29	androvideo-000	0.0000	73	0.0000	54	-	317	0.0000	50
30	anke-004	0.0000	154	0.0011	201	0.0944	35	0.0001	184
31	anke-005	0.0000	166	0.0012	212	0.1228	37	0.0001	197
32	antheus-000	0.0000	111	0.0000	2	0.0000	6	0.0000	72
33	antheus-001	0.0000	47	0.0000	37	-	283	0.0000	45
34	anyvision-004	0.0000	252	0.0017	240	0.1660	40	0.0001	198
35	anyvision-005	0.0000	165	0.0013	220	-	275	0.0000	125
36	asusaics-000	0.0000	35	0.0000	82	-	227	0.0000	20
37	asusaics-001	0.0000	13	0.0000	64	-	203	0.0000	2
38	authenmetric-002	0.0000	122	0.0000	10	-	178	0.0000	82
39	authenmetric-003	0.0000	51	0.0000	39	-	274	0.0000	34
40	aware-005	0.0000	220	0.0020	248	-	218	0.0001	206
41	aware-006	0.0000	199	0.0009	179	-	100	0.0000	128
42	awiros-001	0.0039	327	0.0369	330	-	206	0.0386	338
43	awiros-002	0.0000	278	0.0038	280	-	336	0.0007	286
44	ayftech-001	0.0002	312	0.0046	293	-	98	0.0043	326
45	ayonix-000	0.0053	330	0.0341	327	0.0000	4	0.0113	334
46	beethedata-000	0.0005	319	0.0042	286	-	254	0.0002	212
47	bioidechtechswiss-001	0.0000	215	0.0007	144	-	169	0.0000	115
48	bioidechtechswiss-002	0.0000	174	0.0007	147	-	324	0.0000	118
49	bm-001	0.0000	99	0.0000	31	0.0000	3	0.0000	92
50	boetech-001	0.0087	333	0.0272	320	-	217	0.0032	324
51	bresee-001	0.0000	172	0.0010	193	-	345	0.0002	213
52	bresee-002	0.0000	260	0.0020	251	-	322	0.0008	289
53	camvi-002	0.0000	43	0.0000	36	0.0000	21	0.0000	44
54	camvi-004	0.0000	126	0.0000	93	0.0000	8	0.0000	81
55	canon-002	0.0000	80	0.0000	57	-	302	0.0000	52
56	ceiec-003	0.0000	106	0.0013	226	-	89	0.0001	163
57	ceiec-004	0.0000	137	0.0008	167	-	159	0.0000	122
58	chosun-001	0.0000	123	0.0000	9	-	179	0.0000	83

Table 22: FTE is the proportion of failed template generation attempts. Failures can occur because the software throws an exception, or because the software electively refuses to process the input image. This would typically occur if a face is not detected. FTE is measured as the number of function calls that give EITHER a non-zero error code OR that give a “small” template. This is defined as one whose size is less than 0.3 times the median template size for that algorithm. This second rule is needed because some algorithms incorrectly fail to return a non-zero error code when template generation fails.

<sup>1</sup>The effects of FTE are included in the accuracy results of this report by regarding any template comparison involving a failed template to produce a low similarity score. Thus higher FTE results in higher FNMR and lower FMR.

	Algorithm	Failure to Enrol Rate <sup>1</sup>						
		APPLICATION	BORDER	CHILD-EXPLOIT	MUGSHOT	VISA	WILD	
Name	SEC. 2.3	SEC. 2.4	SEC. 2.1	SEC. 2.5	SEC. 2.2	SEC. 2.6		
59 chosun-002	0.0000	59	0.0000	47	-	269	0.0000	42
60 chtface-002	0.0000	277	0.0021	253	-	279	0.0002	235
61 chtface-003	0.0000	259	0.0018	243	-	325	0.0001	167
62 cib-001	0.0000	103	0.0000	33	-	86	0.0000	65
63 closeli-001	0.0000	81	0.0000	21	-	75	0.0000	60
64 cloudwalk-hr-003	0.0000	177	0.0008	169	-	332	0.0001	166
65 cloudwalk-hr-004	0.0000	148	0.0011	208	-	198	0.0004	258
66 cloudwalk-mt-002	0.0000	207	0.0003	108	-	123	0.0001	153
67 cloudwalk-mt-003	0.0000	143	0.0007	139	-	209	0.0002	220
68 clova-000	0.0000	272	0.0022	254	-	342	0.0006	282
69 cogent-005	0.0000	38	0.0000	87	-	233	0.0000	24
70 cogent-006	0.0000	92	0.0000	27	-	63	0.0000	58
71 cognitec-002	0.0001	296	0.0069	304	-	140	0.0003	252
72 cognitec-003	0.0001	297	0.0194	317	-	331	0.0003	249
73 cor-001	0.0000	175	0.0006	130	-	321	0.0002	233
74 coretech-000	0.0000	18	0.0000	72	-	190	0.0000	10
75 corsight-001	0.0000	191	0.0006	133	-	66	0.0001	202
76 csc-002	0.0015	324	0.0033	271	-	107	0.0006	284
77 csc-003	0.0015	325	0.0033	270	-	104	0.0006	283
78 ctbcbank-000	0.0001	298	0.0051	297	0.3285	48	0.0011	299
79 ctbcbank-001	0.0000	280	0.0036	279	-	182	0.0005	275
80 cubox-001	0.0000	72	0.0000	51	-	311	0.0000	47
81 cubox-002	0.0000	229	0.0006	132	-	298	0.0002	232
82 cuhkee-001	0.0000	180	0.0011	207	-	300	0.0000	99
83 cybercore-000	0.0000	214	0.0073	307	-	165	0.0001	175
84 cyberextruder-001	0.0029	326	0.0293	321	0.5338	54	0.0024	314
85 cyberextruder-002	0.0013	323	0.0840	336	0.2672	47	0.0027	320
86 cyberlink-006	0.0000	115	0.0005	120	-	133	0.0000	97
87 cyberlink-007	0.0000	26	0.0003	104	-	247	0.0000	95
88 dahua-005	0.0000	29	0.0000	92	-	243	0.0000	124
89 dahua-006	0.0000	133	0.0000	89	-	171	0.0000	139
90 decatur-000	0.0000	222	0.0020	247	-	188	0.0004	265
91 deepglint-002	0.0000	151	0.0004	116	0.0669	32	0.0002	227
92 deepglint-003	0.0000	159	0.0004	115	-	290	0.0002	228
93 deepsea-001	0.0000	129	0.0000	15	0.0000	9	0.0000	87
94 deepsense-000	0.0000	21	0.0006	134	-	252	0.0000	106
95 dermalog-006	0.0005	318	0.0031	268	0.1797	41	0.0013	303
96 dermalog-008	0.0000	274	0.0031	267	-	318	0.0006	279
97 didiglobalface-001	0.0000	192	0.0012	209	0.2175	43	0.0000	145
98 digitalbarriers-002	0.0001	302	0.0045	290	-	184	0.0028	322
99 dps-000	0.0000	120	0.0000	6	-	115	0.0000	69
100 dsk-000	0.0000	34	0.0000	80	0.0000	13	0.0000	19
101 einetworks-000	0.0000	279	0.0017	239	-	87	0.0002	223
102 ekin-002	0.0000	141	0.0000	94	-	152	0.0000	98
103 enfave-000	0.0000	91	0.0012	217	-	64	0.0000	131
104 eocortex-000	0.0095	334	0.0602	333	-	84	0.0094	333
105 ercacat-001	0.0000	49	0.0005	121	-	273	0.0000	130
106 expasoft-001	0.0000	12	0.0000	69	-	204	0.0000	7
107 expasoft-002	0.0000	58	0.0000	43	-	257	0.0000	39
108 f8-001	0.0003	314	0.0059	302	0.2026	42	0.0035	325
109 facesoft-000	0.0000	27	0.0000	76	0.0000	17	0.0000	31
110 facetag-000	0.0000	14	0.0000	66	-	200	0.0000	4
111 facex-001	0.0001	309	0.0360	328	-	170	0.0047	329
112 facex-002	0.0001	308	0.0360	329	-	237	0.0047	328
113 farfaces-001	0.0000	276	0.0007	146	-	281	0.0003	245
114 fiberhome-nanjing-002	0.0000	237	0.0006	135	-	185	0.0001	172
115 fiberhome-nanjing-003	0.0000	100	0.0004	114	-	93	0.0000	63
116 fincore-000	0.0000	153	0.0008	171	-	239	0.0001	151

Table 23: FTE is the proportion of failed template generation attempts. Failures can occur because the software throws an exception, or because the software electively refuses to process the input image. This would typically occur if a face is not detected. FTE is measured as the number of function calls that give EITHER a non-zero error code OR that give a “small” template. This is defined as one whose size is less than 0.3 times the median template size for that algorithm. This second rule is needed because some algorithms incorrectly fail to return a non-zero error code when template generation fails.

<sup>1</sup> The effects of FTE are included in the accuracy results of this report by regarding any template comparison involving a failed template to produce a low similarity score. Thus higher FTE results in higher FNMR and lower FMR.

	Algorithm	Failure to Enrol Rate <sup>1</sup>											
		APPLICATION	BORDER	CHILD-EXPLOIT	MUGSHOT	VISA	WILD	SEC. 2.3	SEC. 2.4	SEC. 2.1	SEC. 2.5	SEC. 2.2	SEC. 2.6
117	fujitsulab-002	0.0000	76	0.0009	177	-	310	0.0001	193	0.0003	112	0.0003	110
118	fujitsulab-003	0.0000	52	0.0008	163	-	266	0.0001	183	0.0001	97	0.0003	106
119	geo-001	0.0000	197	0.0011	200	-	112	0.0000	141	0.0004	178	0.0007	203
120	geo-002	0.0000	198	0.0015	230	-	101	0.0001	148	0.0004	230	0.0017	236
121	glory-002	0.0003	313	0.0045	289	-	148	0.0015	307	0.0011	304	0.0557	314
122	glory-003	0.0000	241	0.0027	261	-	201	0.0004	257	0.0005	250	0.0244	296
123	gorilla-006	0.0000	89	0.0006	137	-	57	0.0000	108	0.0003	120	0.0003	113
124	gorilla-007	0.0000	184	0.0009	187	-	77	0.0001	169	0.0004	206	0.0004	150
125	griaule-000	0.0000	285	0.0026	260	-	167	0.0004	268	0.0010	294	0.0023	244
126	hertasecurity-000	0.0133	337	0.0077	309	-	139	0.0025	317	0.0243	340	0.0171	287
127	hik-001	0.0000	114	0.0000	96	-	129	0.0000	76	0.0000	16	0.0000	48
128	hyperverge-001	0.0000	293	0.0072	305	-	95	0.0015	309	0.0014	313	0.0042	252
129	hyperverge-002	0.0000	39	0.0008	162	-	291	0.0002	234	0.0004	172	0.0004	164
130	icm-002	0.0000	3	0.0001	97	-	222	0.0000	14	0.0000	92	0.0000	79
131	icthtc-000	0.0001	307	0.0047	295	-	197	0.0028	323	0.0029	327	0.0086	270
132	id3-006	0.0000	240	0.0009	186	-	223	0.0004	260	0.0005	268	0.0008	209
133	id3-007	0.0000	160	0.0041	284	-	297	0.0001	185	0.0004	195	0.0052	260
134	idemia-007	0.0000	116	0.0004	117	-	131	0.0000	105	0.0003	136	0.0003	115
135	idemia-008	0.0000	95	0.0004	118	-	113	0.0000	104	0.0003	135	0.0003	117
136	iit-002	0.0000	283	0.0021	252	-	162	0.0009	296	0.0005	275	0.0443	309
137	iit-003	0.0000	168	0.0008	170	-	262	0.0000	120	0.0004	151	0.0069	265
138	imagus-002	0.0000	247	0.0018	241	-	150	0.0000	132	0.0004	201	0.0296	300
139	imagus-003	0.0000	56	0.0000	42	-	259	0.0000	37	0.0000	71	0.0000	1
140	imperial-000	0.0000	125	0.0000	11	-	174	0.0000	84	0.0000	31	0.0000	60
141	imperial-002	0.0000	36	0.0000	81	0.0000	12	0.0000	21	0.0000	53	0.0000	30
142	incode-008	0.0000	227	0.0009	182	-	327	0.0002	216	0.0004	169	0.0007	204
143	incode-009	0.0000	234	0.0009	181	-	124	0.0002	217	0.0004	166	0.0007	205
144	innefulabs-000	0.0000	211	0.0024	256	-	172	0.0003	246	0.0005	263	0.0004	151
145	innovativetechnologyltd-001	0.0001	306	0.0050	296	-	294	0.0024	316	0.0025	322	0.0055	261
146	innovativetechnologyltd-002	0.0000	243	0.0046	292	-	70	0.0057	332	0.0005	266	0.0247	298
147	innovatrics-006	0.0000	196	0.0009	185	0.0350	27	0.0000	127	0.0004	147	0.0003	132
148	innovatrics-007	0.0000	204	0.0007	153	-	128	0.0001	149	0.0003	121	0.0003	120
149	insightface-000	0.0000	17	0.0000	71	-	191	0.0000	9	0.0000	37	0.0000	17
150	intellিলoudai-001	0.0000	69	0.0000	52	-	315	0.0000	48	0.0000	86	0.0001	87
151	intellিলoudai-002	0.0000	61	0.0008	164	-	338	0.0000	121	0.0004	146	0.0012	224
152	intellifusion-001	0.0000	212	0.0005	123	0.0949	36	0.0001	165	0.0003	138	0.0005	180
153	intellifusion-002	0.0000	62	0.0000	95	-	337	0.0000	90	0.0000	90	0.0001	88
154	intellivision-001	0.0042	328	0.0296	322	0.5495	55	0.0048	330	0.0042	331	0.1358	332
155	intellivision-002	0.0000	294	0.0046	291	-	160	0.0012	300	0.0005	279	0.0146	283
156	intelresearch-003	0.0000	187	0.0006	127	-	81	0.0000	111	0.0004	160	0.0003	135
157	intelresearch-004	0.0000	173	0.0006	128	-	343	0.0000	110	0.0004	163	0.0003	124
158	intsysmsu-001	0.0000	4	0.0010	192	-	211	0.0001	178	0.0004	192	0.0004	160
159	intsysmsu-002	0.0000	67	0.0010	191	-	326	0.0001	180	0.0004	197	0.0004	159
160	ionetworks-000	0.0000	78	0.0016	236	-	307	0.0004	254	0.0005	252	0.0004	165
161	iqface-000	0.0000	75	0.0000	55	0.0000	22	0.0000	51	0.0000	80	0.0000	10
162	iqface-003	0.0000	281	0.0076	308	-	62	0.0006	280	0.0005	278	0.0069	264
163	irex-000	0.0000	255	0.0009	184	-	177	0.0000	134	0.0005	245	0.0003	131
164	isap-001	0.0000	93	0.0000	28	-	61	0.0000	59	0.0000	5	0.0000	68
165	isap-002	0.0000	138	0.0000	20	-	145	0.0000	79	0.0000	22	0.0000	52
166	isityou-000	0.0068	332	0.0316	325	0.4714	51	0.0023	312	0.0010	297	0.0663	317
167	isystems-001	0.0000	287	0.0035	276	0.1421	39	0.0010	298	0.0007	289	0.0128	278
168	isystems-002	0.0000	286	0.0035	277	0.1421	38	0.0010	297	0.0007	288	0.0128	279
169	itmo-006	0.0000	140	0.0015	231	-	143	0.0004	266	0.0004	189	0.0006	193
170	itmo-007	0.0000	77	0.0009	176	-	309	0.0003	253	0.0000	83	0.0004	147
171	ivacognitive-001	0.0000	230	0.0011	203	-	303	0.0001	160	0.0004	233	0.0011	218
172	iws-000	0.0005	320	0.0650	334	-	106	0.0024	315	0.0012	305	0.0936	322
173	kakao-004	0.0000	33	0.0000	85	-	229	0.0000	23	0.0000	56	0.0000	34
174	kakao-005	0.0000	20	0.0000	91	-	253	0.0000	27	0.0000	94	0.0000	44

Table 24: FTE is the proportion of failed template generation attempts. Failures can occur because the software throws an exception, or because the software electively refuses to process the input image. This would typically occur if a face is not detected. FTE is measured as the number of function calls that give EITHER a non-zero error code OR that give a “small” template. This is defined as one whose size is less than 0.3 times the median template size for that algorithm. This second rule is needed because some algorithms incorrectly fail to return a non-zero error code when template generation fails.

<sup>1</sup>The effects of FTE are included in the accuracy results of this report by regarding any template comparison involving a failed template to produce a low similarity score. Thus higher FTE results in higher FNMR and lower FMR.

	Algorithm	Failure to Enrol Rate <sup>1</sup>											
		APPLICATION	BORDER	CHILD-EXPLOIT	MUGSHOT	VISA	WILD	SEC. 2.3	SEC. 2.4	SEC. 2.1	SEC. 2.5	SEC. 2.2	SEC. 2.6
175	kakaopay-001	0.0000	224	0.0013	224	-	276	0.0001	162	0.0004	235	0.0078	267
176	kedacom-000	0.0000	74	0.0000	53	0.0000	23	0.0000	49	0.0000	87	0.0000	13
177	kiwitech-000	0.0000	157	0.0009	174	-	232	0.0004	263	0.0005	248	0.0004	167
178	kneron-003	0.0239	339	0.0306	323	0.4883	53	0.0044	327	0.0016	316	0.1823	336
179	kneron-005	0.0000	289	0.0226	318	-	256	0.0006	278	0.0005	259	0.0097	274
180	kookmin-001	0.0000	132	0.0000	17	-	164	0.0000	89	0.0000	26	0.0000	55
181	kookmin-002	0.0000	96	0.0000	30	-	103	0.0000	68	0.0000	12	0.0000	74
182	lemalabs-001	0.0000	44	0.0005	124	-	280	0.0002	221	0.0004	153	0.0004	141
183	line-000	0.0000	55	0.0000	41	-	261	0.0000	36	0.0000	67	0.0000	80
184	lookman-002	0.0000	54	0.0000	40	-	263	0.0000	35	0.0000	68	0.0000	4
185	lookman-004	0.0000	86	0.0000	25	0.0000	1	0.0000	56	0.0000	2	0.0000	67
186	luxand-000	0.0000	84	0.0000	23	-	69	0.0000	62	0.0000	6	0.0000	70
187	megvii-002	0.0000	117	0.0006	129	0.0274	26	0.0054	331	0.0004	155	0.0126	277
188	megvii-003	0.0000	205	0.0010	197	-	132	0.0002	231	0.0004	220	0.0011	223
189	meituan-000	0.0000	42	0.0001	99	-	295	0.0000	102	0.0002	101	0.0001	90
190	meiya-001	0.0000	284	0.0028	264	-	333	0.0004	267	0.0010	298	0.0025	246
191	microfocus-001	0.0001	305	0.0053	299	0.0791	33	0.0008	292	0.0016	314	0.0220	292
192	microfocus-002	0.0001	303	0.0053	300	0.0791	34	0.0008	291	0.0016	315	0.0220	291
193	minivision-000	0.0000	1	0.0000	58	-	221	0.0000	12	0.0000	50	0.0000	27
194	mobai-000	0.0000	256	0.0114	314	-	192	0.0003	248	0.0012	307	0.1242	330
195	mobai-001	0.0000	225	0.0040	282	-	265	0.0001	186	0.0012	306	0.0523	312
196	mobbl-000	0.0116	336	0.0720	335	-	135	0.0119	335	0.0063	334	0.1136	328
197	mobbl-001	0.0000	282	0.0052	298	-	186	0.0002	209	0.0005	270	0.0181	289
198	moreedian-000	0.0000	149	0.0009	173	-	250	0.0004	264	0.0005	249	0.0004	168
199	mvision-001	0.0000	131	0.0000	16	-	166	0.0000	88	0.0000	25	0.0000	56
200	nazhiai-000	0.0000	94	0.0000	29	-	109	0.0000	67	0.0000	13	0.0000	75
201	neosystems-001	0.0000	97	0.0000	90	-	105	0.0013	304	0.9994	344	0.0002	104
202	neosystems-002	0.0000	5	0.0000	60	-	215	0.0000	15	0.0000	47	0.0000	26
203	netbridgetech-001	0.0000	112	0.0000	3	-	134	0.0000	73	0.0000	19	0.0000	49
204	netbridgetech-002	0.0000	121	0.0000	7	-	118	0.0000	70	0.0000	15	0.0000	47
205	neurotechnology-011	0.0000	226	0.0013	219	-	319	0.0002	210	0.0003	139	0.0020	242
206	neurotechnology-012	0.0000	275	0.0010	199	-	127	0.0001	196	0.0004	188	0.0005	179
207	nhn-001	0.0000	194	0.0019	244	-	111	0.0001	170	0.0004	237	0.0020	243
208	nhn-002	0.0000	83	0.0004	119	-	79	0.0000	119	0.0003	115	0.0003	109
209	nodeflux-002	0.0000	201	0.0261	319	-	96	0.0008	290	0.0005	267	0.0008	212
210	notiontag-000	0.0000	30	0.0000	79	0.0000	15	0.0000	18	0.0000	60	0.0000	38
211	notiontag-001	0.0000	79	0.0000	56	-	305	0.0027	321	0.0000	81	0.0132	282
212	nsensecorp-001	0.0000	292	0.0024	255	-	210	0.0014	306	0.0101	337	0.0375	306
213	nsensecorp-002	0.0000	179	0.0009	175	-	314	0.0003	237	0.0011	299	0.0178	288
214	ntechlab-009	0.0000	251	0.0009	180	-	341	0.0001	199	0.0004	144	0.0005	172
215	ntechlab-010	0.0000	161	0.0005	122	-	277	0.0001	182	0.0004	152	0.0006	185
216	null-000	-	346	-	341	-	108	-	345	-	345	-	345
217	null-082	-	343	-	345	-	207	-	342	-	346	-	343
218	omnigarde-000	0.0000	152	0.0008	159	-	240	0.0000	112	0.0004	193	0.0003	134
219	omnigarde-001	0.0000	195	0.0008	158	-	110	0.0000	114	0.0004	187	0.0003	136
220	openface-001	0.0000	266	0.0104	313	-	235	0.0004	259	0.0006	284	0.0856	320
221	oz-002	0.0000	41	0.0003	106	-	296	0.0000	107	0.0003	127	0.0002	101
222	oz-003	0.0000	104	0.0002	101	-	85	0.0000	96	0.0003	106	0.0002	96
223	papsav1923-001	0.0000	210	0.0007	148	-	120	0.0001	177	0.0002	103	0.0005	175
224	paravision-004	0.0000	254	0.0007	156	0.0570	29	0.0002	222	0.0004	179	0.0008	208
225	paravision-008	0.0000	46	0.0010	190	-	286	0.0001	171	0.0004	145	0.0003	133
226	pensees-001	0.0000	217	0.0000	19	-	163	0.0000	78	0.0000	24	0.0000	54
227	pixelall-005	0.0000	9	0.0000	63	-	196	0.0000	1	0.0000	40	0.0000	18
228	pixelall-006	0.0000	7	0.0000	61	-	214	0.0000	16	0.0000	49	0.0000	24
229	psl-007	0.0000	190	0.0007	138	-	72	0.0000	135	0.0003	129	0.0003	123
230	psl-008	0.0000	178	0.0003	107	-	329	0.0000	101	0.0003	128	0.0002	103
231	ptakuratsatu-000	0.0000	219	0.0007	154	-	149	0.0001	150	0.0003	122	0.0003	121
232	pxl-001	0.0000	295	0.0044	288	-	301	0.0005	272	0.0022	320	0.0323	302

Table 25: FTE is the proportion of failed template generation attempts. Failures can occur because the software throws an exception, or because the software electively refuses to process the input image. This would typically occur if a face is not detected. FTE is measured as the number of function calls that give EITHER a non-zero error code OR that give a “small” template. This is defined as one whose size is less than 0.3 times the median template size for that algorithm. This second rule is needed because some algorithms incorrectly fail to return a non-zero error code when template generation fails.

<sup>1</sup> The effects of FTE are included in the accuracy results of this report by regarding any template comparison involving a failed template to produce a low similarity score. Thus higher FTE results in higher FNMR and lower FMR.

	Algorithm	Failure to Enrol Rate <sup>1</sup>											
		Name	APPLICATION	BORDER	CHILD-EXPLOIT	MUGSHOT	VISA	WILD	SEC. 2.3	SEC. 2.4	SEC. 2.1	SEC. 2.5	SEC. 2.2
233	pyramid-000	0.0001	301	0.0041	285	-	228	0.0005	271	0.0007	290	0.0015	232
234	qnap-000	0.0000	45	0.0007	155	-	288	0.0002	215	0.0002	98	0.0003	107
235	quantasoft-003	0.0000	258	0.0015	233	-	245	0.0005	270	0.0006	282	0.0088	272
236	rankone-010	0.0000	28	0.0000	77	-	248	0.0000	30	0.0000	63	0.0000	42
237	rankone-011	0.0000	10	0.0000	67	-	205	0.0000	6	0.0000	44	0.0000	23
238	realnetworks-002	0.0000	246	0.0003	111	-	168	0.0004	255	0.0003	117	0.0004	161
239	realnetworks-004	0.0000	186	0.0003	105	-	82	0.0000	91	0.0002	105	0.0003	116
240	regula-000	0.0000	130	0.0000	13	-	181	0.0000	86	0.0000	33	0.0000	64
241	remarkai-001	0.0000	53	0.0000	45	-	264	0.0000	40	0.0000	72	0.0000	81
242	remarkai-003	0.0000	189	0.0007	145	-	74	0.0000	133	0.0004	154	0.0004	154
243	rendip-000	0.0000	245	0.0016	235	-	122	0.0002	218	0.0004	242	0.0013	229
244	rokid-000	0.0000	105	0.0072	306	-	91	0.0001	174	0.0005	258	0.0354	305
245	rokid-001	0.0000	19	0.0013	222	-	189	0.0000	11	0.0000	38	0.0007	202
246	s1-002	0.0000	232	0.0089	310	-	67	0.0001	191	0.0005	262	0.0571	315
247	s1-003	0.0000	139	0.0002	103	-	146	0.0007	285	0.0003	113	0.0415	308
248	saffe-001	0.0000	23	0.0000	74	0.0000	19	0.0000	28	0.0000	66	0.0000	45
249	saffe-002	0.0000	57	0.0000	44	-	258	0.0000	38	0.0000	69	0.0000	3
250	samtech-001	0.0001	300	0.0032	269	-	193	0.0004	262	0.0008	291	0.0013	227
251	scanovate-001	0.0208	338	0.2388	338	-	241	0.0024	313	0.0014	312	0.2751	337
252	scanovate-002	0.0000	221	0.0018	242	-	225	0.0000	144	0.0004	239	0.0008	210
253	securifai-001	0.0000	128	0.0000	14	-	183	0.0000	94	0.0000	34	0.0017	237
254	securifai-003	0.0000	88	0.0000	24	-	59	0.0000	55	0.0000	1	0.0005	178
255	sensetime-004	0.0000	202	0.0011	206	-	90	0.0000	93	0.0004	177	0.0003	129
256	sensetime-005	0.0000	6	0.0004	113	-	213	0.0000	117	0.0003	123	0.0002	102
257	sertis-000	0.0000	85	0.0007	150	-	71	0.0000	147	0.0004	164	0.0004	149
258	sertis-002	0.0000	98	0.0007	142	-	94	0.0000	140	0.0004	165	0.0004	146
259	seventhsense-000	0.0000	218	0.0006	136	-	144	0.0001	155	0.0004	190	0.0003	128
260	shaman-000	0.0000	24	0.0000	75	0.0000	16	0.0000	29	0.0000	61	0.0000	40
261	shaman-001	0.0000	110	0.0000	1	0.0000	7	0.0000	71	0.0000	17	0.0000	76
262	shu-002	0.0000	233	0.0010	194	-	125	0.0005	269	0.0004	228	0.0007	201
263	shu-003	0.0000	134	0.0007	141	-	155	0.0001	157	0.0003	119	0.0004	170
264	siat-002	0.0000	145	0.0012	216	0.0616	30	0.0000	129	0.0004	180	0.0048	257
265	siat-004	0.0000	144	0.0011	205	-	208	0.0000	116	0.0004	175	0.0003	125
266	sjtu-003	0.0000	113	0.0005	125	-	142	0.0000	138	0.0003	116	0.0003	127
267	sjtu-004	0.0000	82	0.0000	22	-	76	0.0000	61	0.0003	114	0.0000	71
268	sktelecom-000	0.0000	209	0.0008	166	-	114	0.0000	136	0.0004	199	0.0013	228
269	smartengines-000	0.0066	331	0.0150	316	-	278	0.0022	311	0.0013	310	0.0826	318
270	smilart-002	0.0000	290	0.0036	278	0.2422	46	-	343	0.0011	302	-	341
271	smilart-003	0.0003	315	0.0100	312	-	80	0.0014	305	0.0013	311	0.0555	313
272	sodec-000	0.0000	37	0.0000	88	-	236	0.0000	25	0.0000	59	0.0000	37
273	sqisoft-001	0.0000	66	0.0003	110	-	340	0.0000	103	0.0003	140	0.0003	112
274	stauq-000	0.0000	109	0.0000	5	-	136	0.0000	75	0.0000	21	0.0000	50
275	starhybrid-001	0.0001	304	0.0033	273	0.2340	45	0.0009	295	0.0023	321	0.0044	253
276	suprema-000	0.0000	235	0.0017	238	-	117	0.0002	225	0.0004	207	0.0020	241
277	supremaid-001	0.0000	206	0.0020	249	-	130	0.0001	181	0.0004	238	0.0045	255
278	synesis-006	0.0000	119	0.0003	112	-	116	0.0000	137	0.0003	107	0.0002	99
279	synesis-007	0.0000	176	0.0013	221	-	323	0.0002	229	0.0004	182	0.0005	173
280	synology-000	0.0000	127	0.0000	8	-	173	0.0000	80	0.0000	27	0.0000	58
281	synology-002	0.0000	136	0.0000	18	-	161	0.0000	77	0.0000	23	0.0000	53
282	sztu-000	0.0000	2	0.0000	59	-	224	0.0000	13	0.0000	51	0.0000	28
283	sztu-001	0.0000	63	0.0000	48	-	335	0.0000	53	0.0000	89	0.0000	14
284	tech5-004	0.0000	200	0.0008	160	-	97	0.0003	239	0.0004	234	0.0006	187
285	tech5-005	0.0000	164	0.0007	157	-	270	0.0000	113	0.0004	213	0.0049	258
286	techsign-000	0.0007	321	0.0334	326	-	88	0.0020	310	0.0011	301	0.0170	286
287	tevian-006	0.0000	48	0.0012	213	-	285	0.0003	244	0.0005	264	0.0007	200
288	tevian-007	0.0000	213	0.0015	234	-	180	0.0002	224	0.0004	202	0.0008	207
289	tiger-003	0.0000	170	-	343	0.0619	31	0.0001	188	0.0004	173	0.0082	269
290	tiger-005	0.0000	150	0.0009	183	-	246	0.0001	168	0.0004	171	0.0004	166

Table 26: FTE is the proportion of failed template generation attempts. Failures can occur because the software throws an exception, or because the software electively refuses to process the input image. This would typically occur if a face is not detected. FTE is measured as the number of function calls that give EITHER a non-zero error code OR that give a “small” template. This is defined as one whose size is less than 0.3 times the median template size for that algorithm. This second rule is needed because some algorithms incorrectly fail to return a non-zero error code when template generation fails.

<sup>1</sup> The effects of FTE are included in the accuracy results of this report by regarding any template comparison involving a failed template to produce a low similarity score. Thus higher FTE results in higher FNMR and lower FMR.

Name	Algorithm	Failure to Enrol Rate <sup>1</sup>									
		APPLICATION		BORDER		CHILD-EXPLOIT		MUGSHOT		VISA	
		SEC. 2.3	SEC. 2.4	SEC. 2.1	SEC. 2.5	SEC. 2.2	SEC. 2.6				
291	tinkoff-001	0.0000	231	0.0008	165	-	73	0.0001	195	0.0004	170
292	tongyi-005	0.0000	22	0.0000	73	0.0000	18	0.0000	26	0.0000	65
293	toshiba-002	0.0000	16	0.0000	70	0.0000	10	0.0000	8	0.0000	36
294	toshiba-003	0.0000	65	0.0001	98	-	344	0.0001	189	0.0001	96
295	trueface-001	0.0000	228	0.0038	281	-	328	0.0007	287	0.0005	265
296	trueface-002	0.0000	223	0.0046	294	-	255	0.0003	236	0.0005	272
297	tuputech-000	0.0003	316	0.0116	315	-	119	-	346	0.0081	336
298	twface-000	0.0000	8	0.0000	62	-	212	0.0000	17	0.0000	48
299	ulsee-001	0.0000	25	0.0000	78	-	249	0.0000	32	0.0000	64
300	ultinous-000	-	344	-	346	0.0007	24	-	340	0.0003	125
301	ultinous-001	-	342	-	344	0.0007	25	-	341	0.0003	126
302	uluface-002	0.0000	11	0.0000	68	0.0000	11	0.0000	5	0.0000	45
303	uluface-003	0.0000	118	0.0001	100	-	126	0.0002	208	0.0002	100
304	upc-001	0.0000	271	0.0003	109	0.0450	28	0.0003	238	0.0003	137
305	vcog-002	-	345	-	340	0.2209	44	-	344	0.0019	318
306	vd-001	0.0000	288	0.0030	266	-	151	0.0004	261	0.0009	292
307	vd-002	0.0000	31	0.0000	84	-	231	0.0000	22	0.0000	57
308	veridas-004	0.0000	268	0.0026	259	-	320	0.0001	190	0.0005	256
309	veridas-006	0.0000	265	0.0026	258	-	216	0.0001	187	0.0005	255
310	verihubs-inteligensia-000	0.0000	181	0.0029	265	-	299	0.0001	159	0.0004	214
311	via-000	0.0000	102	0.0000	32	0.0000	5	0.0000	64	0.0000	11
312	via-001	0.0000	60	0.0000	46	-	267	0.0000	41	0.0000	73
313	videmo-000	0.0000	236	0.0019	245	-	175	0.0003	247	0.0012	308
314	videonetics-001	0.0004	317	0.0309	324	0.4799	52	0.0015	308	0.0010	296
315	videonetics-002	0.0000	239	0.0459	332	0.4598	50	0.0006	281	0.0005	277
316	vigilantsolutions-010	0.0000	261	0.0028	262	-	154	0.0001	164	0.0004	149
317	vigilantsolutions-011	0.0000	257	0.0028	263	-	251	0.0001	161	0.0004	150
318	vinai-000	0.0000	124	0.0000	12	-	176	0.0000	85	0.0000	32
319	vion-000	0.0050	329	0.0392	331	0.6388	56	0.0130	336	0.0078	335
320	visage-000	0.0000	273	0.0054	301	-	187	0.0009	293	0.0006	281
321	visionbox-001	0.0000	291	0.0033	272	-	220	0.0005	277	0.0011	303
322	visionbox-002	0.0000	68	0.0017	237	-	316	0.0000	126	0.0004	243
323	visionlabs-009	0.0000	216	0.0010	188	-	157	0.0001	154	0.0004	191
324	visionlabs-010	0.0000	250	0.0009	178	-	268	0.0001	200	0.0004	194
325	visteam-001	0.0000	249	0.0014	227	-	293	0.0002	214	0.0004	205
326	visteam-002	0.0000	248	0.0014	228	-	242	0.0002	211	0.0004	204
327	vnpt-001	0.0652	341	0.2829	339	-	226	0.2116	339	0.1598	343
328	vnpt-002	0.0000	203	0.0002	102	-	141	0.0003	250	0.0003	108
329	vocord-008	0.0000	163	0.0015	232	-	271	0.0003	251	0.0001	95
330	vocord-009	0.0000	169	0.0006	131	-	339	0.0001	204	0.0003	110
331	vts-000	0.0000	242	0.0011	202	-	282	0.0001	205	0.0004	241
332	winsense-001	0.0000	50	0.0000	38	0.0000	20	0.0000	33	0.0000	75
333	winsense-002	0.0000	108	0.0000	4	-	138	0.0000	74	0.0000	20
334	wuhantianyu-001	0.0000	90	0.0007	143	-	65	0.0001	152	0.0004	185
335	x-laboratory-000	0.0247	340	0.0000	83	0.0000	14	0.0005	276	0.0002	102
336	x-laboratory-001	0.0000	171	0.0012	214	-	334	0.0001	192	0.0004	229
337	xforwardai-001	0.0000	155	0.0007	151	-	244	0.0003	240	0.0004	225
338	xforwardai-002	0.0000	156	0.0007	152	-	234	0.0003	241	0.0004	223
339	xm-000	0.0000	135	0.0007	140	-	156	0.0001	156	0.0003	118
340	yisheng-004	0.0002	311	-	342	0.4279	49	0.0013	302	0.0006	283
341	yitu-003	0.0000	32	0.0000	86	-	230	0.0009	294	0.0000	55
342	yoonik-000	0.0000	185	0.0019	246	-	83	0.0001	173	0.0004	227
343	yoonik-001	0.0000	101	0.0014	229	-	99	0.0001	203	0.0004	219
344	ytu-000	0.0000	158	0.0010	198	-	292	0.0002	230	0.0004	226
345	yuan-001	0.0000	270	0.0010	195	-	147	0.0005	274	0.0005	260
346	yuan-002	0.0000	269	0.0010	196	-	330	0.0005	273	0.0005	261
											0.0005
											181

Table 27: FTE is the proportion of failed template generation attempts. Failures can occur because the software throws an exception, or because the software electively refuses to process the input image. This would typically occur if a face is not detected. FTE is measured as the number of function calls that give EITHER a non-zero error code OR that give a “small” template. This is defined as one whose size is less than 0.3 times the median template size for that algorithm. This second rule is needed because some algorithms incorrectly fail to return a non-zero error code when template generation fails.

<sup>1</sup> The effects of FTE are included in the accuracy results of this report by regarding any template comparison involving a failed template to produce a low similarity score. Thus higher FTE results in higher FNMR and lower FMR.

### 3.4 Recognition accuracy

Core algorithm accuracy is stated via:

▷ **Cooperative subjects**

- The summary table of Figure 21;
- The visa image DETs of Figure 53;
- The mugshot DETs of Figure 70;
- The mugshot ageing profiles of Figure 258;
- The human-difficult pairs of Figure 18

▷ **Non-cooperative subjects**

- The photojournalism DET of Figure 85
- The child-exploitation DET of Figure 88;
- The child-exploitation CMC of Figure 92.

Figure 208 shows dependence of false match rate on algorithm score threshold. This allows a deployer to set a threshold to target a particular false match rate appropriate to the security objectives of the application.

Figure 173 likewise shows FMR(T) but for mugshots, and specially four subsets of the population.

Note that in both the mugshot and visa sets false match rates vary with the ethnicity, age, and sex, of the enrollee and impostor. For example figure 110 summarizes FMR for impostors paired from four groups black females, black males, white females, white males.



Figure 4: The Figure shows, in blue, algorithms that correctly separate the 12 genuine and 8 impostor pairs used in the May 2018 paper Face recognition accuracy of forensic examiners, superrecognizers, and face recognition algorithms (Phillips et al. [1]). In red are algorithms that are imperfect. Some algorithms fail only because they failed to make a template e.g. due to face detection failure (shown as a triangle). Others fail because the pairs were selected for that study because they had been difficult for three leading algorithms used in FRVT 2006. Caution: Given the small sample size ( $n=20$ ) the figure may change substantially if larger or different sets were used. The images can be downloaded from the [Supplemental Information](#) page provided with that publication.

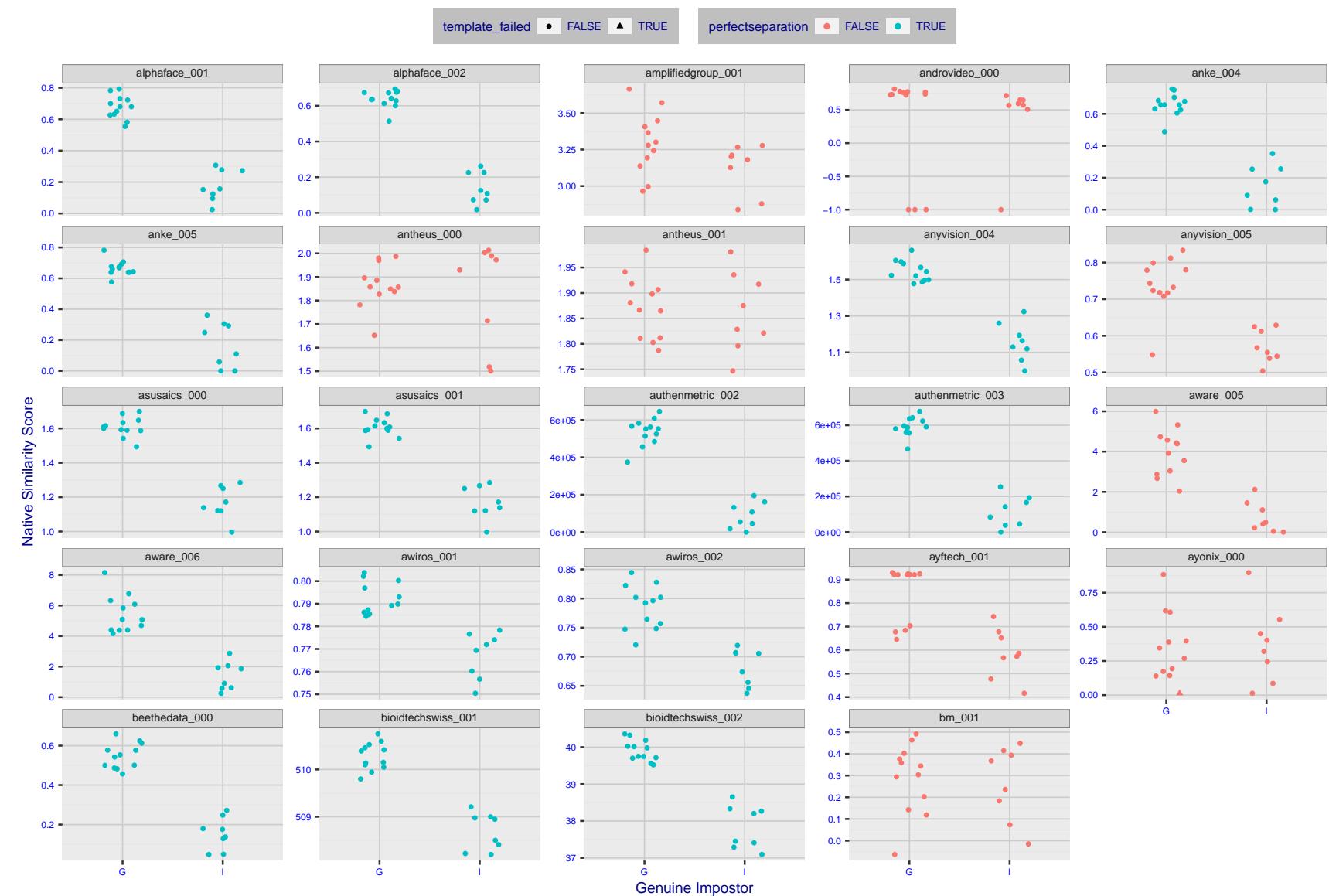


Figure 5: The Figure shows, in blue, algorithms that correctly separate the 12 genuine and 8 impostor pairs used in the May 2018 paper Face recognition accuracy of forensic examiners, superrecognizers, and face recognition algorithms (Phillips et al. [1]). In red are algorithms that are imperfect. Some algorithms fail only because they failed to make a template e.g. due to face detection failure (shown as a triangle). Others fail because the pairs were selected for that study because they had been difficult for three leading algorithms used in FRVT 2006. Caution: Given the small sample size ( $n=20$ ) the figure may change substantially if larger or different sets were used. The images can be downloaded from the [Supplemental Information](#) page provided with that publication.

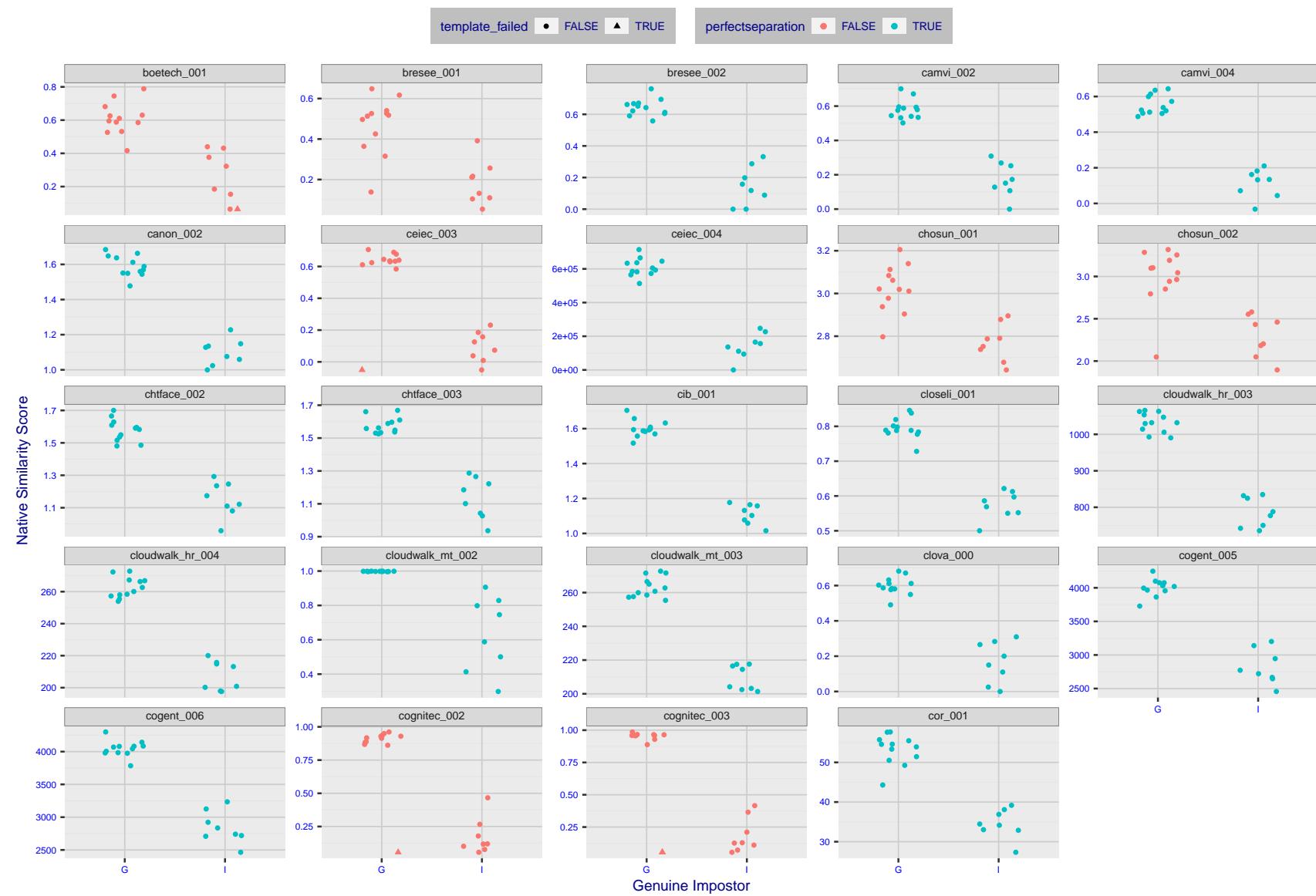


Figure 6: The Figure shows, in blue, algorithms that correctly separate the 12 genuine and 8 impostor pairs used in the May 2018 paper [Face recognition accuracy of forensic examiners, superrecognizers, and face recognition algorithms](#) (Phillips et al. [1]). In red are algorithms that imperfect. Some algorithms fail only because they failed to make a template e.g. due to face detection failure (shown as a triangle). Others fail because the pairs were selected for that study because they had been difficult for three leading algorithms used in FRVT 2006. Caution: Given the small sample size ( $n=20$ ) the figure may change substantially if larger or different sets were used. The images can be downloaded from the [Supplemental Information](#) page provided with that publication.

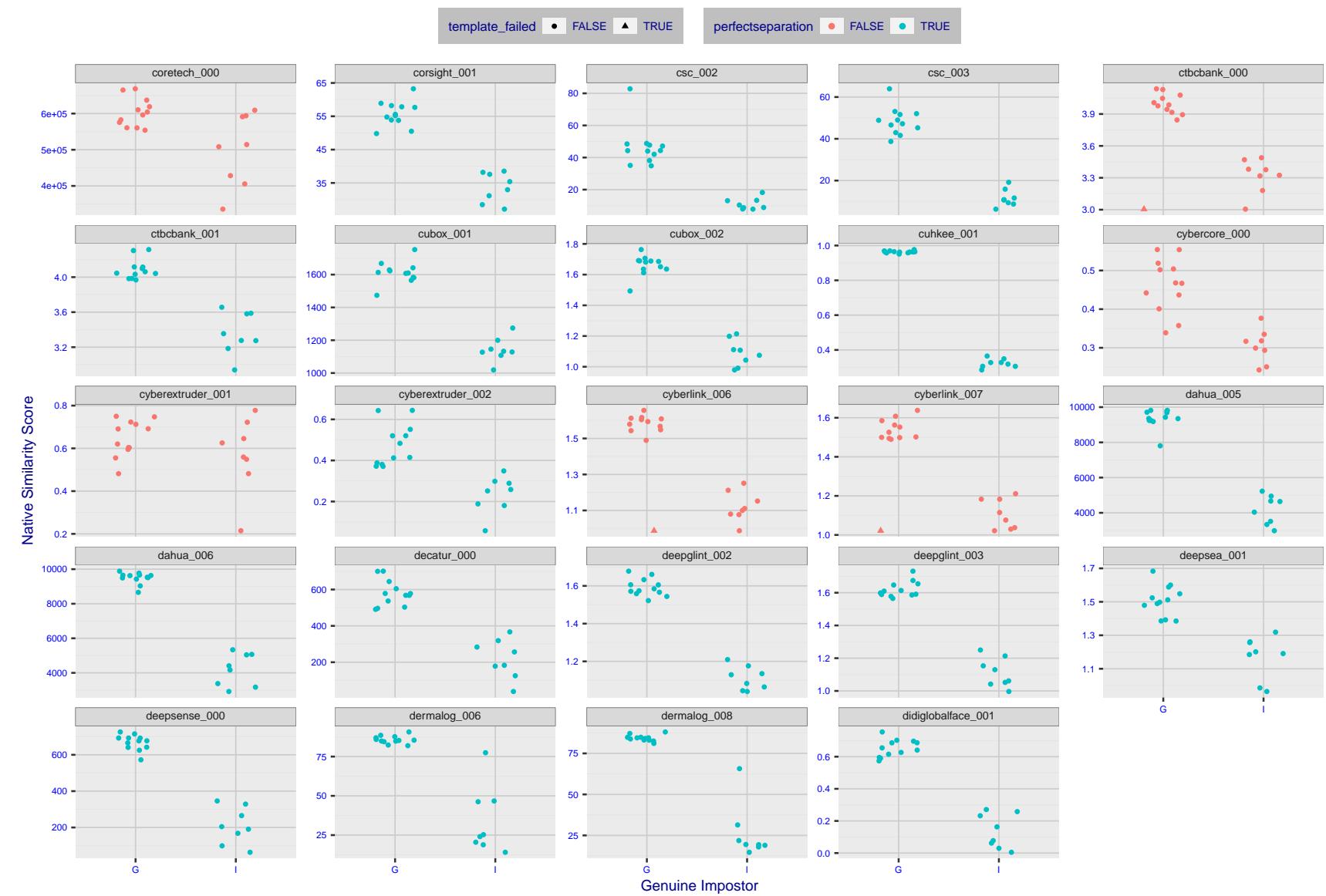


Figure 7: The Figure shows, in blue, algorithms that correctly separate the 12 genuine and 8 impostor pairs used in the May 2018 paper [Face recognition accuracy of forensic examiners, superrecognizers, and face recognition algorithms](#) (Phillips et al. [1]). In red are algorithms that are imperfect. Some algorithms fail only because they failed to make a template e.g. due to face detection failure (shown as a triangle). Others fail because the pairs were selected for that study because they had been difficult for three leading algorithms used in FRVT 2006. Caution: Given the small sample size ( $n=20$ ) the figure may change substantially if larger or different sets were used. The images can be downloaded from the [Supplemental Information](#) page provided with that publication.

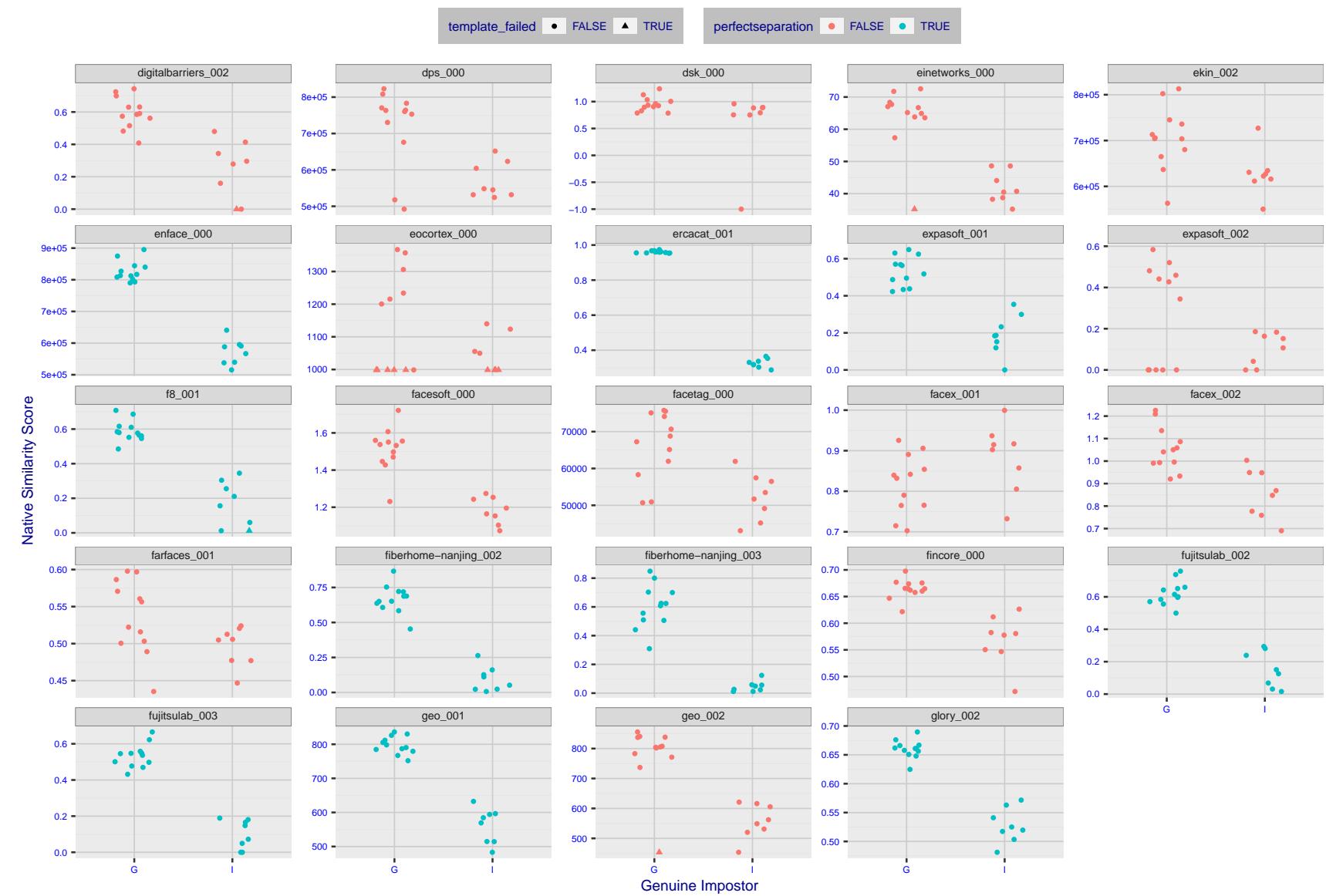


Figure 8: The Figure shows, in blue, algorithms that correctly separate the 12 genuine and 8 impostor pairs used in the May 2018 paper [Face recognition accuracy of forensic examiners, superrecognizers, and face recognition algorithms](#) (Phillips et al. [1]). In red are algorithms that are imperfect. Some algorithms fail only because they failed to make a template e.g. due to face detection failure (shown as a triangle). Others fail because the pairs were selected for that study because they had been difficult for three leading algorithms used in FRVT 2006. Caution: Given the small sample size ( $n=20$ ) the figure may change substantially if larger or different sets were used. The images can be downloaded from the [Supplemental Information](#) page provided with that publication.

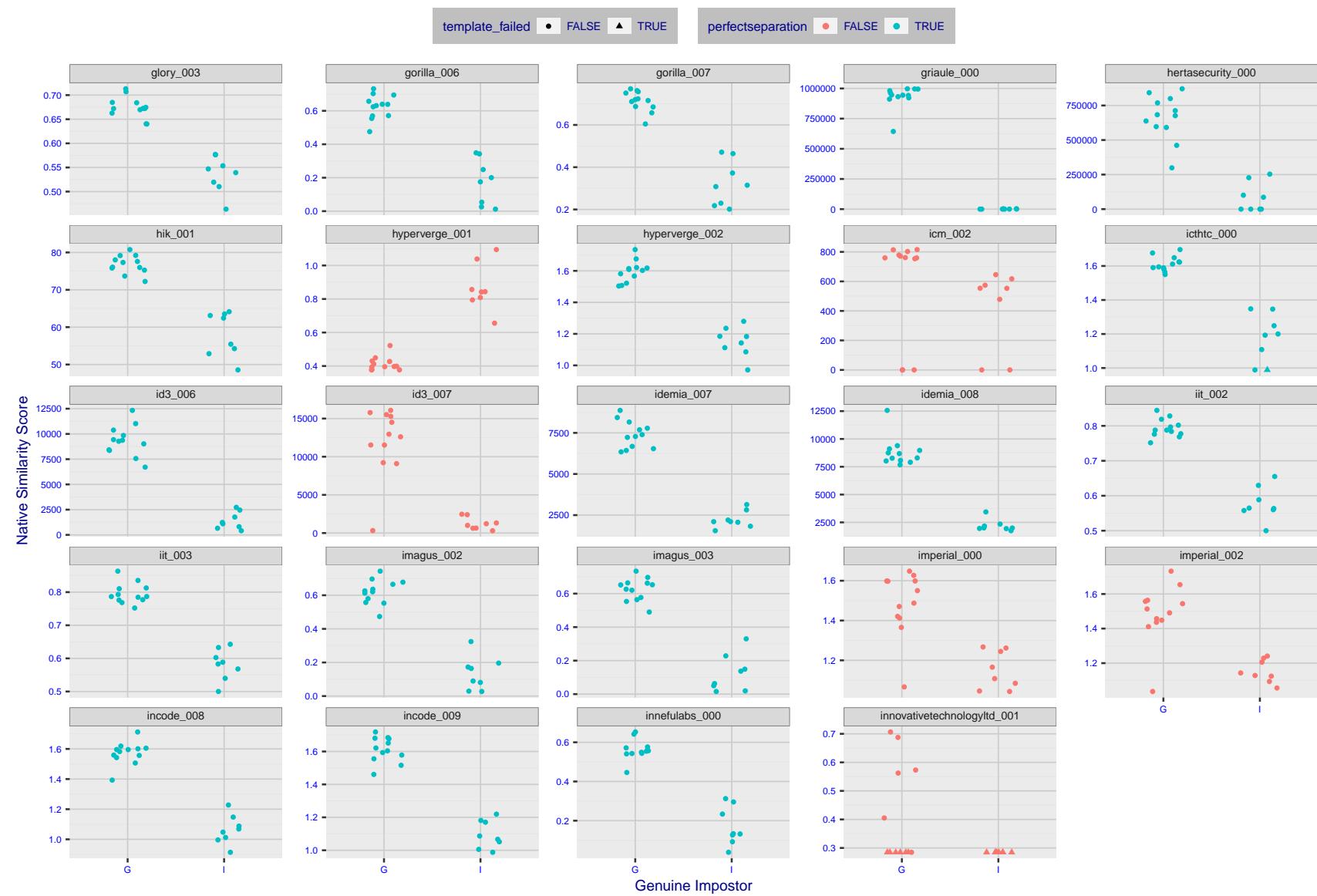


Figure 9: The Figure shows, in blue, algorithms that correctly separate the 12 genuine and 8 impostor pairs used in the May 2018 paper [Face recognition accuracy of forensic examiners, superrecognizers, and face recognition algorithms](#) (Phillips et al. [1]). In red are algorithms that imperfect. Some algorithms fail only because they failed to make a template e.g. due to face detection failure (shown as a triangle). Others fail because the pairs were selected for that study because they had been difficult for three leading algorithms used in FRVT 2006. Caution: Given the small sample size ( $n=20$ ) the figure may change substantially if larger or different sets were used. The images can be downloaded from the [Supplemental Information](#) page provided with that publication.

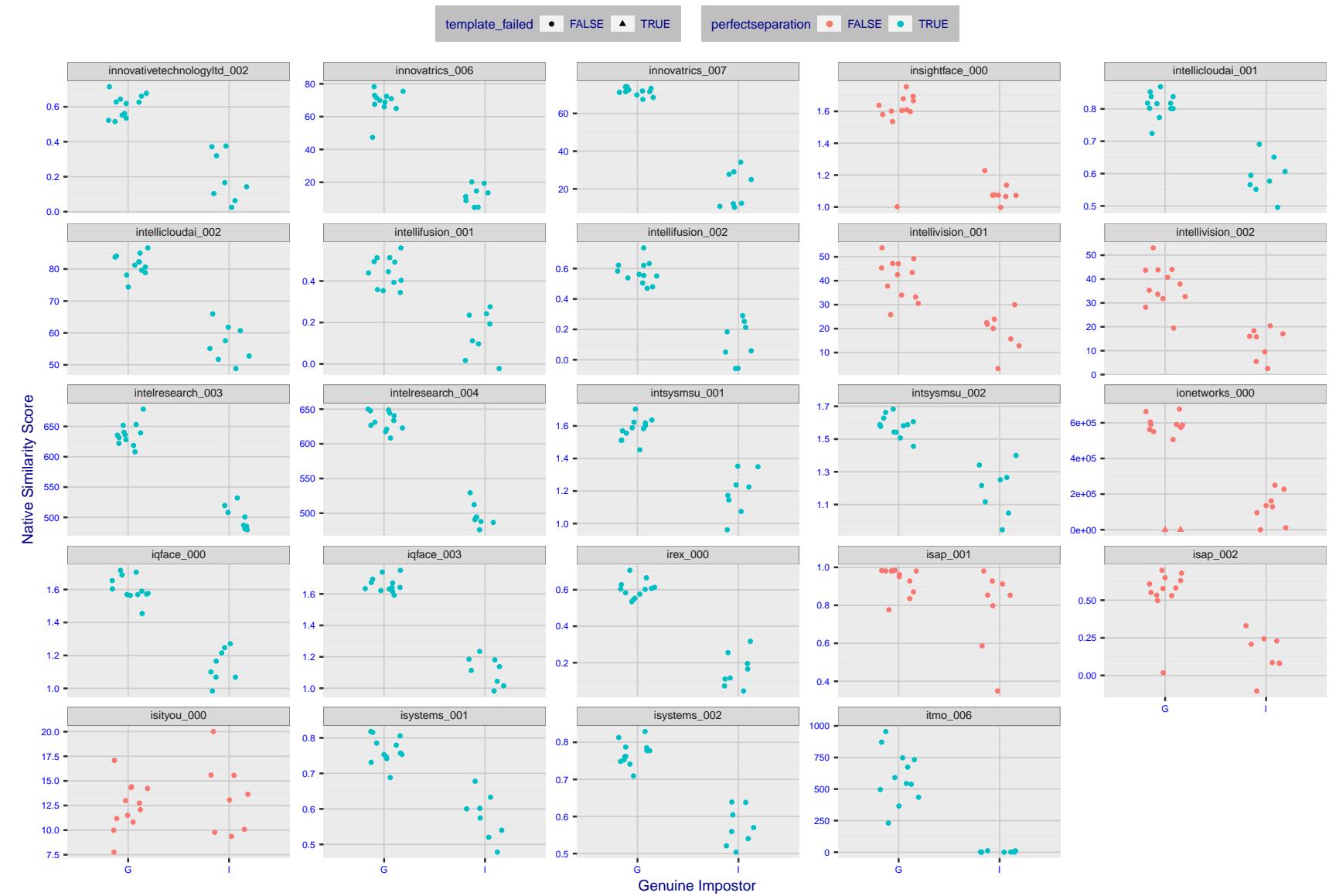


Figure 10: The Figure shows, in blue, algorithms that correctly separate the 12 genuine and 8 impostor pairs used in the May 2018 paper [Face recognition accuracy of forensic examiners, superrecognizers, and face recognition algorithms](#) (Phillips et al. [1]). In red are algorithms that are imperfect. Some algorithms fail only because they failed to make a template e.g. due to face detection failure (shown as a triangle). Others fail because the pairs were selected for that study because they had been difficult for three leading algorithms used in FRVT 2006. Caution: Given the small sample size ( $n=20$ ) the figure may change substantially if larger or different sets were used. The images can be downloaded from the [Supplemental Information](#) page provided with that publication.

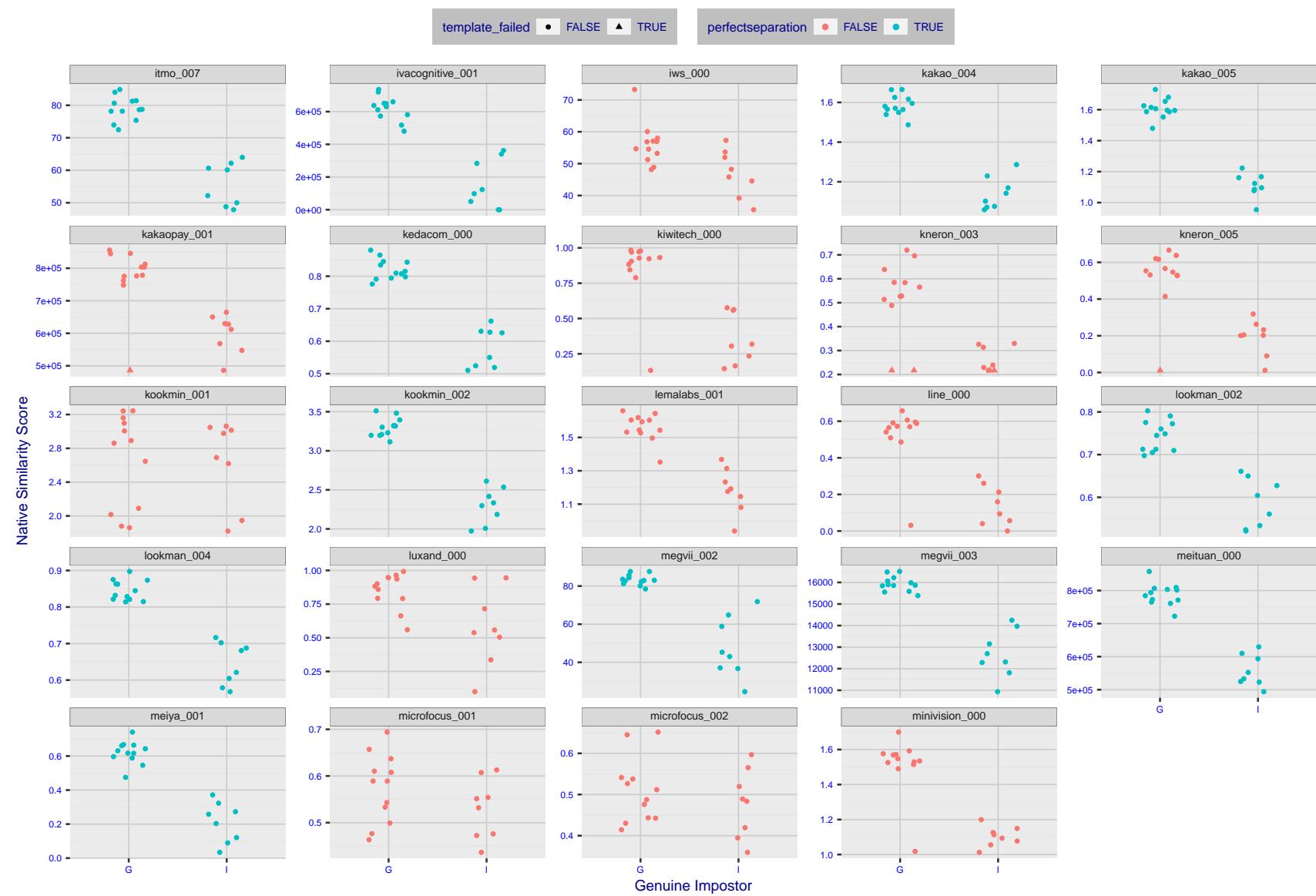


Figure 11: The Figure shows, in blue, algorithms that correctly separate the 12 genuine and 8 impostor pairs used in the May 2018 paper Face recognition accuracy of forensic examiners, superrecognizers, and face recognition algorithms (Phillips et al. [1]). In red are algorithms that are imperfect. Some algorithms fail only because they failed to make a template e.g. due to face detection failure (shown as a triangle). Others fail because the pairs were selected for that study because they had been difficult for three leading algorithms used in FRVT 2006. Caution: Given the small sample size ( $n=20$ ) the figure may change substantially if larger or different sets were used. The images can be downloaded from the [Supplemental Information](#) page provided with that publication.



Figure 12: The Figure shows, in blue, algorithms that correctly separate the 12 genuine and 8 impostor pairs used in the May 2018 paper Face recognition accuracy of forensic examiners, superrecognizers, and face recognition algorithms (Phillips et al. [1]). In red are algorithms that are imperfect. Some algorithms fail only because they failed to make a template e.g. due to face detection failure (shown as a triangle). Others fail because the pairs were selected for that study because they had been difficult for three leading algorithms used in FRVT 2006. Caution: Given the small sample size ( $n=20$ ) the figure may change substantially if larger or different sets were used. The images can be downloaded from the [Supplemental Information](#) page provided with that publication.

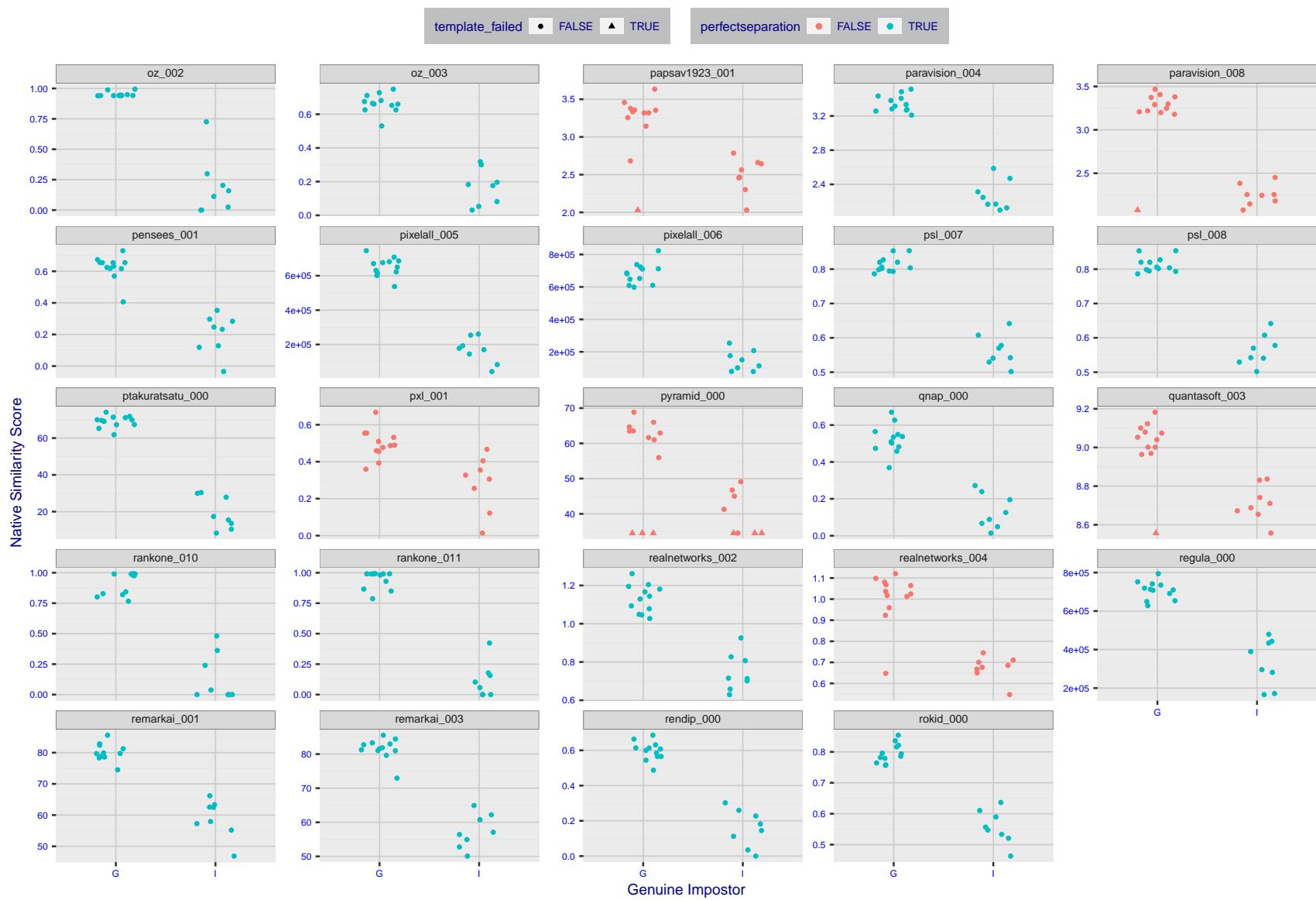


Figure 13: The Figure shows, in blue, algorithms that correctly separate the 12 genuine and 8 impostor pairs used in the May 2018 paper [Face recognition accuracy of forensic examiners, superrecognizers, and face recognition algorithms](#) (Phillips et al. [1]). In red are algorithms that are imperfect. Some algorithms fail only because they failed to make a template e.g. due to face detection failure (shown as a triangle). Others fail because the pairs were selected for that study because they had been difficult for three leading algorithms used in FRVT 2006. Caution: Given the small sample size ( $n=20$ ) the figure may change substantially if larger or different sets were used. The images can be downloaded from the [Supplemental Information](#) page provided with that publication.

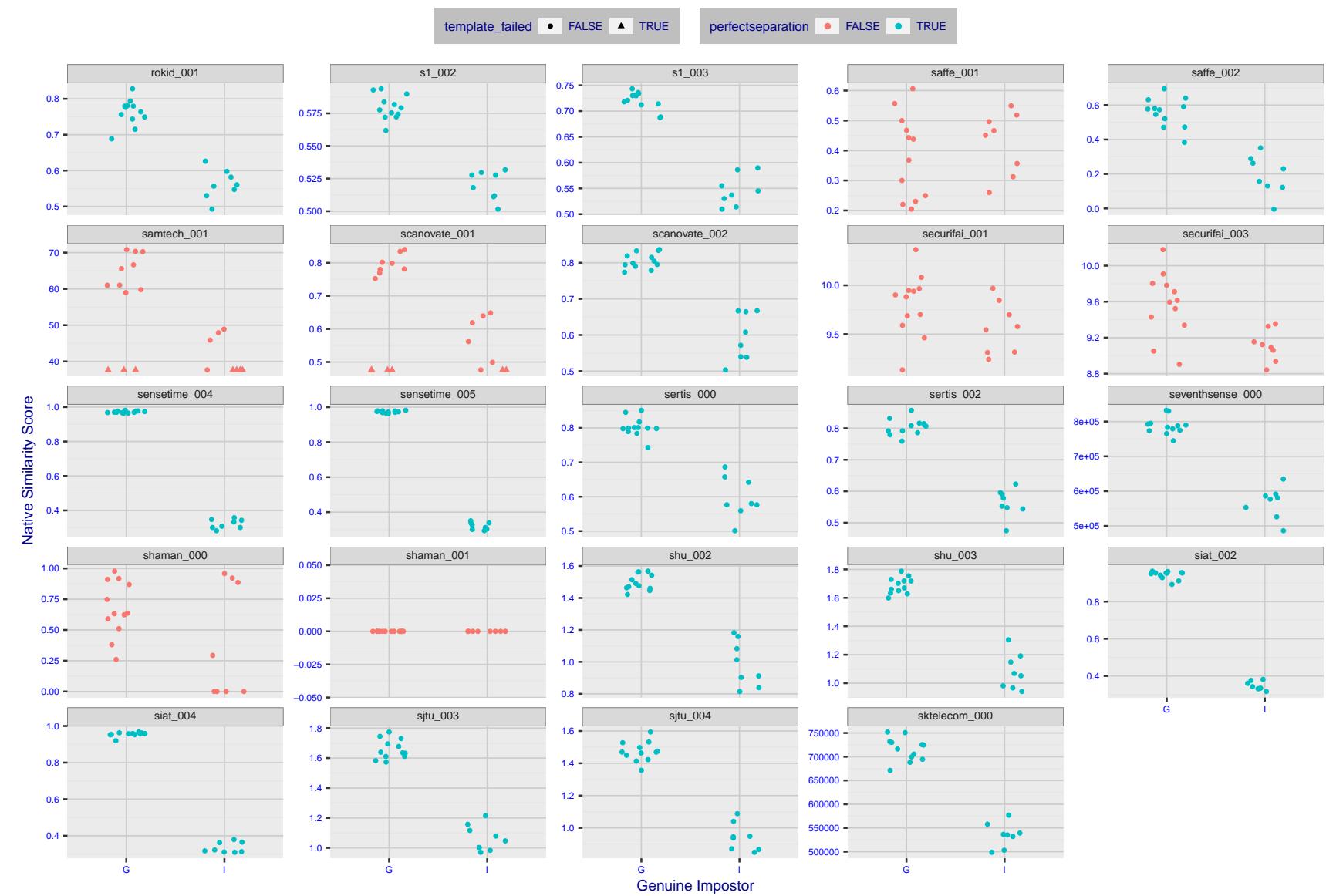


Figure 14: The Figure shows, in blue, algorithms that correctly separate the 12 genuine and 8 impostor pairs used in the May 2018 paper [Face recognition accuracy of forensic examiners, superrecognizers, and face recognition algorithms](#) (Phillips et al. [1]). In red are algorithms that are imperfect. Some algorithms fail only because they failed to make a template e.g. due to face detection failure (shown as a triangle). Others fail because the pairs were selected for that study because they had been difficult for three leading algorithms used in FRVT 2006. Caution: Given the small sample size ( $n=20$ ) the figure may change substantially if larger or different sets were used. The images can be downloaded from the [Supplemental Information](#) page provided with that publication.

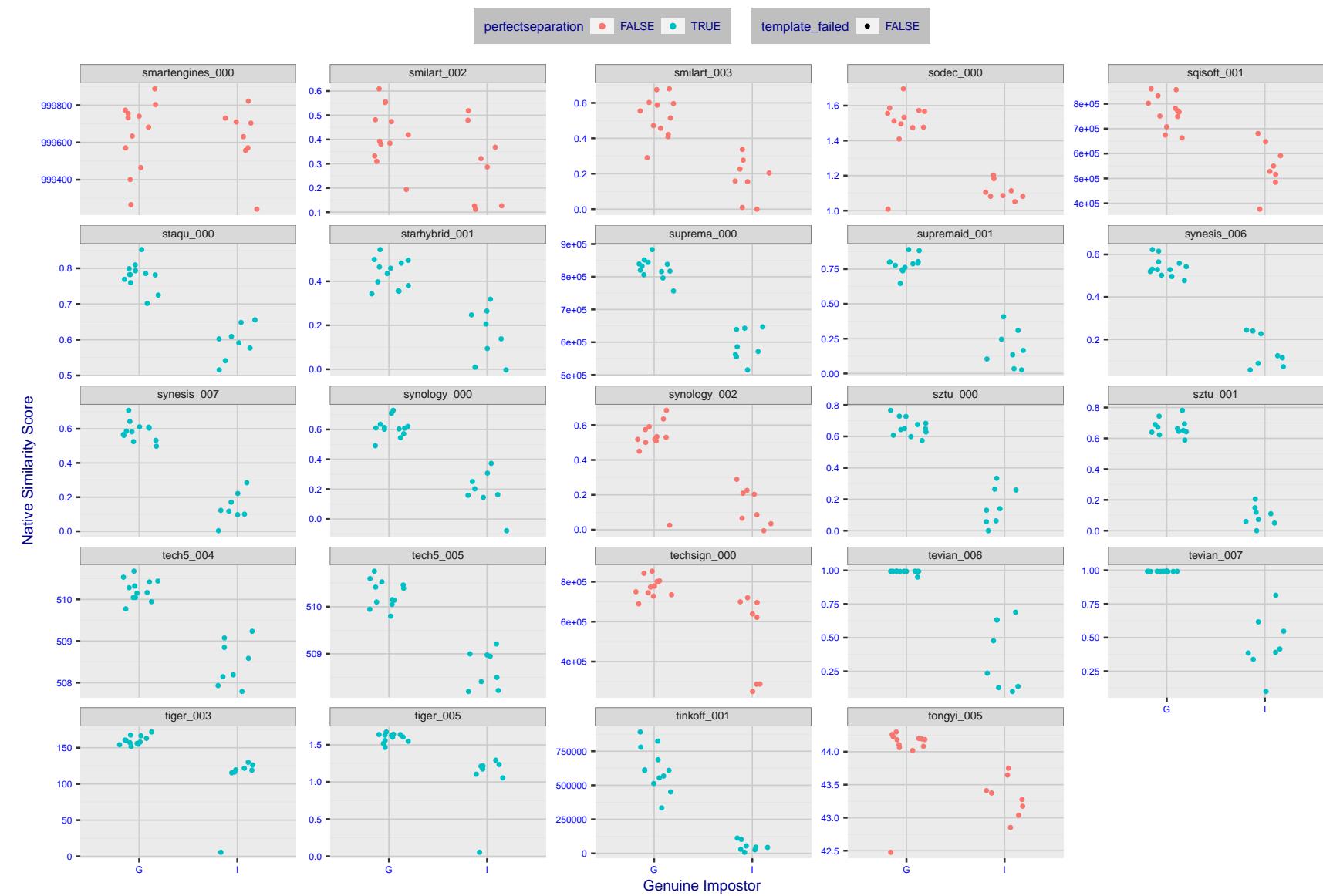


Figure 15: The Figure shows, in blue, algorithms that correctly separate the 12 genuine and 8 impostor pairs used in the May 2018 paper [Face recognition accuracy of forensic examiners, superrecognizers, and face recognition algorithms](#) (Phillips et al. [1]). In red are algorithms that are imperfect. Some algorithms fail only because they failed to make a template e.g. due to face detection failure (shown as a triangle). Others fail because the pairs were selected for that study because they had been difficult for three leading algorithms used in FRVT 2006. Caution: Given the small sample size ( $n=20$ ) the figure may change substantially if larger or different sets were used. The images can be downloaded from the [Supplemental Information](#) page provided with that publication.



Figure 16: The Figure shows, in blue, algorithms that correctly separate the 12 genuine and 8 impostor pairs used in the May 2018 paper [Face recognition accuracy of forensic examiners, superrecognizers, and face recognition algorithms](#) (Phillips et al. [1]). In red are algorithms that are imperfect. Some algorithms fail only because they failed to make a template e.g. due to face detection failure (shown as a triangle). Others fail because the pairs were selected for that study because they had been difficult for three leading algorithms used in FRVT 2006. Caution: Given the small sample size ( $n=20$ ) the figure may change substantially if larger or different sets were used. The images can be downloaded from the [Supplemental Information](#) page provided with that publication.

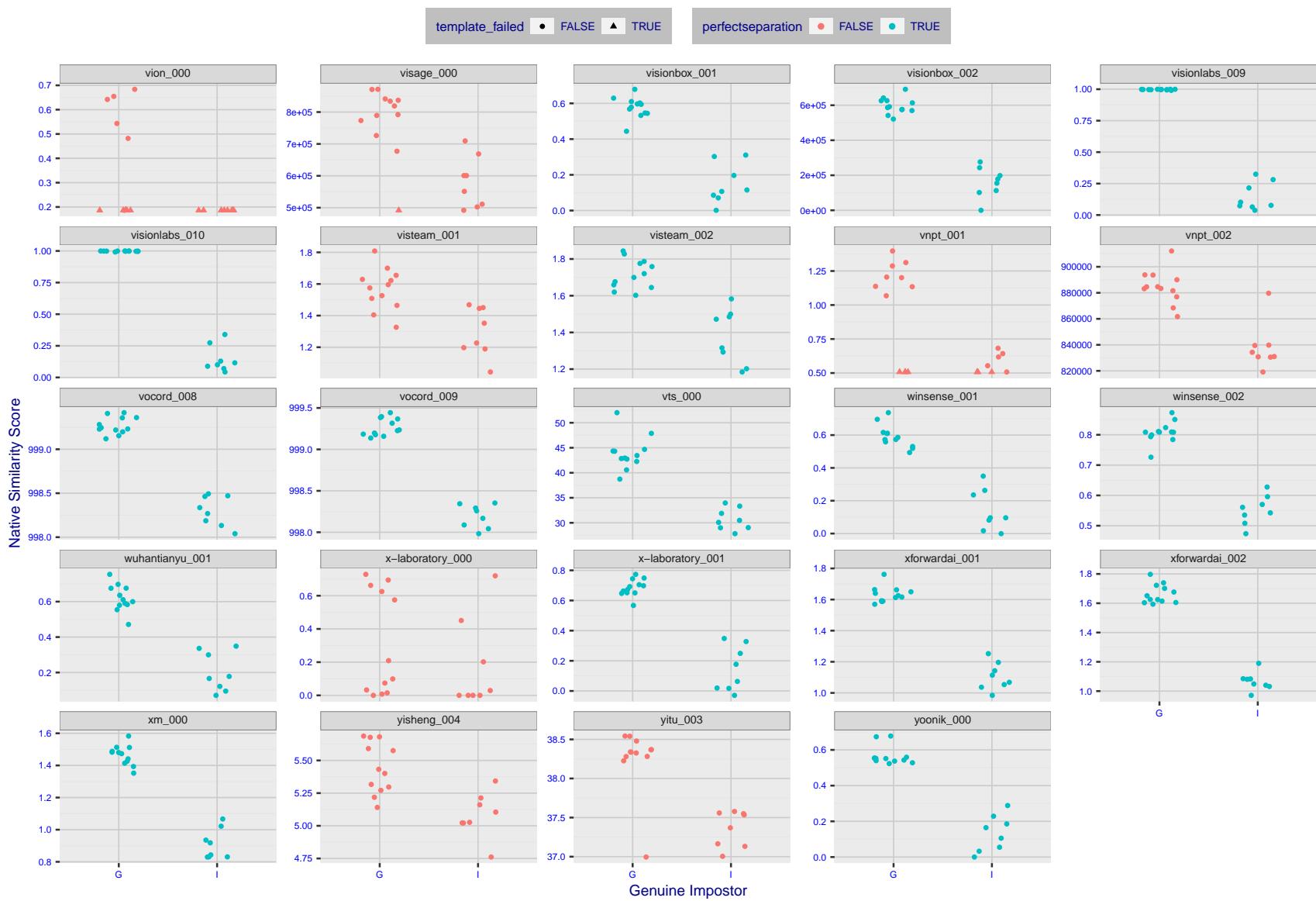


Figure 17: The Figure shows, in blue, algorithms that correctly separate the 12 genuine and 8 impostor pairs used in the May 2018 paper Face recognition accuracy of forensic examiners, superrecognizers, and face recognition algorithms (Phillips et al. [1]). In red are algorithms that are imperfect. Some algorithms fail only because they failed to make a template e.g. due to face detection failure (shown as a triangle). Others fail because the pairs were selected for that study because they had been difficult for three leading algorithms used in FRVT 2006. Caution: Given the small sample size ( $n=20$ ) the figure may change substantially if larger or different sets were used. The images can be downloaded from the [Supplemental Information](#) page provided with that publication.

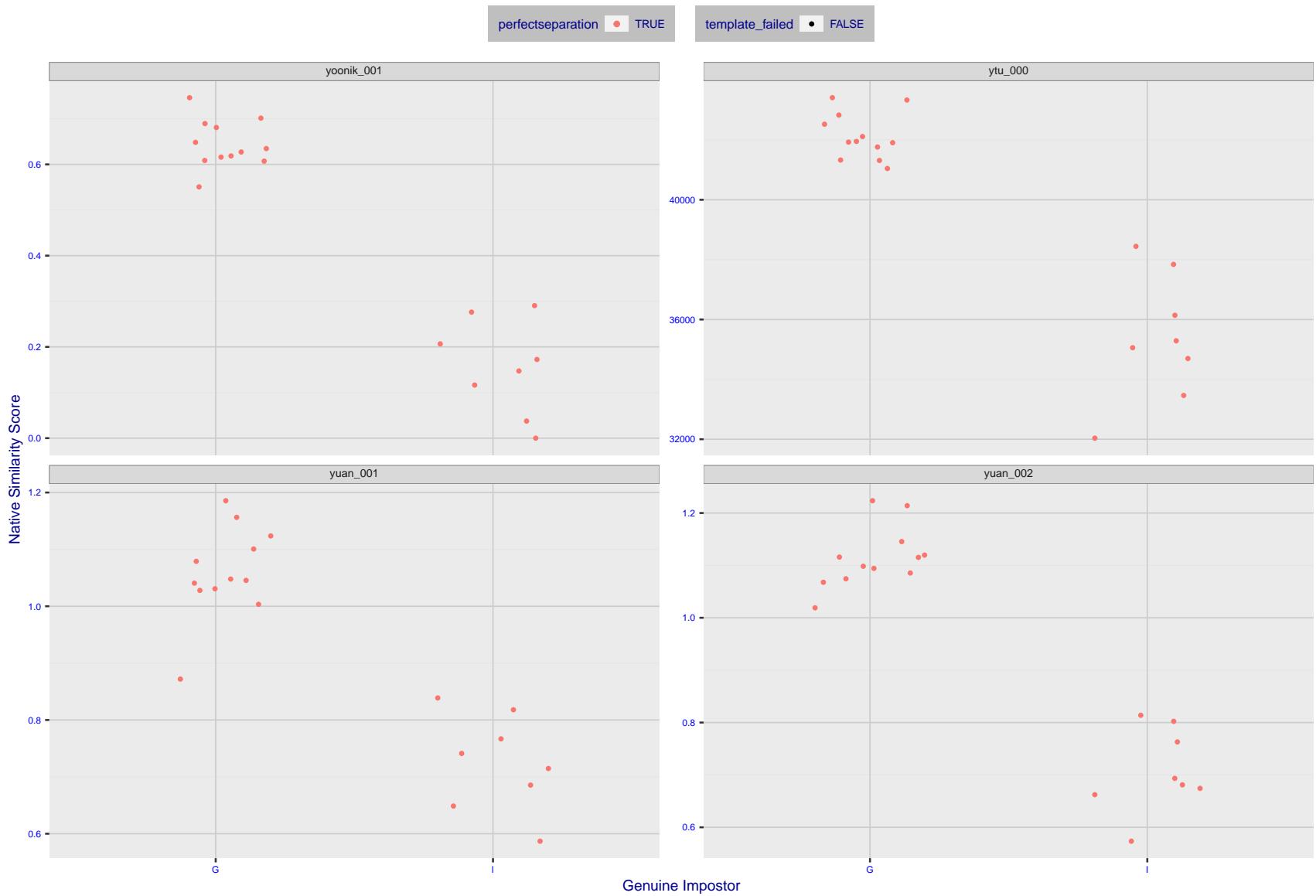


Figure 18: The Figure shows, in blue, algorithms that correctly separate the 12 genuine and 8 impostor pairs used in the May 2018 paper [Face recognition accuracy of forensic examiners, superrecognizers, and face recognition algorithms](#) (Phillips et al. [1]). In red are algorithms that are imperfect. Some algorithms fail only because they failed to make a template e.g. due to face detection failure (shown as a triangle). Others fail because the pairs were selected for that study because they had been difficult for three leading algorithms used in FRVT 2006. Caution: Given the small sample size ( $n=20$ ) the figure may change substantially if larger or different sets were used. The images can be downloaded from the [Supplemental Information](#) page provided with that publication.

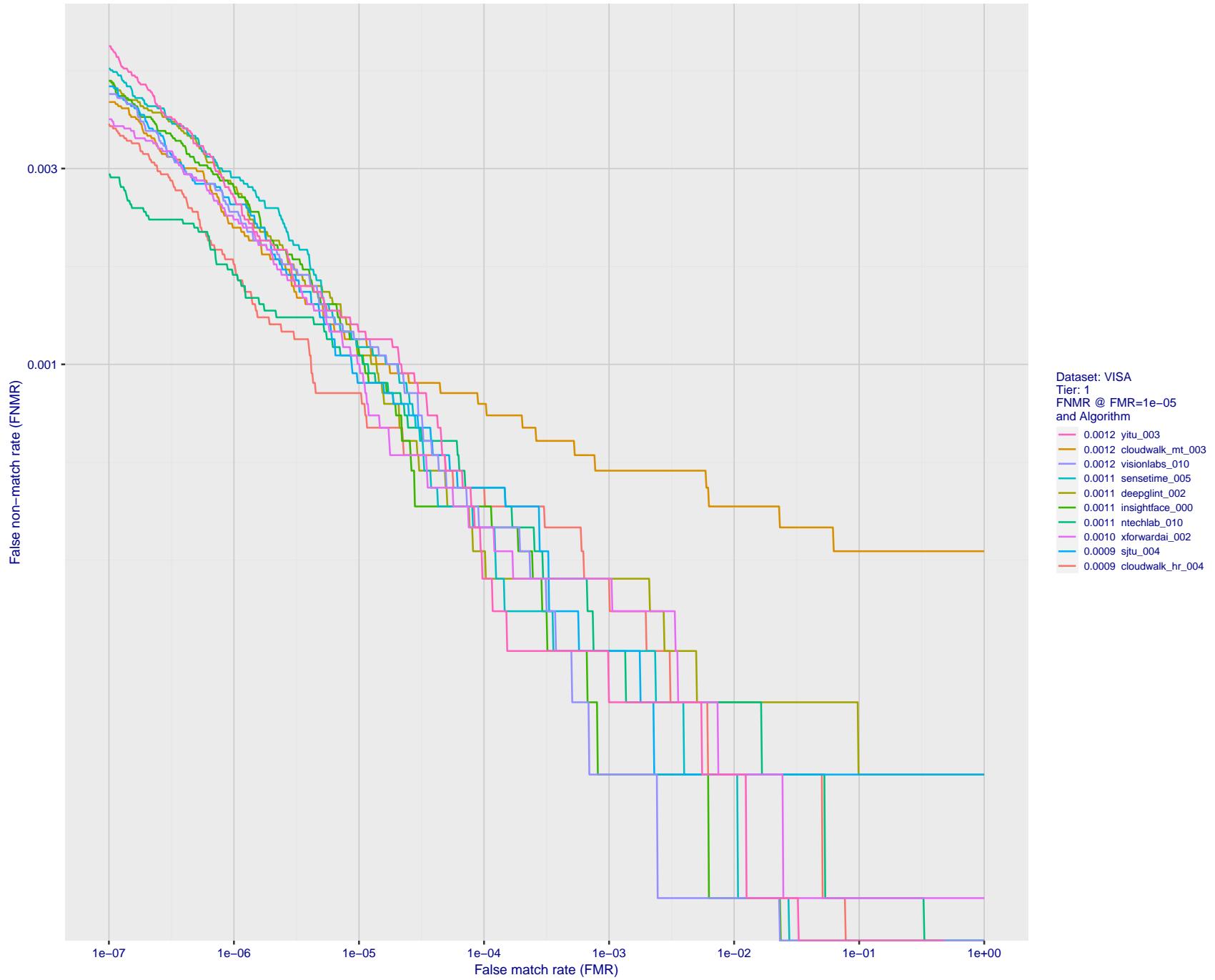


Figure 19: For the visa images, detection error tradeoff (DET) characteristics showing false non-match rate vs. false match rate plotted parametrically on threshold,  $T$ . The scales are logarithmic in order to show many decades of FMR.

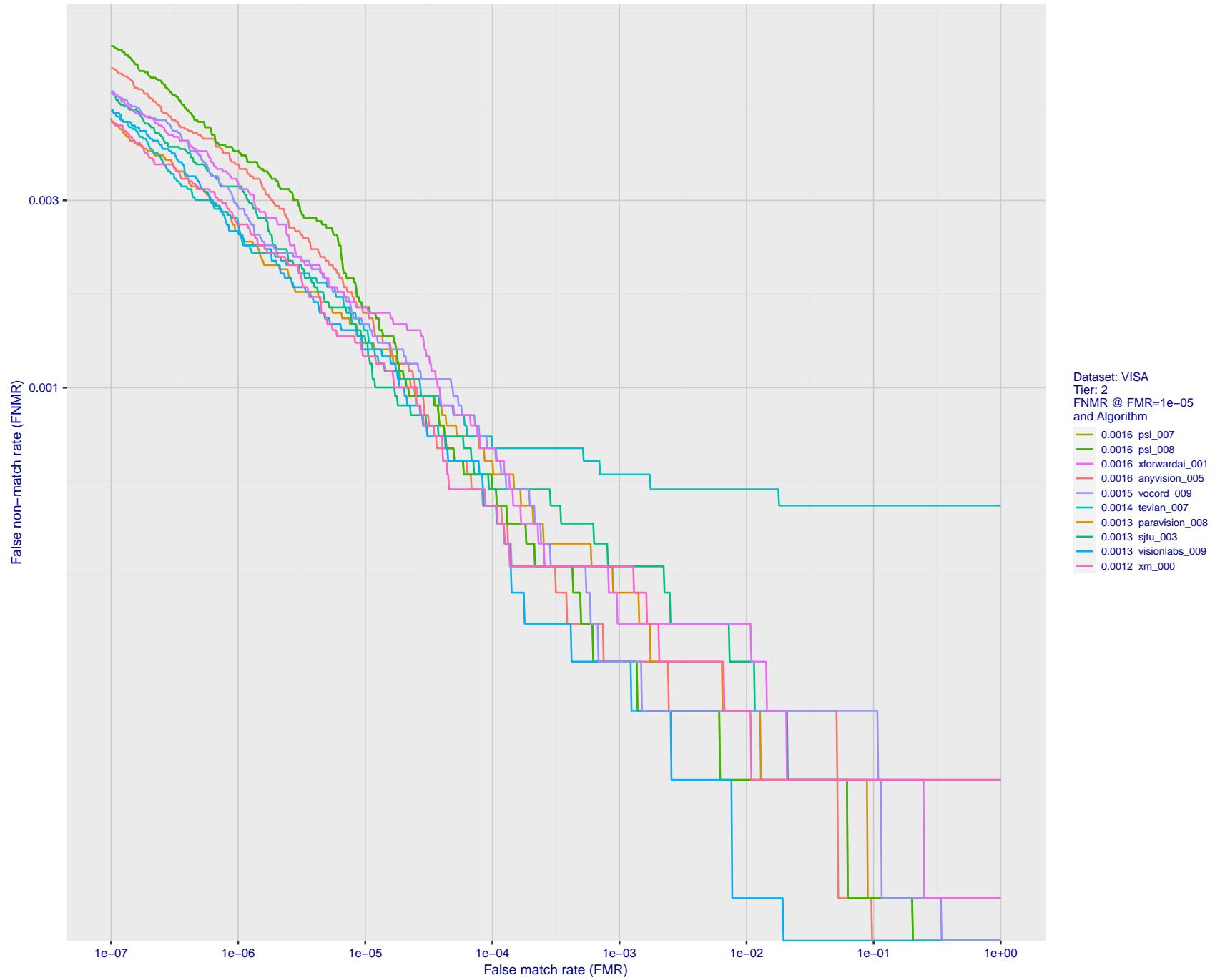


Figure 20: For the visa images, detection error tradeoff (DET) characteristics showing false non-match rate vs. false match rate plotted parametrically on threshold,  $T$ . The scales are logarithmic in order to show many decades of FMR.

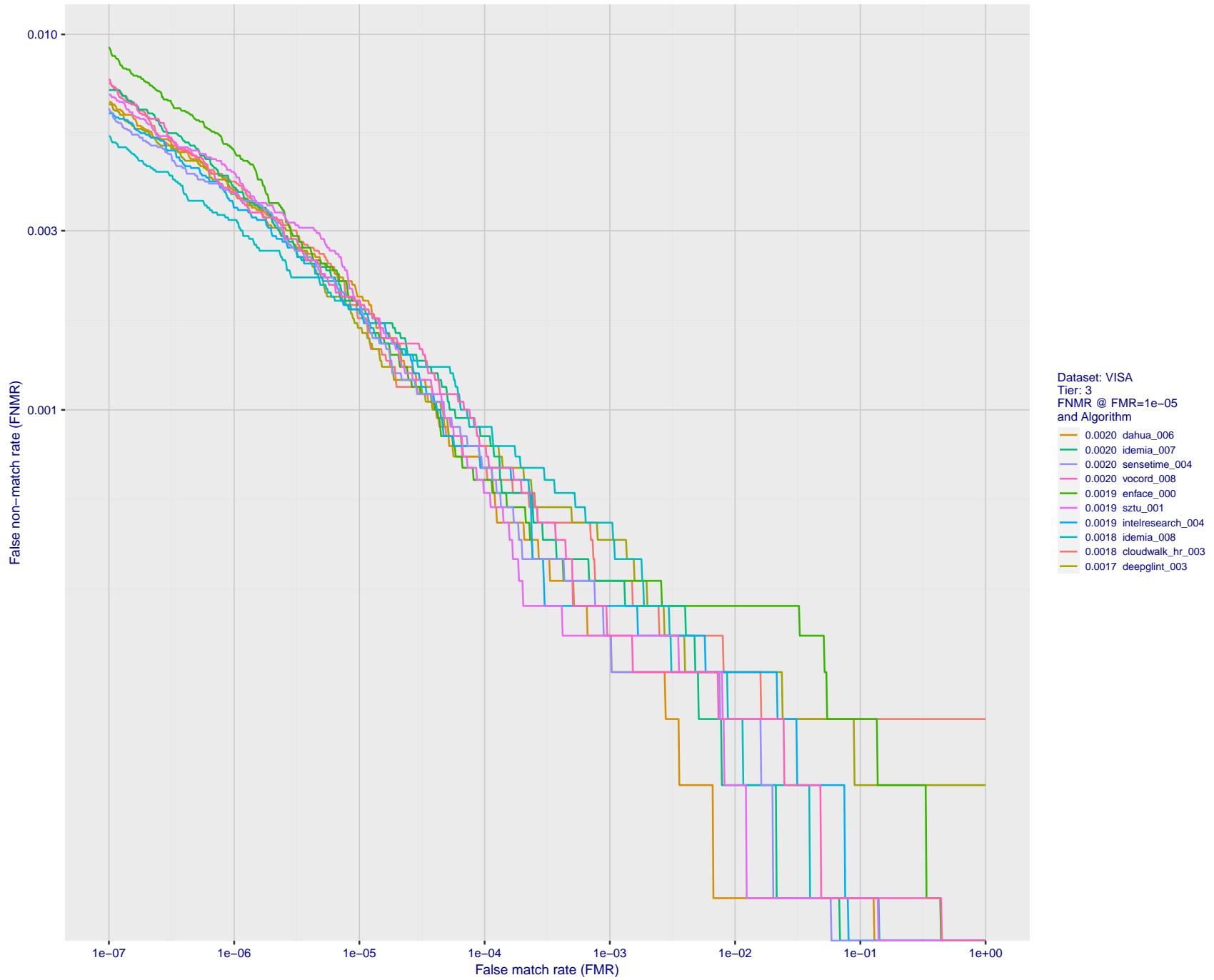


Figure 21: For the visa images, detection error tradeoff (DET) characteristics showing false non-match rate vs. false match rate plotted parametrically on threshold,  $T$ . The scales are logarithmic in order to show many decades of FMR.

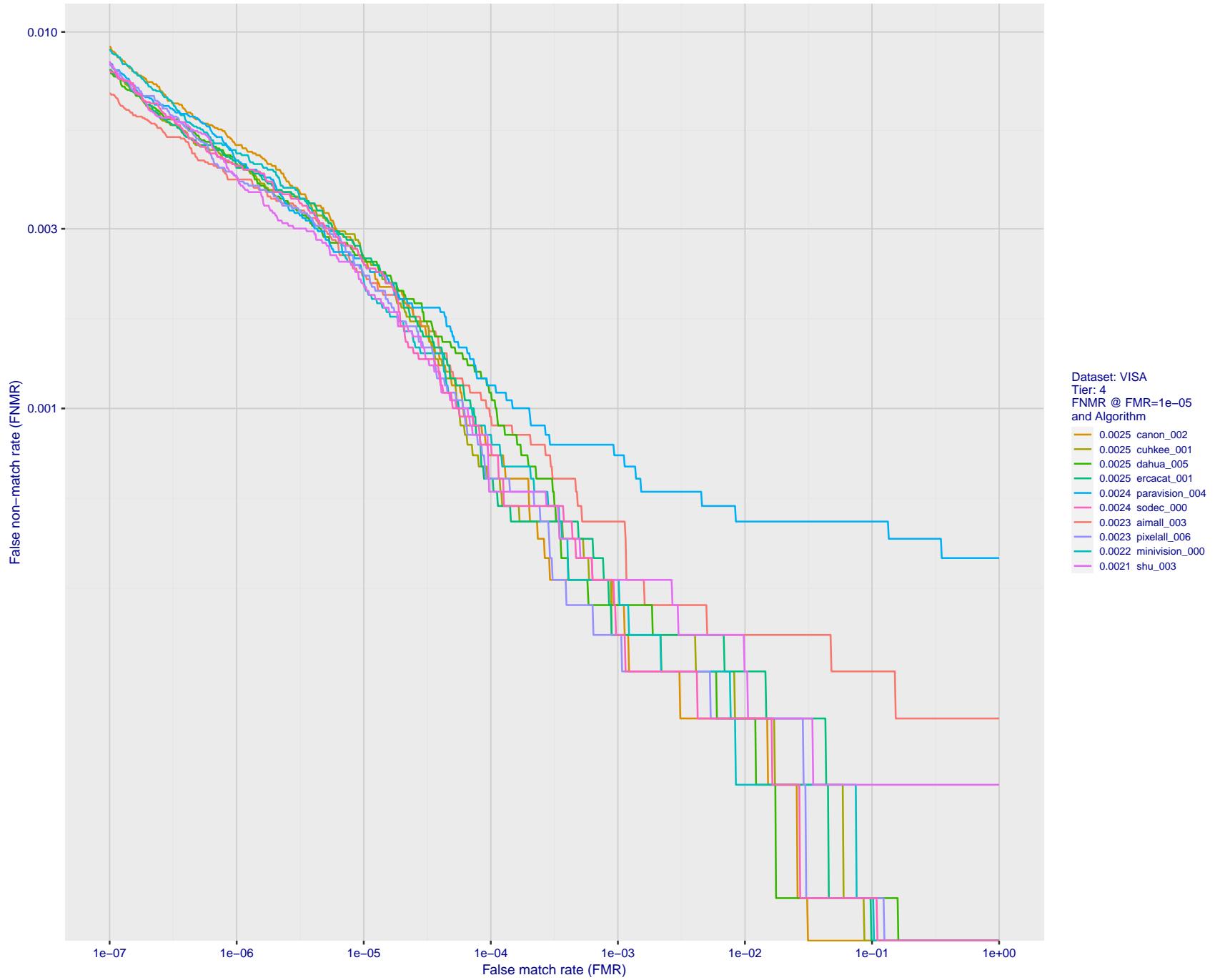


Figure 22: For the visa images, detection error tradeoff (DET) characteristics showing false non-match rate vs. false match rate plotted parametrically on threshold,  $T$ . The scales are logarithmic in order to show many decades of FMR.

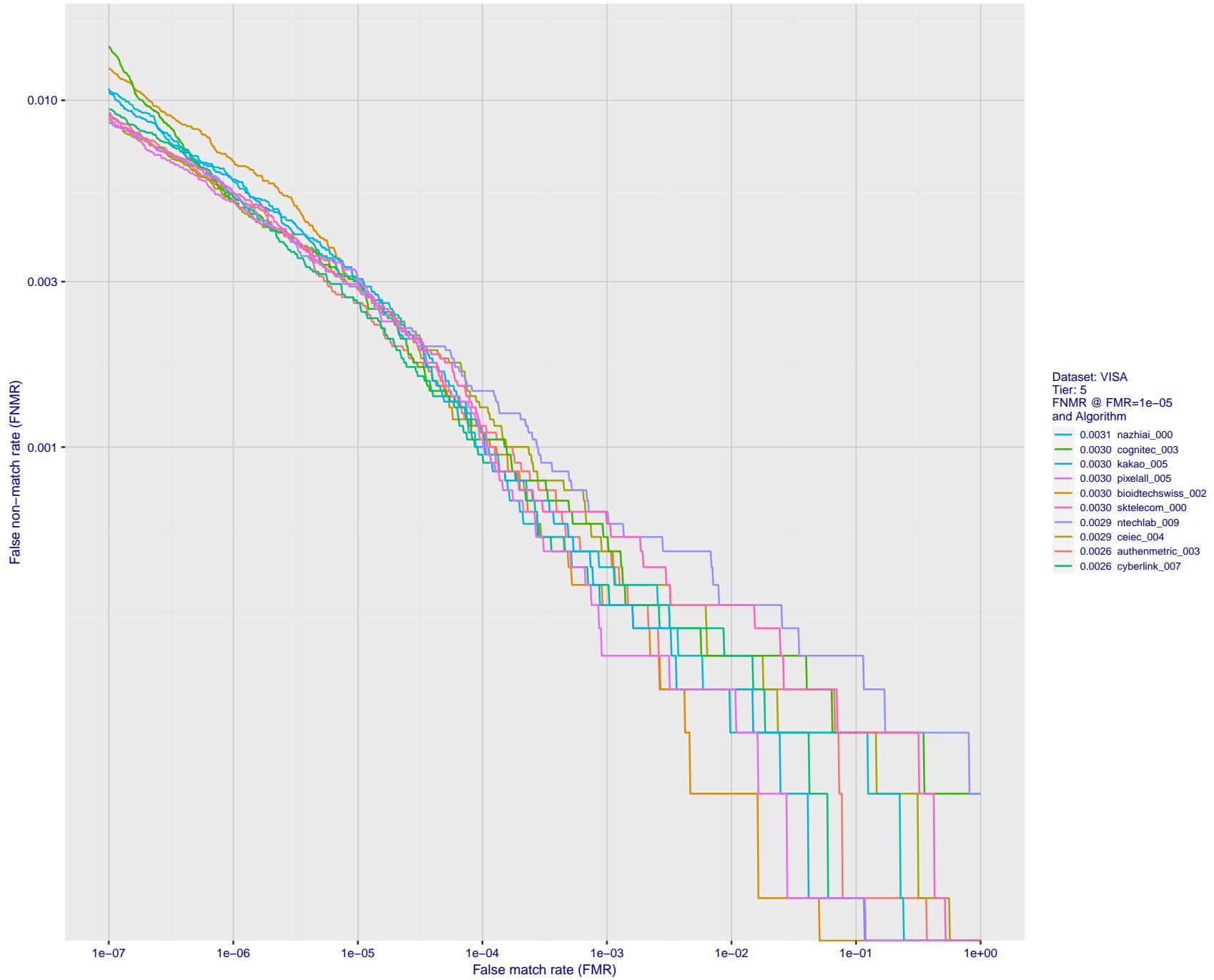


Figure 23: For the visa images, detection error tradeoff (DET) characteristics showing false non-match rate vs. false match rate plotted parametrically on threshold,  $T$ . The scales are logarithmic in order to show many decades of FMR.

2021/09/10 10:17:25

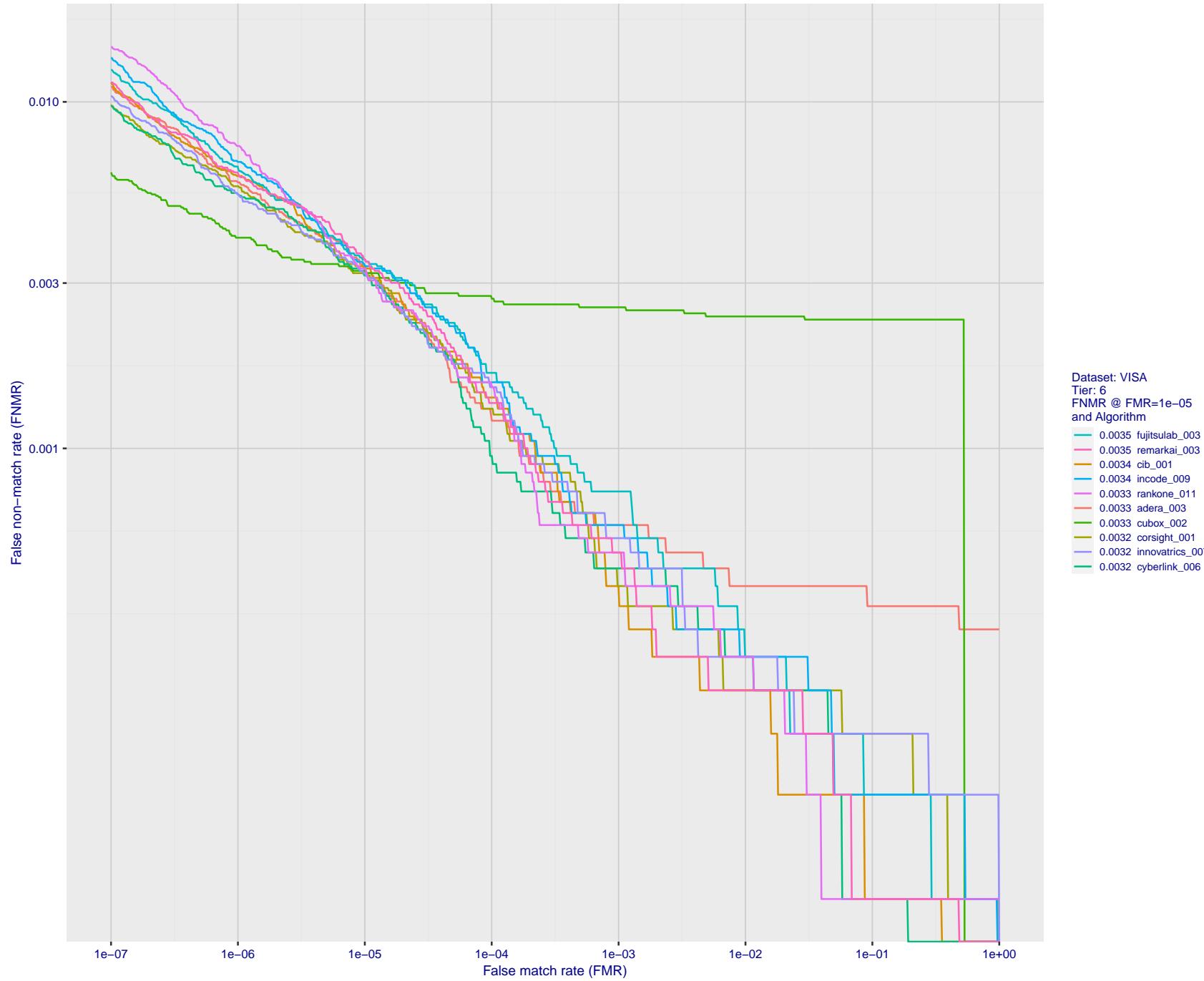


Figure 24: For the visa images, detection error tradeoff (DET) characteristics showing false non-match rate vs. false match rate plotted parametrically on threshold,  $T$ . The scales are logarithmic in order to show many decades of FMR.

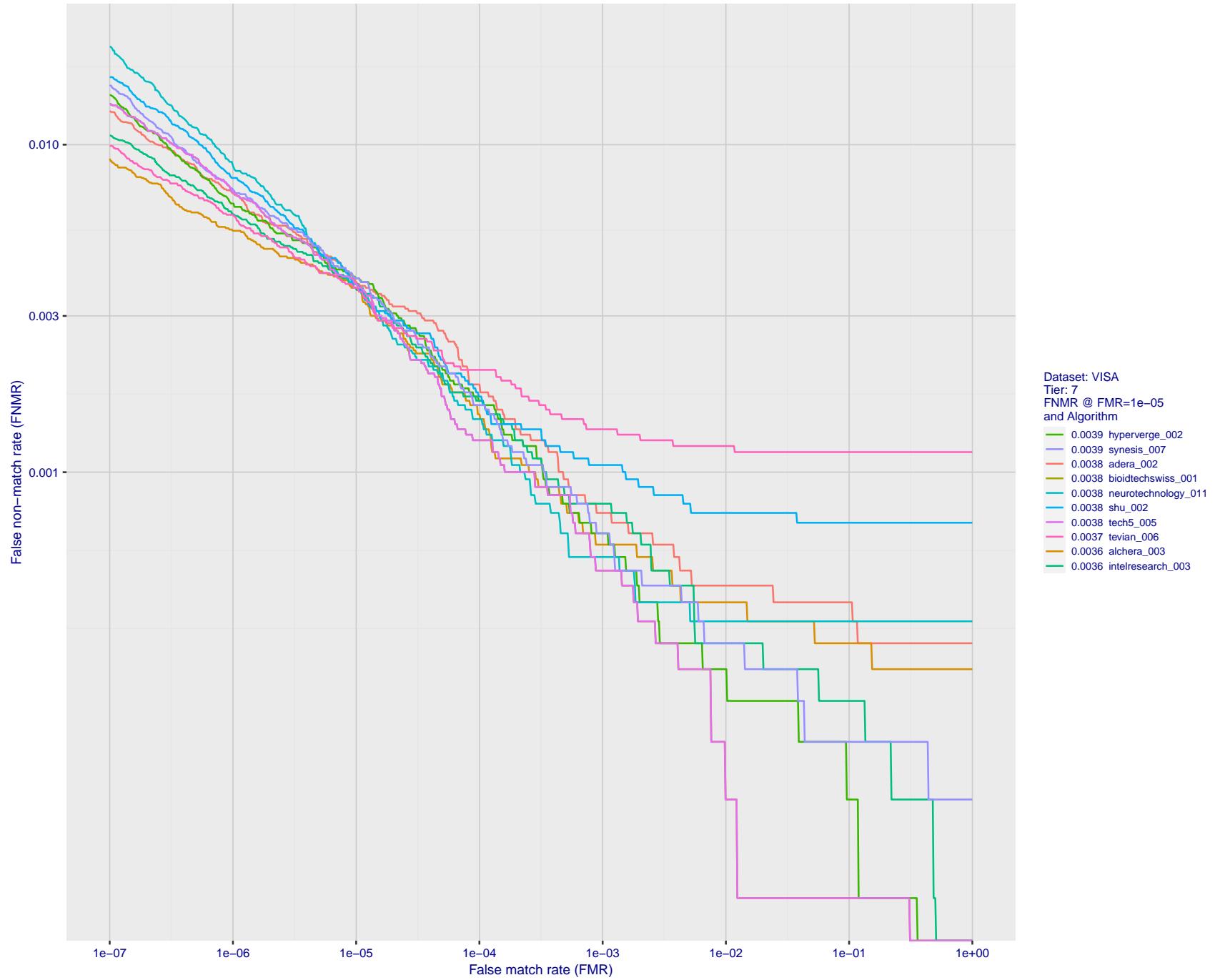


Figure 25: For the visa images, detection error tradeoff (DET) characteristics showing false non-match rate vs. false match rate plotted parametrically on threshold,  $T$ . The scales are logarithmic in order to show many decades of FMR.

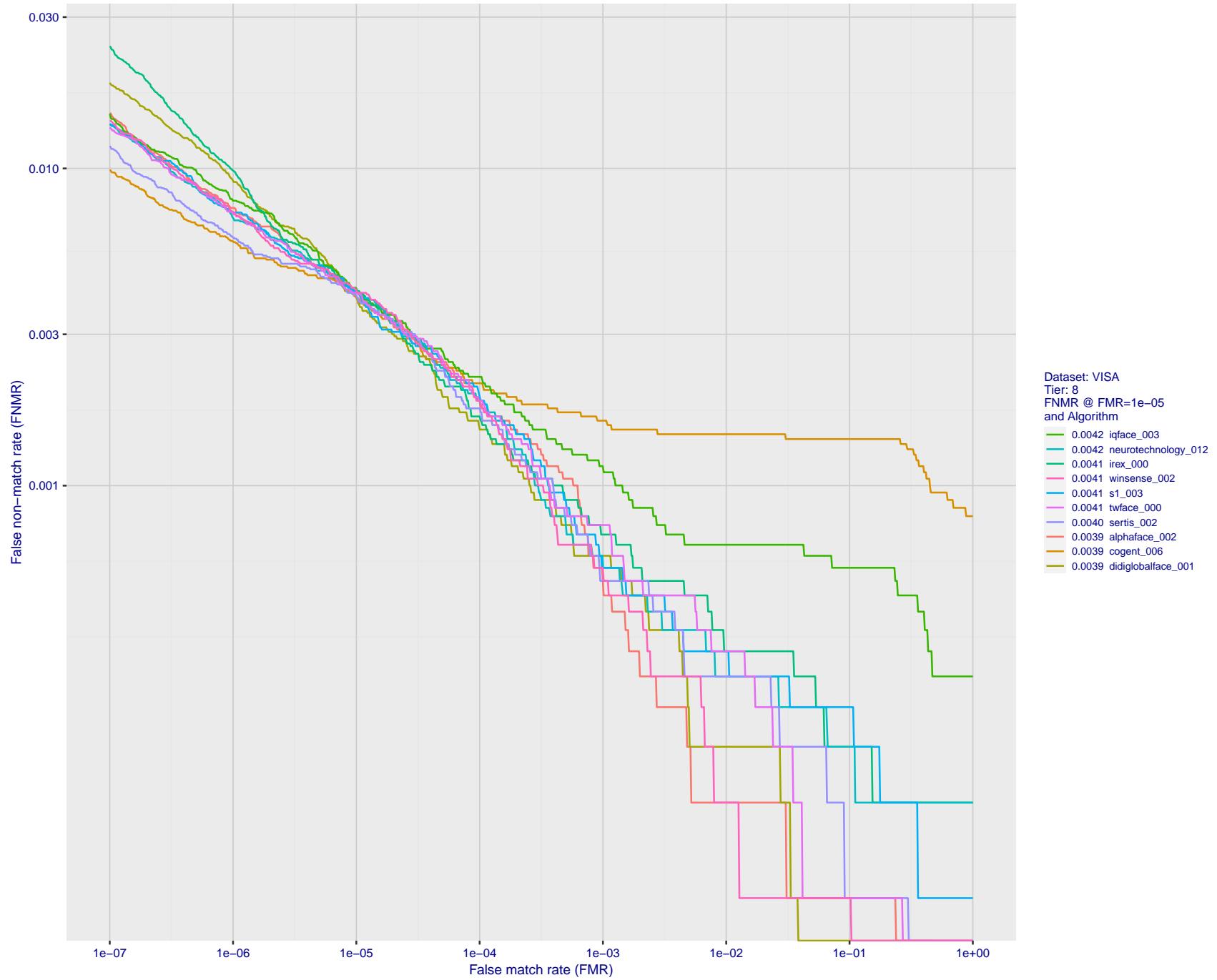


Figure 26: For the visa images, detection error tradeoff (DET) characteristics showing false non-match rate vs. false match rate plotted parametrically on threshold,  $T$ . The scales are logarithmic in order to show many decades of FMR.

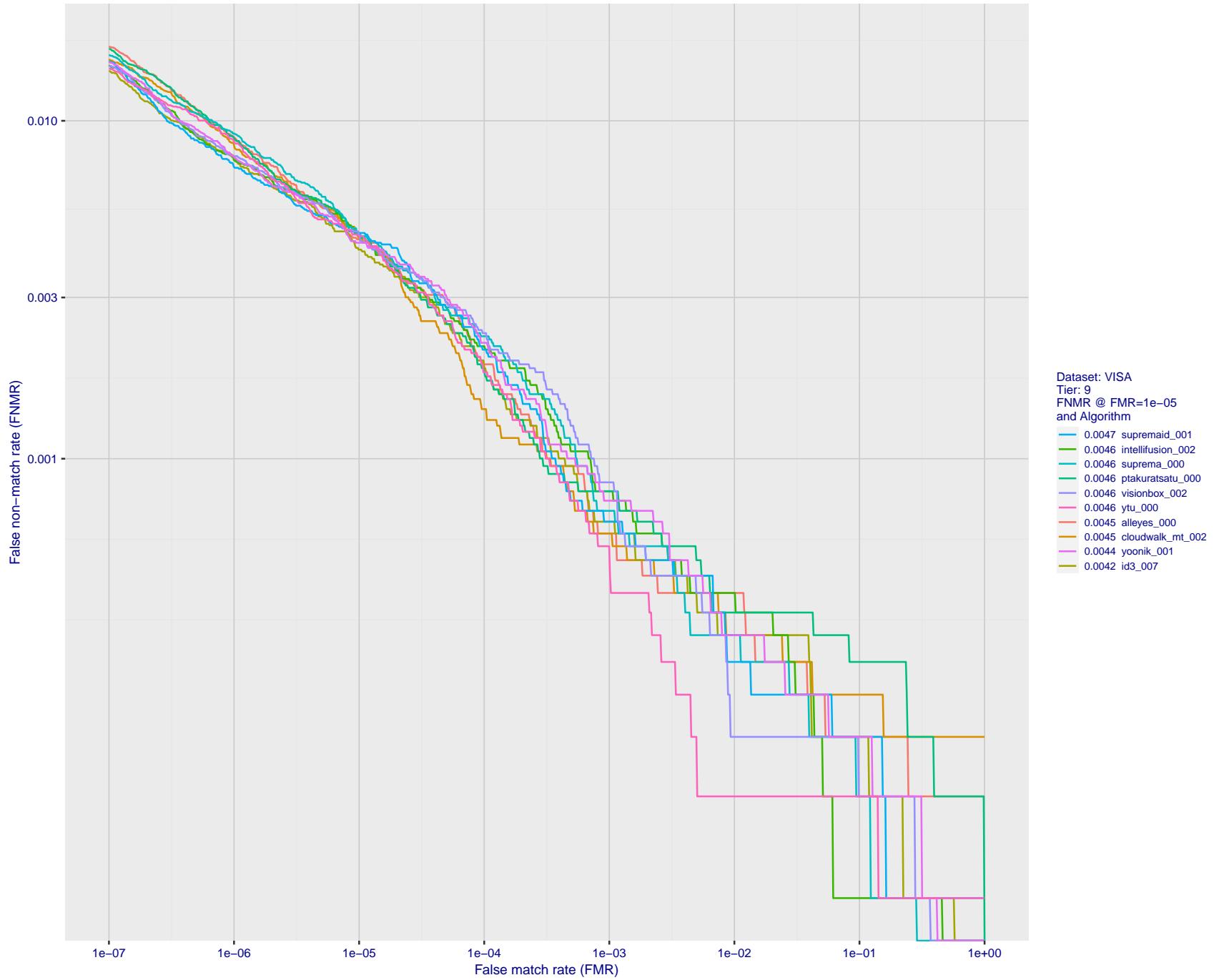


Figure 27: For the visa images, detection error tradeoff (DET) characteristics showing false non-match rate vs. false match rate plotted parametrically on threshold,  $T$ . The scales are logarithmic in order to show many decades of FMR.

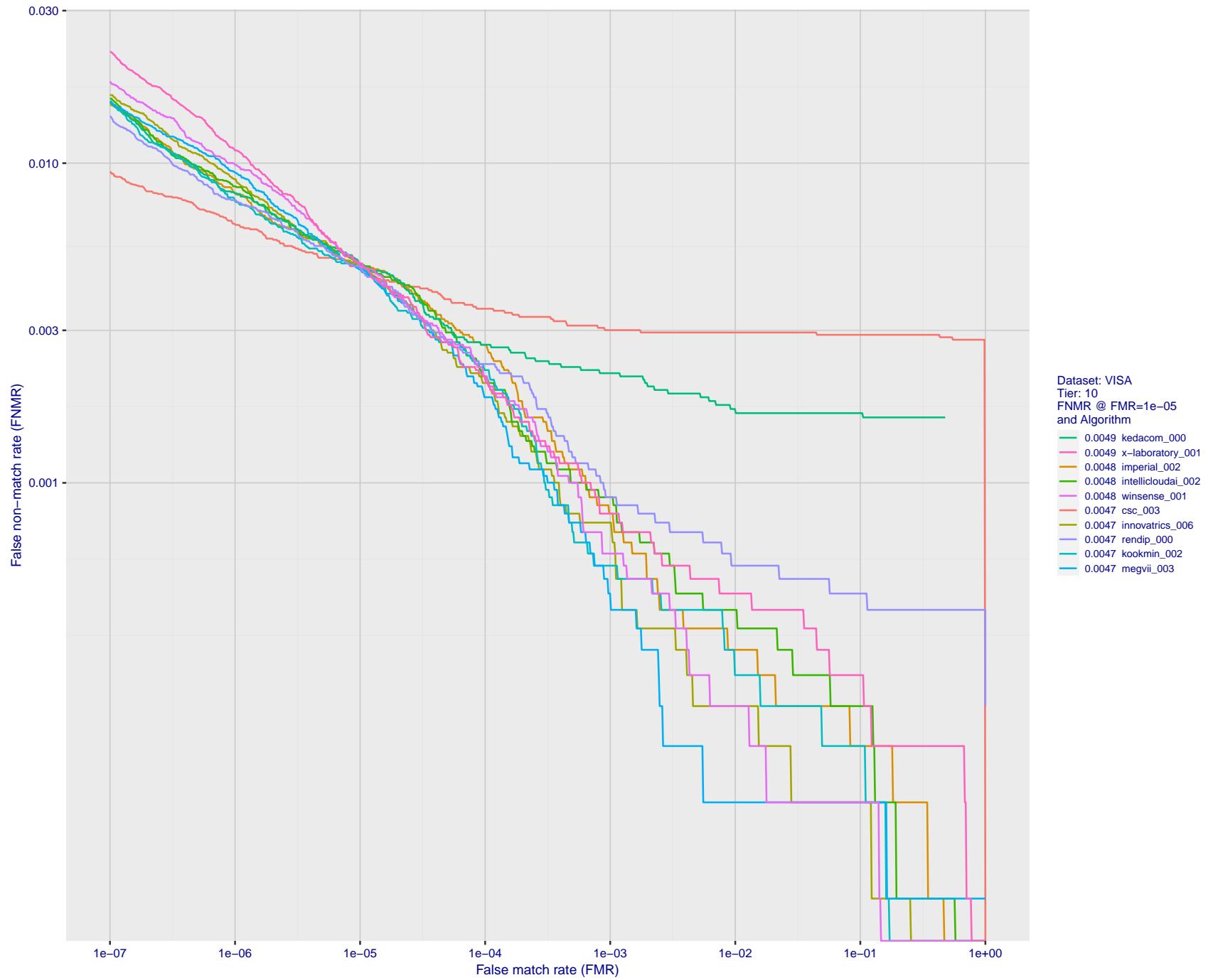


Figure 28: For the visa images, detection error tradeoff (DET) characteristics showing false non-match rate vs. false match rate plotted parametrically on threshold,  $T$ . The scales are logarithmic in order to show many decades of FMR.

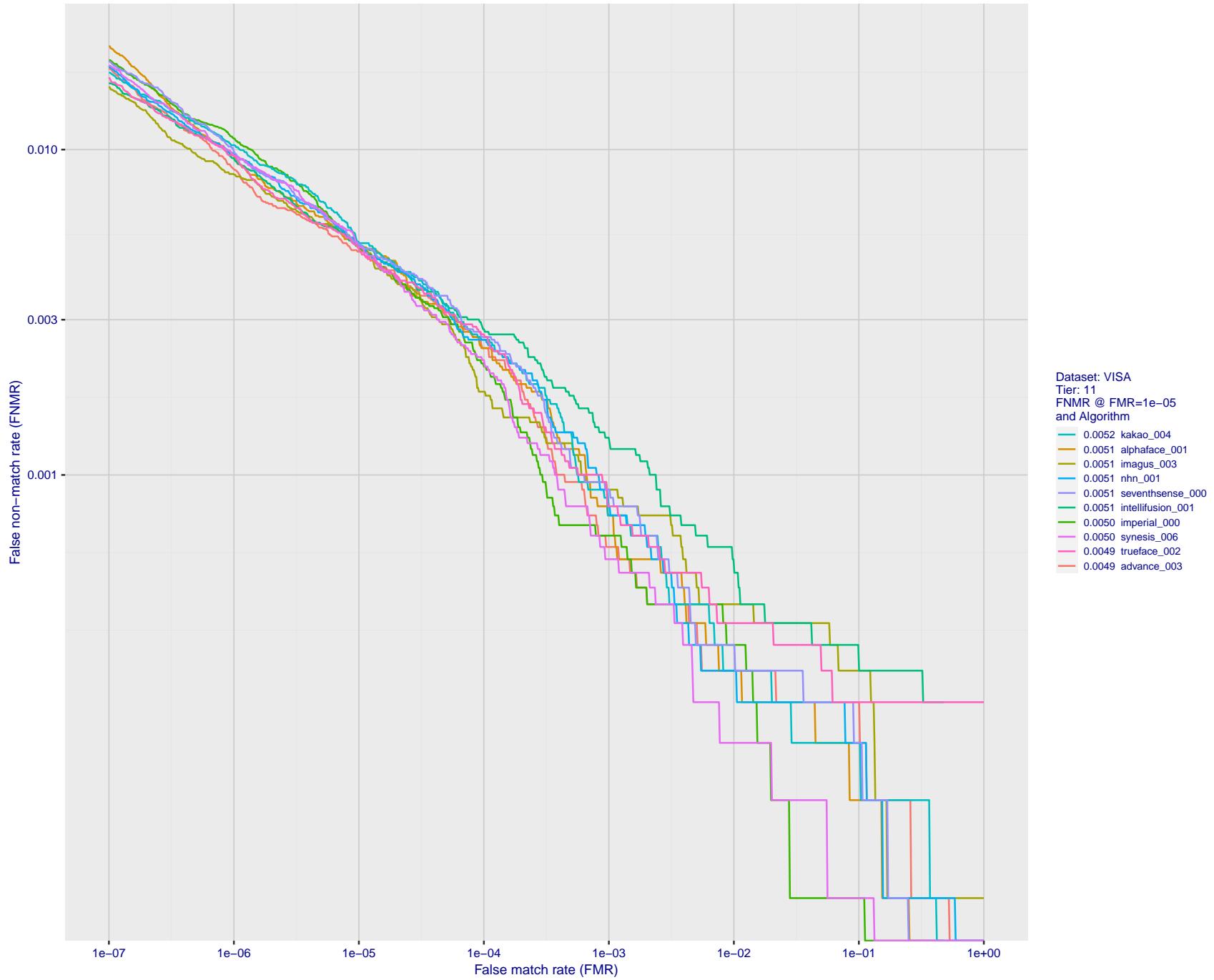


Figure 29: For the visa images, detection error tradeoff (DET) characteristics showing false non-match rate vs. false match rate plotted parametrically on threshold,  $T$ . The scales are logarithmic in order to show many decades of FMR.

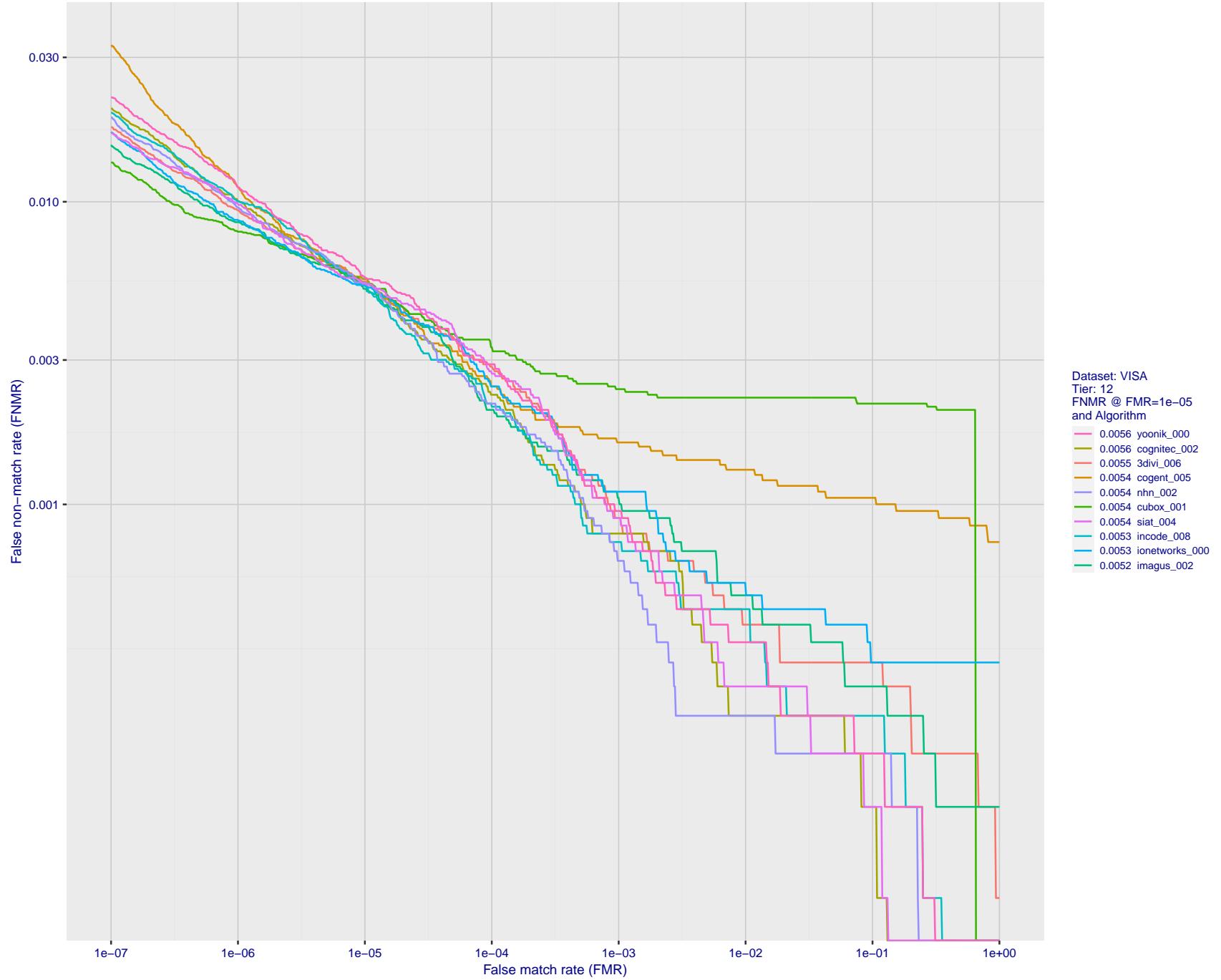


Figure 30: For the visa images, detection error tradeoff (DET) characteristics showing false non-match rate vs. false match rate plotted parametrically on threshold,  $T$ . The scales are logarithmic in order to show many decades of FMR.

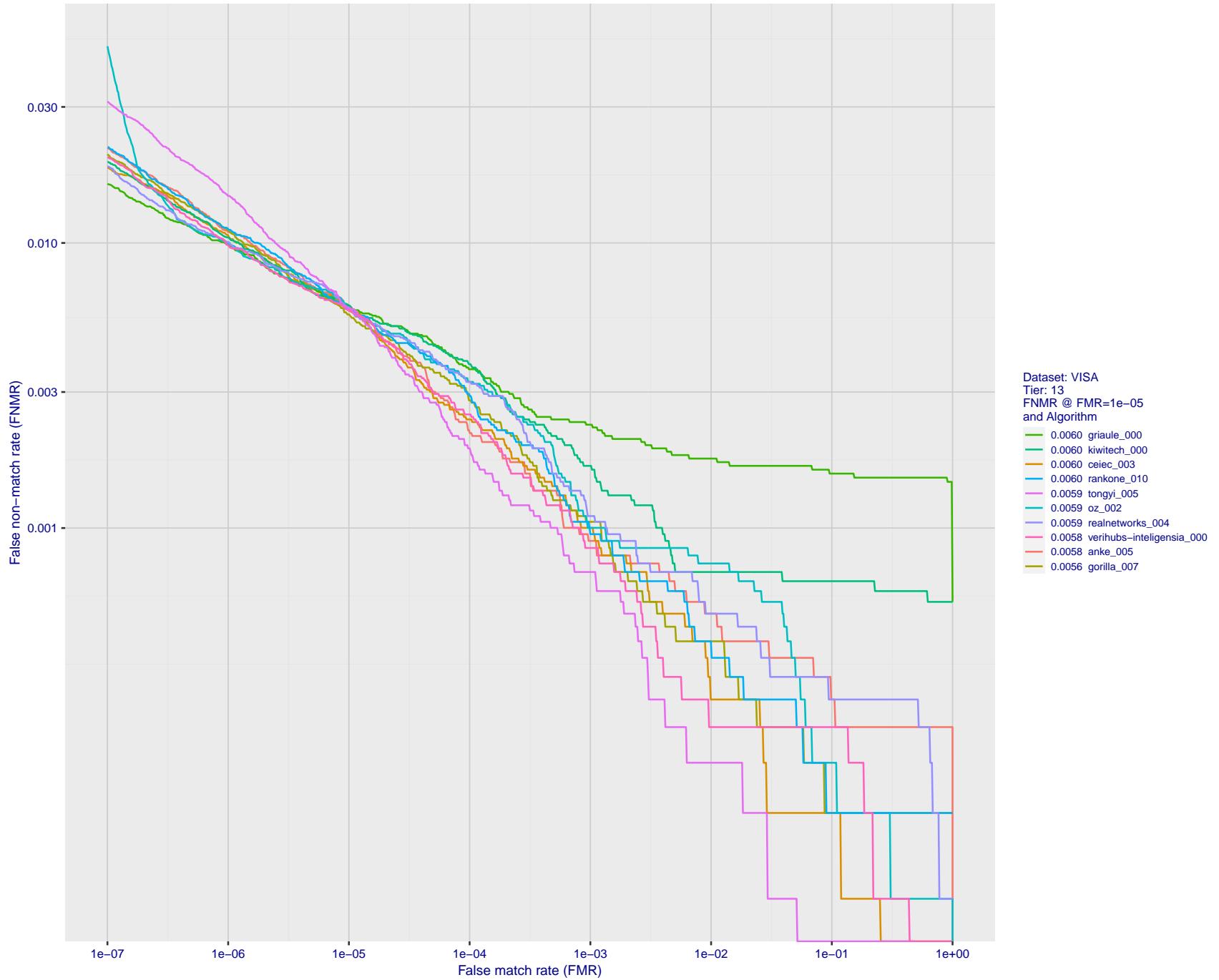


Figure 31: For the visa images, detection error tradeoff (DET) characteristics showing false non-match rate vs. false match rate plotted parametrically on threshold,  $T$ . The scales are logarithmic in order to show many decades of FMR.

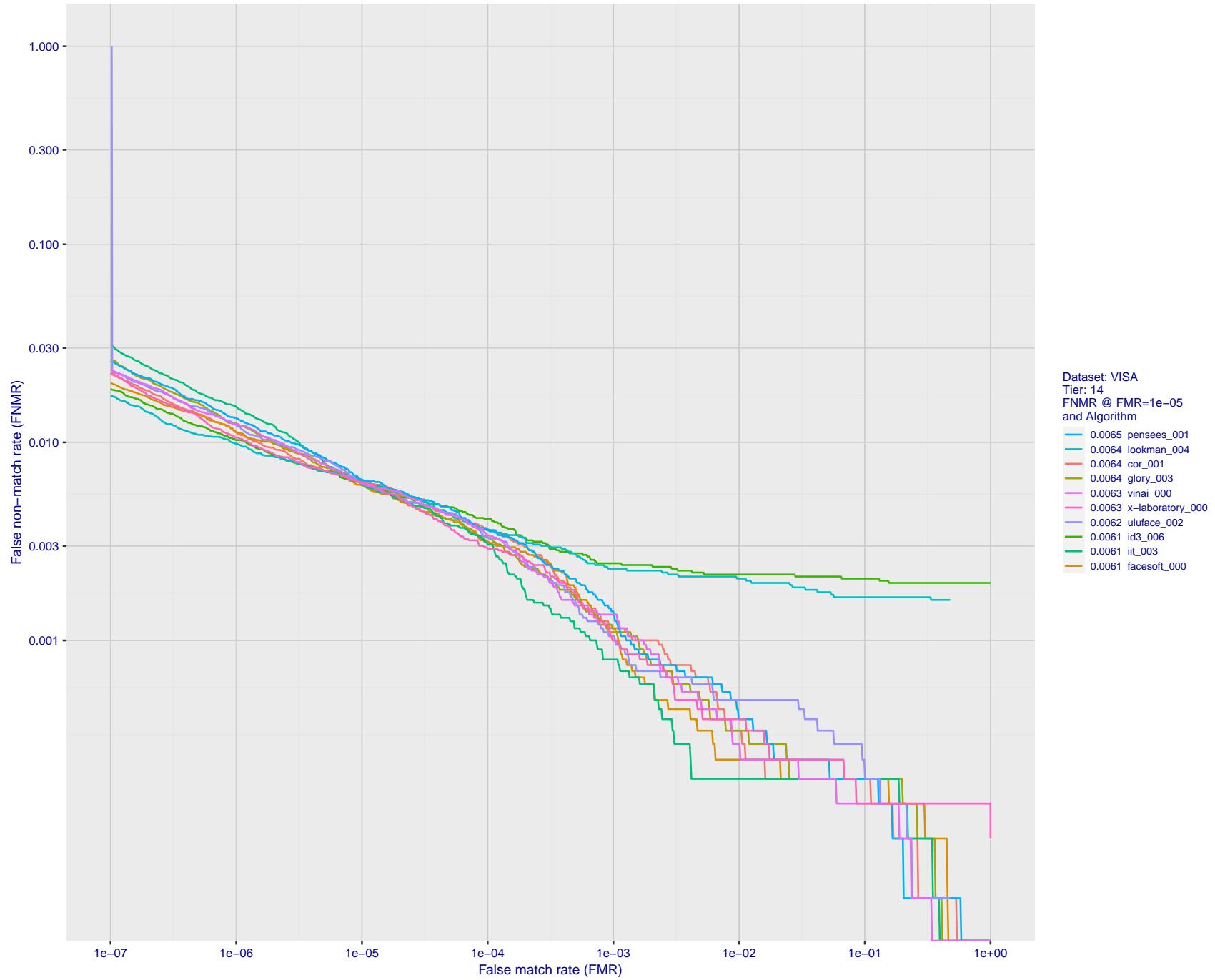


Figure 32: For the visa images, detection error tradeoff (DET) characteristics showing false non-match rate vs. false match rate plotted parametrically on threshold,  $T$ . The scales are logarithmic in order to show many decades of FMR.

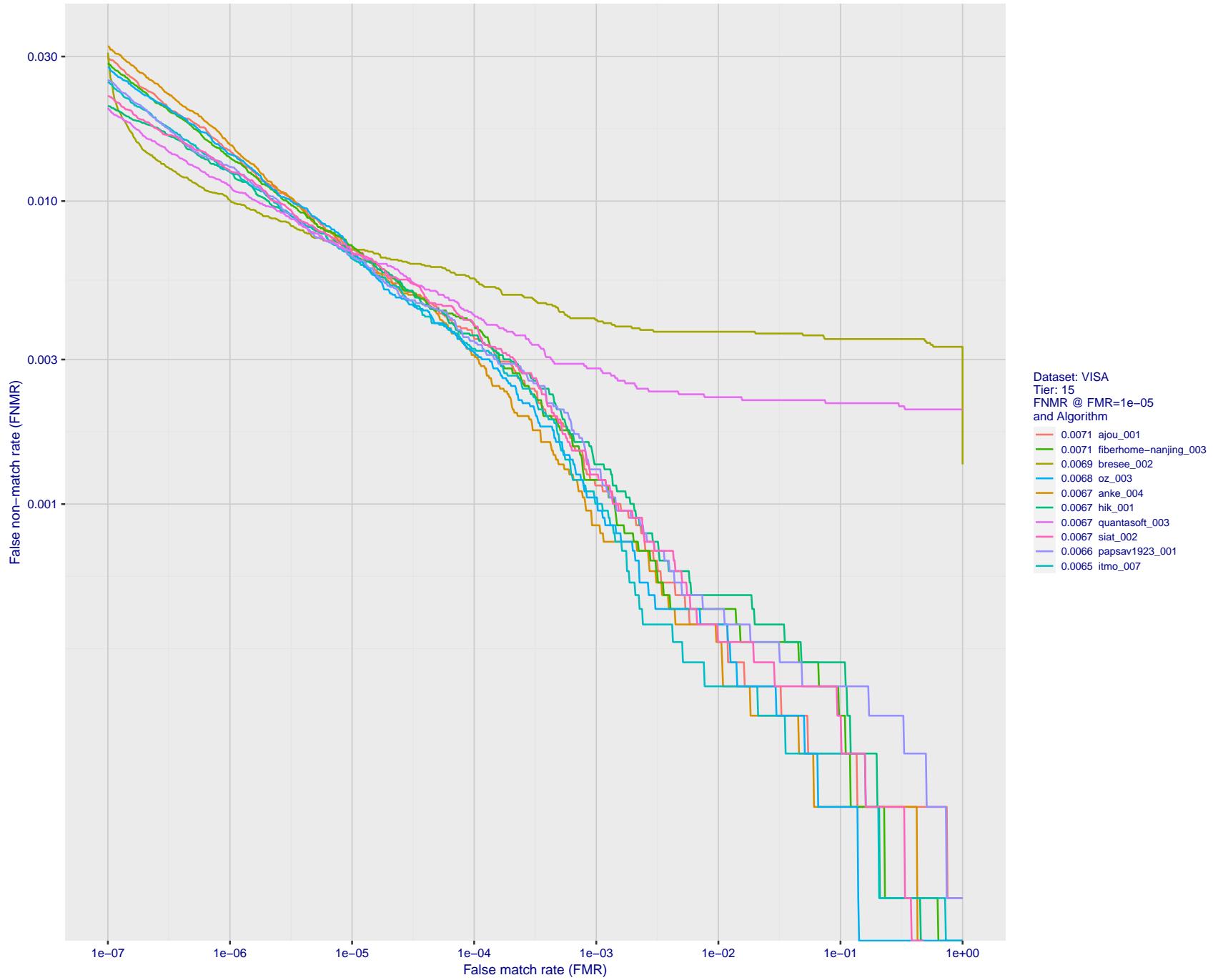


Figure 33: For the visa images, detection error tradeoff (DET) characteristics showing false non-match rate vs. false match rate plotted parametrically on threshold,  $T$ . The scales are logarithmic in order to show many decades of FMR.

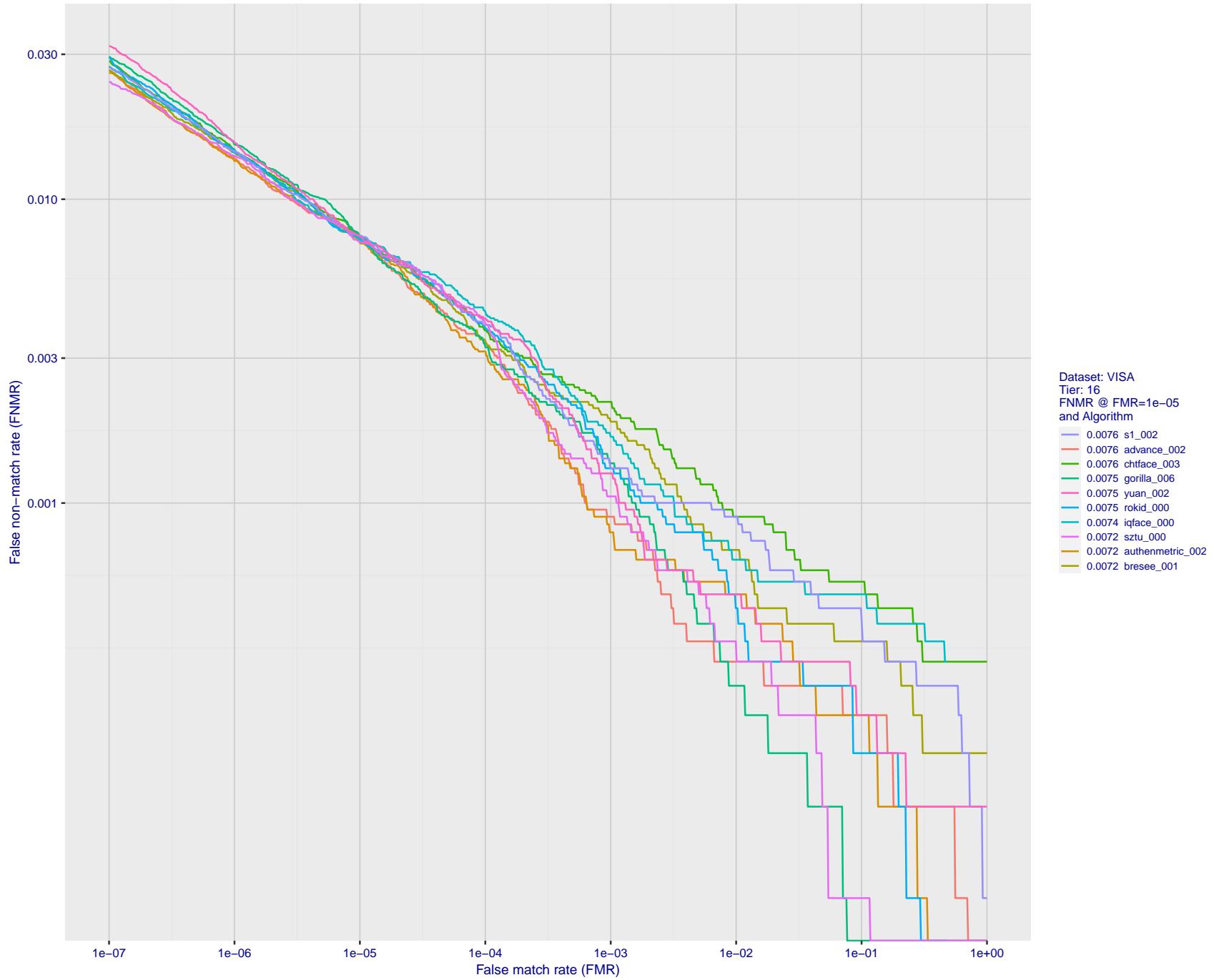


Figure 34: For the visa images, detection error tradeoff (DET) characteristics showing false non-match rate vs. false match rate plotted parametrically on threshold,  $T$ . The scales are logarithmic in order to show many decades of FMR.

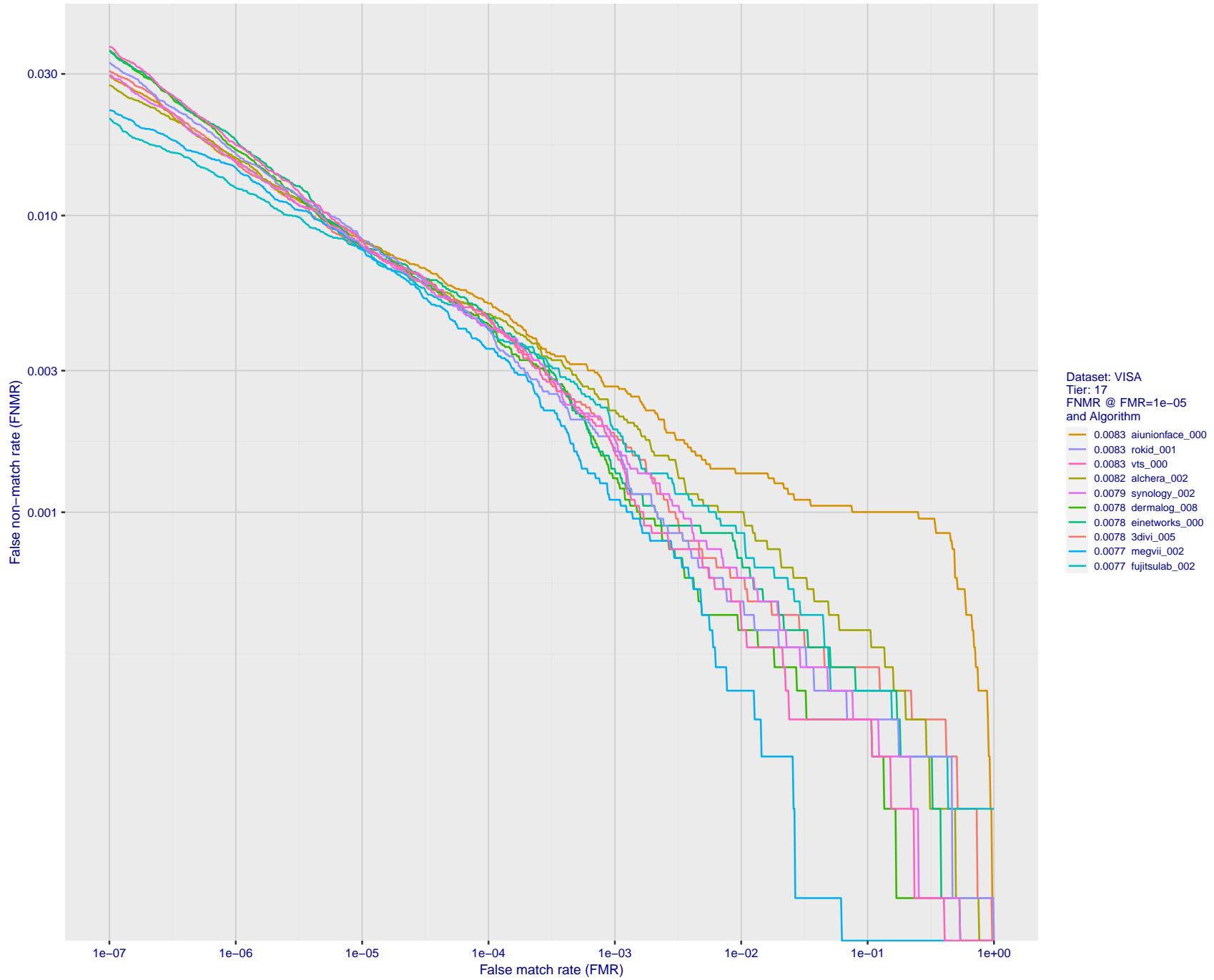


Figure 35: For the visa images, detection error tradeoff (DET) characteristics showing false non-match rate vs. false match rate plotted parametrically on threshold,  $T$ . The scales are logarithmic in order to show many decades of FMR.

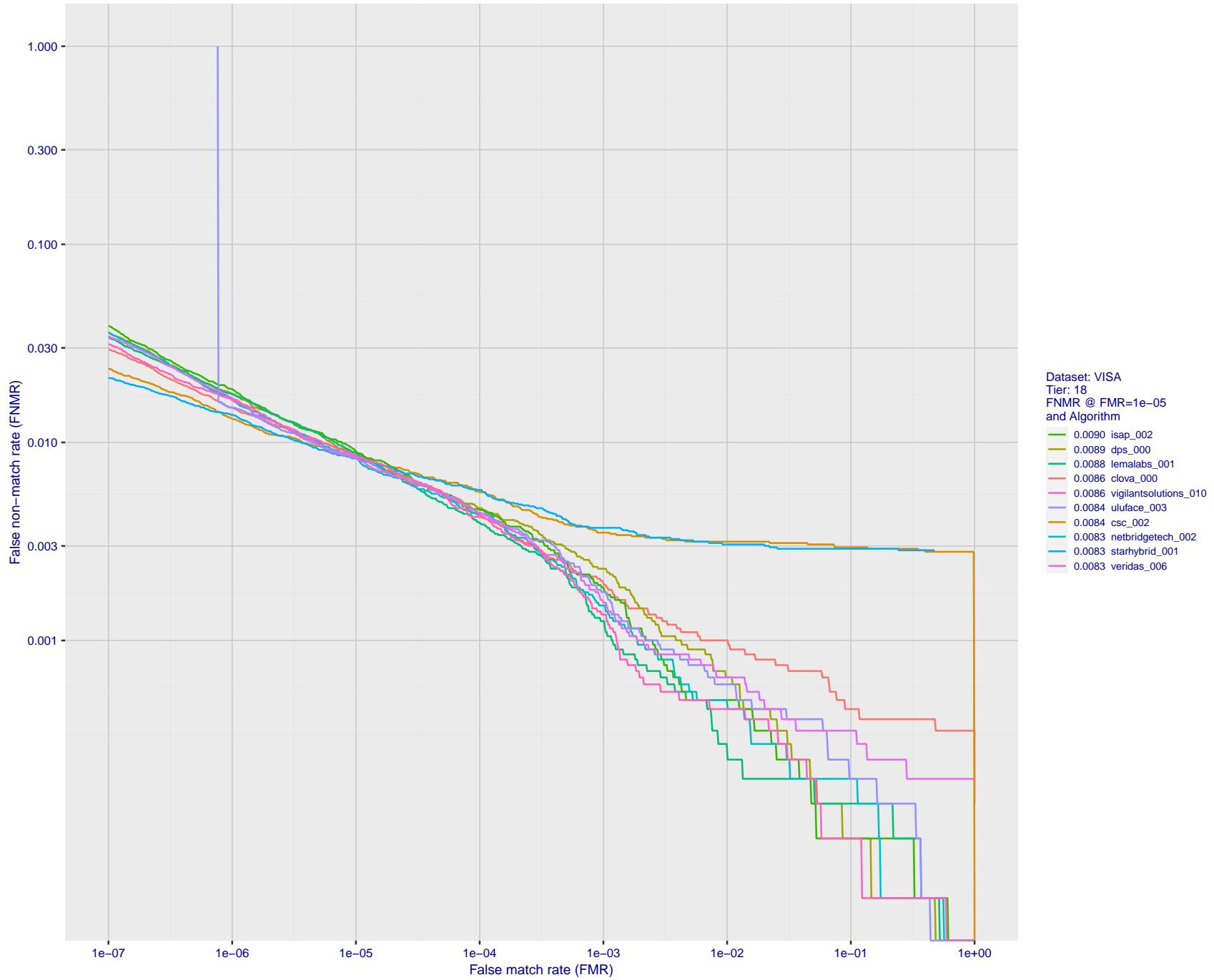


Figure 36: For the visa images, detection error tradeoff (DET) characteristics showing false non-match rate vs. false match rate plotted parametrically on threshold,  $T$ . The scales are logarithmic in order to show many decades of FMR.

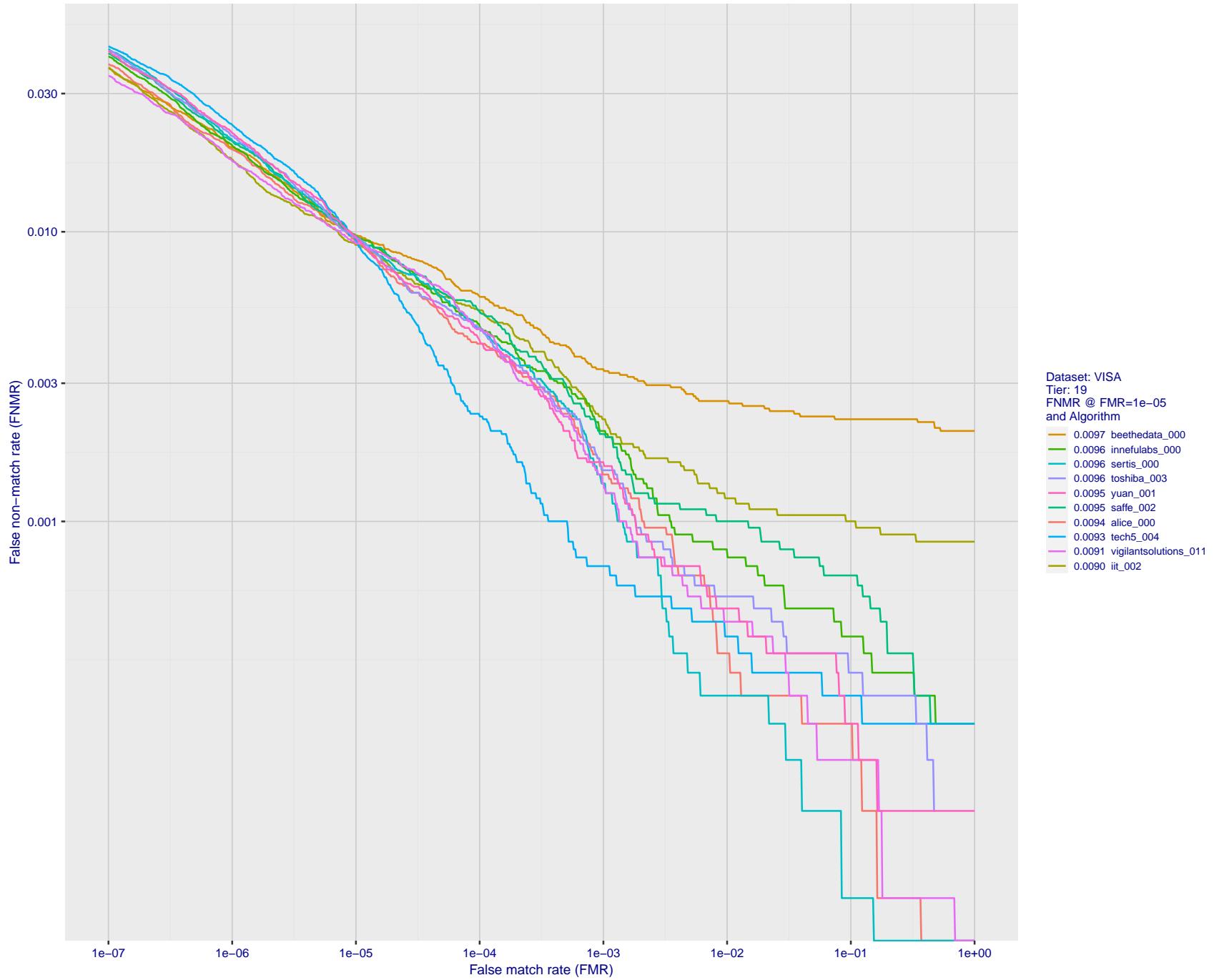
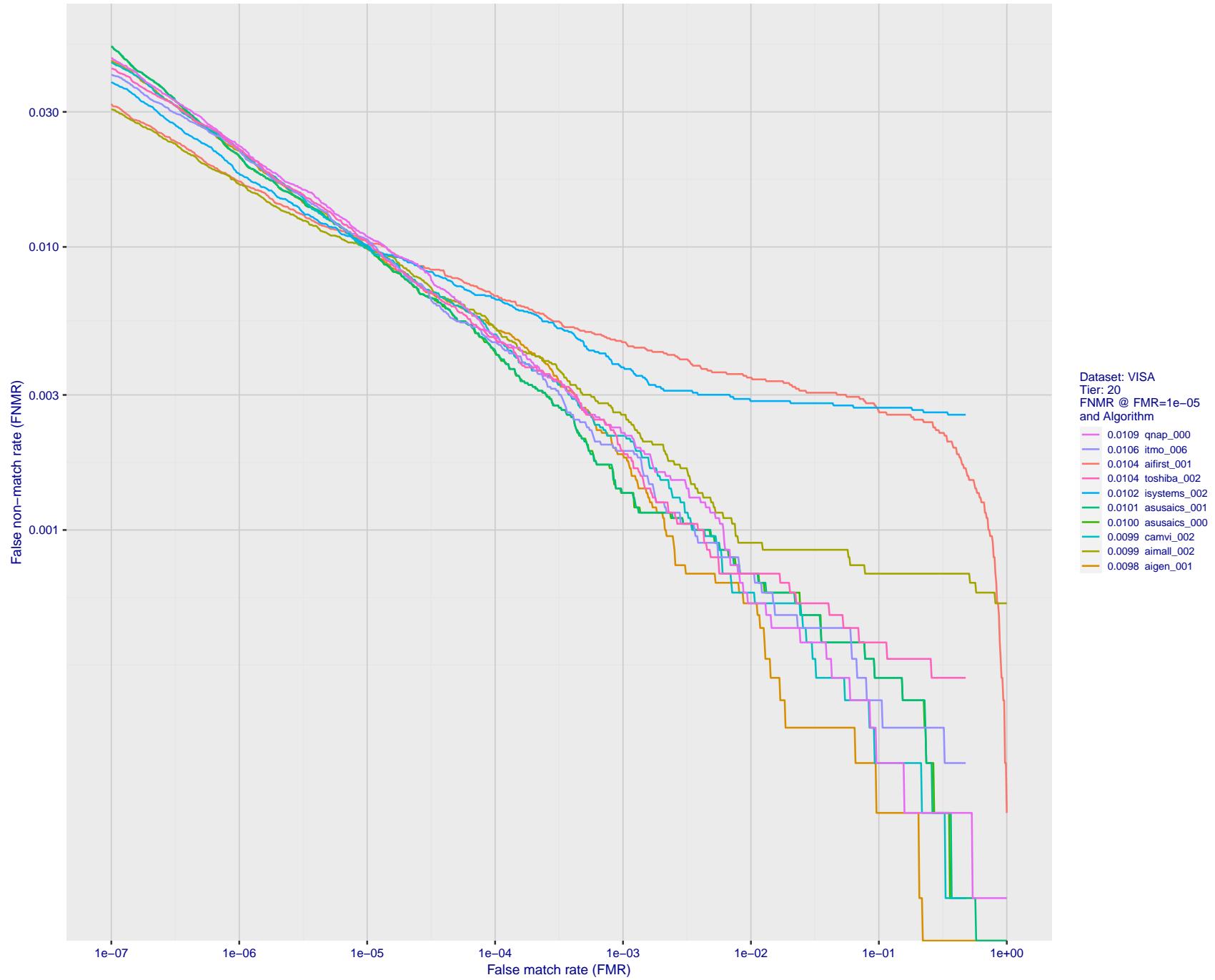


Figure 37: For the visa images, detection error tradeoff (DET) characteristics showing false non-match rate vs. false match rate plotted parametrically on threshold,  $T$ . The scales are logarithmic in order to show many decades of FMR.



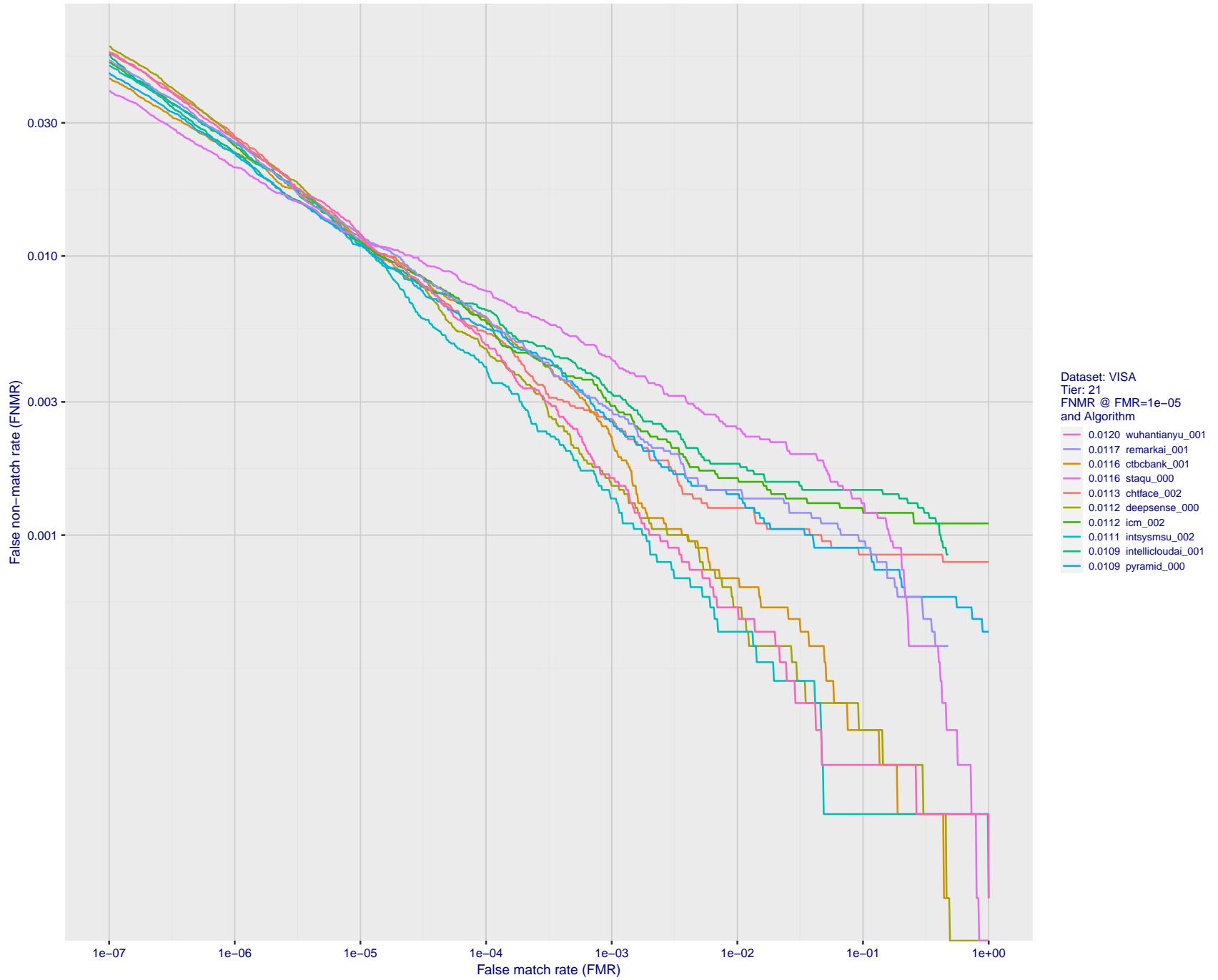


Figure 39: For the visa images, detection error tradeoff (DET) characteristics showing false non-match rate vs. false match rate plotted parametrically on threshold,  $T$ . The scales are logarithmic in order to show many decades of FMR.

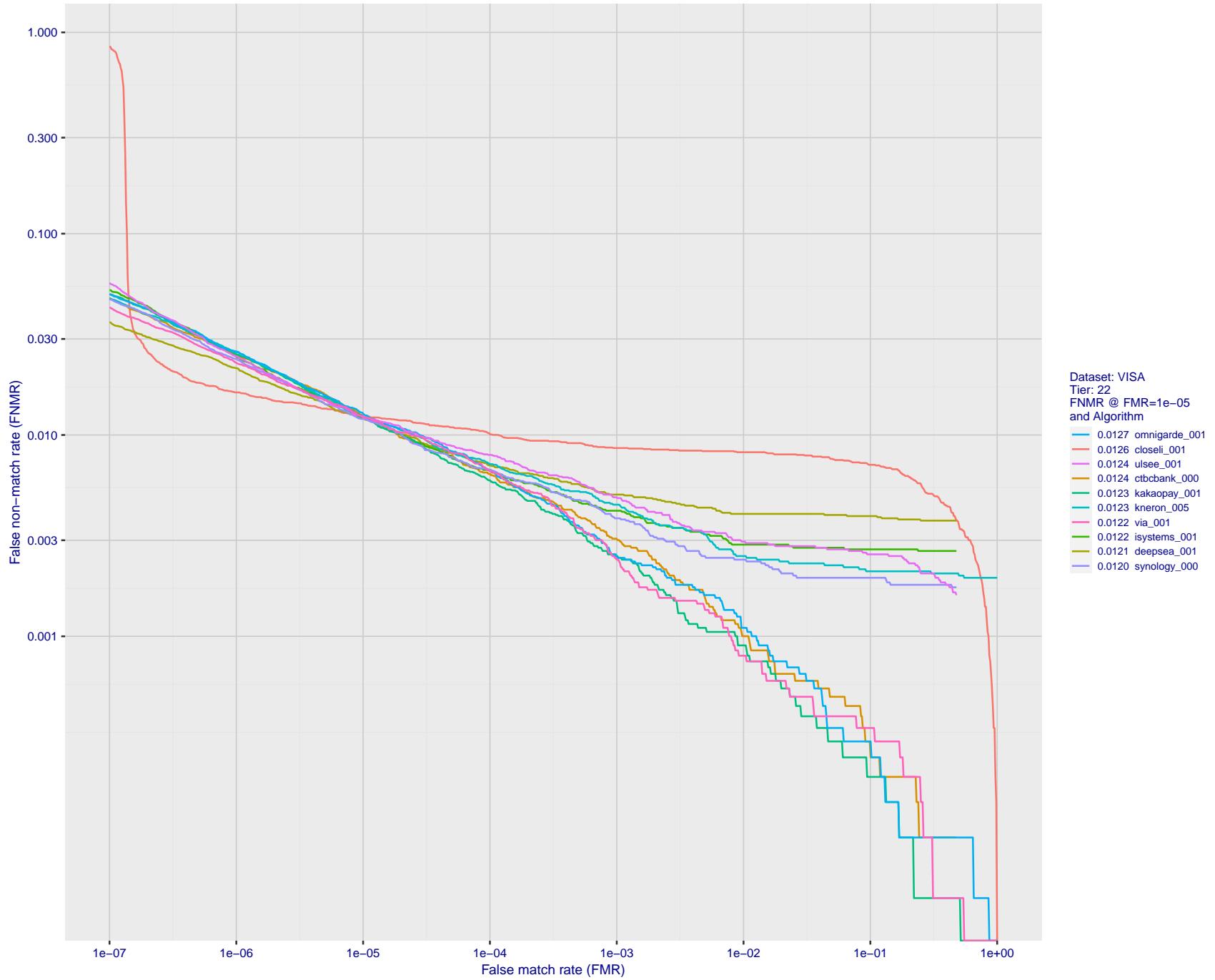


Figure 40: For the visa images, detection error tradeoff (DET) characteristics showing false non-match rate vs. false match rate plotted parametrically on threshold,  $T$ . The scales are logarithmic in order to show many decades of FMR.

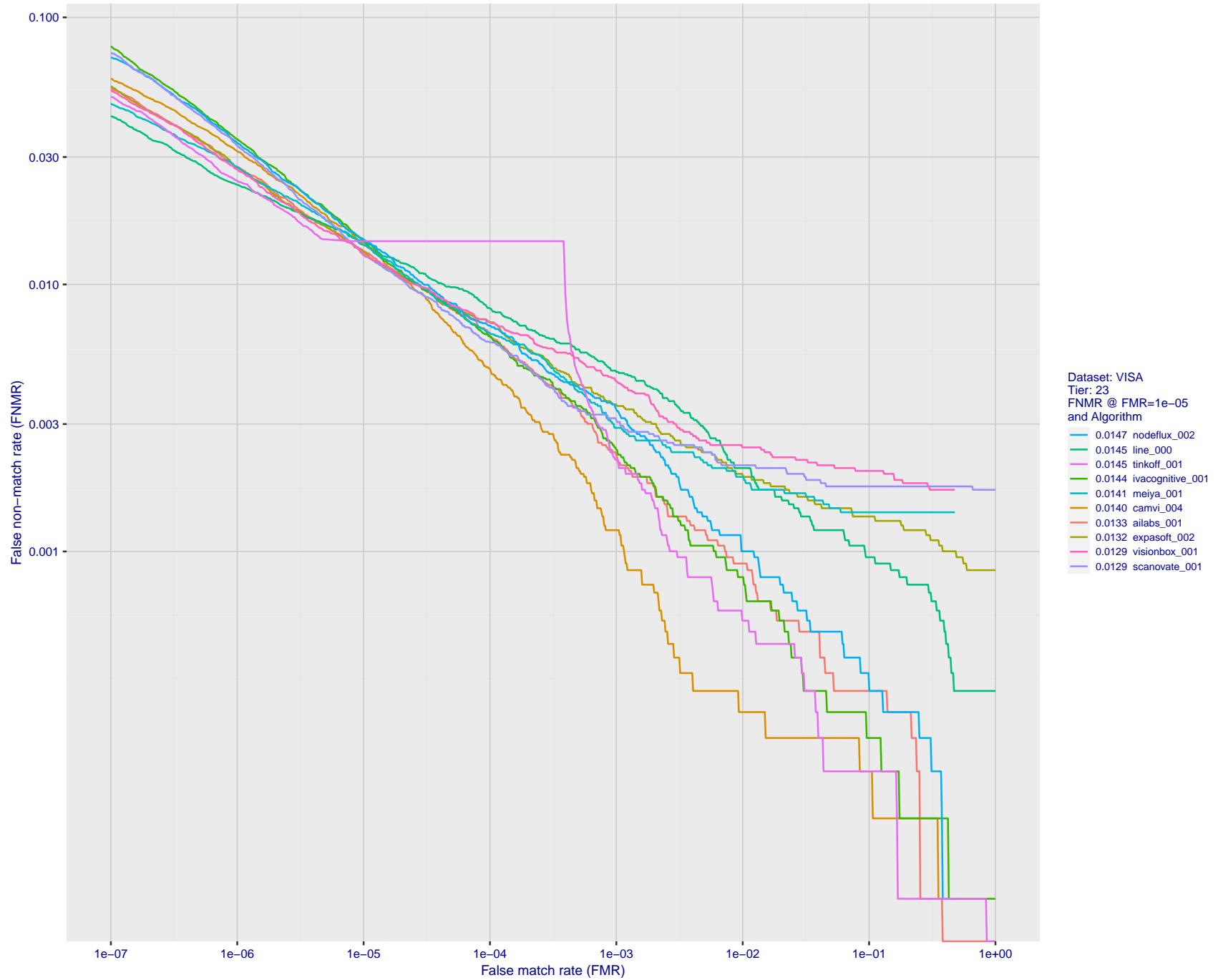


Figure 41: For the visa images, detection error tradeoff (DET) characteristics showing false non-match rate vs. false match rate plotted parametrically on threshold,  $T$ . The scales are logarithmic in order to show many decades of FMR.

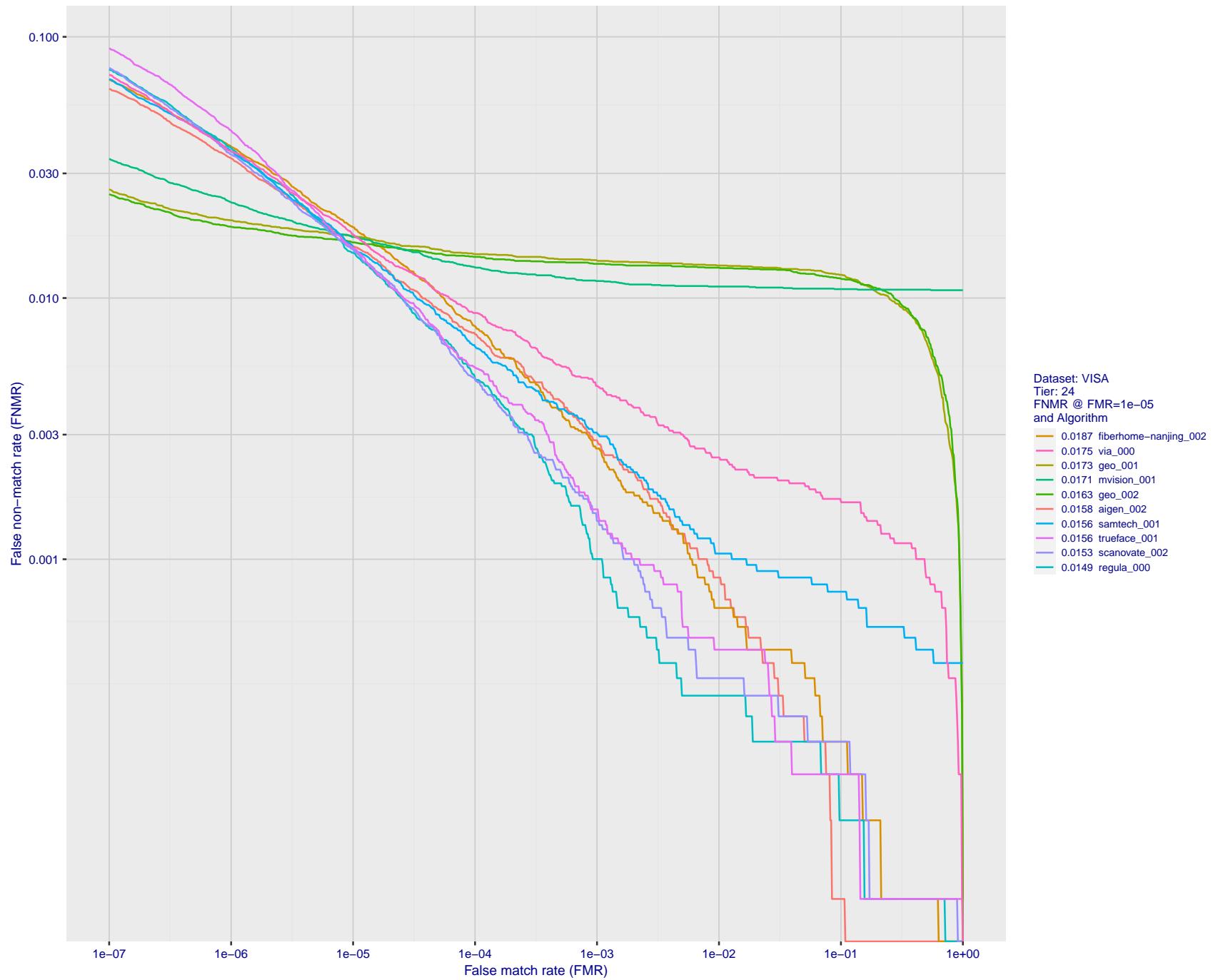


Figure 42: For the visa images, detection error tradeoff (DET) characteristics showing false non-match rate vs. false match rate plotted parametrically on threshold,  $T$ . The scales are logarithmic in order to show many decades of FMR.

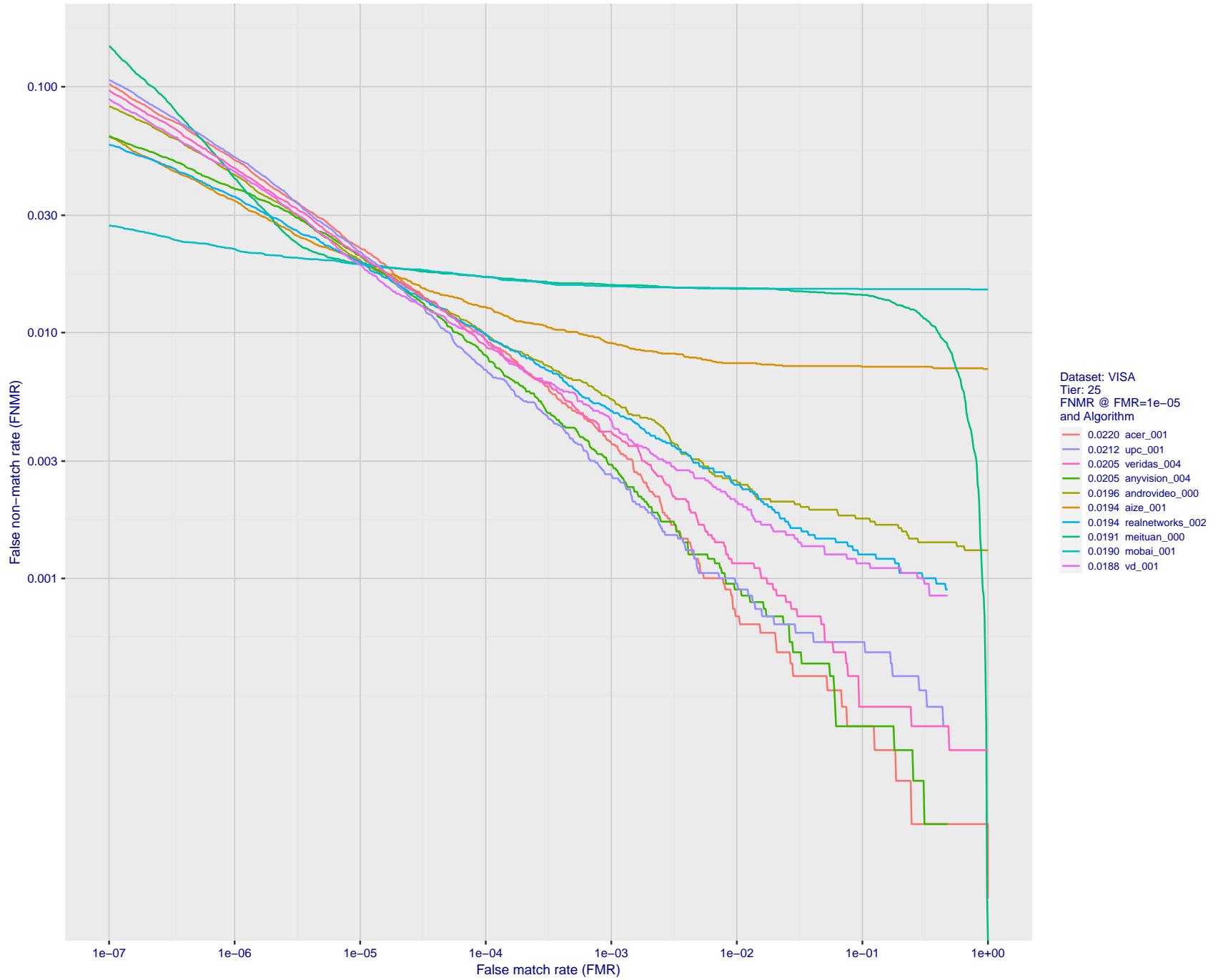


Figure 43: For the visa images, detection error tradeoff (DET) characteristics showing false non-match rate vs. false match rate plotted parametrically on threshold,  $T$ . The scales are logarithmic in order to show many decades of FMR.

2021/09/10 10:17:25

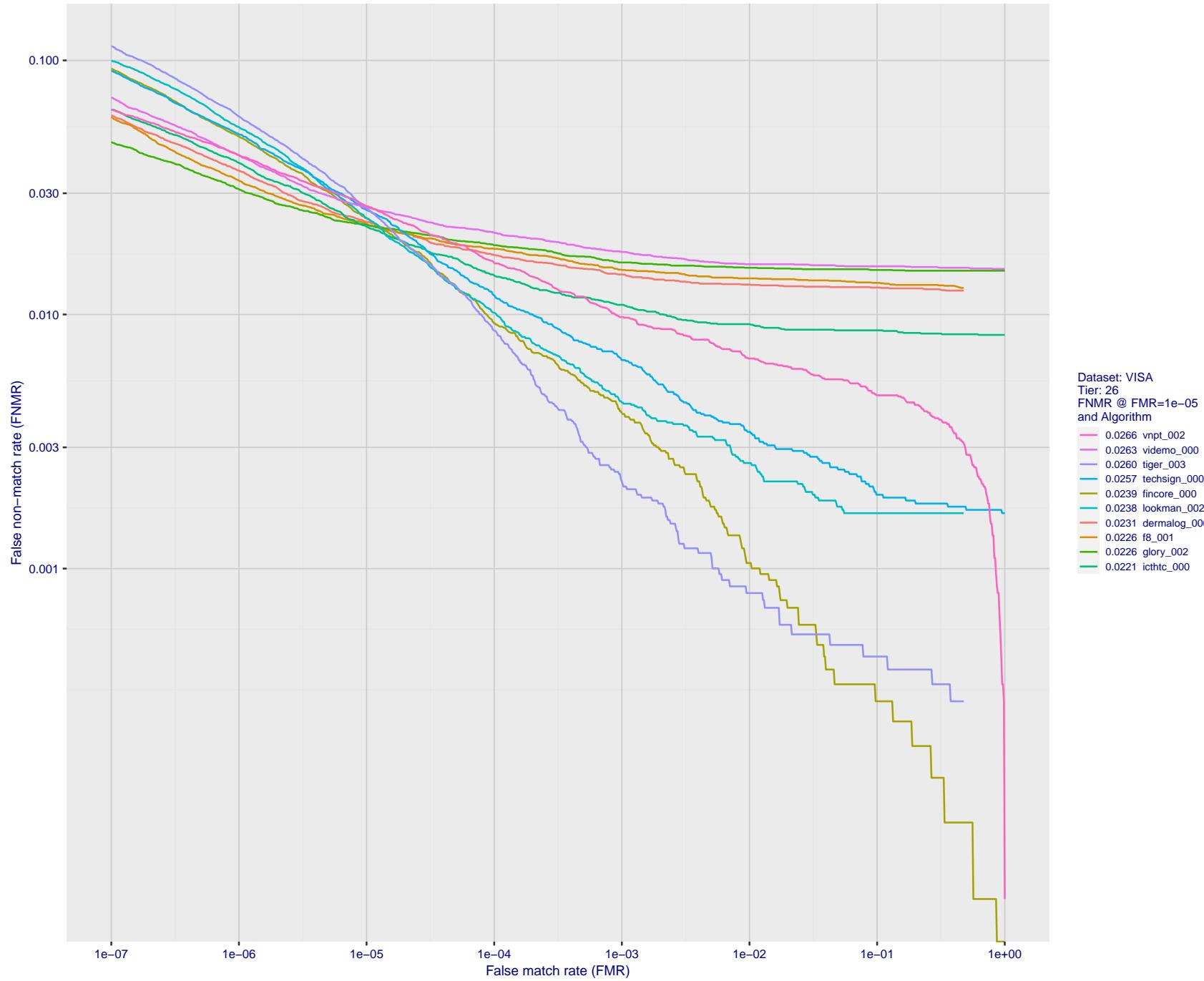


Figure 44: For the visa images, detection error tradeoff (DET) characteristics showing false non-match rate vs. false match rate plotted parametrically on threshold,  $T$ . The scales are logarithmic in order to show many decades of FMR.

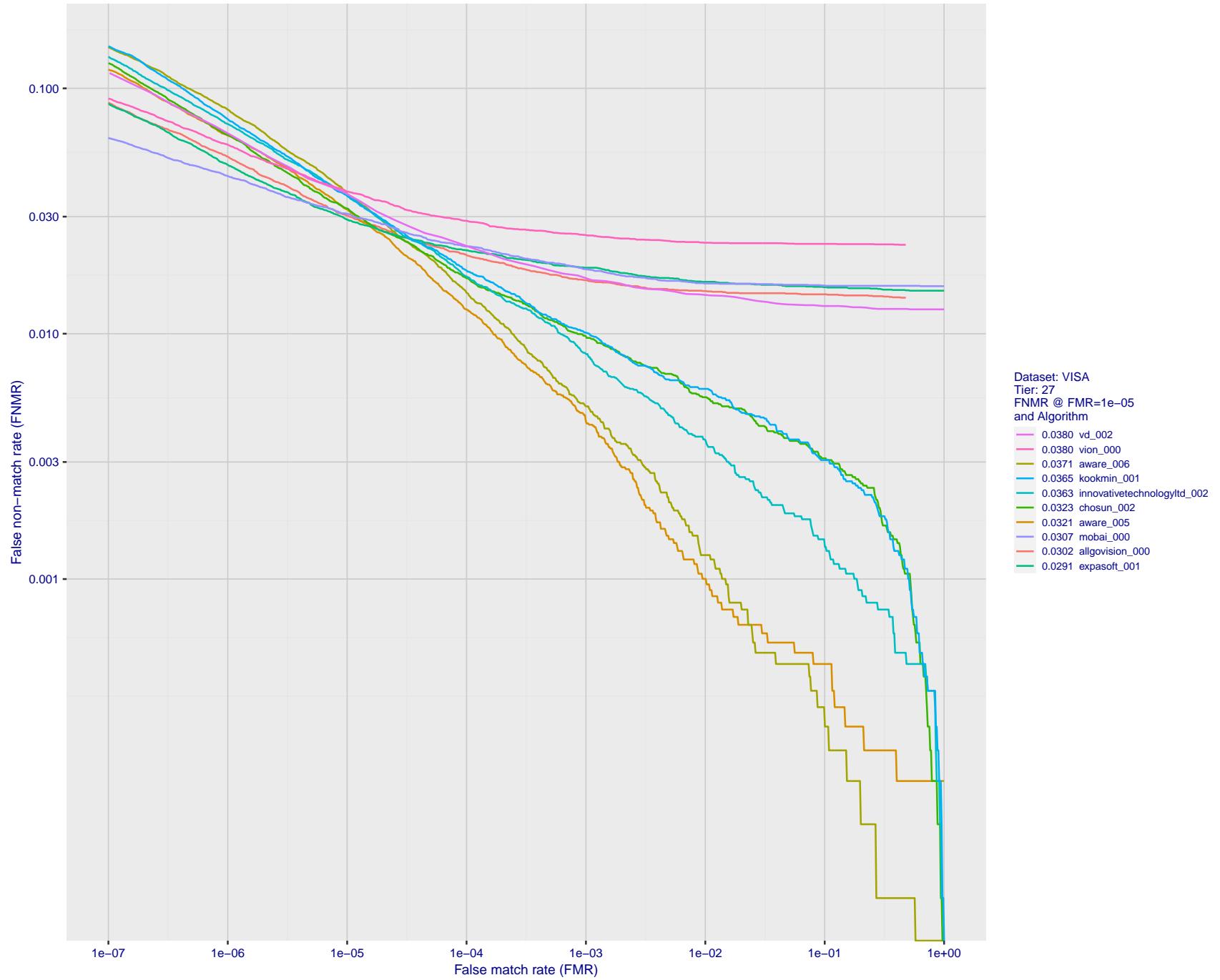


Figure 45: For the visa images, detection error tradeoff (DET) characteristics showing false non-match rate vs. false match rate plotted parametrically on threshold,  $T$ . The scales are logarithmic in order to show many decades of FMR.

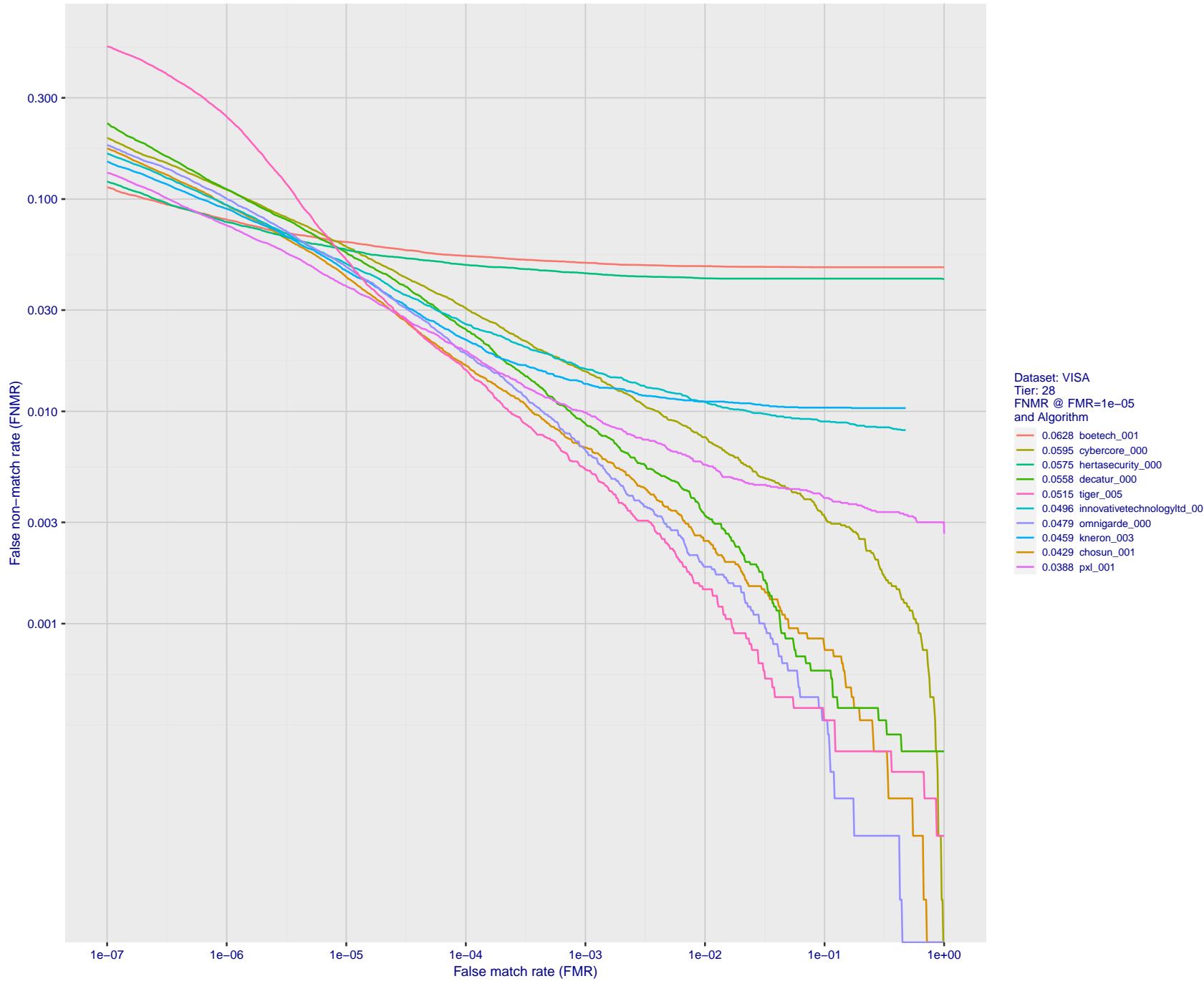


Figure 46: For the visa images, detection error tradeoff (DET) characteristics showing false non-match rate vs. false match rate plotted parametrically on threshold,  $T$ . The scales are logarithmic in order to show many decades of FMR.

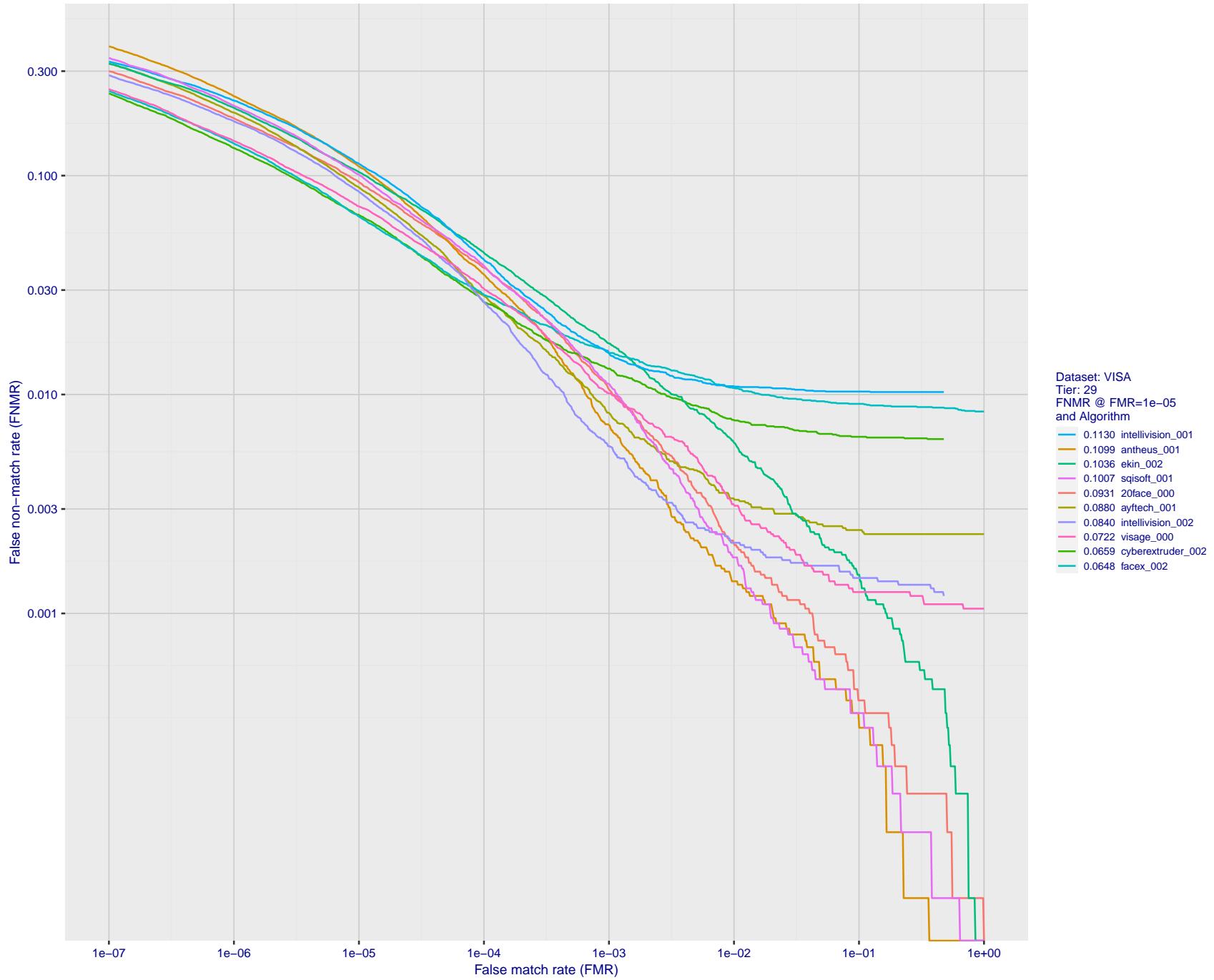


Figure 47: For the visa images, detection error tradeoff (DET) characteristics showing false non-match rate vs. false match rate plotted parametrically on threshold,  $T$ . The scales are logarithmic in order to show many decades of FMR.

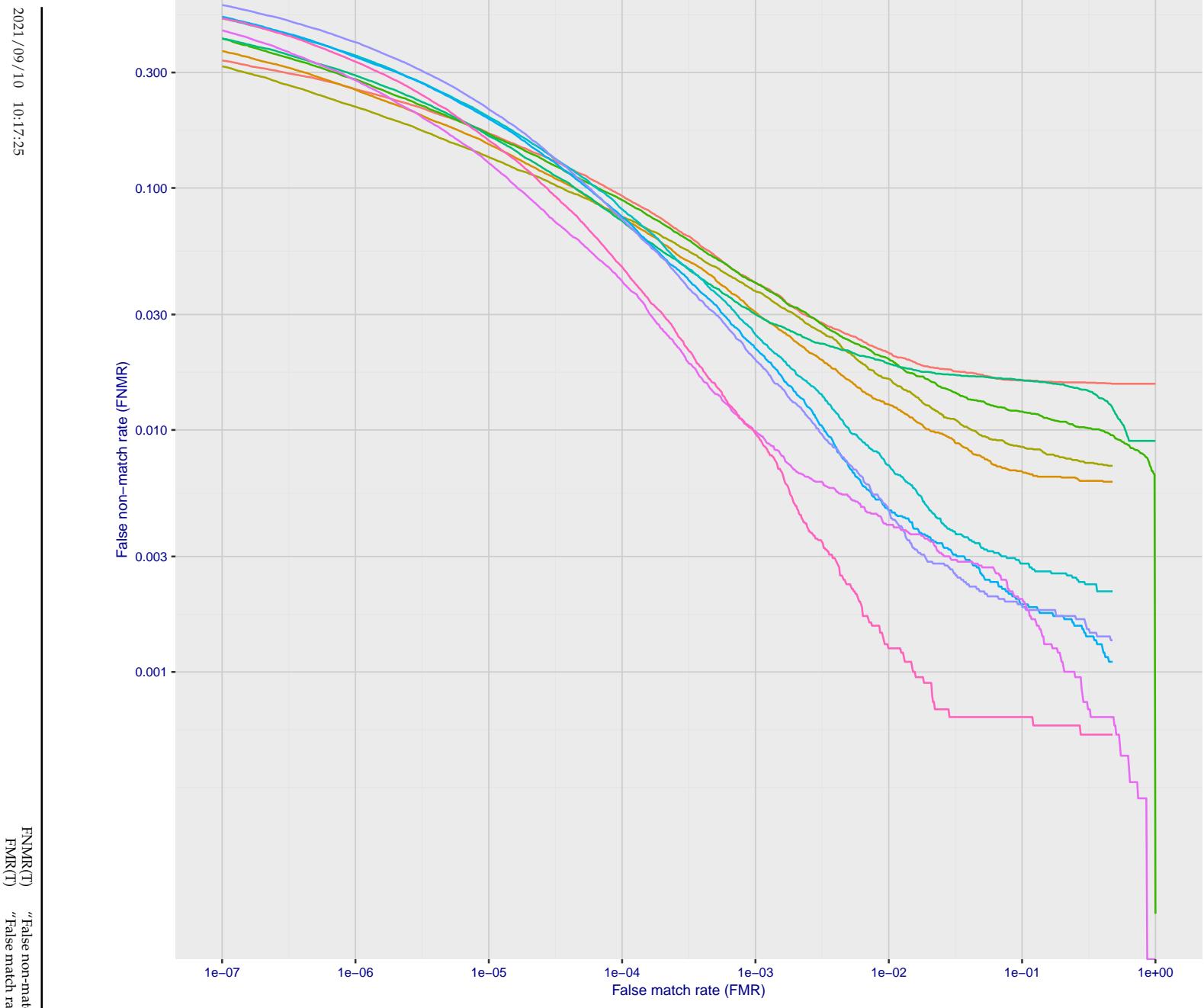


Figure 48: For the visa images, detection error tradeoff (DET) characteristics showing false non-match rate vs. false match rate plotted parametrically on threshold,  $T$ . The scales are logarithmic in order to show many decades of FMR.

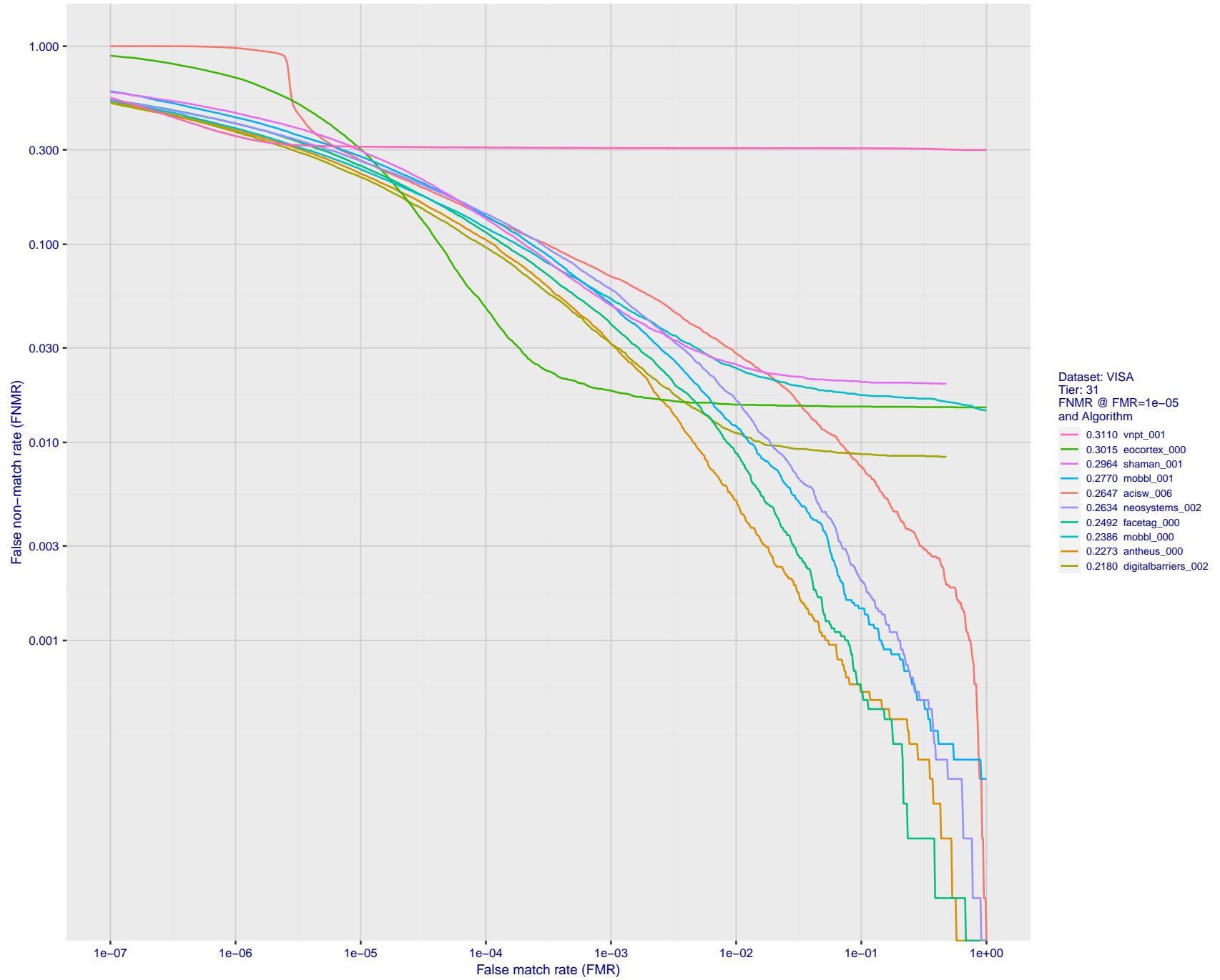


Figure 49: For the visa images, detection error tradeoff (DET) characteristics showing false non-match rate vs. false match rate plotted parametrically on threshold,  $T$ . The scales are logarithmic in order to show many decades of FMR.

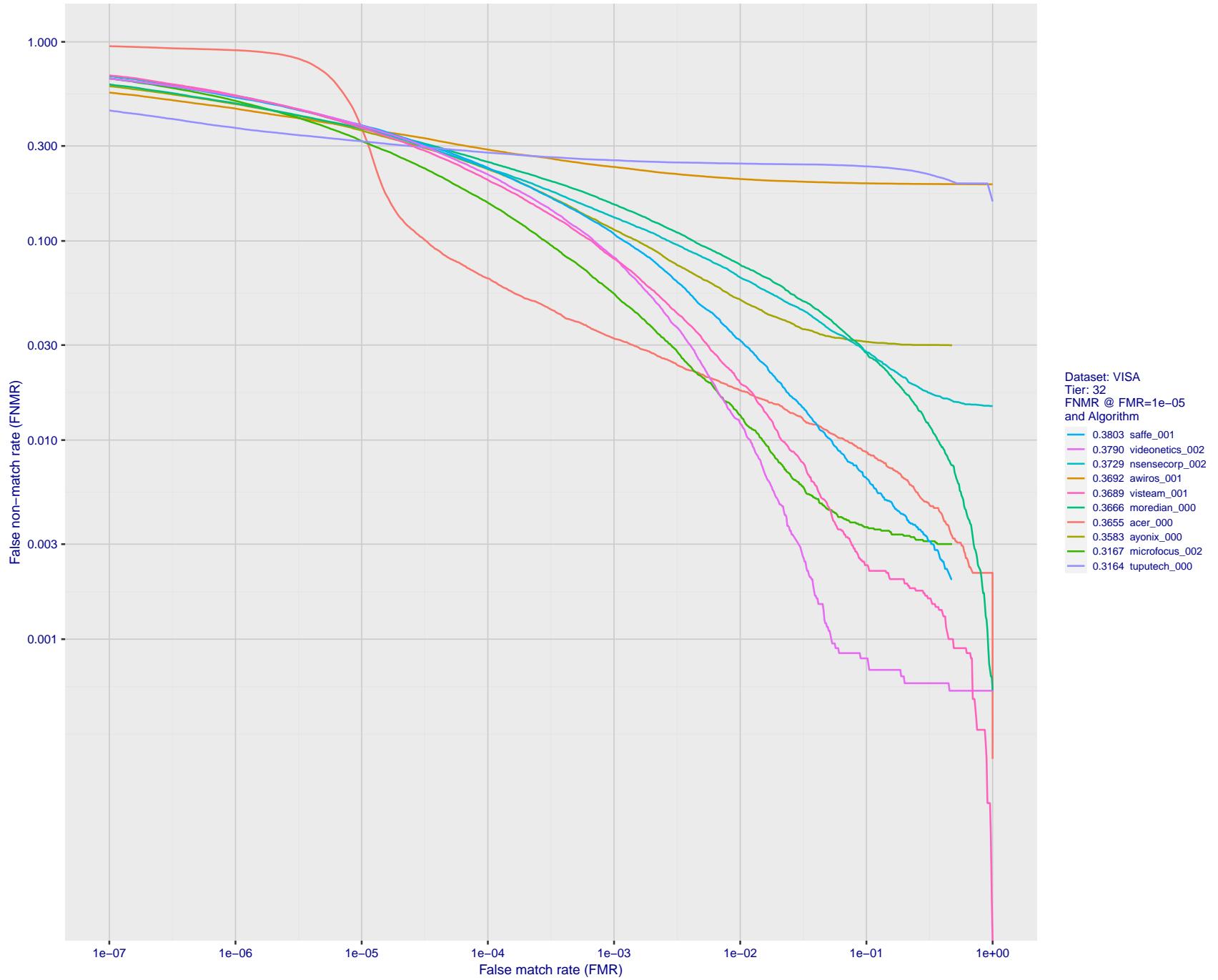


Figure 50: For the visa images, detection error tradeoff (DET) characteristics showing false non-match rate vs. false match rate plotted parametrically on threshold,  $T$ . The scales are logarithmic in order to show many decades of FMR.

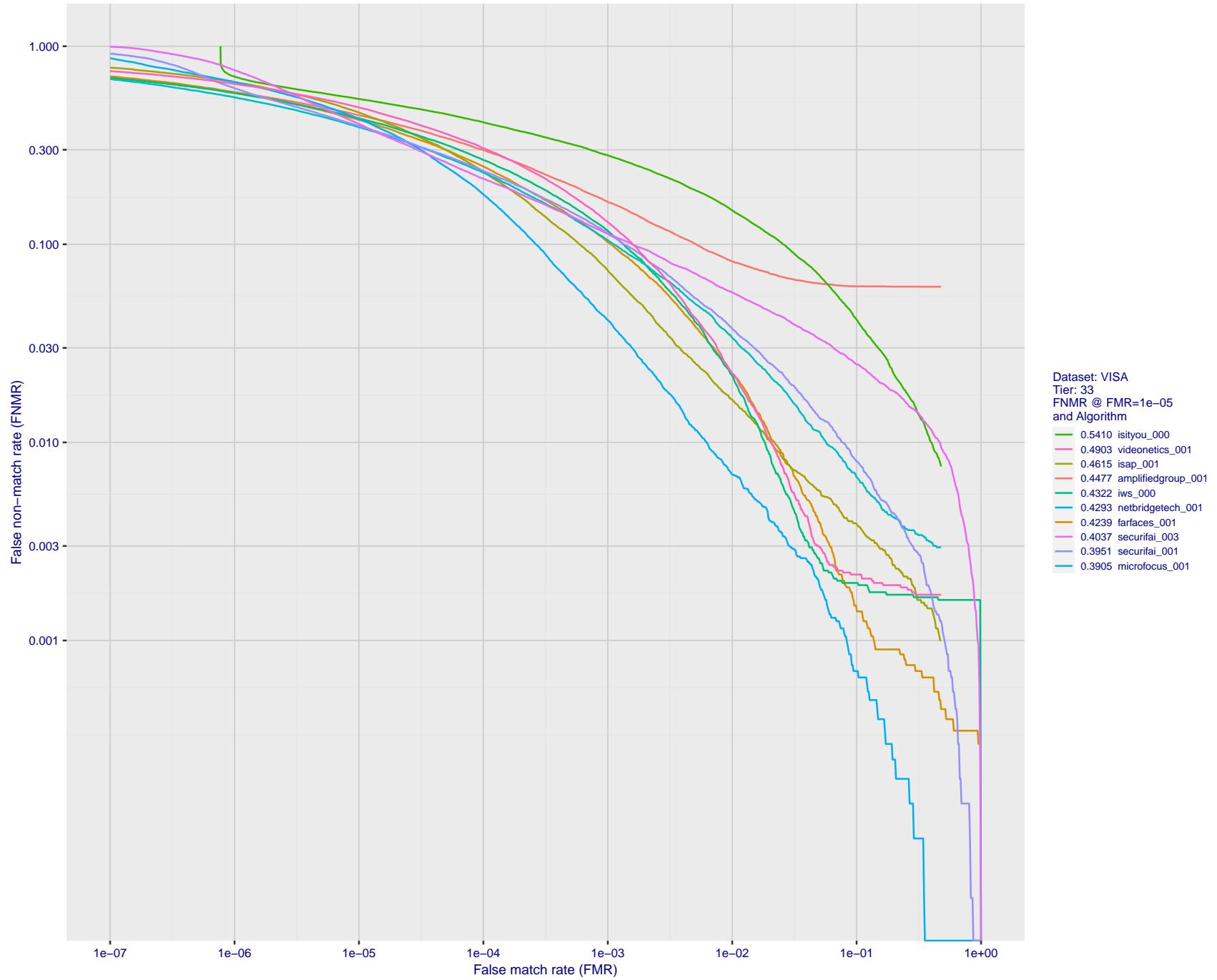


Figure 51: For the visa images, detection error tradeoff (DET) characteristics showing false non-match rate vs. false match rate plotted parametrically on threshold,  $T$ . The scales are logarithmic in order to show many decades of FMR.

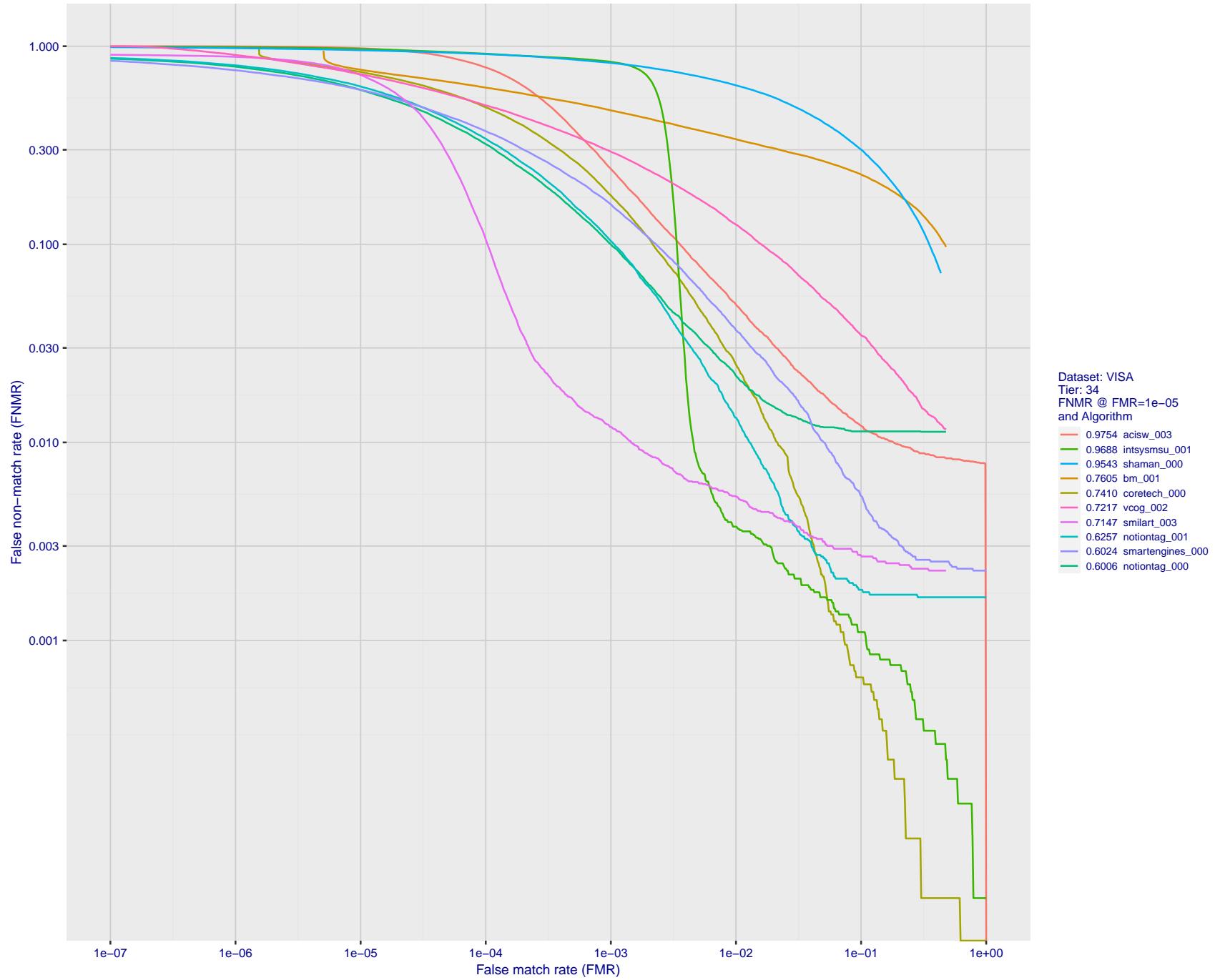


Figure 52: For the visa images, detection error tradeoff (DET) characteristics showing false non-match rate vs. false match rate plotted parametrically on threshold,  $T$ . The scales are logarithmic in order to show many decades of FMR.

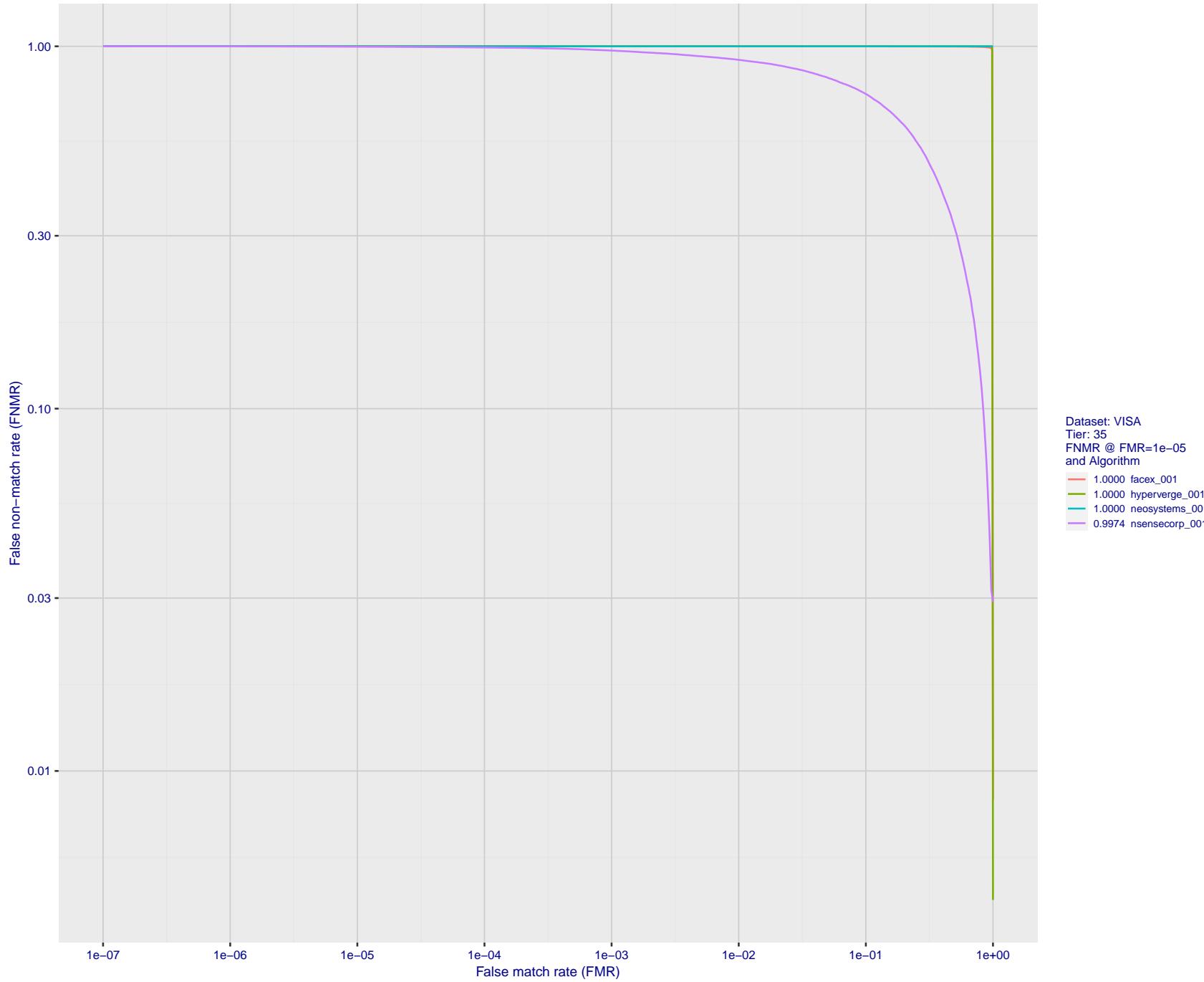


Figure 53: For the visa images, detection error tradeoff (DET) characteristics showing false non-match rate vs. false match rate plotted parametrically on threshold,  $T$ . The scales are logarithmic in order to show many decades of FMR.

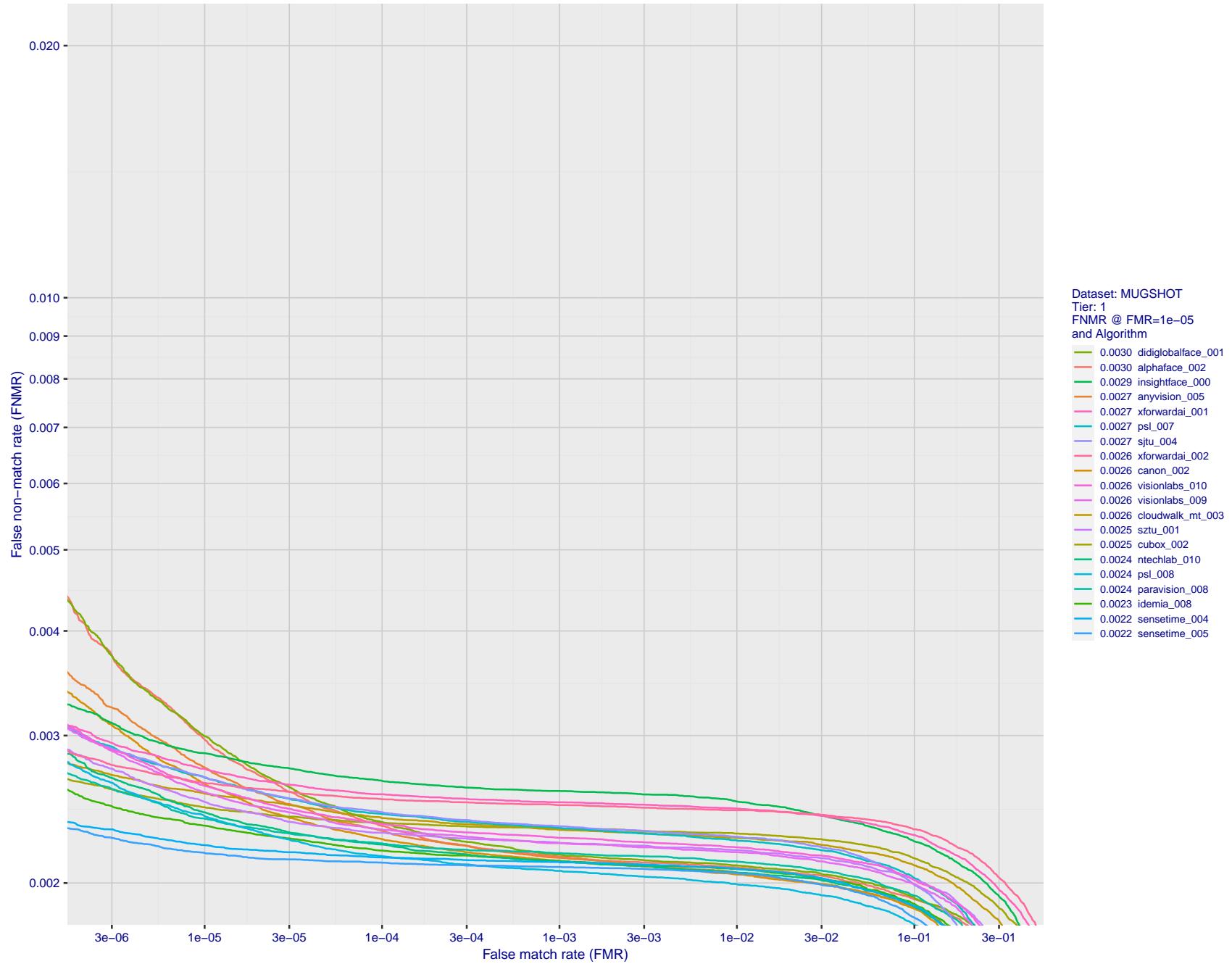


Figure 54: For the mugshot images, detection error tradeoff (DET) characteristics showing false non-match rate vs. false match rate plotted parametrically on threshold,  $T$ . The scales are logarithmic in order to show decades of FMR.

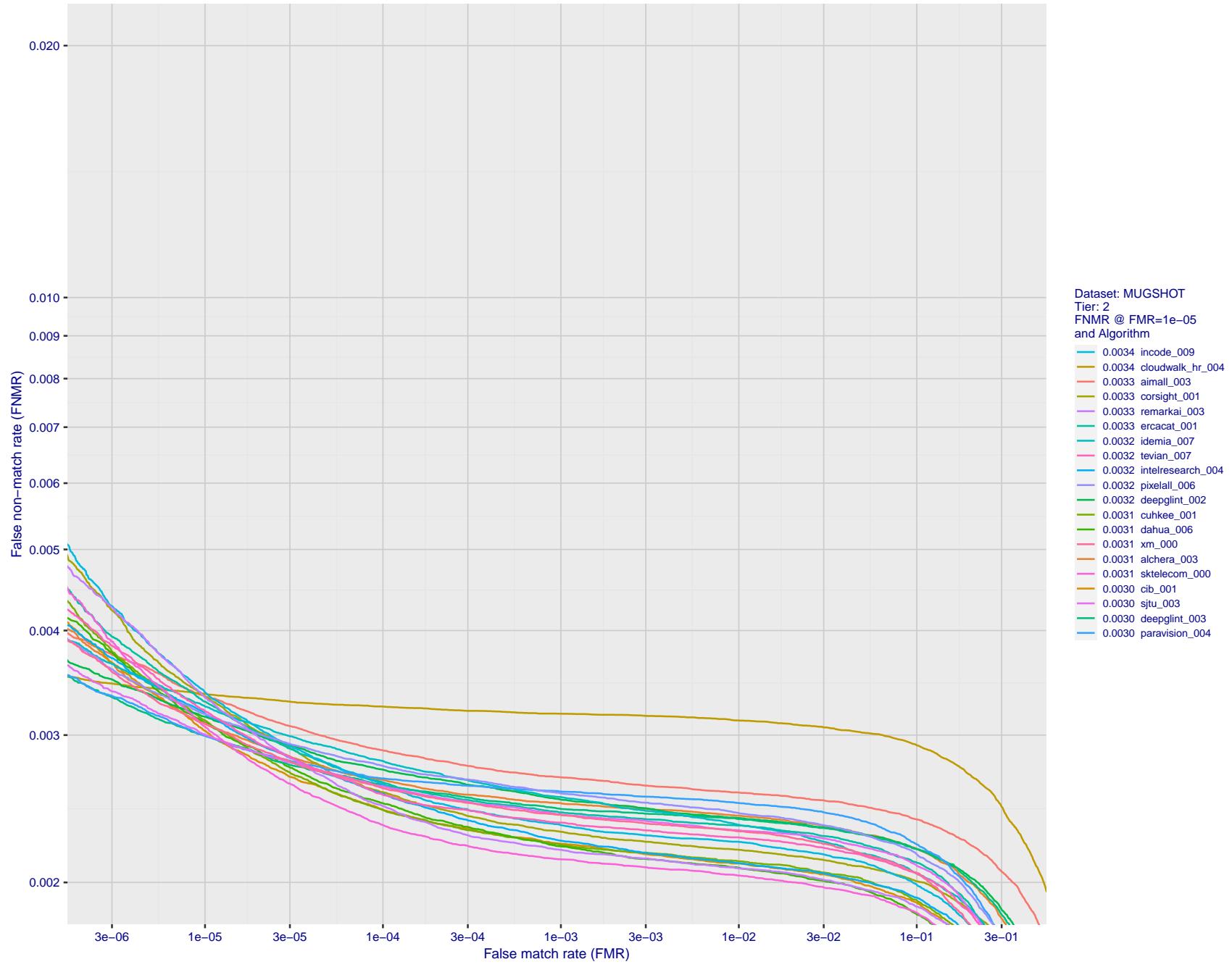


Figure 55: For the mugshot images, detection error tradeoff (DET) characteristics showing false non-match rate vs. false match rate plotted parametrically on threshold,  $T$ . The scales are logarithmic in order to show decades of FMR.

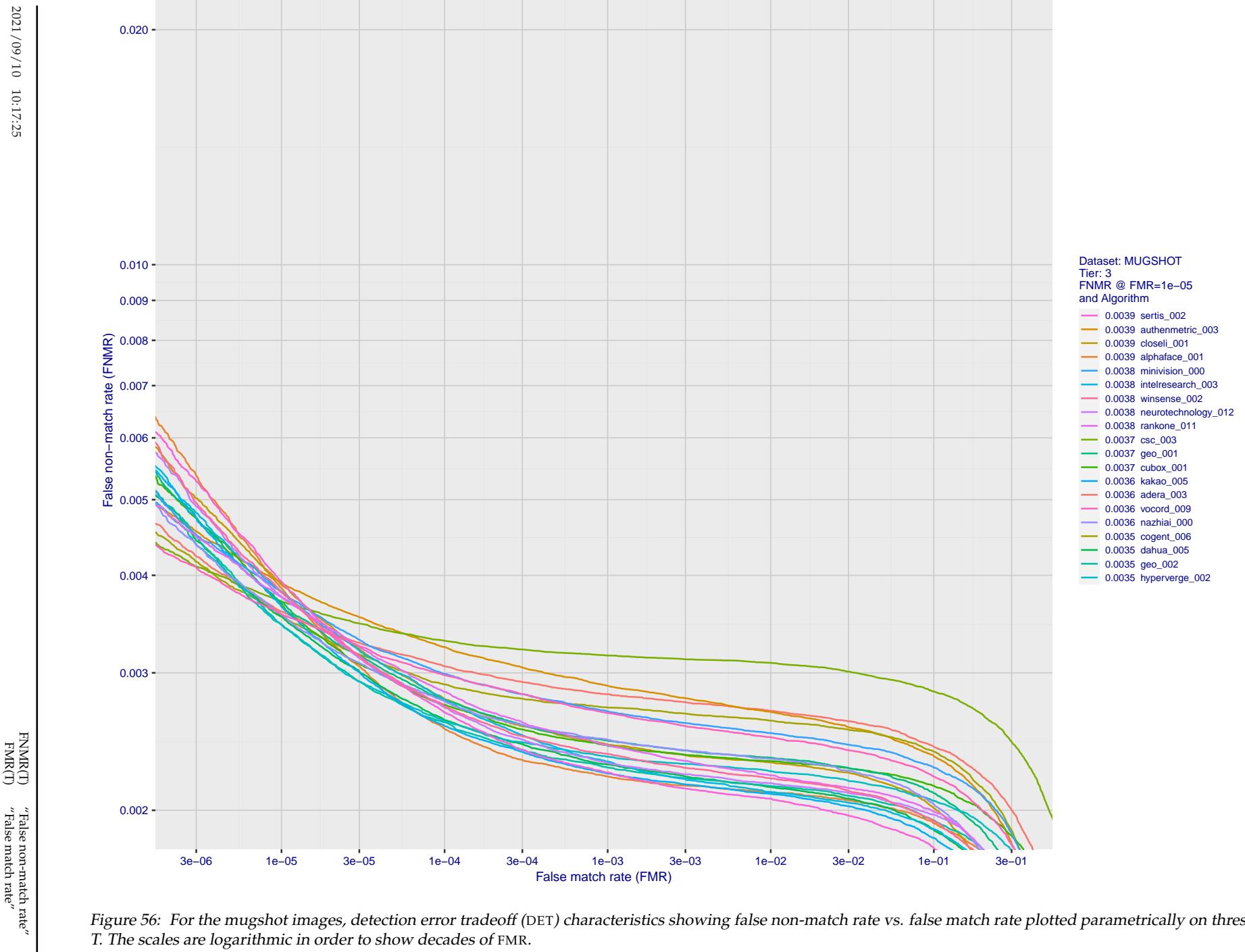


Figure 56: For the mugshot images, detection error tradeoff (DET) characteristics showing false non-match rate vs. false match rate plotted parametrically on threshold,  $T$ . The scales are logarithmic in order to show decades of FMR.

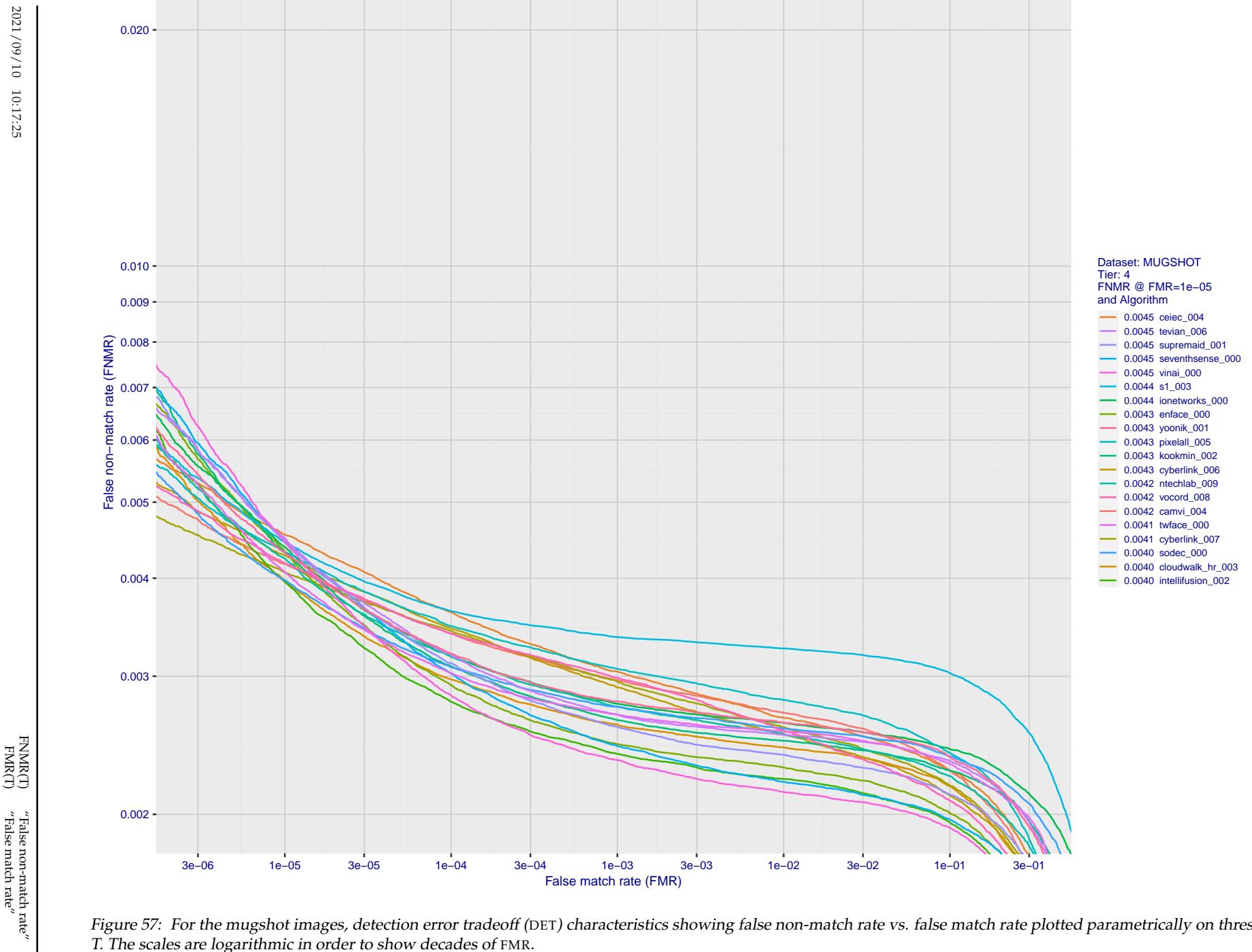


Figure 57: For the mugshot images, detection error tradeoff (DET) characteristics showing false non-match rate vs. false match rate plotted parametrically on threshold,  $T$ . The scales are logarithmic in order to show decades of FMR.

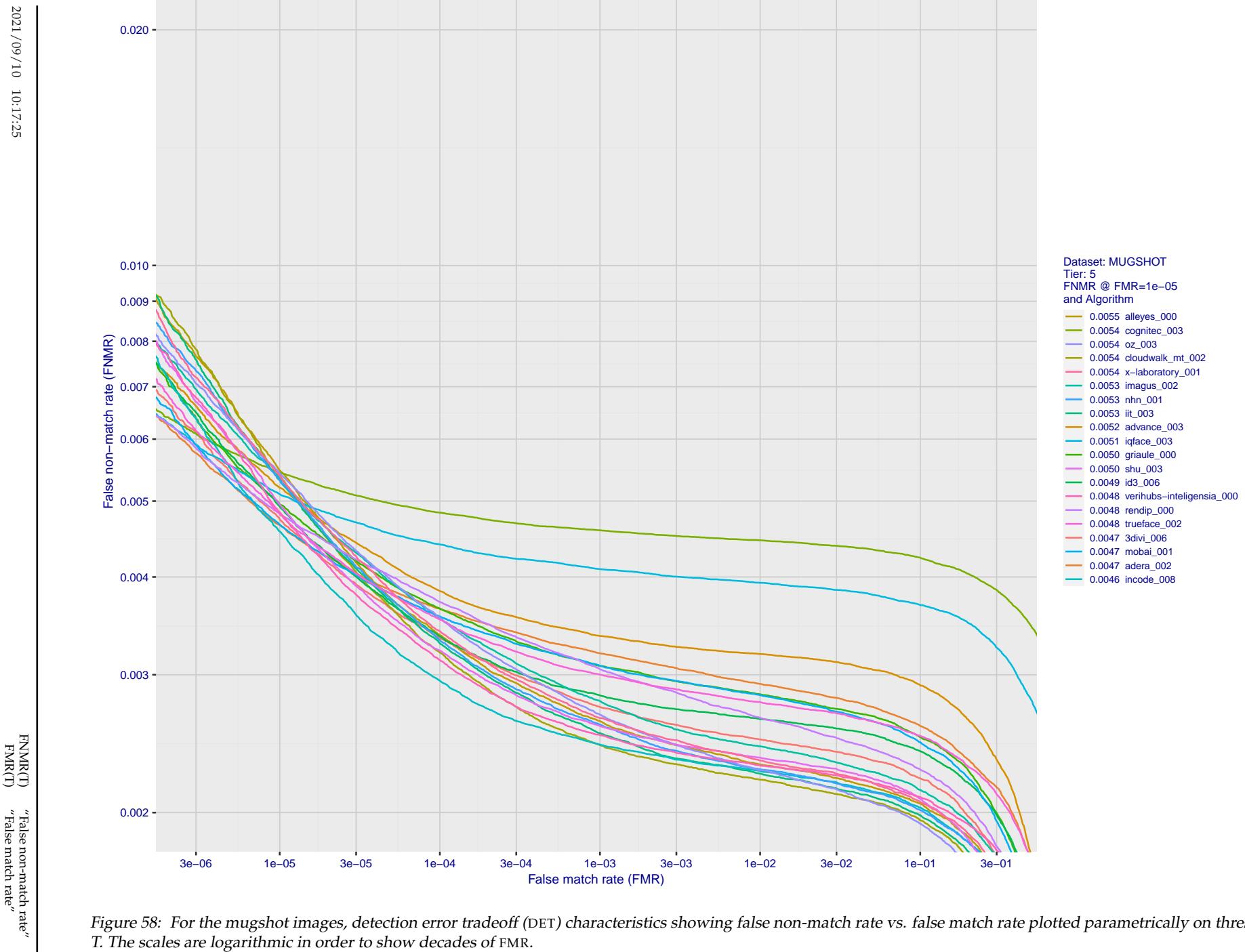


Figure 58: For the mugshot images, detection error tradeoff (DET) characteristics showing false non-match rate vs. false match rate plotted parametrically on threshold,  $T$ . The scales are logarithmic in order to show decades of FMR.

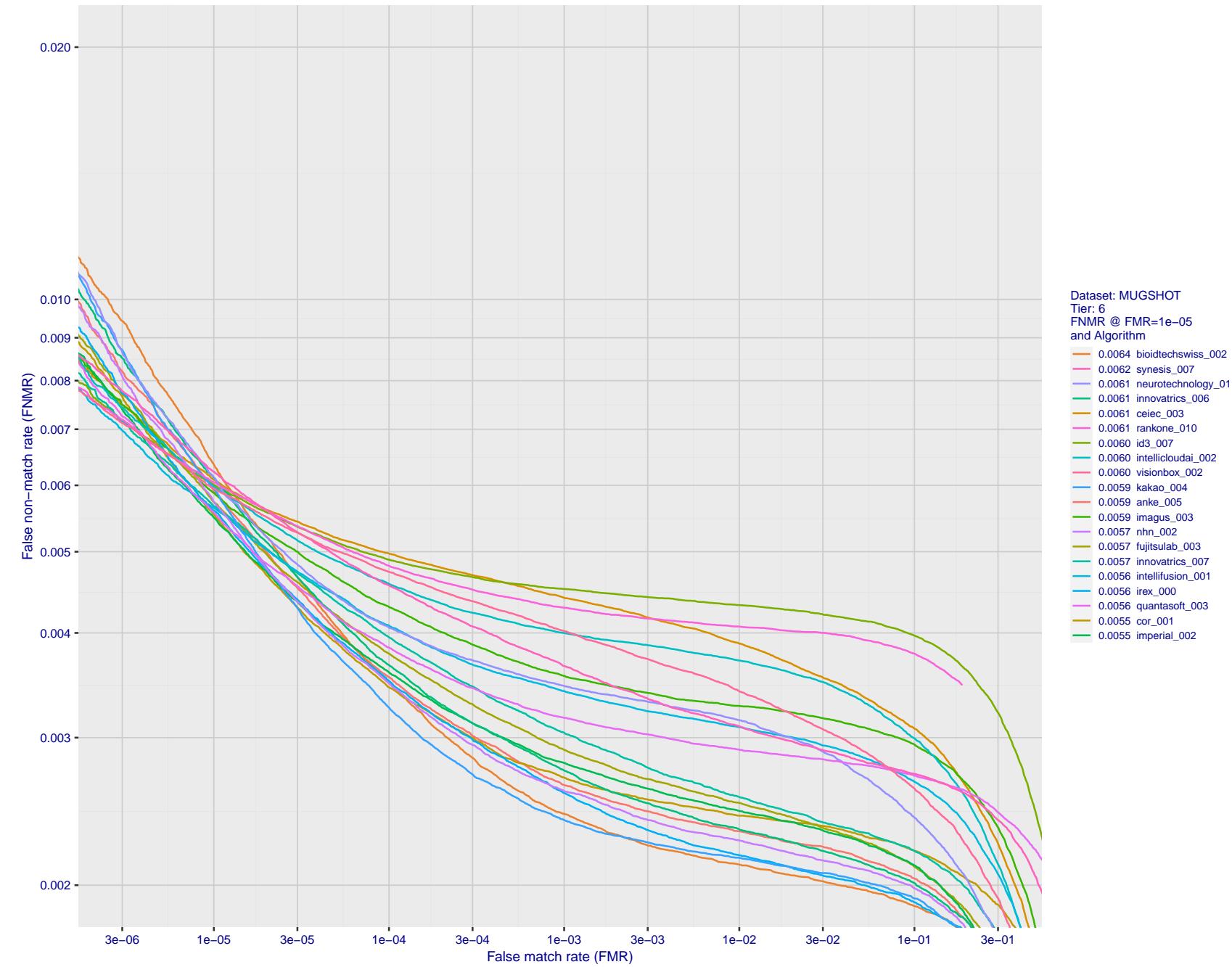
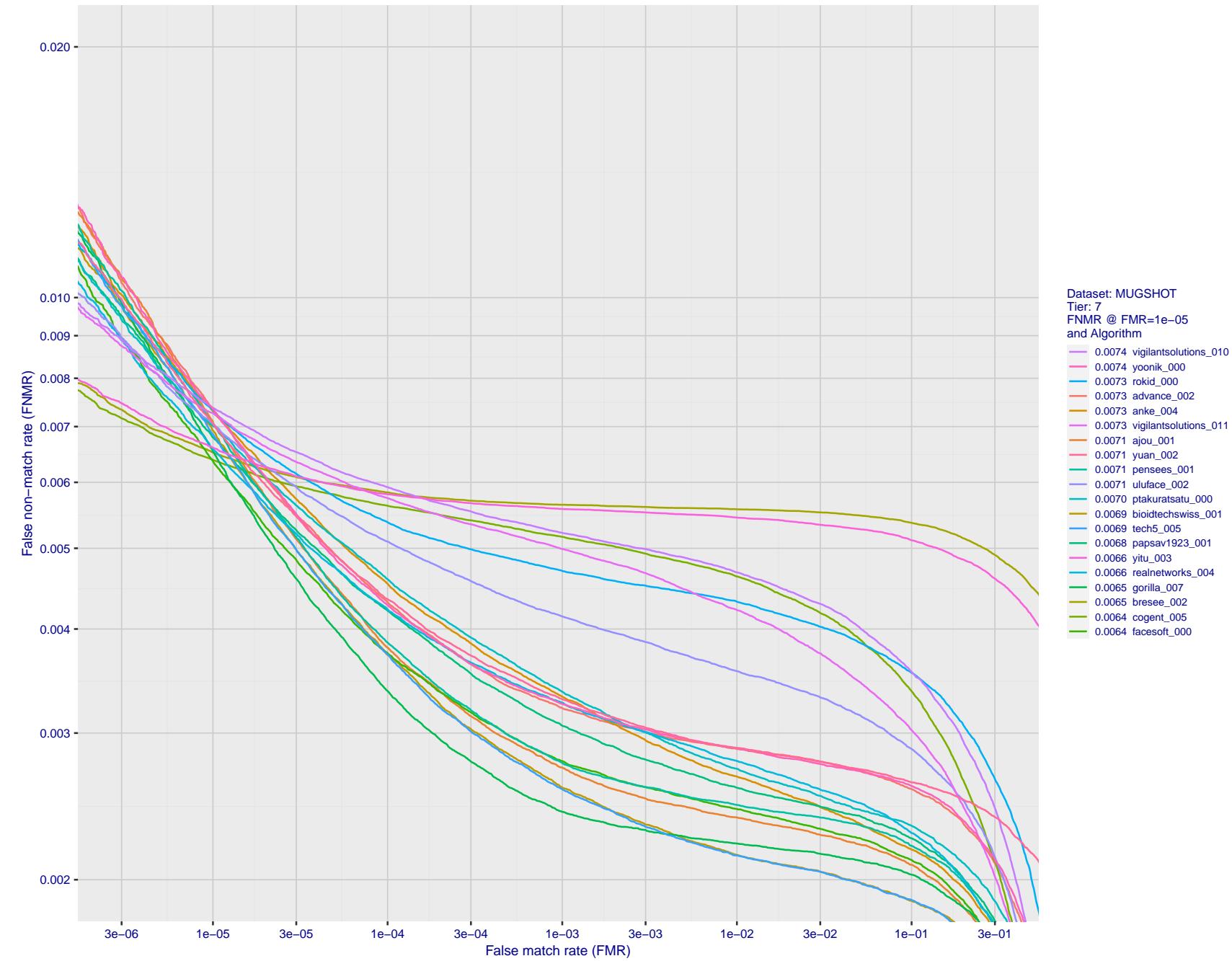


Figure 59: For the mugshot images, detection error tradeoff (DET) characteristics showing false non-match rate vs. false match rate plotted parametrically on threshold,  $T$ . The scales are logarithmic in order to show decades of FMR.



FNMR( $T$ )  
FMR( $T$ )  
"False non-match rate"  
"False match rate"

Figure 60: For the mugshot images, detection error tradeoff (DET) characteristics showing false non-match rate vs. false match rate plotted parametrically on threshold,  $T$ . The scales are logarithmic in order to show decades of FMR.

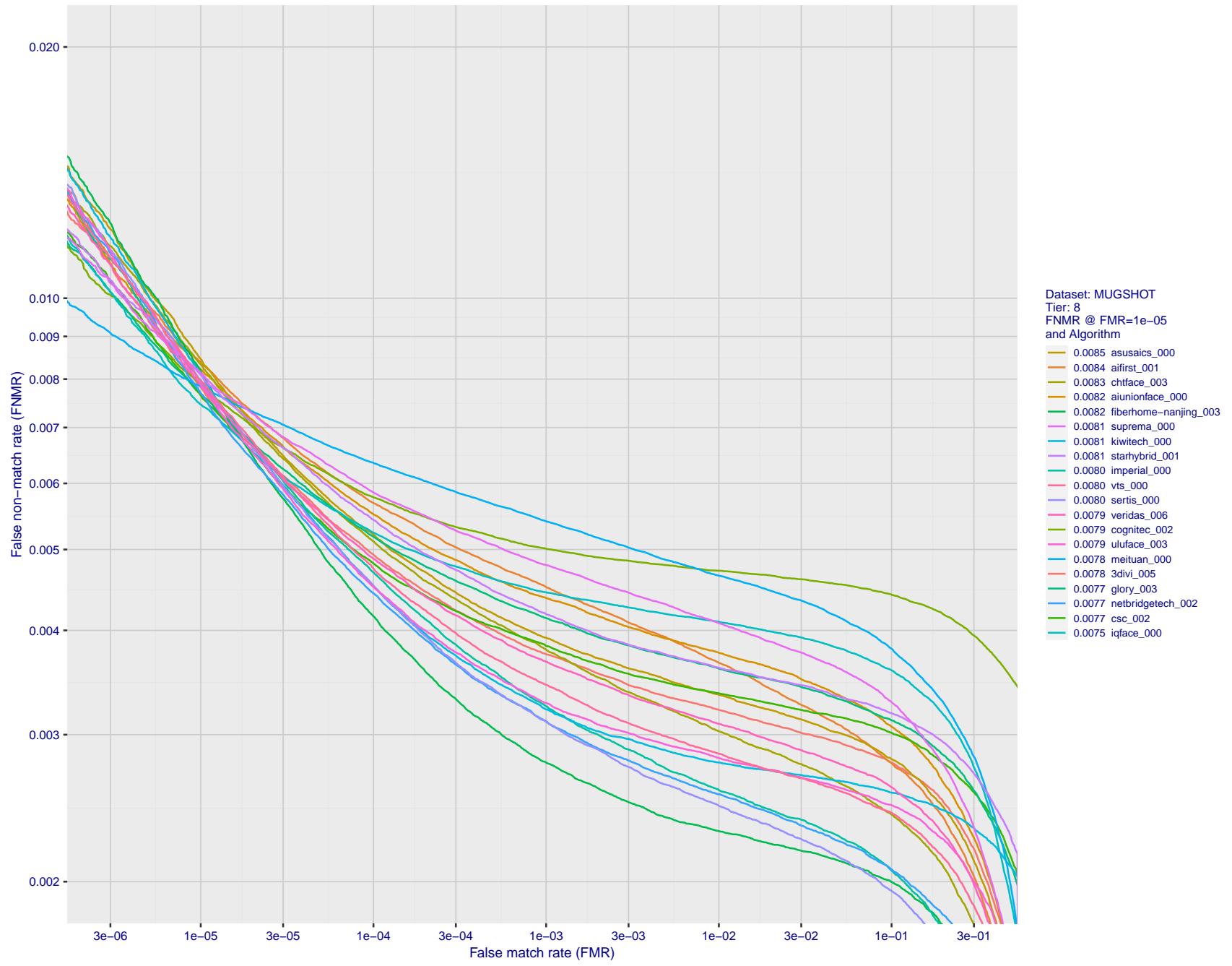


Figure 61: For the mugshot images, detection error tradeoff (DET) characteristics showing false non-match rate vs. false match rate plotted parametrically on threshold,  $T$ . The scales are logarithmic in order to show decades of FMR.

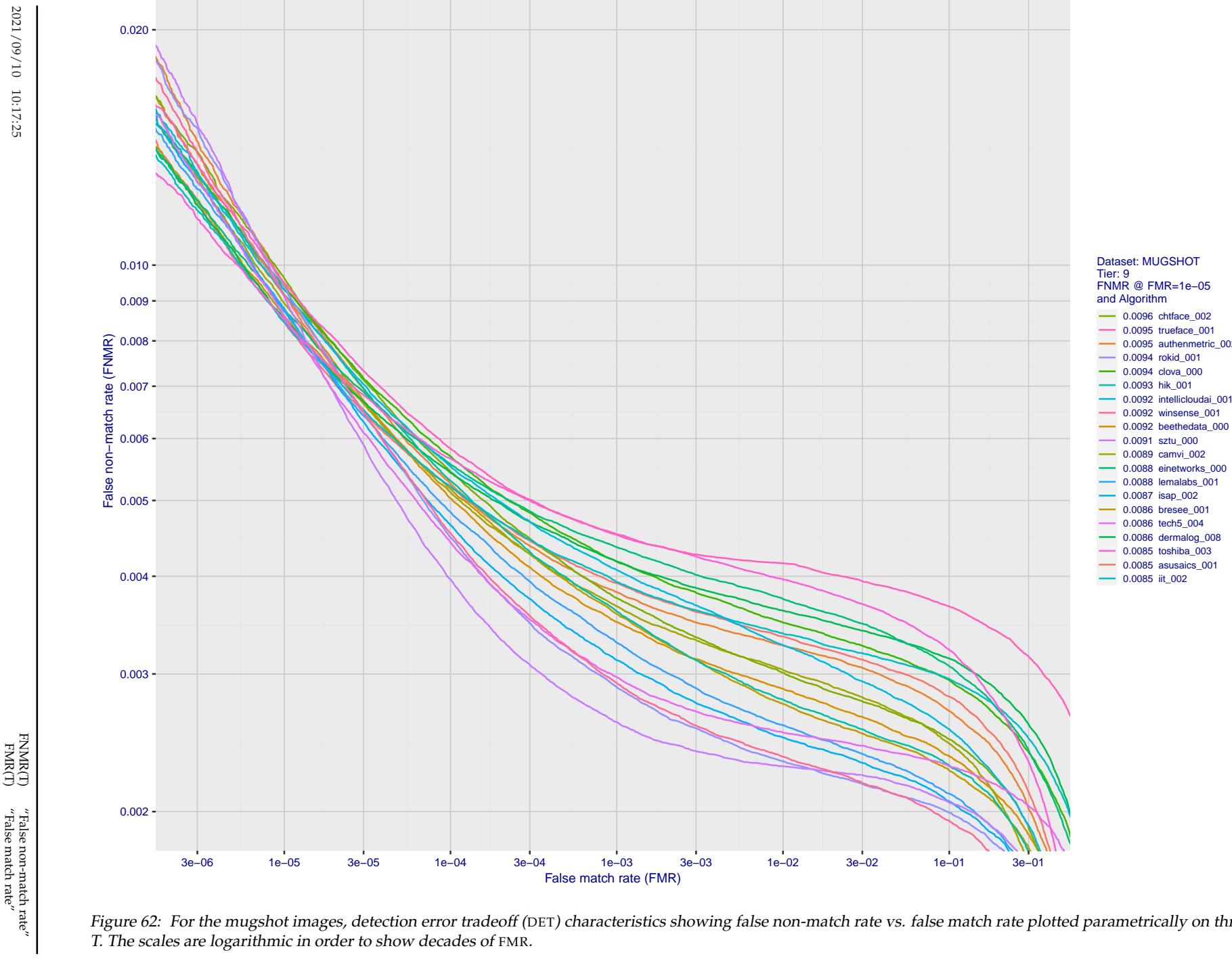


Figure 62: For the mugshot images, detection error tradeoff (DET) characteristics showing false non-match rate vs. false match rate plotted parametrically on threshold,  $T$ . The scales are logarithmic in order to show decades of FMR.

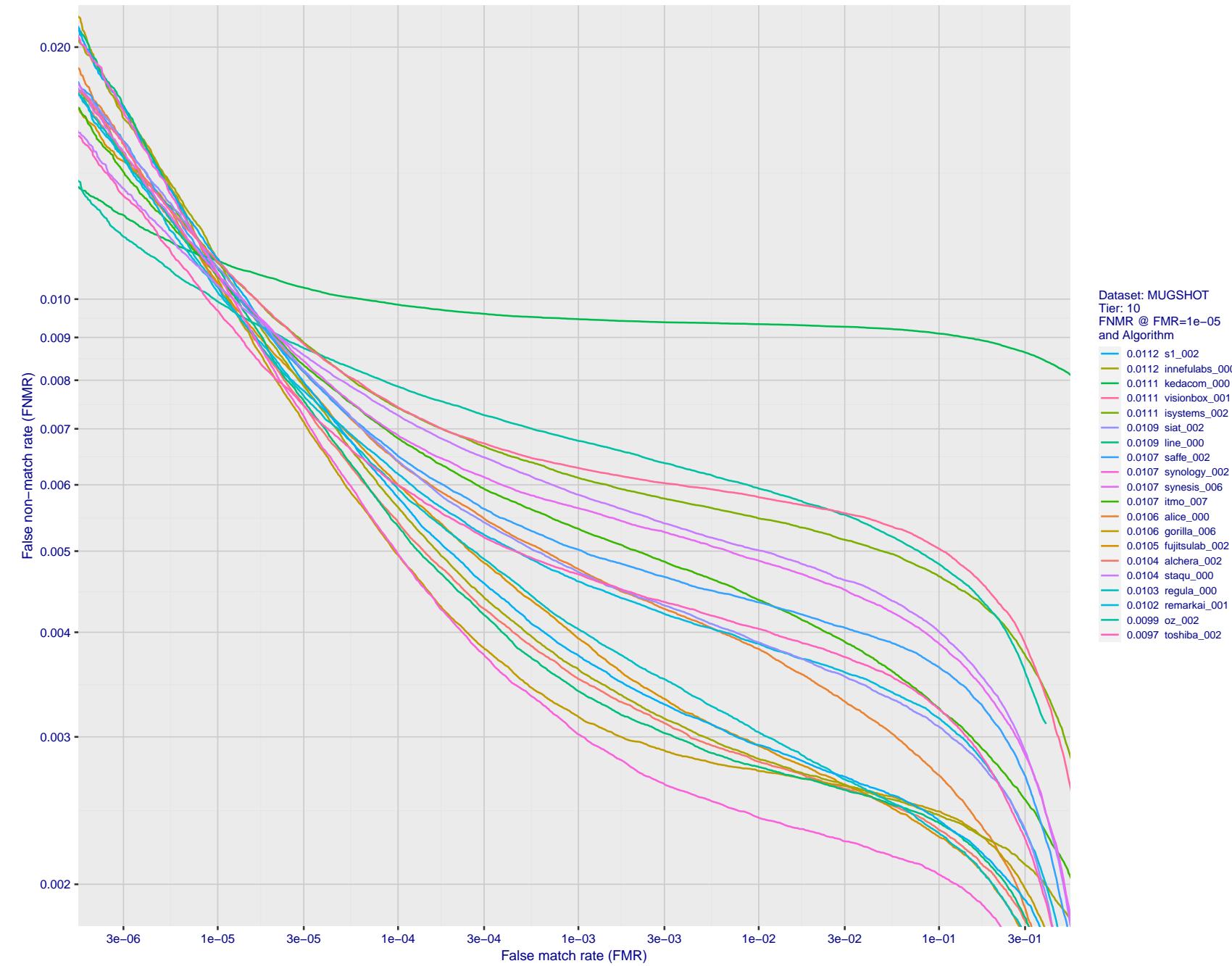


Figure 63: For the mugshot images, detection error tradeoff (DET) characteristics showing false non-match rate vs. false match rate plotted parametrically on threshold,  $T$ . The scales are logarithmic in order to show decades of FMR.

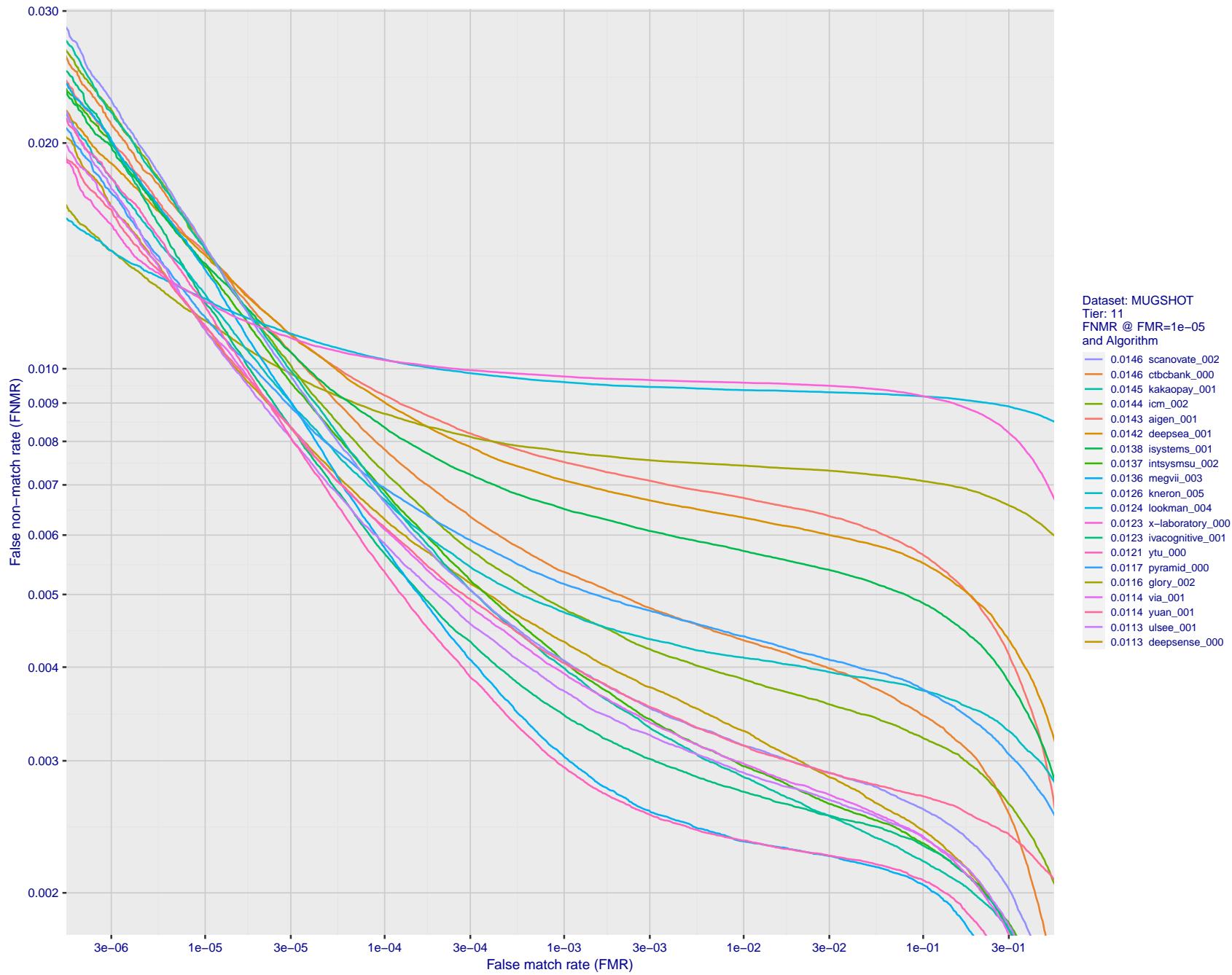


Figure 64: For the mugshot images, detection error tradeoff (DET) characteristics showing false non-match rate vs. false match rate plotted parametrically on threshold,  $T$ . The scales are logarithmic in order to show decades of FMR.

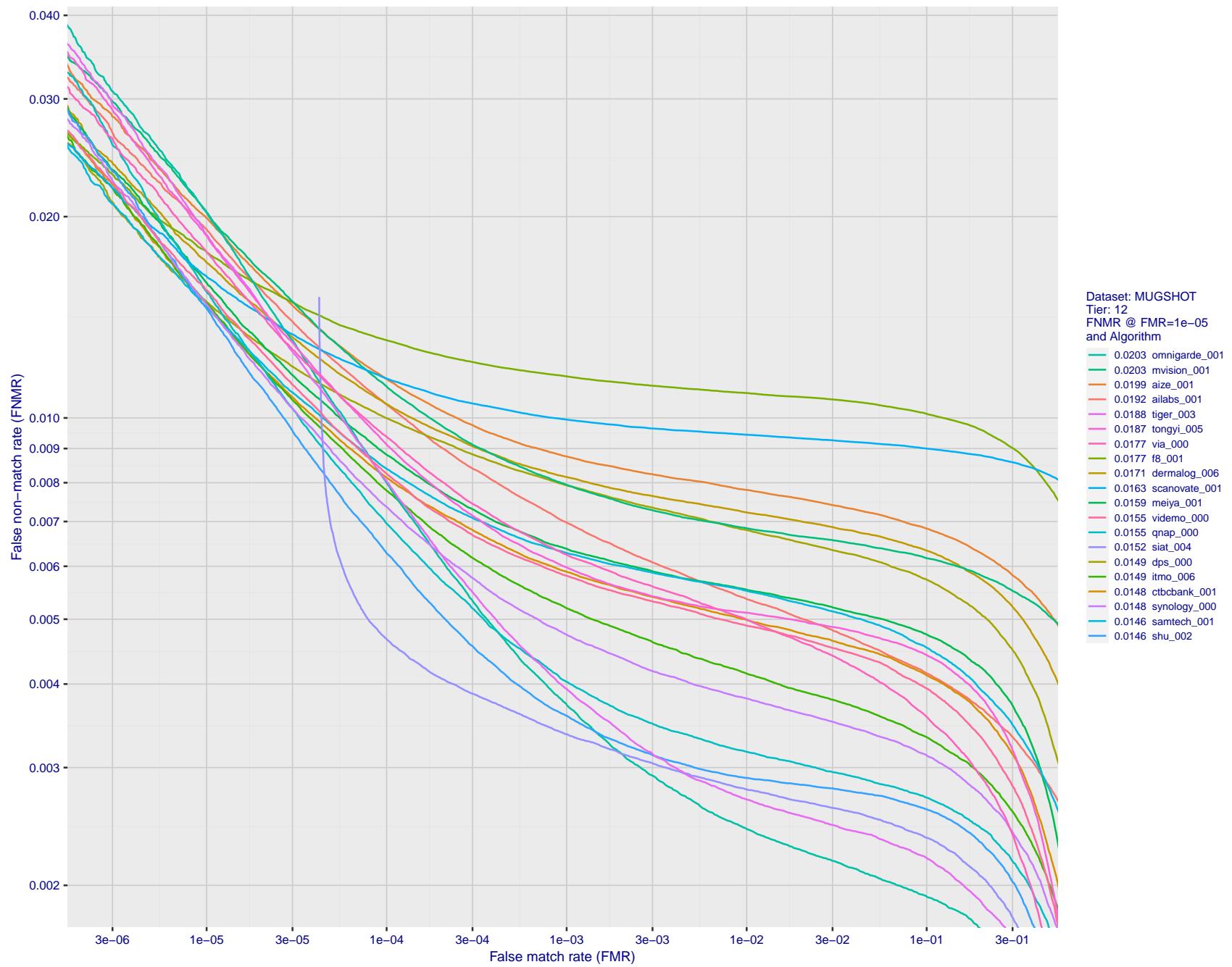
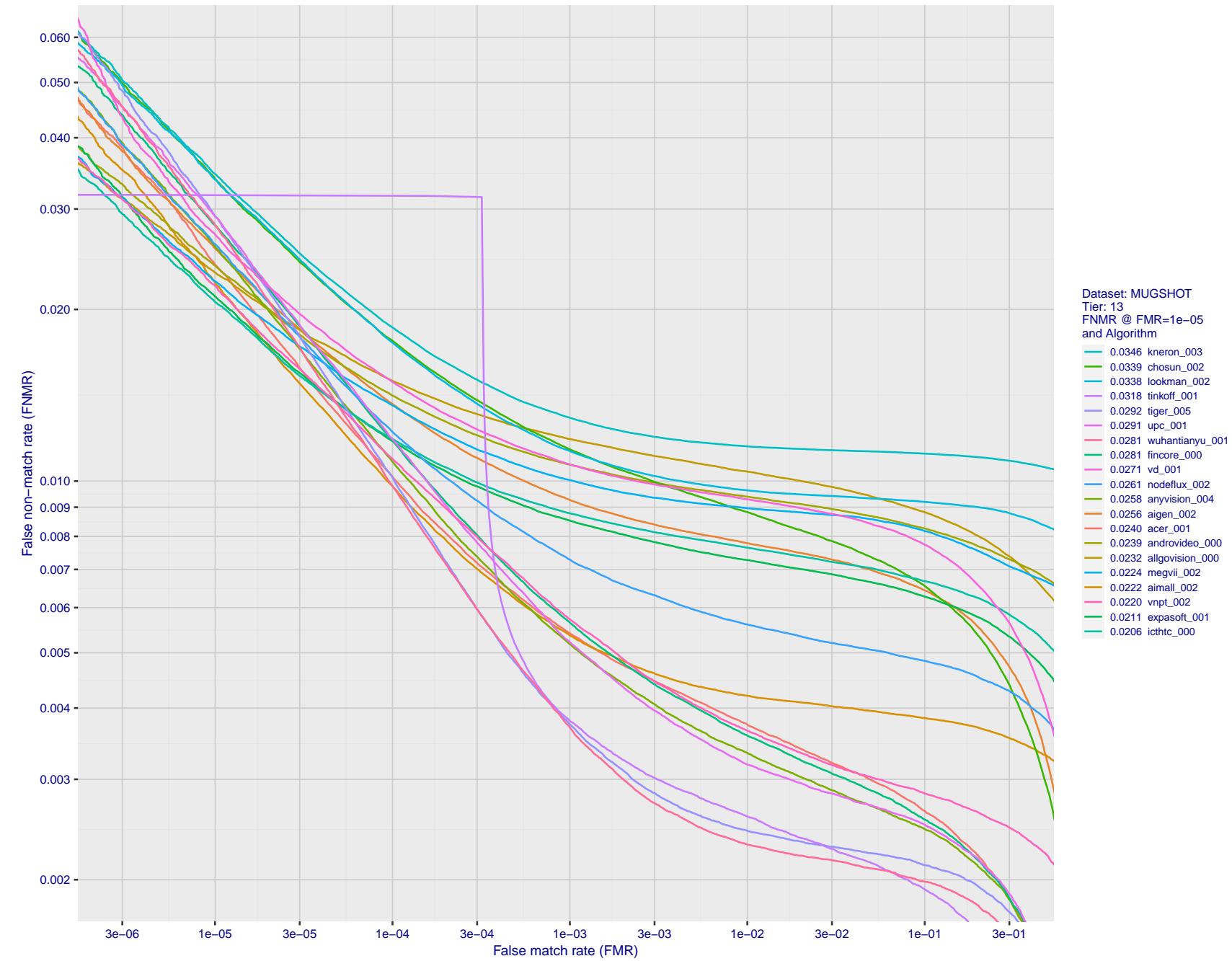


Figure 65: For the mugshot images, detection error tradeoff (DET) characteristics showing false non-match rate vs. false match rate plotted parametrically on threshold,  $T$ . The scales are logarithmic in order to show decades of FMR.



FNMR( $T$ )  
 "False non-match rate"  
 "False match rate"

Figure 66: For the mugshot images, detection error tradeoff (DET) characteristics showing false non-match rate vs. false match rate plotted parametrically on threshold,  $T$ . The scales are logarithmic in order to show decades of FMR.

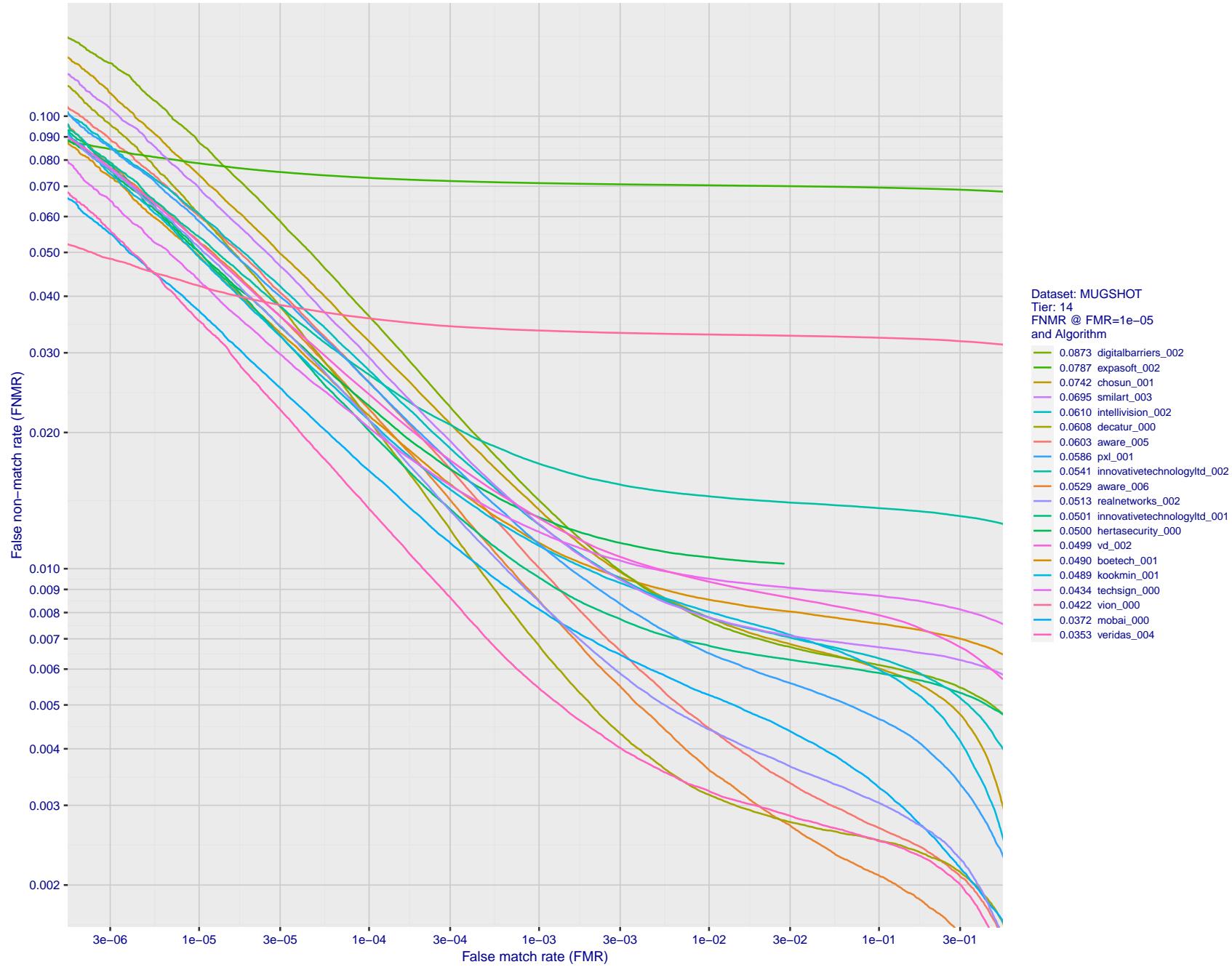


Figure 67: For the mugshot images, detection error tradeoff (DET) characteristics showing false non-match rate vs. false match rate plotted parametrically on threshold,  $T$ . The scales are logarithmic in order to show decades of FMR.

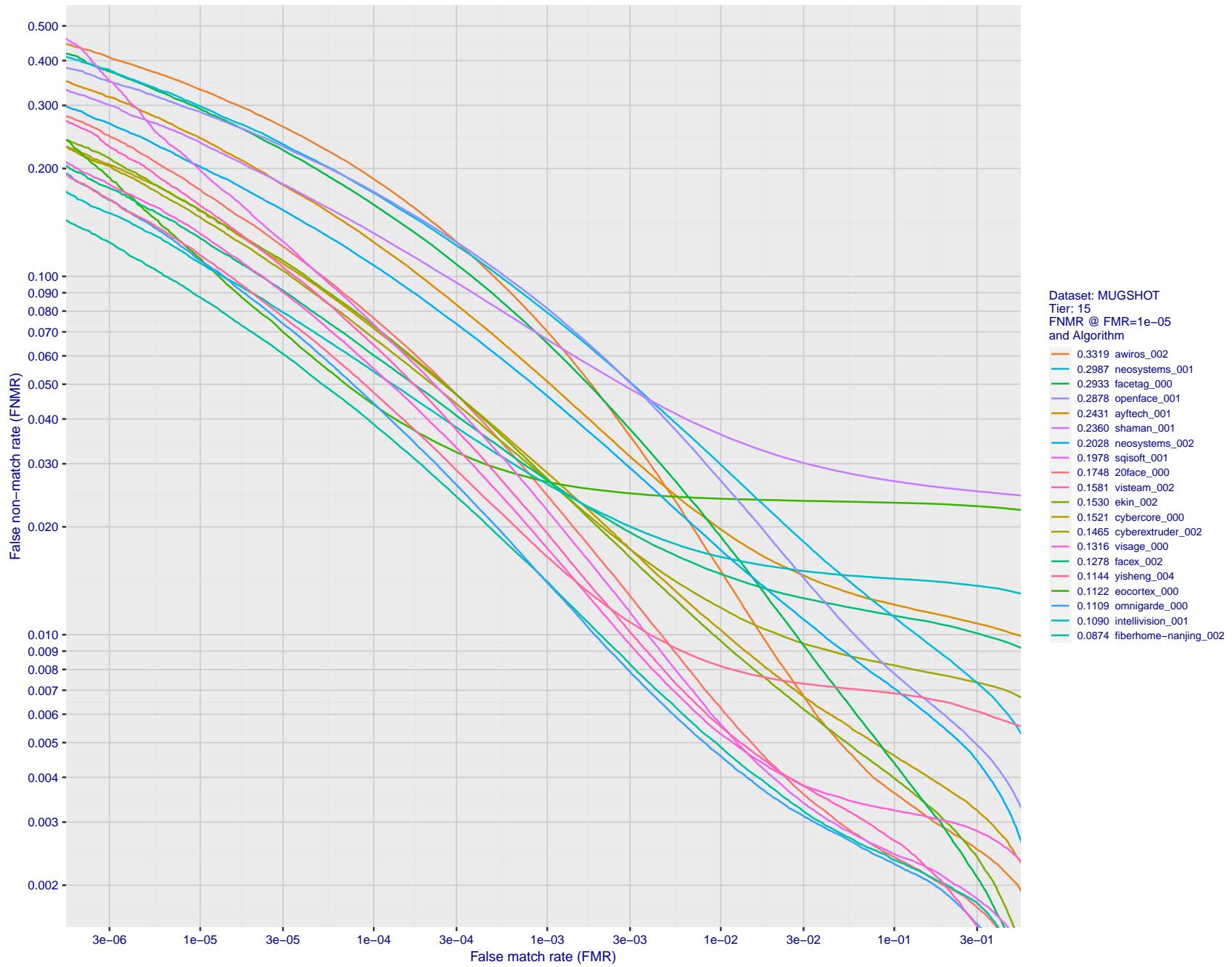
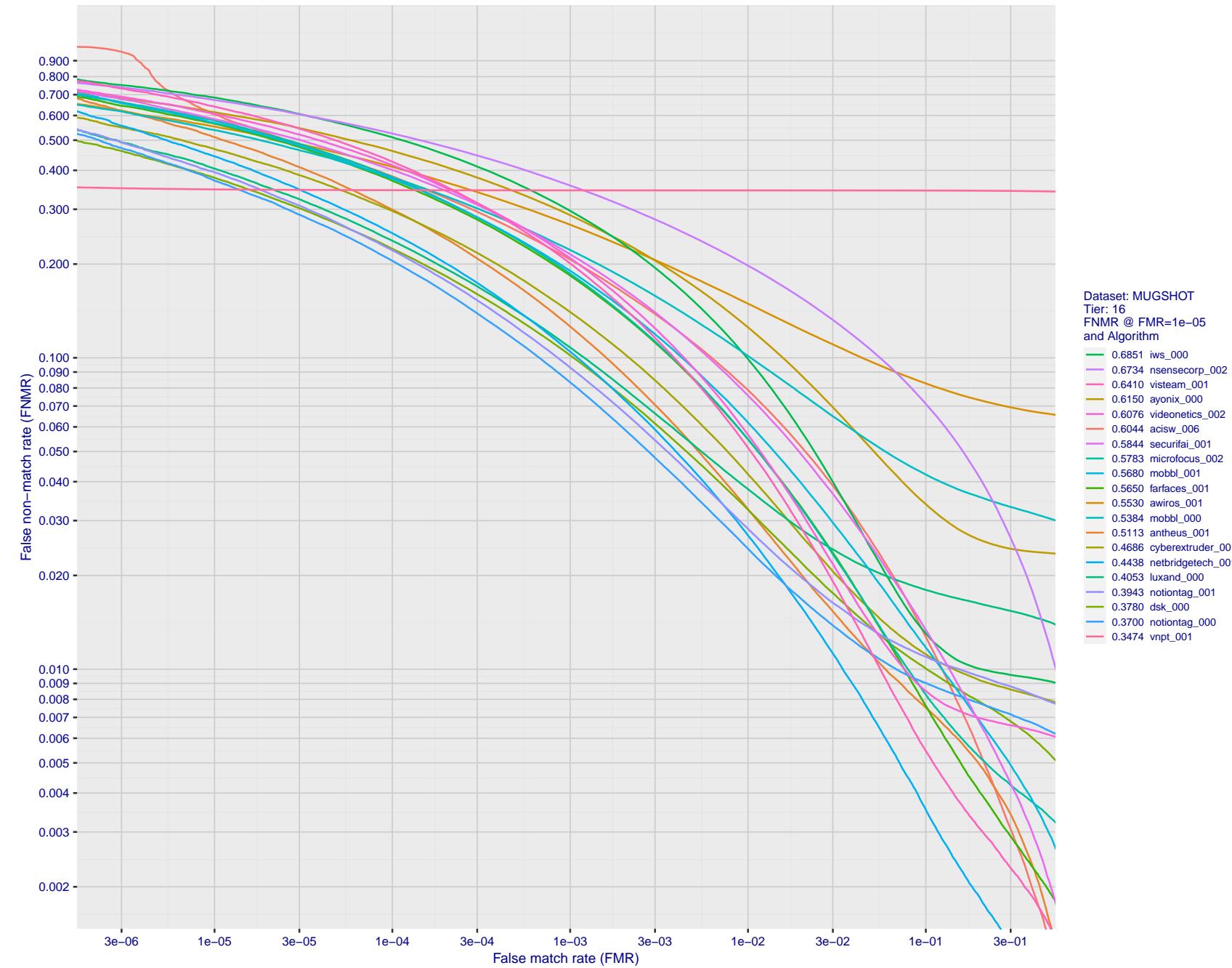


Figure 68: For the mugshot images, detection error tradeoff (DET) characteristics showing false non-match rate vs. false match rate plotted parametrically on threshold,  $T$ . The scales are logarithmic in order to show decades of FMR.



FNMR(T)  
FMR(T)  
"False non-match rate"  
"False match rate"

Figure 69: For the mugshot images, detection error tradeoff (DET) characteristics showing false non-match rate vs. false match rate plotted parametrically on threshold, T. The scales are logarithmic in order to show decades of FMR.

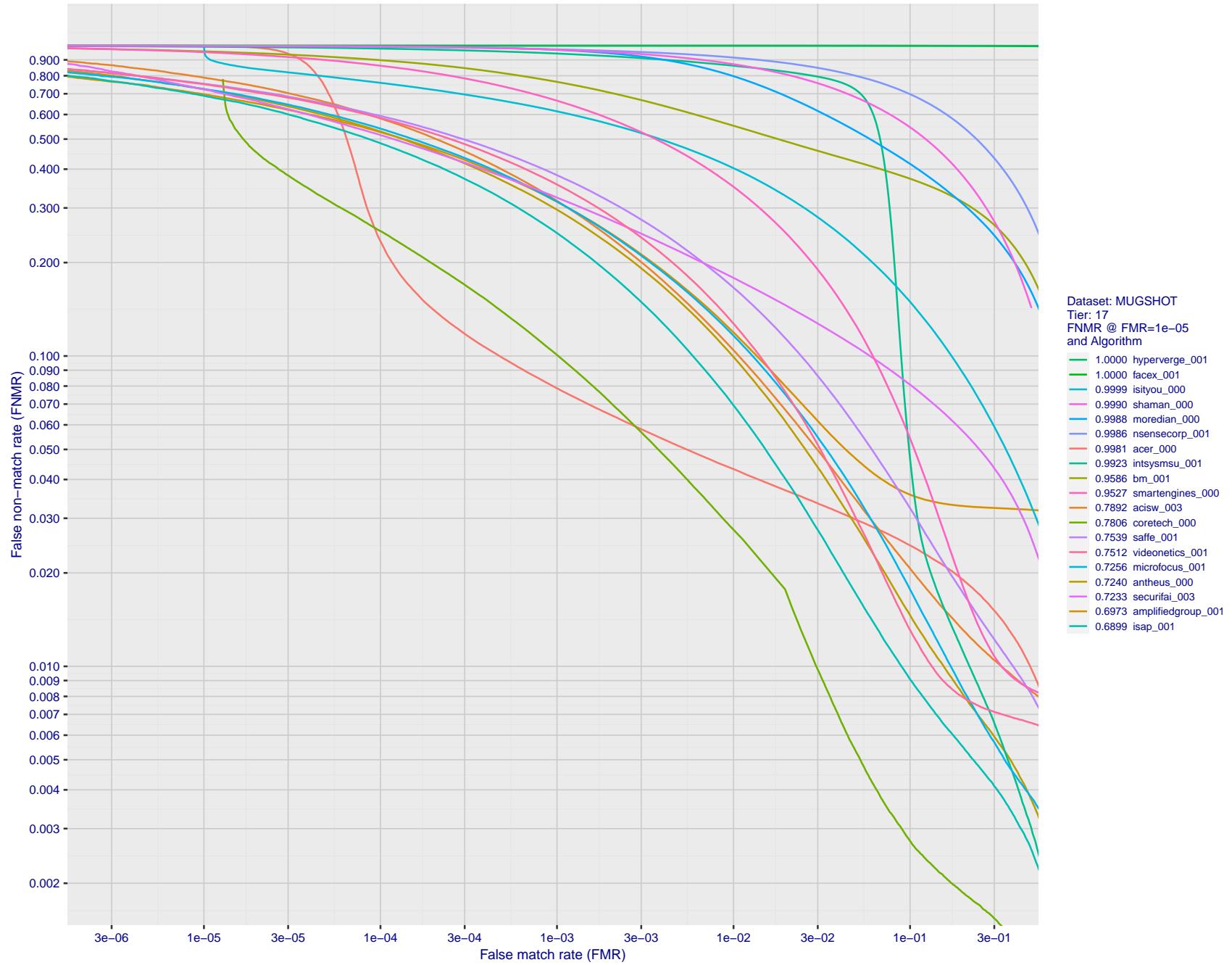


Figure 70: For the mugshot images, detection error tradeoff (DET) characteristics showing false non-match rate vs. false match rate plotted parametrically on threshold,  $T$ . The scales are logarithmic in order to show decades of FMR.

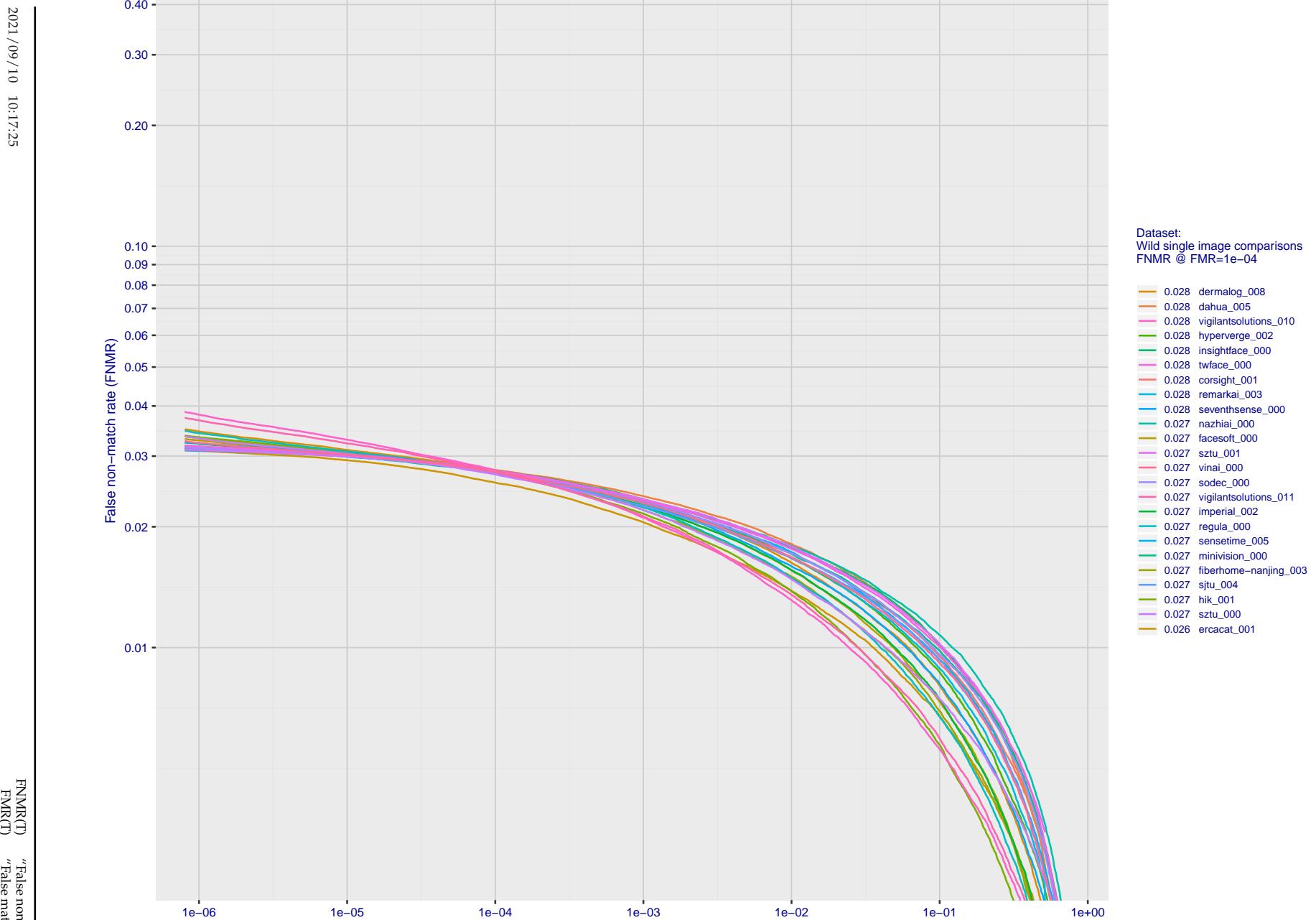


Figure 71: For the 2018 wild image comparisons, detection error tradeoff (DET) characteristics showing false non-match rate vs. false match rate plotted parametrically on threshold, T. The scales are logarithmic in order to show several decades of FMR.

2021/09/10 10:17:25

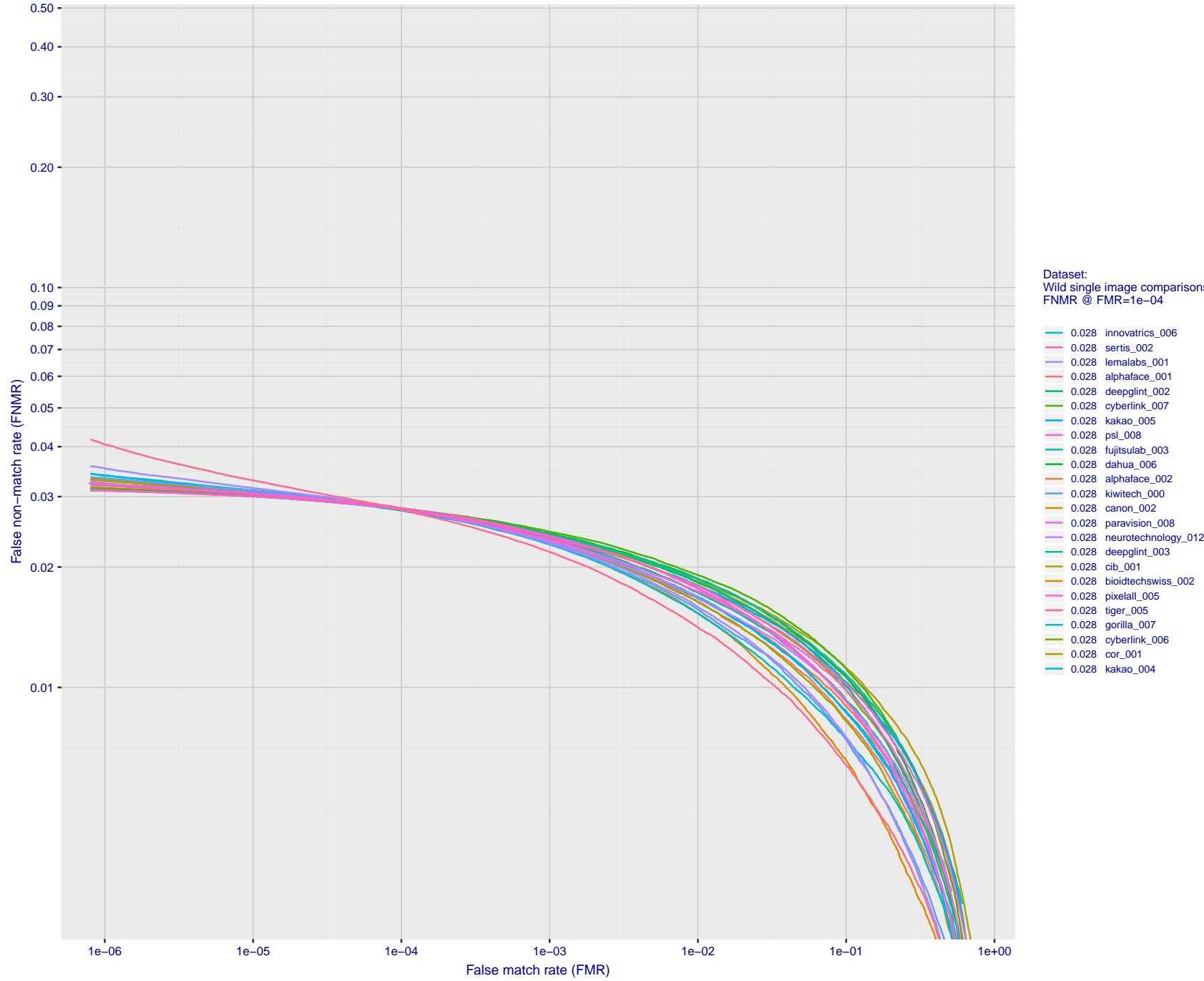


Figure 72: For the 2018 wild image comparisons, detection error tradeoff (DET) characteristics showing false non-match rate vs. false match rate plotted parametrically on threshold, T. The scales are logarithmic in order to show several decades of FMR.

2021/09/10 10:17:25

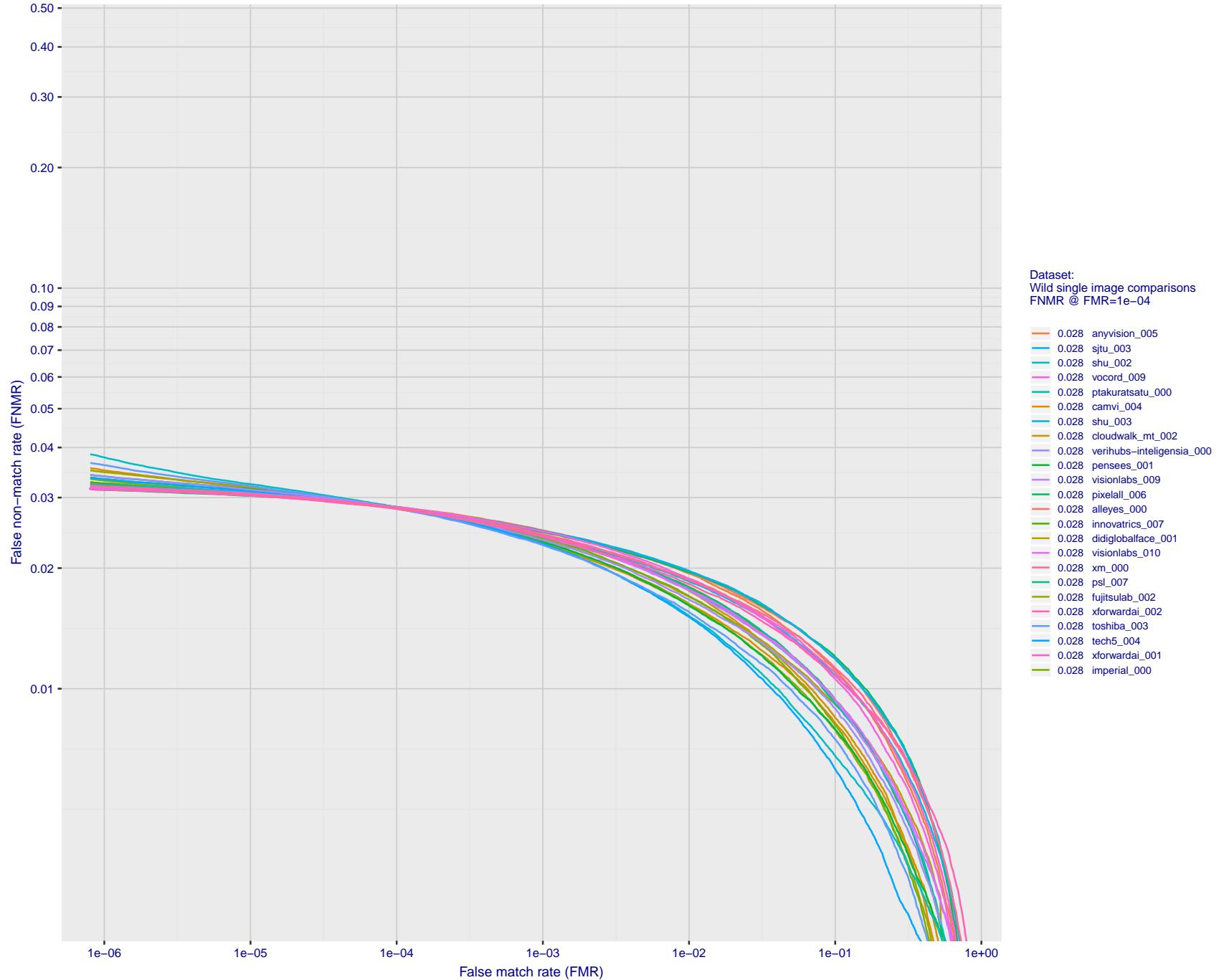


Figure 73: For the 2018 wild image comparisons, detection error tradeoff (DET) characteristics showing false non-match rate vs. false match rate plotted parametrically on threshold, T. The scales are logarithmic in order to show several decades of FMR.

2021/09/10 10:17:25

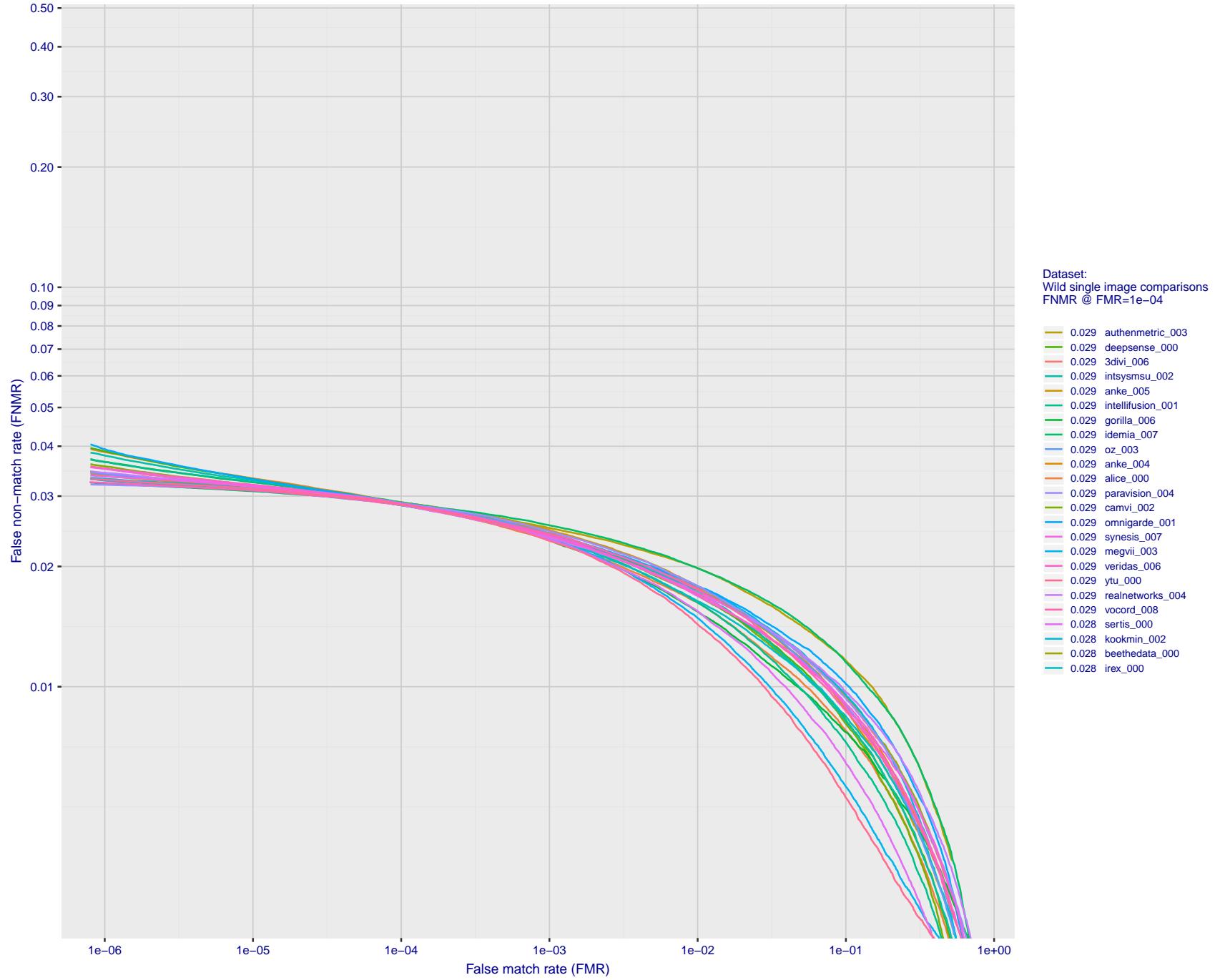


Figure 74: For the 2018 wild image comparisons, detection error tradeoff (DET) characteristics showing false non-match rate vs. false match rate plotted parametrically on threshold, T. The scales are logarithmic in order to show several decades of FMR.

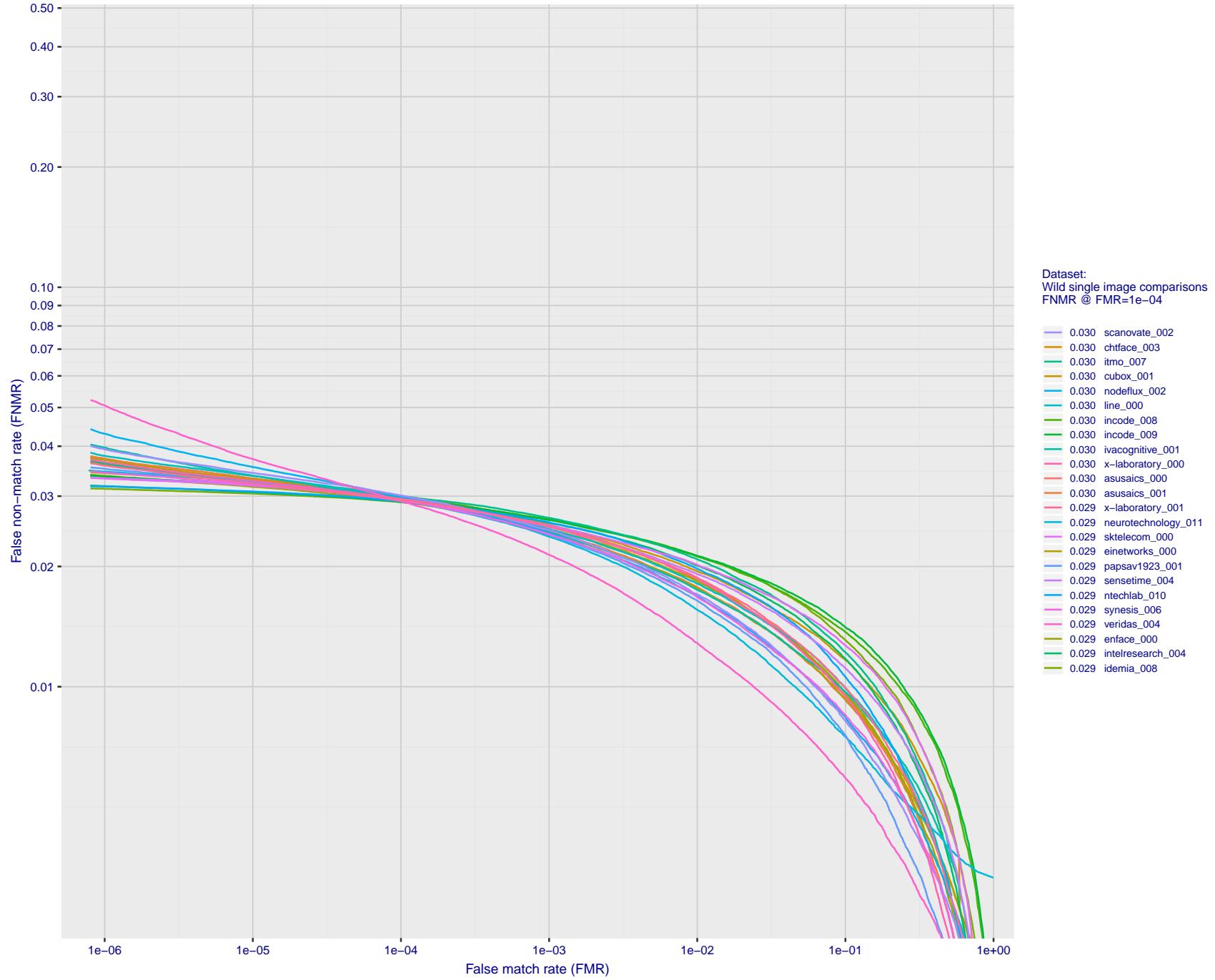


Figure 75: For the 2018 wild image comparisons, detection error tradeoff (DET) characteristics showing false non-match rate vs. false match rate plotted parametrically on threshold, T. The scales are logarithmic in order to show several decades of FMR.

2021/09/10 10:17:25

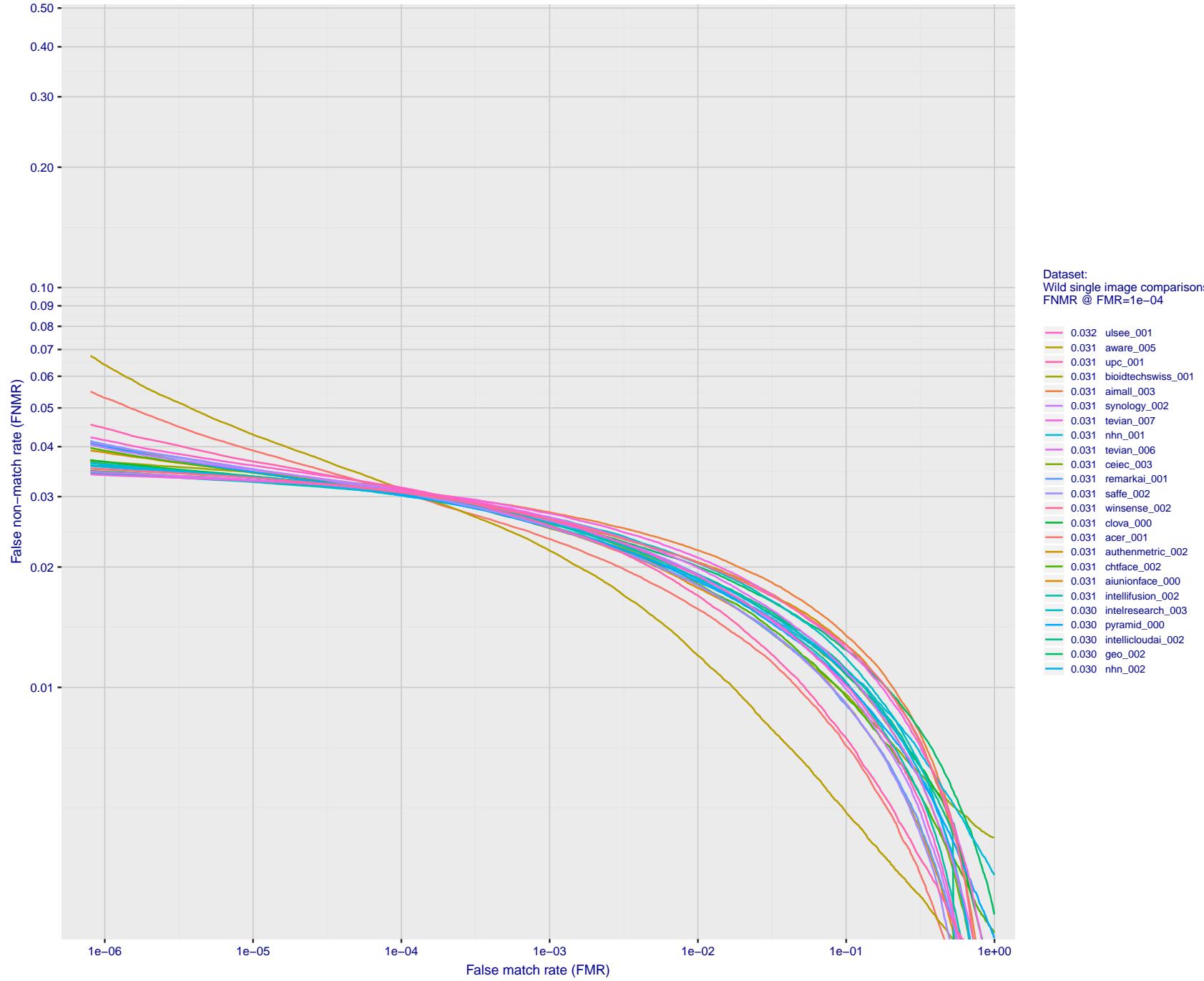


Figure 76: For the 2018 wild image comparisons, detection error tradeoff (DET) characteristics showing false non-match rate vs. false match rate plotted parametrically on threshold, T. The scales are logarithmic in order to show several decades of FMR.

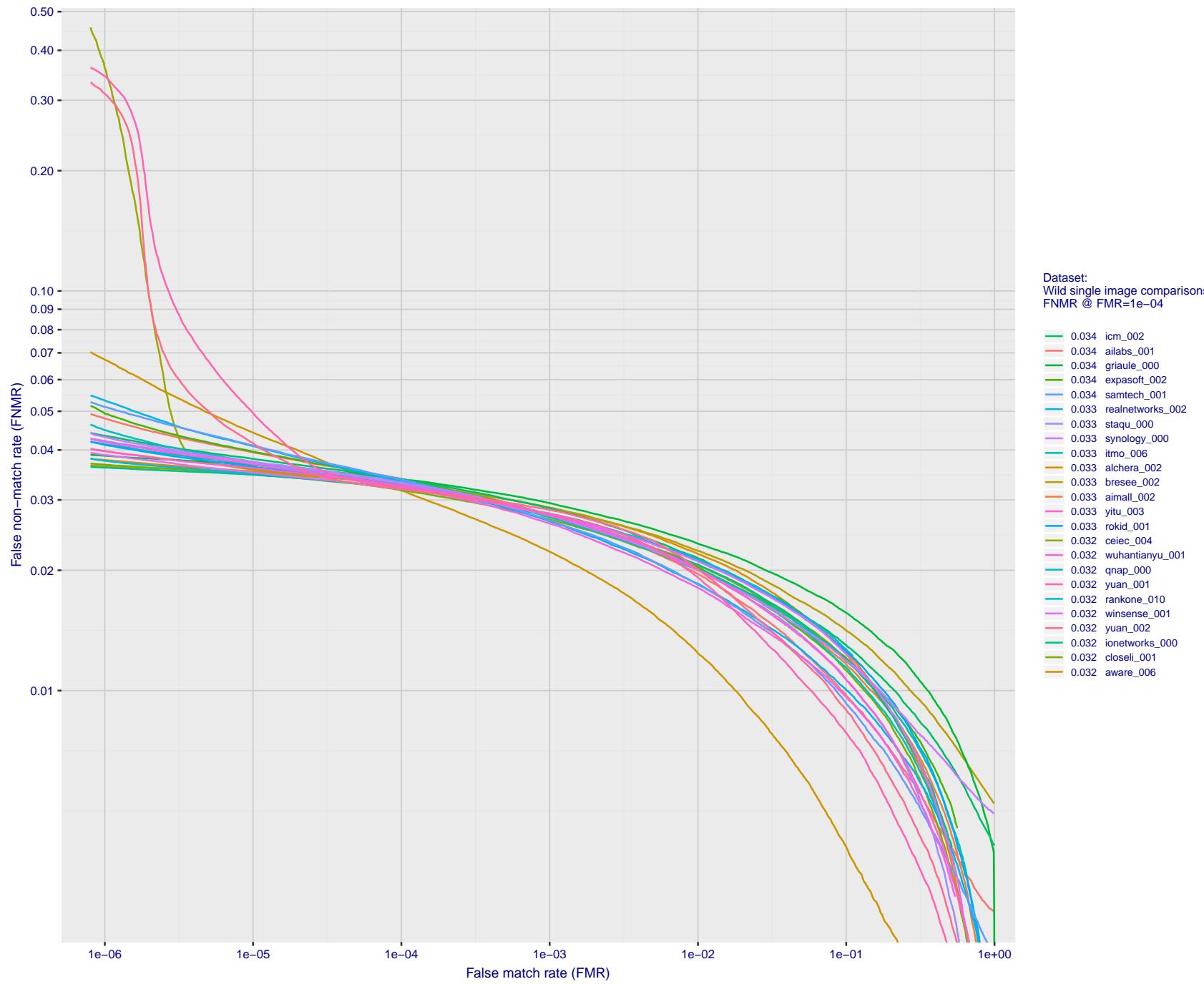


Figure 77: For the 2018 wild image comparisons, detection error tradeoff (DET) characteristics showing false non-match rate vs. false match rate plotted parametrically on threshold,  $T$ . The scales are logarithmic in order to show several decades of FMR.

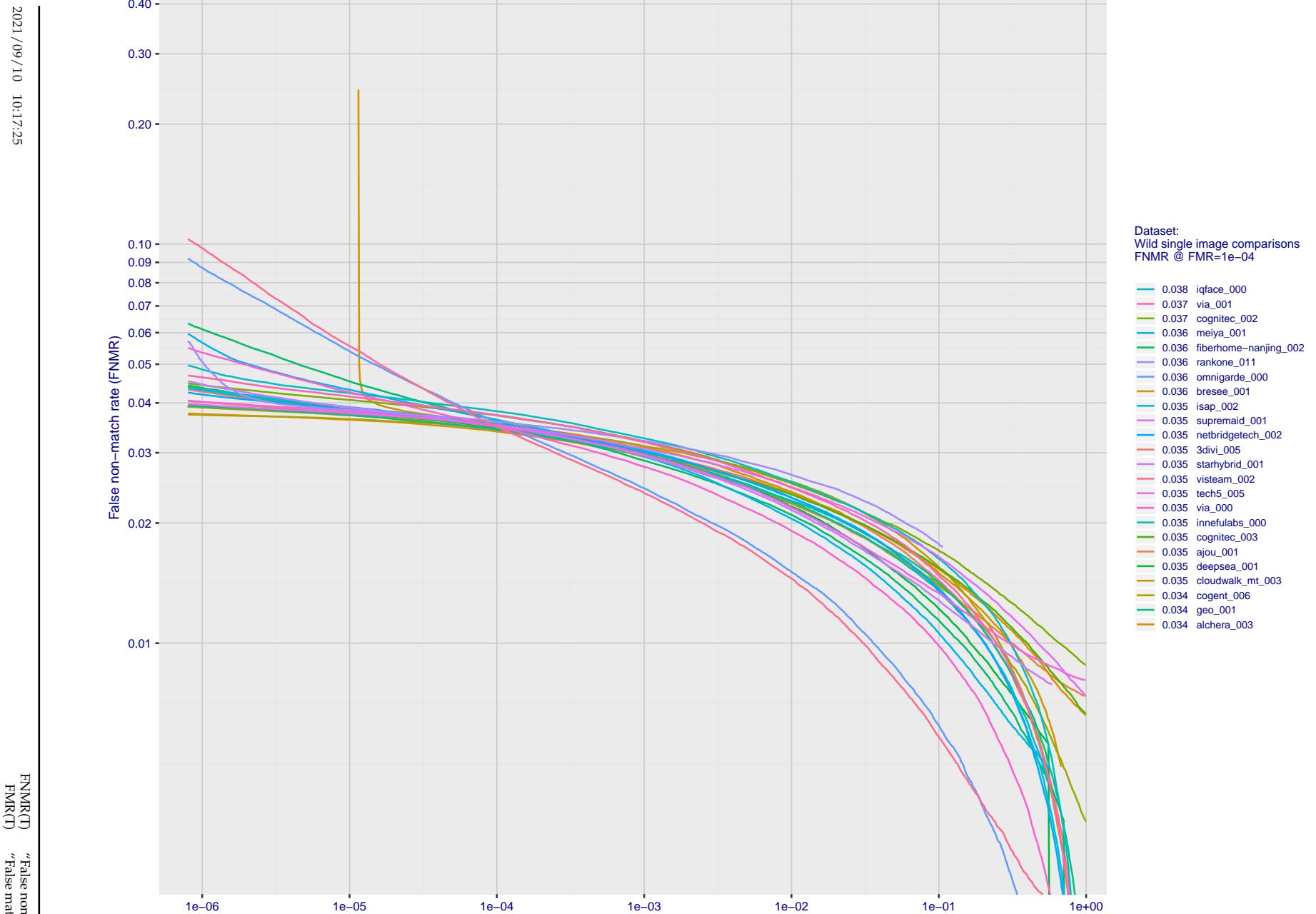


Figure 78: For the 2018 wild image comparisons, detection error tradeoff (DET) characteristics showing false non-match rate vs. false match rate plotted parametrically on threshold, T. The scales are logarithmic in order to show several decades of FMR.

2021/09/10 10:17:25

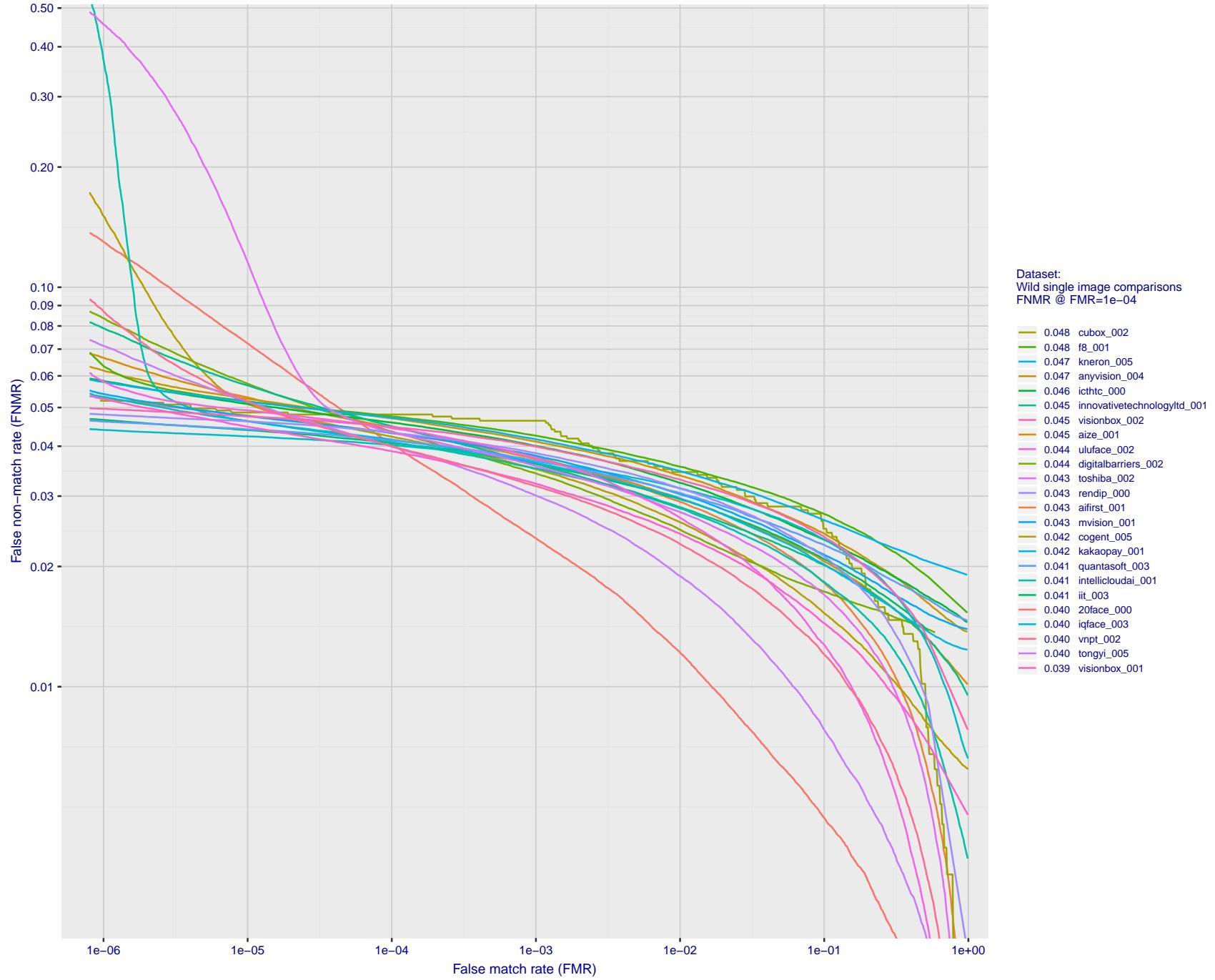


Figure 79: For the 2018 wild image comparisons, detection error tradeoff (DET) characteristics showing false non-match rate vs. false match rate plotted parametrically on threshold,  $T$ . The scales are logarithmic in order to show several decades of FMR.

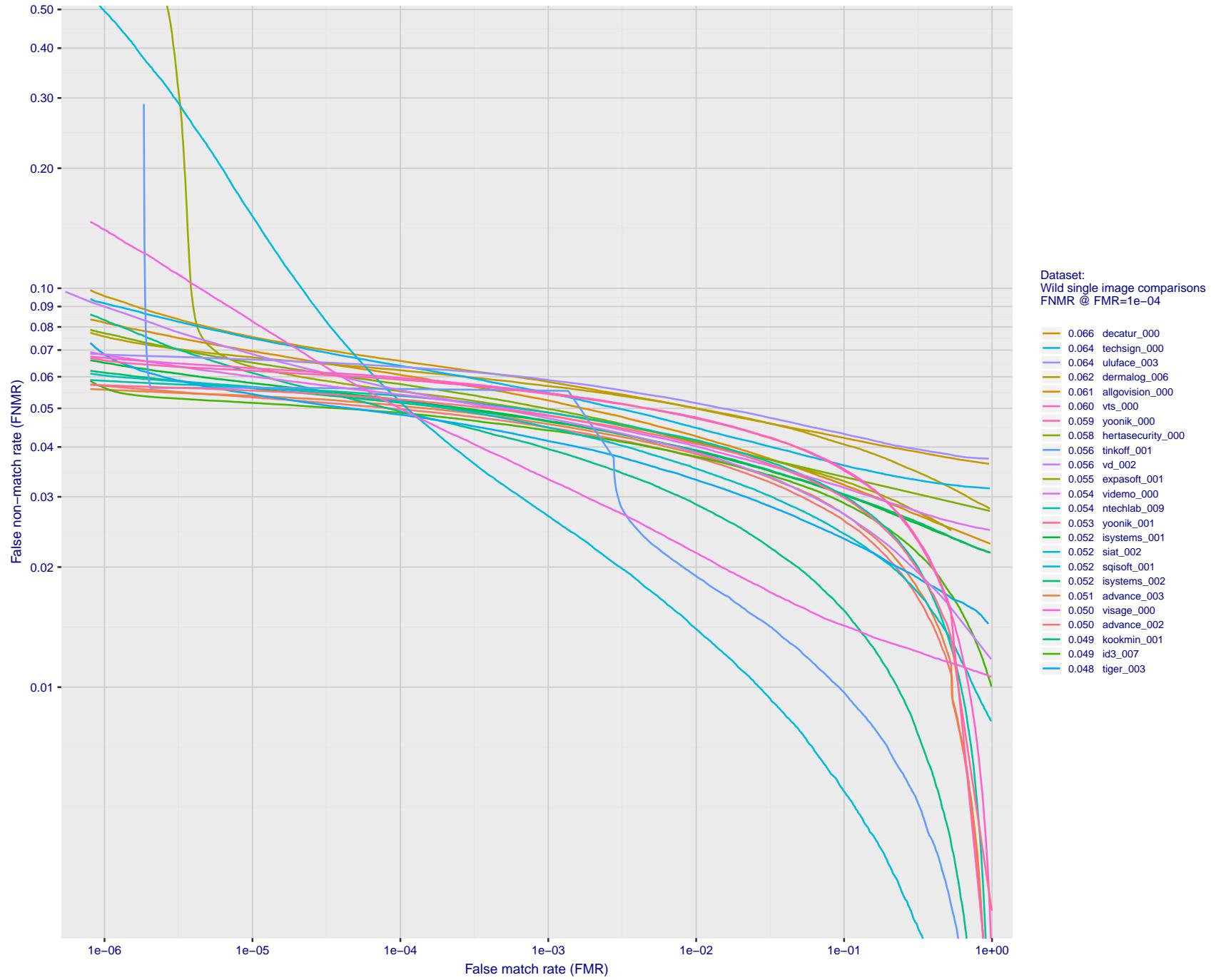


Figure 80: For the 2018 wild image comparisons, detection error tradeoff (DET) characteristics showing false non-match rate vs. false match rate plotted parametrically on threshold,  $T$ . The scales are logarithmic in order to show several decades of FMR.

2021/09/10 10:17:25

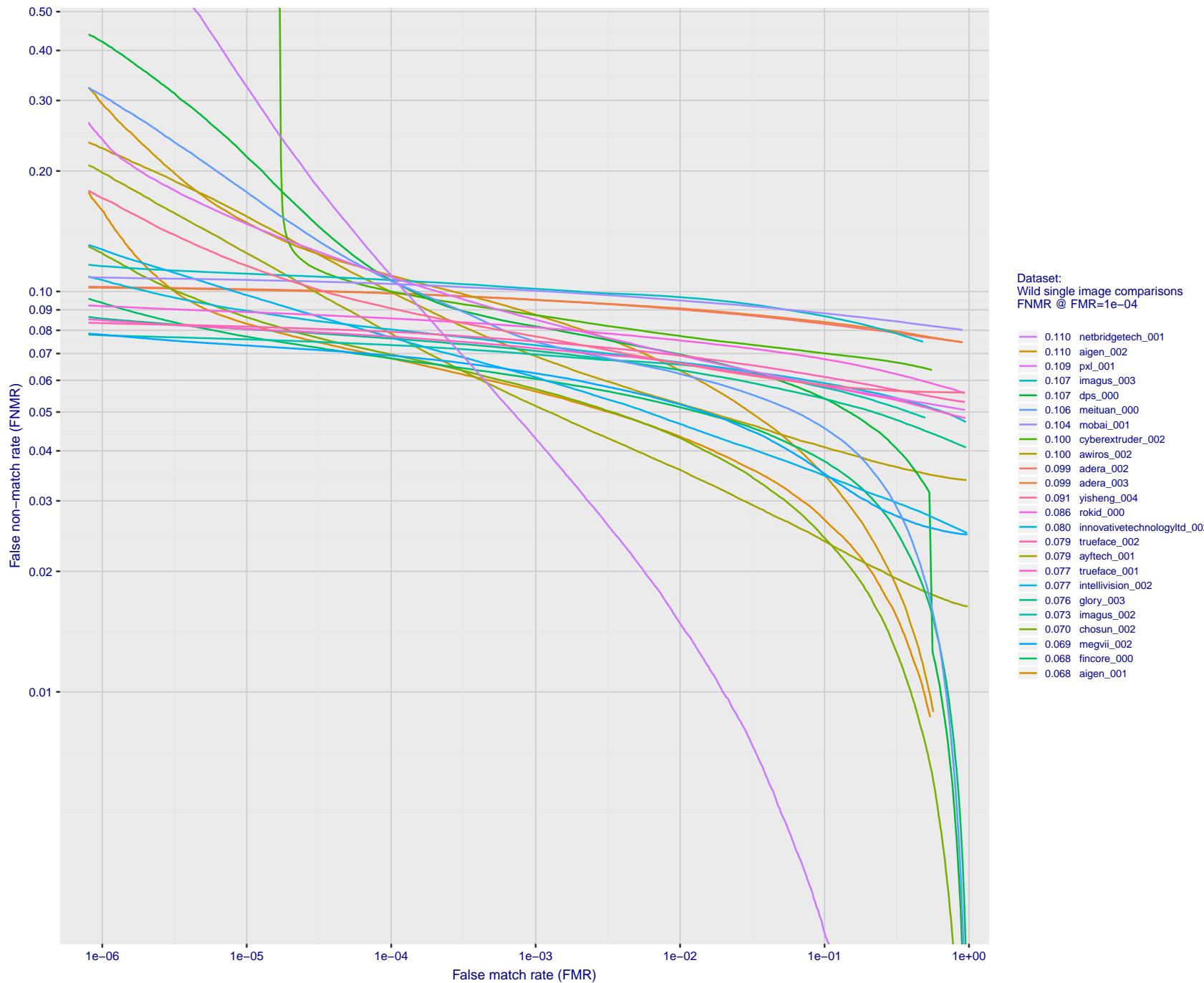


Figure 81: For the 2018 wild image comparisons, detection error tradeoff (DET) characteristics showing false non-match rate vs. false match rate plotted parametrically on threshold,  $T$ . The scales are logarithmic in order to show several decades of FMR.

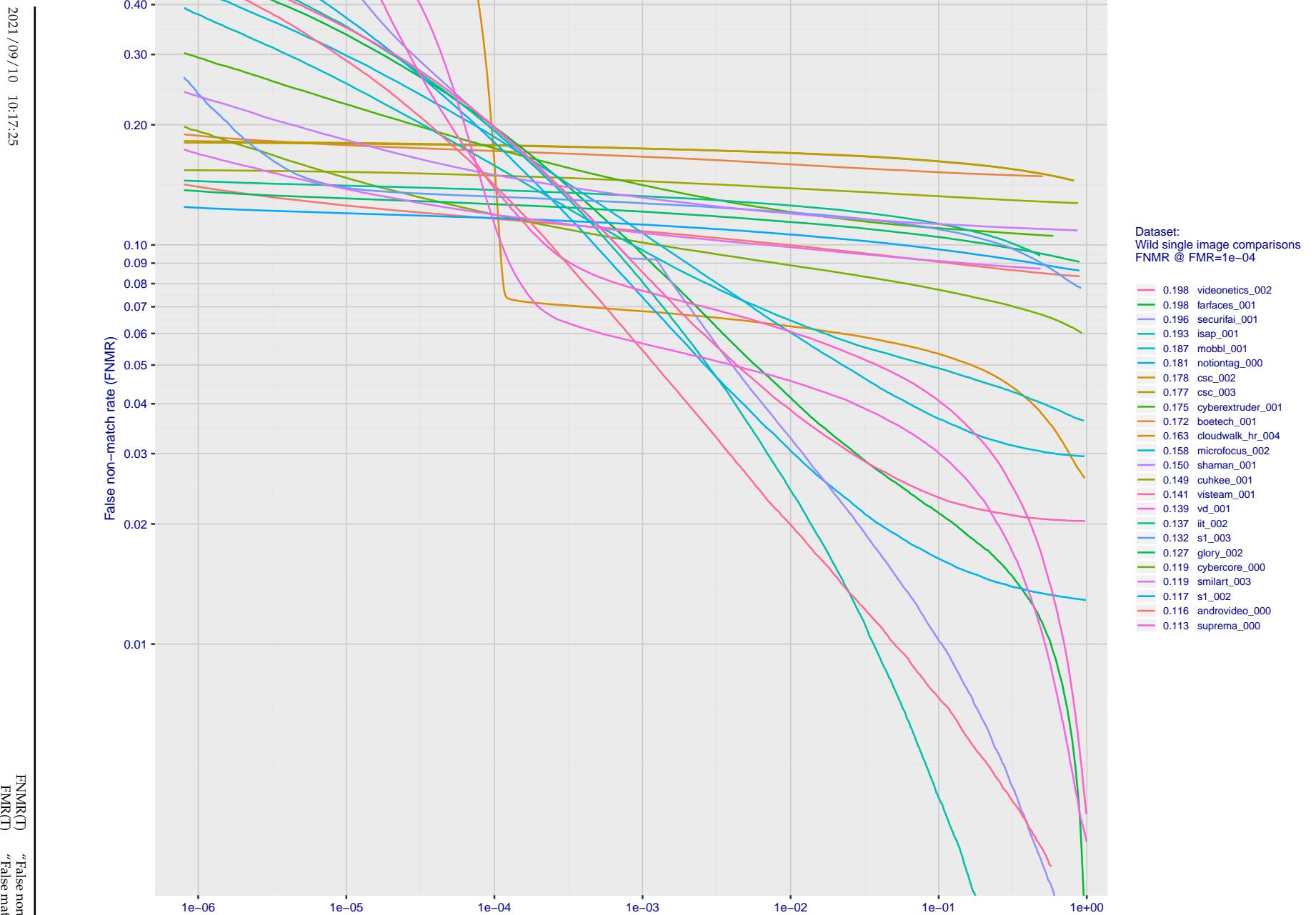


Figure 82: For the 2018 wild image comparisons, detection error tradeoff (DET) characteristics showing false non-match rate vs. false match rate plotted parametrically on threshold,  $T$ . The scales are logarithmic in order to show several decades of FMR.

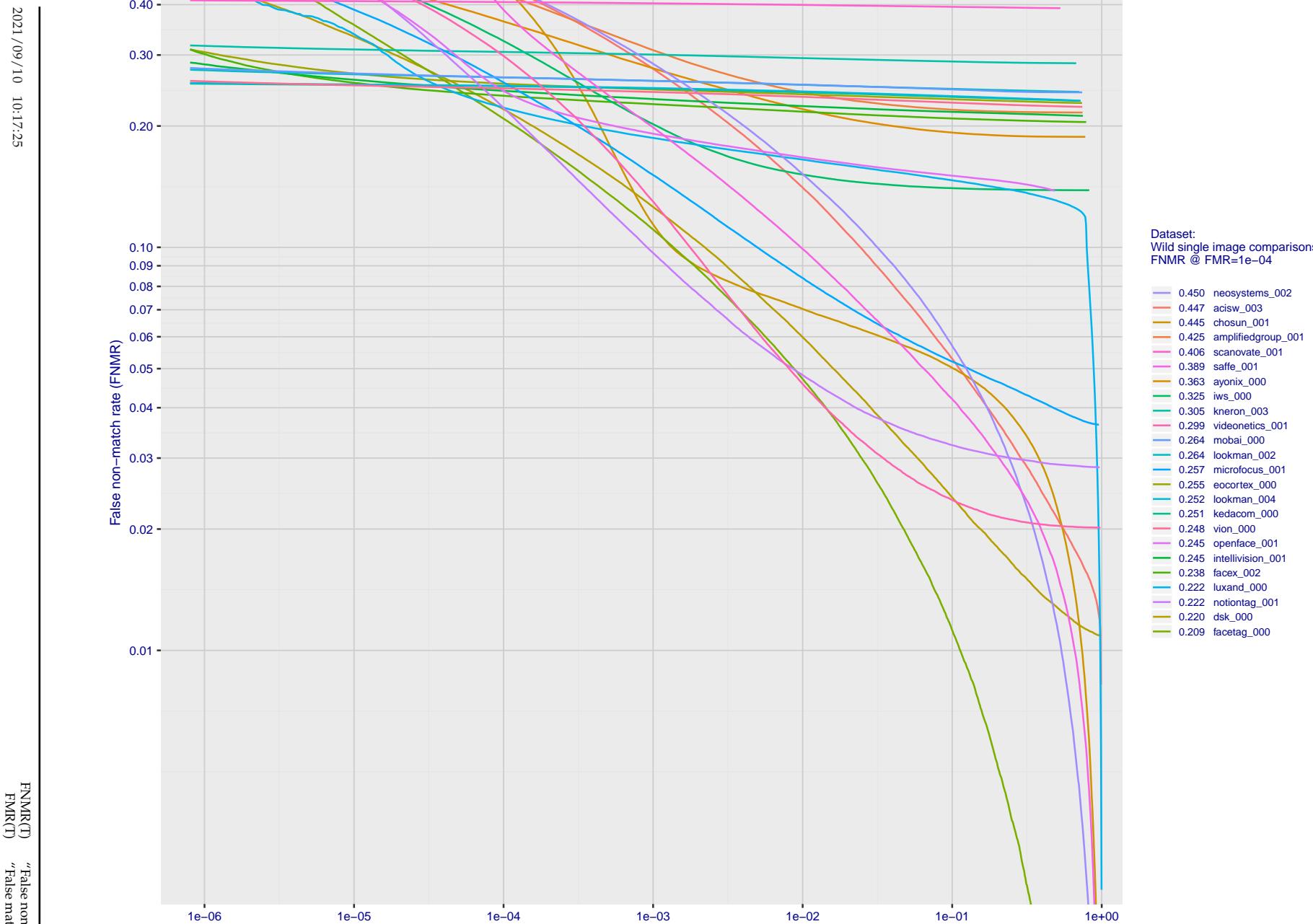
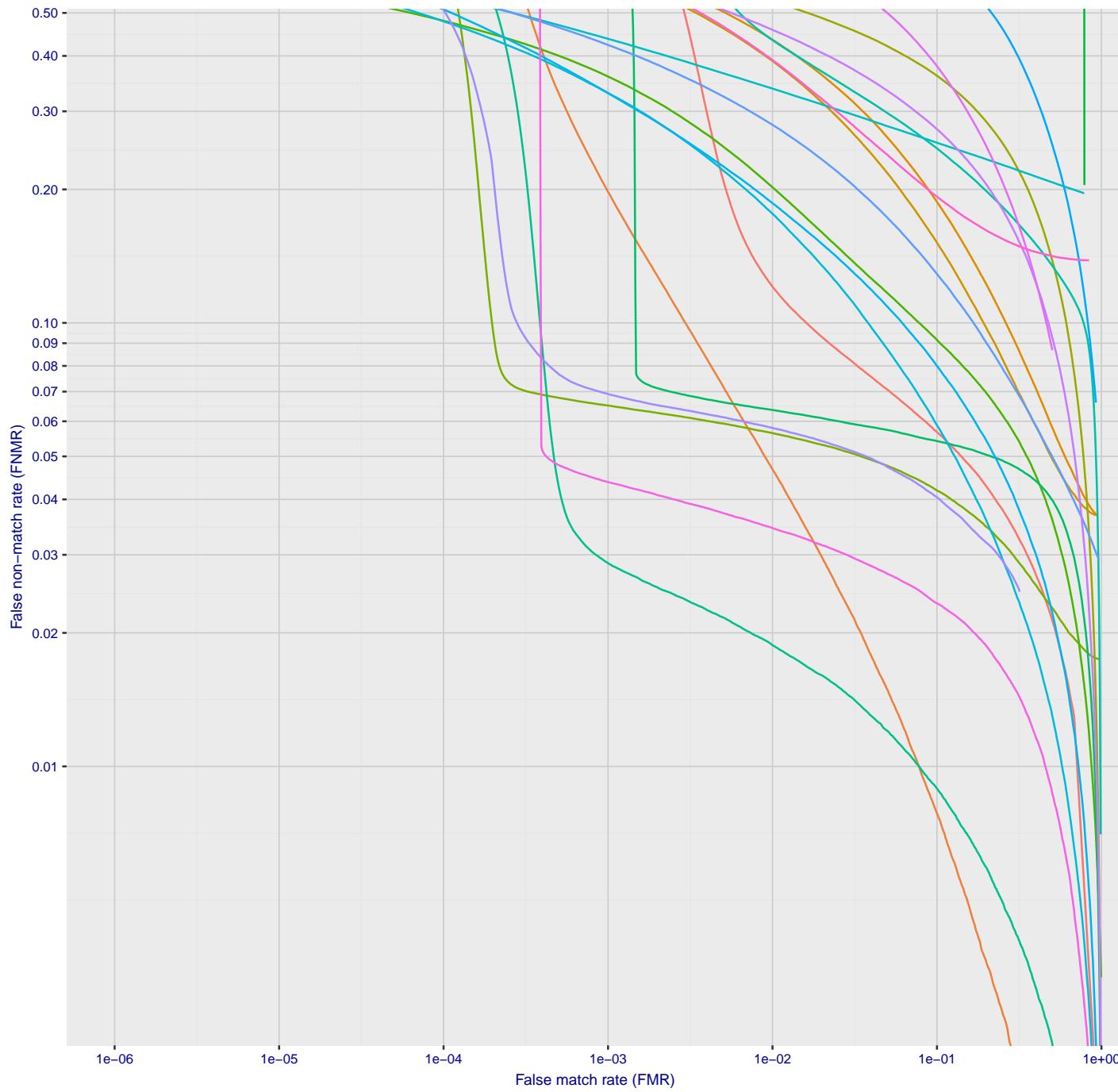


Figure 83: For the 2018 wild image comparisons, detection error tradeoff (DET) characteristics showing false non-match rate vs. false match rate plotted parametrically on threshold, T. The scales are logarithmic in order to show several decades of FMR.

2021/09/10 10:17:25



Dataset:  
Wild single image comparisons  
FNMR @ FMR=1e-04

1.000	isityou_000
1.000	facex_001
1.000	siat_004
0.999	acisw_006
0.994	id3_006
0.993	bm_001
0.986	nsensecorp_001
0.984	acer_000
0.958	shaman_000
0.942	tuputech_000
0.833	securifai_003
0.800	smartengines_000
0.787	intsysmsu_001
0.767	antheus_000
0.759	antheus_001
0.721	cloudwalk_hr_003
0.558	awiros_001
0.553	nsensecorp_002
0.547	mobbl_000
0.534	vpt_001
0.509	neosystems_001
0.508	oz_002
0.480	ekin_002
0.479	moreidian_000

FNMR(T)  
"False non-match rate"  
"False match rate"

Figure 84: For the 2018 wild image comparisons, detection error tradeoff (DET) characteristics showing false non-match rate vs. false match rate plotted parametrically on threshold, T. The scales are logarithmic in order to show several decades of FMR.

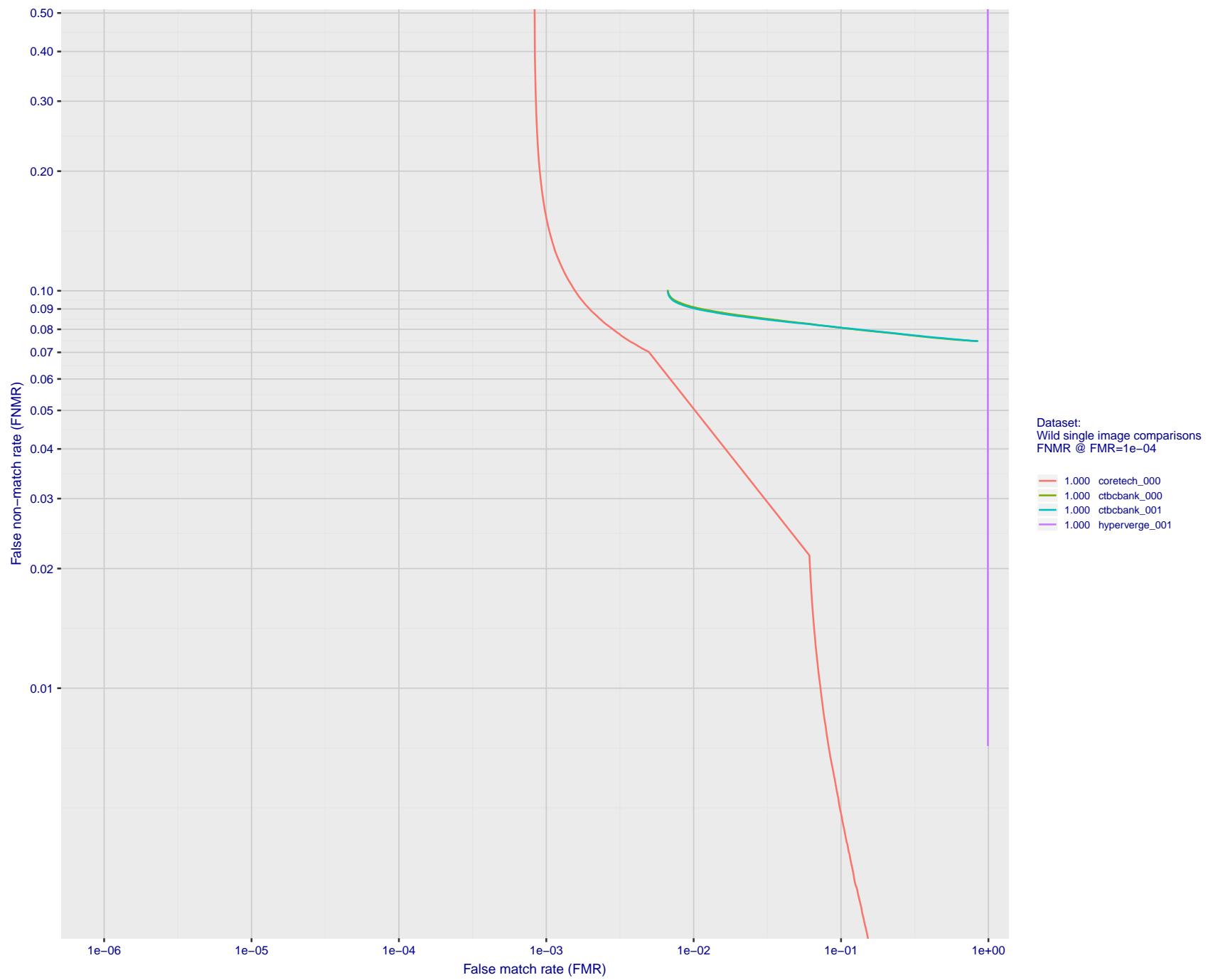


Figure 85: For the 2018 wild image comparisons, detection error tradeoff (DET) characteristics showing false non-match rate vs. false match rate plotted parametrically on threshold,  $T$ . The scales are logarithmic in order to show several decades of FMR.

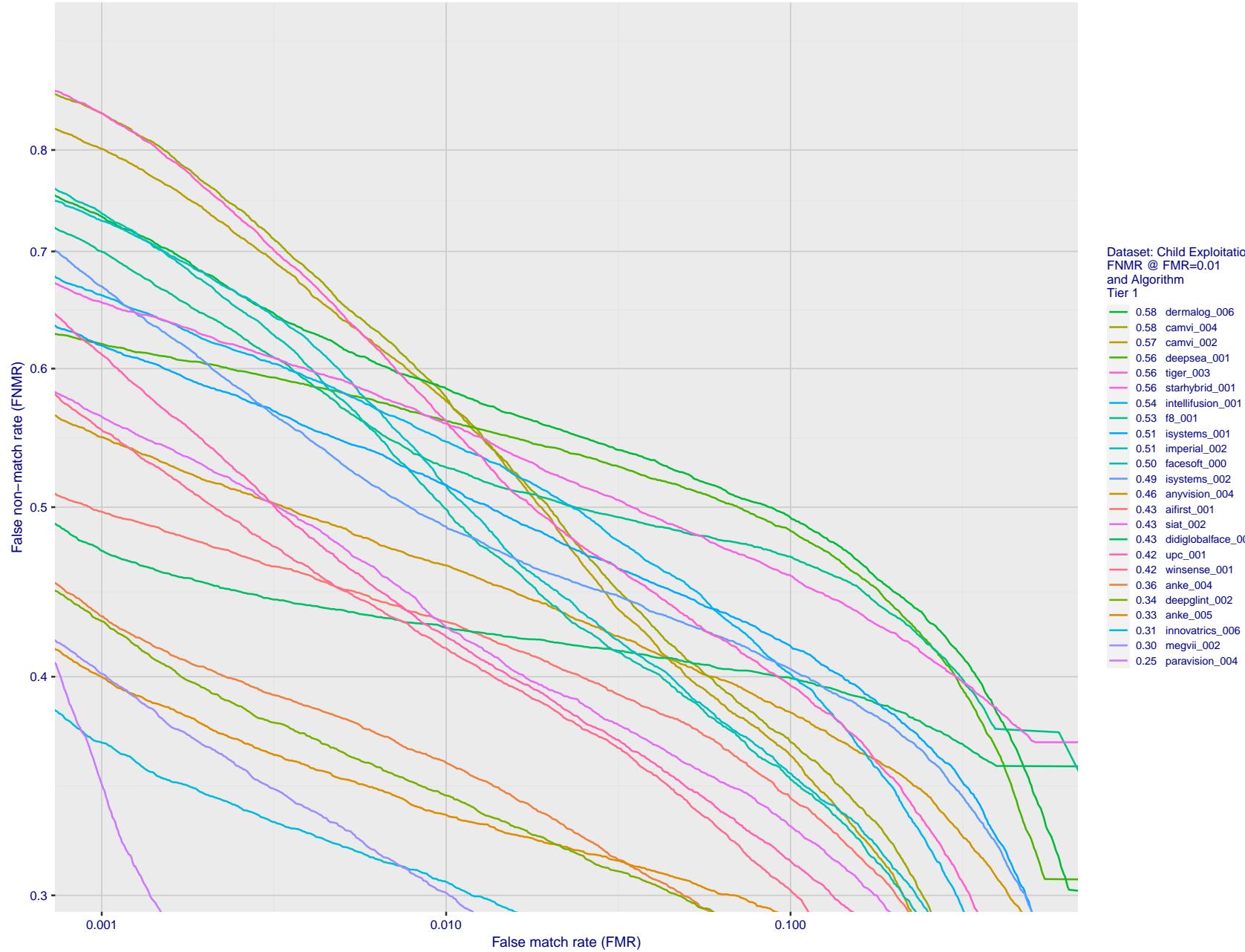


Figure 86: For child exploitation images, detection error tradeoff (DET) characteristics showing false non-match rate vs. false match rate plotted parametrically on threshold, T. The scales are logarithmic in order to show many decades of FMR. Accuracy is poor because many images have adverse quality characteristics, and because detection and enrollment fails.

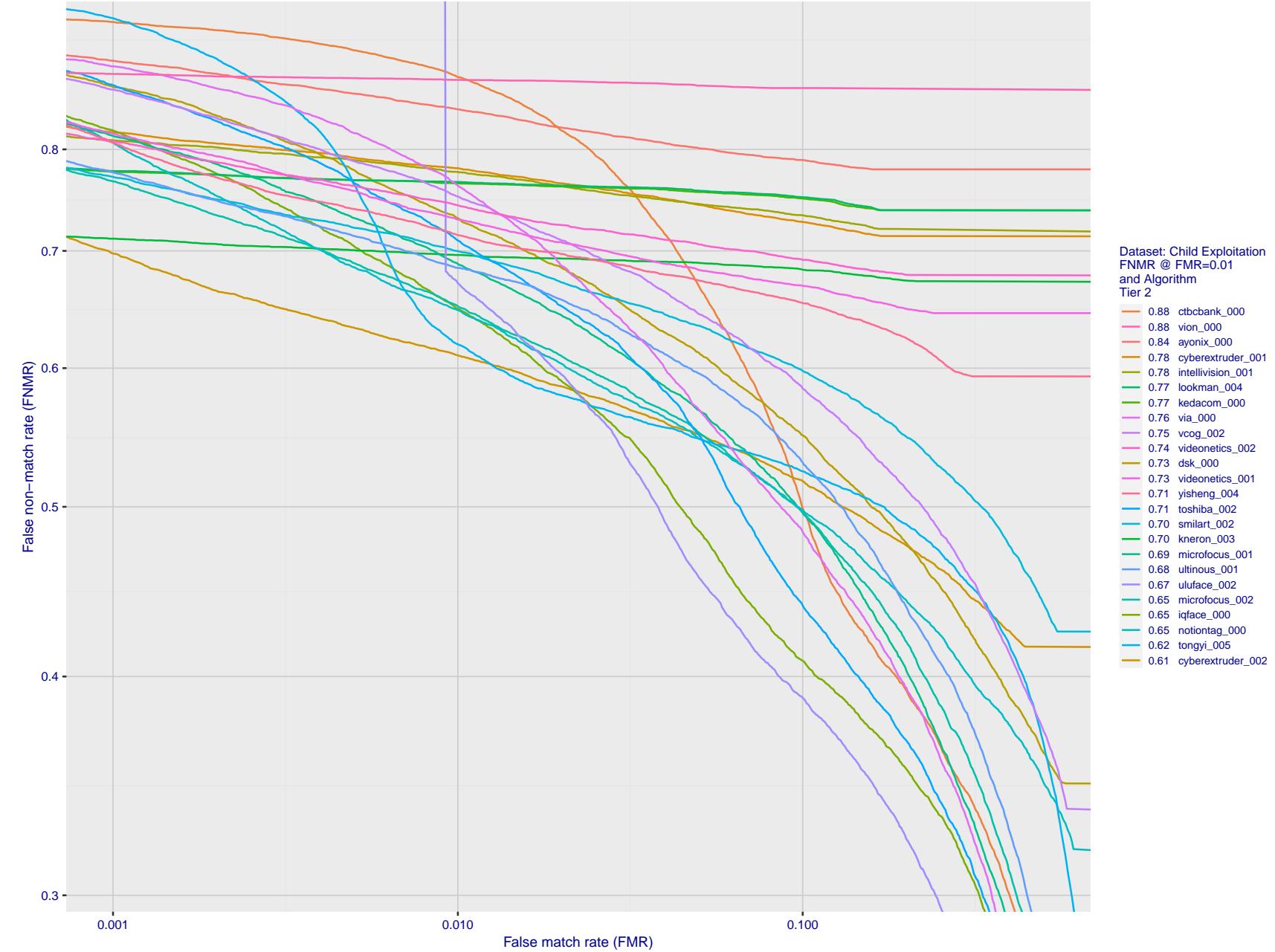


Figure 87: For child exploitation images, detection error tradeoff (DET) characteristics showing false non-match rate vs. false match rate plotted parametrically on threshold,  $T$ . The scales are logarithmic in order to show many decades of FMR. Accuracy is poor because many images have adverse quality characteristics, and because detection and enrollment fails.

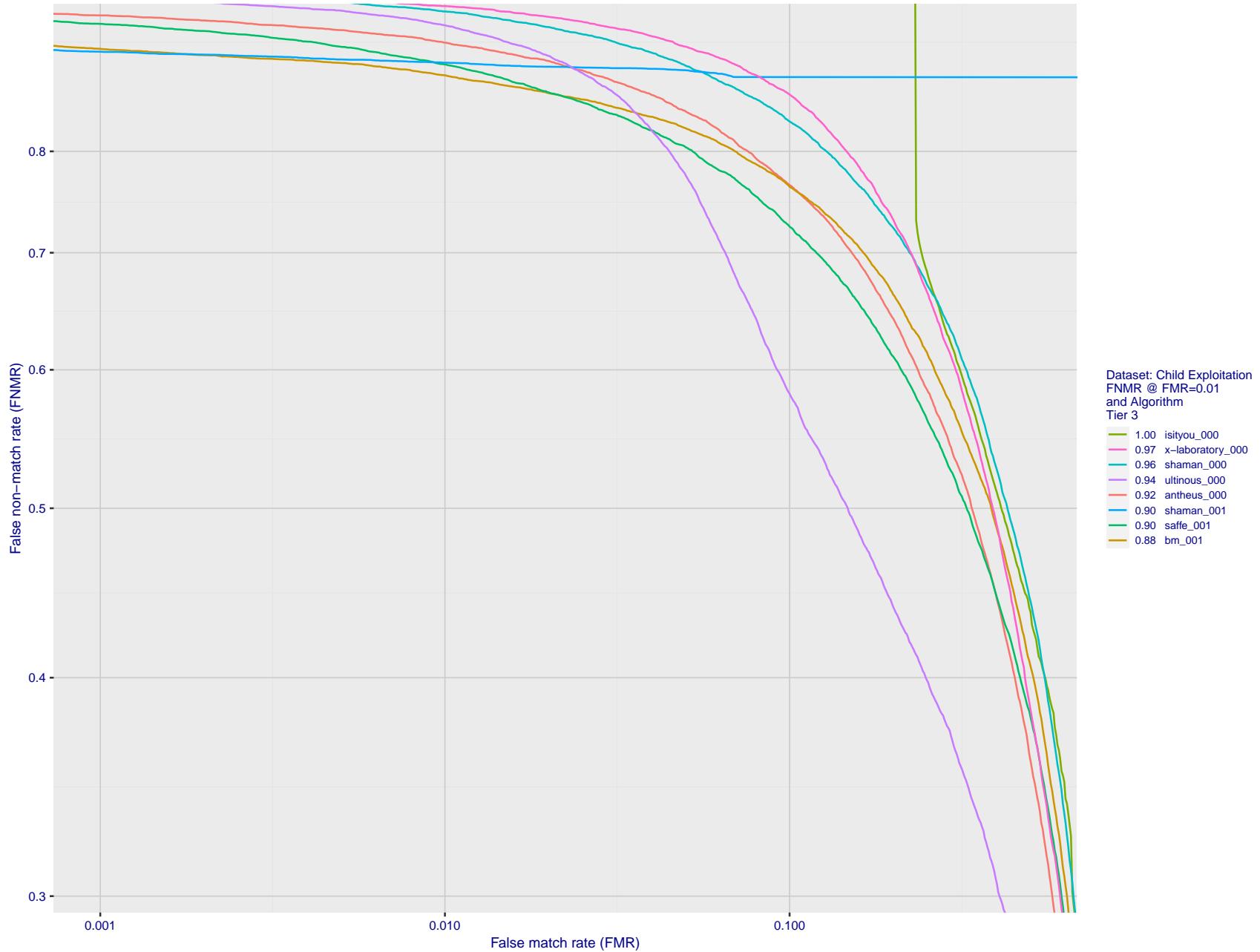


Figure 88: For child exploitation images, detection error tradeoff (DET) characteristics showing false non-match rate vs. false match rate plotted parametrically on threshold,  $T$ . The scales are logarithmic in order to show many decades of FMR. Accuracy is poor because many images have adverse quality characteristics, and because detection and enrollment fails.

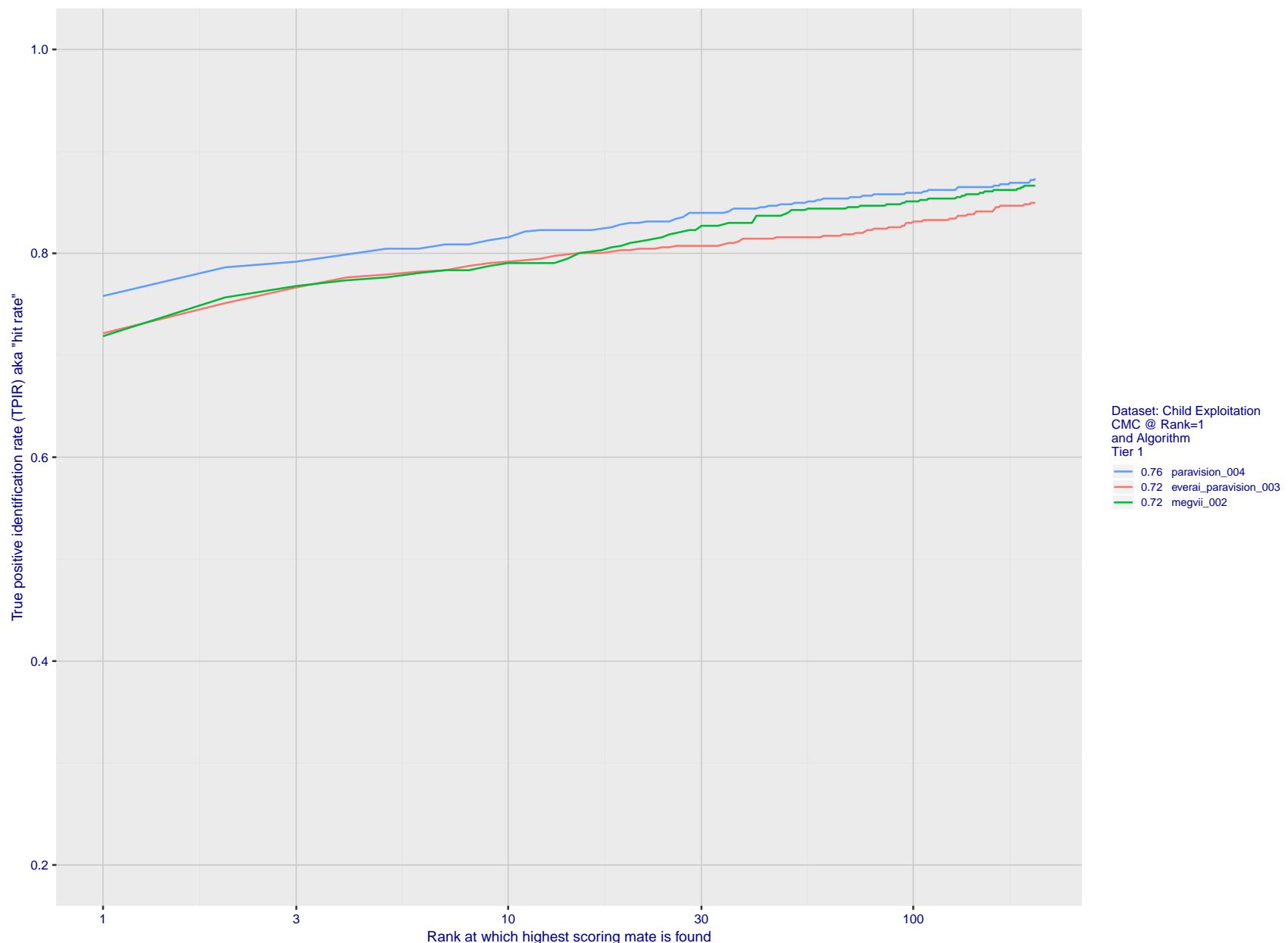


Figure 89: For child exploitation images, cumulative match characteristics (CMC) showing true positive identification rate vs. rank. This is simulation of a one-to-many search experiment - see discussion in section 3.2. The scales are logarithmic in order to show the effect of long candidate lists. Accuracy is poor but much improved relative to the 1:1 DETs of Fig. 88 because a search can succeed if any of a subject's several enrolled images matches the search image with a high score.

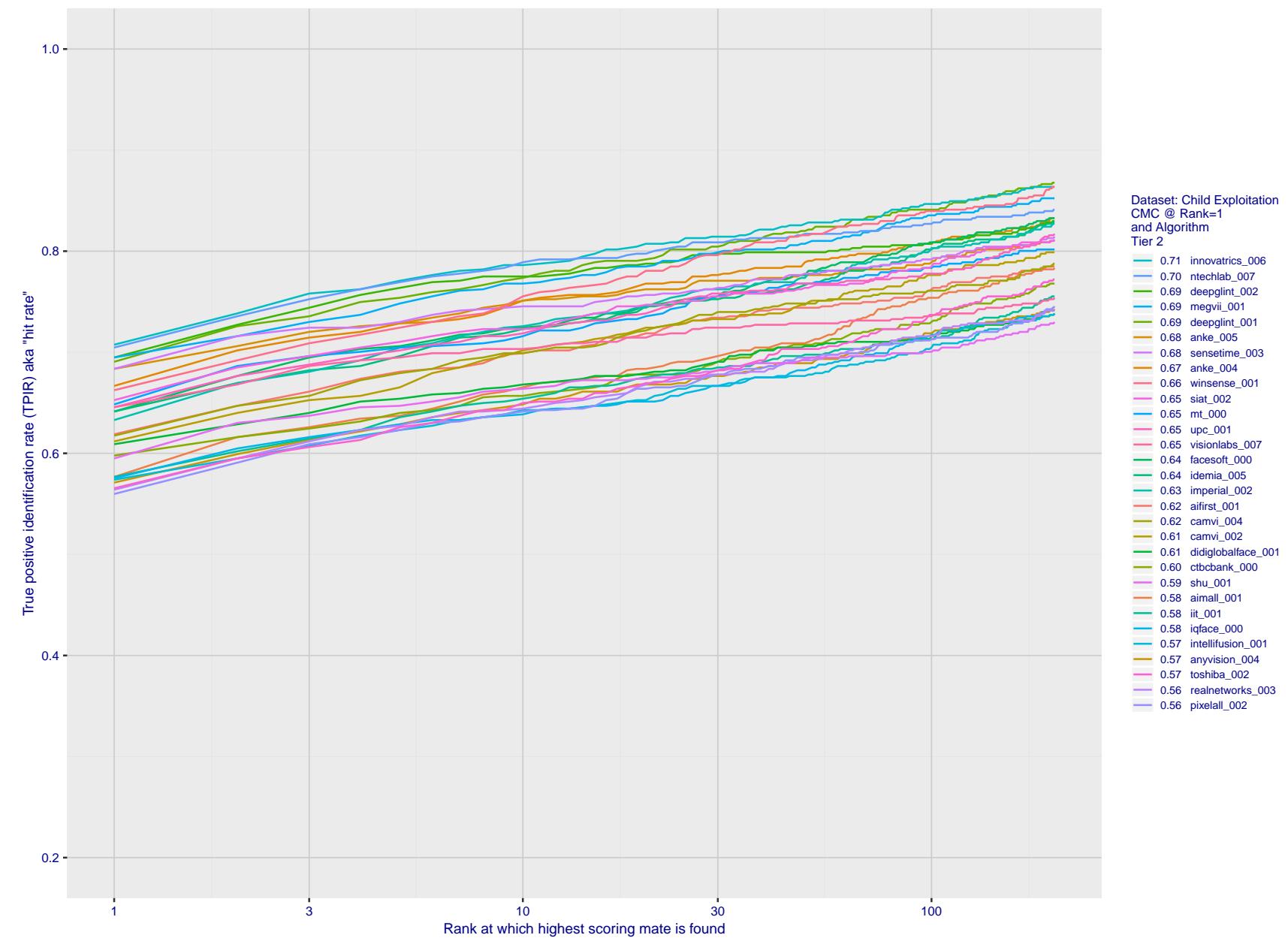


Figure 90: For child exploitation images, cumulative match characteristics (CMC) showing true positive identification rate vs. rank. This is simulation of a one-to-many search experiment - see discussion in section 3.2. The scales are logarithmic in order to show the effect of long candidate lists. Accuracy is poor but much improved relative to the 1:1 DETs of Fig. 88 because a search can succeed if any of a subject's several enrolled images matches the search image with a high score.

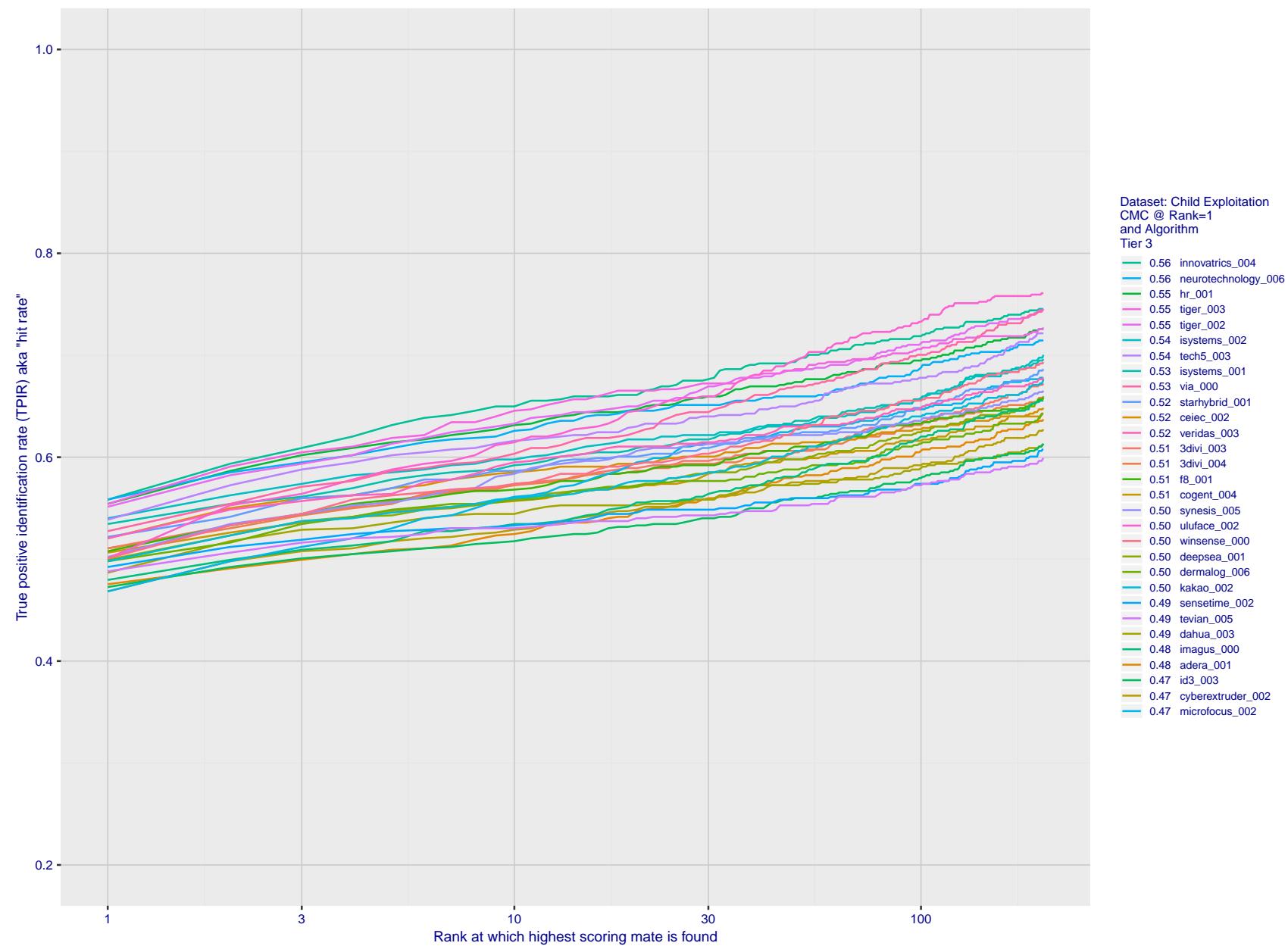


Figure 91: For child exploitation images, cumulative match characteristics (CMC) showing true positive identification rate vs. rank. This is simulation of a one-to-many search experiment - see discussion in section 3.2. The scales are logarithmic in order to show the effect of long candidate lists. Accuracy is poor but much improved relative to the 1:1 DETs of Fig. 88 because a search can succeed if any of a subject's several enrolled images matches the search image with a high score.

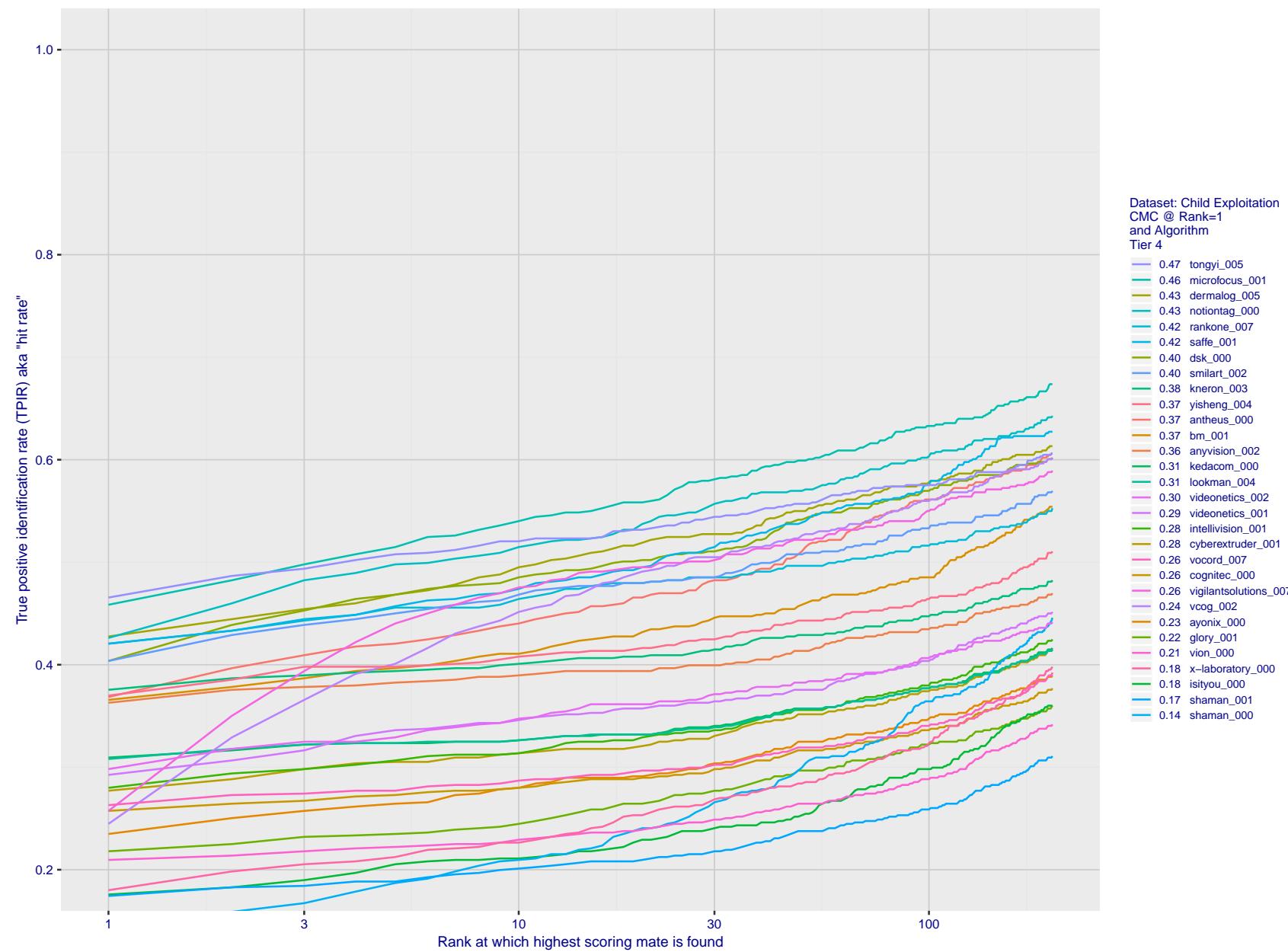


Figure 92: For child exploitation images, cumulative match characteristics (CMC) showing true positive identification rate vs. rank. This is simulation of a one-to-many search experiment - see discussion in section 3.2. The scales are logarithmic in order to show the effect of long candidate lists. Accuracy is poor but much improved relative to the 1:1 DETs of Fig. 88 because a search can succeed if any of a subject's several enrolled images matches the search image with a high score.

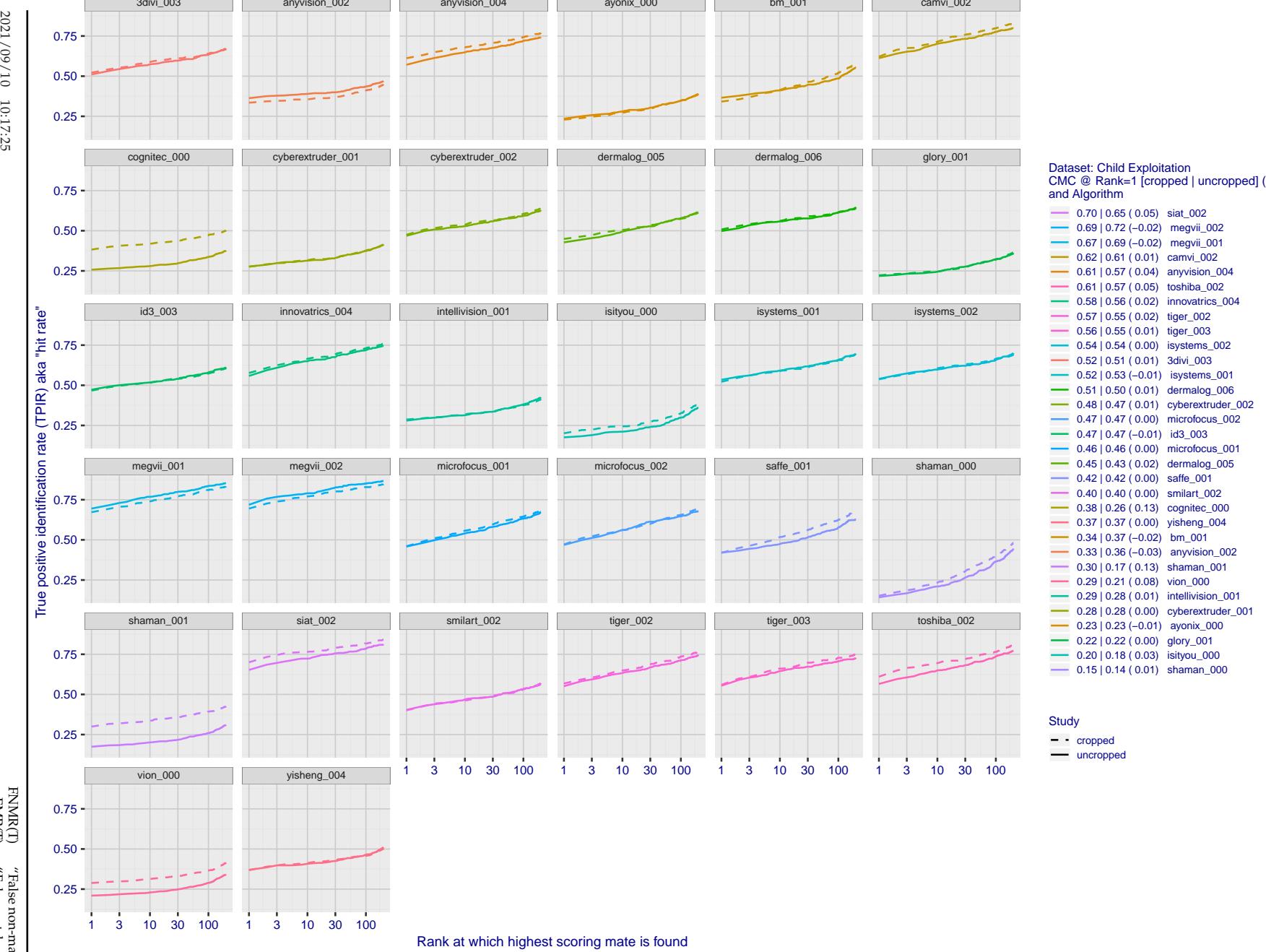


Figure 93: For child exploitation images, cumulative match characteristics (CMC) showing true positive identification rate vs. rank for two cases: 1. Whole image provided to the algorithm; 2. Human annotated rectangular region, cropped and provided to the algorithm. The difference between the traces is associated with detection of difficult faces, and fine localization.

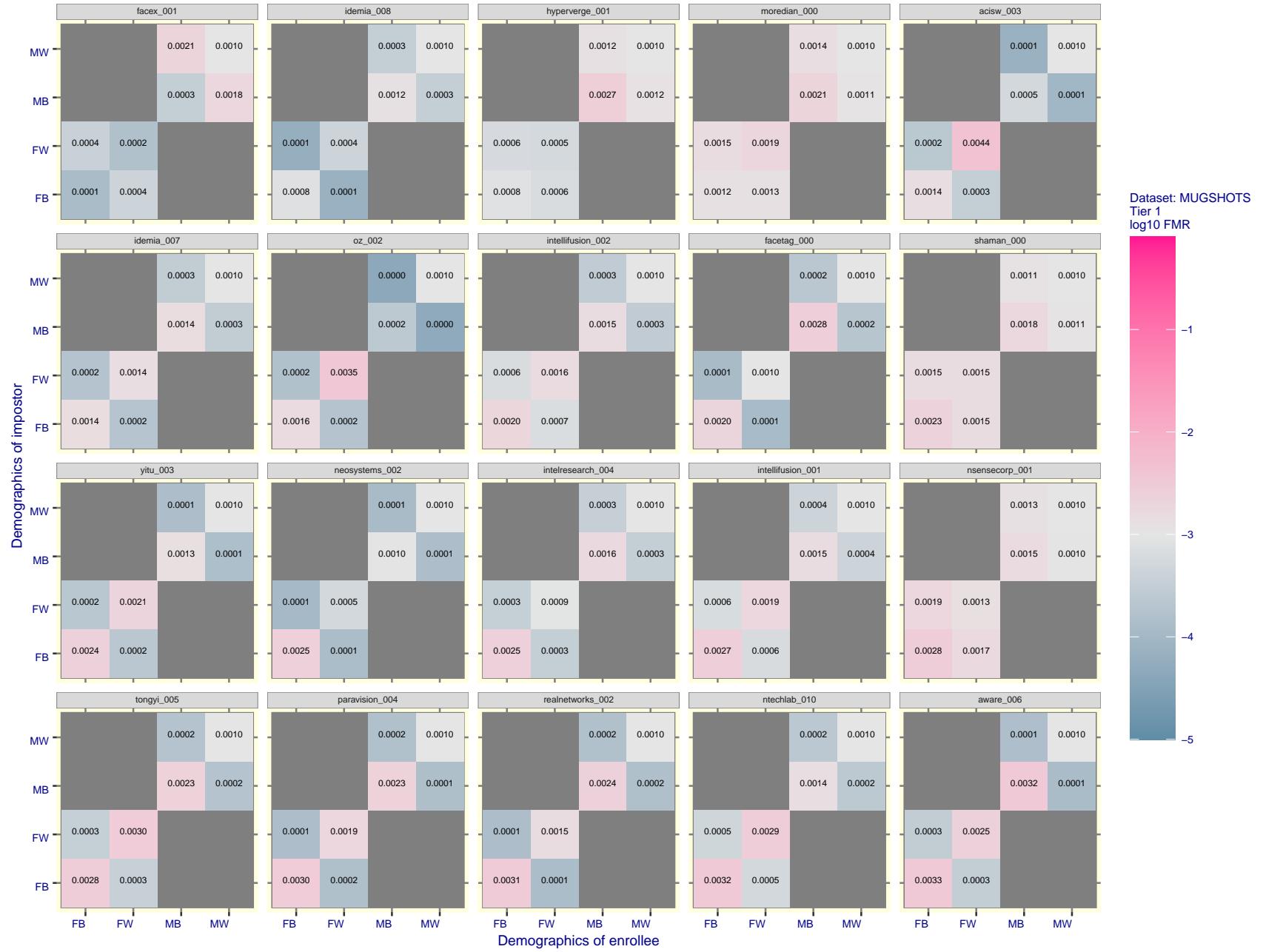


Figure 94: For the mugshot images, FMR for same-sex impostor pairs of images annotated with codes for black female, black male, white female, white male. The threshold is set for each algorithm to give FMR = 0.001 for white males which is the demographic that usually gives the lowest FMR. This means the top right box is the same color in all panels. The panels are sorted over multiple pages in order of FMR on black females, which is the demographic that usually gives the highest FMR.

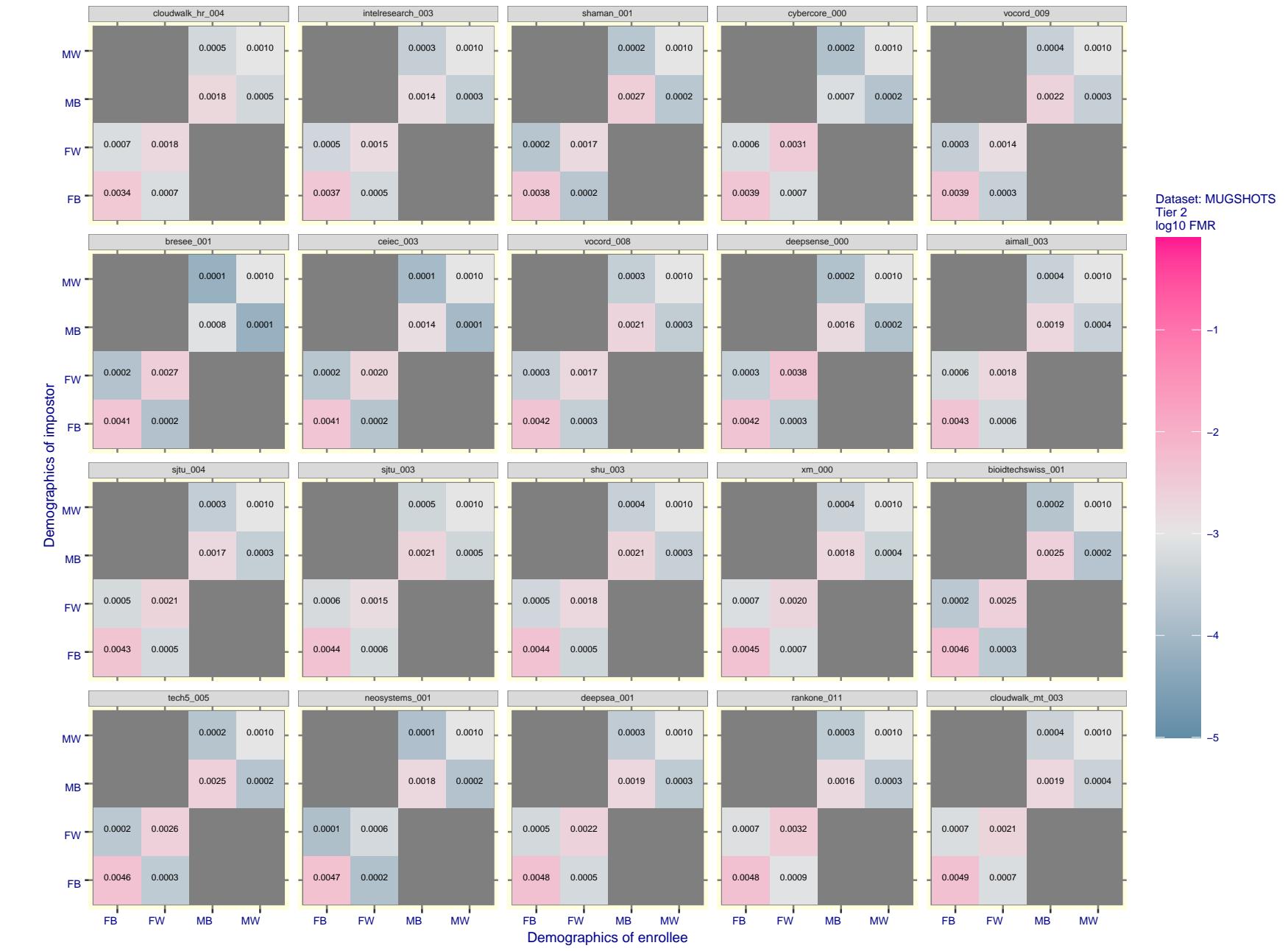


Figure 95: For the mugshot images, FMR for same-sex impostor pairs of images annotated with codes for black female, black male, white female, white male. The threshold is set for each algorithm to give  $FMR = 0.001$  for white males which is the demographic that usually gives the lowest FMR. This means the top right box is the same color in all panels. The panels are sorted over multiple pages in order of FMR on black females, which is the demographic that usually gives the highest FMR.

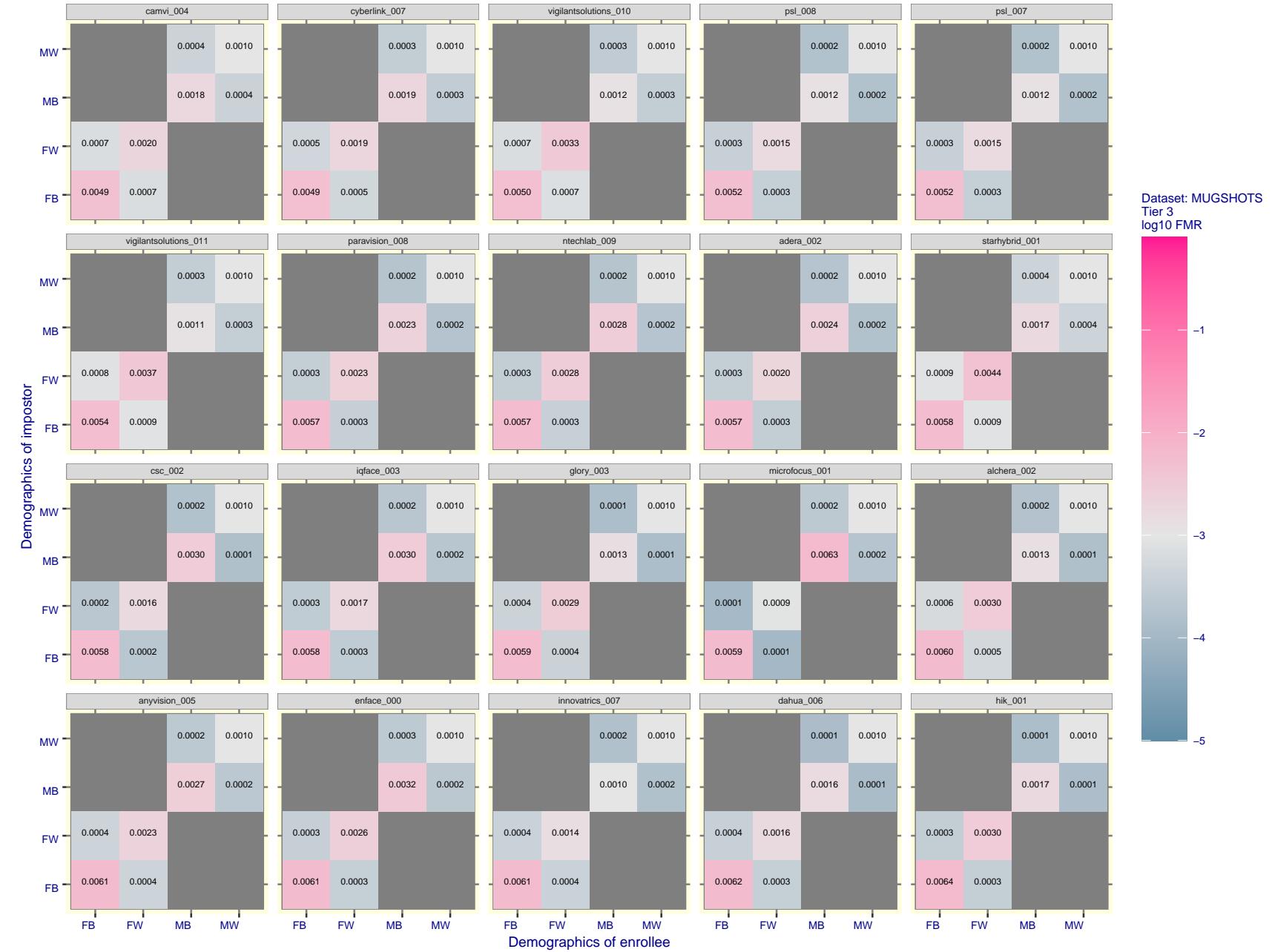


Figure 96: For the mugshot images, FMR for same-sex impostor pairs of images annotated with codes for black female, black male, white female, white male. The threshold is set for each algorithm to give FMR = 0.001 for white males which is the demographic that usually gives the lowest FMR. This means the top right box is the same color in all panels. The panels are sorted over multiple pages in order of FMR on black females, which is the demographic that usually gives the highest FMR.

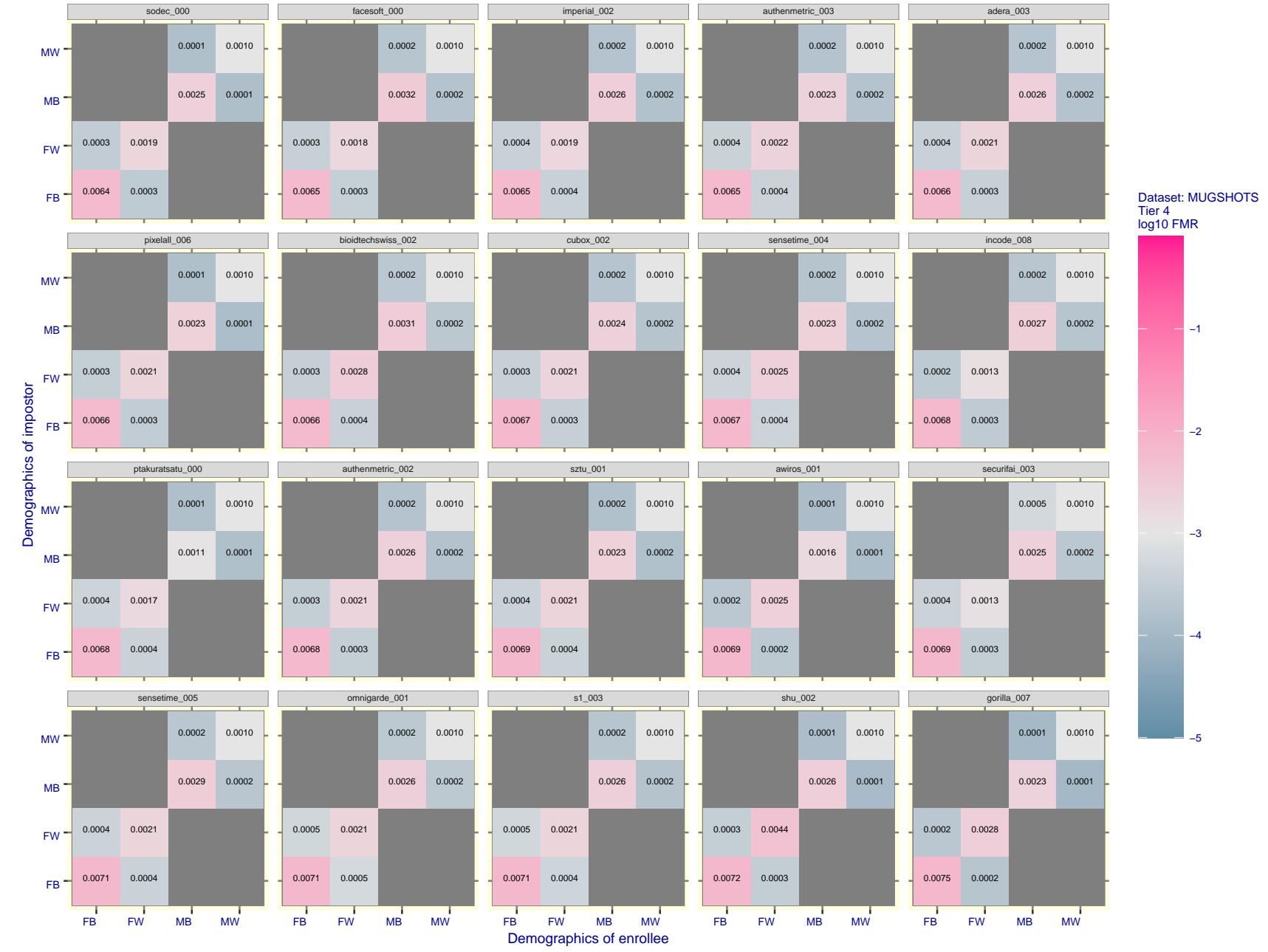


Figure 97: For the mugshot images, FMR for same-sex impostor pairs of images annotated with codes for black female, black male, white female, white male. The threshold is set for each algorithm to give  $\text{FMR} = 0.001$  for white males which is the demographic that usually gives the lowest FMR. This means the top right box is the same color in all panels. The panels are sorted over multiple pages in order of FMR on black females, which is the demographic that usually gives the highest FMR.

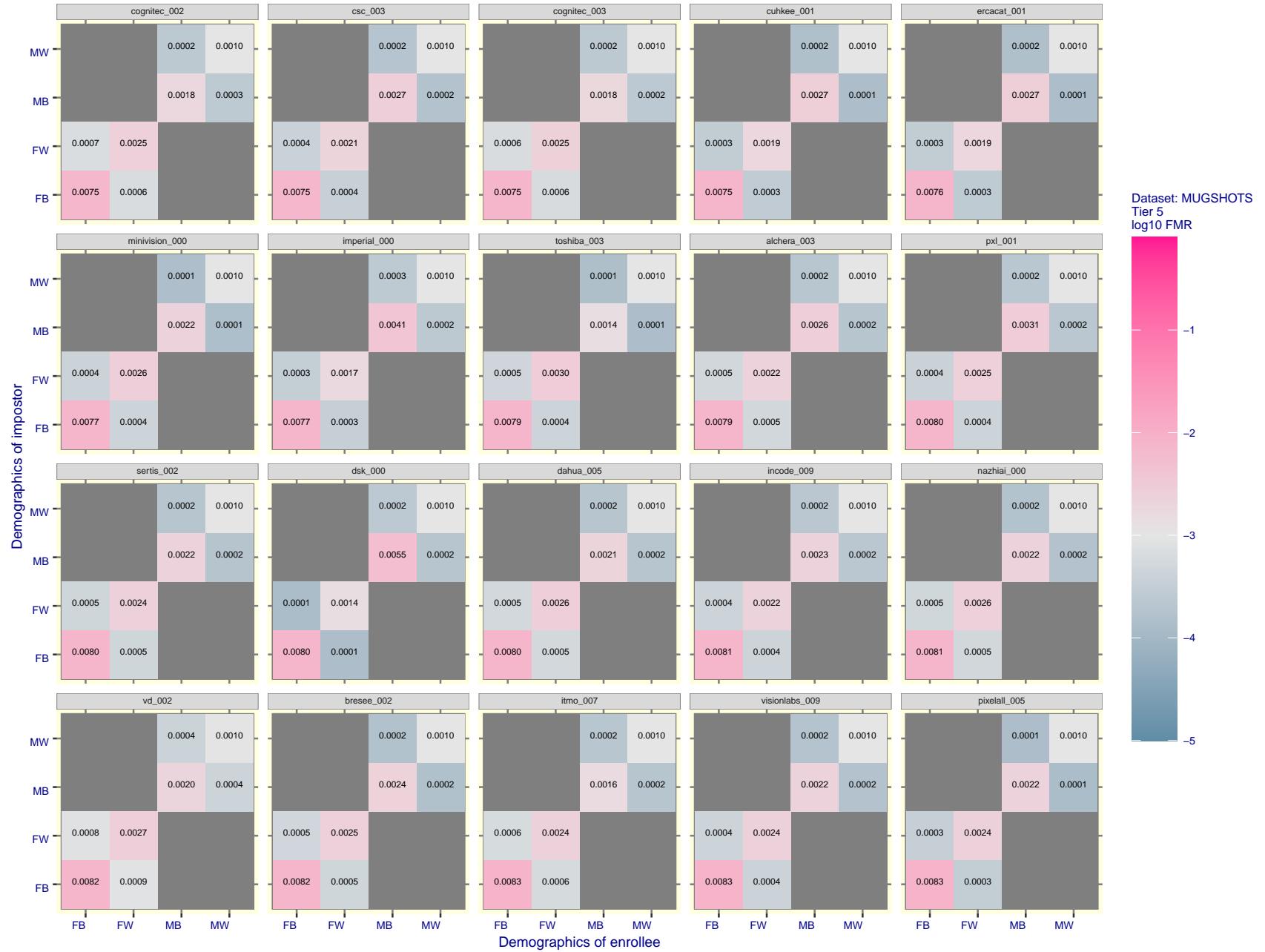


Figure 98: For the mugshot images, FMR for same-sex impostor pairs of images annotated with codes for black female, black male, white female, white male. The threshold is set for each algorithm to give FMR = 0.001 for white males which is the demographic that usually gives the lowest FMR. This means the top right box is the same color in all panels. The panels are sorted over multiple pages in order of FMR on black females, which is the demographic that usually gives the highest FMR.

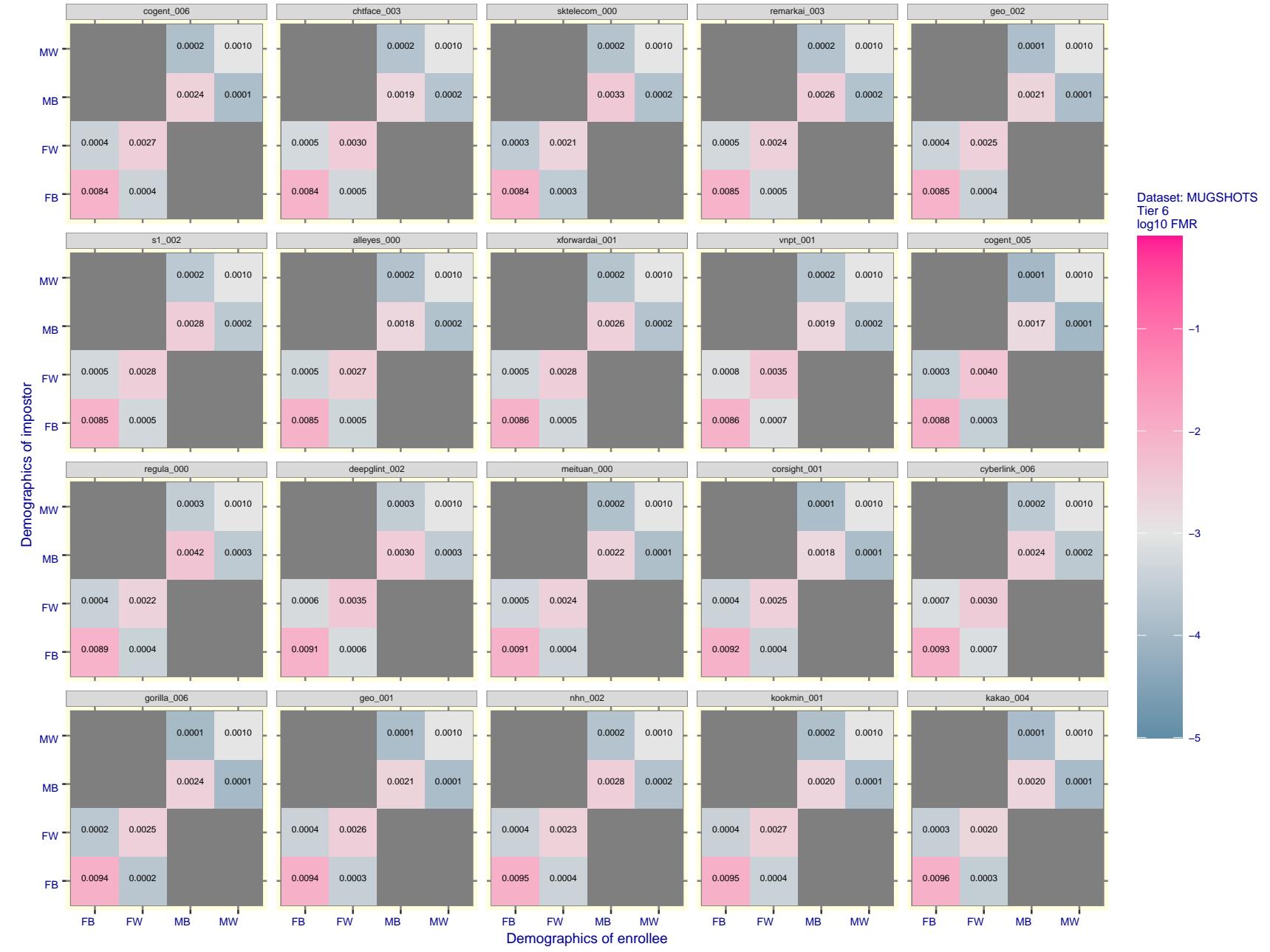


Figure 99: For the mugshot images, FMR for same-sex impostor pairs of images annotated with codes for black female, black male, white female, white male. The threshold is set for each algorithm to give  $FMR = 0.001$  for white males which is the demographic that usually gives the lowest FMR. This means the top right box is the same color in all panels. The panels are sorted over multiple pages in order of FMR on black females, which is the demographic that usually gives the highest FMR.

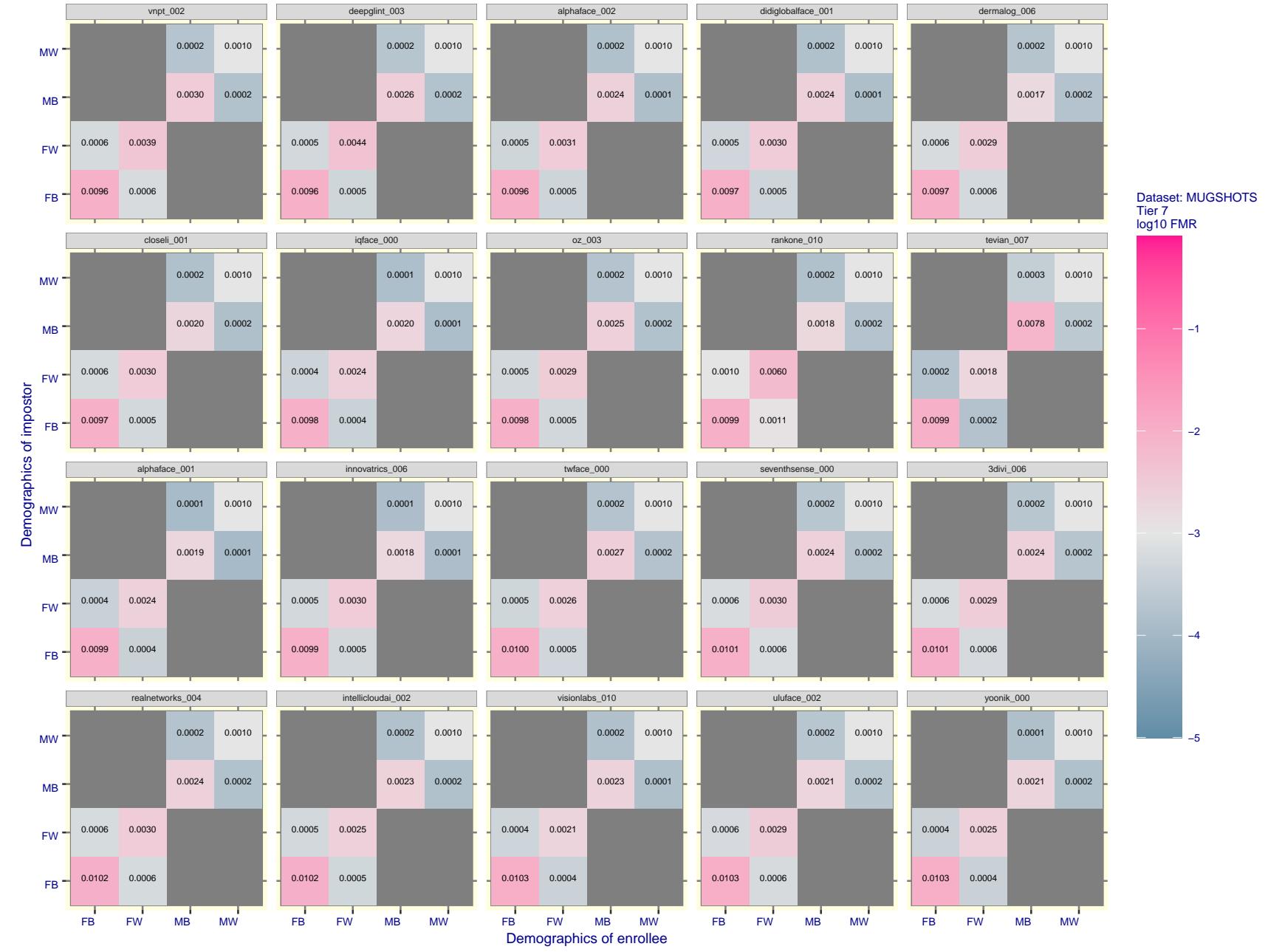


Figure 100: For the mugshot images, FMR for same-sex impostor pairs of images annotated with codes for black female, black male, white female, white male. The threshold is set for each algorithm to give FMR = 0.001 for white males which is the demographic that usually gives the lowest FMR. This means the top right box is the same color in all panels. The panels are sorted over multiple pages in order of FMR on black females, which is the demographic that usually gives the highest FMR.

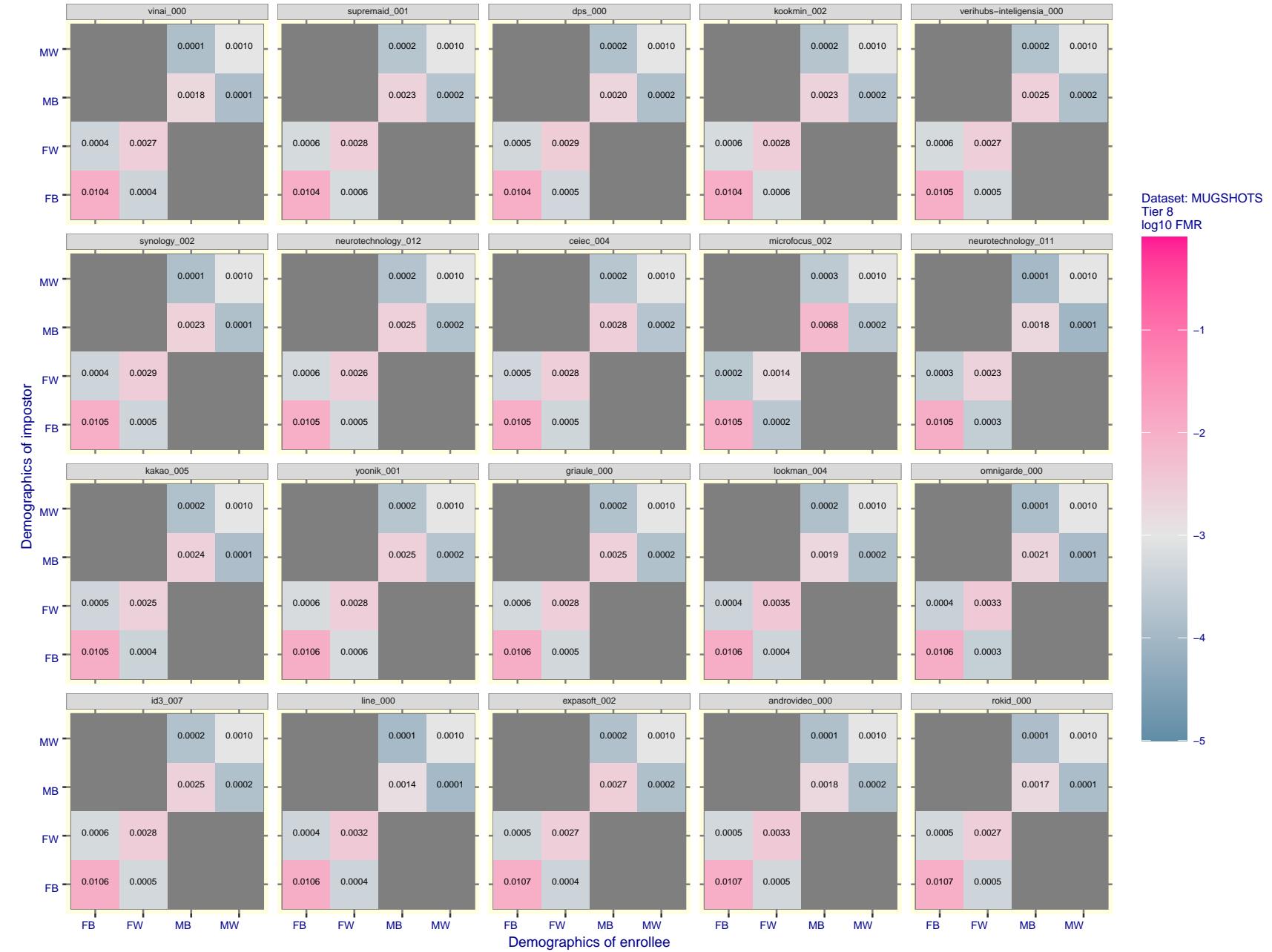


Figure 101: For the mugshot images, FMR for same-sex impostor pairs of images annotated with codes for black female, black male, white female, white male. The threshold is set for each algorithm to give FMR = 0.001 for white males which is the demographic that usually gives the lowest FMR. This means the top right box is the same color in all panels. The panels are sorted over multiple pages in order of FMR on black females, which is the demographic that usually gives the highest FMR.

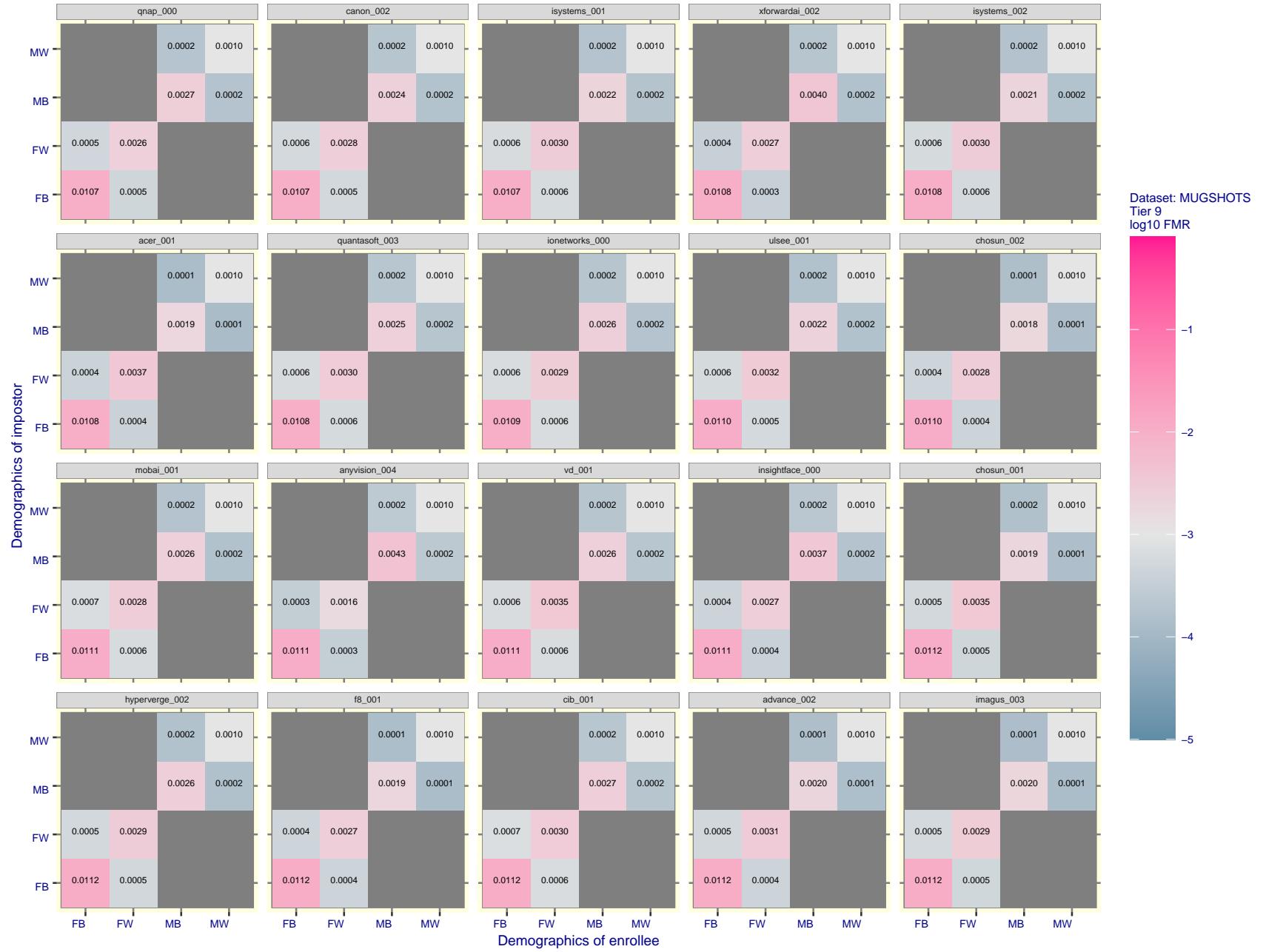


Figure 102: For the mugshot images, FMR for same-sex impostor pairs of images annotated with codes for black female, black male, white female, white male. The threshold is set for each algorithm to give FMR = 0.001 for white males which is the demographic that usually gives the lowest FMR. This means the top right box is the same color in all panels. The panels are sorted over multiple pages in order of FMR on black females, which is the demographic that usually gives the highest FMR.

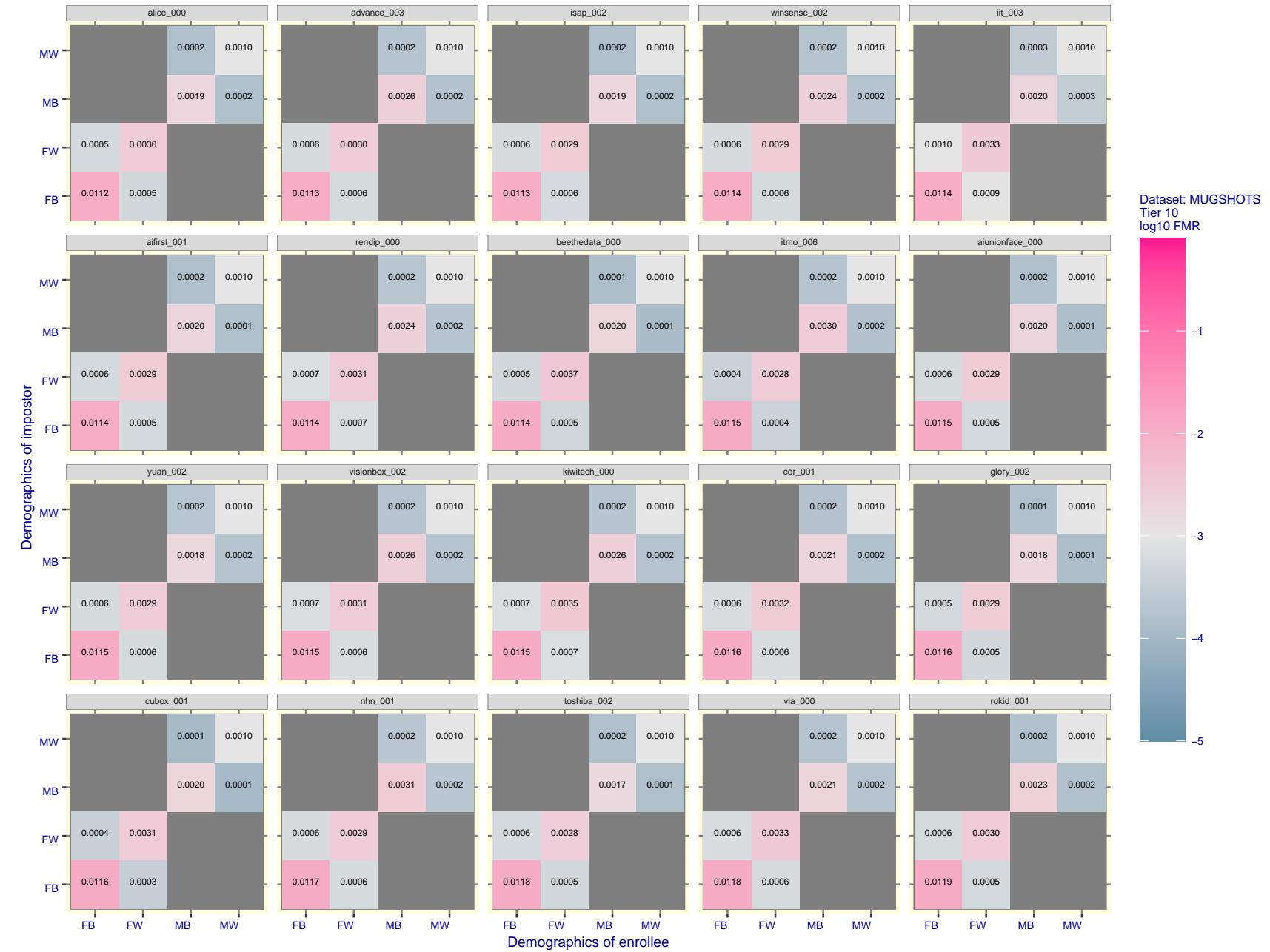


Figure 103: For the mugshot images, FMR for same-sex impostor pairs of images annotated with codes for black female, black male, white female, white male. The threshold is set for each algorithm to give FMR = 0.001 for white males which is the demographic that usually gives the lowest FMR. This means the top right box is the same color in all panels. The panels are sorted over multiple pages in order of FMR on black females, which is the demographic that usually gives the highest FMR.

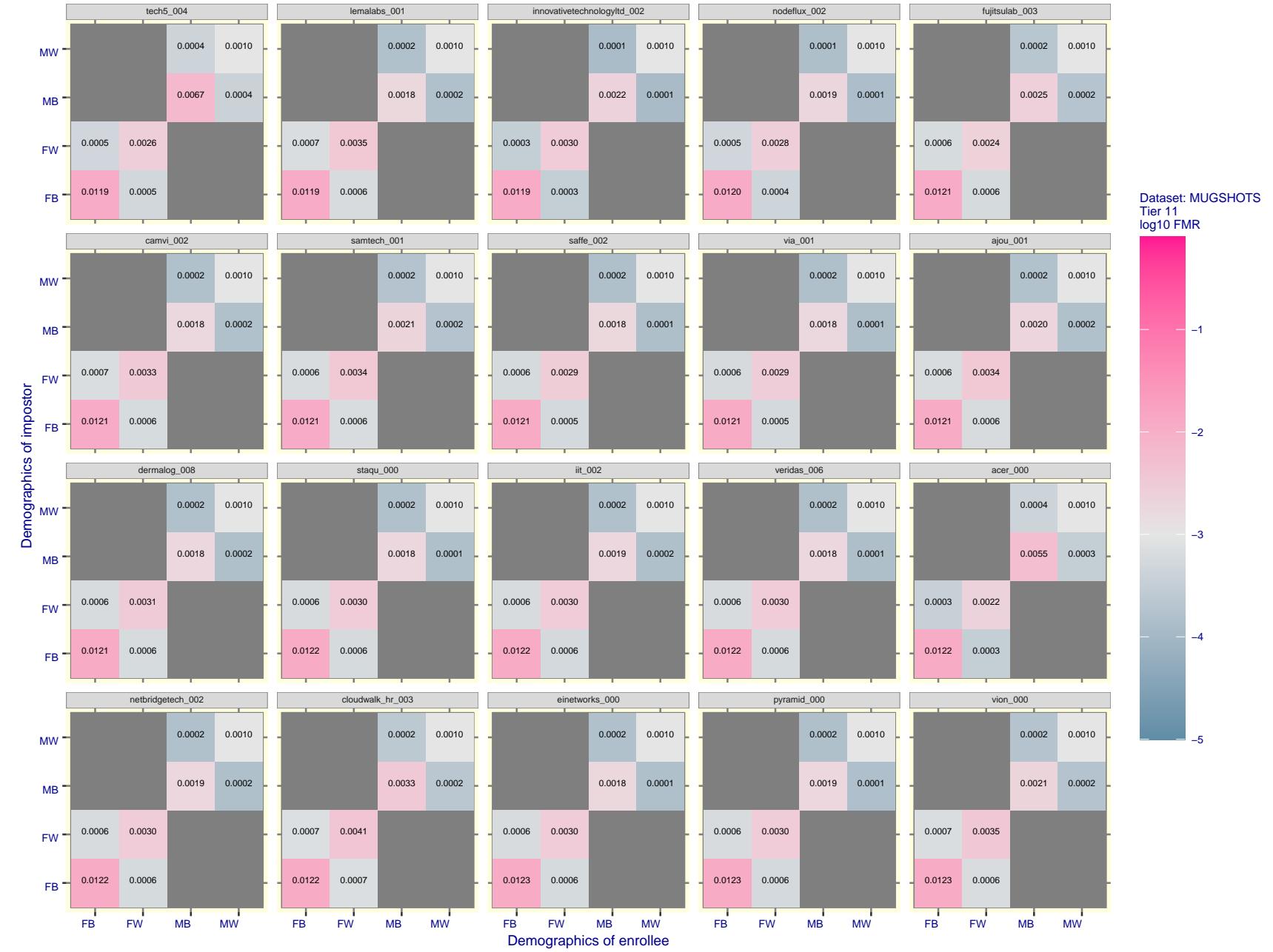


Figure 104: For the mugshot images, FMR for same-sex impostor pairs of images annotated with codes for black female, black male, white female, white male. The threshold is set for each algorithm to give FMR = 0.001 for white males which is the demographic that usually gives the lowest FMR. This means the top right box is the same color in all panels. The panels are sorted over multiple pages in order of FMR on black females, which is the demographic that usually gives the highest FMR.

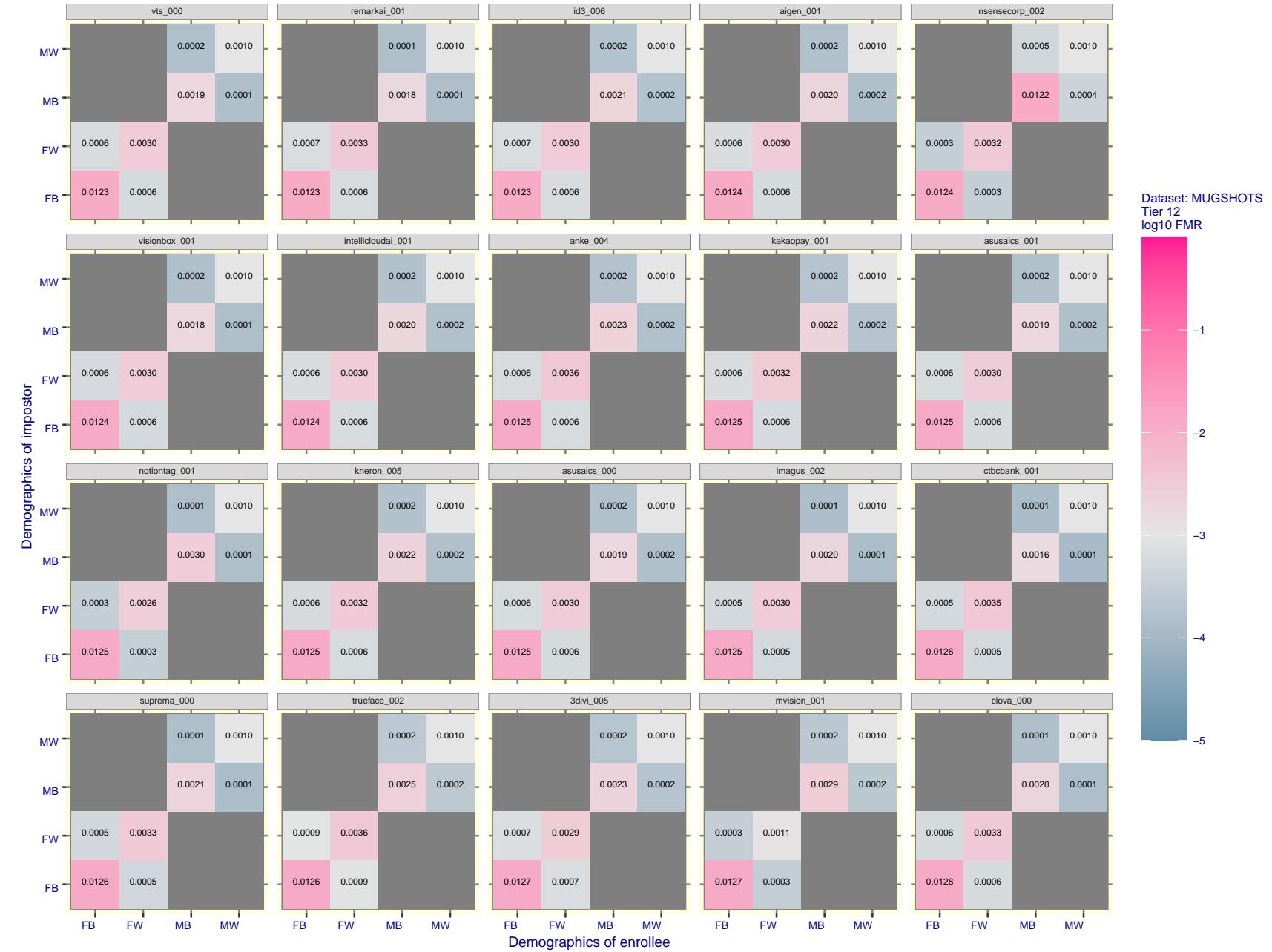


Figure 105: For the mugshot images, FMR for same-sex impostor pairs of images annotated with codes for black female, black male, white female, white male. The threshold is set for each algorithm to give FMR = 0.001 for white males which is the demographic that usually gives the lowest FMR. This means the top right box is the same color in all panels. The panels are sorted over multiple pages in order of FMR on black females, which is the demographic that usually gives the highest FMR.

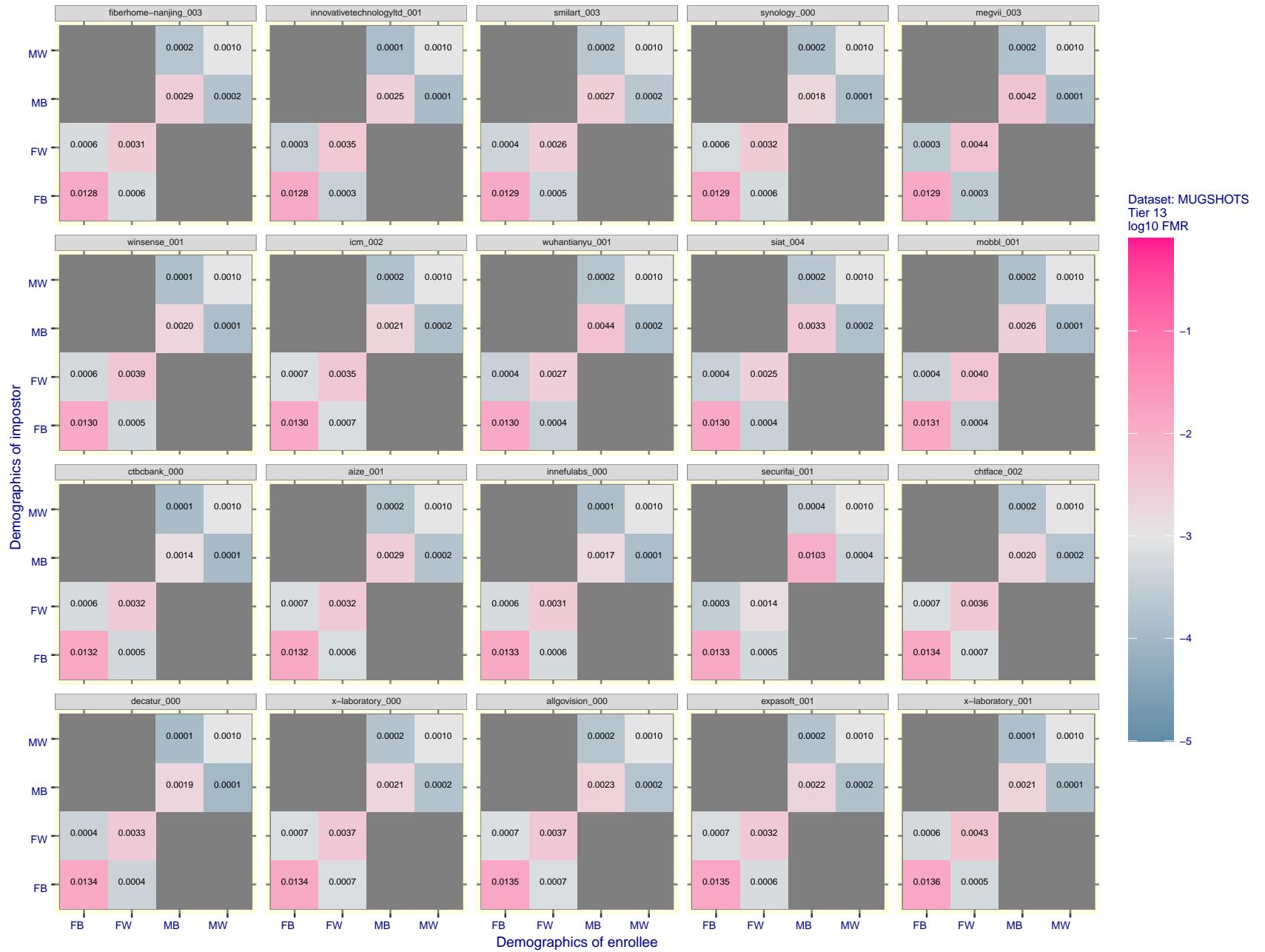


Figure 106: For the mugshot images, FMR for same-sex impostor pairs of images annotated with codes for black female, black male, white female, white male. The threshold is set for each algorithm to give FMR = 0.001 for white males which is the demographic that usually gives the lowest FMR. This means the top right box is the same color in all panels. The panels are sorted over multiple pages in order of FMR on black females, which is the demographic that usually gives the highest FMR.

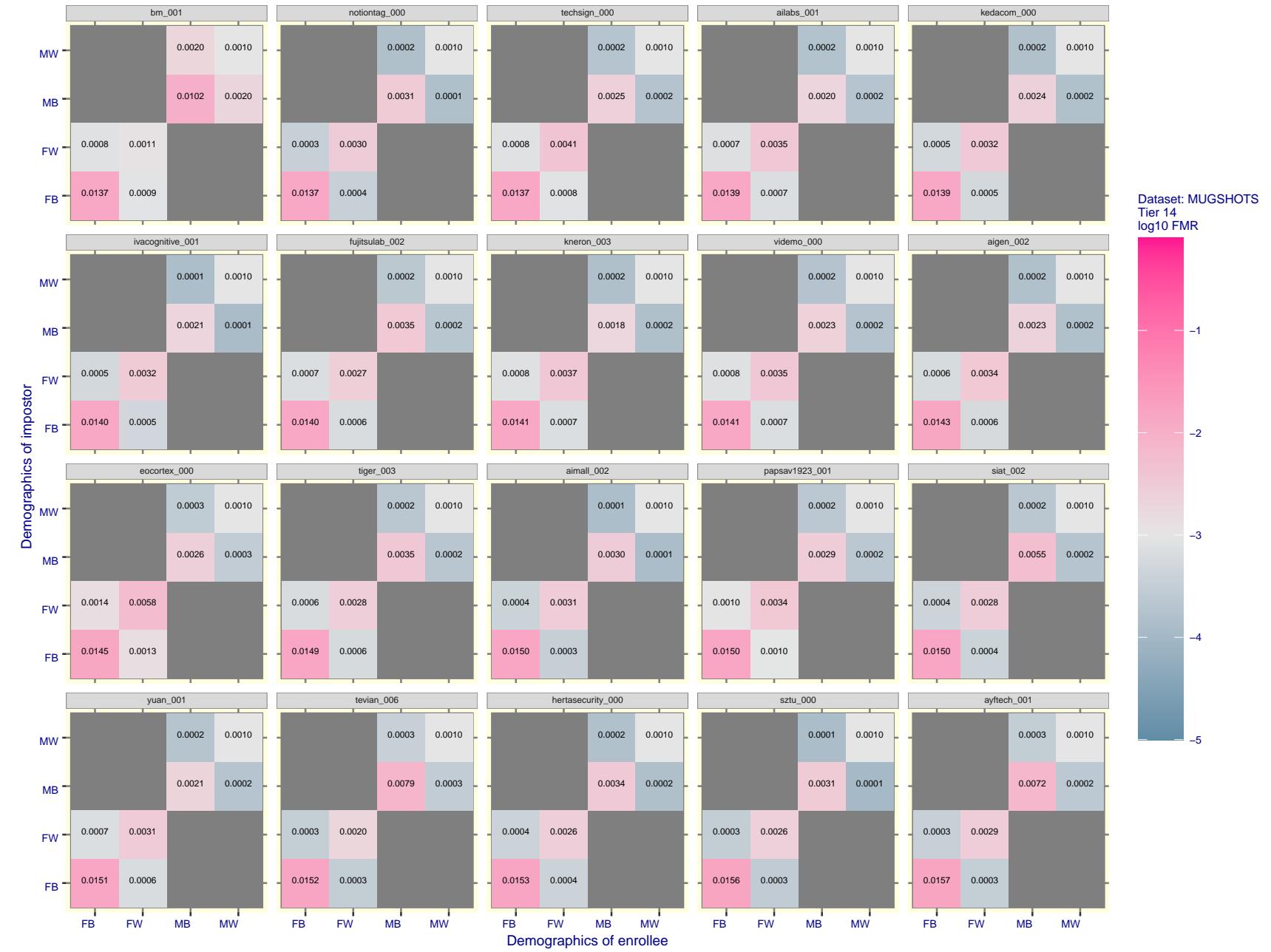


Figure 107: For the mugshot images, FMR for same-sex impostor pairs of images annotated with codes for black female, black male, white female, white male. The threshold is set for each algorithm to give FMR = 0.001 for white males which is the demographic that usually gives the lowest FMR. This means the top right box is the same color in all panels. The panels are sorted over multiple pages in order of FMR on black females, which is the demographic that usually gives the highest FMR.

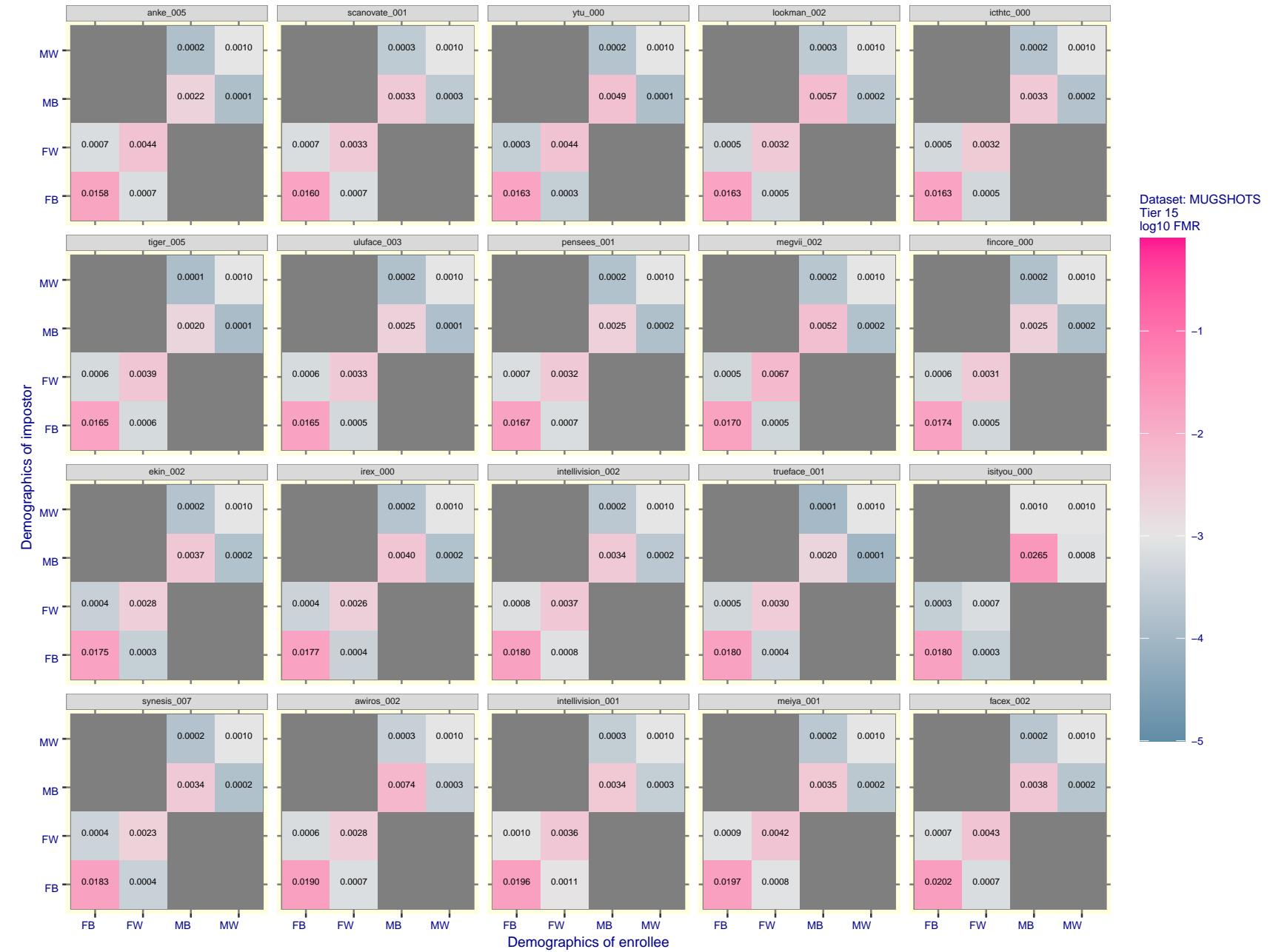


Figure 108: For the mugshot images, FMR for same-sex impostor pairs of images annotated with codes for black female, black male, white female, white male. The threshold is set for each algorithm to give  $FMR = 0.001$  for white males which is the demographic that usually gives the lowest FMR. This means the top right box is the same color in all panels. The panels are sorted over multiple pages in order of FMR on black females, which is the demographic that usually gives the highest FMR.

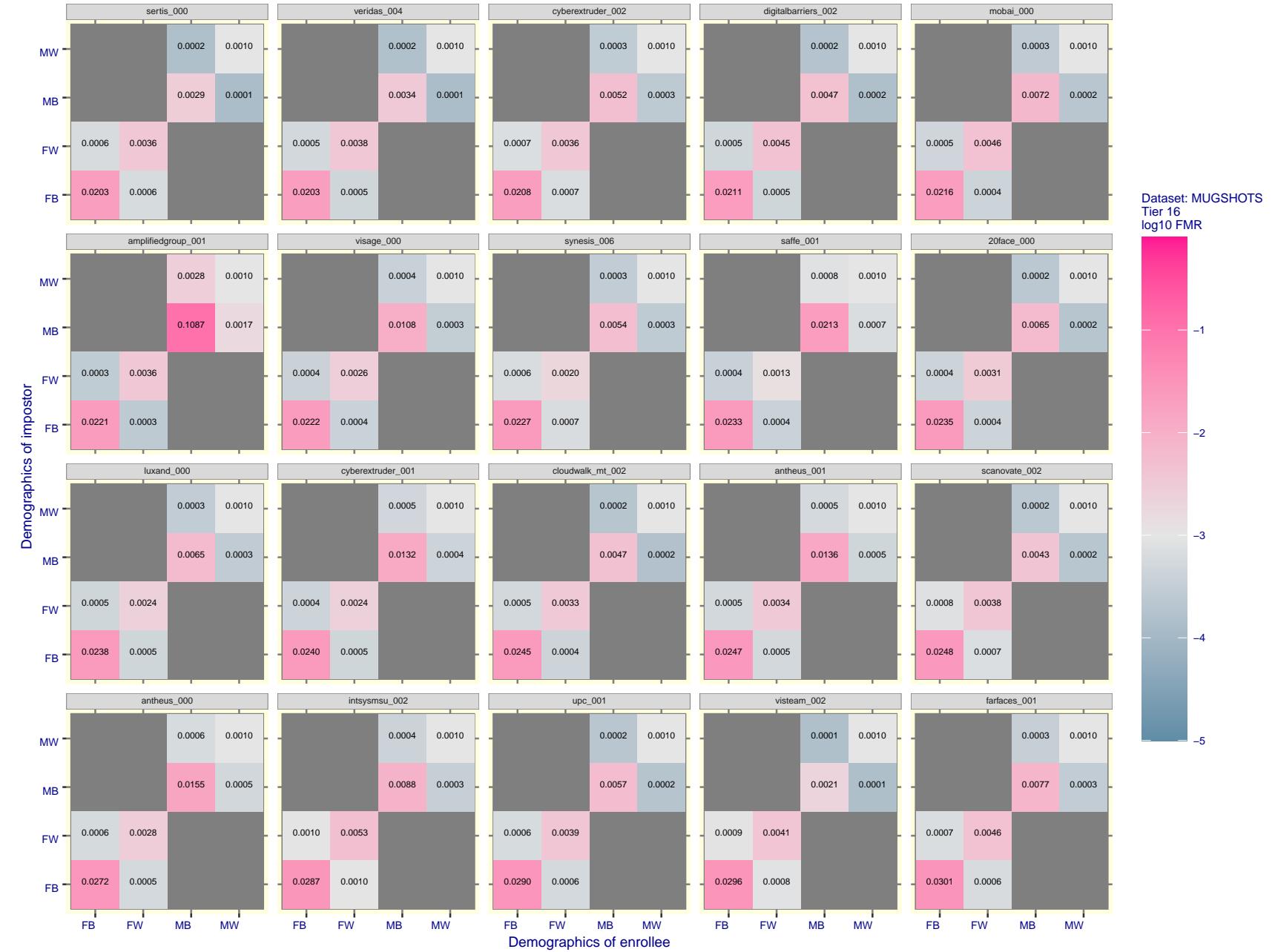


Figure 109: For the mugshot images, FMR for same-sex impostor pairs of images annotated with codes for black female, black male, white female, white male. The threshold is set for each algorithm to give  $FMR = 0.001$  for white males which is the demographic that usually gives the lowest FMR. This means the top right box is the same color in all panels. The panels are sorted over multiple pages in order of FMR on black females, which is the demographic that usually gives the highest FMR.

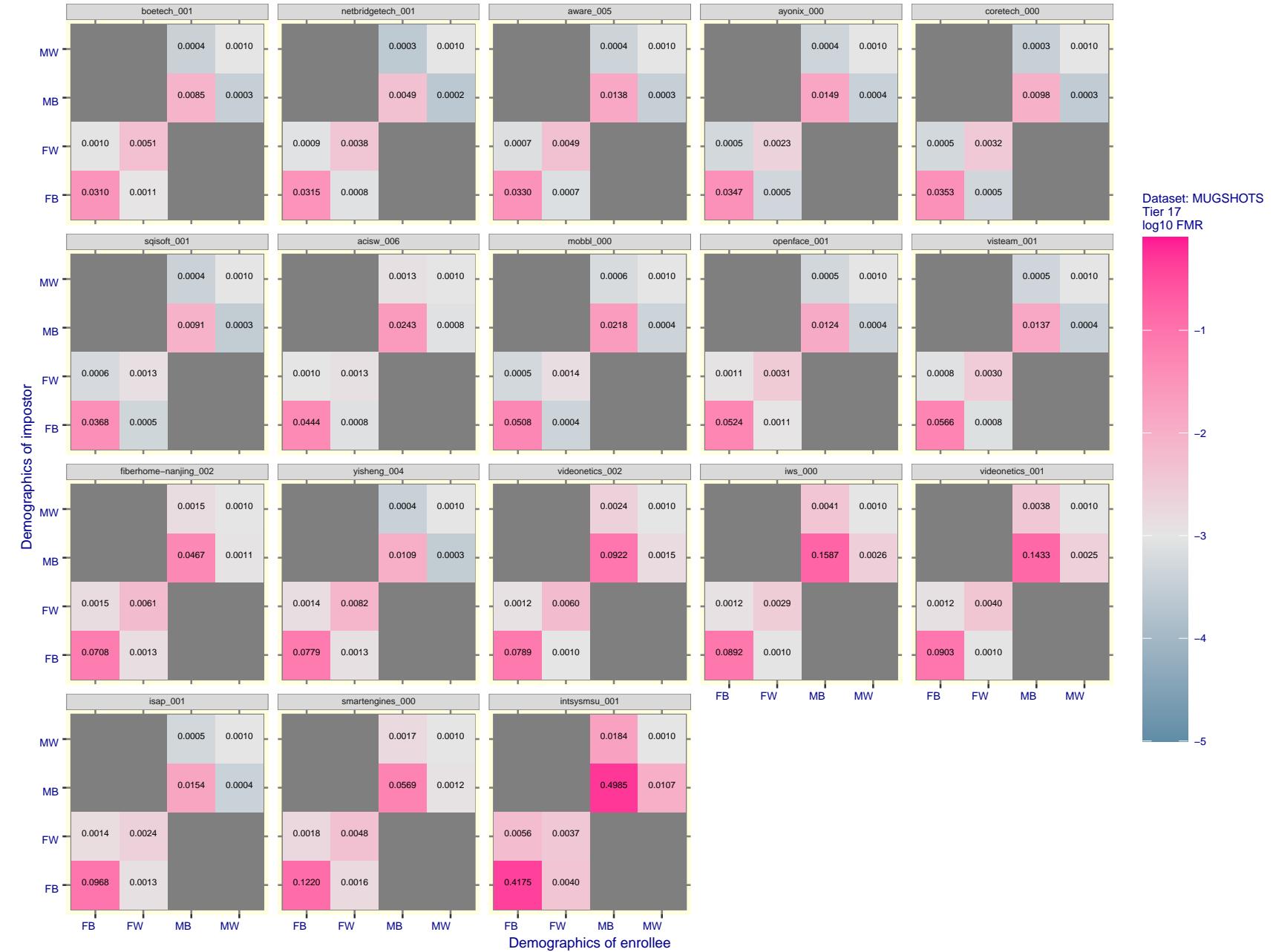


Figure 110: For the mugshot images, FMR for same-sex impostor pairs of images annotated with codes for black female, black male, white female, white male. The threshold is set for each algorithm to give  $\text{FMR} = 0.001$  for white males which is the demographic that usually gives the lowest FMR. This means the top right box is the same color in all panels. The panels are sorted over multiple pages in order of FMR on black females, which is the demographic that usually gives the highest FMR.

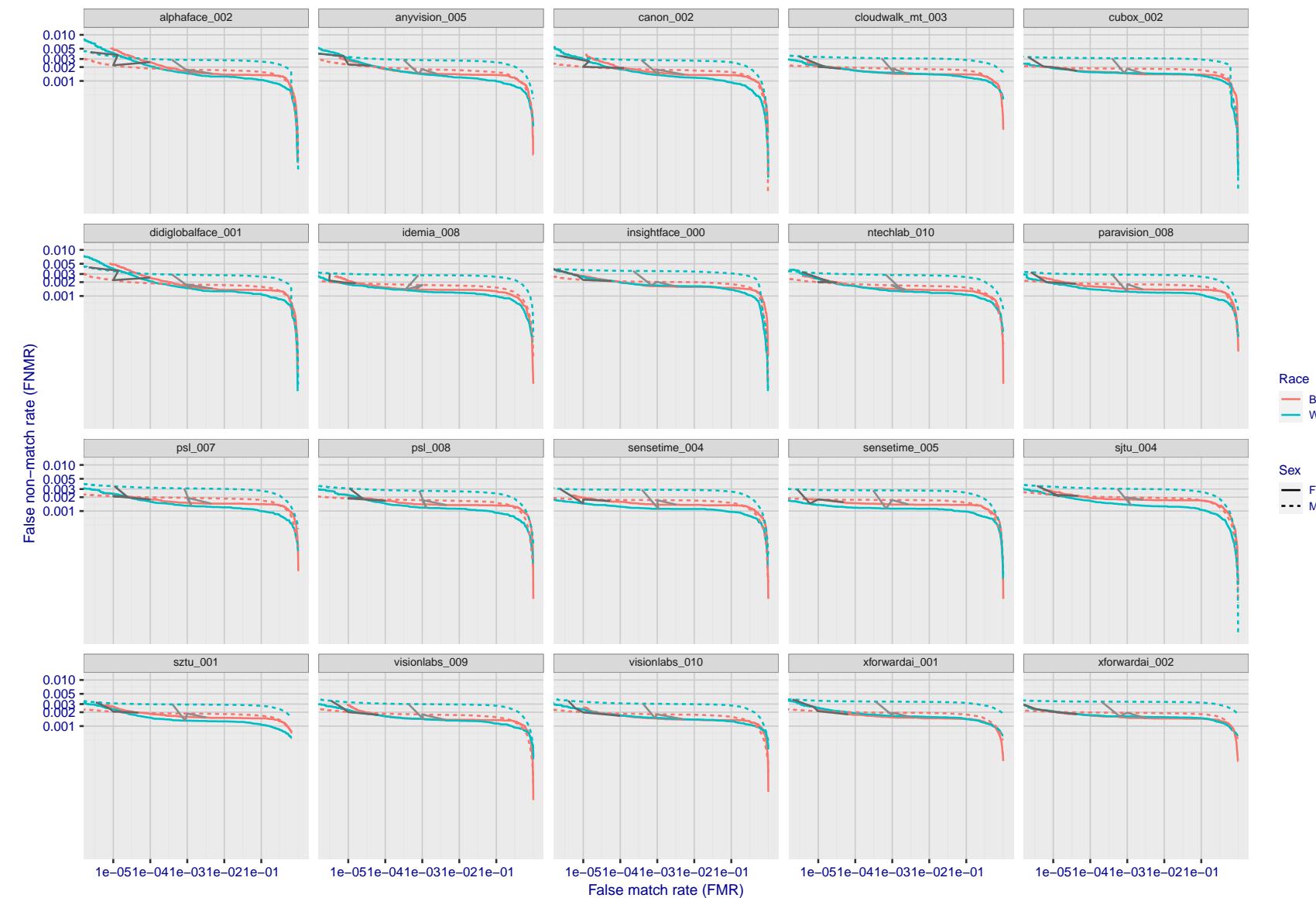


Figure 111: For the mugshot images, error tradeoff characteristics for white females, black females, black males and white males. The Z-shaped grey lines correspond to fixed thresholds, showing both FNMR and FMR vary at one  $T$  value. Note: Many of the plots will naively be read as saying women gives worse error rates than men because the solid traces lie above the dotted ones. However, this is misleading and incomplete: The grey lines show the traces reveal horizontal shifts. Thus for the cogent-003 algorithm FNMR for men is higher than for women at a fixed threshold but, at the same time, FMR is higher for women - see Figure 173. As access control systems almost always operate at a fixed threshold, the naive interpretation is incorrect.

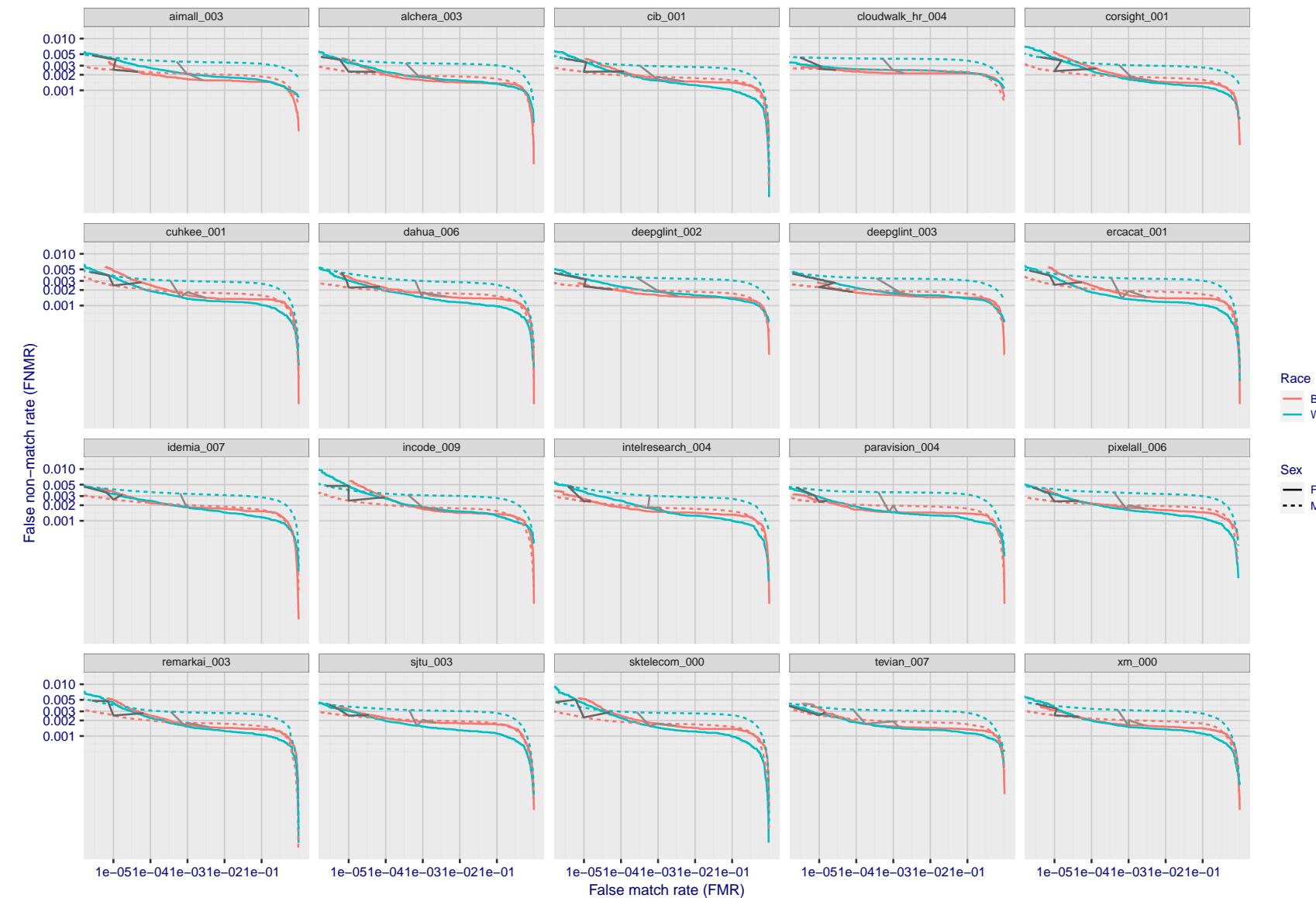


Figure 112: For the mugshot images, error tradeoff characteristics for white females, black females, black males and white males. The Z-shaped grey lines correspond to fixed thresholds, showing both FNMR and FMR vary at one  $T$  value. Note: Many of the plots will naively be read as saying women gives worse error rates than men because the solid traces lie above the dotted ones. However, this is misleading and incomplete: The grey lines show the traces reveal horizontal shifts. Thus for the cogent-003 algorithm FNMR for men is higher than for women at a fixed threshold but, at the same time, FMR is higher for women - see Figure 173. As access control systems almost always operate at a fixed threshold, the naive interpretation is incorrect.

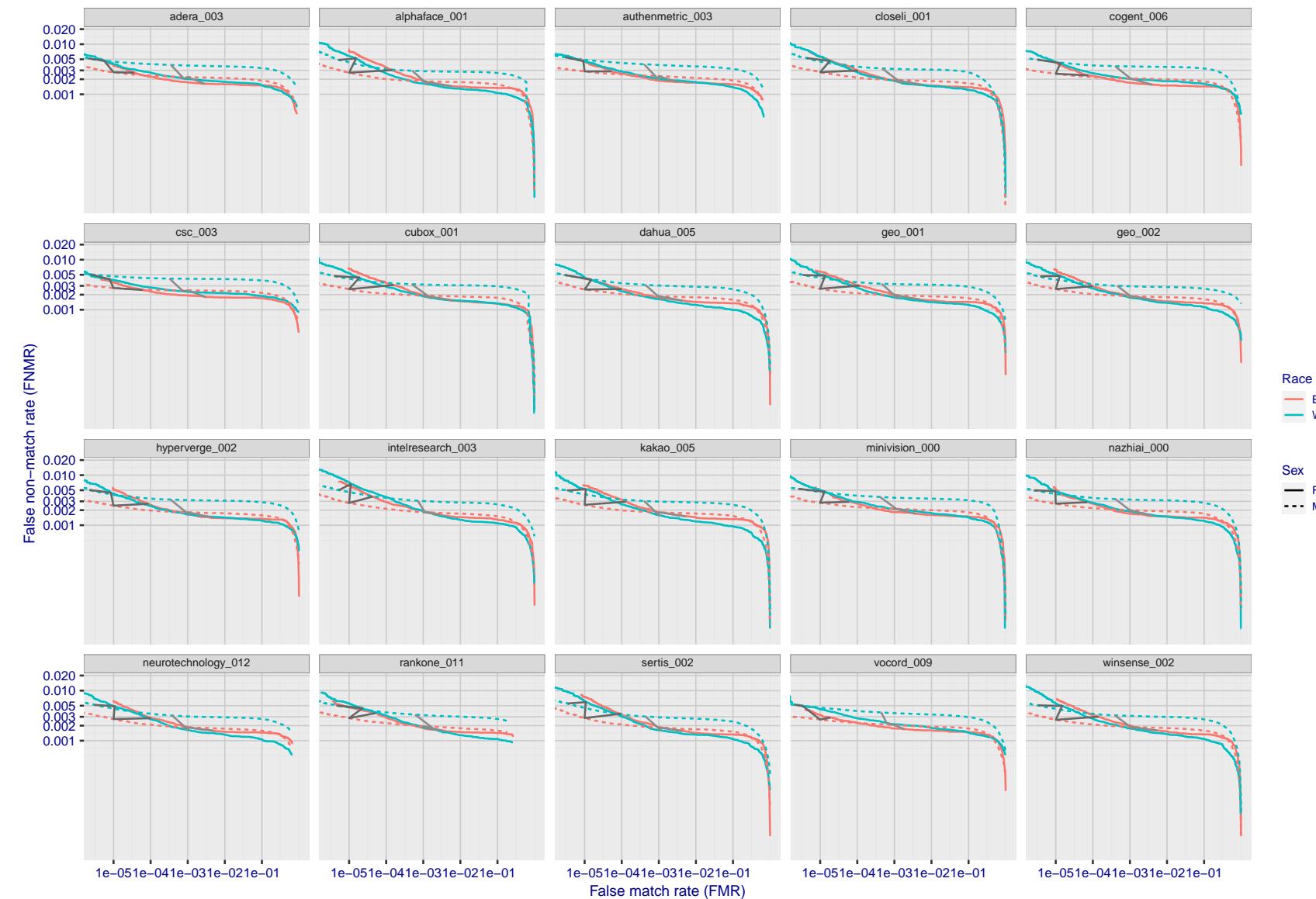


Figure 113: For the mugshot images, error tradeoff characteristics for white females, black females, black males and white males. The Z-shaped grey lines correspond to fixed thresholds, showing both FNMR and FMR vary at one  $T$  value. Note: Many of the plots will naively be read as saying women gives worse error rates than men because the solid traces lie above the dotted ones. However, this is misleading and incomplete: The grey lines show the traces reveal horizontal shifts. Thus for the cogent-003 algorithm FNMR for men is higher than for women at a fixed threshold but, at the same time, FMR is higher for women - see Figure 173. As access control systems almost always operate at a fixed threshold, the naive interpretation is incorrect.

2021/09/10 10:17:25

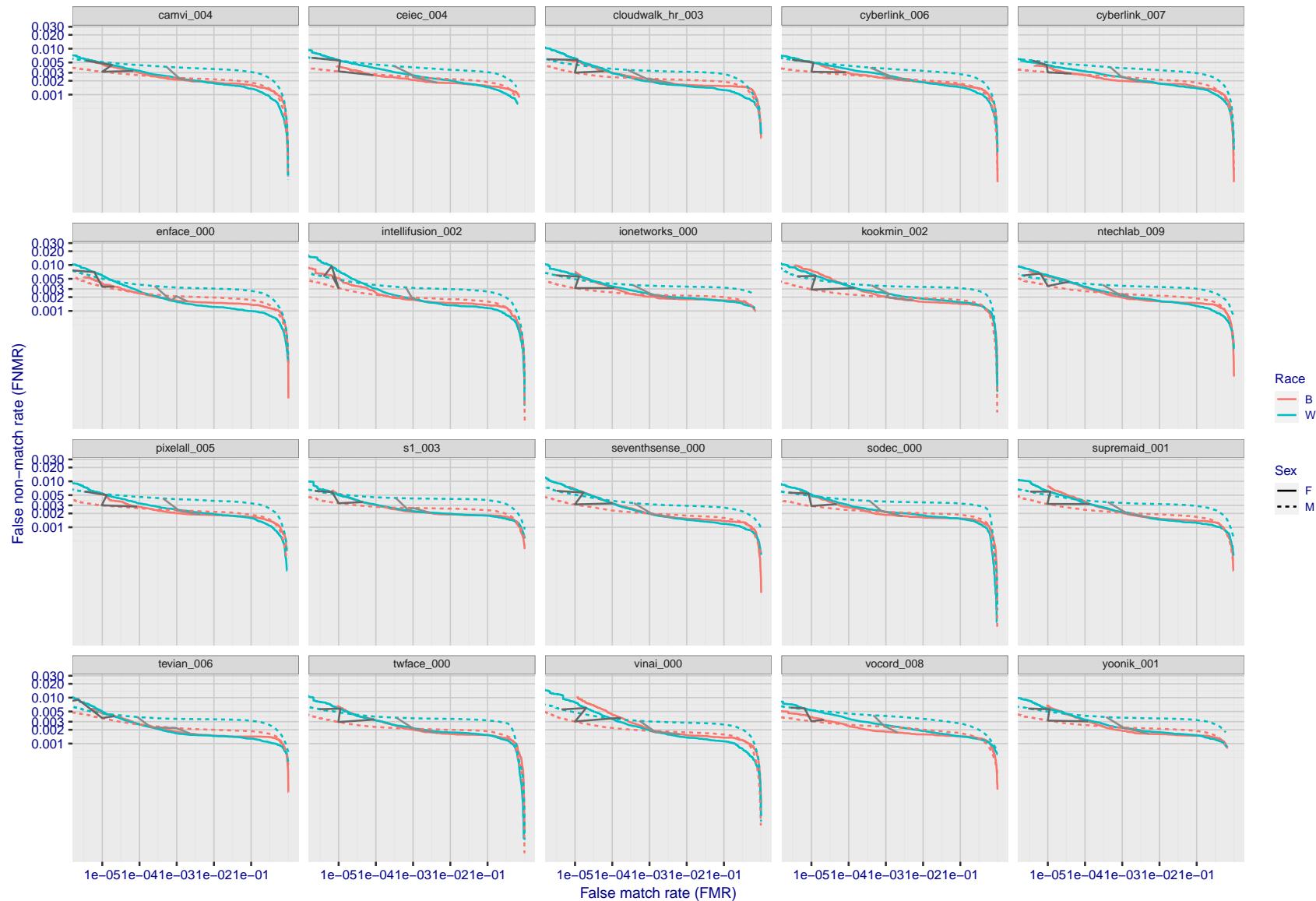


Figure 114: For the mugshot images, error tradeoff characteristics for white females, black females, black males and white males. The Z-shaped grey lines correspond to fixed thresholds, showing both FNMR and FMR vary at one  $T$  value. Note: Many of the plots will naively be read as saying women gives worse error rates than men because the solid traces lie above the dotted ones. However, this is misleading and incomplete: The grey lines show the traces reveal horizontal shifts. Thus for the cogent-003 algorithm FNMR for men is higher than for women at a fixed threshold but, at the same time, FMR is higher for women - see Figure 173. As access control systems almost always operate at a fixed threshold, the naive interpretation is incorrect.

FNMR( $T$ )

"False non-match rate"

FMR( $T$ )

"False match rate"

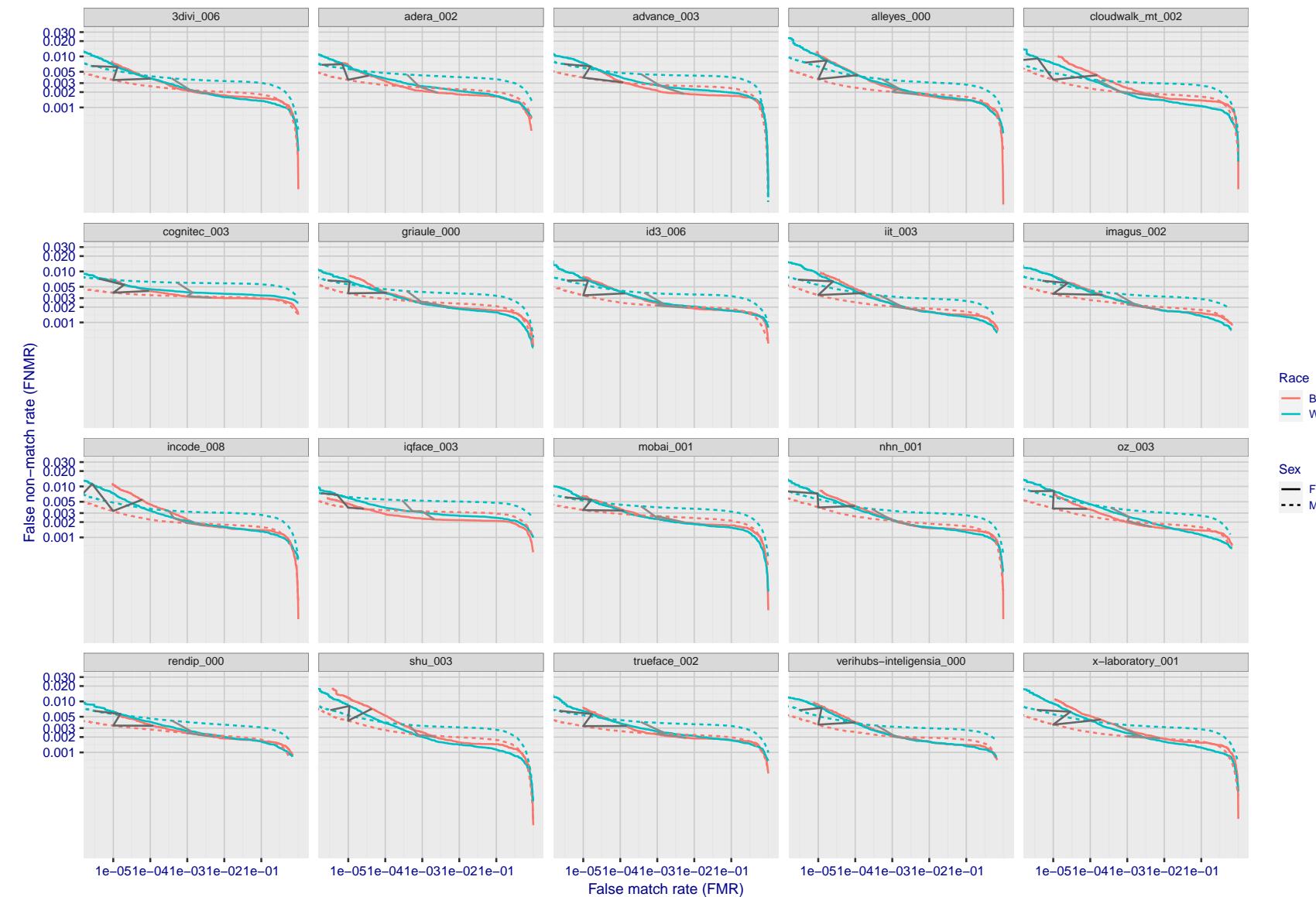


Figure 115: For the mugshot images, error tradeoff characteristics for white females, black females, black males and white males. The Z-shaped grey lines correspond to fixed thresholds, showing both FNMR and FMR vary at one  $T$  value. Note: Many of the plots will naively be read as saying women gives worse error rates than men because the solid traces lie above the dotted ones. However, this is misleading and incomplete: The grey lines show the traces reveal horizontal shifts. Thus for the cogent-003 algorithm FNMR for men is higher than for women at a fixed threshold but, at the same time, FMR is higher for women - see Figure 173. As access control systems almost always operate at a fixed threshold, the naive interpretation is incorrect.

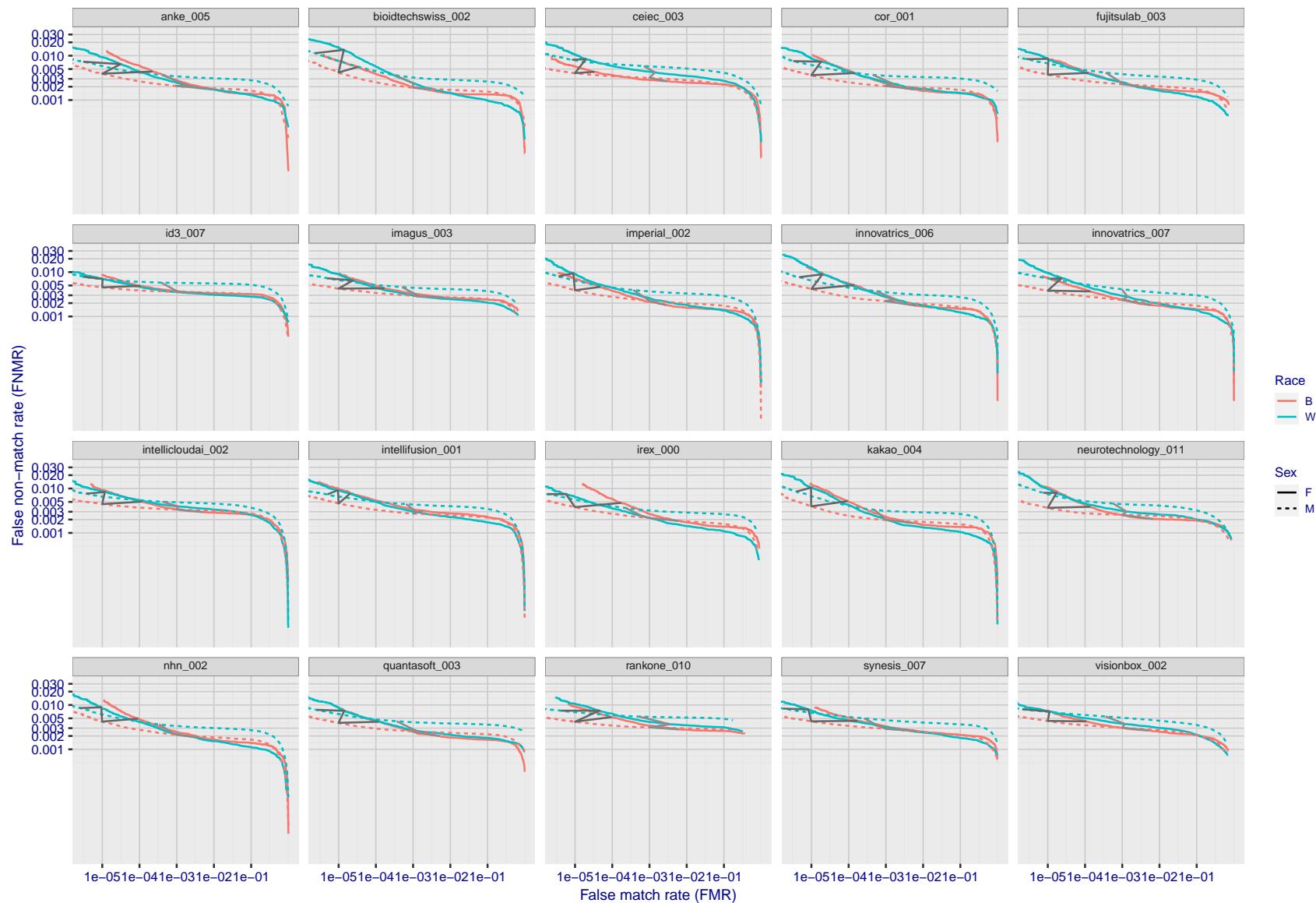


Figure 116: For the mugshot images, error tradeoff characteristics for white females, black females, black males and white males. The Z-shaped grey lines correspond to fixed thresholds, showing both FNMR and FMR vary at one T value. Note: Many of the plots will naively be read as saying women gives worse error rates than men because the solid traces lie above the dotted ones. However, this is misleading and incomplete: The grey lines show the traces reveal horizontal shifts. Thus for the cogent-003 algorithm FNMR for men is higher than for women at a fixed threshold but, at the same time, FMR is higher for women - see Figure 173. As access control systems almost always operate at a fixed threshold, the naive interpretation is incorrect.

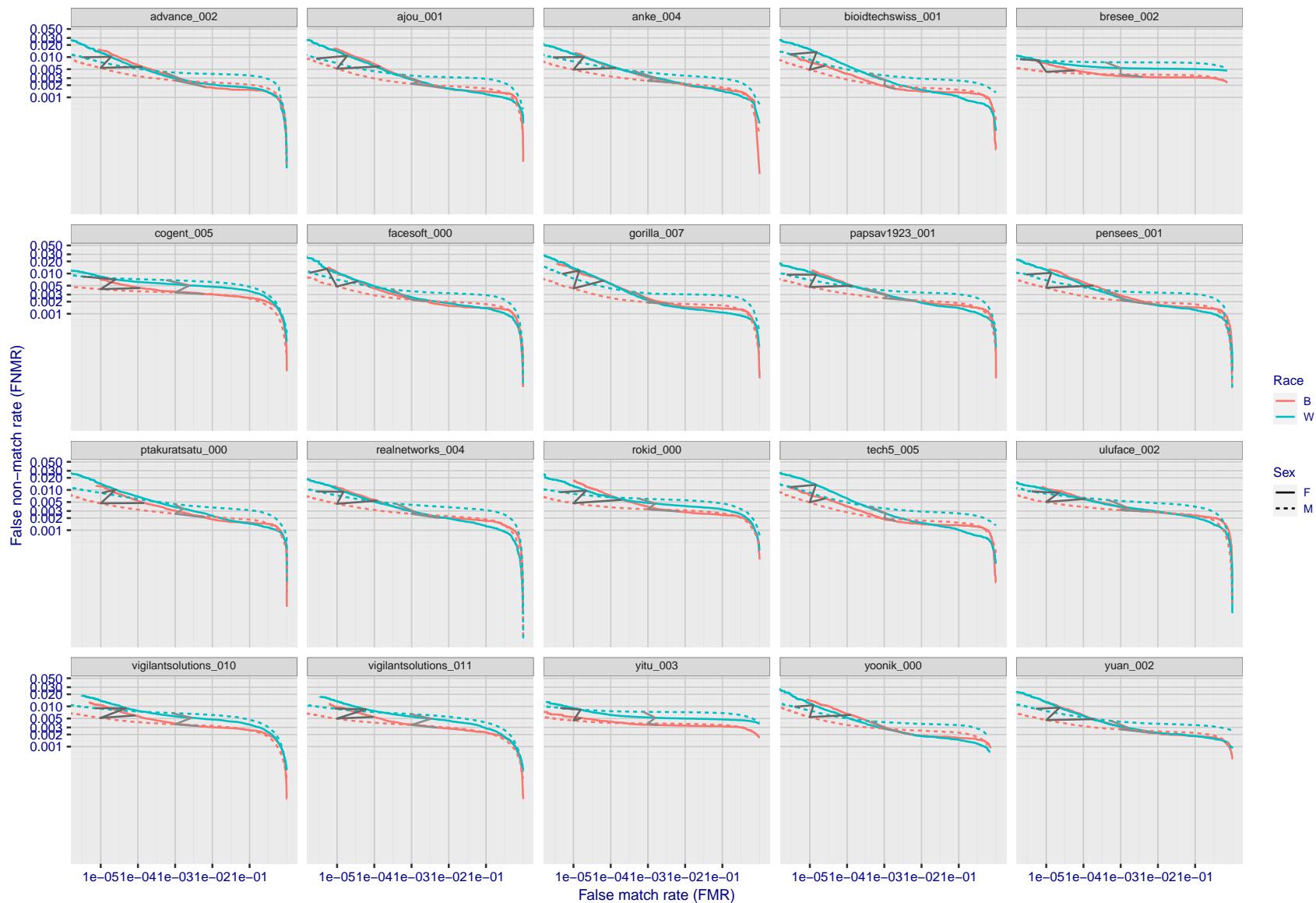


Figure 117: For the mugshot images, error tradeoff characteristics for white females, black females, black males and white males. The Z-shaped grey lines correspond to fixed thresholds, showing both FNMR and FMR vary at one  $T$  value. Note: Many of the plots will naively be read as saying women gives worse error rates than men because the solid traces lie above the dotted ones. However, this is misleading and incomplete: The grey lines show the traces reveal horizontal shifts. Thus for the cogent-003 algorithm FNMR for men is higher than for women at a fixed threshold but, at the same time, FMR is higher for women - see Figure 173. As access control systems almost always operate at a fixed threshold, the naive interpretation is incorrect.

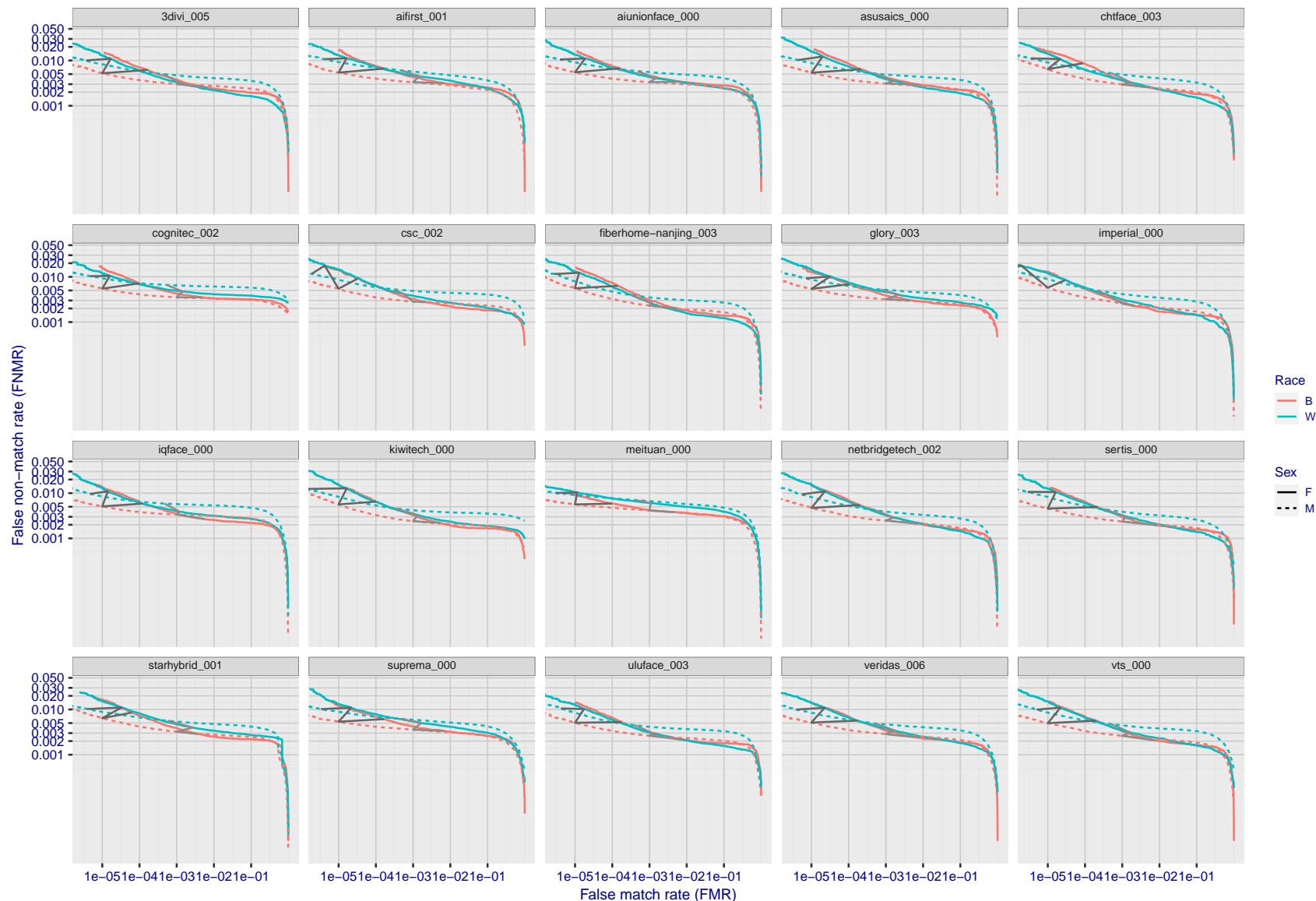


Figure 118: For the mugshot images, error tradeoff characteristics for white females, black females, black males and white males. The Z-shaped grey lines correspond to fixed thresholds, showing both FNMR and FMR vary at one  $T$  value. Note: Many of the plots will naively be read as saying women gives worse error rates than men because the solid traces lie above the dotted ones. However, this is misleading and incomplete: The grey lines show the traces reveal horizontal shifts. Thus for the cogent-003 algorithm FNMR for men is higher than for women at a fixed threshold but, at the same time, FMR is higher for women - see Figure 173. As access control systems almost always operate at a fixed threshold, the naive interpretation is incorrect.

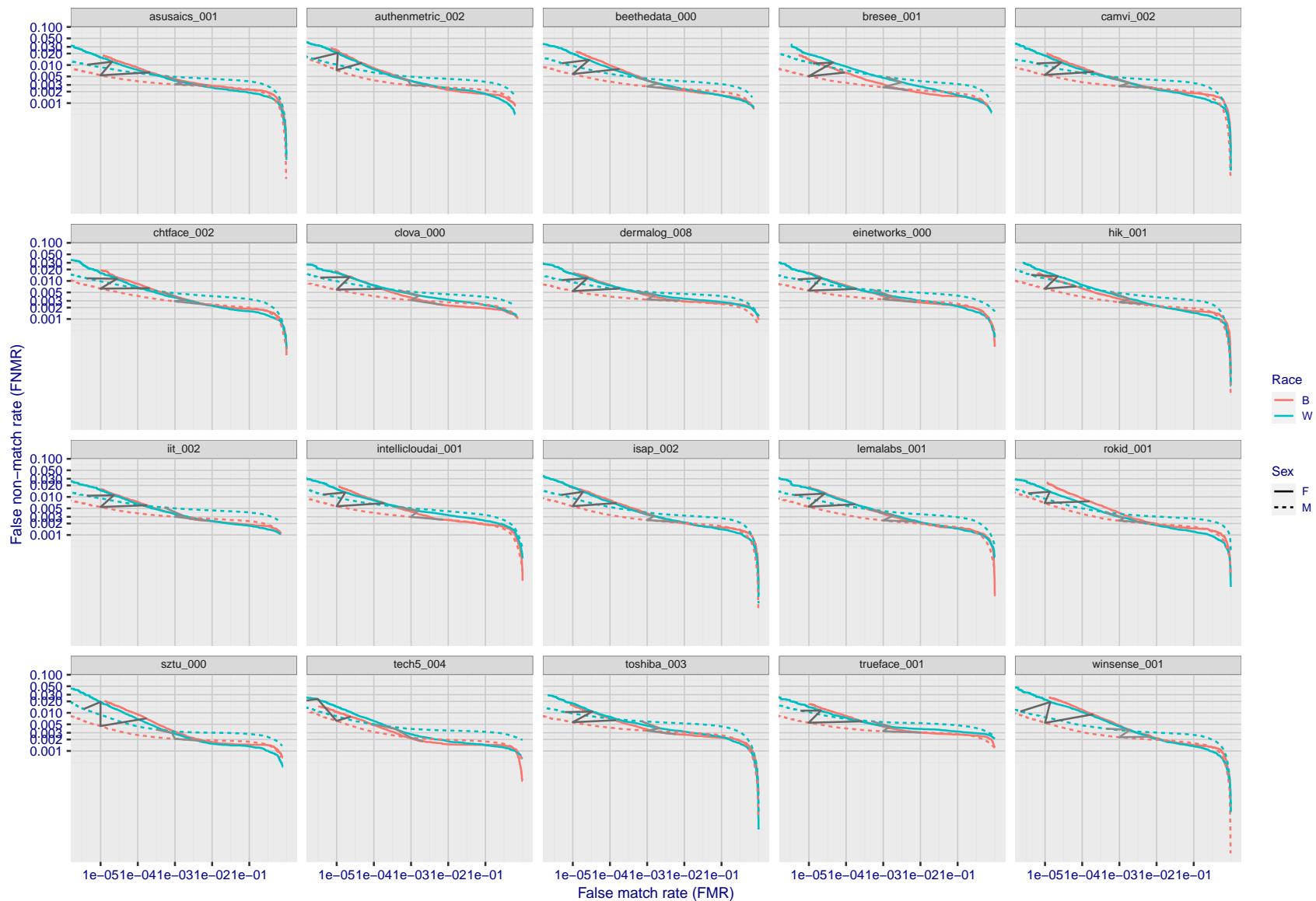


Figure 119: For the mugshot images, error tradeoff characteristics for white females, black females, black males and white males. The Z-shaped grey lines correspond to fixed thresholds, showing both FNMR and FMR vary at one  $T$  value. Note: Many of the plots will naively be read as saying women gives worse error rates than men because the solid traces lie above the dotted ones. However, this is misleading and incomplete: The grey lines show the traces reveal horizontal shifts. Thus for the cogent-003 algorithm FNMR for men is higher than for women at a fixed threshold but, at the same time, FMR is higher for women - see Figure 173. As access control systems almost always operate at a fixed threshold, the naive interpretation is incorrect.

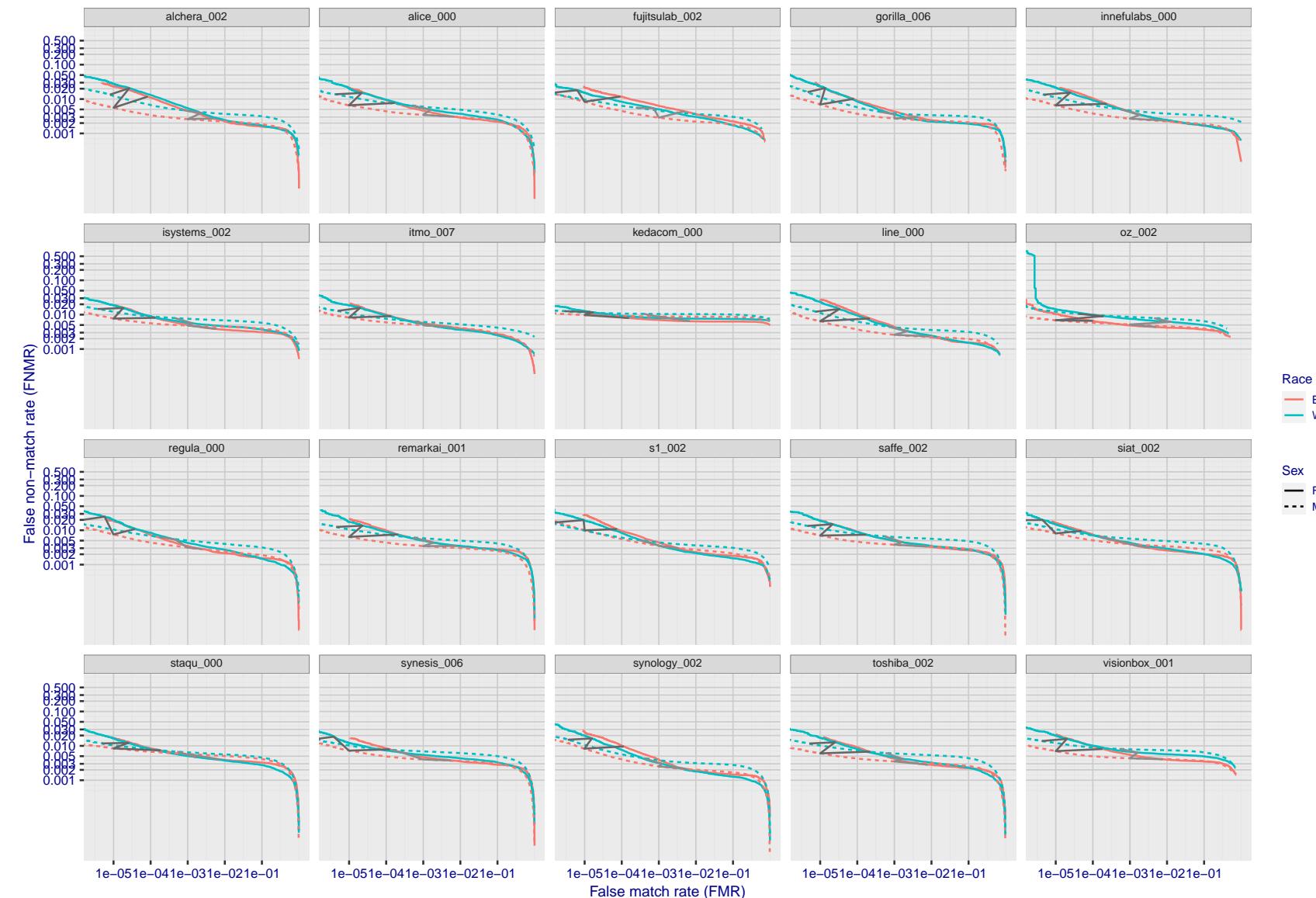


Figure 120: For the mugshot images, error tradeoff characteristics for white females, black females, black males and white males. The Z-shaped grey lines correspond to fixed thresholds, showing both FNMR and FMR vary at one  $T$  value. Note: Many of the plots will naively be read as saying women gives worse error rates than men because the solid traces lie above the dotted ones. However, this is misleading and incomplete: The grey lines show the traces reveal horizontal shifts. Thus for the cogent-003 algorithm FNMR for men is higher than for women at a fixed threshold but, at the same time, FMR is higher for women - see Figure 173. As access control systems almost always operate at a fixed threshold, the naive interpretation is incorrect.

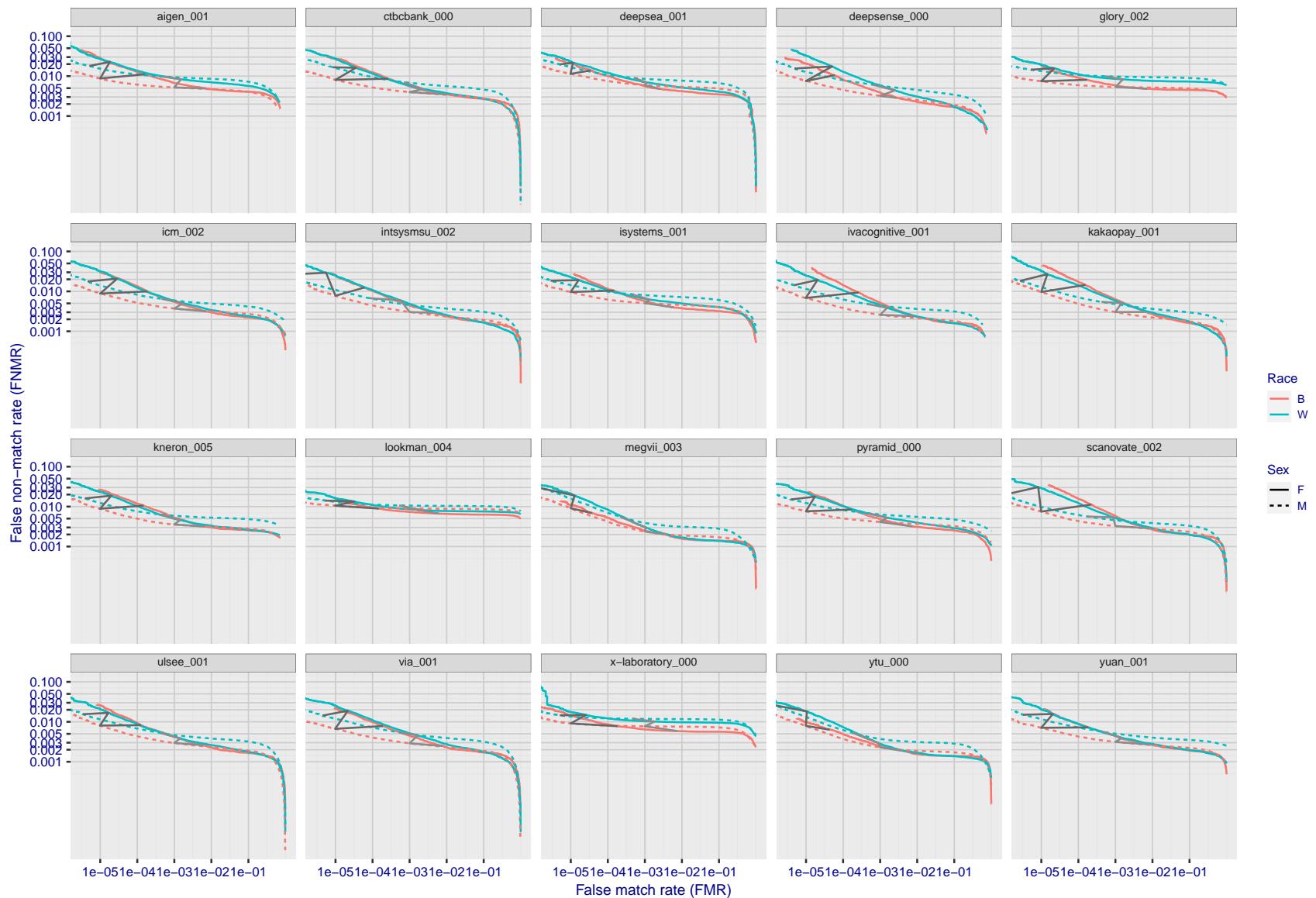


Figure 121: For the mugshot images, error tradeoff characteristics for white females, black females, black males and white males. The Z-shaped grey lines correspond to fixed thresholds, showing both FNMR and FMR vary at one T value. Note: Many of the plots will naively be read as saying women gives worse error rates than men because the solid traces lie above the dotted ones. However, this is misleading and incomplete: The grey lines show the traces reveal horizontal shifts. Thus for the cogent-003 algorithm FNMR for men is higher than for women at a fixed threshold but, at the same time, FMR is higher for women - see Figure 173. As access control systems almost always operate at a fixed threshold, the naive interpretation is incorrect.

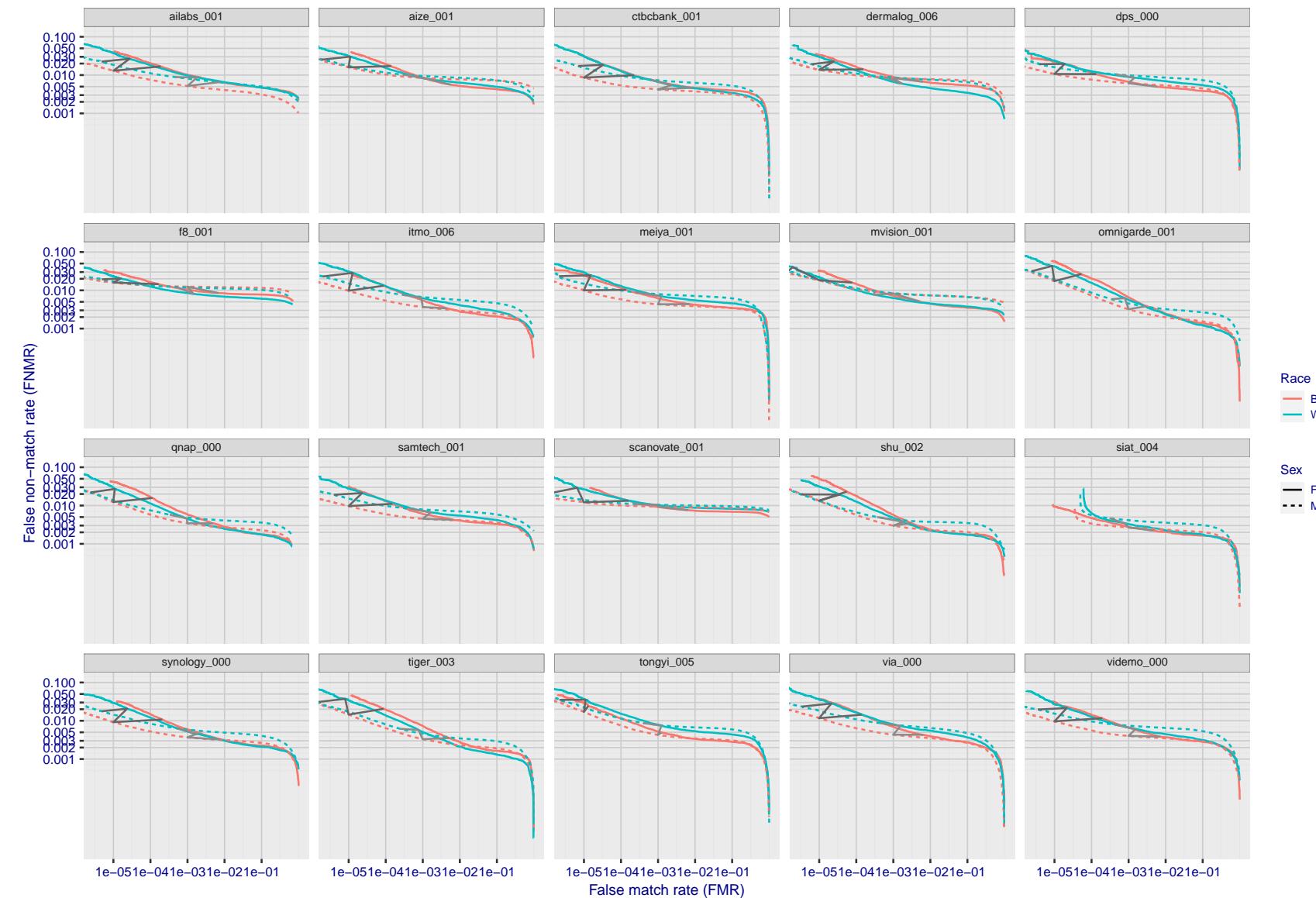


Figure 122: For the mugshot images, error tradeoff characteristics for white females, black females, black males and white males. The Z-shaped grey lines correspond to fixed thresholds, showing both FNMR and FMR vary at one T value. Note: Many of the plots will naively be read as saying women gives worse error rates than men because the solid traces lie above the dotted ones. However, this is misleading and incomplete: The grey lines show the traces reveal horizontal shifts. Thus for the cogent-003 algorithm FNMR for men is higher than for women at a fixed threshold but, at the same time, FMR is higher for women - see Figure 173. As access control systems almost always operate at a fixed threshold, the naive interpretation is incorrect.

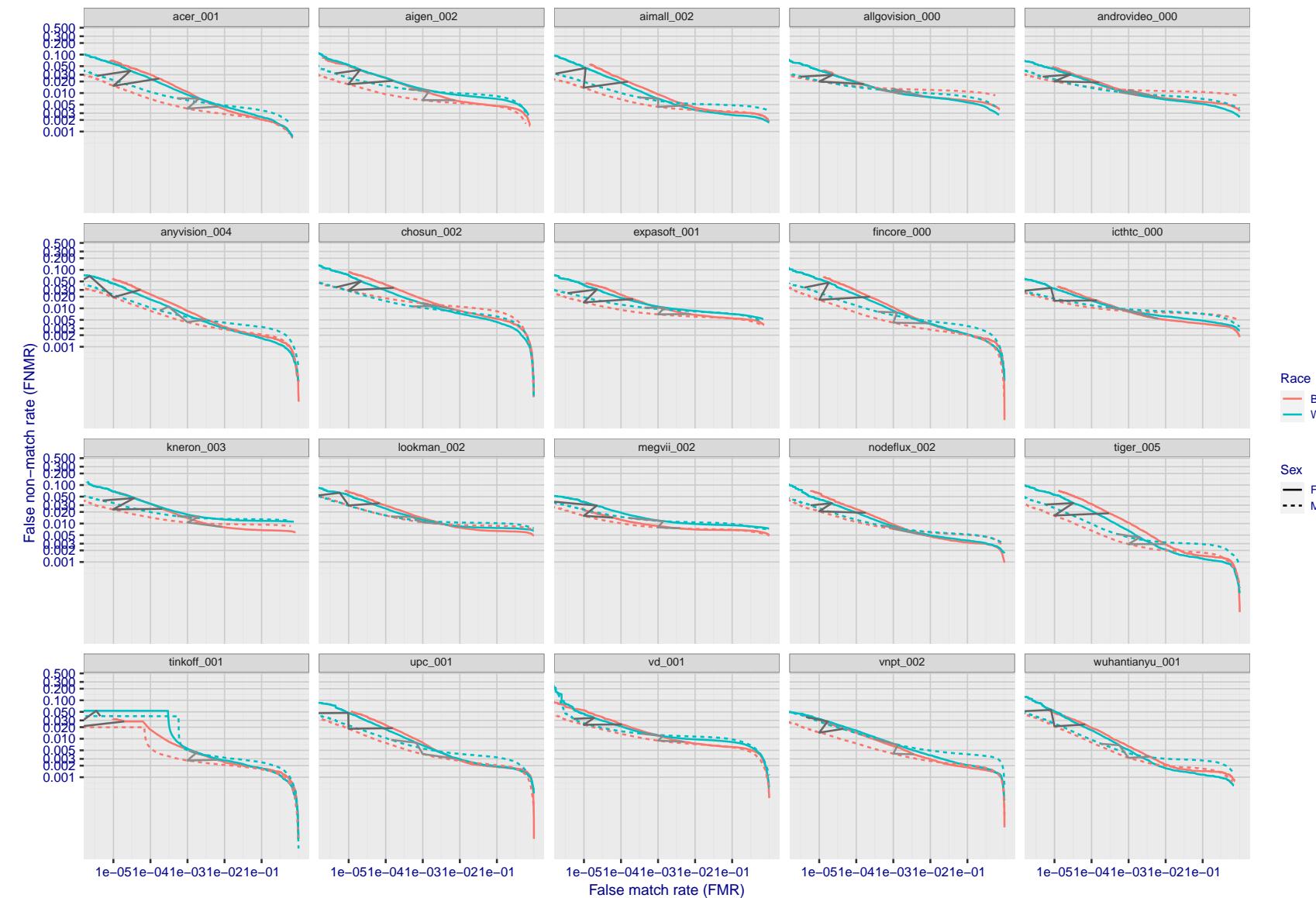


Figure 123: For the mugshot images, error tradeoff characteristics for white females, black females, black males and white males. The Z-shaped grey lines correspond to fixed thresholds, showing both FNMR and FMR vary at one  $T$  value. Note: Many of the plots will naively be read as saying women gives worse error rates than men because the solid traces lie above the dotted ones. However, this is misleading and incomplete: The grey lines show the traces reveal horizontal shifts. Thus for the cogent-003 algorithm FNMR for men is higher than for women at a fixed threshold but, at the same time, FMR is higher for women - see Figure 173. As access control systems almost always operate at a fixed threshold, the naive interpretation is incorrect.

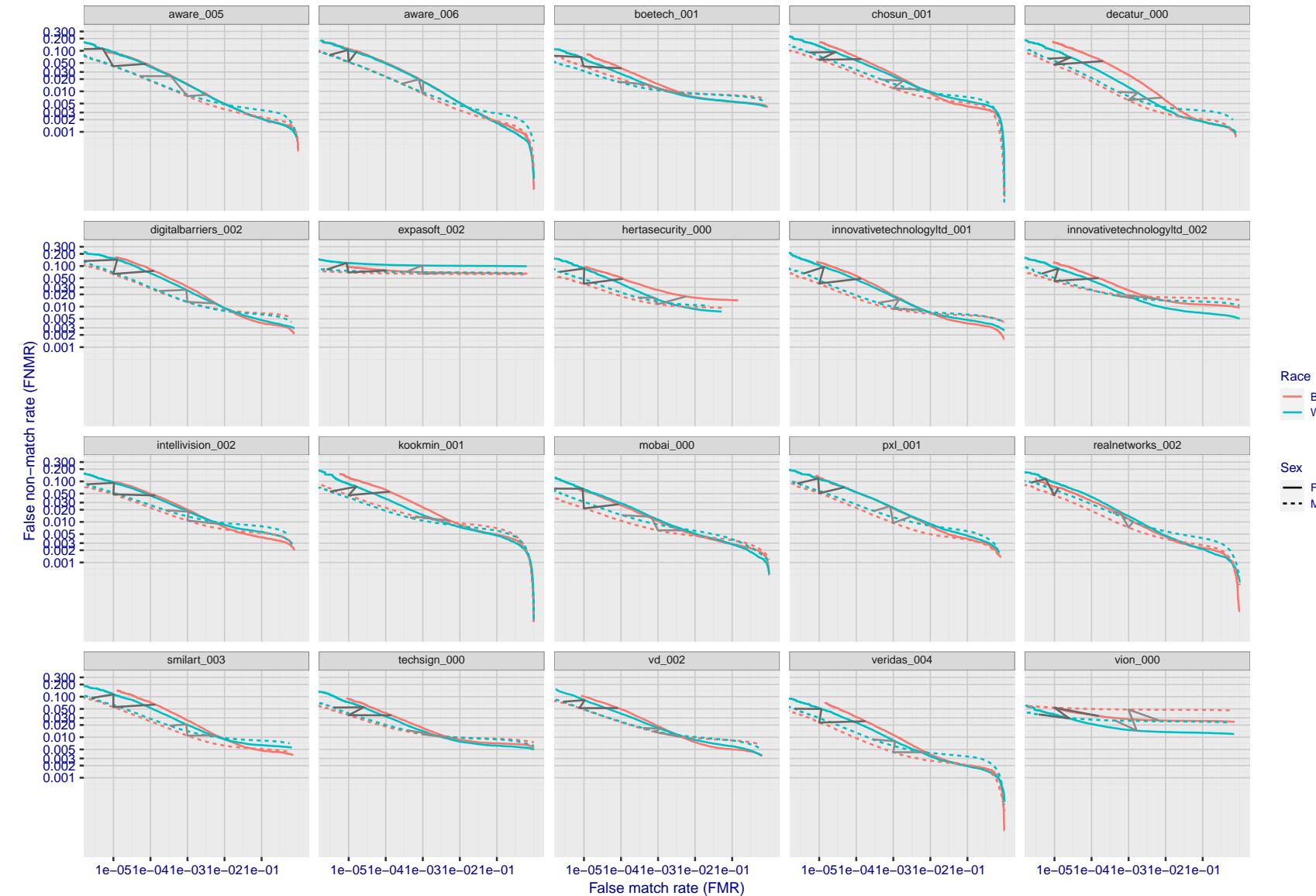


Figure 124: For the mugshot images, error tradeoff characteristics for white females, black females, black males and white males. The Z-shaped grey lines correspond to fixed thresholds, showing both FNMR and FMR vary at one T value. Note: Many of the plots will naively be read as saying women gives worse error rates than men because the solid traces lie above the dotted ones. However, this is misleading and incomplete: The grey lines show the traces reveal horizontal shifts. Thus for the cogent-003 algorithm FNMR for men is higher than for women at a fixed threshold but, at the same time, FMR is higher for women - see Figure 173. As access control systems almost always operate at a fixed threshold, the naive interpretation is incorrect.

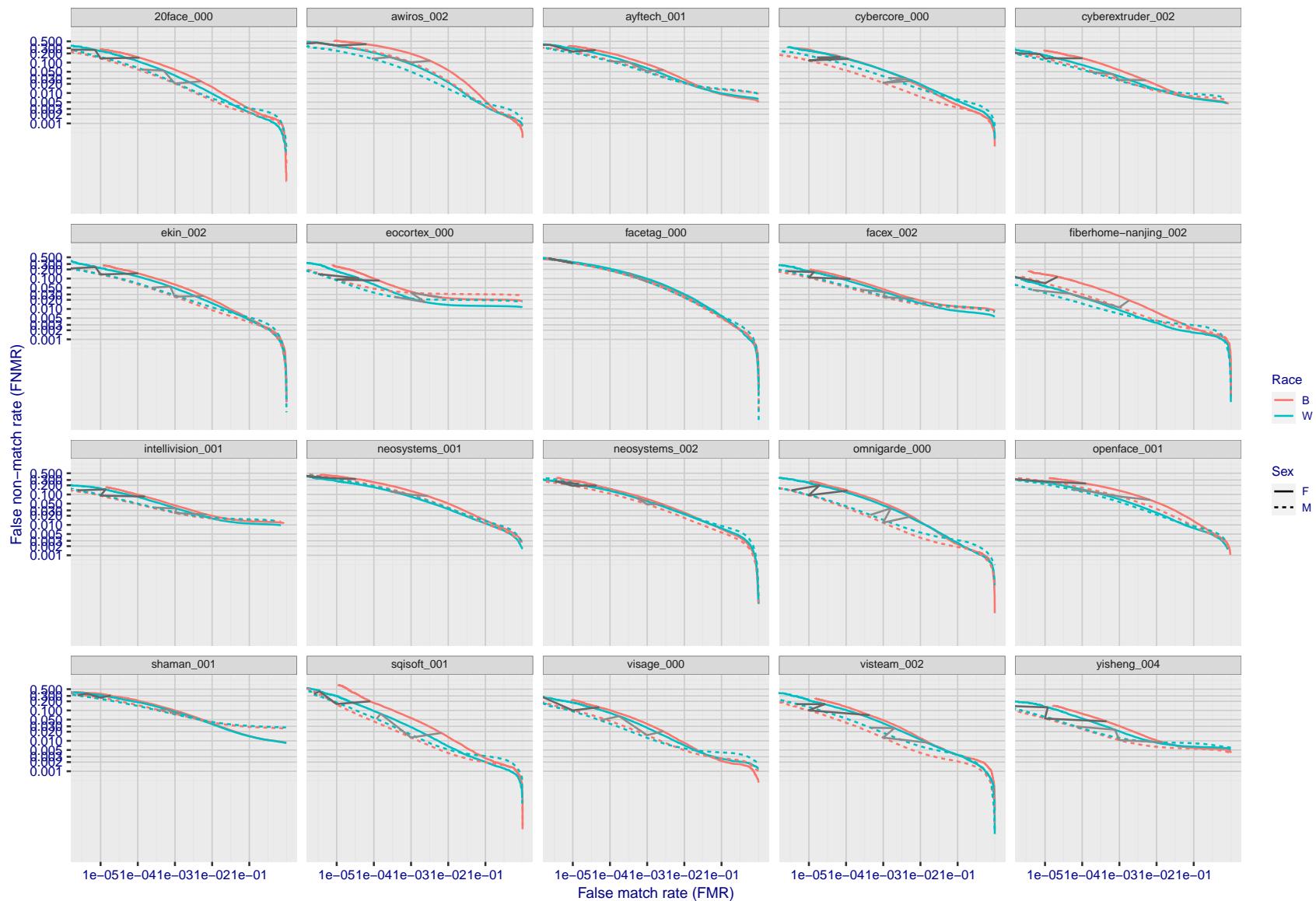


Figure 125: For the mugshot images, error tradeoff characteristics for white females, black females, black males and white males. The Z-shaped grey lines correspond to fixed thresholds, showing both FNMR and FMR vary at one  $T$  value. Note: Many of the plots will naively be read as saying women gives worse error rates than men because the solid traces lie above the dotted ones. However, this is misleading and incomplete: The grey lines show the traces reveal horizontal shifts. Thus for the cogent-003 algorithm FNMR for men is higher than for women at a fixed threshold but, at the same time, FMR is higher for women - see Figure 173. As access control systems almost always operate at a fixed threshold, the naive interpretation is incorrect.

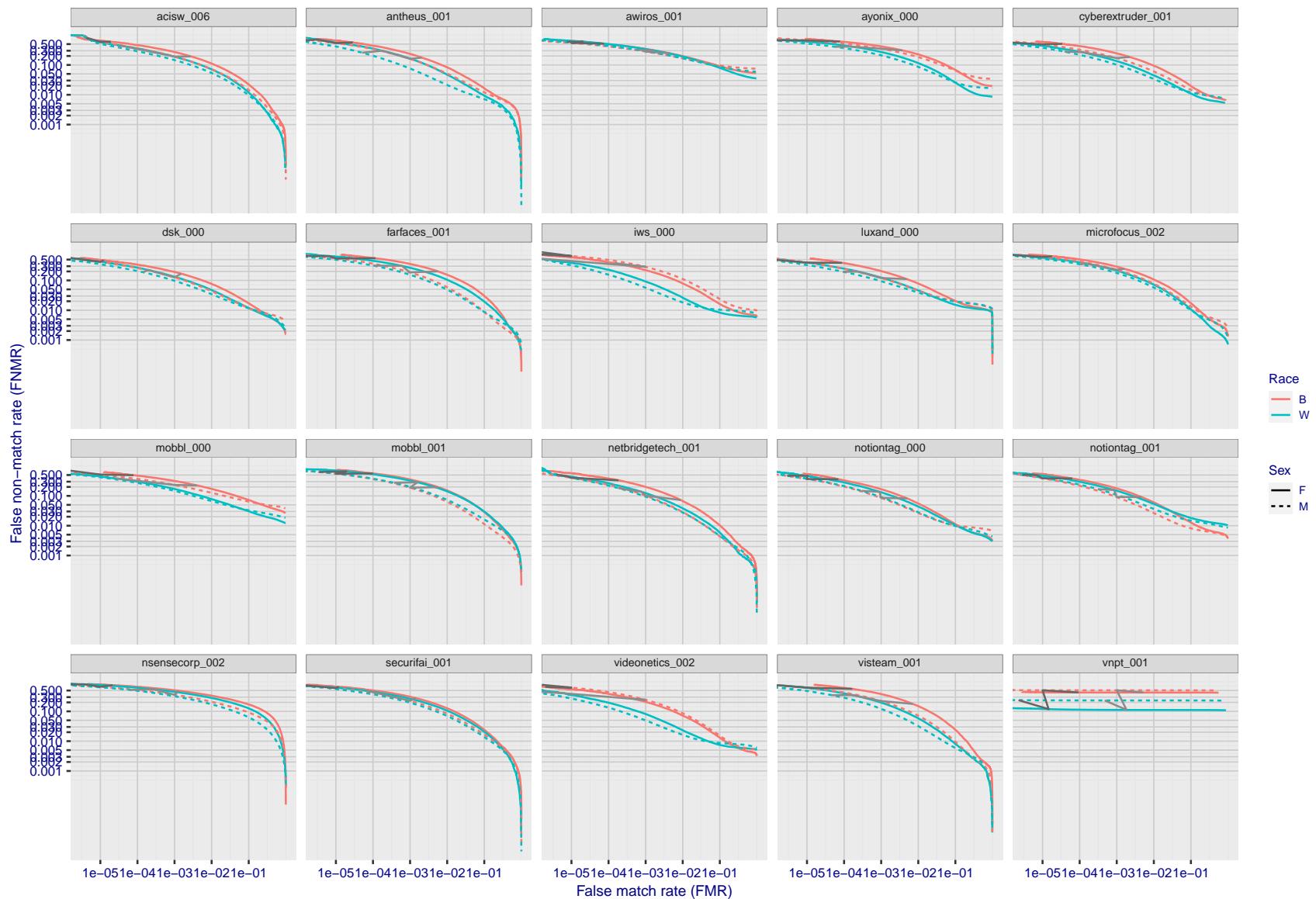


Figure 126: For the mugshot images, error tradeoff characteristics for white females, black females, black males and white males. The Z-shaped grey lines correspond to fixed thresholds, showing both FNMR and FMR vary at one  $T$  value. Note: Many of the plots will naively be read as saying women gives worse error rates than men because the solid traces lie above the dotted ones. However, this is misleading and incomplete: The grey lines show the traces reveal horizontal shifts. Thus for the cogent-003 algorithm FNMR for men is higher than for women at a fixed threshold but, at the same time, FMR is higher for women - see Figure 173. As access control systems almost always operate at a fixed threshold, the naive interpretation is incorrect.

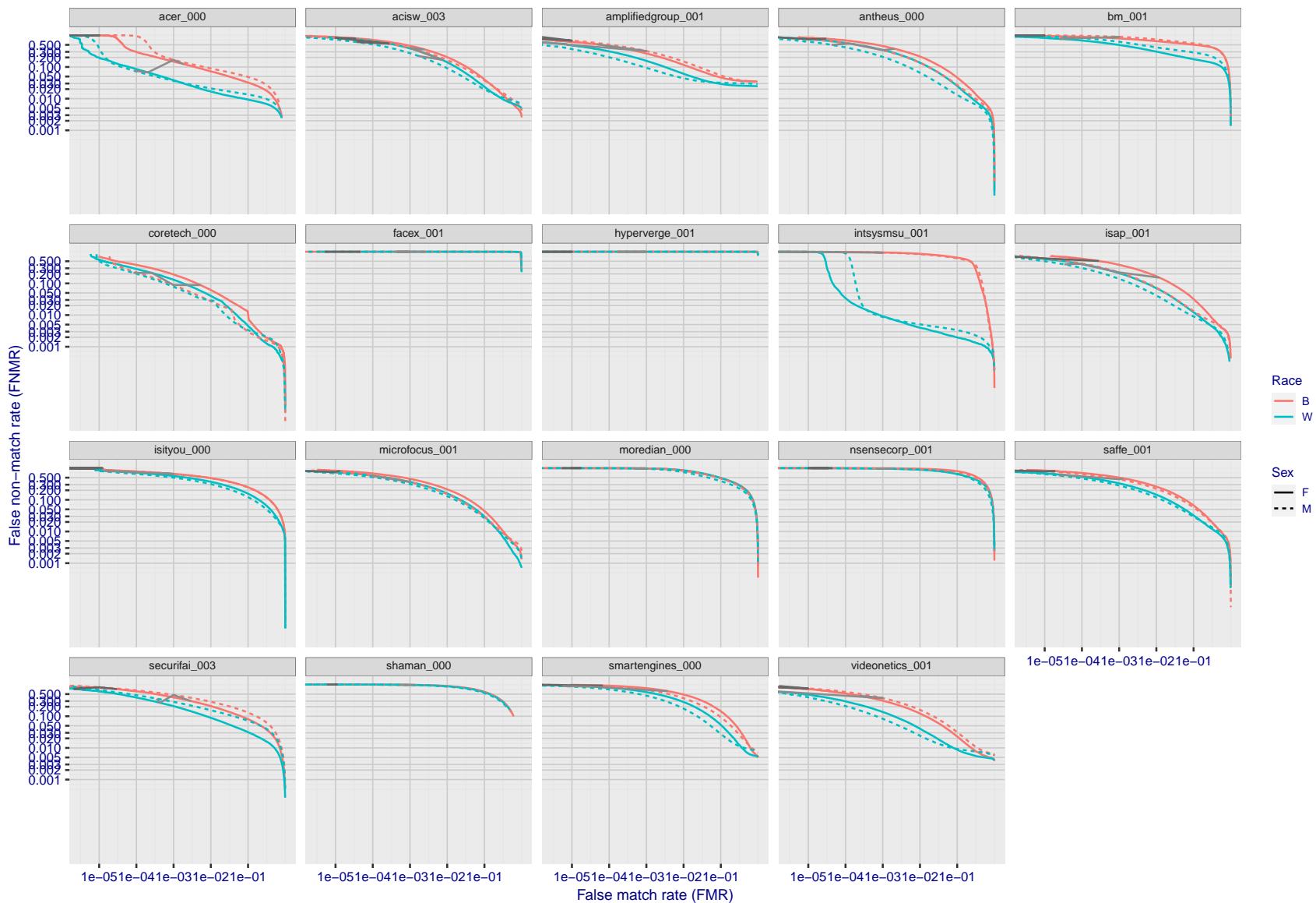


Figure 127: For the mugshot images, error tradeoff characteristics for white females, black females, black males and white males. The Z-shaped grey lines correspond to fixed thresholds, showing both FNMR and FMR vary at one  $T$  value. Note: Many of the plots will naively be read as saying women gives worse error rates than men because the solid traces lie above the dotted ones. However, this is misleading and incomplete: The grey lines show the traces reveal horizontal shifts. Thus for the cogent-003 algorithm FNMR for men is higher than for women at a fixed threshold but, at the same time, FMR is higher for women - see Figure 173. As access control systems almost always operate at a fixed threshold, the naive interpretation is incorrect.

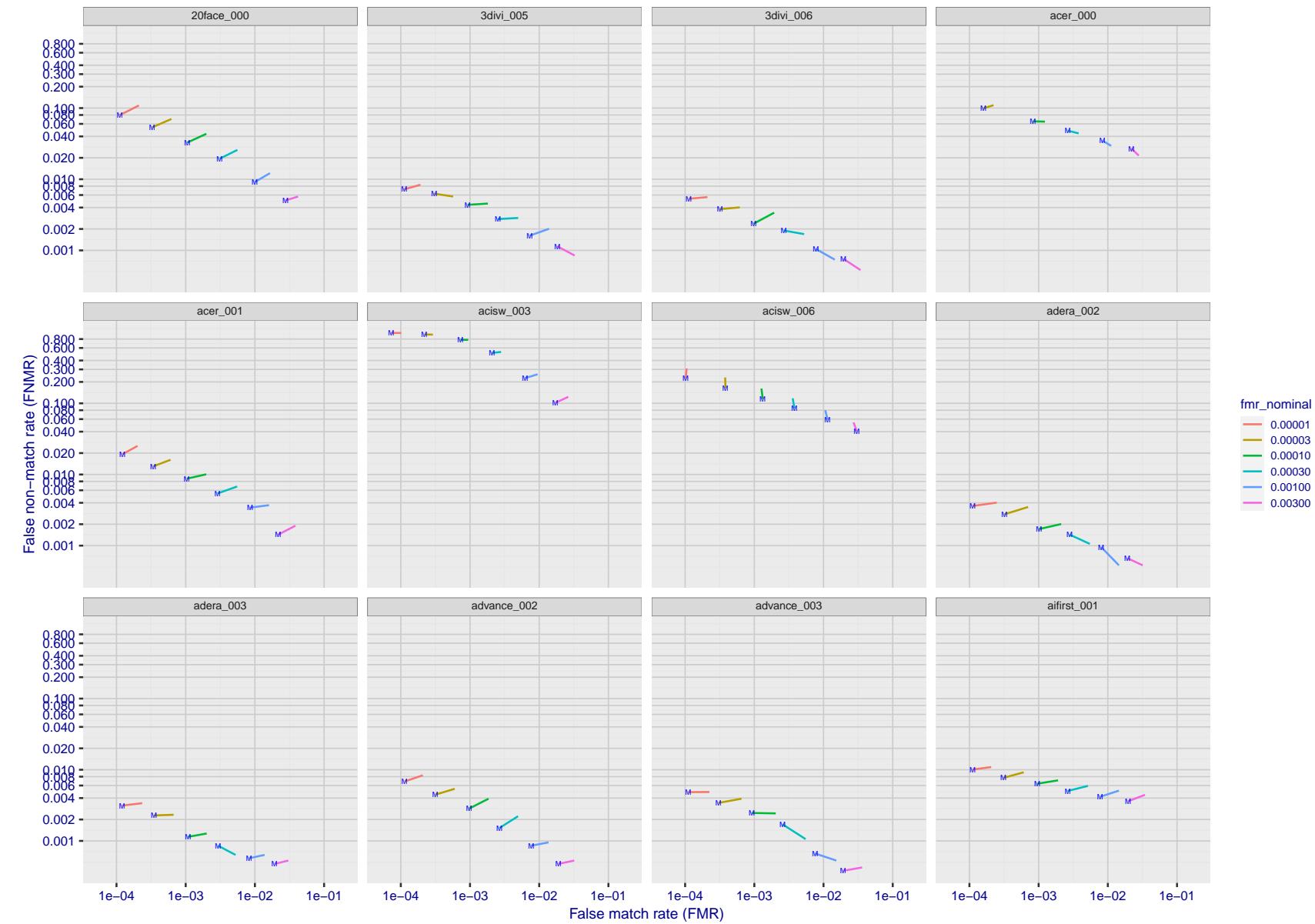


Figure 128: For the visa images, FNMR and FMR at six operating points along the DET characteristic. At each point a line is drawn between  $(FMR, FNMR)_{MALE}$  and  $(FMR, FNMR)_{FEMALE}$  showing how which sex has lower FMR and/or FNMR. The "M" label denotes male, the other end of the line corresponds to female. The six operating thresholds are selected to give the nominal false match rates given in the legend, and are computed over all impostor pairs regardless of age, sex, and place of birth. The plotted FMR values are broadly an order of magnitude larger than the nominal rates because FMR is computed over demographically-matched impostor pairs i.e individuals of the same sex, from the same geographic region (see section 3.6.1), and the same age group (see section 3.6.2).

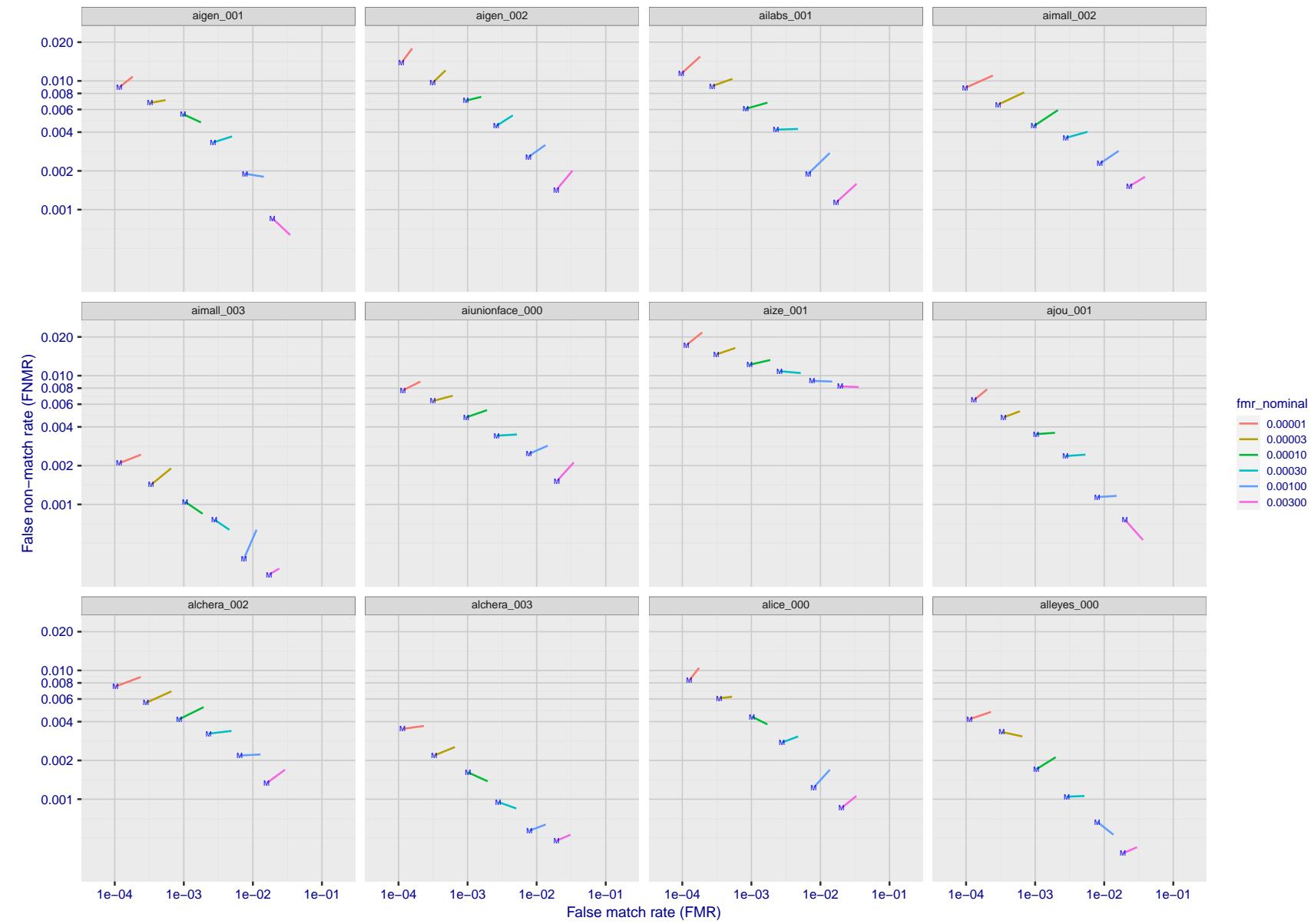


Figure 129: For the visa images, FNMR and FMR at six operating points along the DET characteristic. At each point a line is drawn between  $(FMR, FNMR)_{MALE}$  and  $(FMR, FNMR)_{FEMALE}$  showing how which sex has lower FMR and/or FNMR. The "M" label denotes male, the other end of the line corresponds to female. The six operating thresholds are selected to give the nominal false match rates given in the legend, and are computed over all impostor pairs regardless of age, sex, and place of birth. The plotted FMR values are broadly an order of magnitude larger than the nominal rates because FMR is computed over demographically-matched impostor pairs i.e individuals of the same sex, from the same geographic region (see section 3.6.1), and the same age group (see section 3.6.2).

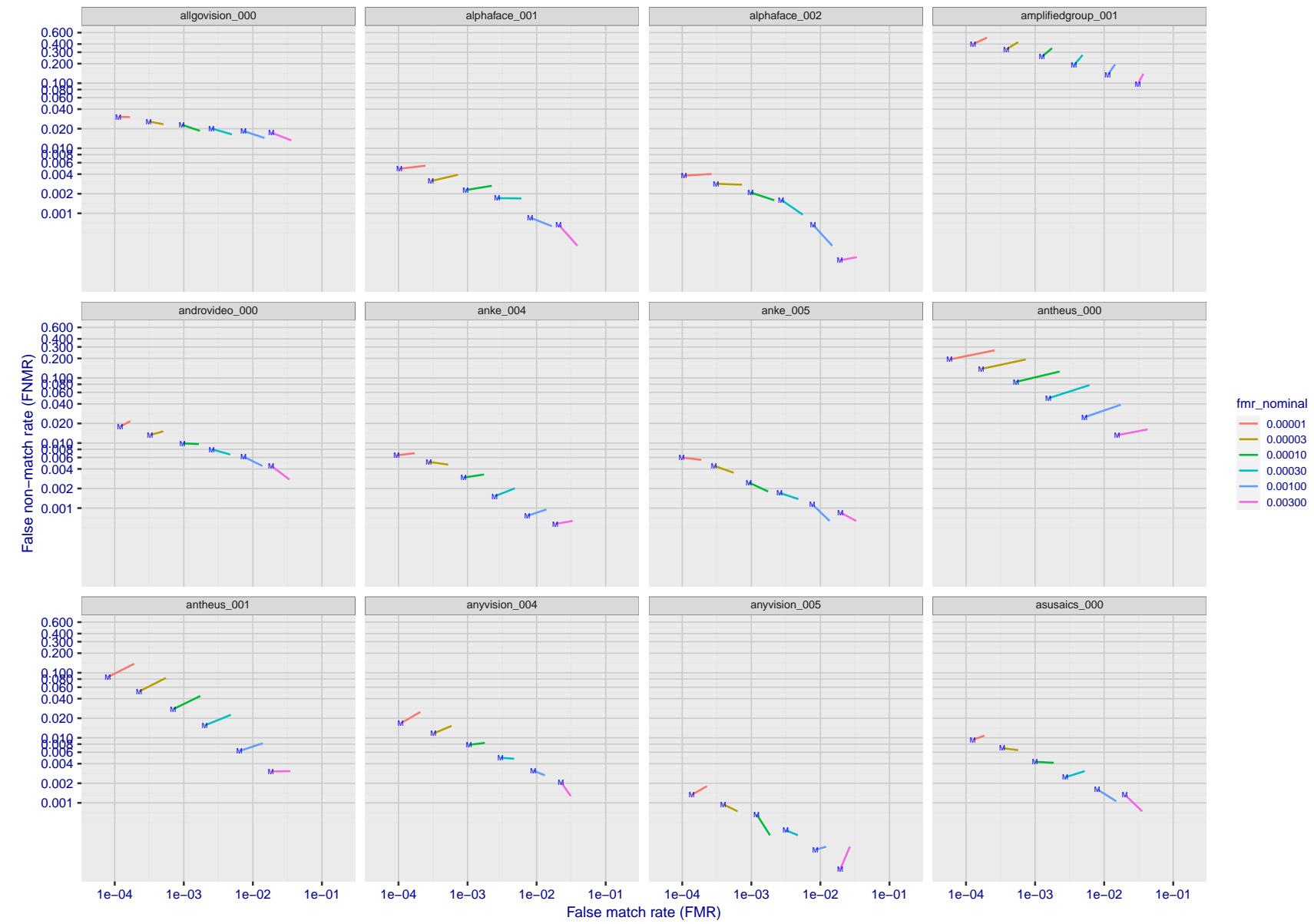


Figure 130: For the visa images, FNMR and FMR at six operating points along the DET characteristic. At each point a line is drawn between  $(FMR, FNMR)_{MALE}$  and  $(FMR, FNMR)_{FEMALE}$  showing how which sex has lower FMR and/or FNMR. The "M" label denotes male, the other end of the line corresponds to female. The six operating thresholds are selected to give the nominal false match rates given in the legend, and are computed over all impostor pairs regardless of age, sex, and place of birth. The plotted FMR values are broadly an order of magnitude larger than the nominal rates because FMR is computed over demographically-matched impostor pairs i.e individuals of the same sex, from the same geographic region (see section 3.6.1), and the same age group (see section 3.6.2).

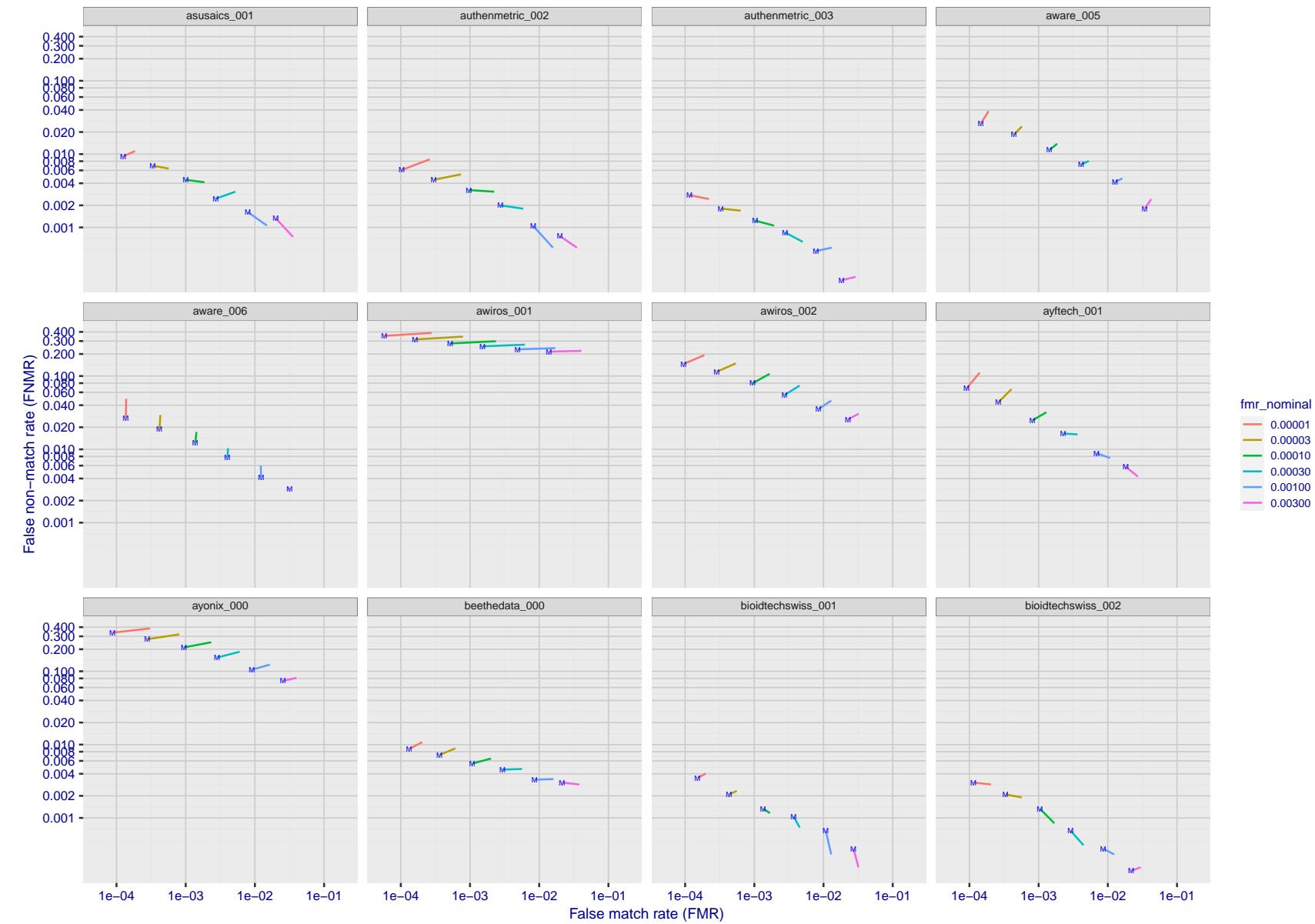


Figure 131: For the visa images, FNMR and FMR at six operating points along the DET characteristic. At each point a line is drawn between  $(FMR, FNMR)_{MALE}$  and  $(FMR, FNMR)_{FEMALE}$  showing how which sex has lower FMR and/or FNMR. The "M" label denotes male, the other end of the line corresponds to female. The six operating thresholds are selected to give the nominal false match rates given in the legend, and are computed over all impostor pairs regardless of age, sex, and place of birth. The plotted FMR values are broadly an order of magnitude larger than the nominal rates because FMR is computed over demographically-matched impostor pairs i.e individuals of the same sex, from the same geographic region (see section 3.6.1), and the same age group (see section 3.6.2).

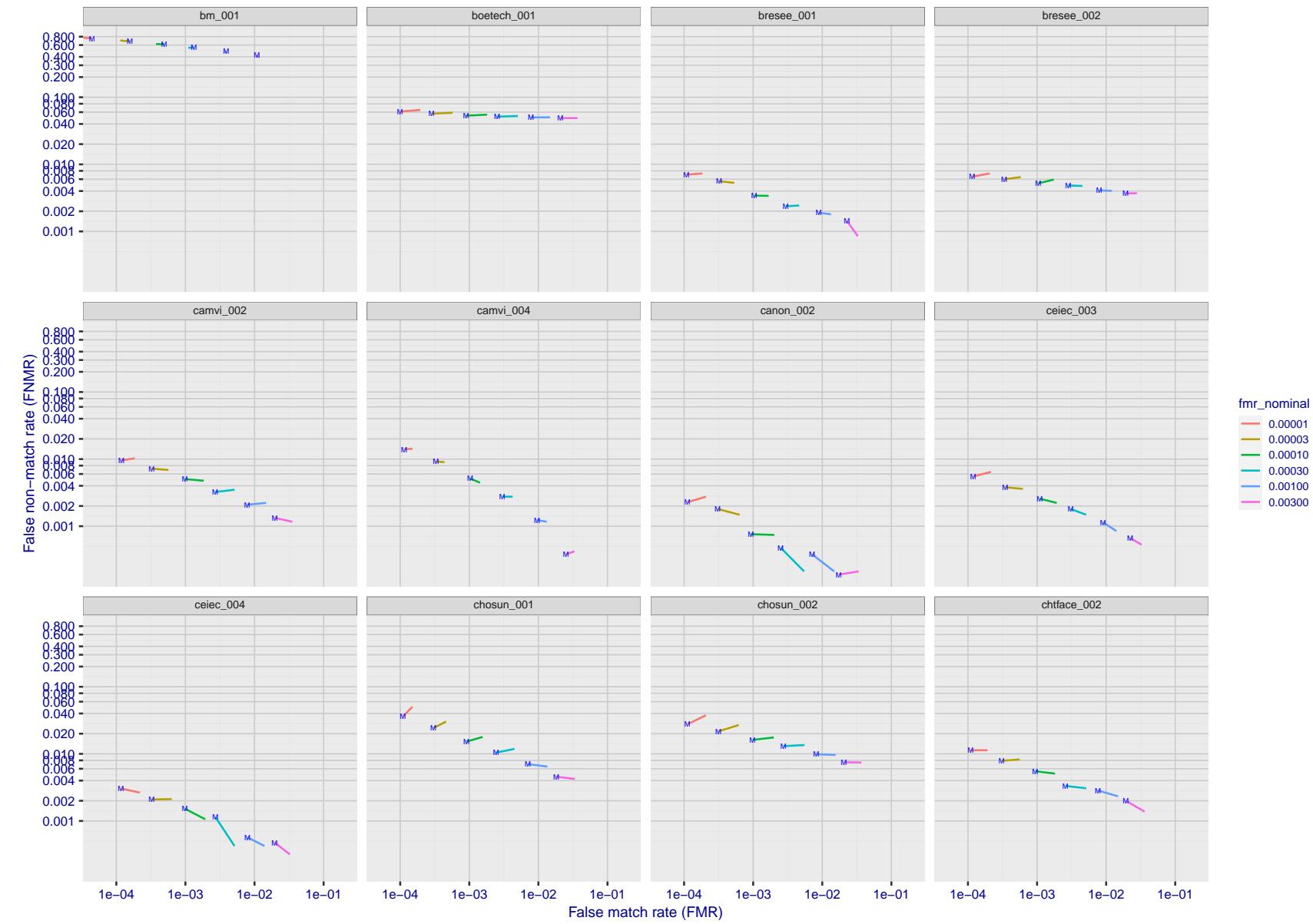


Figure 132: For the visa images, FNMR and FMR at six operating points along the DET characteristic. At each point a line is drawn between  $(FMR, FNMR)_{MALE}$  and  $(FMR, FNMR)_{FEMALE}$  showing how which sex has lower FMR and/or FNMR. The "M" label denotes male, the other end of the line corresponds to female. The six operating thresholds are selected to give the nominal false match rates given in the legend, and are computed over all impostor pairs regardless of age, sex, and place of birth. The plotted FMR values are broadly an order of magnitude larger than the nominal rates because FMR is computed over demographically-matched impostor pairs i.e individuals of the same sex, from the same geographic region (see section 3.6.1), and the same age group (see section 3.6.2).

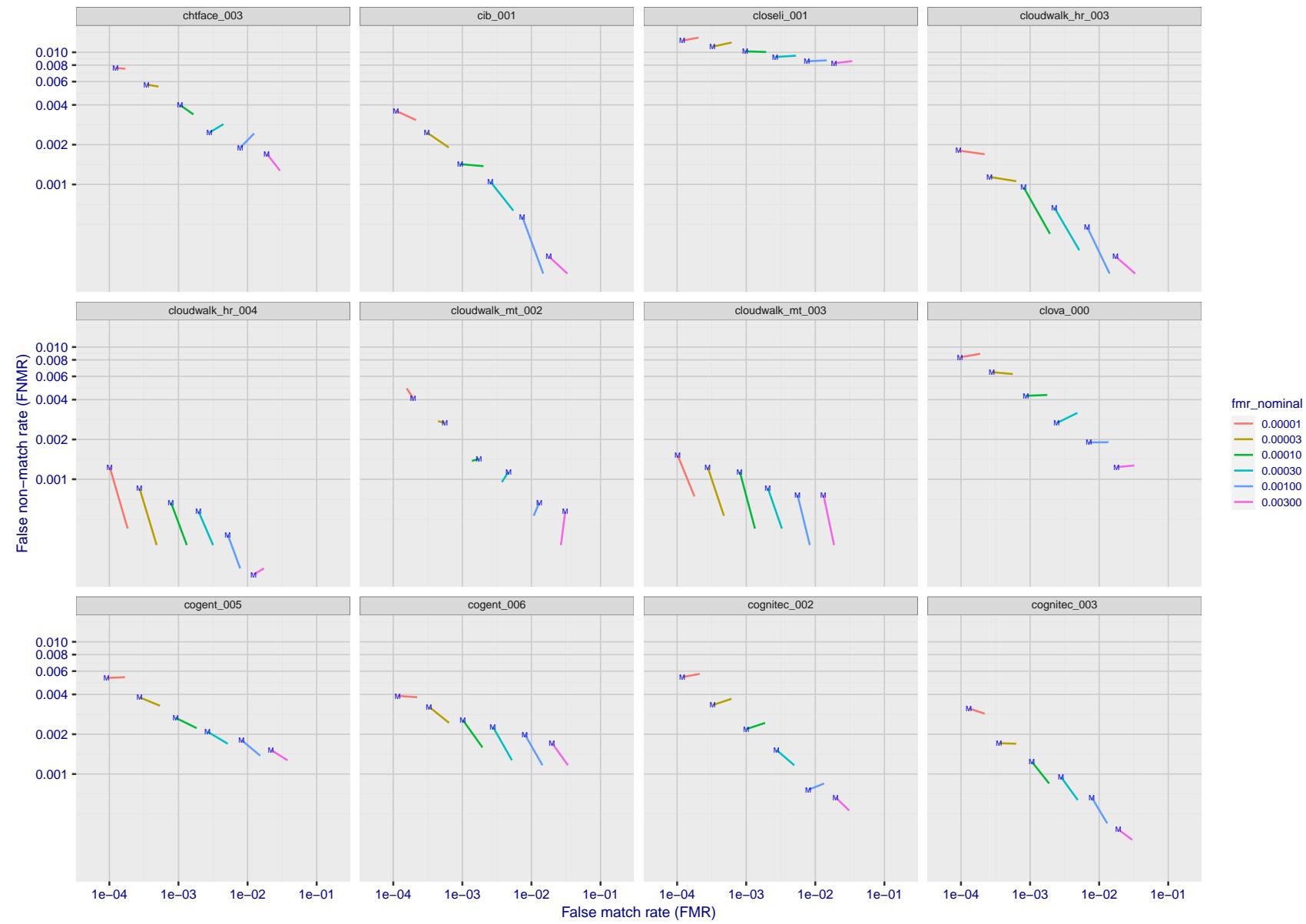


Figure 133: For the visa images, FNMR and FMR at six operating points along the DET characteristic. At each point a line is drawn between  $(FMR, FNMR)_{MALE}$  and  $(FMR, FNMR)_{FEMALE}$  showing how which sex has lower FMR and/or FNMR. The "M" label denotes male, the other end of the line corresponds to female. The six operating thresholds are selected to give the nominal false match rates given in the legend, and are computed over all impostor pairs regardless of age, sex, and place of birth. The plotted FMR values are broadly an order of magnitude larger than the nominal rates because FMR is computed over demographically-matched impostor pairs i.e individuals of the same sex, from the same geographic region (see section 3.6.1), and the same age group (see section 3.6.2).

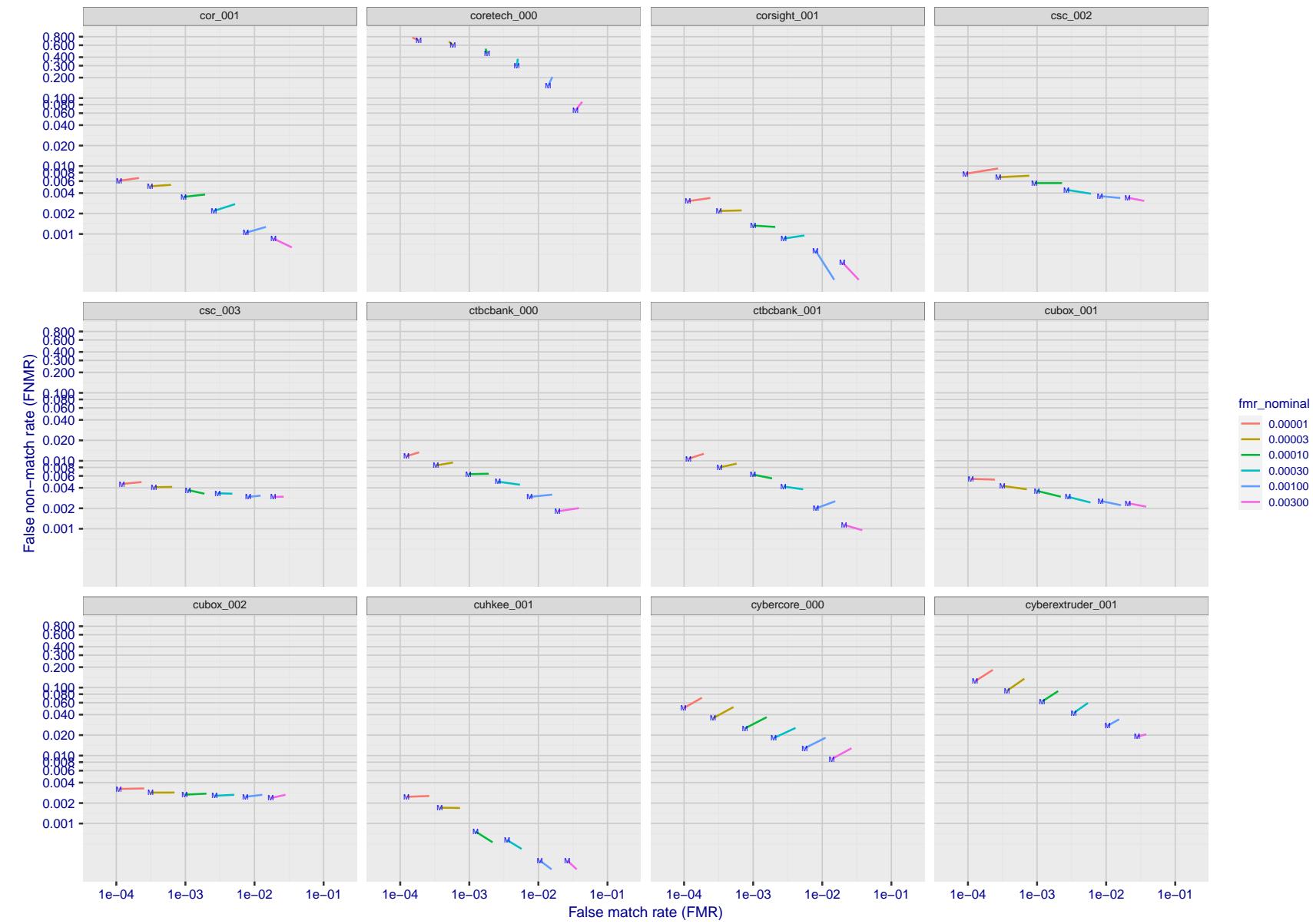


Figure 134: For the visa images, FNMR and FMR at six operating points along the DET characteristic. At each point a line is drawn between  $(FMR, FNMR)_{MALE}$  and  $(FMR, FNMR)_{FEMALE}$  showing how which sex has lower FMR and/or FNMR. The "M" label denotes male, the other end of the line corresponds to female. The six operating thresholds are selected to give the nominal false match rates given in the legend, and are computed over all impostor pairs regardless of age, sex, and place of birth. The plotted FMR values are broadly an order of magnitude larger than the nominal rates because FMR is computed over demographically-matched impostor pairs i.e individuals of the same sex, from the same geographic region (see section 3.6.1), and the same age group (see section 3.6.2).

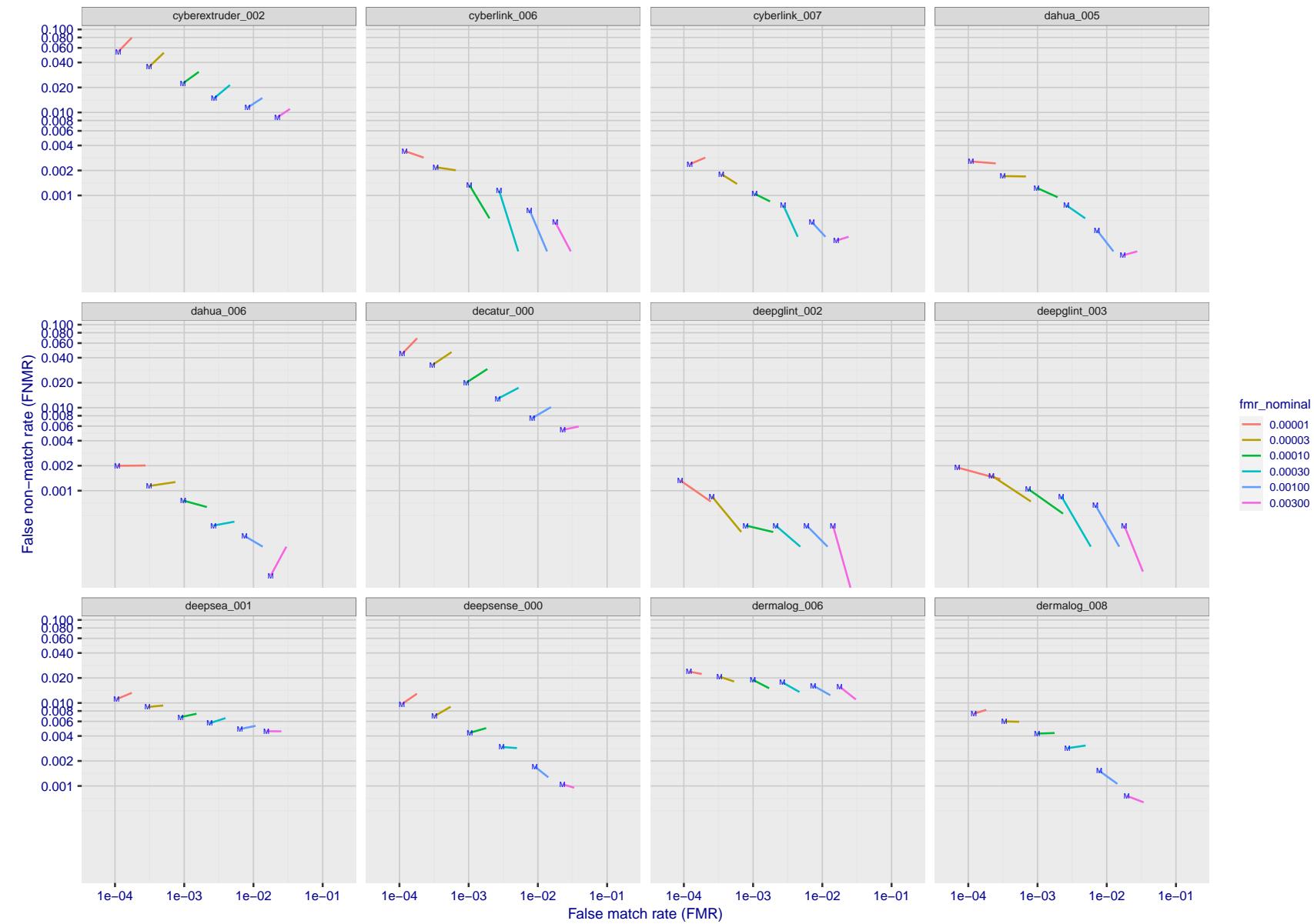


Figure 135: For the visa images, FNMR and FMR at six operating points along the DET characteristic. At each point a line is drawn between  $(FMR, FNMR)_{MALE}$  and  $(FMR, FNMR)_{FEMALE}$  showing how which sex has lower FMR and/or FNMR. The "M" label denotes male, the other end of the line corresponds to female. The six operating thresholds are selected to give the nominal false match rates given in the legend, and are computed over all impostor pairs regardless of age, sex, and place of birth. The plotted FMR values are broadly an order of magnitude larger than the nominal rates because FMR is computed over demographically-matched impostor pairs i.e individuals of the same sex, from the same geographic region (see section 3.6.1), and the same age group (see section 3.6.2).

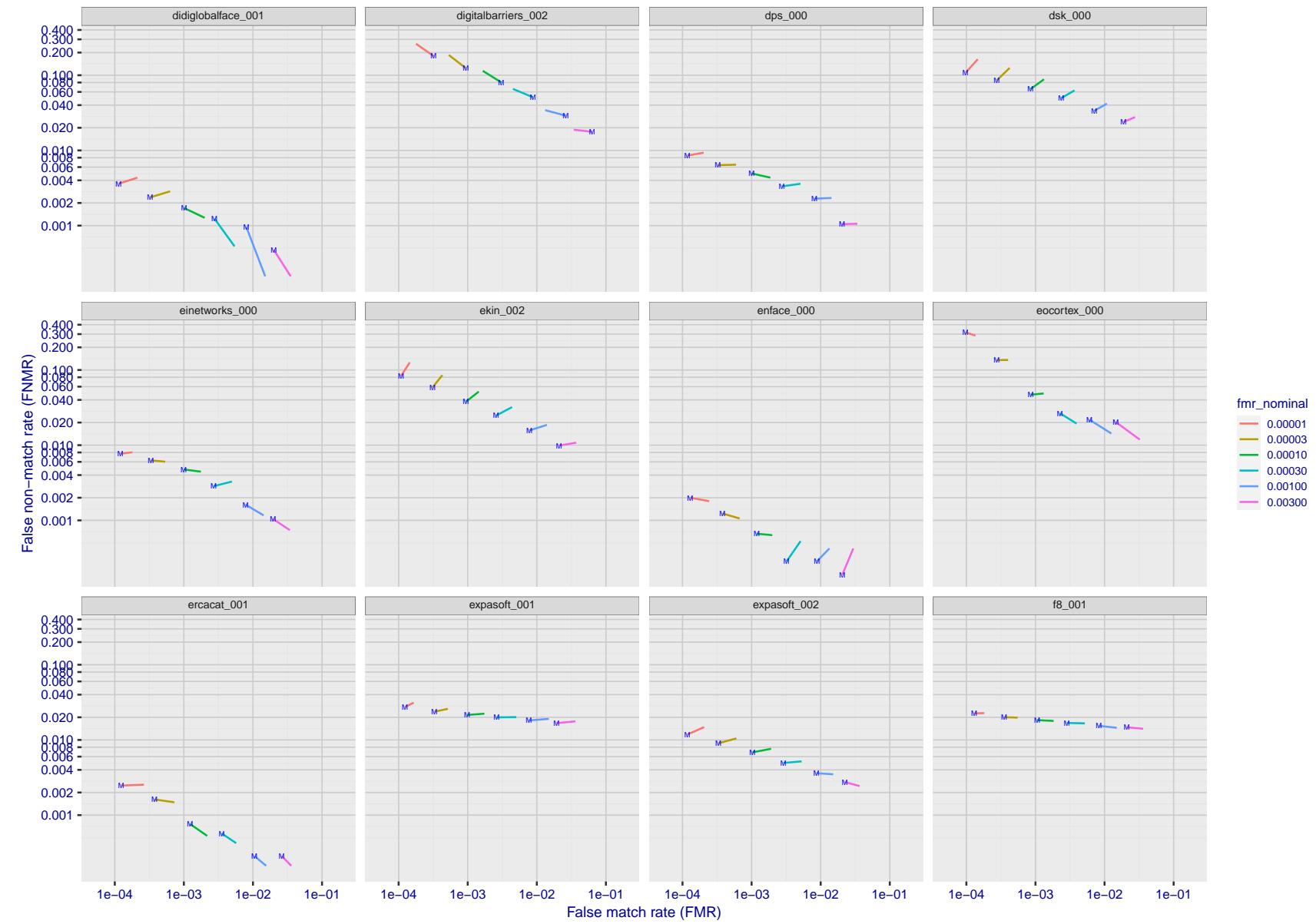


Figure 136: For the visa images, FNMR and FMR at six operating points along the DET characteristic. At each point a line is drawn between  $(FMR, FNMR)_{MALE}$  and  $(FMR, FNMR)_{FEMALE}$  showing how which sex has lower FMR and/or FNMR. The "M" label denotes male, the other end of the line corresponds to female. The six operating thresholds are selected to give the nominal false match rates given in the legend, and are computed over all impostor pairs regardless of age, sex, and place of birth. The plotted FMR values are broadly an order of magnitude larger than the nominal rates because FMR is computed over demographically-matched impostor pairs i.e individuals of the same sex, from the same geographic region (see section 3.6.1), and the same age group (see section 3.6.2).

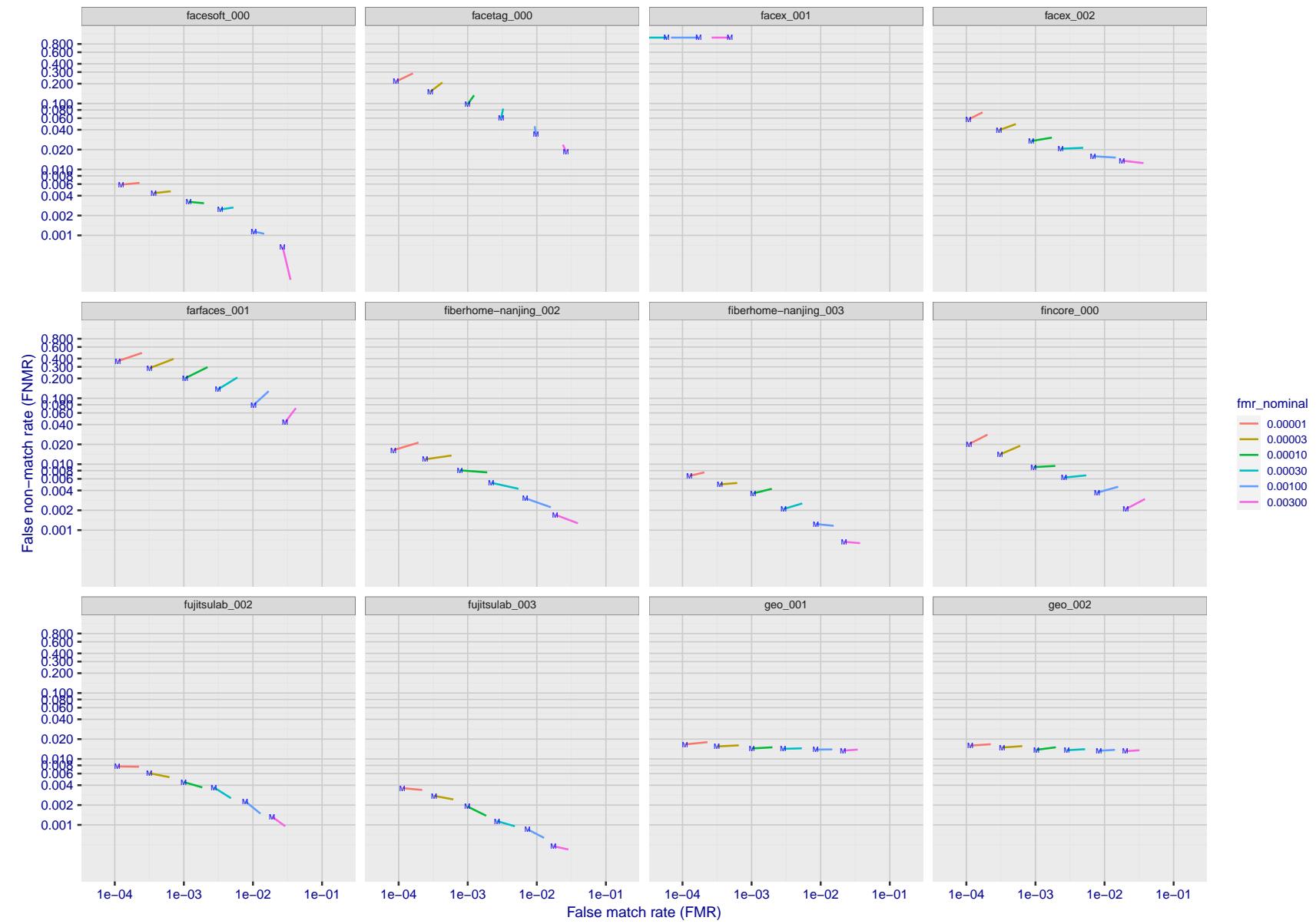


Figure 137: For the visa images, FNMR and FMR at six operating points along the DET characteristic. At each point a line is drawn between  $(FMR, FNMR)_{MALE}$  and  $(FMR, FNMR)_{FEMALE}$  showing how which sex has lower FMR and/or FNMR. The "M" label denotes male, the other end of the line corresponds to female. The six operating thresholds are selected to give the nominal false match rates given in the legend, and are computed over all impostor pairs regardless of age, sex, and place of birth. The plotted FMR values are broadly an order of magnitude larger than the nominal rates because FMR is computed over demographically-matched impostor pairs i.e individuals of the same sex, from the same geographic region (see section 3.6.1), and the same age group (see section 3.6.2).

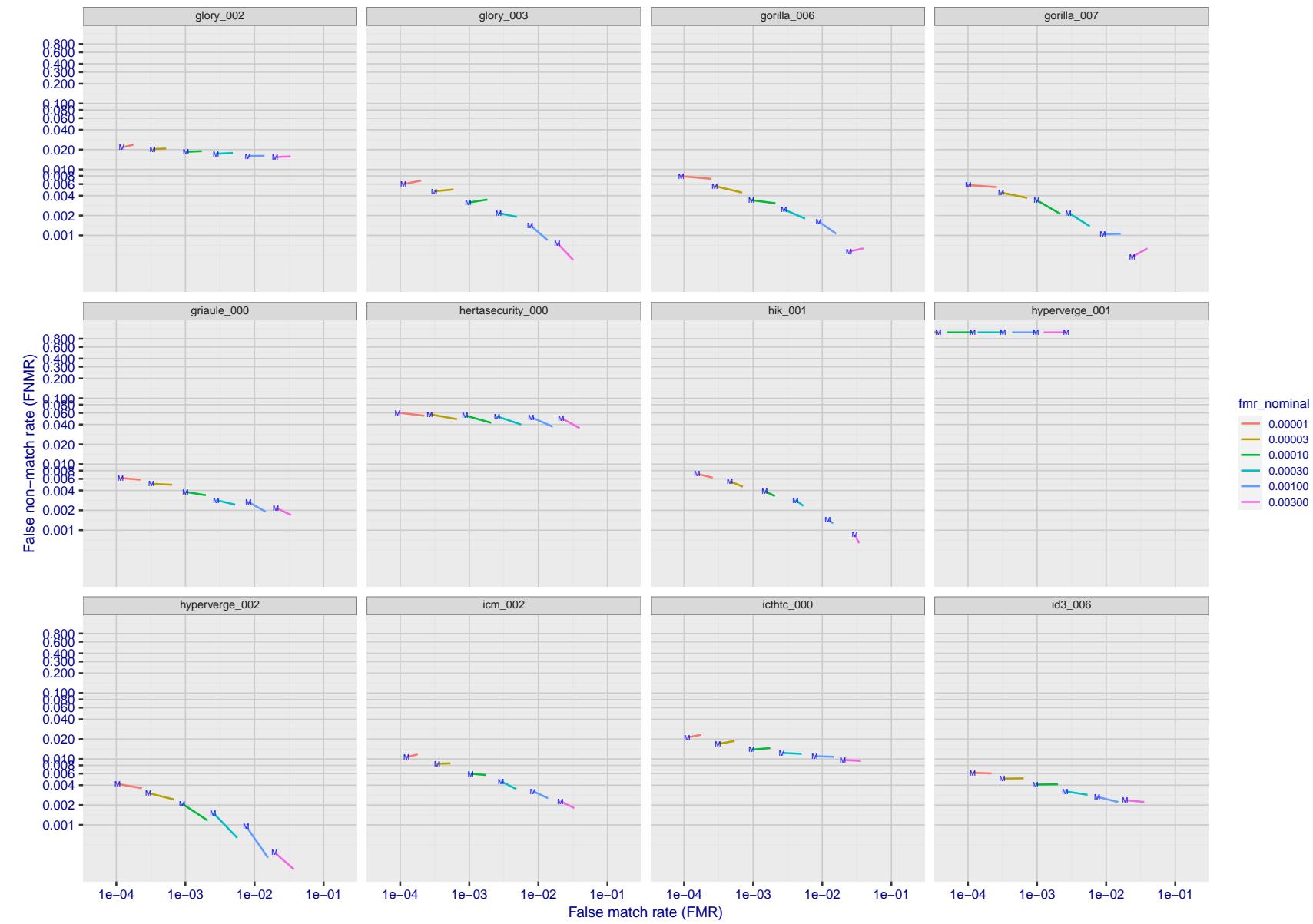


Figure 138: For the visa images, FNMR and FMR at six operating points along the DET characteristic. At each point a line is drawn between  $(FMR, FNMR)_{MALE}$  and  $(FMR, FNMR)_{FEMALE}$  showing how which sex has lower FMR and/or FNMR. The "M" label denotes male, the other end of the line corresponds to female. The six operating thresholds are selected to give the nominal false match rates given in the legend, and are computed over all impostor pairs regardless of age, sex, and place of birth. The plotted FMR values are broadly an order of magnitude larger than the nominal rates because FMR is computed over demographically-matched impostor pairs i.e individuals of the same sex, from the same geographic region (see section 3.6.1), and the same age group (see section 3.6.2).

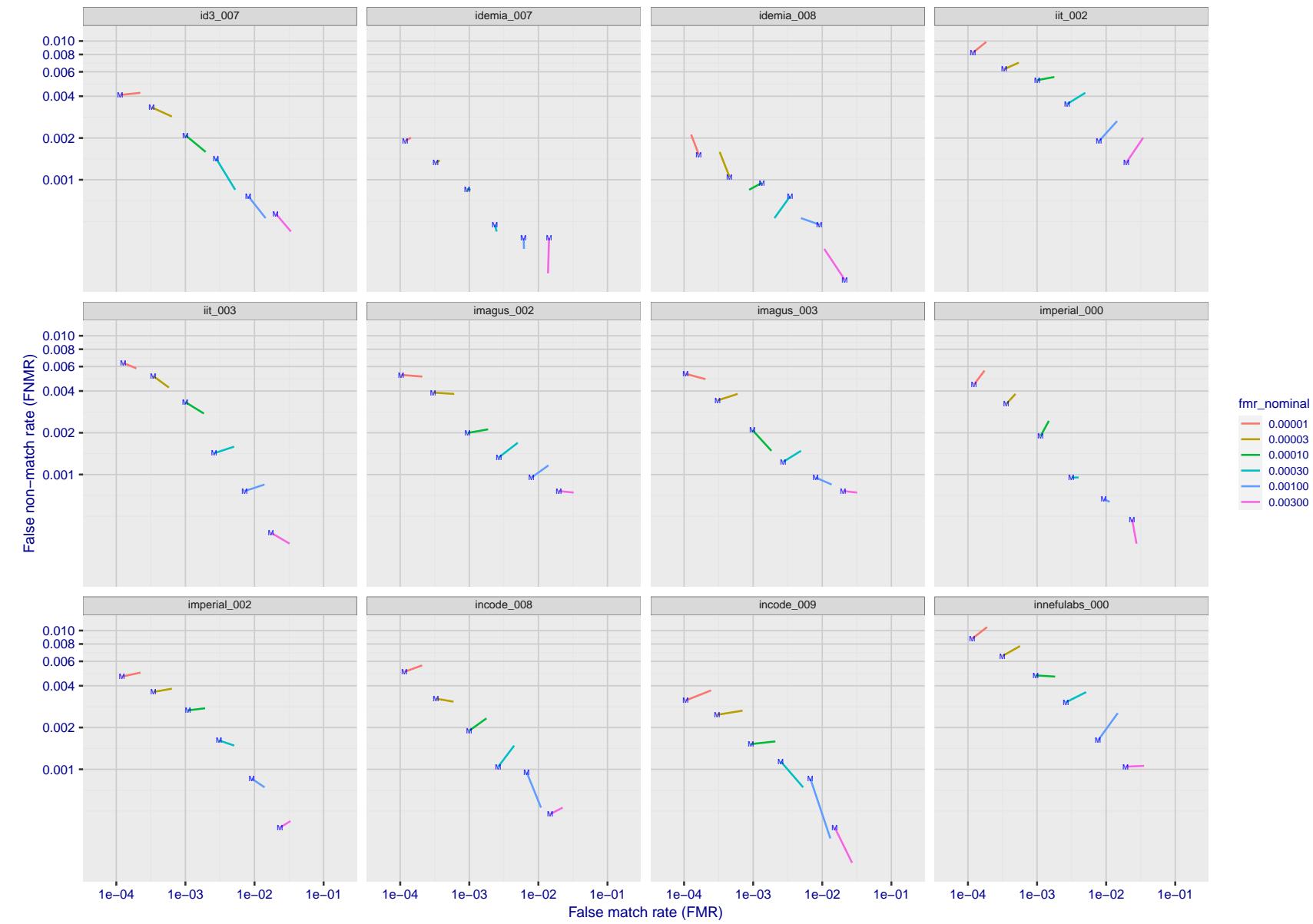


Figure 139: For the visa images, FNMR and FMR at six operating points along the DET characteristic. At each point a line is drawn between  $(FMR, FNMR)_{MALE}$  and  $(FMR, FNMR)_{FEMALE}$  showing how which sex has lower FMR and/or FNMR. The "M" label denotes male, the other end of the line corresponds to female. The six operating thresholds are selected to give the nominal false match rates given in the legend, and are computed over all impostor pairs regardless of age, sex, and place of birth. The plotted FMR values are broadly an order of magnitude larger than the nominal rates because FMR is computed over demographically-matched impostor pairs i.e individuals of the same sex, from the same geographic region (see section 3.6.1), and the same age group (see section 3.6.2).

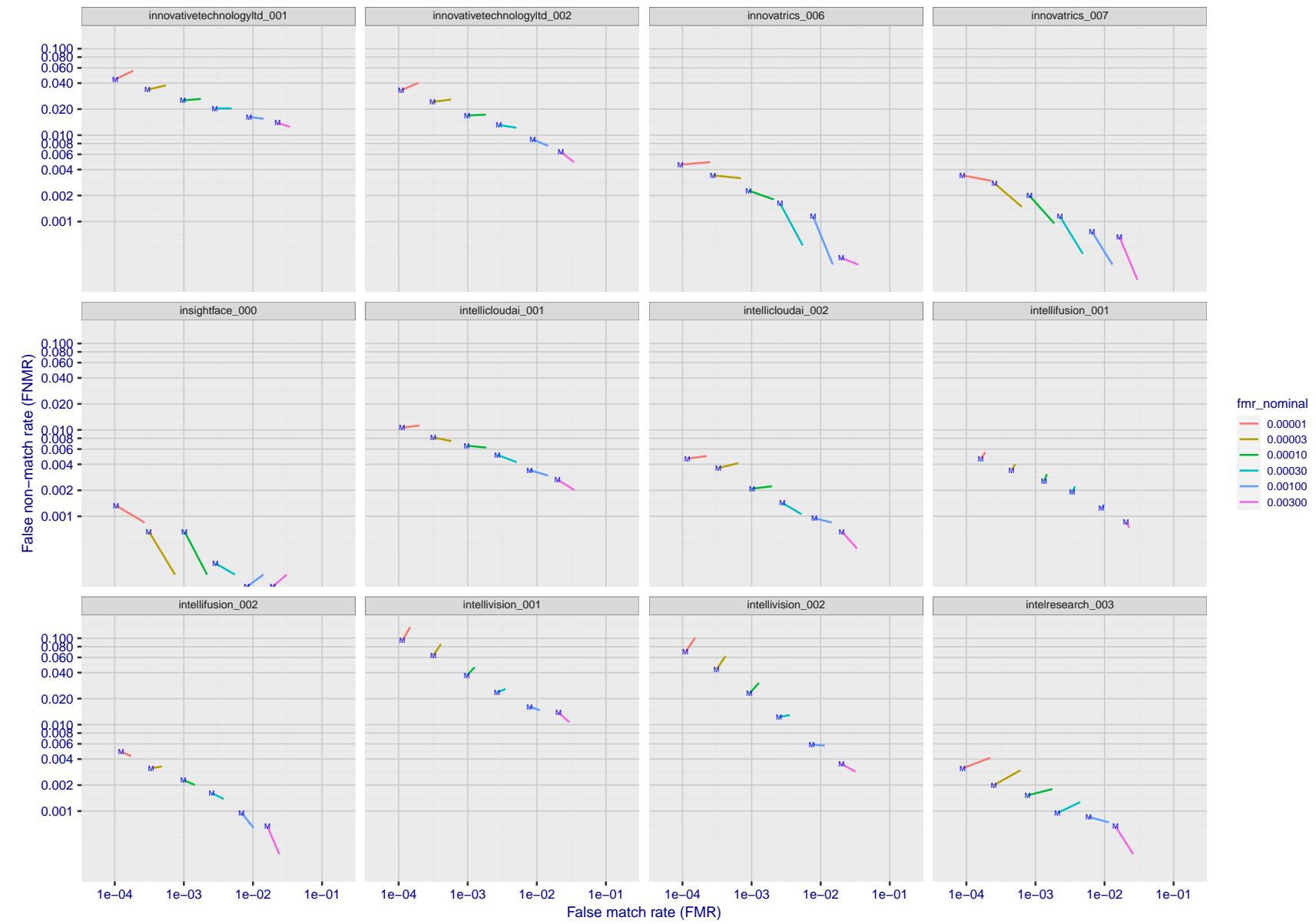


Figure 140: For the visa images, FNMR and FMR at six operating points along the DET characteristic. At each point a line is drawn between  $(FMR, FNMR)_{MALE}$  and  $(FMR, FNMR)_{FEMALE}$  showing how which sex has lower FMR and/or FNMR. The "M" label denotes male, the other end of the line corresponds to female. The six operating thresholds are selected to give the nominal false match rates given in the legend, and are computed over all impostor pairs regardless of age, sex, and place of birth. The plotted FMR values are broadly an order of magnitude larger than the nominal rates because FMR is computed over demographically-matched impostor pairs i.e individuals of the same sex, from the same geographic region (see section 3.6.1), and the same age group (see section 3.6.2).

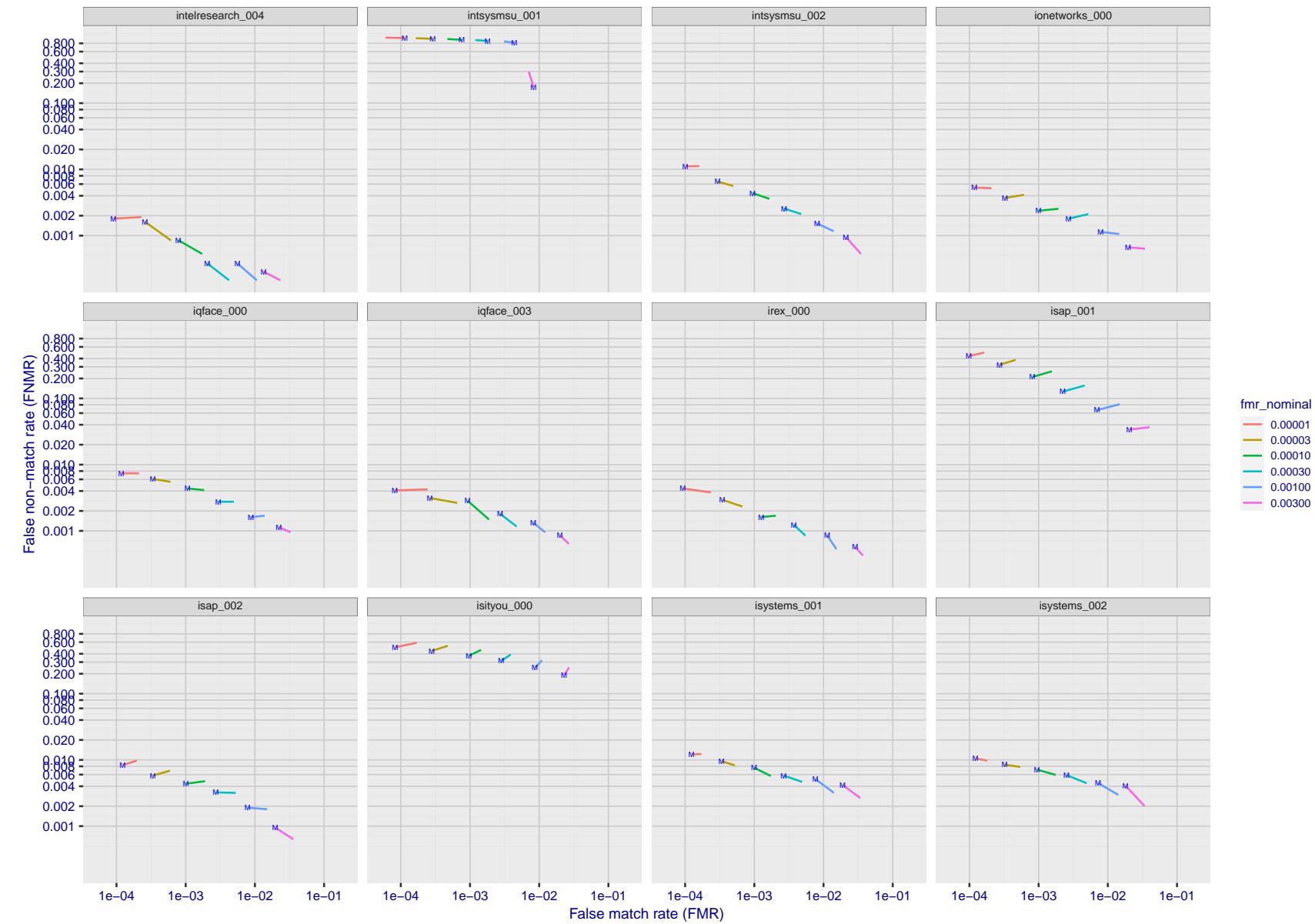


Figure 141: For the visa images, FNMR and FMR at six operating points along the DET characteristic. At each point a line is drawn between  $(FMR, FNMR)_{MALE}$  and  $(FMR, FNMR)_{FEMALE}$  showing how which sex has lower FMR and/or FNMR. The "M" label denotes male, the other end of the line corresponds to female. The six operating thresholds are selected to give the nominal false match rates given in the legend, and are computed over all impostor pairs regardless of age, sex, and place of birth. The plotted FMR values are broadly an order of magnitude larger than the nominal rates because FMR is computed over demographically-matched impostor pairs i.e individuals of the same sex, from the same geographic region (see section 3.6.1), and the same age group (see section 3.6.2).

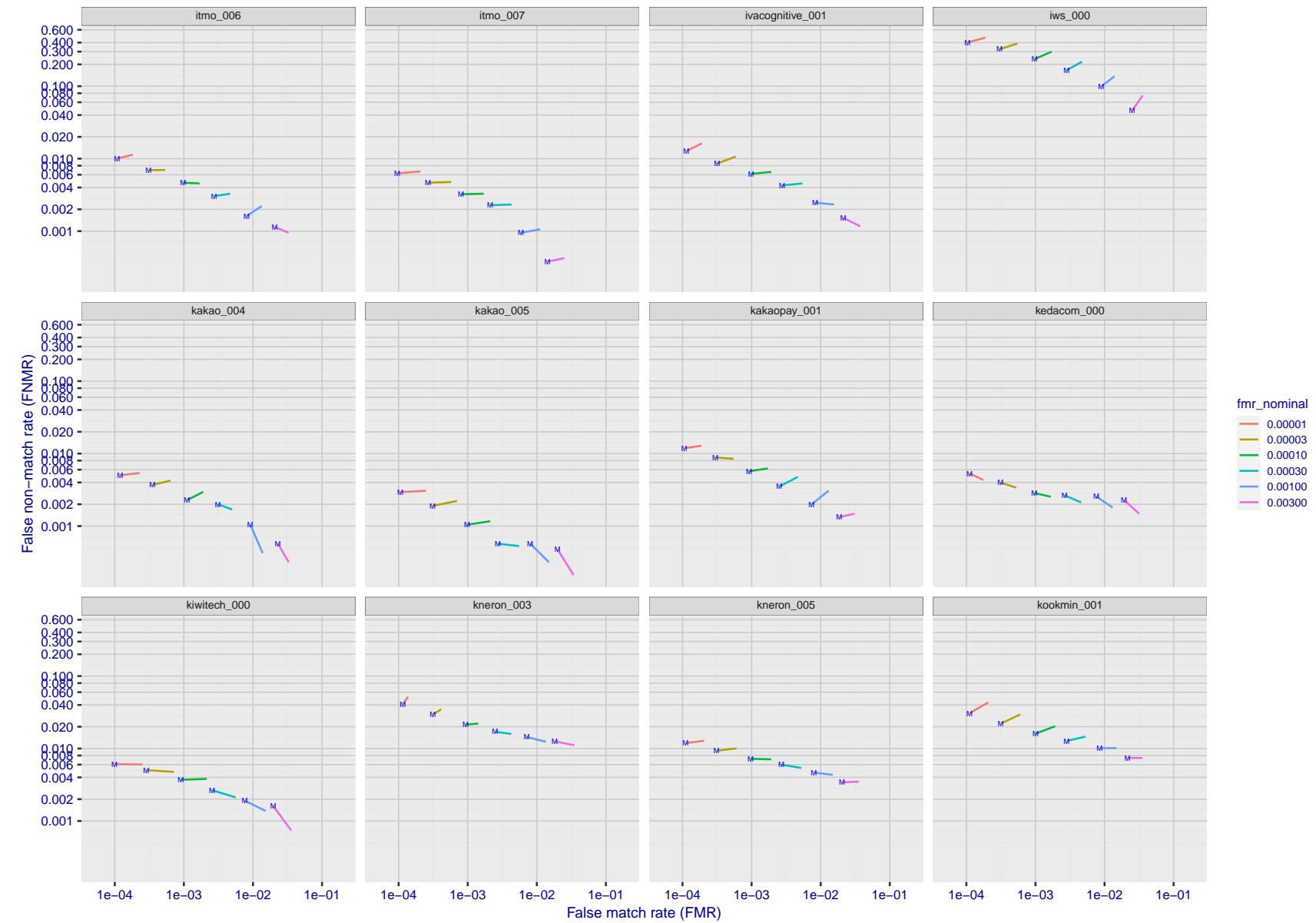


Figure 142: For the visa images, FNMR and FMR at six operating points along the DET characteristic. At each point a line is drawn between  $(FMR, FNMR)_{MALE}$  and  $(FMR, FNMR)_{FEMALE}$  showing how which sex has lower FMR and/or FNMR. The "M" label denotes male, the other end of the line corresponds to female. The six operating thresholds are selected to give the nominal false match rates given in the legend, and are computed over all impostor pairs regardless of age, sex, and place of birth. The plotted FMR values are broadly an order of magnitude larger than the nominal rates because FMR is computed over demographically-matched impostor pairs i.e individuals of the same sex, from the same geographic region (see section 3.6.1), and the same age group (see section 3.6.2).

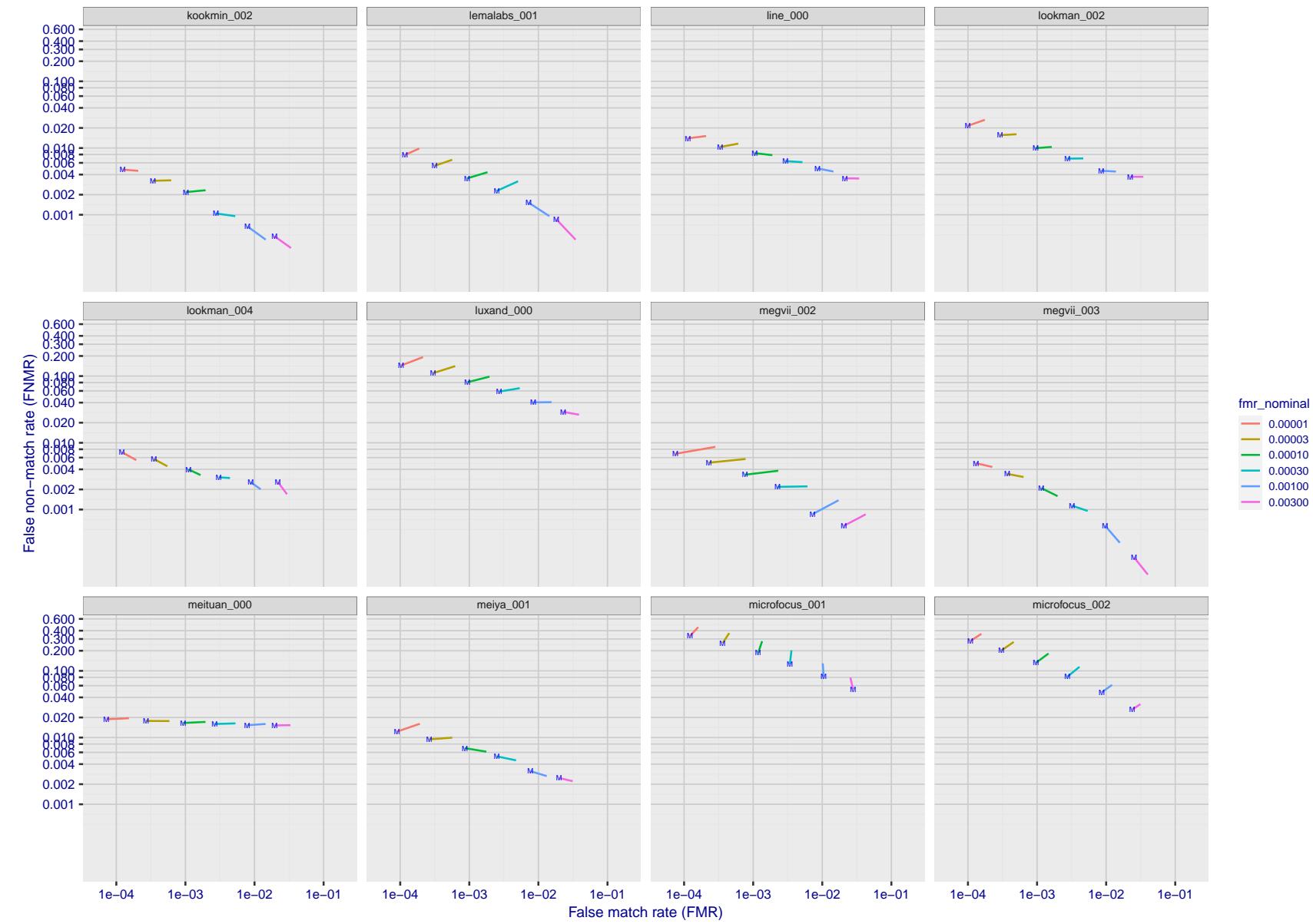


Figure 143: For the visa images, FNMR and FMR at six operating points along the DET characteristic. At each point a line is drawn between  $(FMR, FNMR)_{MALE}$  and  $(FMR, FNMR)_{FEMALE}$  showing how which sex has lower FMR and/or FNMR. The "M" label denotes male, the other end of the line corresponds to female. The six operating thresholds are selected to give the nominal false match rates given in the legend, and are computed over all impostor pairs regardless of age, sex, and place of birth. The plotted FMR values are broadly an order of magnitude larger than the nominal rates because FMR is computed over demographically-matched impostor pairs i.e individuals of the same sex, from the same geographic region (see section 3.6.1), and the same age group (see section 3.6.2).

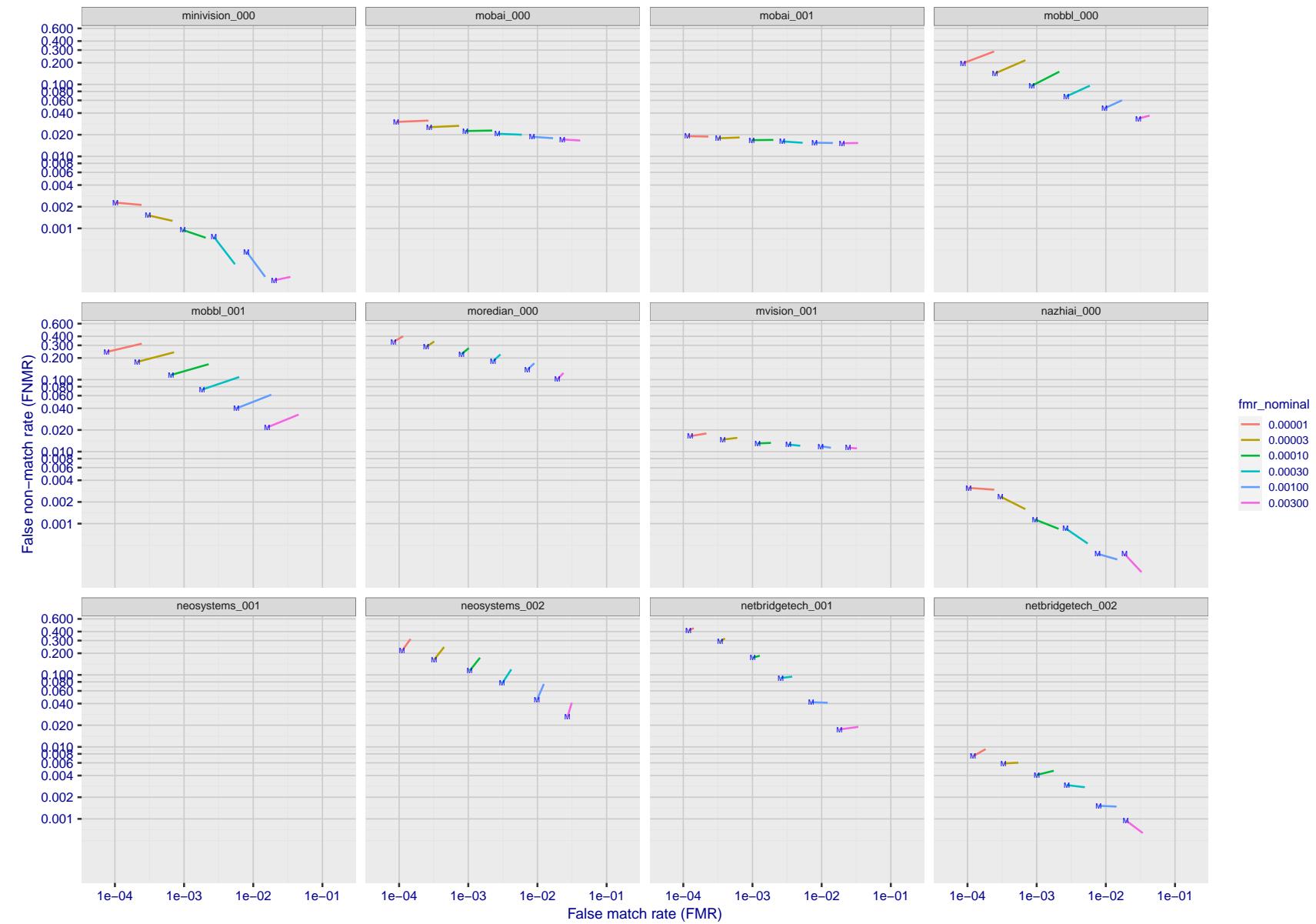


Figure 144: For the visa images, FNMR and FMR at six operating points along the DET characteristic. At each point a line is drawn between  $(FMR, FNMR)_{MALE}$  and  $(FMR, FNMR)_{FEMALE}$  showing how which sex has lower FMR and/or FNMR. The "M" label denotes male, the other end of the line corresponds to female. The six operating thresholds are selected to give the nominal false match rates given in the legend, and are computed over all impostor pairs regardless of age, sex, and place of birth. The plotted FMR values are broadly an order of magnitude larger than the nominal rates because FMR is computed over demographically-matched impostor pairs i.e individuals of the same sex, from the same geographic region (see section 3.6.1), and the same age group (see section 3.6.2).

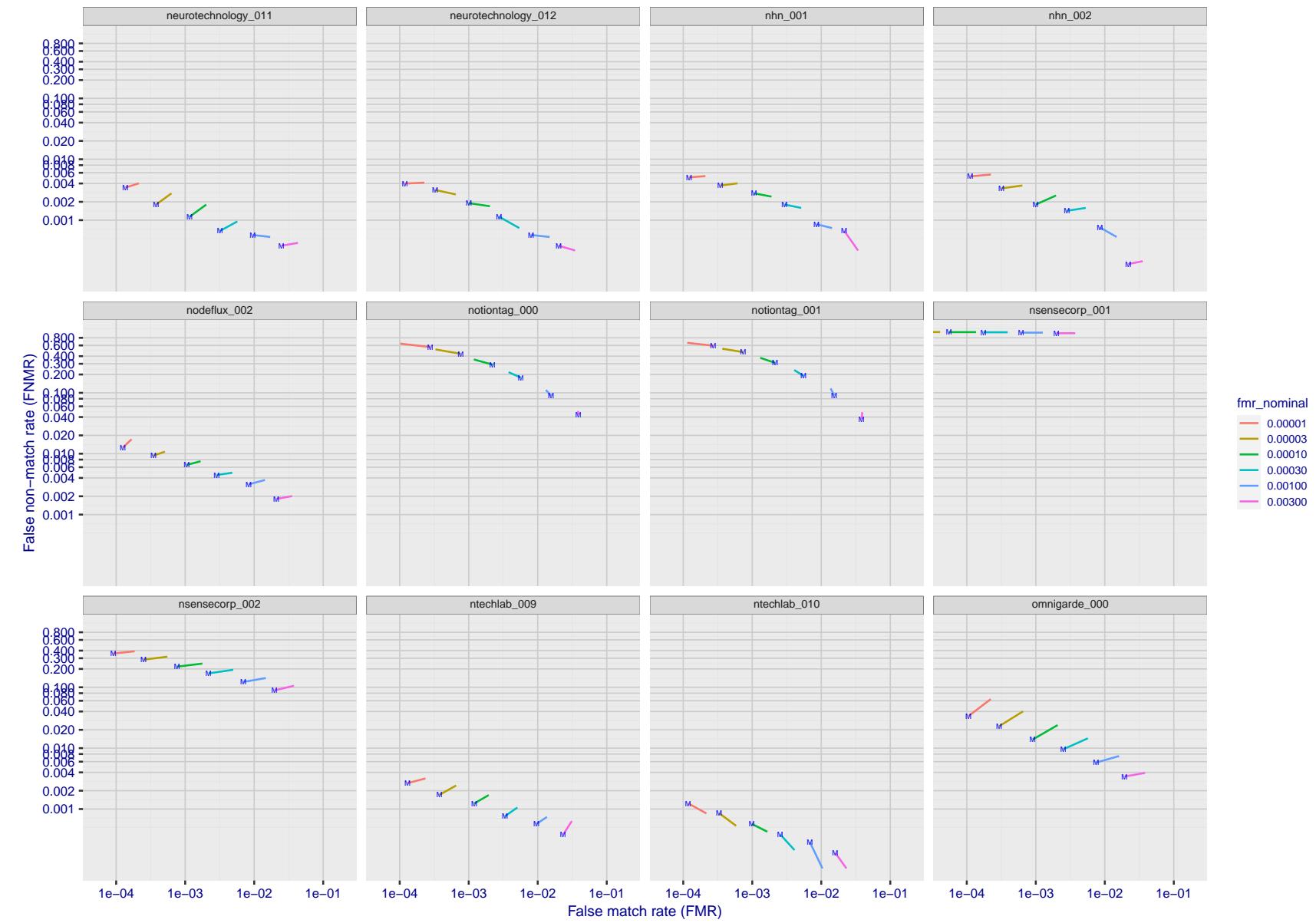


Figure 145: For the visa images, FNMR and FMR at six operating points along the DET characteristic. At each point a line is drawn between  $(FMR, FNMR)_{MALE}$  and  $(FMR, FNMR)_{FEMALE}$  showing how which sex has lower FMR and/or FNMR. The "M" label denotes male, the other end of the line corresponds to female. The six operating thresholds are selected to give the nominal false match rates given in the legend, and are computed over all impostor pairs regardless of age, sex, and place of birth. The plotted FMR values are broadly an order of magnitude larger than the nominal rates because FMR is computed over demographically-matched impostor pairs i.e individuals of the same sex, from the same geographic region (see section 3.6.1), and the same age group (see section 3.6.2).

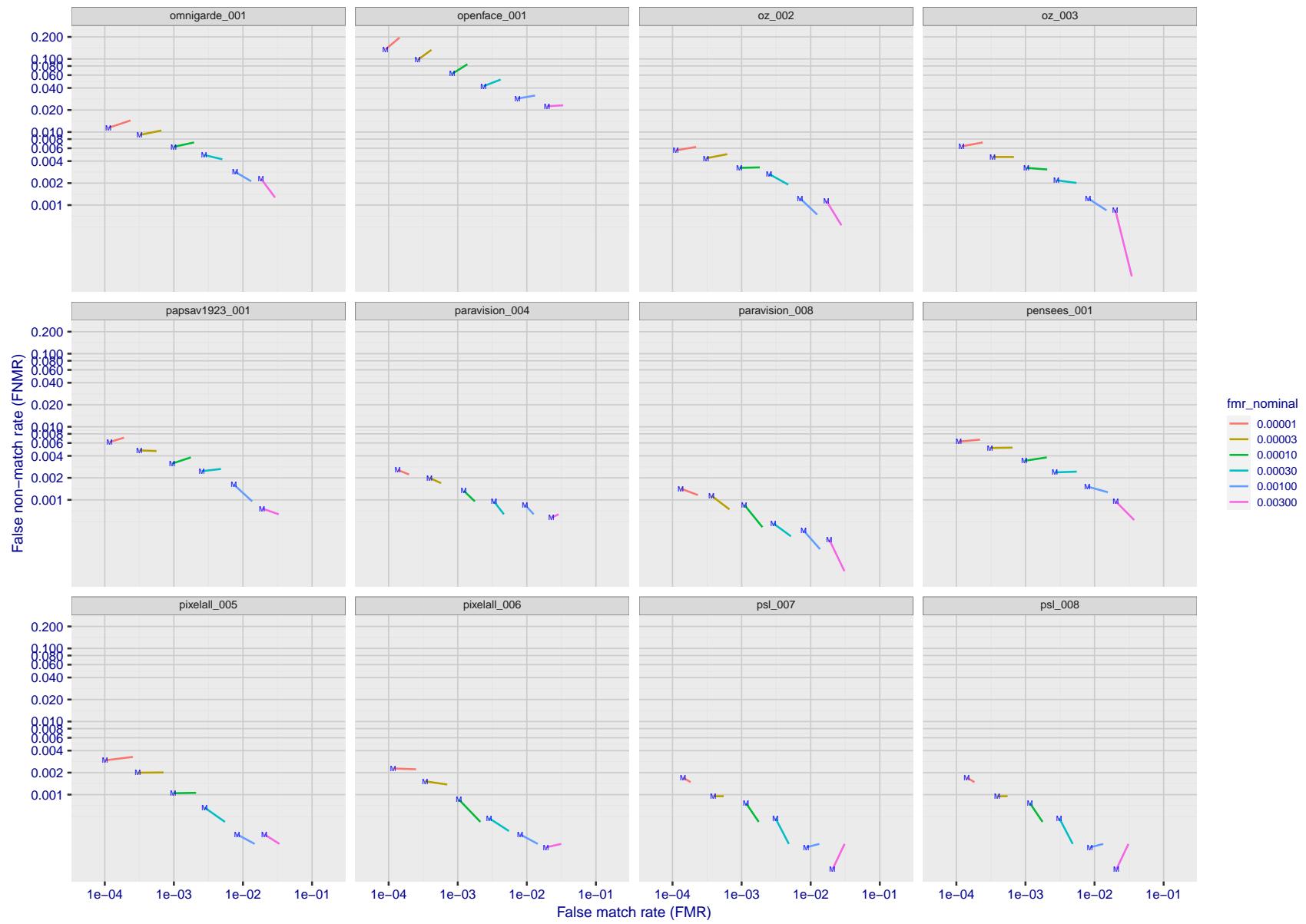


Figure 146: For the visa images, FNMR and FMR at six operating points along the DET characteristic. At each point a line is drawn between  $(FMR, FNMR)_{MALE}$  and  $(FMR, FNMR)_{FEMALE}$  showing how which sex has lower FMR and/or FNMR. The "M" label denotes male, the other end of the line corresponds to female. The six operating thresholds are selected to give the nominal false match rates given in the legend, and are computed over all impostor pairs regardless of age, sex, and place of birth. The plotted FMR values are broadly an order of magnitude larger than the nominal rates because FMR is computed over demographically-matched impostor pairs i.e individuals of the same sex, from the same geographic region (see section 3.6.1), and the same age group (see section 3.6.2).

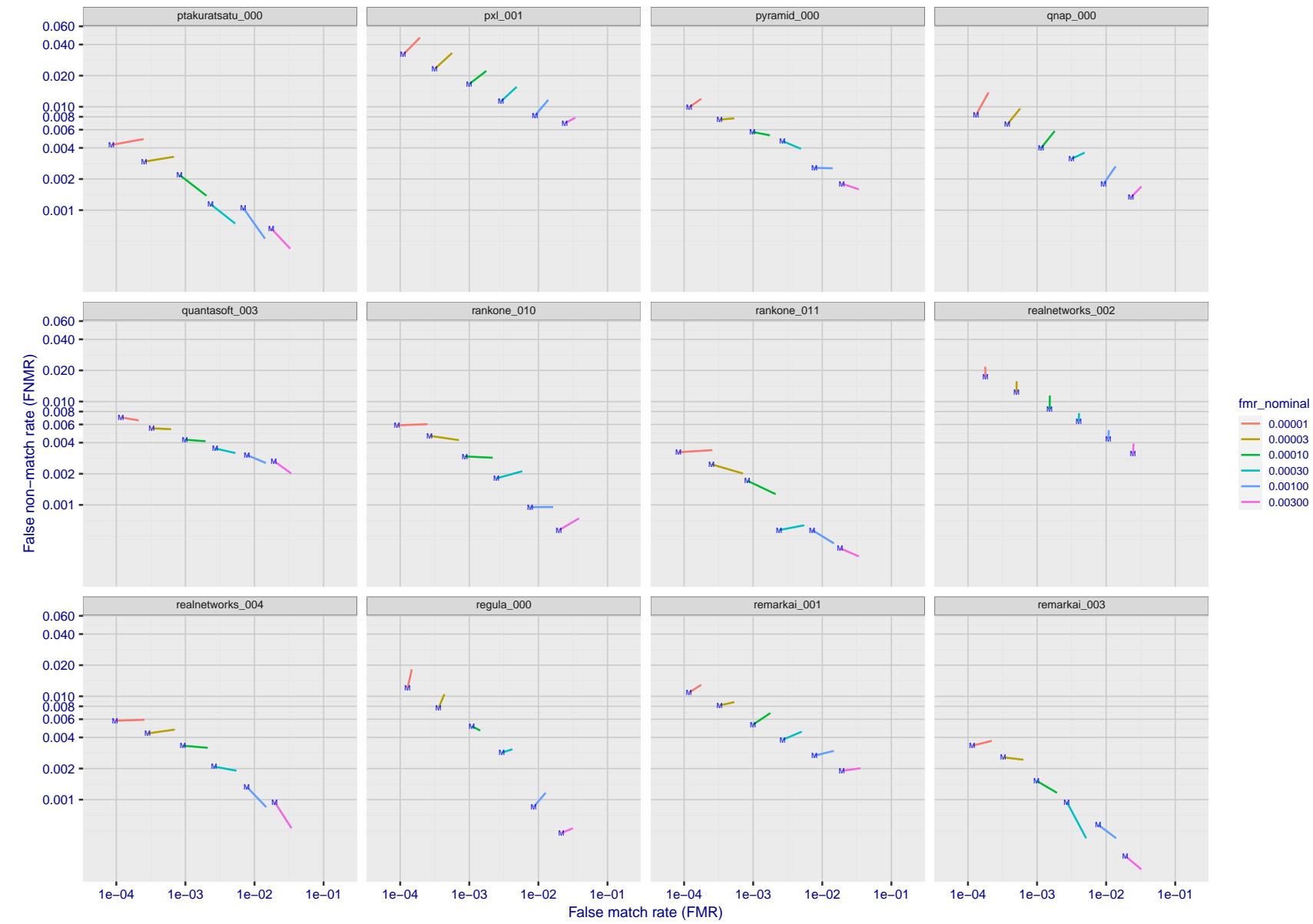


Figure 147: For the visa images, FNMR and FMR at six operating points along the DET characteristic. At each point a line is drawn between  $(FMR, FNMR)_{MALE}$  and  $(FMR, FNMR)_{FEMALE}$  showing how which sex has lower FMR and/or FNMR. The "M" label denotes male, the other end of the line corresponds to female. The six operating thresholds are selected to give the nominal false match rates given in the legend, and are computed over all impostor pairs regardless of age, sex, and place of birth. The plotted FMR values are broadly an order of magnitude larger than the nominal rates because FMR is computed over demographically-matched impostor pairs i.e individuals of the same sex, from the same geographic region (see section 3.6.1), and the same age group (see section 3.6.2).

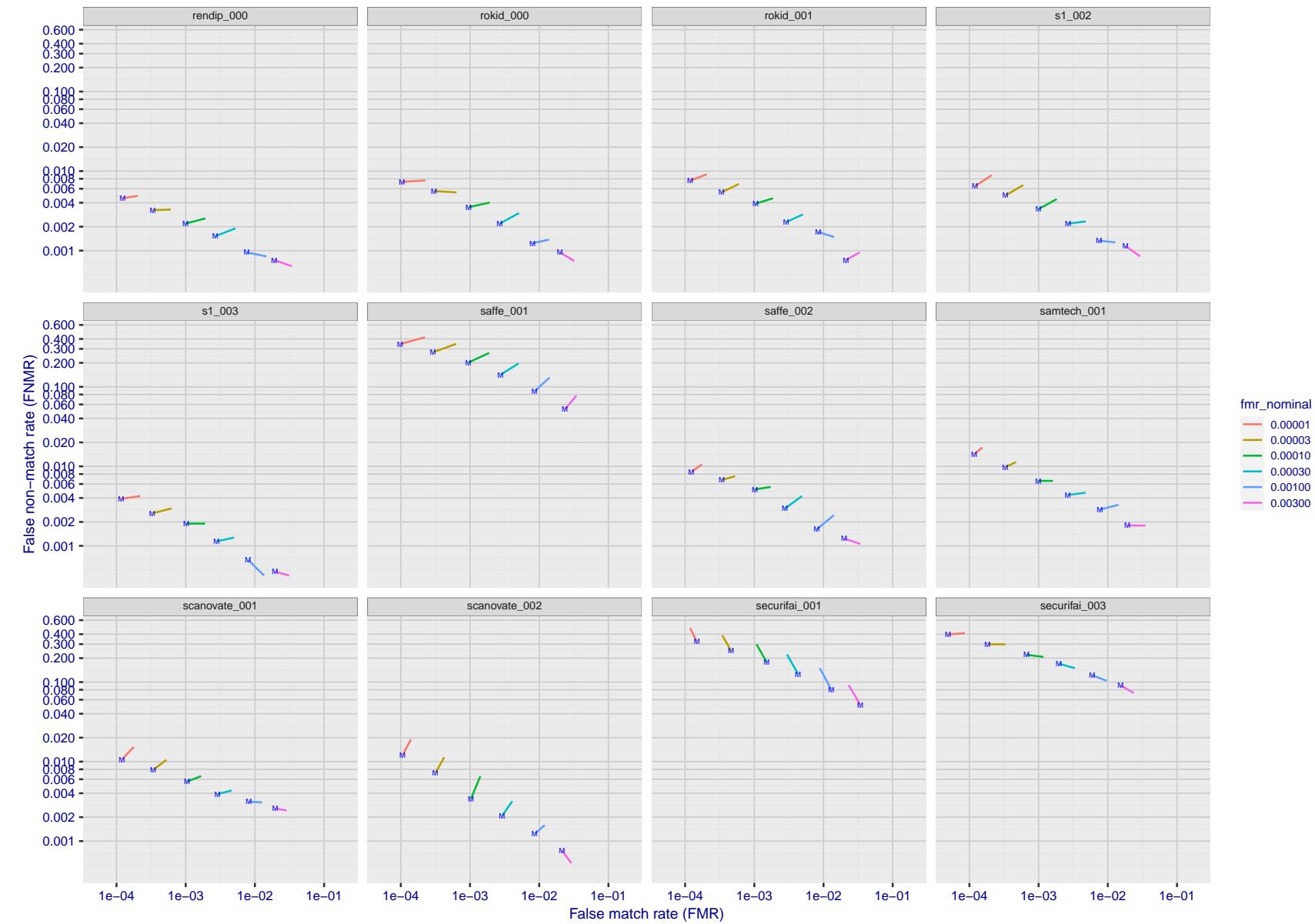


Figure 148: For the visa images, FNMR and FMR at six operating points along the DET characteristic. At each point a line is drawn between  $(FMR, FNMR)_{MALE}$  and  $(FMR, FNMR)_{FEMALE}$  showing how which sex has lower FMR and/or FNMR. The "M" label denotes male, the other end of the line corresponds to female. The six operating thresholds are selected to give the nominal false match rates given in the legend, and are computed over all impostor pairs regardless of age, sex, and place of birth. The plotted FMR values are broadly an order of magnitude larger than the nominal rates because FMR is computed over demographically-matched impostor pairs i.e individuals of the same sex, from the same geographic region (see section 3.6.1), and the same age group (see section 3.6.2).

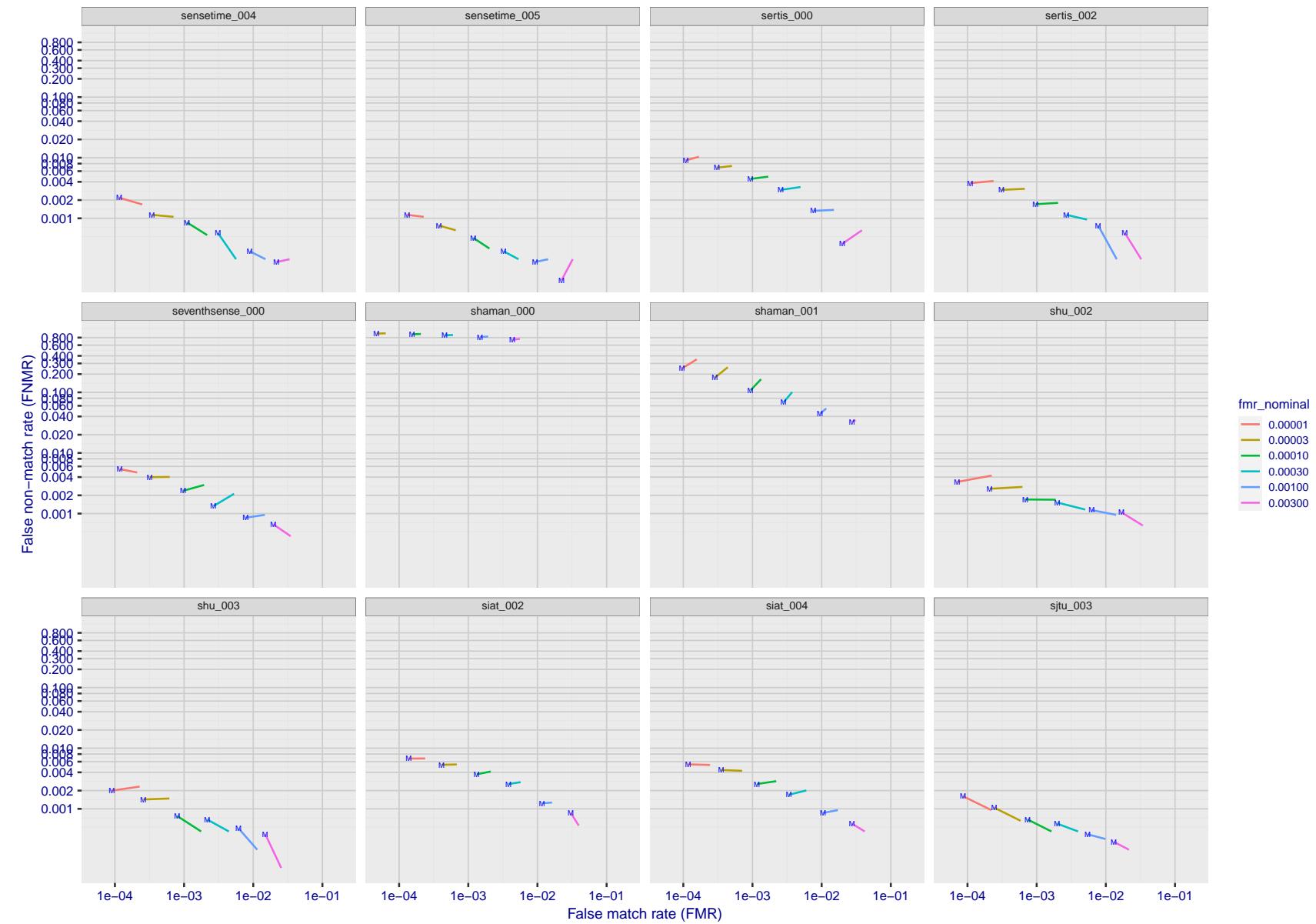


Figure 149: For the visa images, FNMR and FMR at six operating points along the DET characteristic. At each point a line is drawn between  $(FMR, FNMR)_{MALE}$  and  $(FMR, FNMR)_{FEMALE}$  showing how which sex has lower FMR and/or FNMR. The "M" label denotes male, the other end of the line corresponds to female. The six operating thresholds are selected to give the nominal false match rates given in the legend, and are computed over all impostor pairs regardless of age, sex, and place of birth. The plotted FMR values are broadly an order of magnitude larger than the nominal rates because FMR is computed over demographically-matched impostor pairs i.e individuals of the same sex, from the same geographic region (see section 3.6.1), and the same age group (see section 3.6.2).

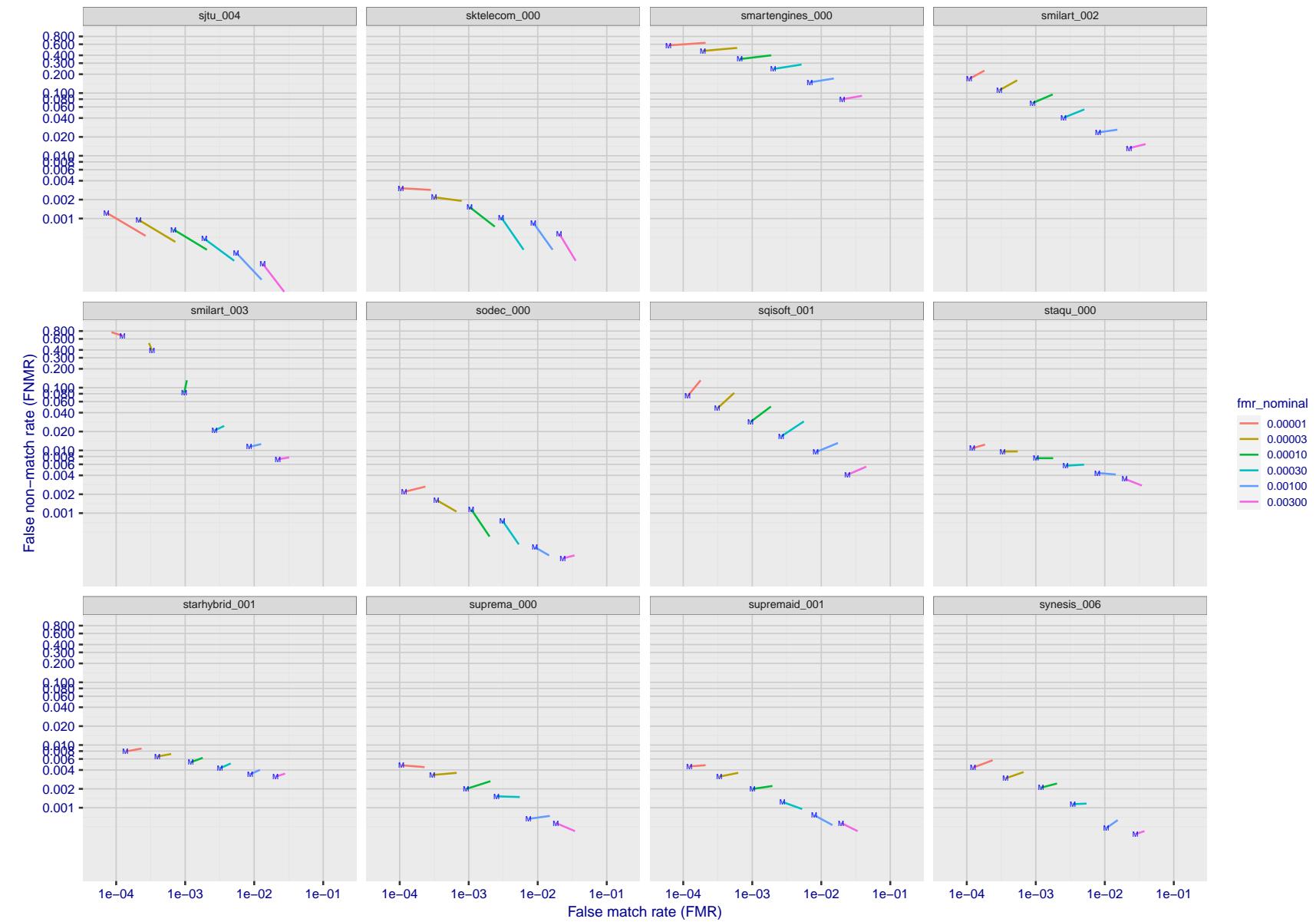


Figure 150: For the visa images, FNMR and FMR at six operating points along the DET characteristic. At each point a line is drawn between  $(FMR, FNMR)_{MALE}$  and  $(FMR, FNMR)_{FEMALE}$  showing how which sex has lower FMR and/or FNMR. The "M" label denotes male, the other end of the line corresponds to female. The six operating thresholds are selected to give the nominal false match rates given in the legend, and are computed over all impostor pairs regardless of age, sex, and place of birth. The plotted FMR values are broadly an order of magnitude larger than the nominal rates because FMR is computed over demographically-matched impostor pairs i.e individuals of the same sex, from the same geographic region (see section 3.6.1), and the same age group (see section 3.6.2).

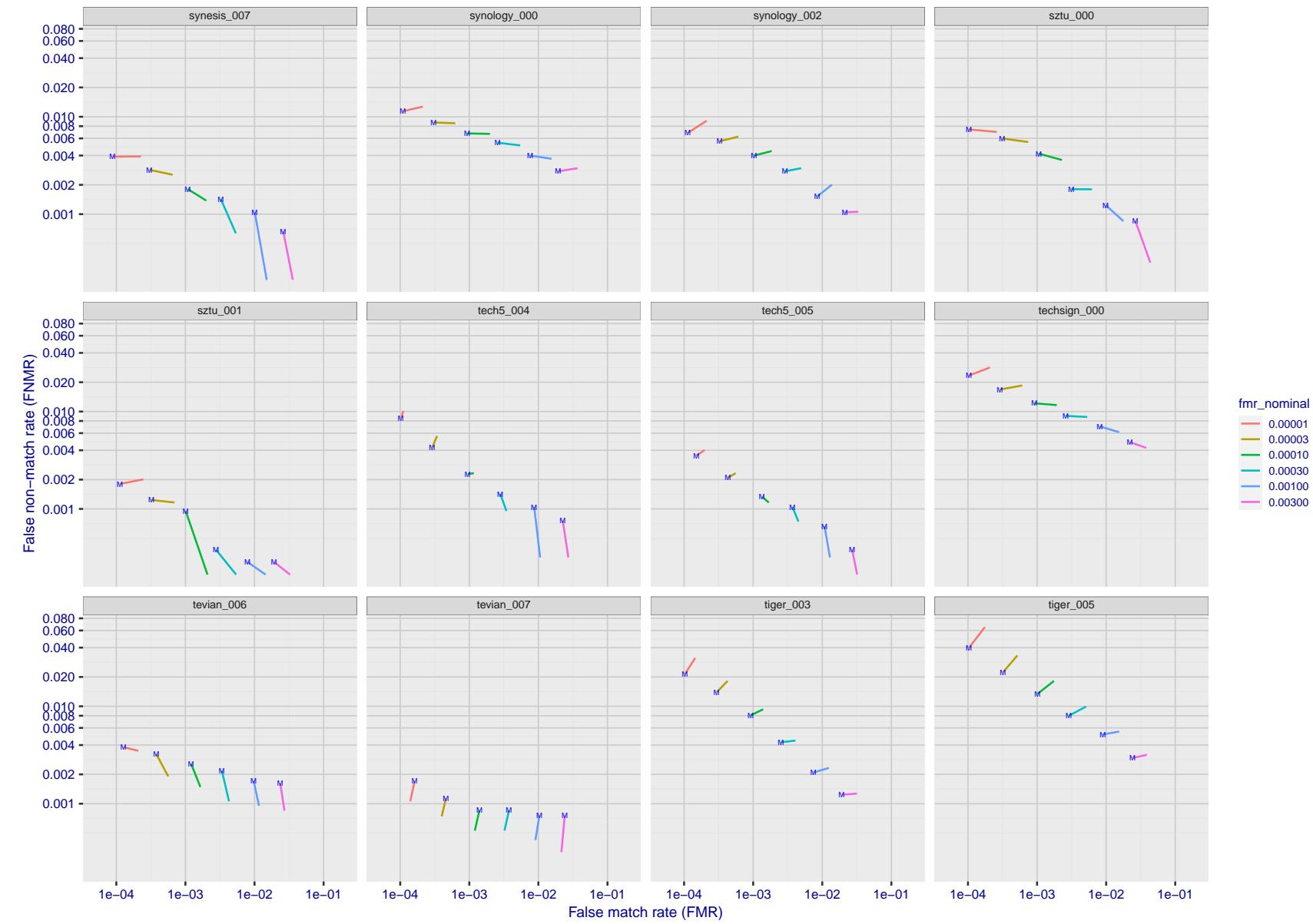


Figure 151: For the visa images, FNMR and FMR at six operating points along the DET characteristic. At each point a line is drawn between  $(FMR, FNMR)_{MALE}$  and  $(FMR, FNMR)_{FEMALE}$  showing how which sex has lower FMR and/or FNMR. The "M" label denotes male, the other end of the line corresponds to female. The six operating thresholds are selected to give the nominal false match rates given in the legend, and are computed over all impostor pairs regardless of age, sex, and place of birth. The plotted FMR values are broadly an order of magnitude larger than the nominal rates because FMR is computed over demographically-matched impostor pairs i.e individuals of the same sex, from the same geographic region (see section 3.6.1), and the same age group (see section 3.6.2).

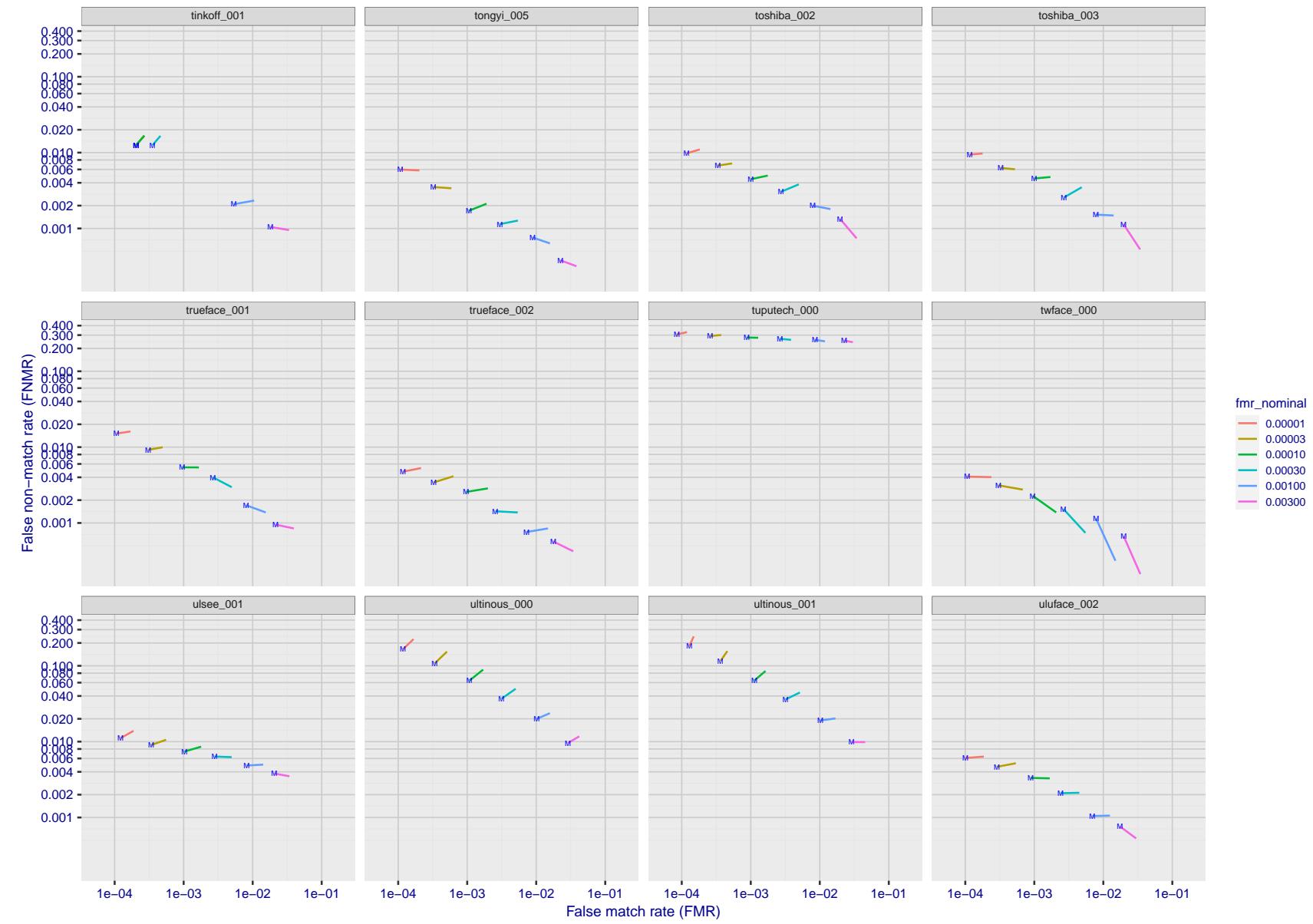


Figure 152: For the visa images, FNMR and FMR at six operating points along the DET characteristic. At each point a line is drawn between  $(FMR, FNMR)_{MALE}$  and  $(FMR, FNMR)_{FEMALE}$  showing how which sex has lower FMR and/or FNMR. The "M" label denotes male, the other end of the line corresponds to female. The six operating thresholds are selected to give the nominal false match rates given in the legend, and are computed over all impostor pairs regardless of age, sex, and place of birth. The plotted FMR values are broadly an order of magnitude larger than the nominal rates because FMR is computed over demographically-matched impostor pairs i.e individuals of the same sex, from the same geographic region (see section 3.6.1), and the same age group (see section 3.6.2).

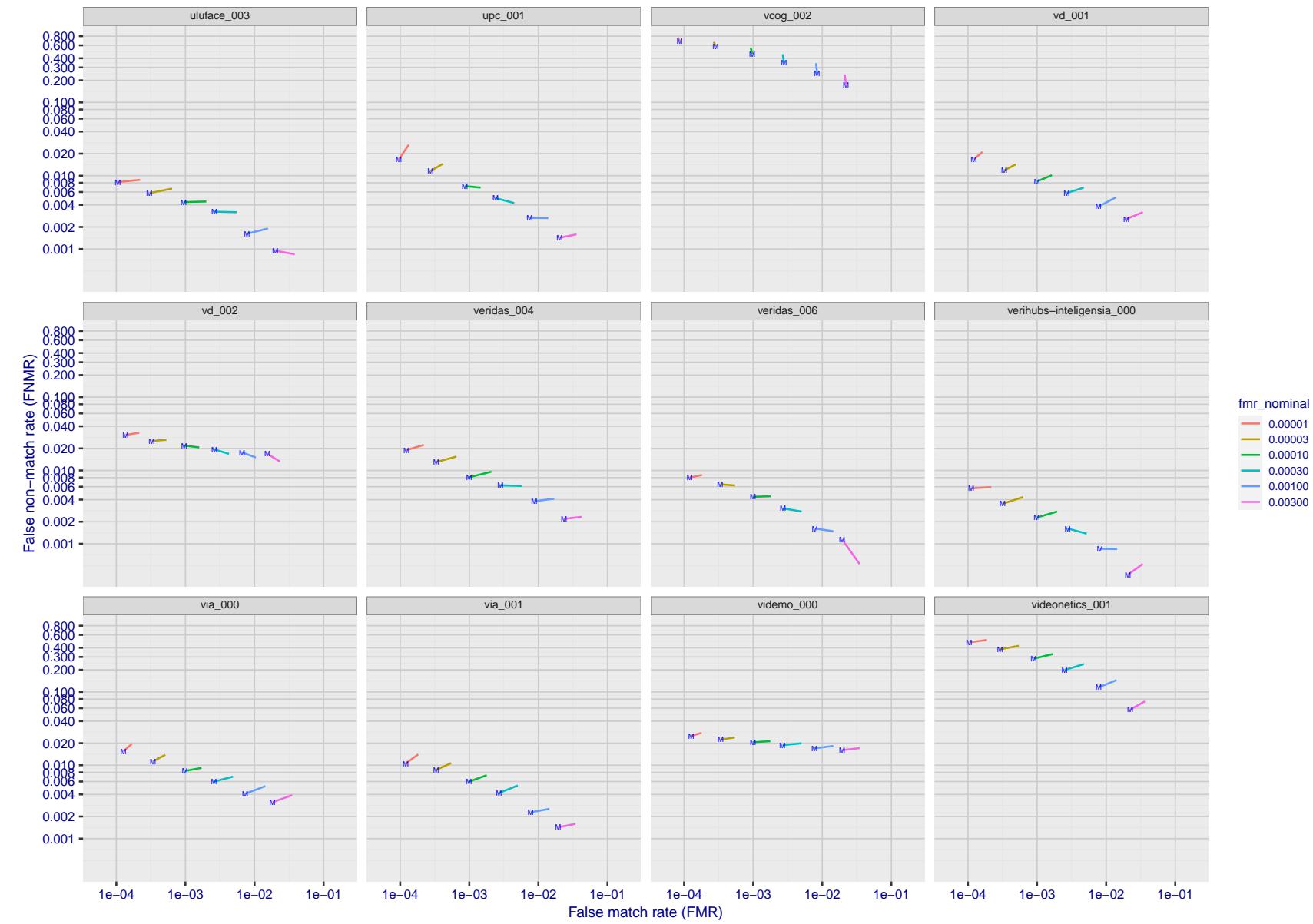


Figure 153: For the visa images, FNMR and FMR at six operating points along the DET characteristic. At each point a line is drawn between  $(FMR, FNMR)_{MALE}$  and  $(FMR, FNMR)_{FEMALE}$  showing how which sex has lower FMR and/or FNMR. The "M" label denotes male, the other end of the line corresponds to female. The six operating thresholds are selected to give the nominal false match rates given in the legend, and are computed over all impostor pairs regardless of age, sex, and place of birth. The plotted FMR values are broadly an order of magnitude larger than the nominal rates because FMR is computed over demographically-matched impostor pairs i.e individuals of the same sex, from the same geographic region (see section 3.6.1), and the same age group (see section 3.6.2).

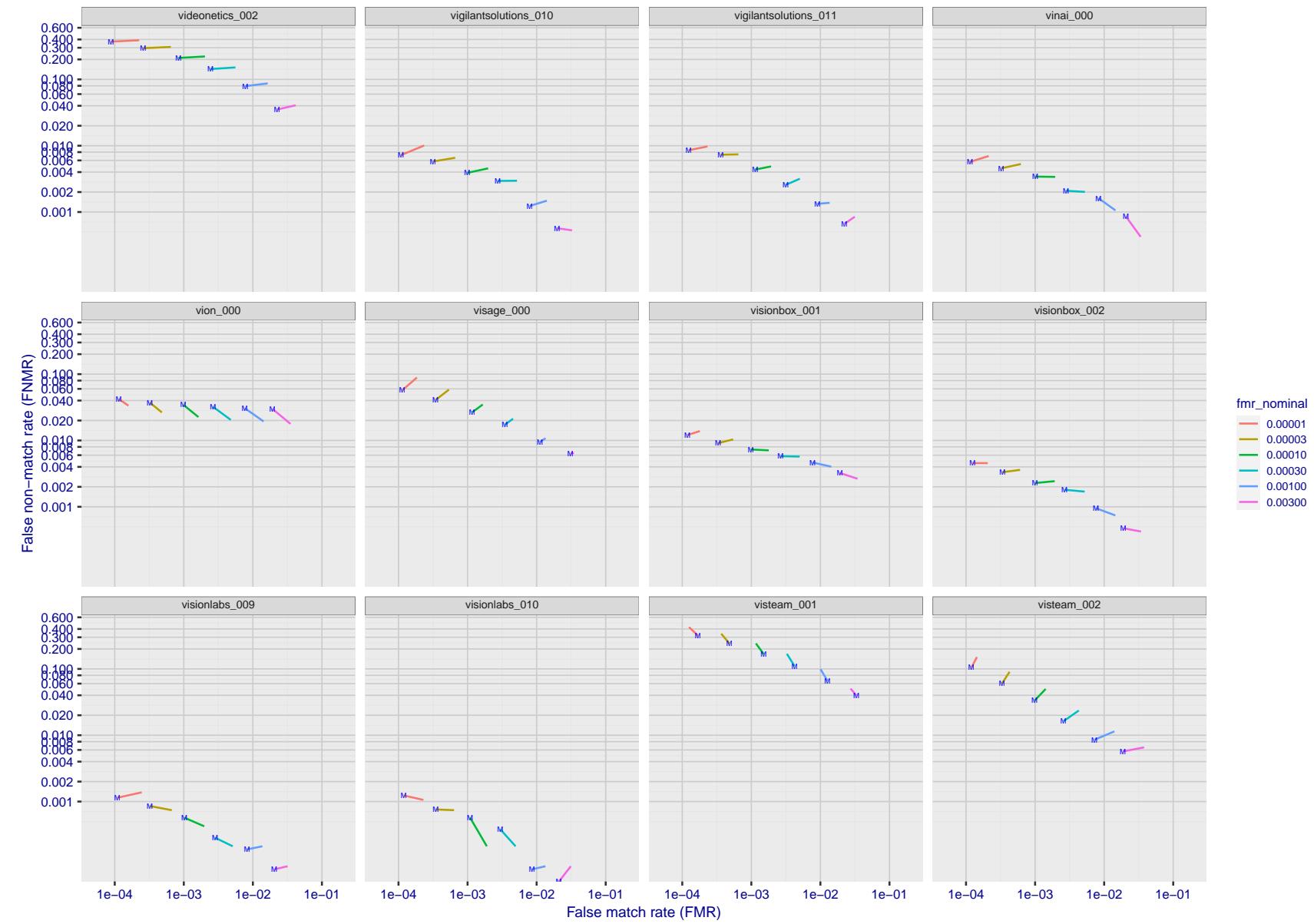


Figure 154: For the visa images, FNMR and FMR at six operating points along the DET characteristic. At each point a line is drawn between  $(FMR, FNMR)_{MALE}$  and  $(FMR, FNMR)_{FEMALE}$  showing how which sex has lower FMR and/or FNMR. The "M" label denotes male, the other end of the line corresponds to female. The six operating thresholds are selected to give the nominal false match rates given in the legend, and are computed over all impostor pairs regardless of age, sex, and place of birth. The plotted FMR values are broadly an order of magnitude larger than the nominal rates because FMR is computed over demographically-matched impostor pairs i.e individuals of the same sex, from the same geographic region (see section 3.6.1), and the same age group (see section 3.6.2).

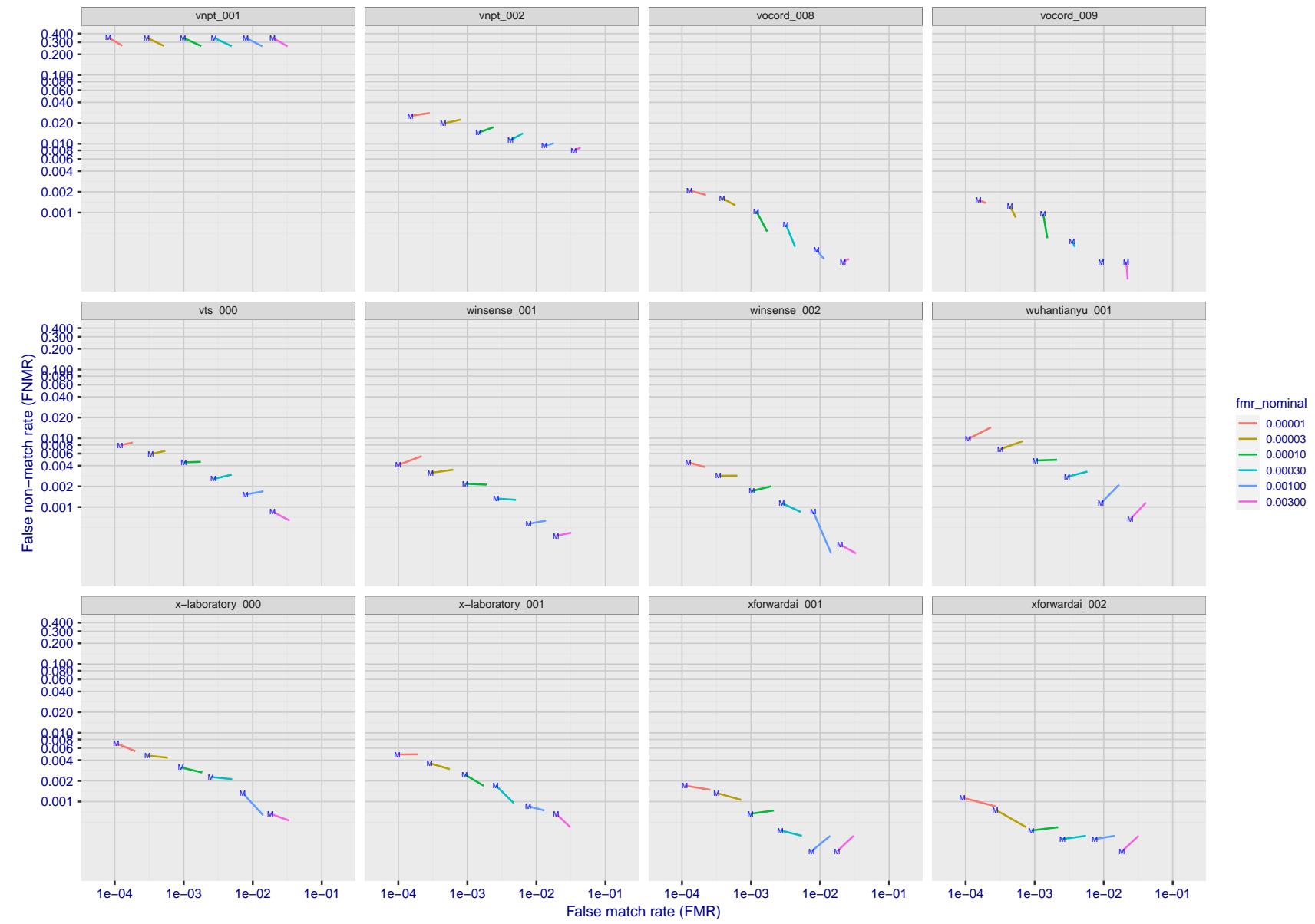


Figure 155: For the visa images, FNMR and FMR at six operating points along the DET characteristic. At each point a line is drawn between  $(FMR, FNMR)_{MALE}$  and  $(FMR, FNMR)_{FEMALE}$  showing how which sex has lower FMR and/or FNMR. The "M" label denotes male, the other end of the line corresponds to female. The six operating thresholds are selected to give the nominal false match rates given in the legend, and are computed over all impostor pairs regardless of age, sex, and place of birth. The plotted FMR values are broadly an order of magnitude larger than the nominal rates because FMR is computed over demographically-matched impostor pairs i.e individuals of the same sex, from the same geographic region (see section 3.6.1), and the same age group (see section 3.6.2).

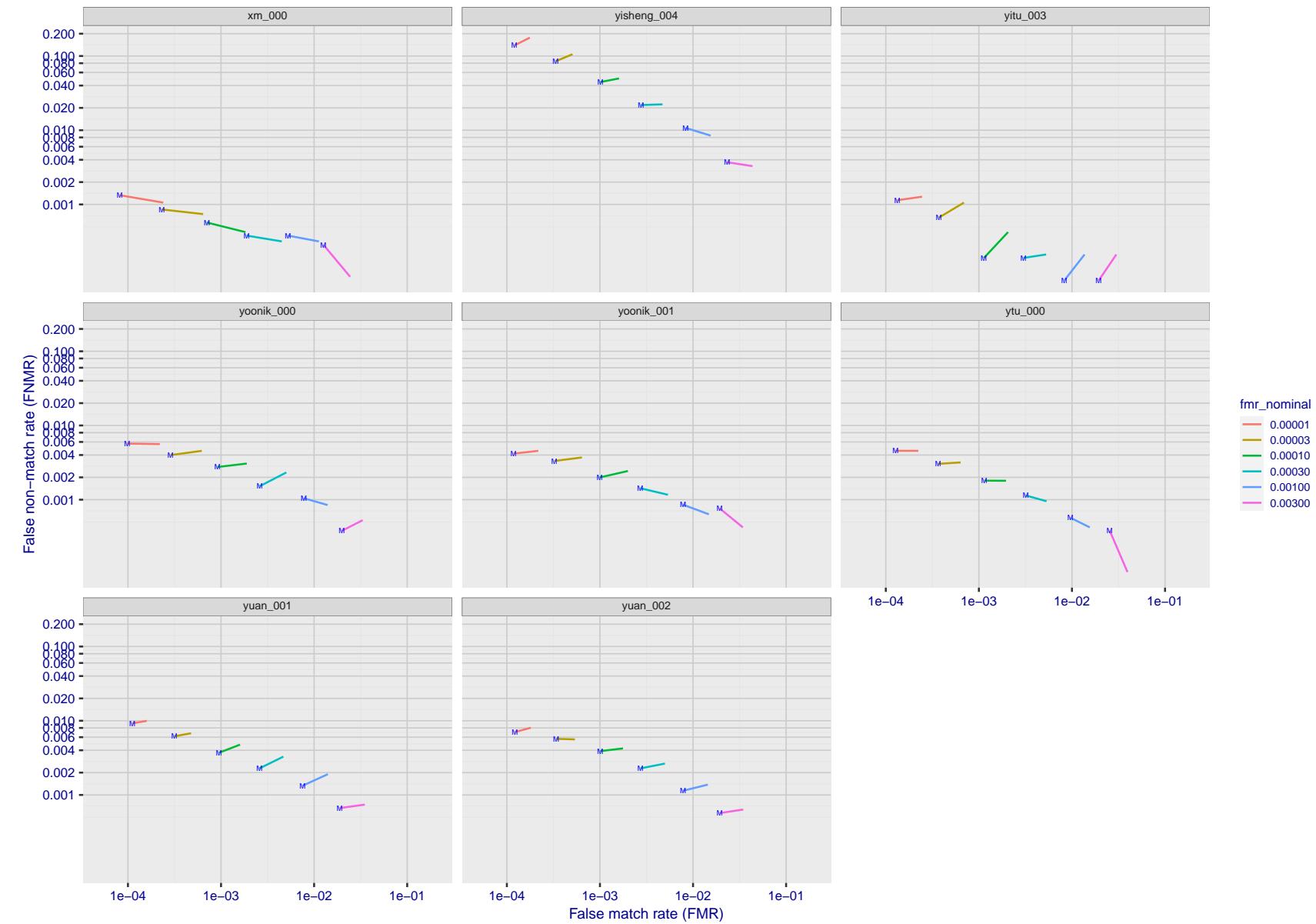


Figure 156: For the visa images, FNMR and FMR at six operating points along the DET characteristic. At each point a line is drawn between  $(FMR, FNMR)_{MALE}$  and  $(FMR, FNMR)_{FEMALE}$  showing how which sex has lower FMR and/or FNMR. The "M" label denotes male, the other end of the line corresponds to female. The six operating thresholds are selected to give the nominal false match rates given in the legend, and are computed over all impostor pairs regardless of age, sex, and place of birth. The plotted FMR values are broadly an order of magnitude larger than the nominal rates because FMR is computed over demographically-matched impostor pairs i.e individuals of the same sex, from the same geographic region (see section 3.6.1), and the same age group (see section 3.6.2).

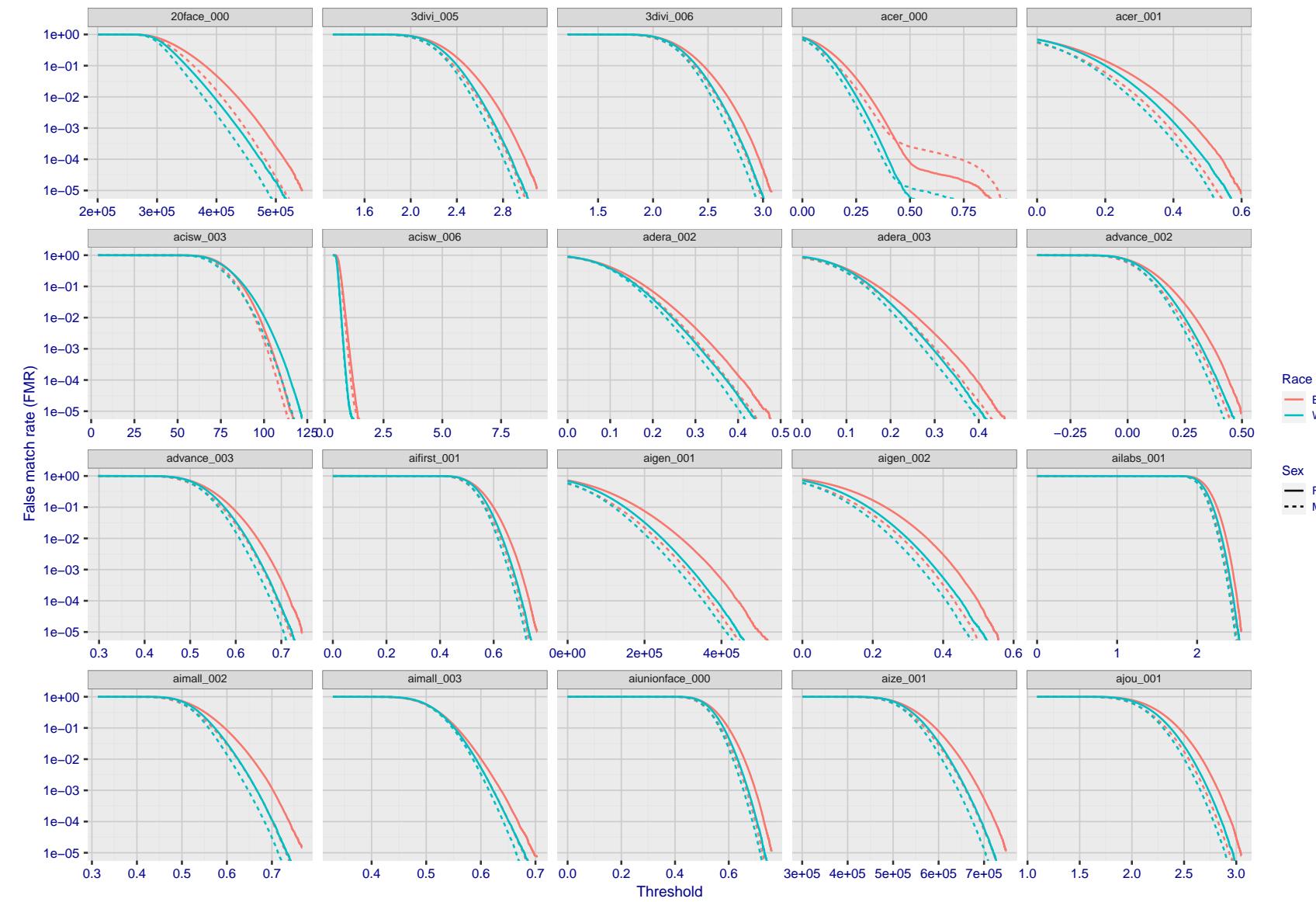


Figure 157: For the mugshot images, the false match calibration curves show false match rate vs. threshold. Separate curves appear for white females, black females, black males and white males.

2021/09/10 10:17:25

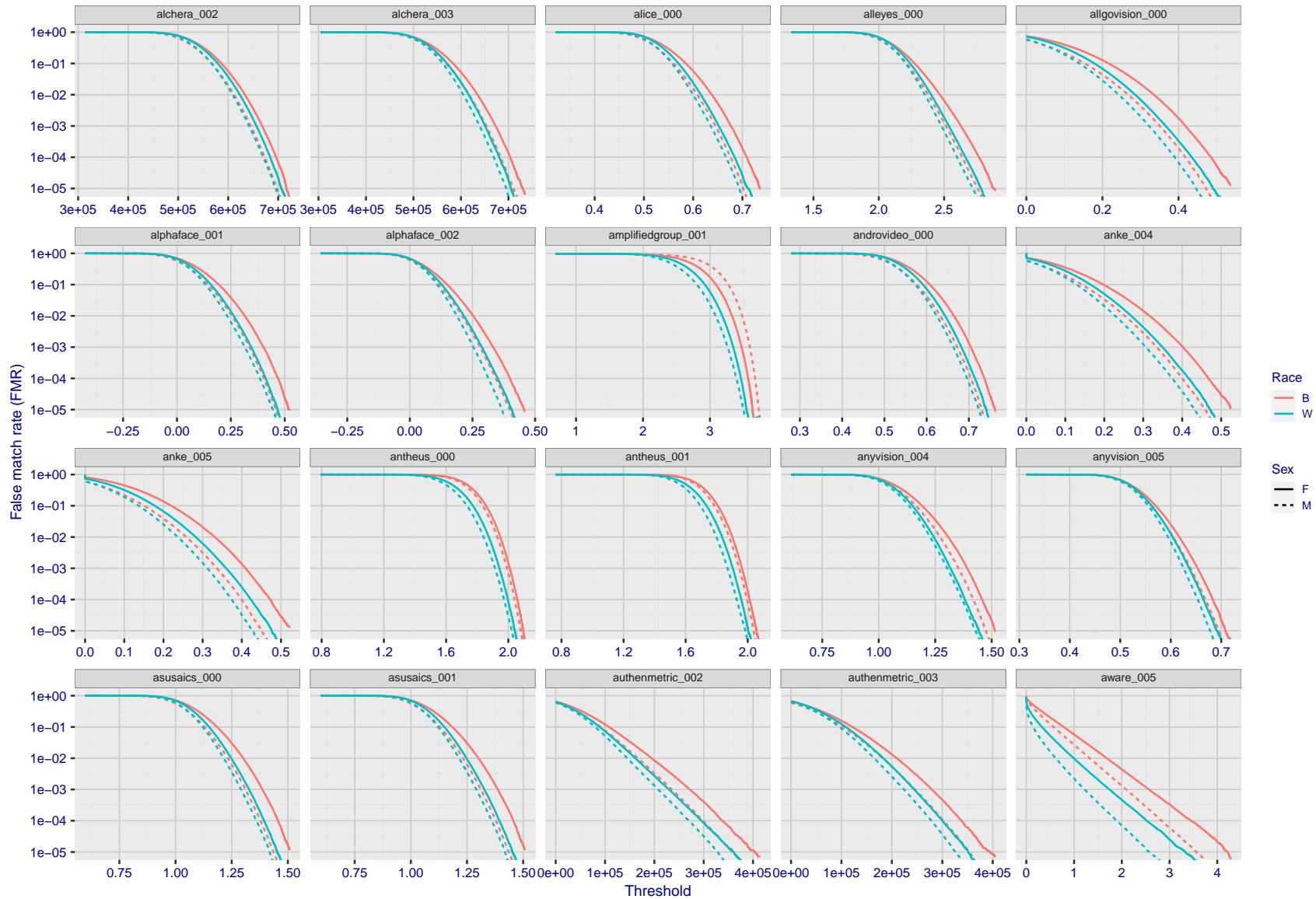


Figure 158: For the mugshot images, the false match calibration curves show false match rate vs. threshold. Separate curves appear for white females, black females, black males and white males.

FNMR(T)  
"False non-match rate"  
"False match rate"

2021/09/10 10:17:25

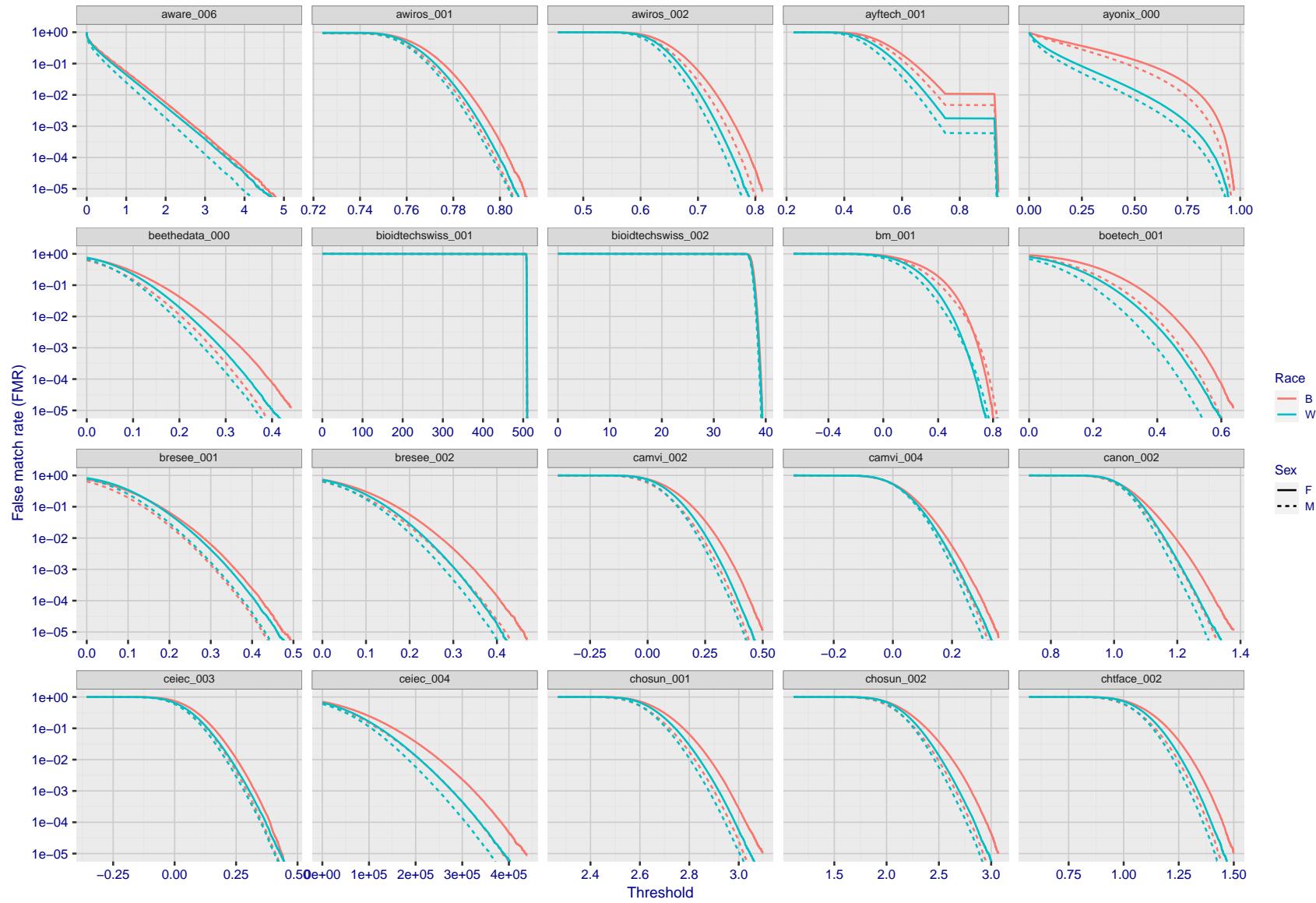


Figure 159: For the mugshot images, the false match calibration curves show false match rate vs. threshold. Separate curves appear for white females, black females, black males and white males.

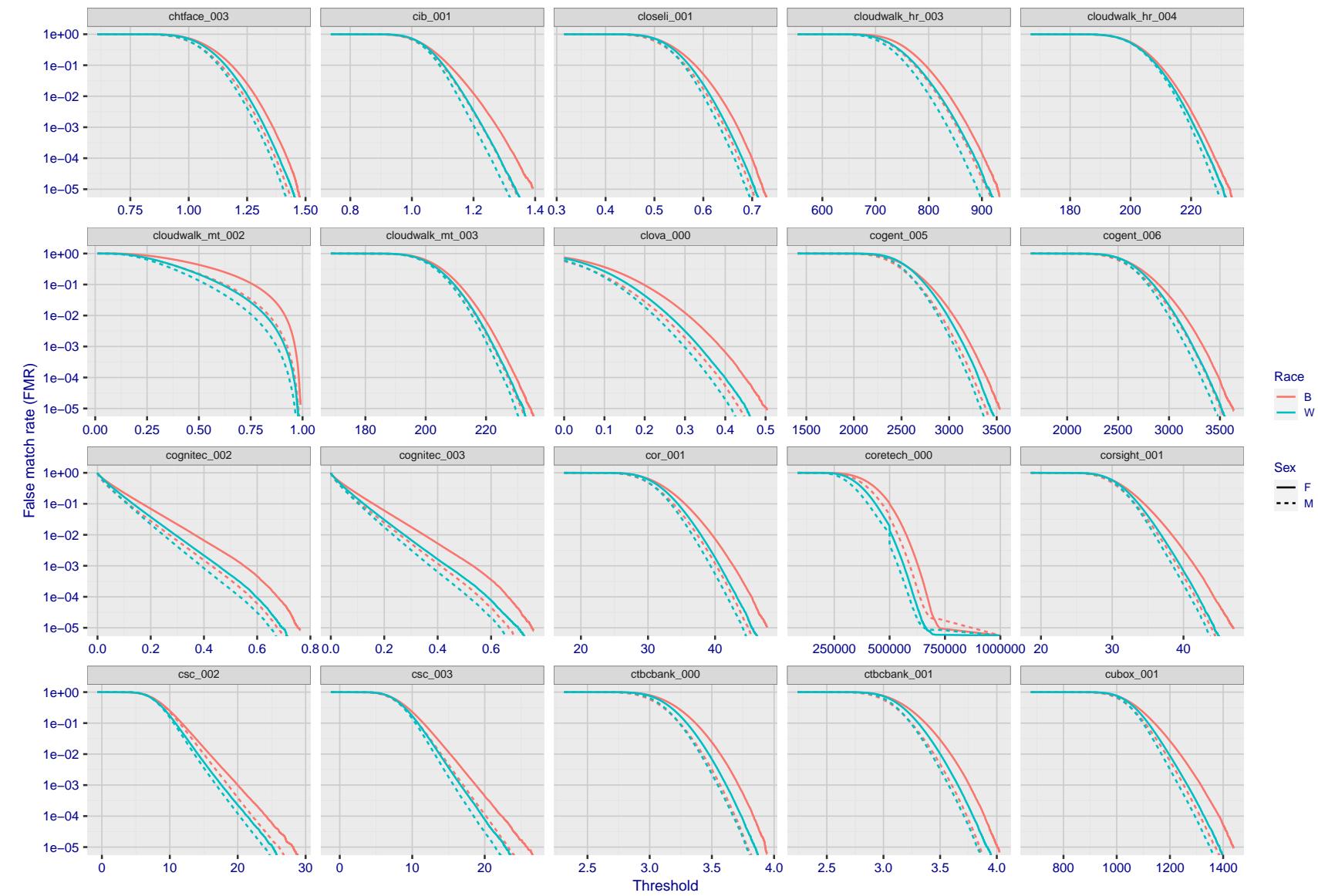


Figure 160: For the mugshot images, the false match calibration curves show false match rate vs. threshold. Separate curves appear for white females, black females, black males and white males.

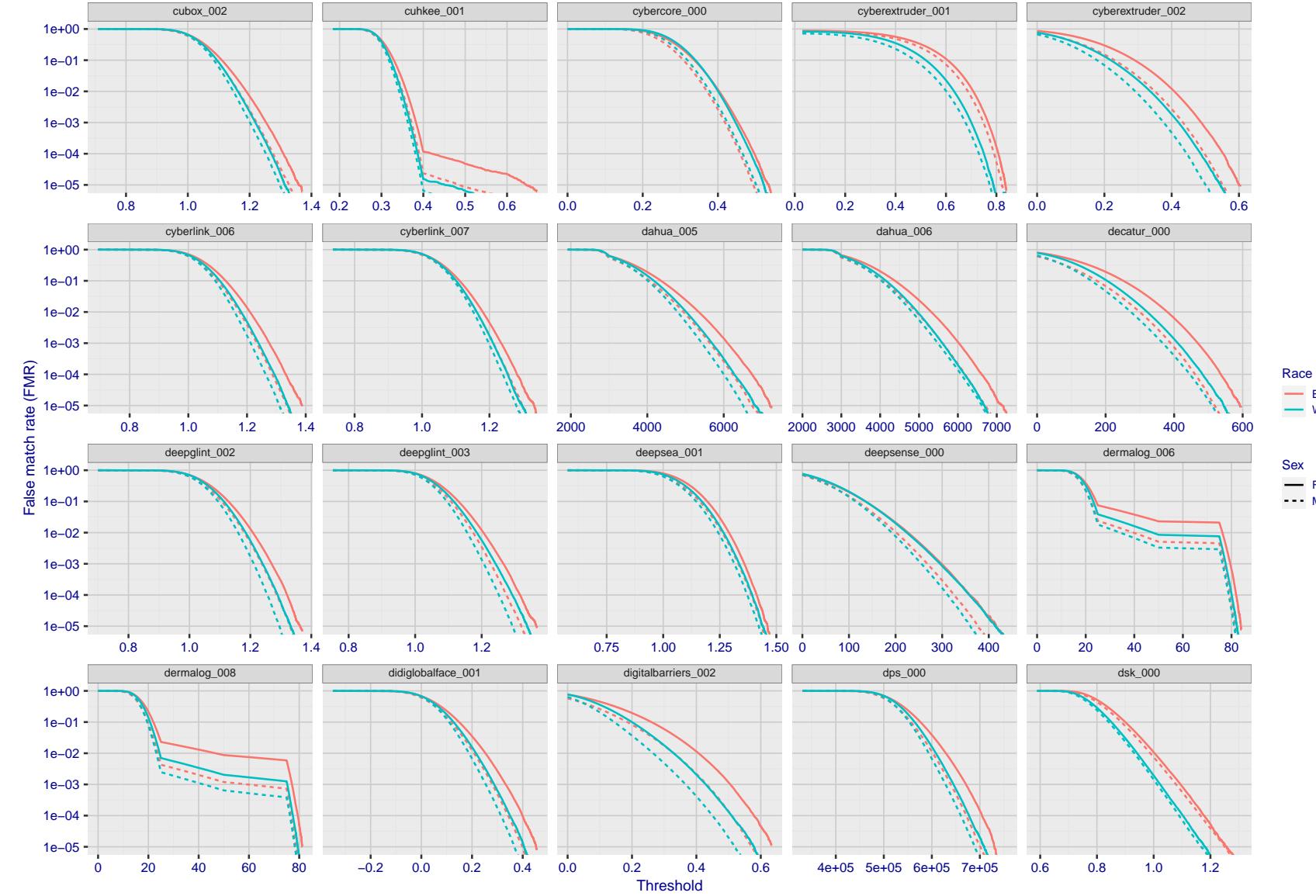


Figure 161: For the mugshot images, the false match calibration curves show false match rate vs. threshold. Separate curves appear for white females, black females, black males and white males.

2021/09/10 10:17:25

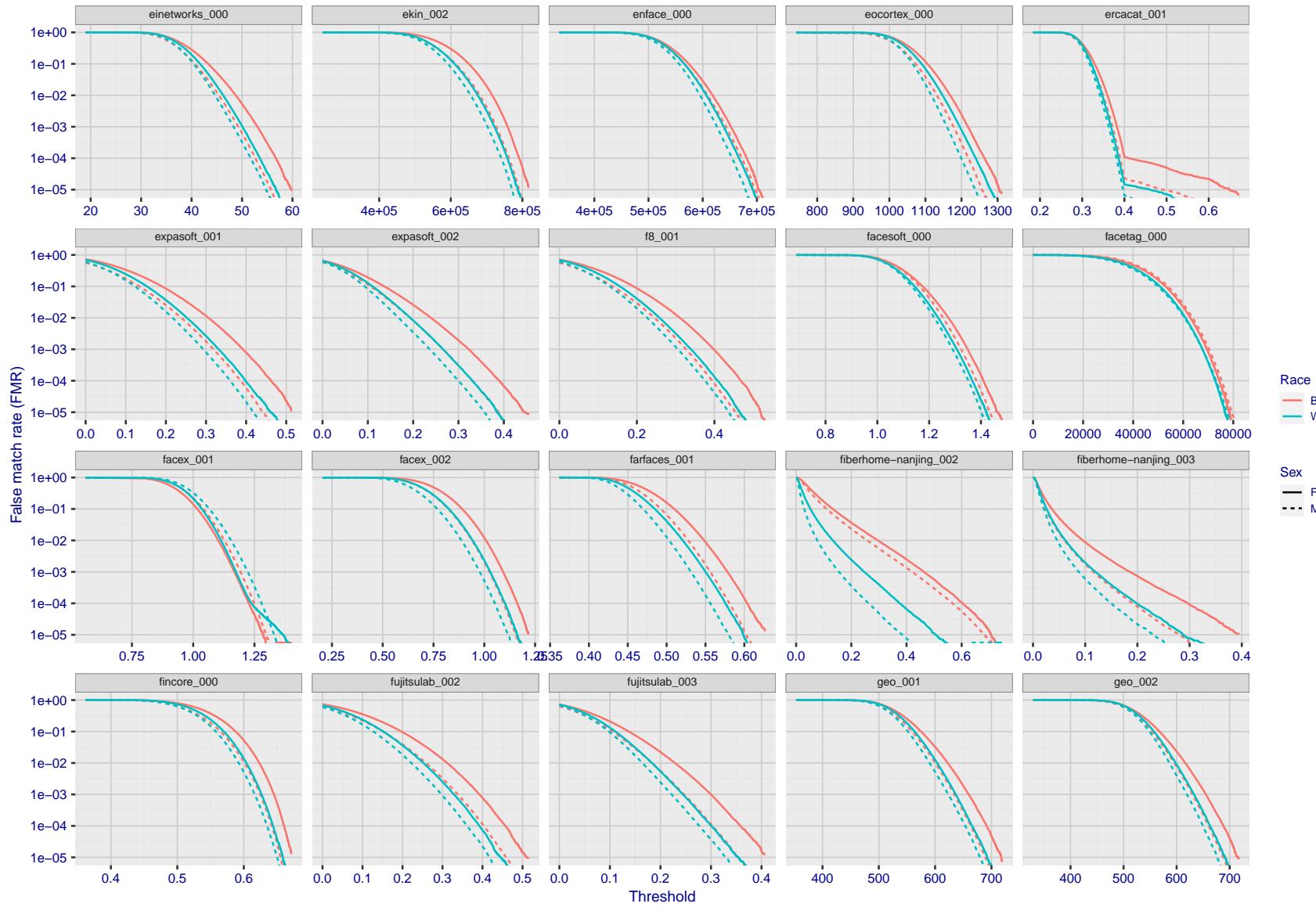


Figure 162: For the mugshot images, the false match calibration curves show false match rate vs. threshold. Separate curves appear for white females, black females, black males and white males.

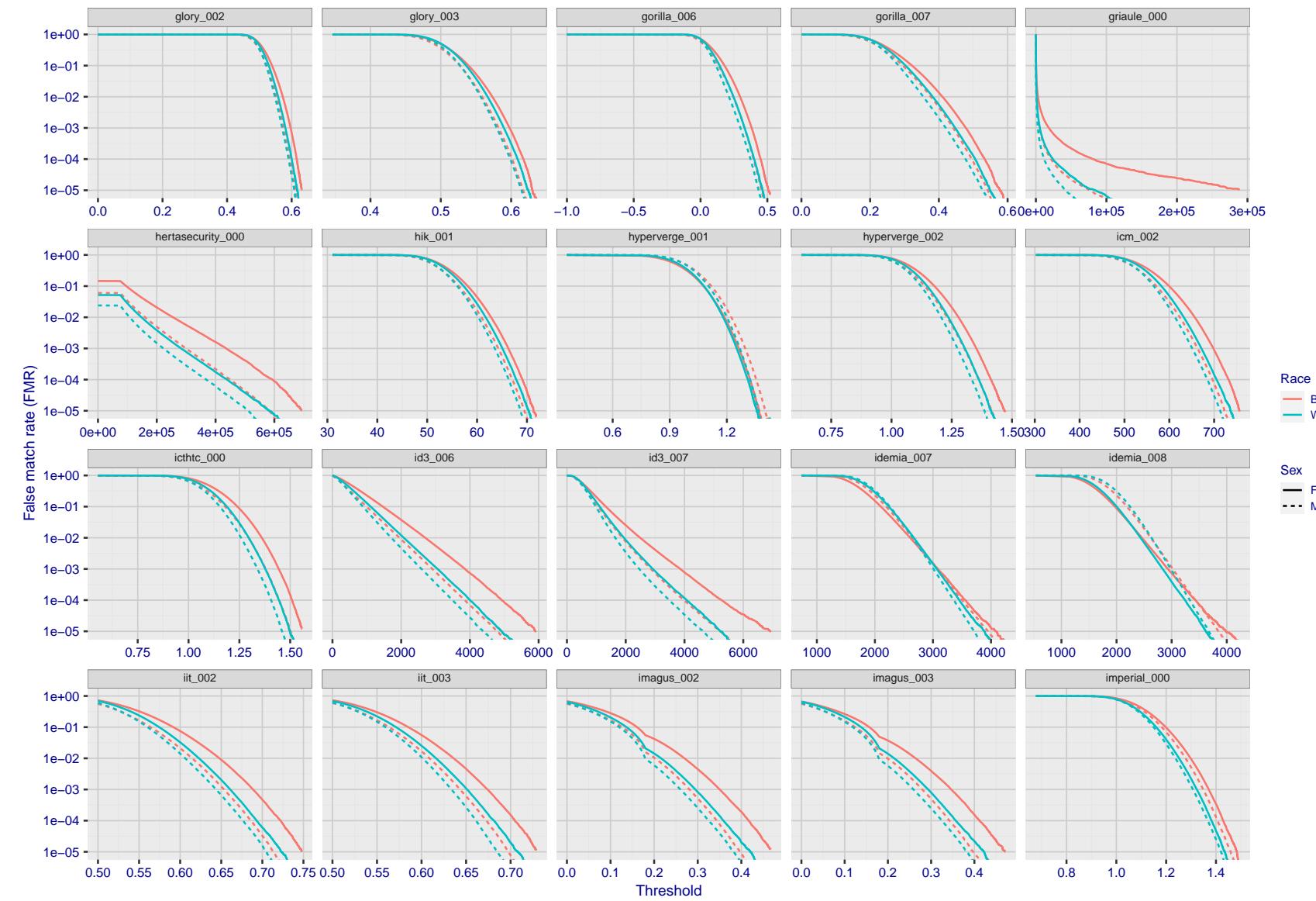


Figure 163: For the mugshot images, the false match calibration curves show false match rate vs. threshold. Separate curves appear for white females, black females, black males and white males.

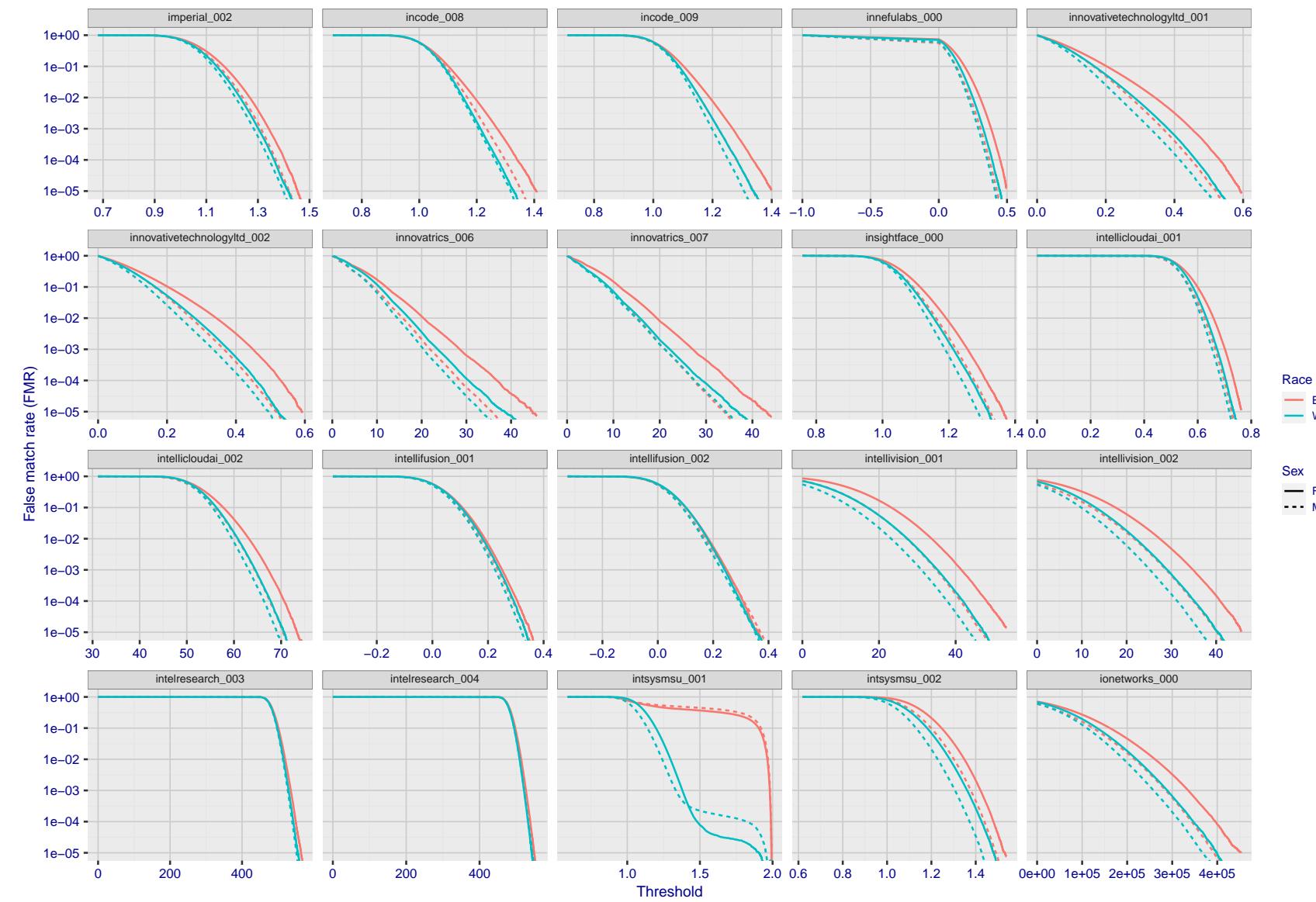


Figure 164: For the mugshot images, the false match calibration curves show false match rate vs. threshold. Separate curves appear for white females, black females, black males and white males.

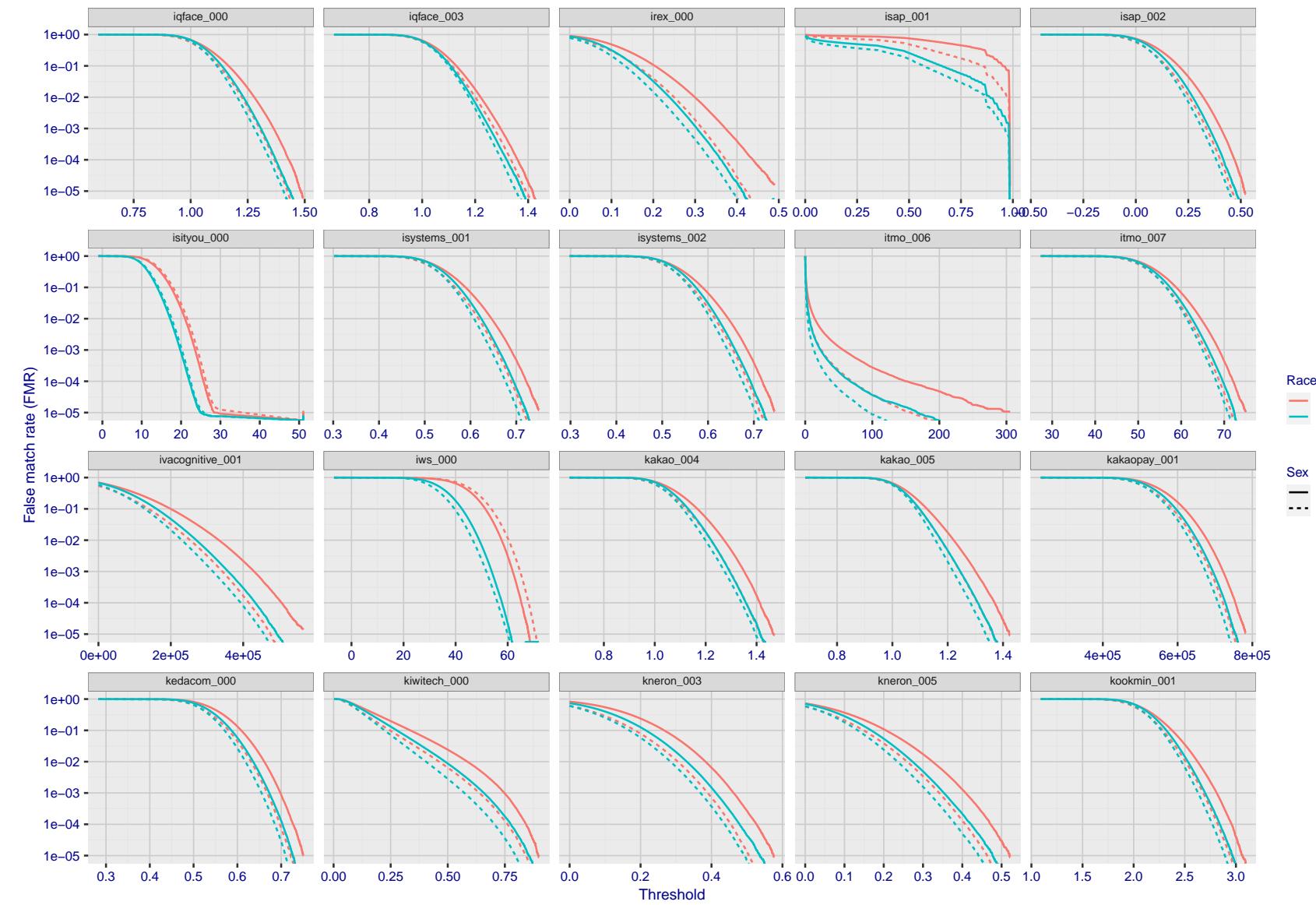


Figure 165: For the mugshot images, the false match calibration curves show false match rate vs. threshold. Separate curves appear for white females, black females, black males and white males.

2021/09/10 10:17:25

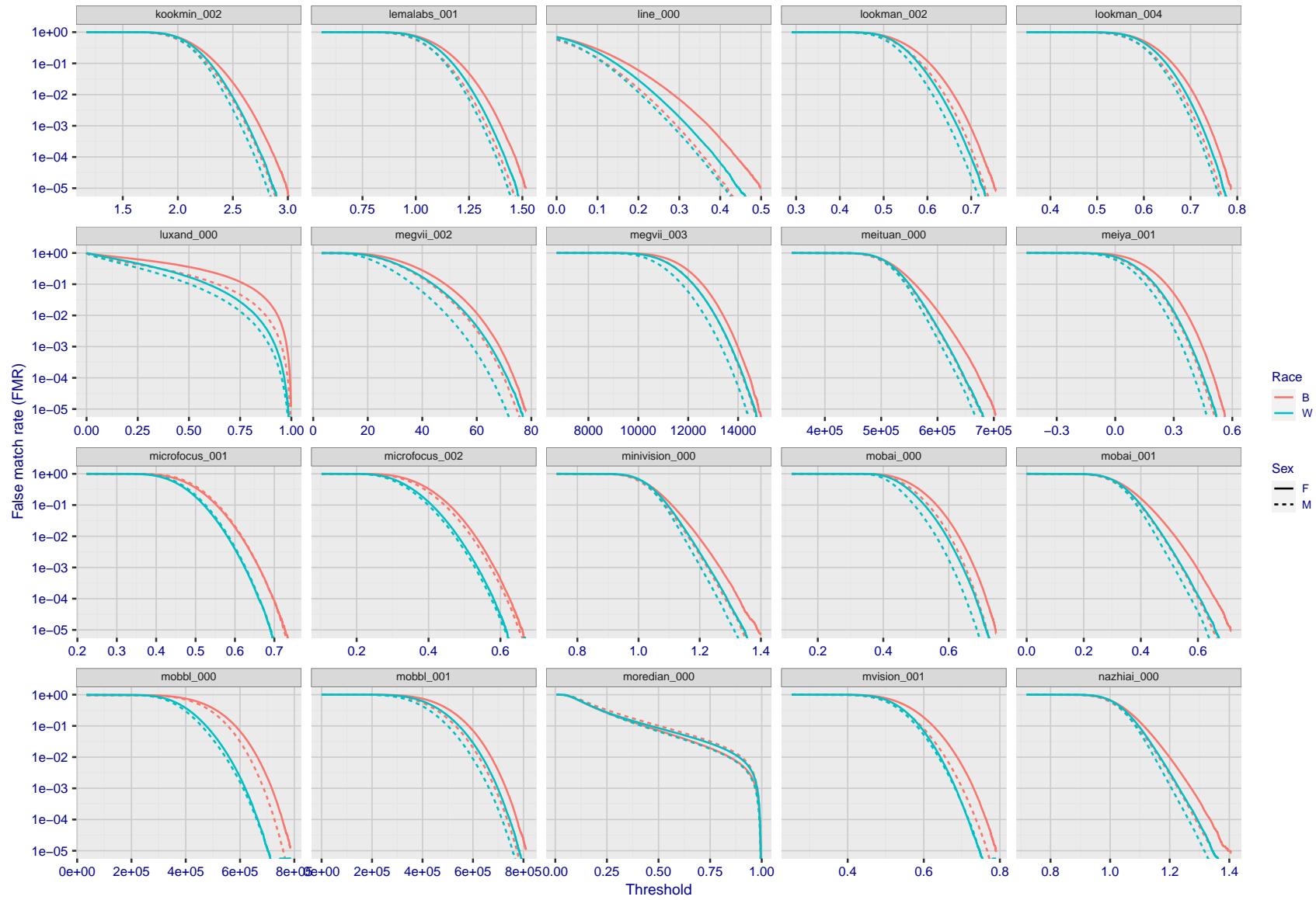


Figure 166: For the mugshot images, the false match calibration curves show false match rate vs. threshold. Separate curves appear for white females, black females, black males and white males.

FNMR(T)  
"False non-match rate"  
"False match rate"

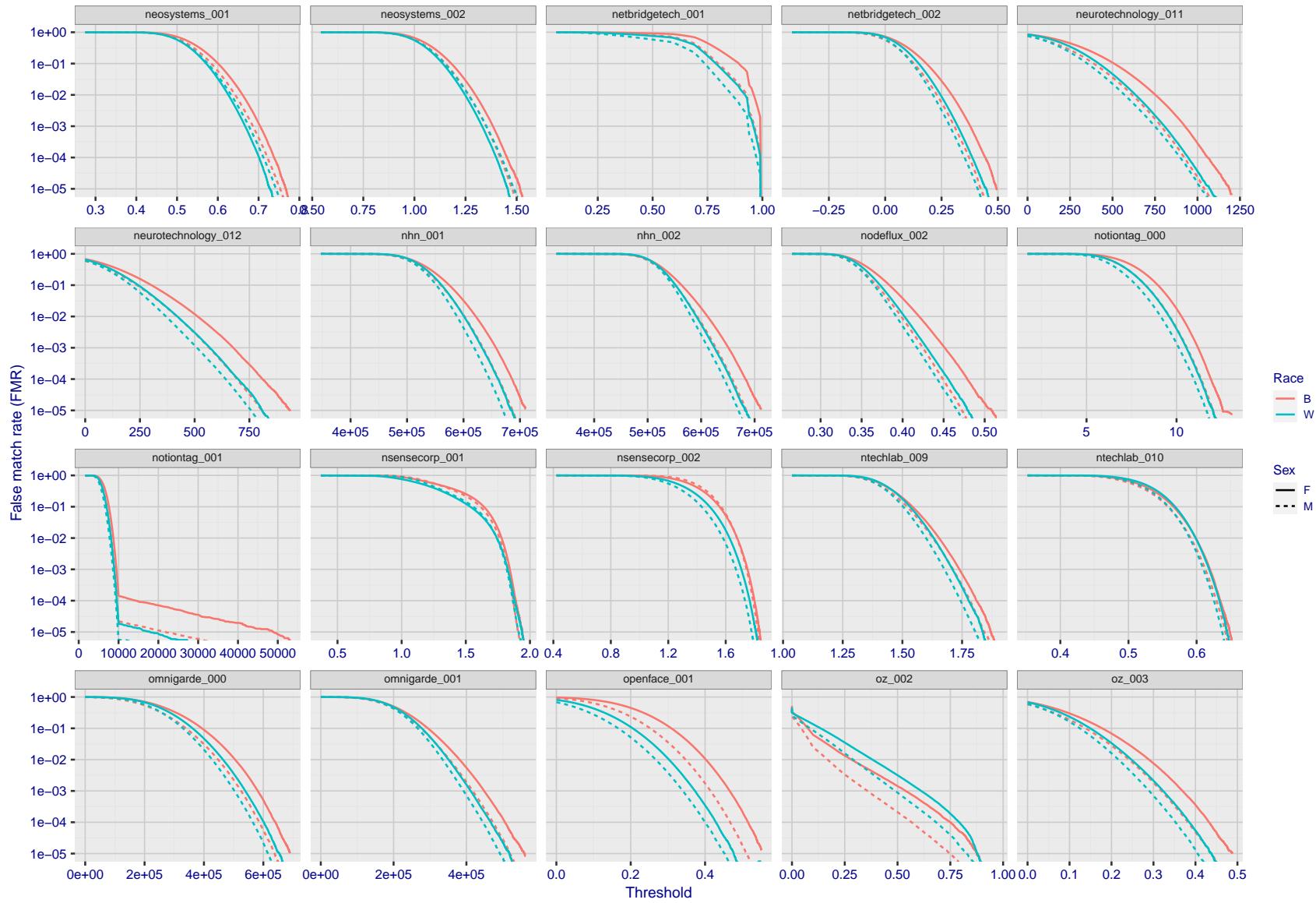


Figure 167: For the mugshot images, the false match calibration curves show false match rate vs. threshold. Separate curves appear for white females, black females, black males and white males.

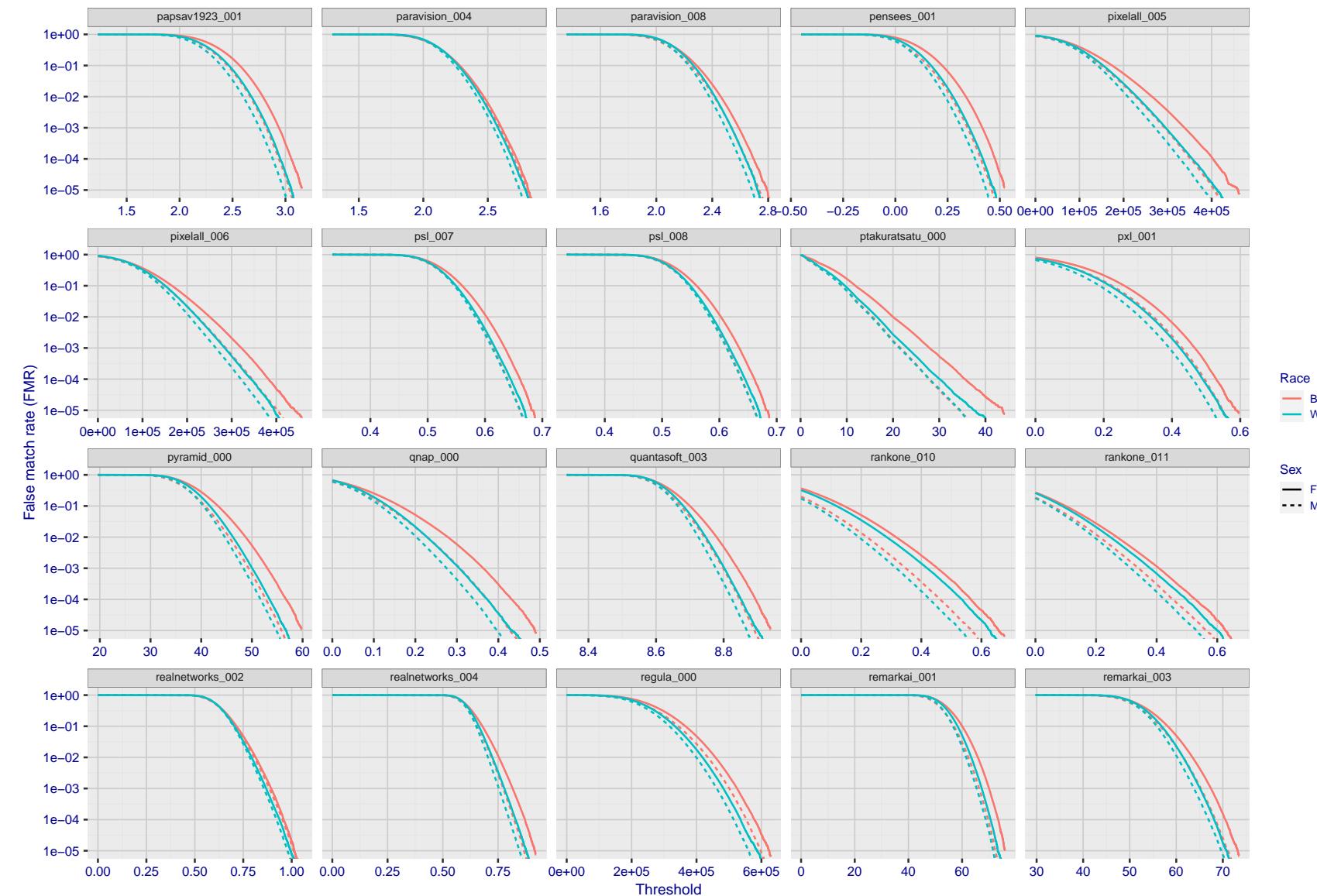


Figure 168: For the mugshot images, the false match calibration curves show false match rate vs. threshold. Separate curves appear for white females, black females, black males and white males.

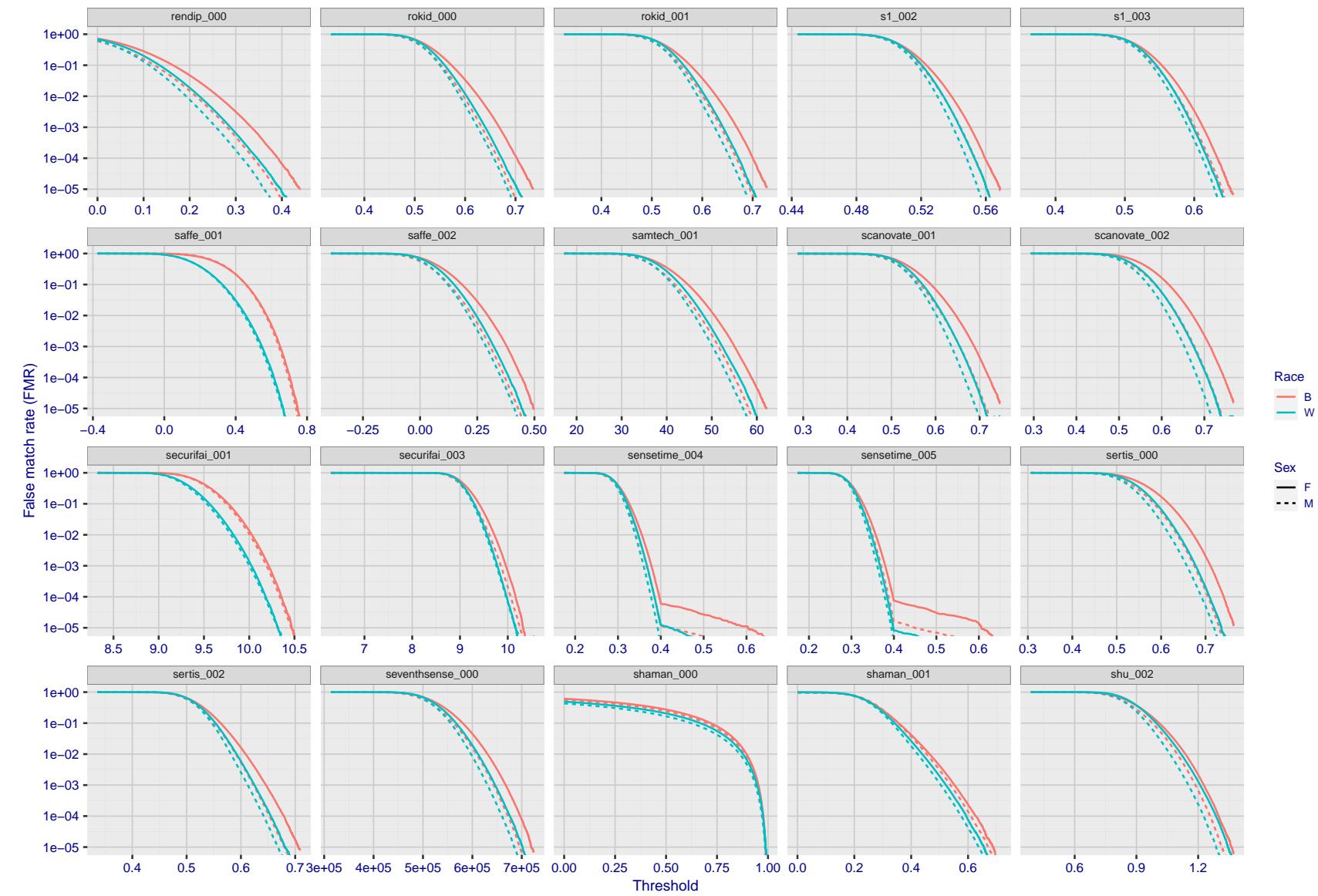


Figure 169: For the mugshot images, the false match calibration curves show false match rate vs. threshold. Separate curves appear for white females, black females, black males and white males.

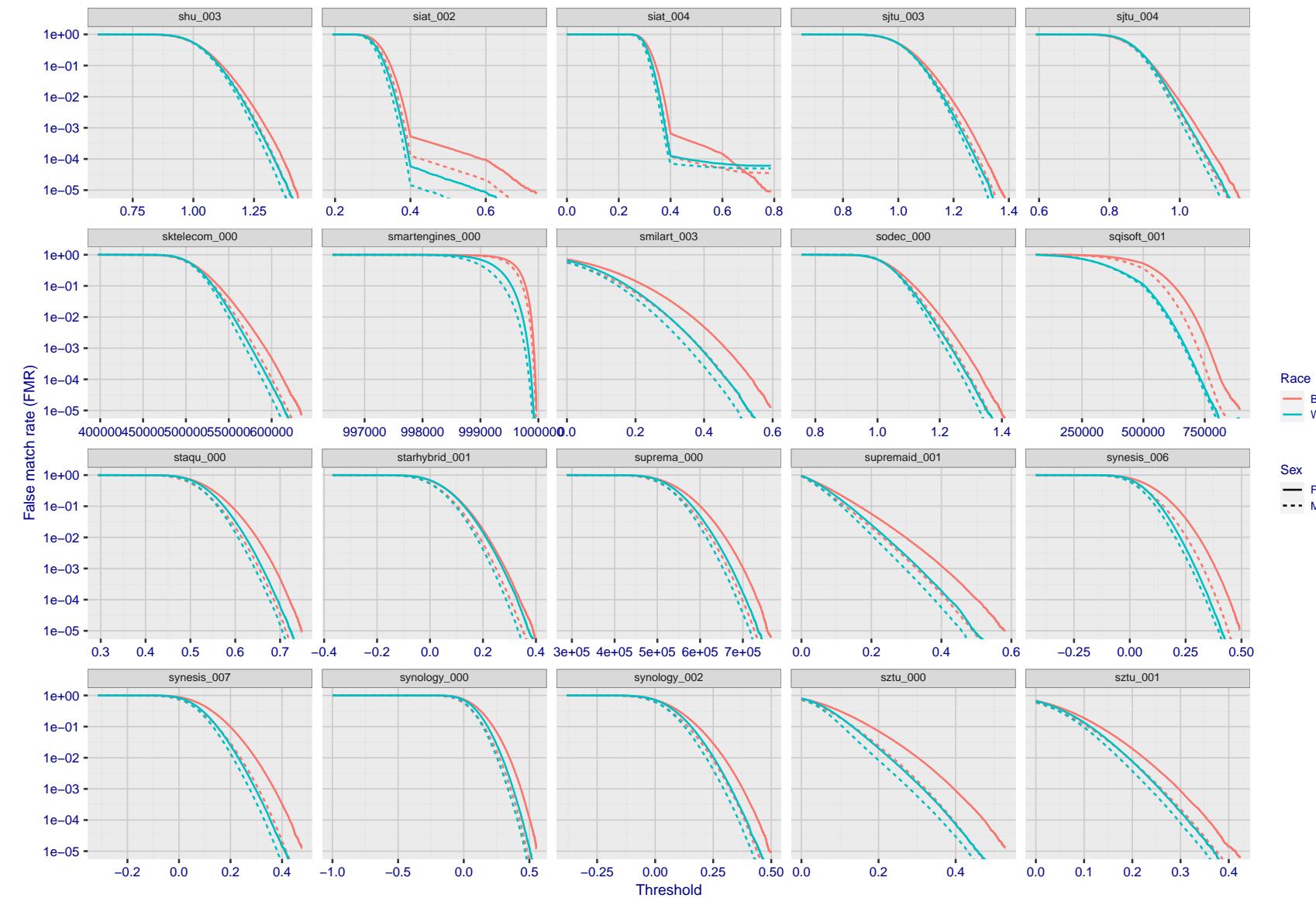


Figure 170: For the mugshot images, the false match calibration curves show false match rate vs. threshold. Separate curves appear for white females, black females, black males and white males.

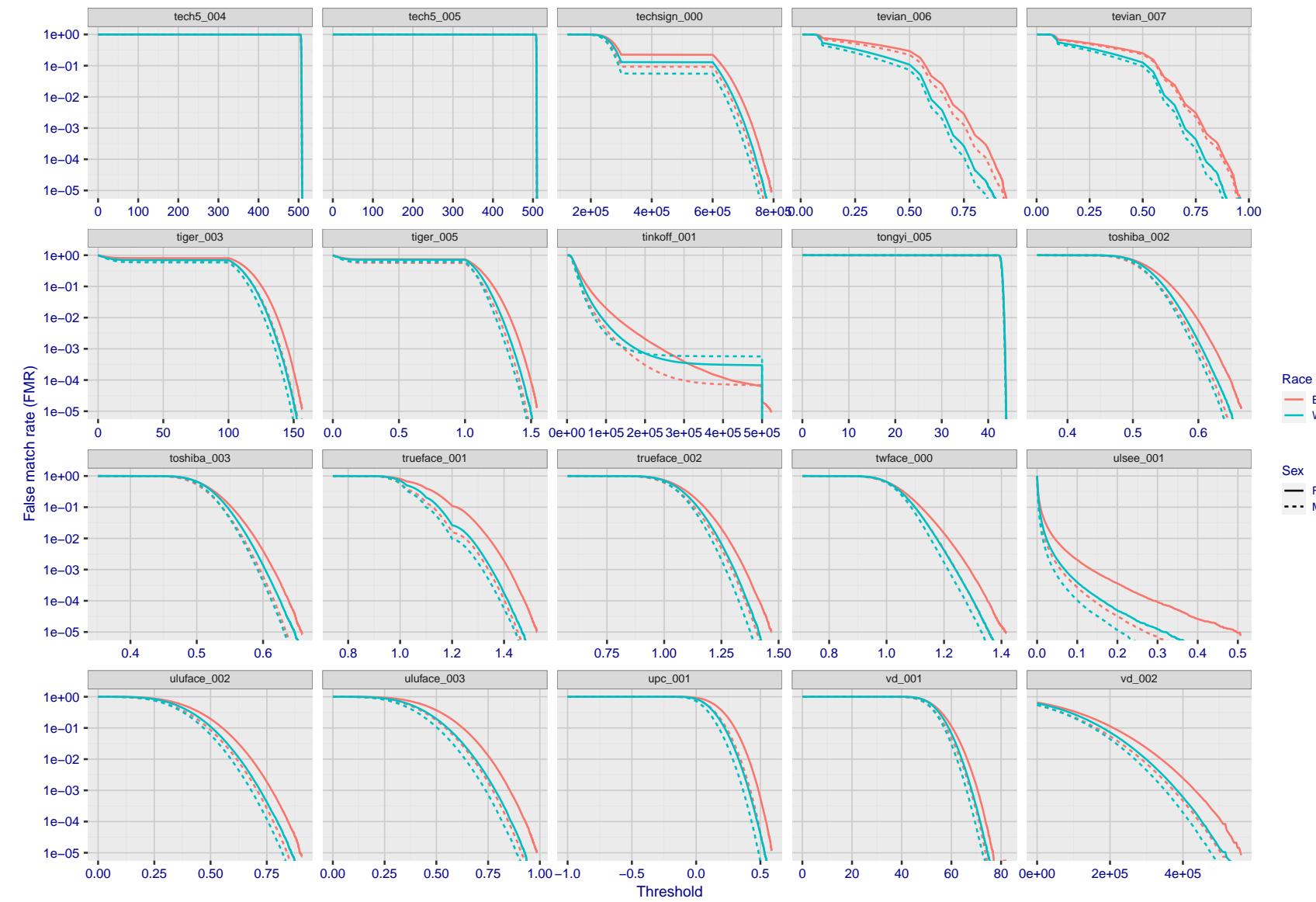


Figure 171: For the mugshot images, the false match calibration curves show false match rate vs. threshold. Separate curves appear for white females, black females, black males and white males.

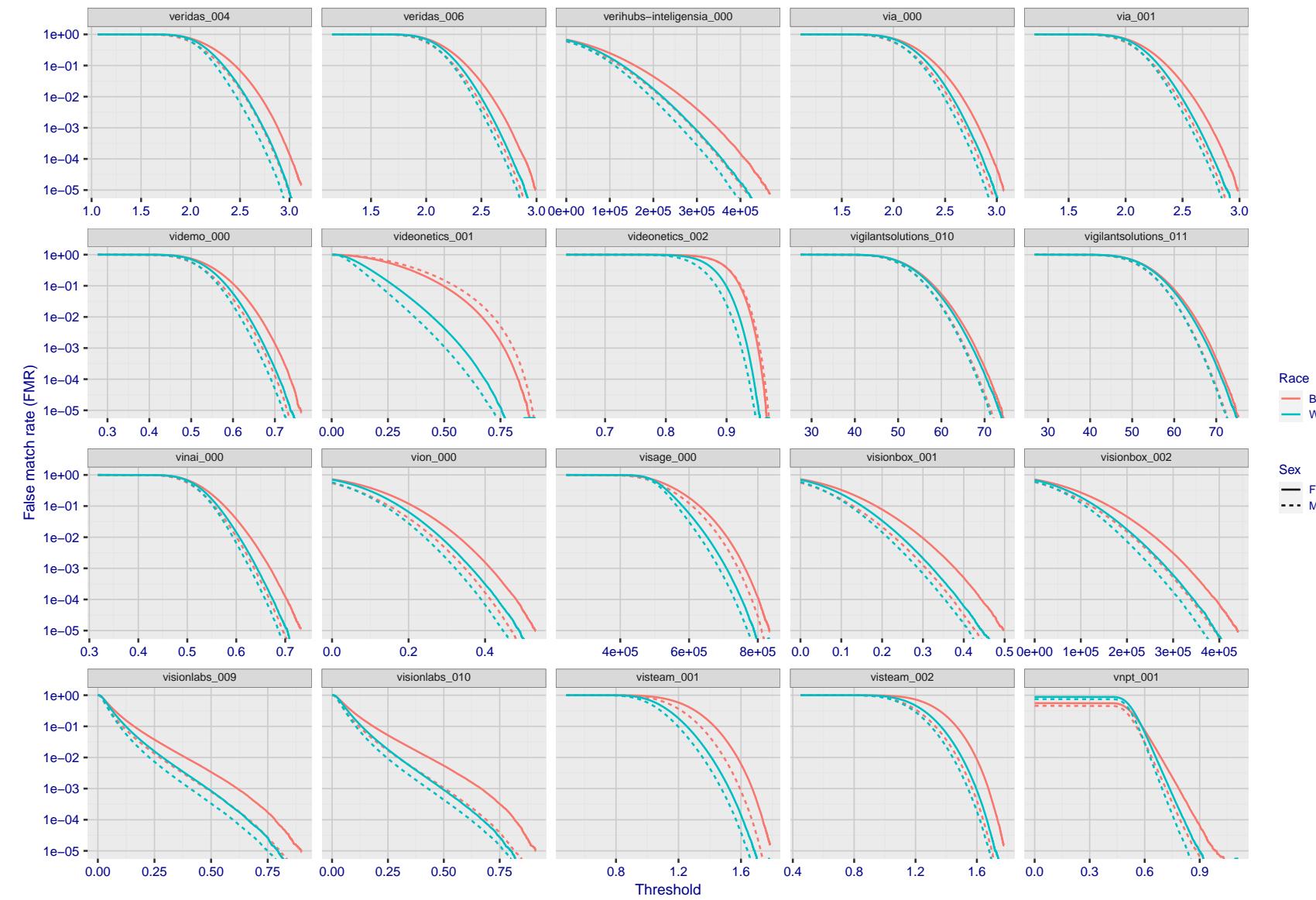
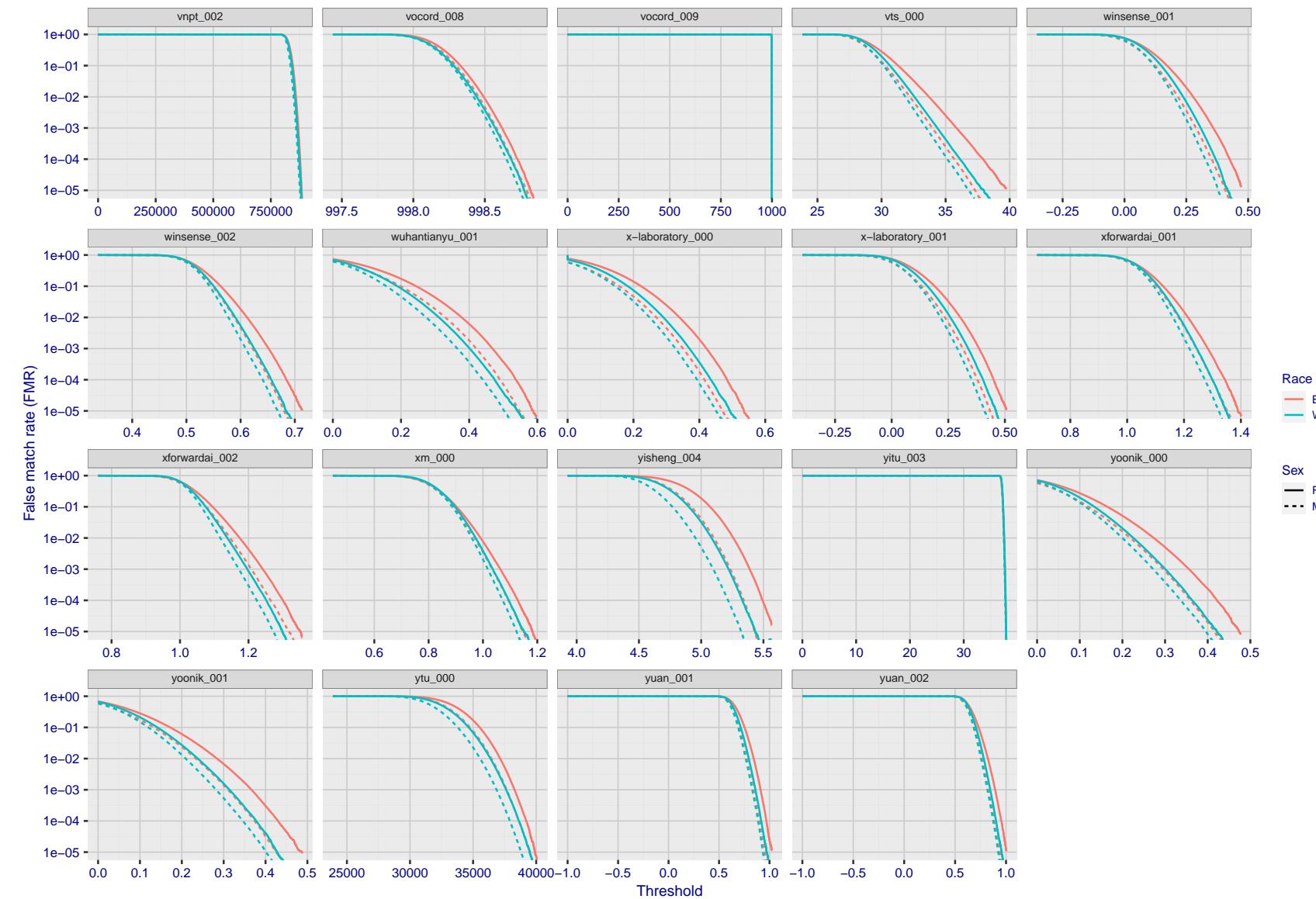


Figure 172: For the mugshot images, the false match calibration curves show false match rate vs. threshold. Separate curves appear for white females, black females, black males and white males.



FNMR(T)  
"False non-match rate"  
"False match rate"

Figure 173: For the mugshot images, the false match calibration curves show false match rate vs. threshold. Separate curves appear for white females, black females, black males and white males.

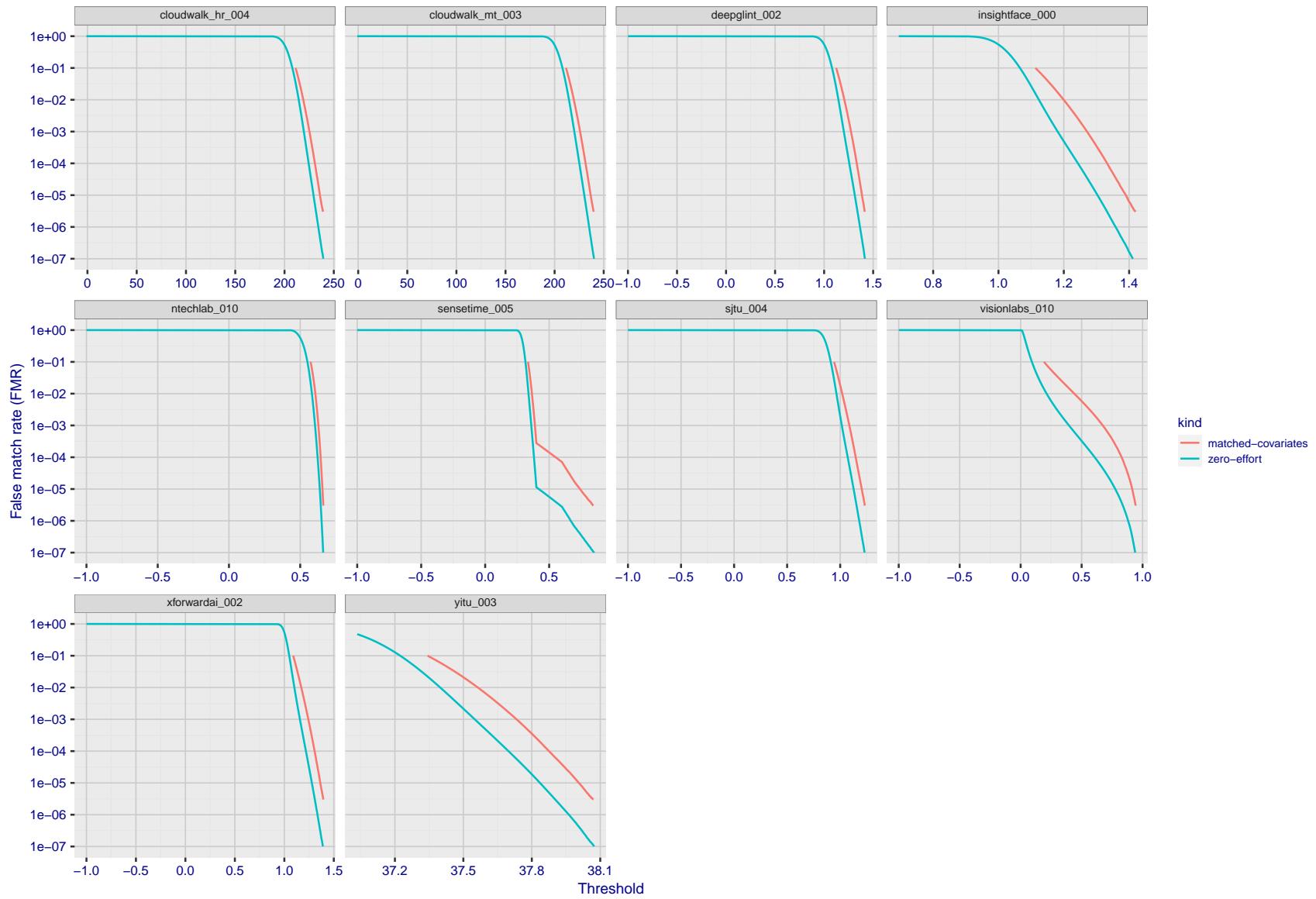


Figure 174: For the visa images, the false match calibration curves show FMR vs. threshold,  $T$ . The blue (lower) curves are for zero-effort impostors (i.e. comparing all images against all). The red (upper) curves are for persons of the same-sex, same-age, and same national-origin. This shows that FMR is underestimated (by a factor of 10 or more) by using a zero-effort impostor calculation to calibrate  $T$ . As shown later (sec. 3.6), FMR is higher for demographic-matched impostors.

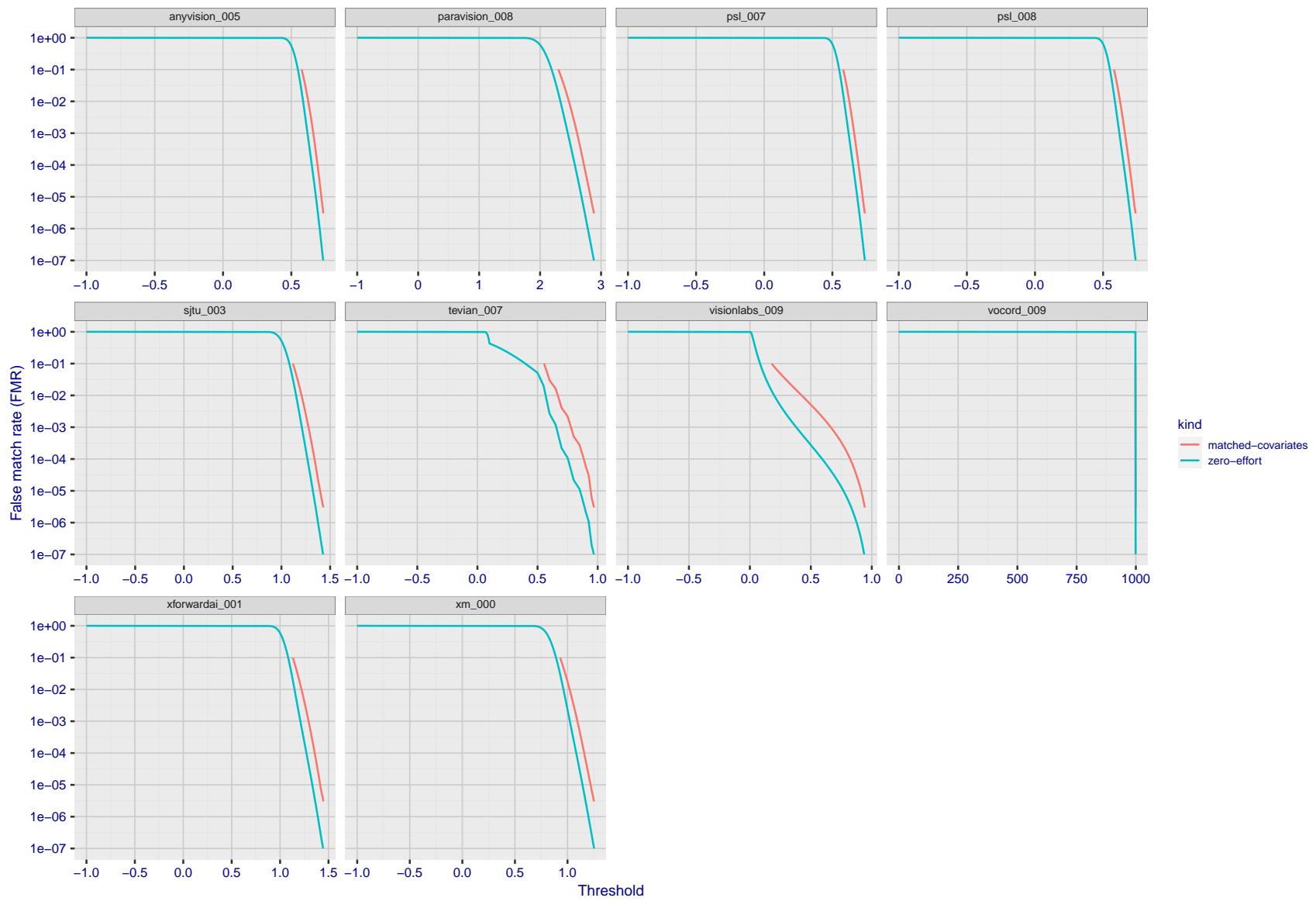


Figure 175: For the visa images, the false match calibration curves show FMR vs. threshold,  $T$ . The blue (lower) curves are for zero-effort impostors (i.e. comparing all images against all). The red (upper) curves are for persons of the same-sex, same-age, and same national-origin. This shows that FMR is underestimated (by a factor of 10 or more) by using a zero-effort impostor calculation to calibrate  $T$ . As shown later (sec. 3.6), FMR is higher for demographic-matched impostors.

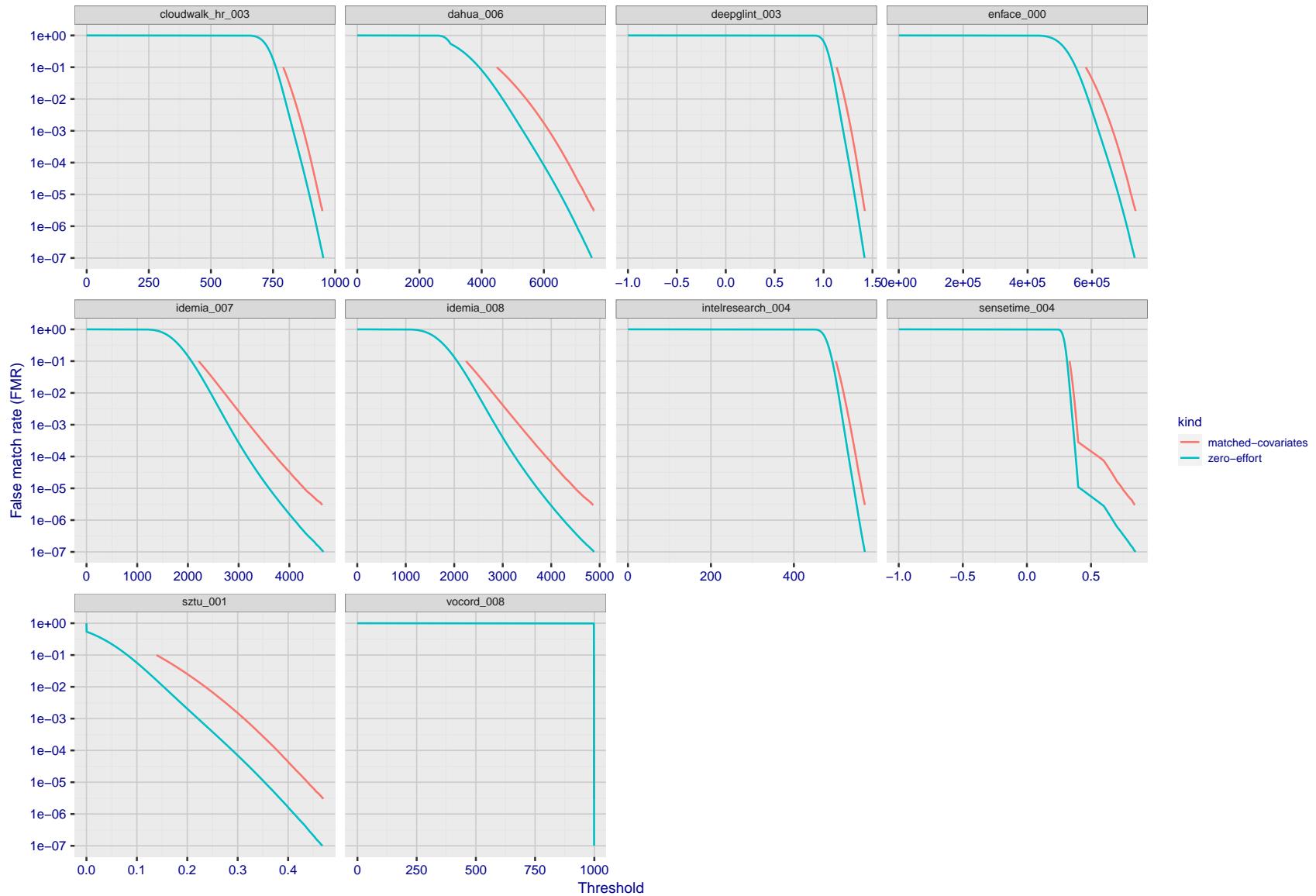


Figure 176: For the visa images, the false match calibration curves show FMR vs. threshold,  $T$ . The blue (lower) curves are for zero-effort impostors (i.e. comparing all images against all). The red (upper) curves are for persons of the same-sex, same-age, and same national-origin. This shows that FMR is underestimated (by a factor of 10 or more) by using a zero-effort impostor calculation to calibrate  $T$ . As shown later (sec. 3.6), FMR is higher for demographic-matched impostors.

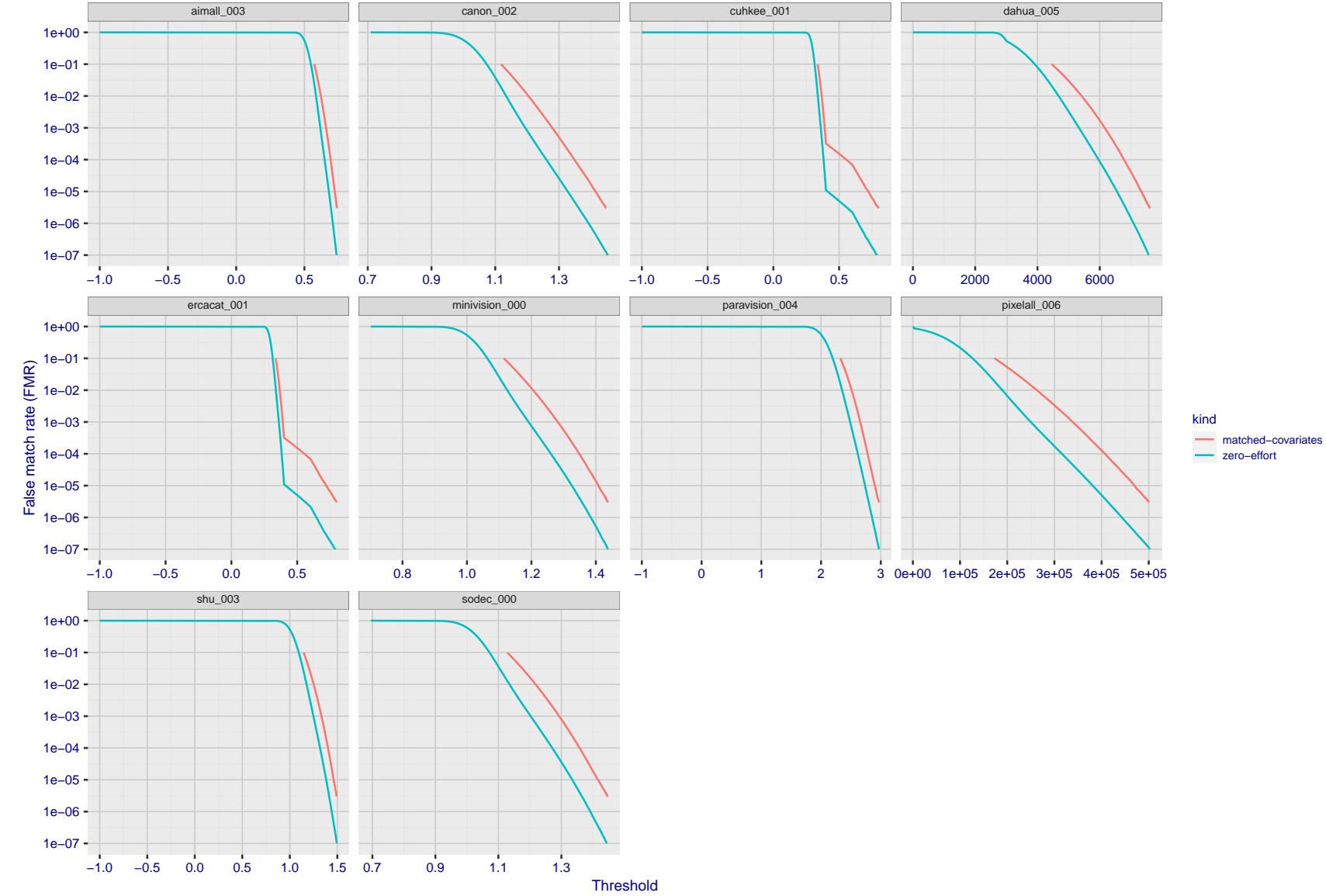


Figure 177: For the visa images, the false match calibration curves show FMR vs. threshold,  $T$ . The blue (lower) curves are for zero-effort impostors (i.e. comparing all images against all). The red (upper) curves are for persons of the same-sex, same-age, and same national-origin. This shows that FMR is underestimated (by a factor of 10 or more) by using a zero-effort impostor calculation to calibrate  $T$ . As shown later (sec. 3.6), FMR is higher for demographic-matched impostors.

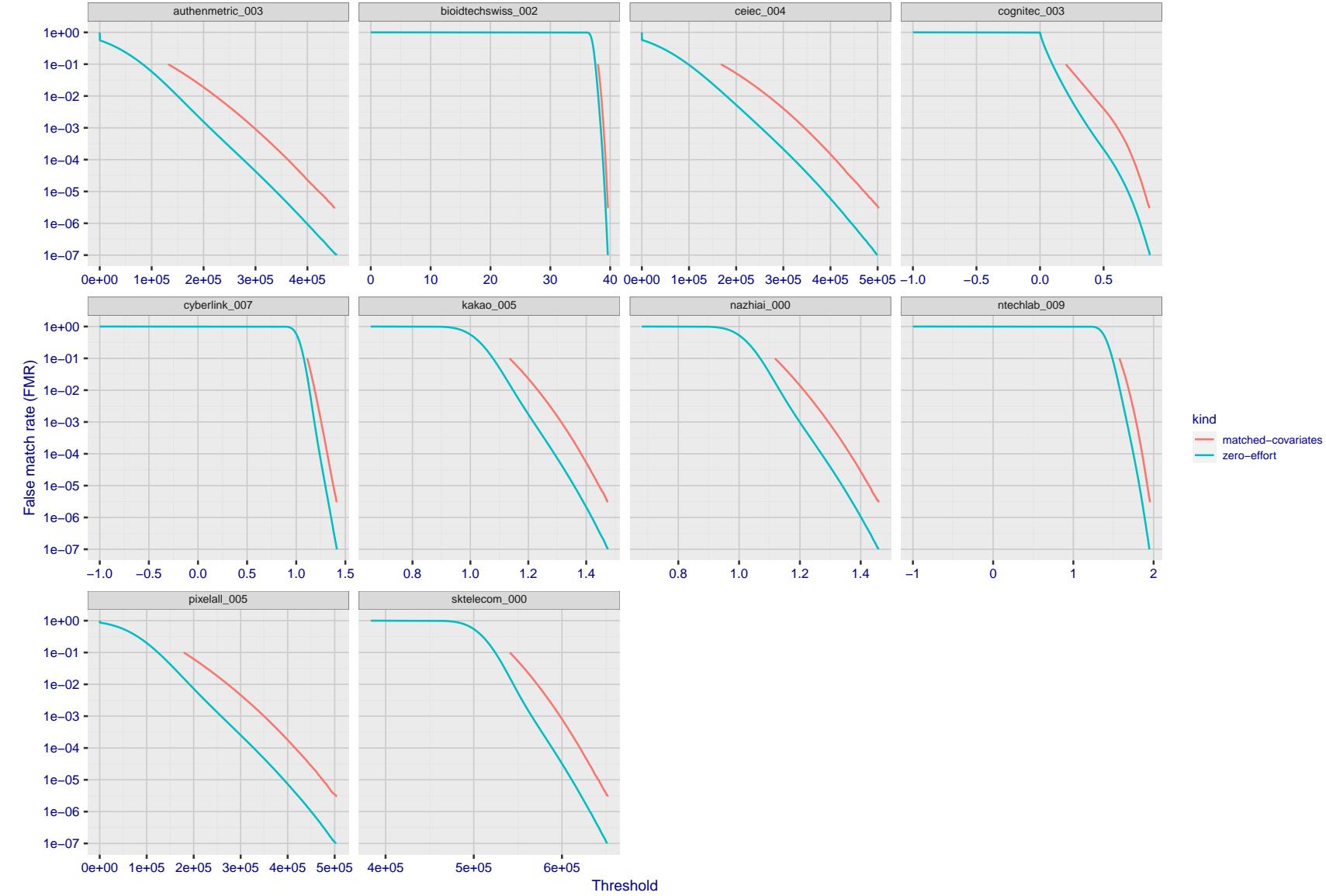


Figure 178: For the visa images, the false match calibration curves show FMR vs. threshold,  $T$ . The blue (lower) curves are for zero-effort impostors (i.e. comparing all images against all). The red (upper) curves are for persons of the same-sex, same-age, and same national-origin. This shows that FMR is underestimated (by a factor of 10 or more) by using a zero-effort impostor calculation to calibrate  $T$ . As shown later (sec. 3.6), FMR is higher for demographic-matched impostors.

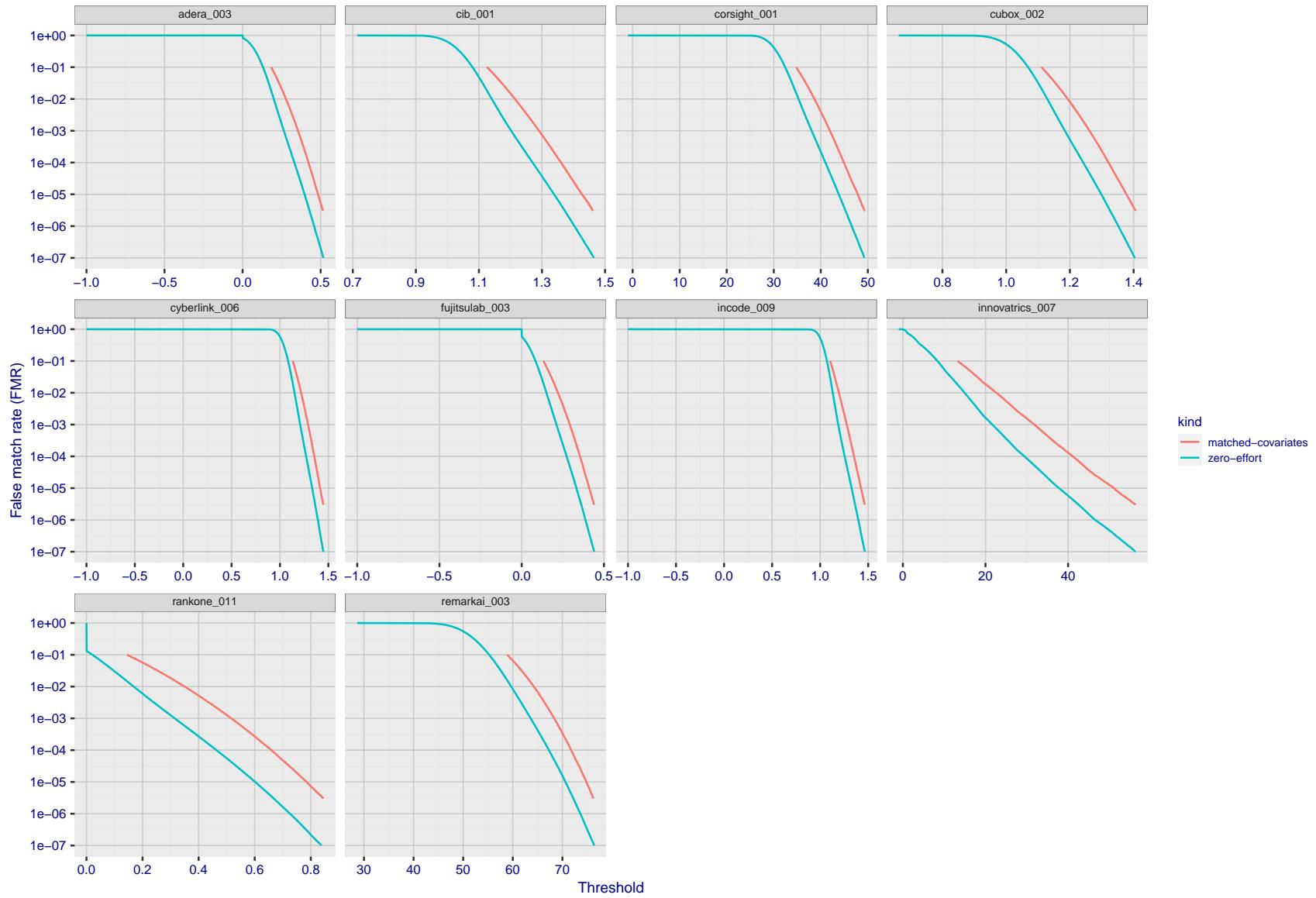


Figure 179: For the visa images, the false match calibration curves show FMR vs. threshold,  $T$ . The blue (lower) curves are for zero-effort impostors (i.e. comparing all images against all). The red (upper) curves are for persons of the same-sex, same-age, and same national-origin. This shows that FMR is underestimated (by a factor of 10 or more) by using a zero-effort impostor calculation to calibrate  $T$ . As shown later (sec. 3.6), FMR is higher for demographic-matched impostors.

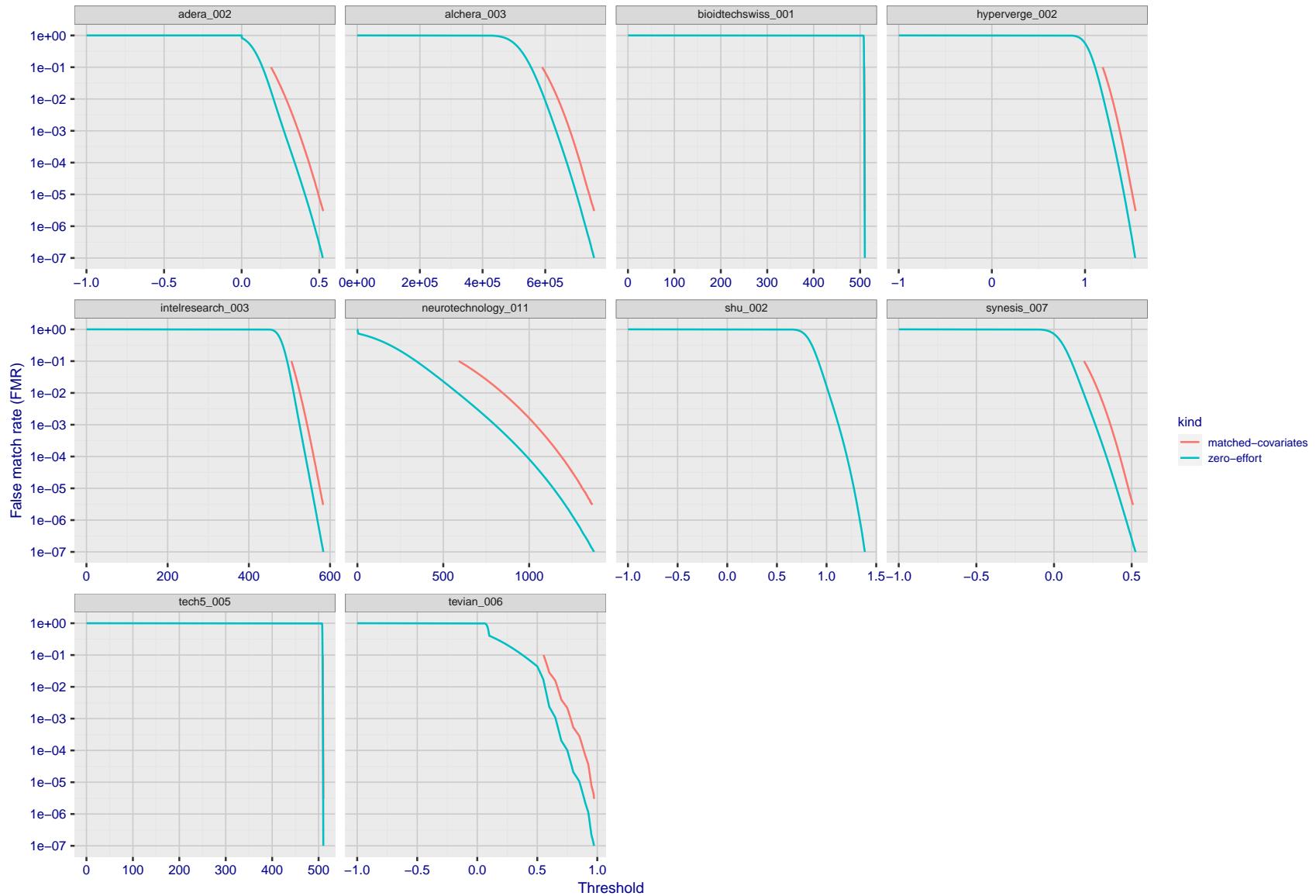


Figure 180: For the visa images, the false match calibration curves show FMR vs. threshold,  $T$ . The blue (lower) curves are for zero-effort impostors (i.e. comparing all images against all). The red (upper) curves are for persons of the same-sex, same-age, and same national-origin. This shows that FMR is underestimated (by a factor of 10 or more) by using a zero-effort impostor calculation to calibrate  $T$ . As shown later (sec. 3.6), FMR is higher for demographic-matched impostors.

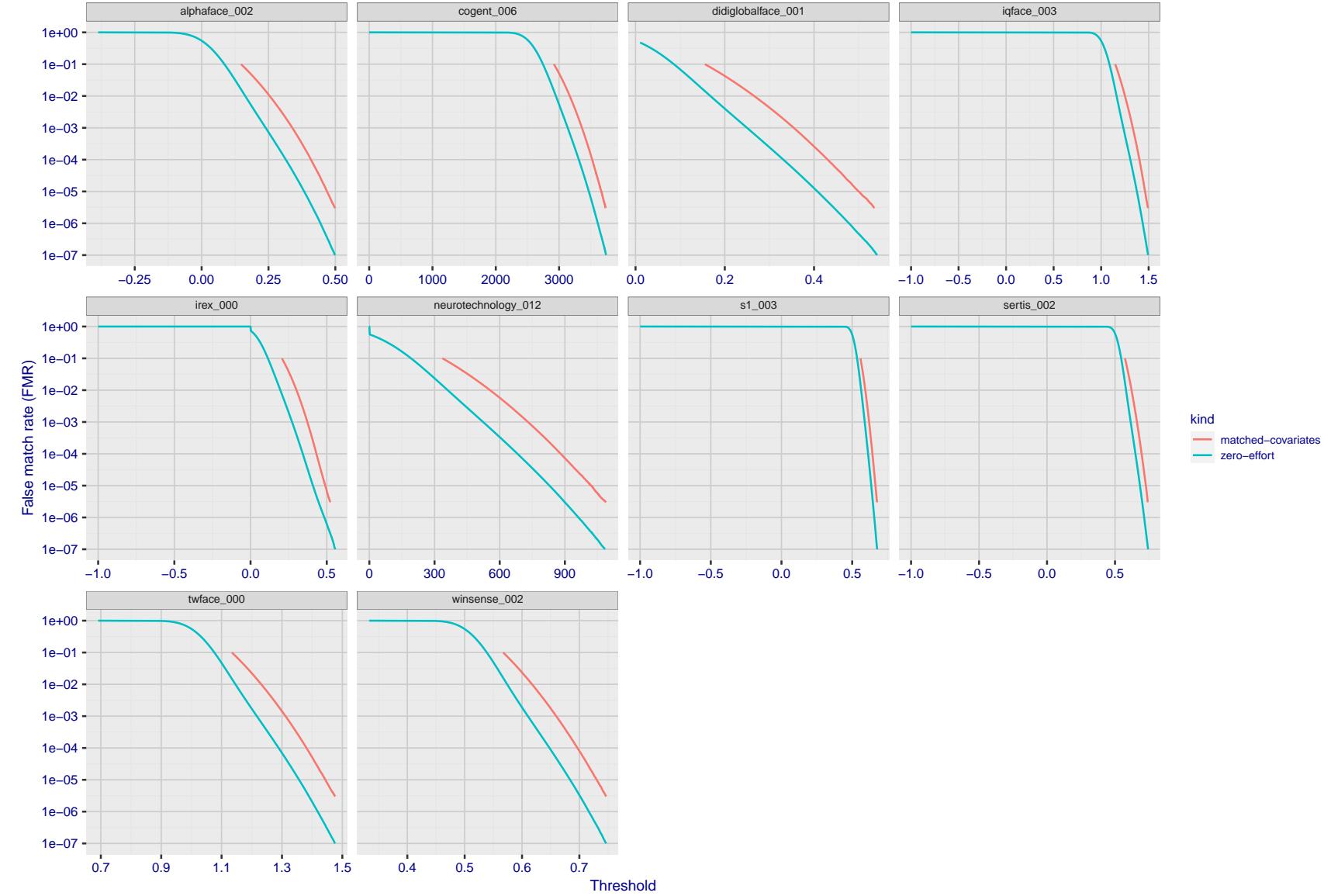


Figure 181: For the visa images, the false match calibration curves show FMR vs. threshold,  $T$ . The blue (lower) curves are for zero-effort impostors (i.e. comparing all images against all). The red (upper) curves are for persons of the same-sex, same-age, and same national-origin. This shows that FMR is underestimated (by a factor of 10 or more) by using a zero-effort impostor calculation to calibrate  $T$ . As shown later (sec. 3.6), FMR is higher for demographic-matched impostors.

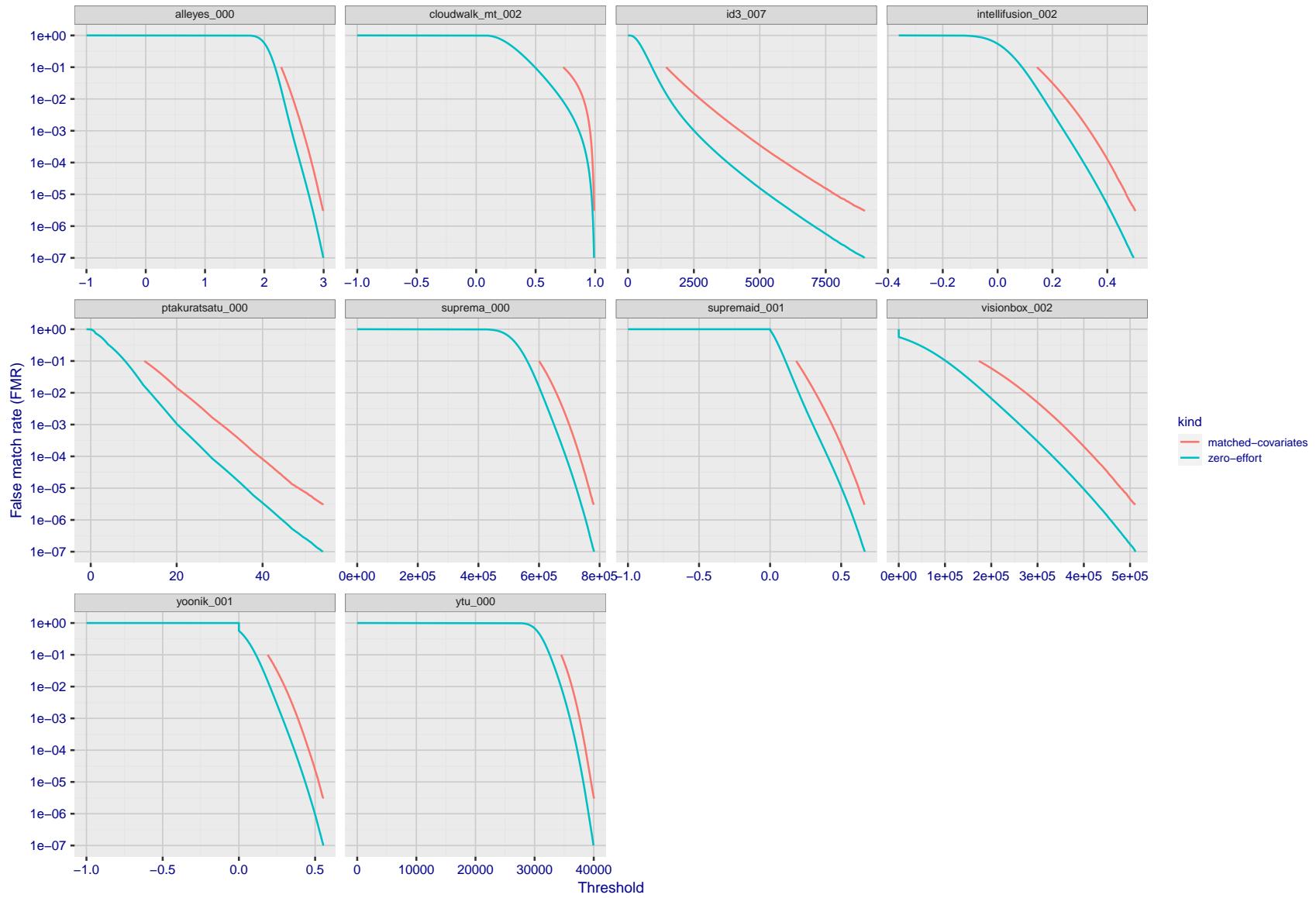


Figure 182: For the visa images, the false match calibration curves show FMR vs. threshold,  $T$ . The blue (lower) curves are for zero-effort impostors (i.e. comparing all images against all). The red (upper) curves are for persons of the same-sex, same-age, and same national-origin. This shows that FMR is underestimated (by a factor of 10 or more) by using a zero-effort impostor calculation to calibrate  $T$ . As shown later (sec. 3.6), FMR is higher for demographic-matched impostors.

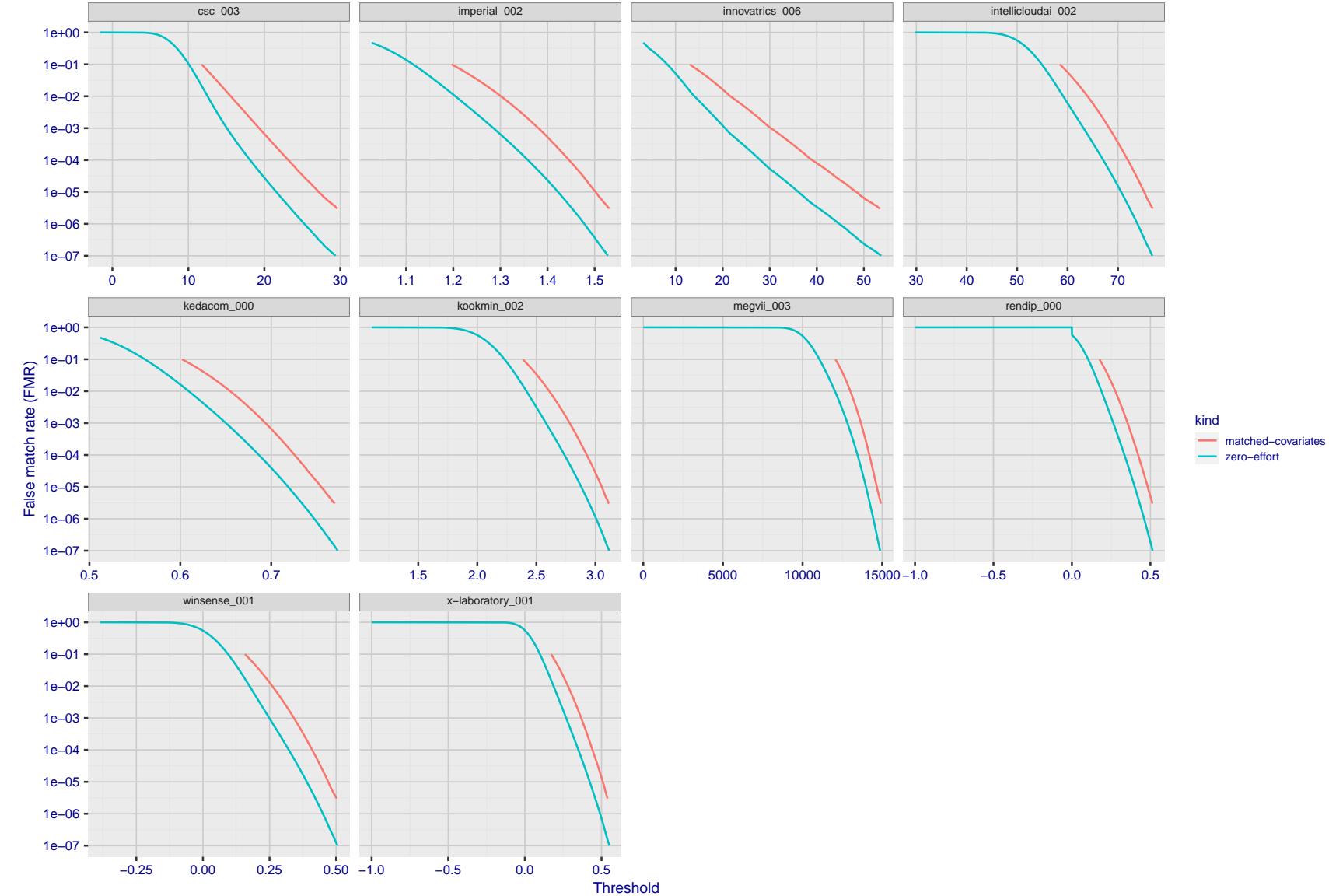


Figure 183: For the visa images, the false match calibration curves show FMR vs. threshold,  $T$ . The blue (lower) curves are for zero-effort impostors (i.e. comparing all images against all). The red (upper) curves are for persons of the same-sex, same-age, and same national-origin. This shows that FMR is underestimated (by a factor of 10 or more) by using a zero-effort impostor calculation to calibrate  $T$ . As shown later (sec. 3.6), FMR is higher for demographic-matched impostors.

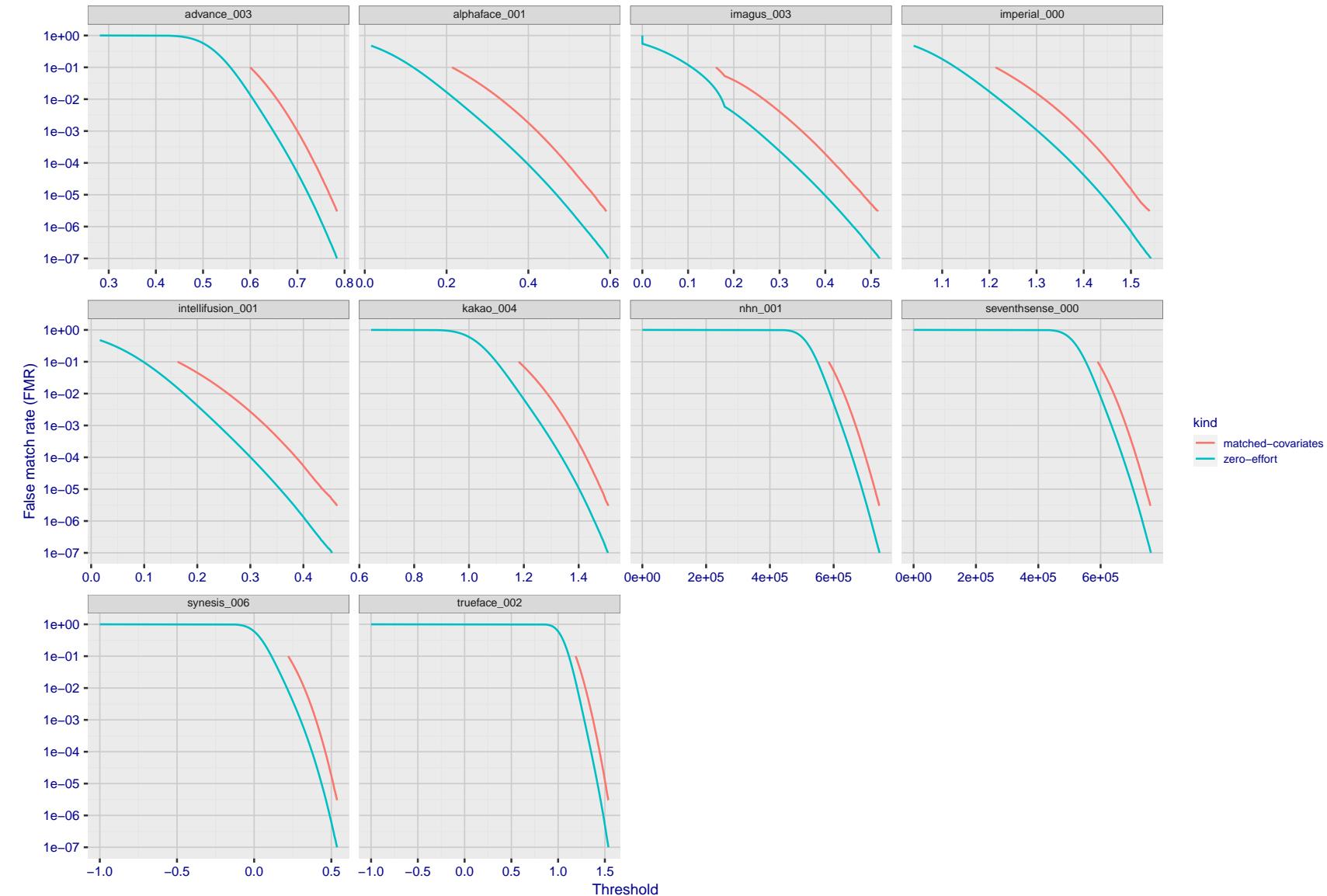


Figure 184: For the visa images, the false match calibration curves show FMR vs. threshold,  $T$ . The blue (lower) curves are for zero-effort impostors (i.e. comparing all images against all). The red (upper) curves are for persons of the same-sex, same-age, and same national-origin. This shows that FMR is underestimated (by a factor of 10 or more) by using a zero-effort impostor calculation to calibrate  $T$ . As shown later (sec. 3.6), FMR is higher for demographic-matched impostors.

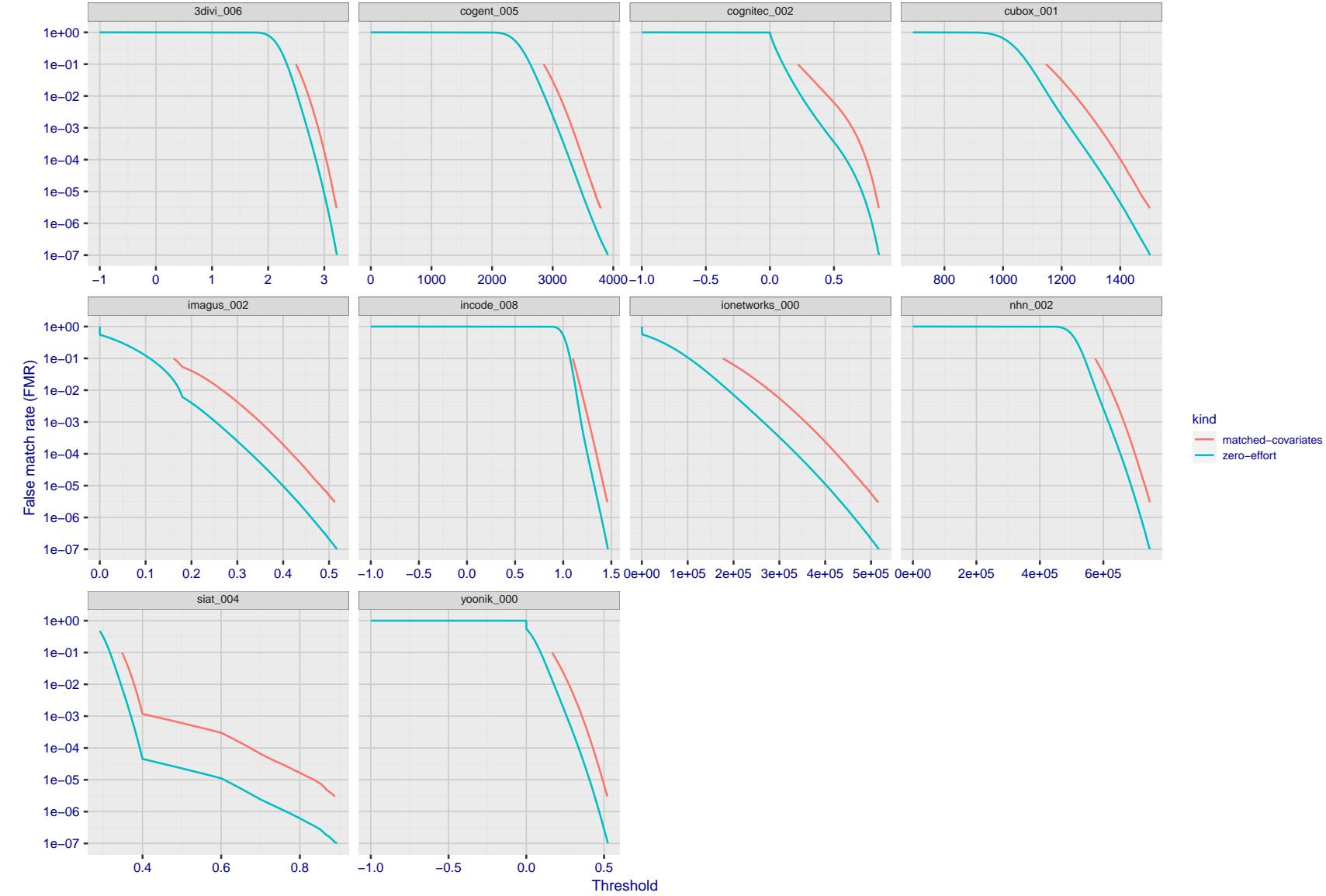


Figure 185: For the visa images, the false match calibration curves show FMR vs. threshold,  $T$ . The blue (lower) curves are for zero-effort impostors (i.e. comparing all images against all). The red (upper) curves are for persons of the same-sex, same-age, and same national-origin. This shows that FMR is underestimated (by a factor of 10 or more) by using a zero-effort impostor calculation to calibrate  $T$ . As shown later (sec. 3.6), FMR is higher for demographic-matched impostors.

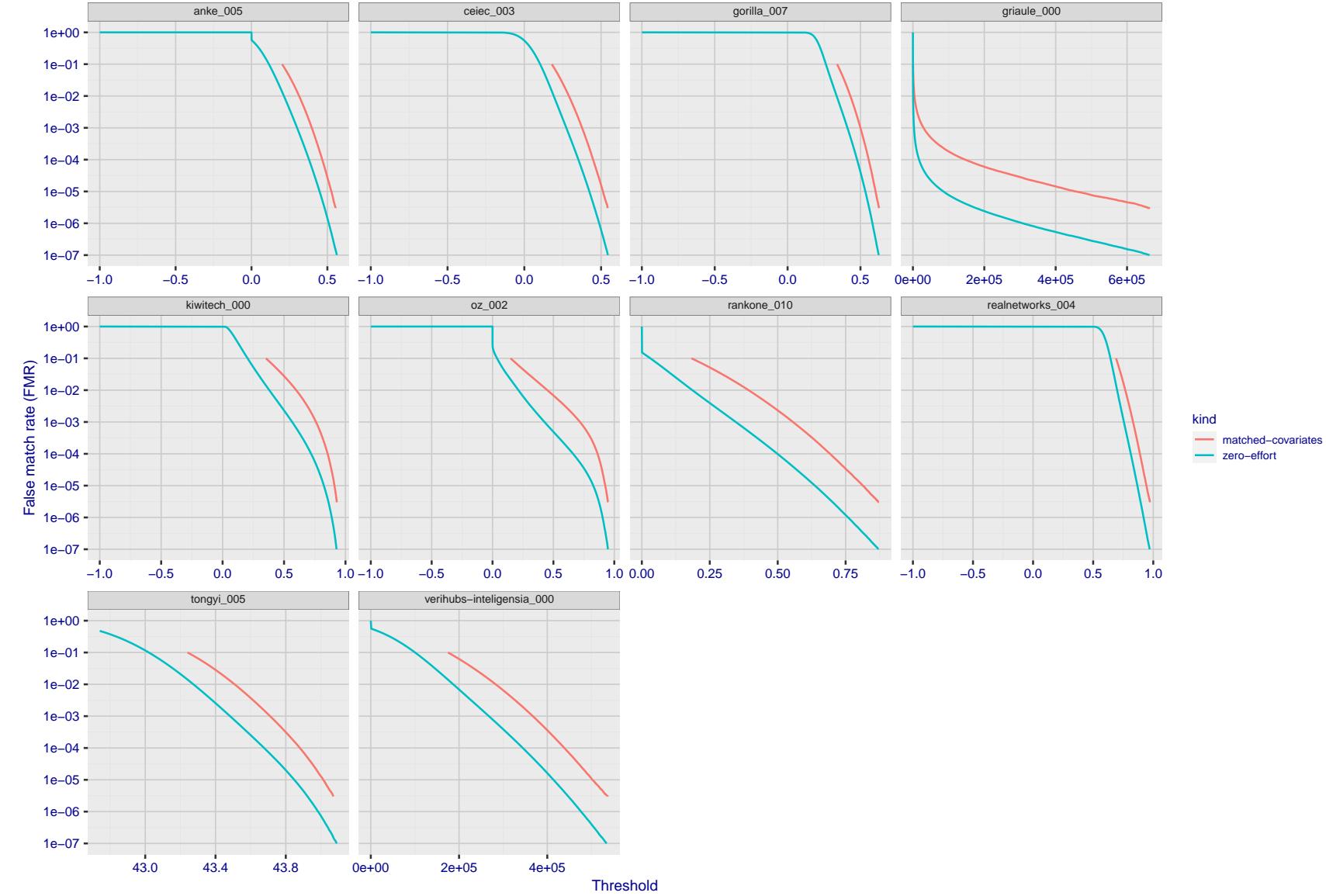


Figure 186: For the visa images, the false match calibration curves show FMR vs. threshold,  $T$ . The blue (lower) curves are for zero-effort impostors (i.e. comparing all images against all). The red (upper) curves are for persons of the same-sex, same-age, and same national-origin. This shows that FMR is underestimated (by a factor of 10 or more) by using a zero-effort impostor calculation to calibrate  $T$ . As shown later (sec. 3.6), FMR is higher for demographic-matched impostors.

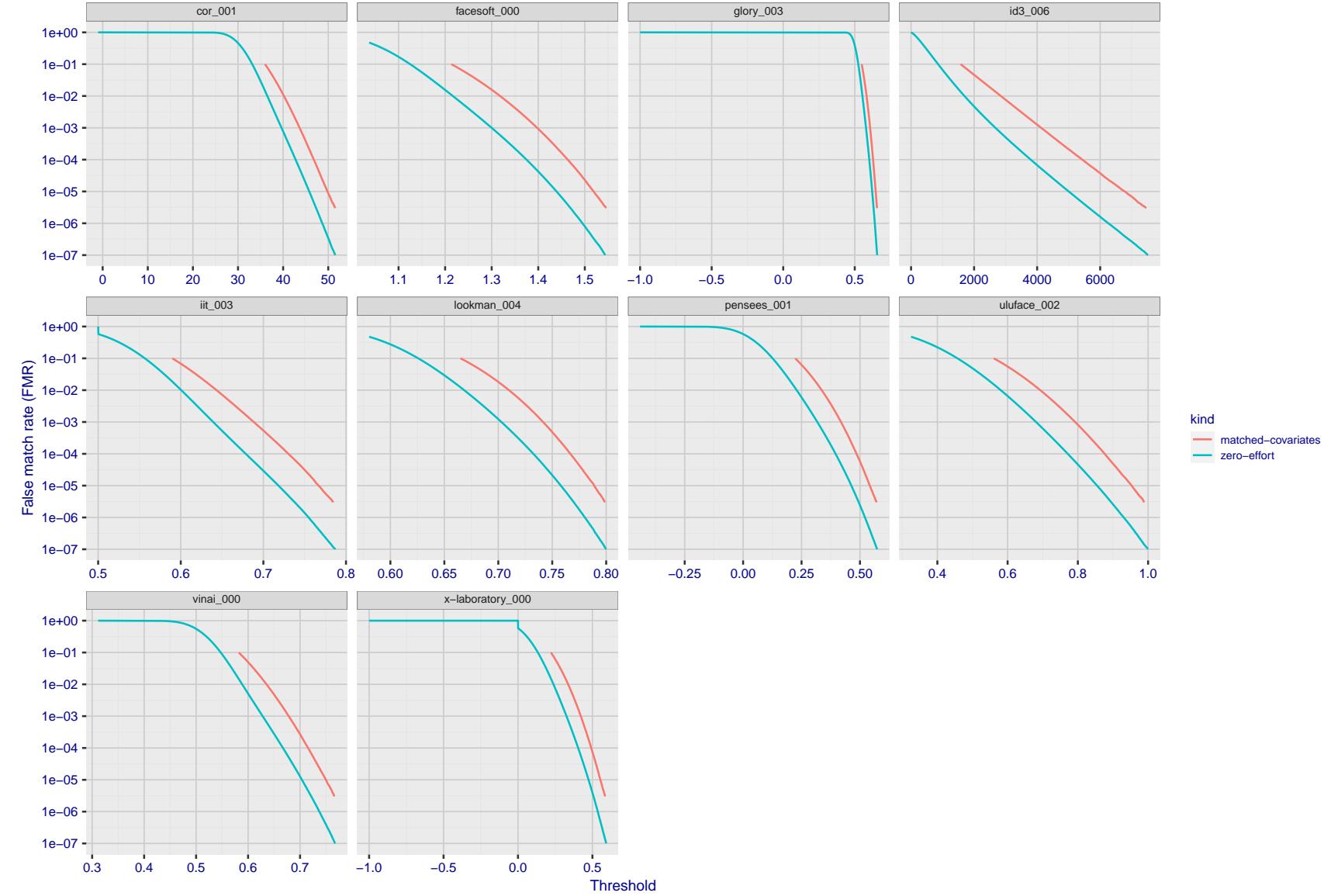


Figure 187: For the visa images, the false match calibration curves show FMR vs. threshold,  $T$ . The blue (lower) curves are for zero-effort impostors (i.e. comparing all images against all). The red (upper) curves are for persons of the same-sex, same-age, and same national-origin. This shows that FMR is underestimated (by a factor of 10 or more) by using a zero-effort impostor calculation to calibrate  $T$ . As shown later (sec. 3.6), FMR is higher for demographic-matched impostors.

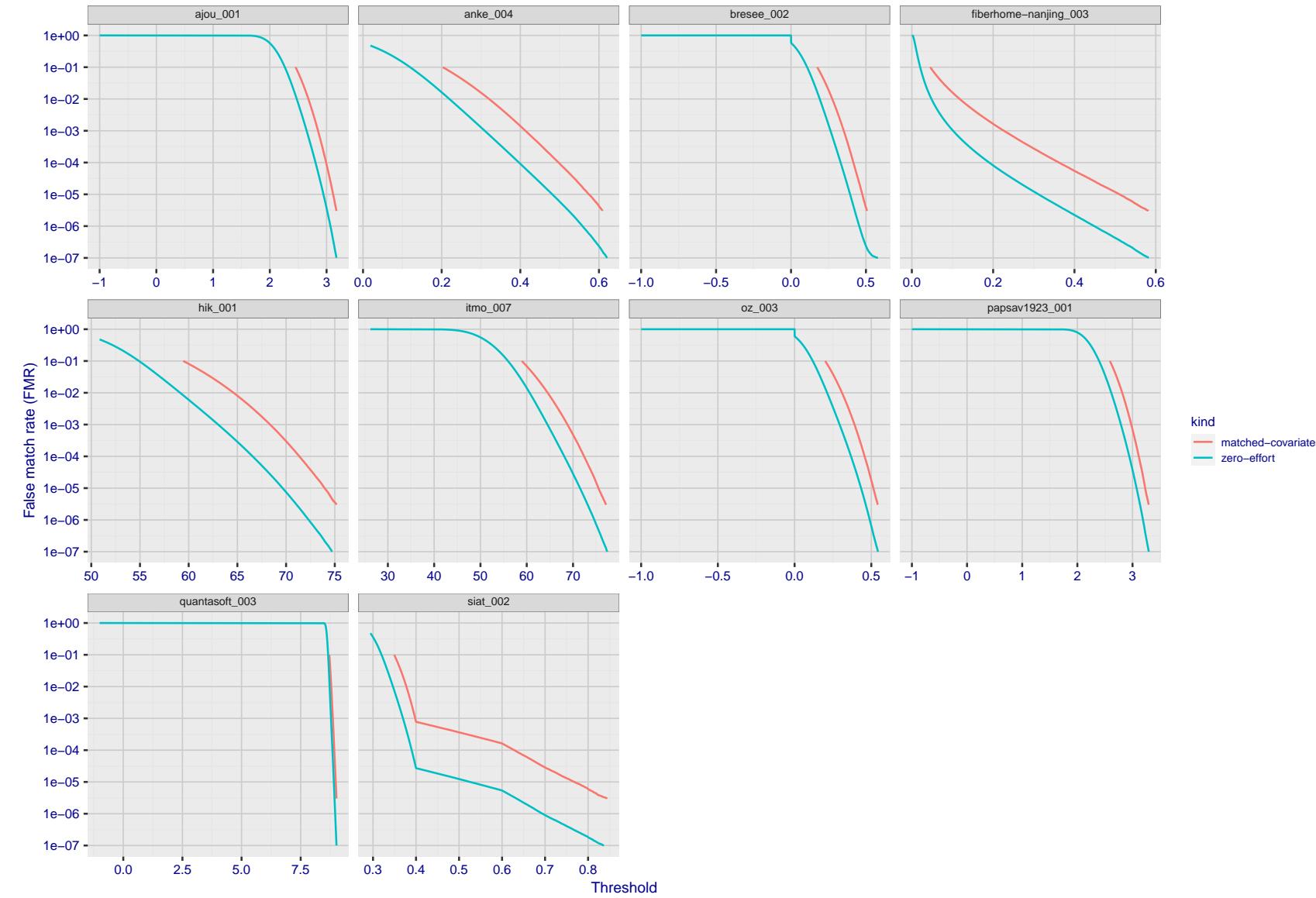


Figure 188: For the visa images, the false match calibration curves show FMR vs. threshold,  $T$ . The blue (lower) curves are for zero-effort impostors (i.e. comparing all images against all). The red (upper) curves are for persons of the same-sex, same-age, and same national-origin. This shows that FMR is underestimated (by a factor of 10 or more) by using a zero-effort impostor calculation to calibrate  $T$ . As shown later (sec. 3.6), FMR is higher for demographic-matched impostors.

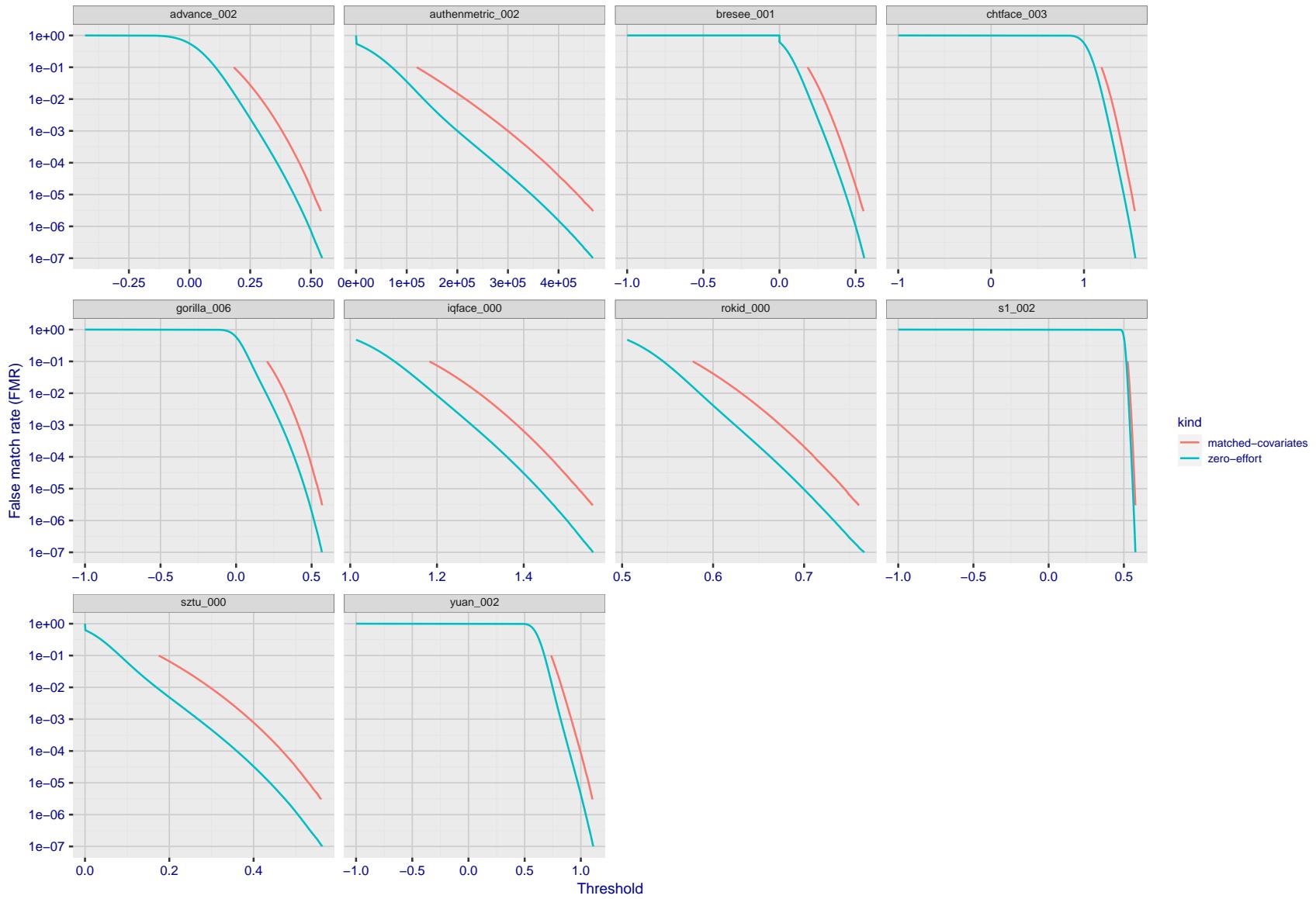


Figure 189: For the visa images, the false match calibration curves show FMR vs. threshold,  $T$ . The blue (lower) curves are for zero-effort impostors (i.e. comparing all images against all). The red (upper) curves are for persons of the same-sex, same-age, and same national-origin. This shows that FMR is underestimated (by a factor of 10 or more) by using a zero-effort impostor calculation to calibrate  $T$ . As shown later (sec. 3.6), FMR is higher for demographic-matched impostors.

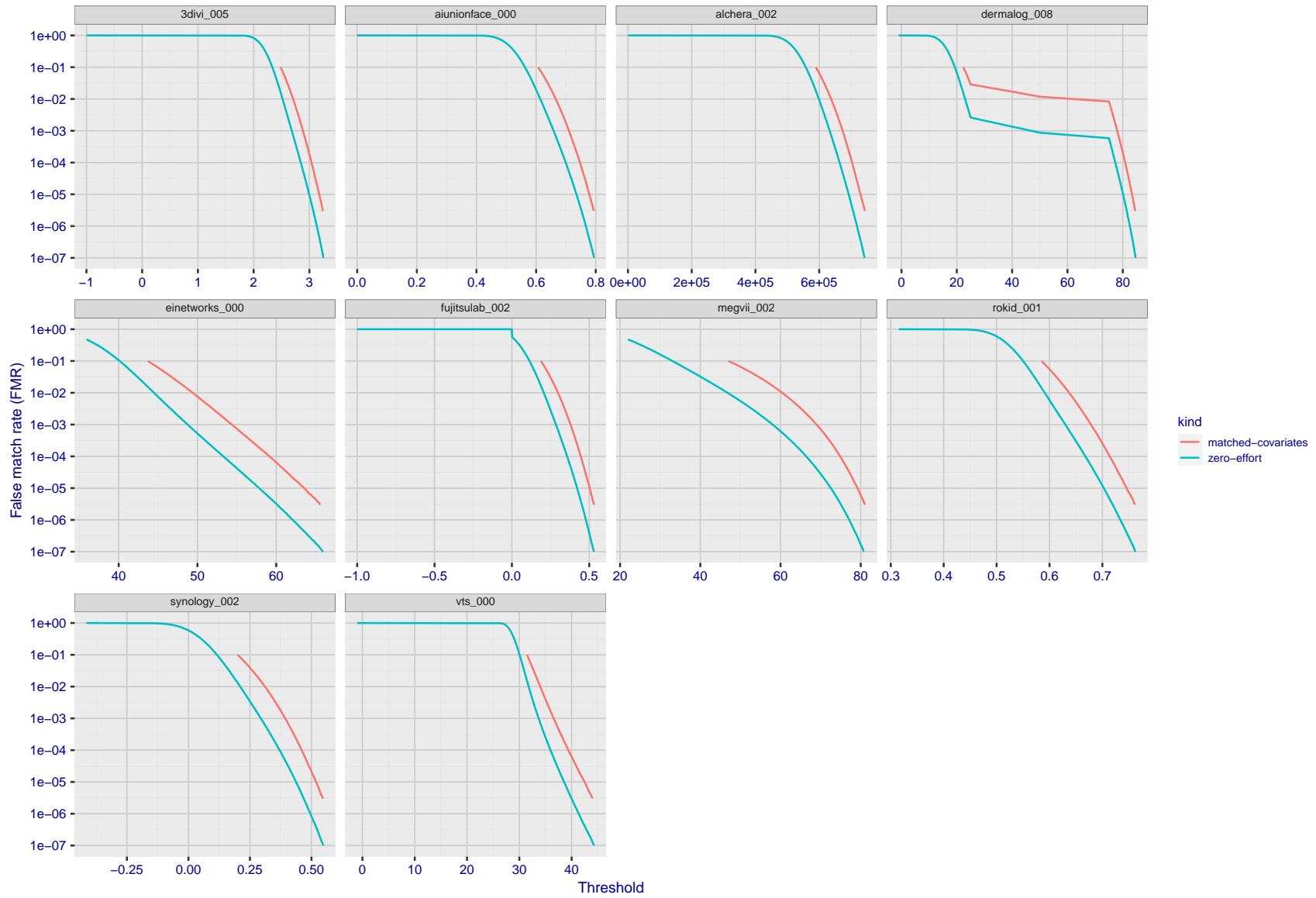


Figure 190: For the visa images, the false match calibration curves show FMR vs. threshold,  $T$ . The blue (lower) curves are for zero-effort impostors (i.e. comparing all images against all). The red (upper) curves are for persons of the same-sex, same-age, and same national-origin. This shows that FMR is underestimated (by a factor of 10 or more) by using a zero-effort impostor calculation to calibrate  $T$ . As shown later (sec. 3.6), FMR is higher for demographic-matched impostors.

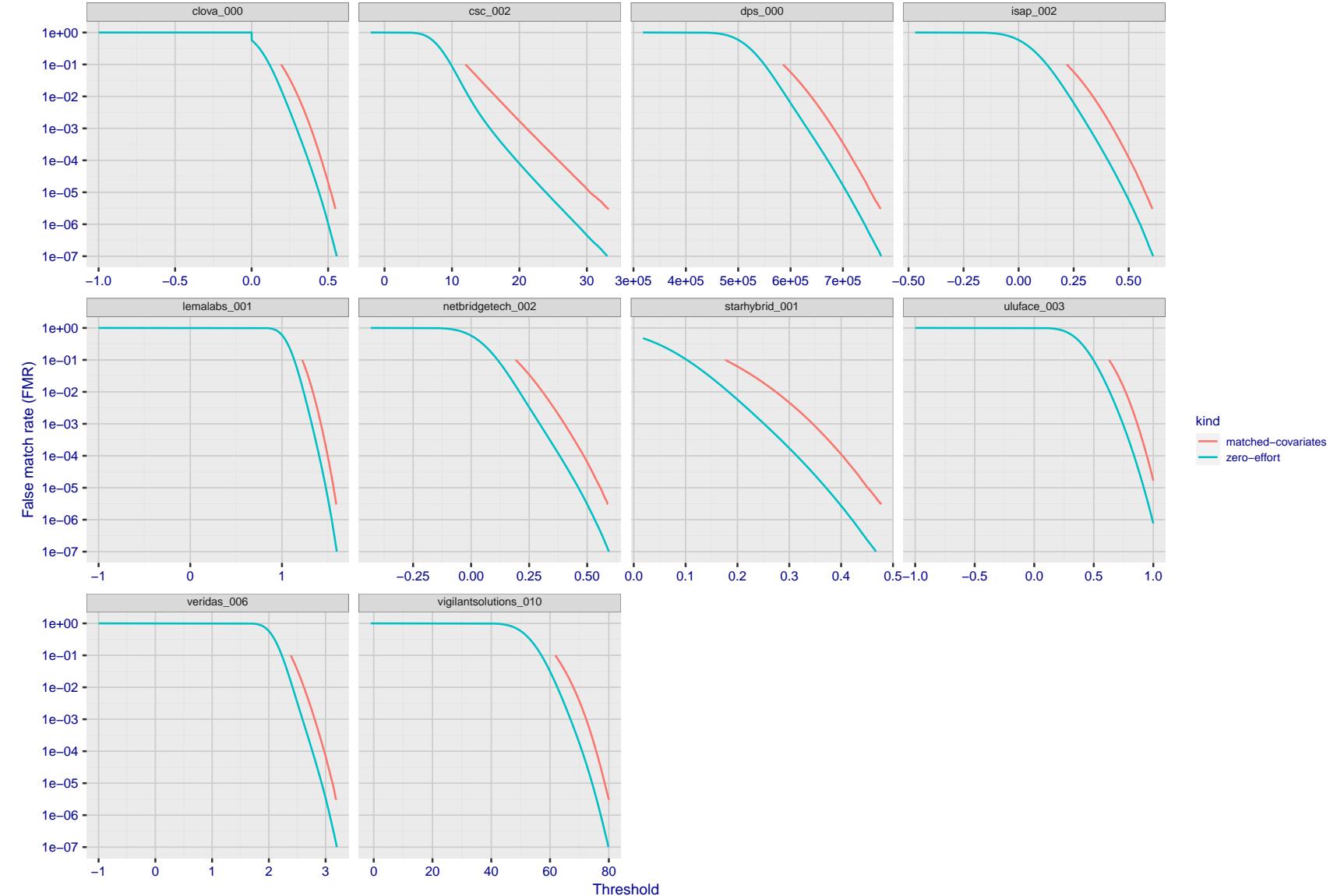


Figure 191: For the visa images, the false match calibration curves show FMR vs. threshold,  $T$ . The blue (lower) curves are for zero-effort impostors (i.e. comparing all images against all). The red (upper) curves are for persons of the same-sex, same-age, and same national-origin. This shows that FMR is underestimated (by a factor of 10 or more) by using a zero-effort impostor calculation to calibrate  $T$ . As shown later (sec. 3.6), FMR is higher for demographic-matched impostors.

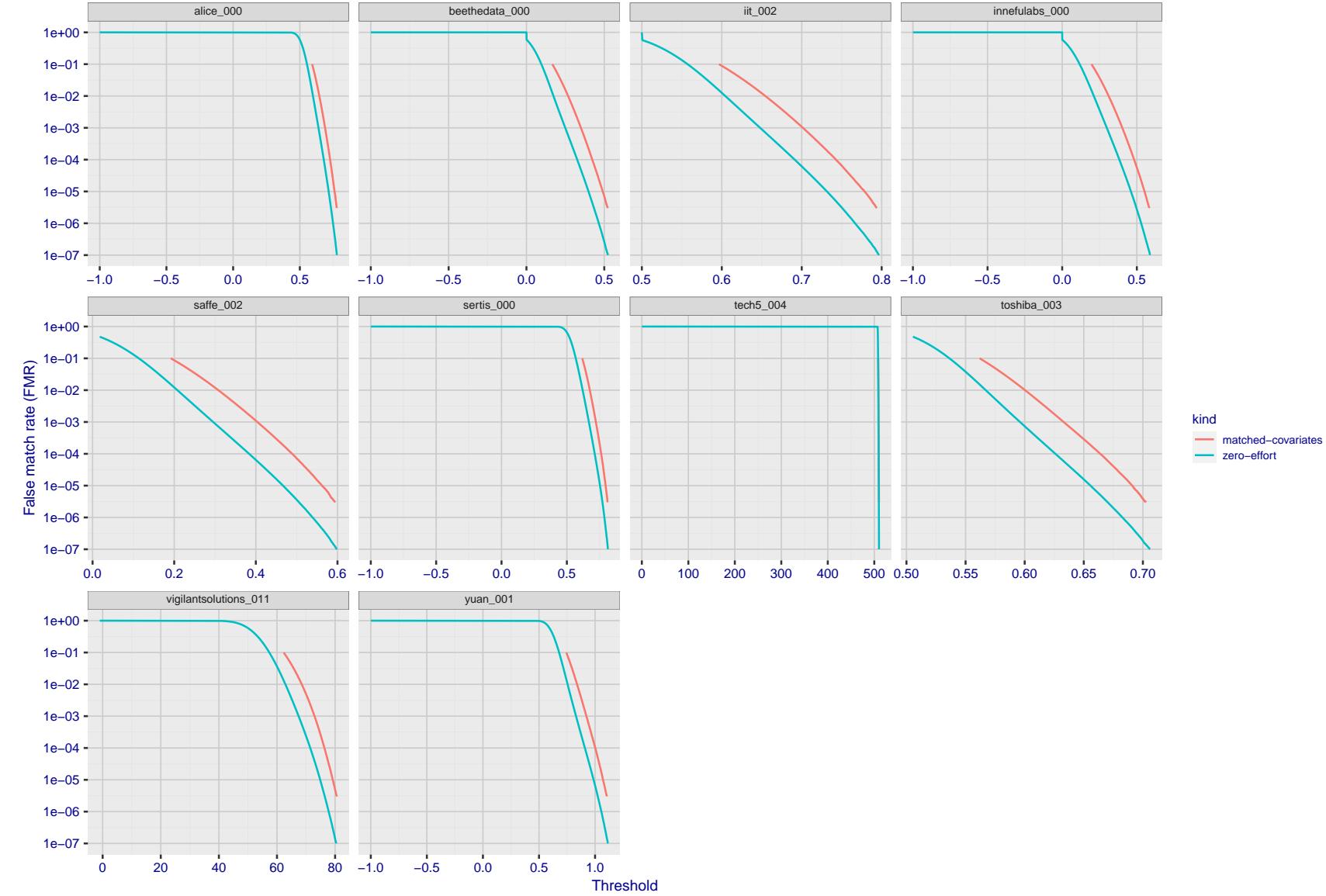


Figure 192: For the visa images, the false match calibration curves show FMR vs. threshold,  $T$ . The blue (lower) curves are for zero-effort impostors (i.e. comparing all images against all). The red (upper) curves are for persons of the same-sex, same-age, and same national-origin. This shows that FMR is underestimated (by a factor of 10 or more) by using a zero-effort impostor calculation to calibrate  $T$ . As shown later (sec. 3.6), FMR is higher for demographic-matched impostors.

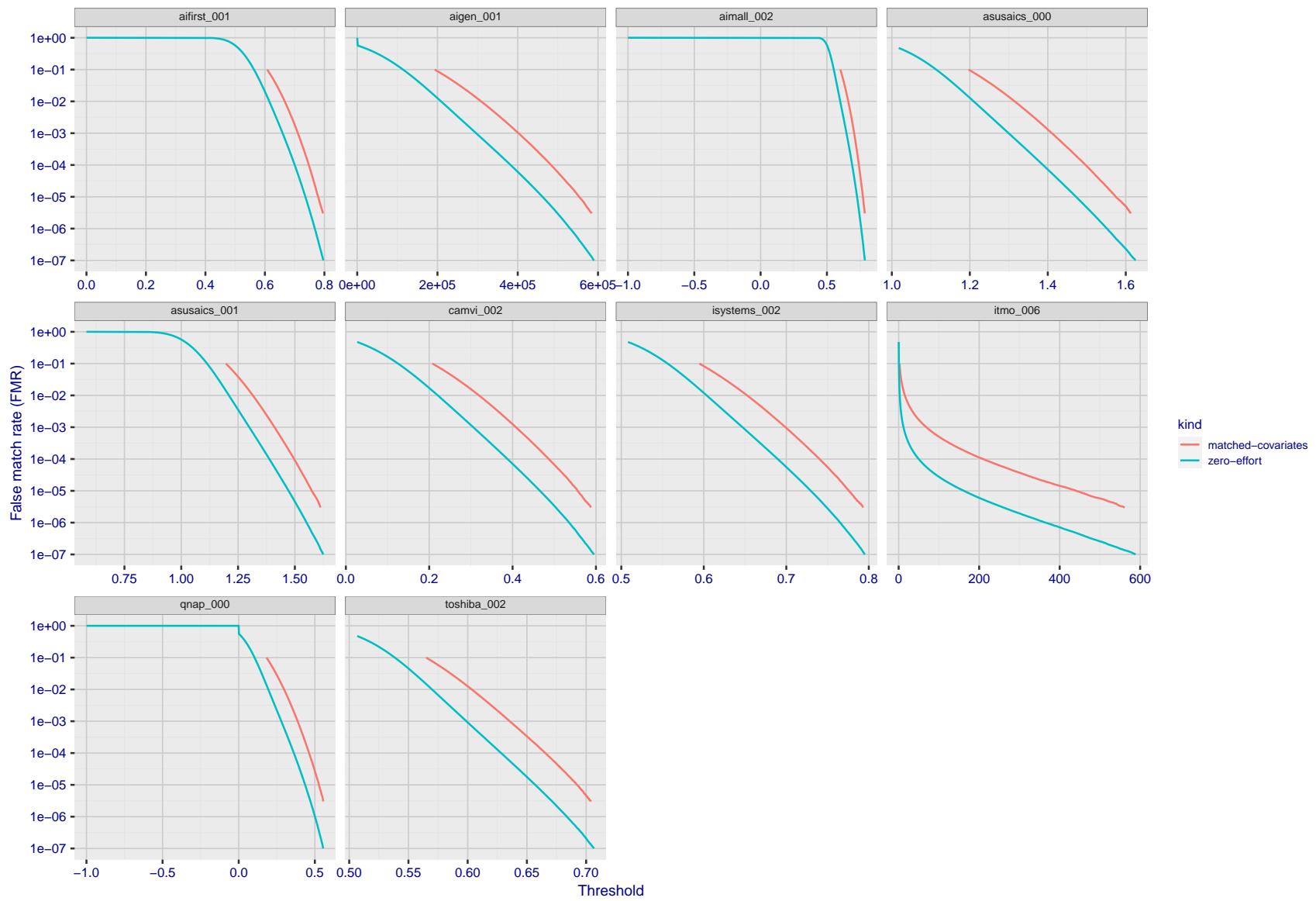


Figure 193: For the visa images, the false match calibration curves show FMR vs. threshold,  $T$ . The blue (lower) curves are for zero-effort impostors (i.e. comparing all images against all). The red (upper) curves are for persons of the same-sex, same-age, and same national-origin. This shows that FMR is underestimated (by a factor of 10 or more) by using a zero-effort impostor calculation to calibrate  $T$ . As shown later (sec. 3.6), FMR is higher for demographic-matched impostors.

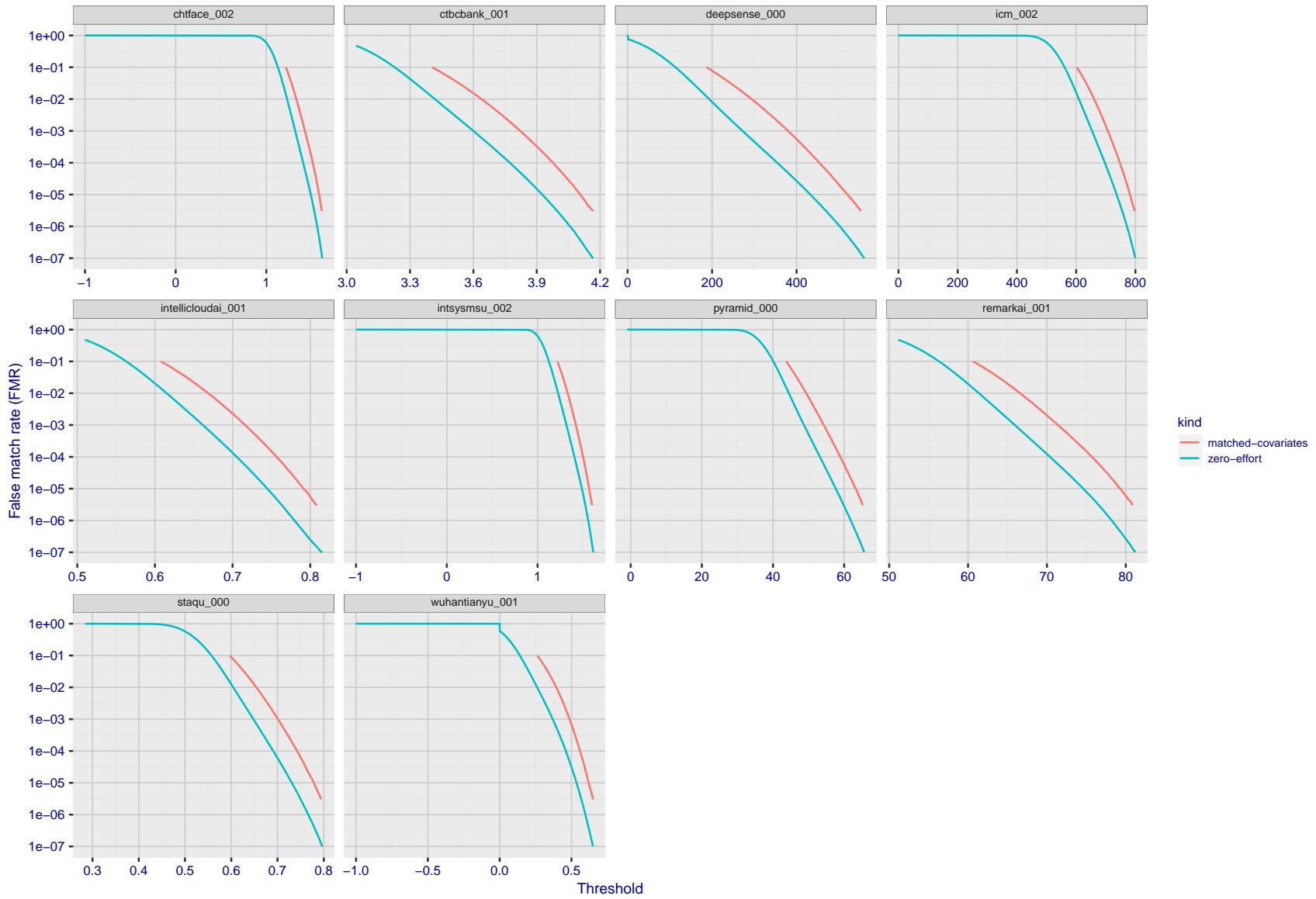


Figure 194: For the visa images, the false match calibration curves show FMR vs. threshold,  $T$ . The blue (lower) curves are for zero-effort impostors (i.e. comparing all images against all). The red (upper) curves are for persons of the same-sex, same-age, and same national-origin. This shows that FMR is underestimated (by a factor of 10 or more) by using a zero-effort impostor calculation to calibrate  $T$ . As shown later (sec. 3.6), FMR is higher for demographic-matched impostors.

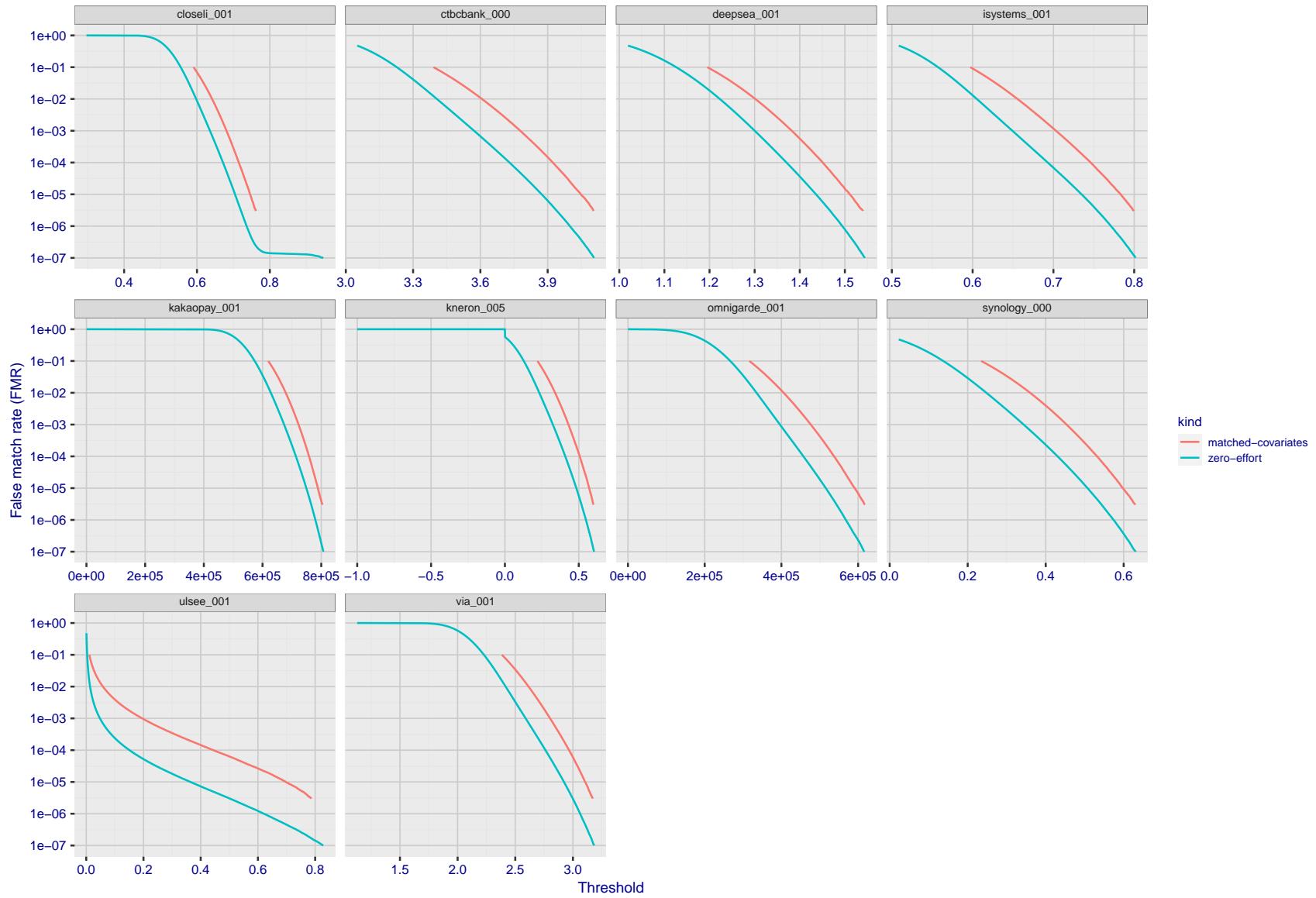


Figure 195: For the visa images, the false match calibration curves show FMR vs. threshold,  $T$ . The blue (lower) curves are for zero-effort impostors (i.e. comparing all images against all). The red (upper) curves are for persons of the same-sex, same-age, and same national-origin. This shows that FMR is underestimated (by a factor of 10 or more) by using a zero-effort impostor calculation to calibrate  $T$ . As shown later (sec. 3.6), FMR is higher for demographic-matched impostors.

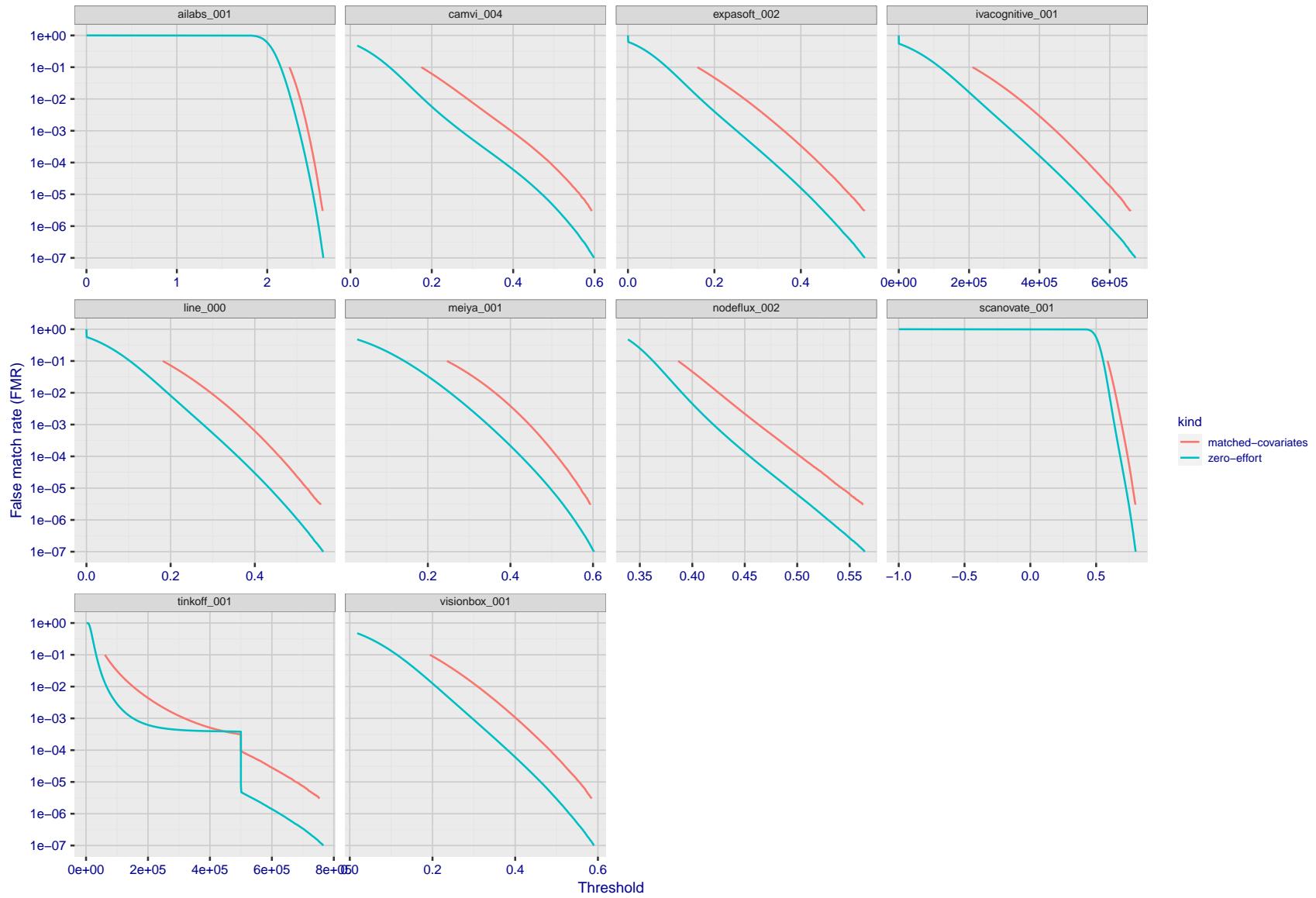


Figure 196: For the visa images, the false match calibration curves show FMR vs. threshold,  $T$ . The blue (lower) curves are for zero-effort impostors (i.e. comparing all images against all). The red (upper) curves are for persons of the same-sex, same-age, and same national-origin. This shows that FMR is underestimated (by a factor of 10 or more) by using a zero-effort impostor calculation to calibrate  $T$ . As shown later (sec. 3.6), FMR is higher for demographic-matched impostors.

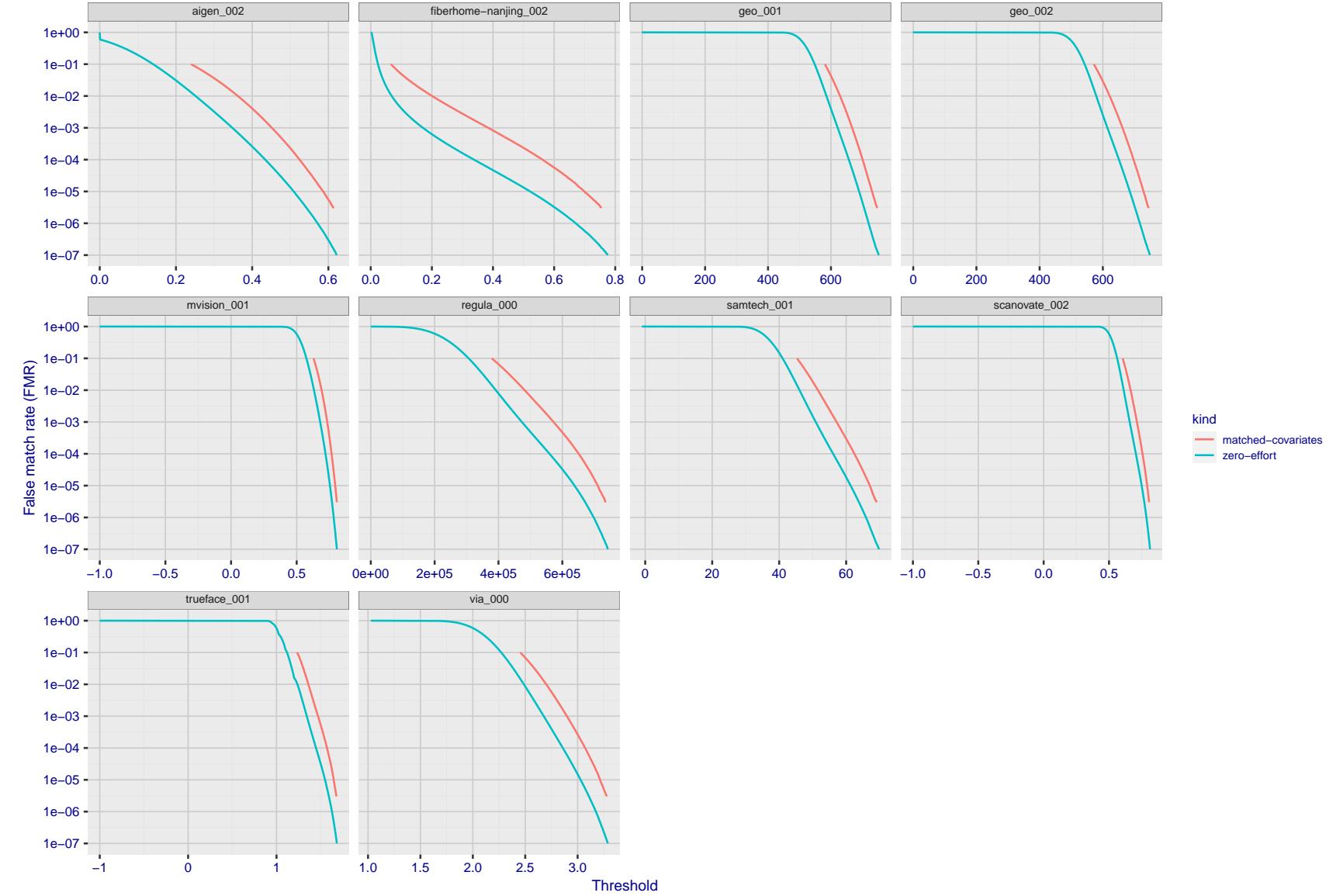


Figure 197: For the visa images, the false match calibration curves show FMR vs. threshold,  $T$ . The blue (lower) curves are for zero-effort impostors (i.e. comparing all images against all). The red (upper) curves are for persons of the same-sex, same-age, and same national-origin. This shows that FMR is underestimated (by a factor of 10 or more) by using a zero-effort impostor calculation to calibrate  $T$ . As shown later (sec. 3.6), FMR is higher for demographic-matched impostors.

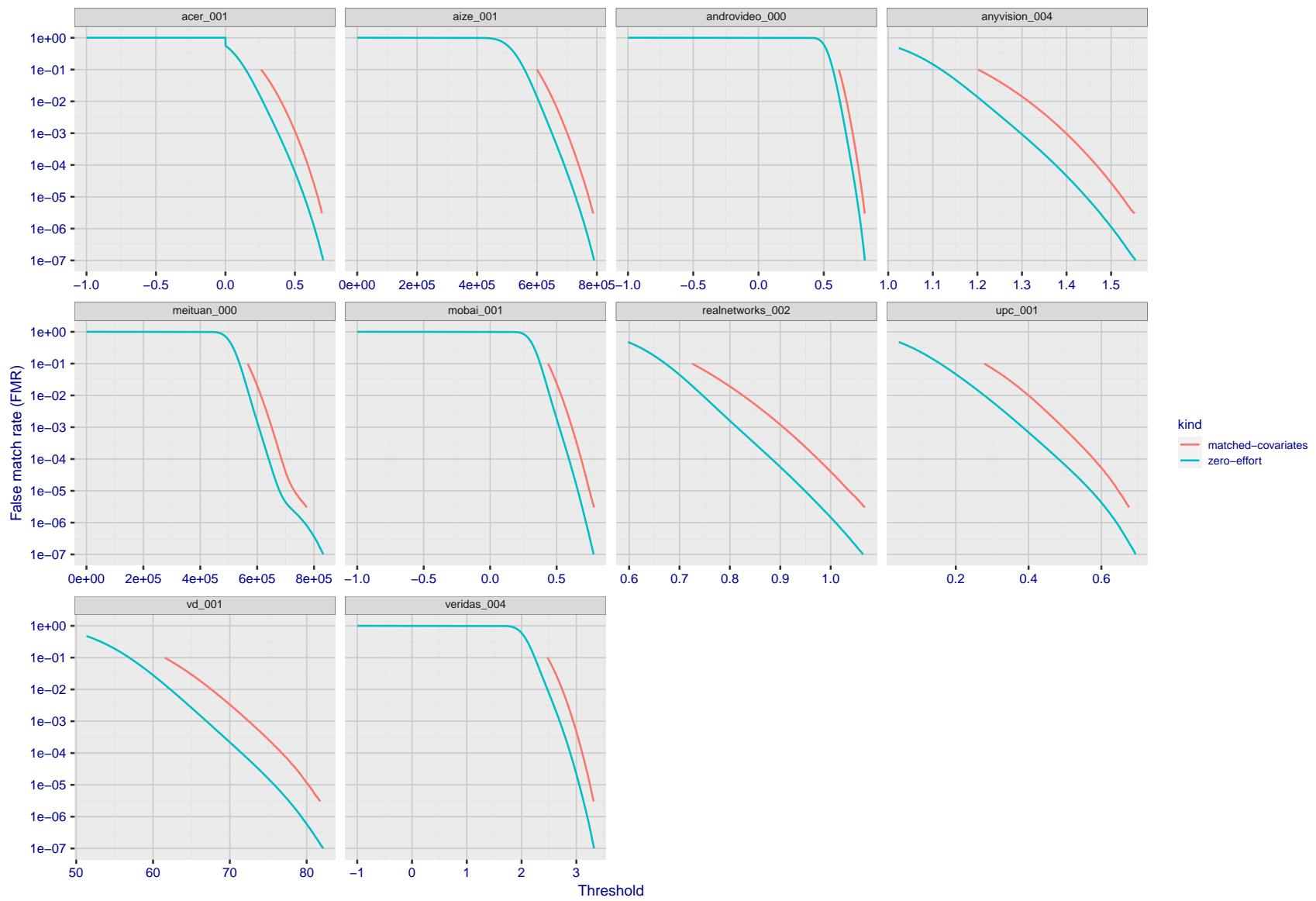


Figure 198: For the visa images, the false match calibration curves show FMR vs. threshold,  $T$ . The blue (lower) curves are for zero-effort impostors (i.e. comparing all images against all). The red (upper) curves are for persons of the same-sex, same-age, and same national-origin. This shows that FMR is underestimated (by a factor of 10 or more) by using a zero-effort impostor calculation to calibrate  $T$ . As shown later (sec. 3.6), FMR is higher for demographic-matched impostors.

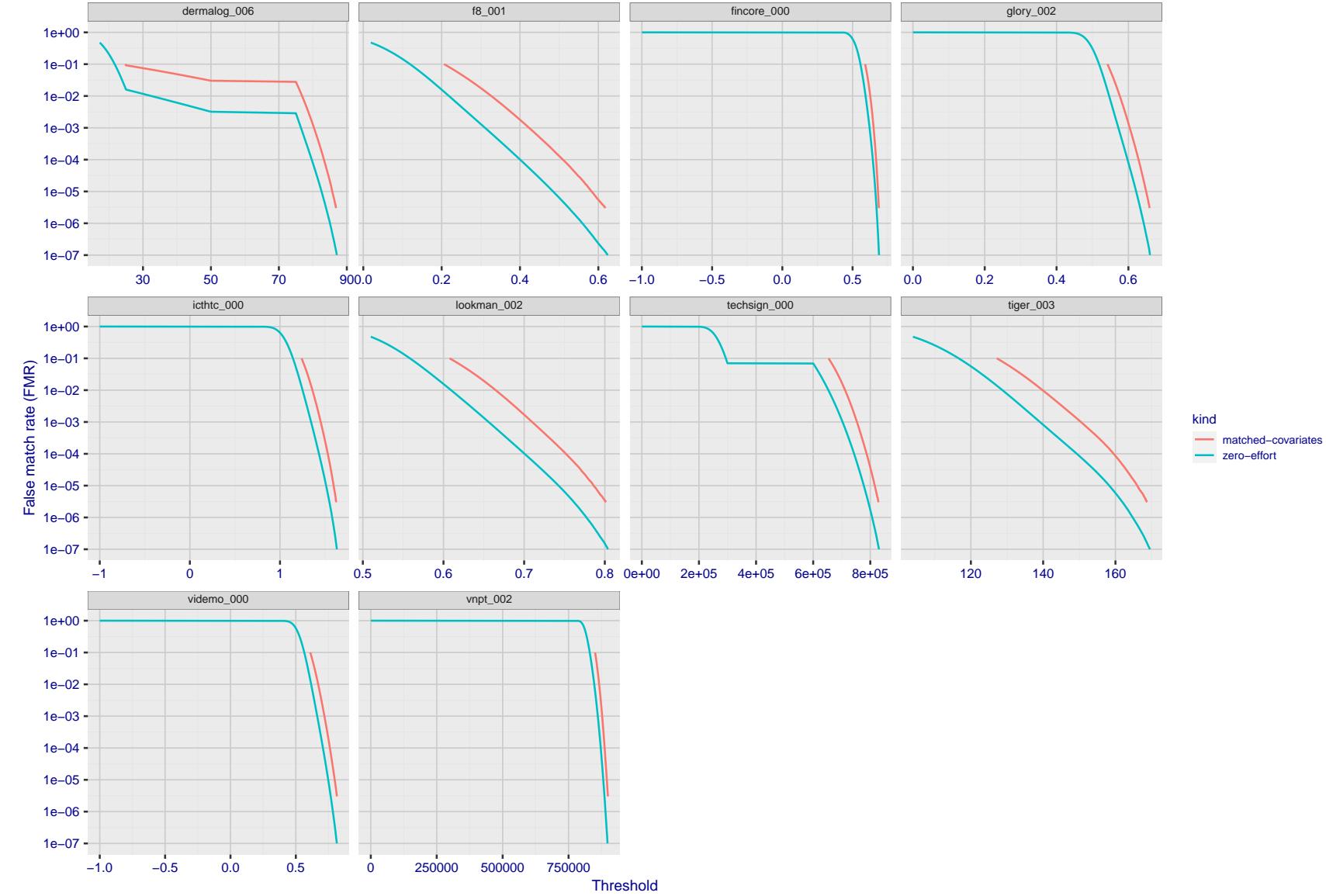


Figure 199: For the visa images, the false match calibration curves show FMR vs. threshold,  $T$ . The blue (lower) curves are for zero-effort impostors (i.e. comparing all images against all). The red (upper) curves are for persons of the same-sex, same-age, and same national-origin. This shows that FMR is underestimated (by a factor of 10 or more) by using a zero-effort impostor calculation to calibrate  $T$ . As shown later (sec. 3.6), FMR is higher for demographic-matched impostors.

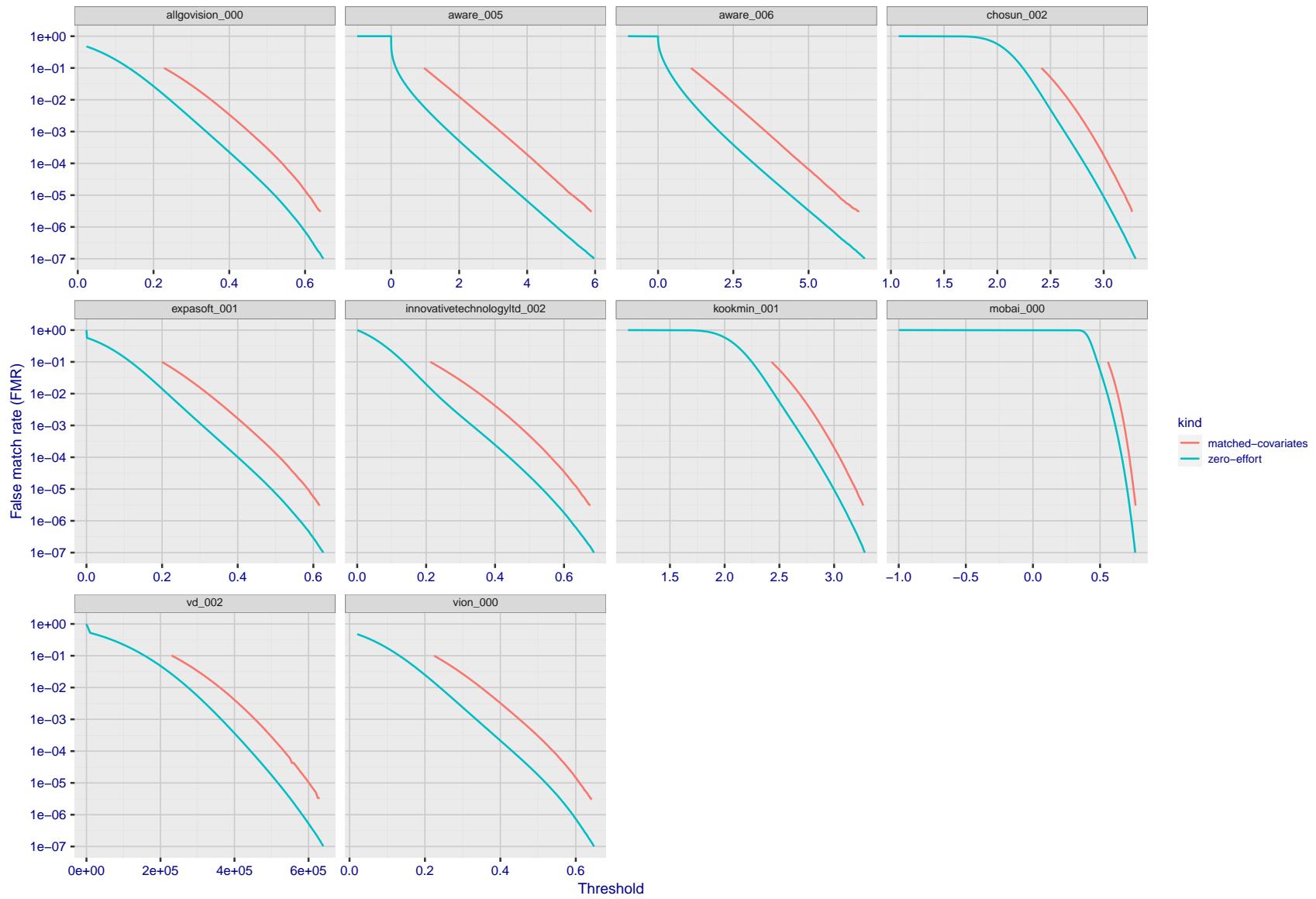


Figure 200: For the visa images, the false match calibration curves show FMR vs. threshold,  $T$ . The blue (lower) curves are for zero-effort impostors (i.e. comparing all images against all). The red (upper) curves are for persons of the same-sex, same-age, and same national-origin. This shows that FMR is underestimated (by a factor of 10 or more) by using a zero-effort impostor calculation to calibrate  $T$ . As shown later (sec. 3.6), FMR is higher for demographic-matched impostors.

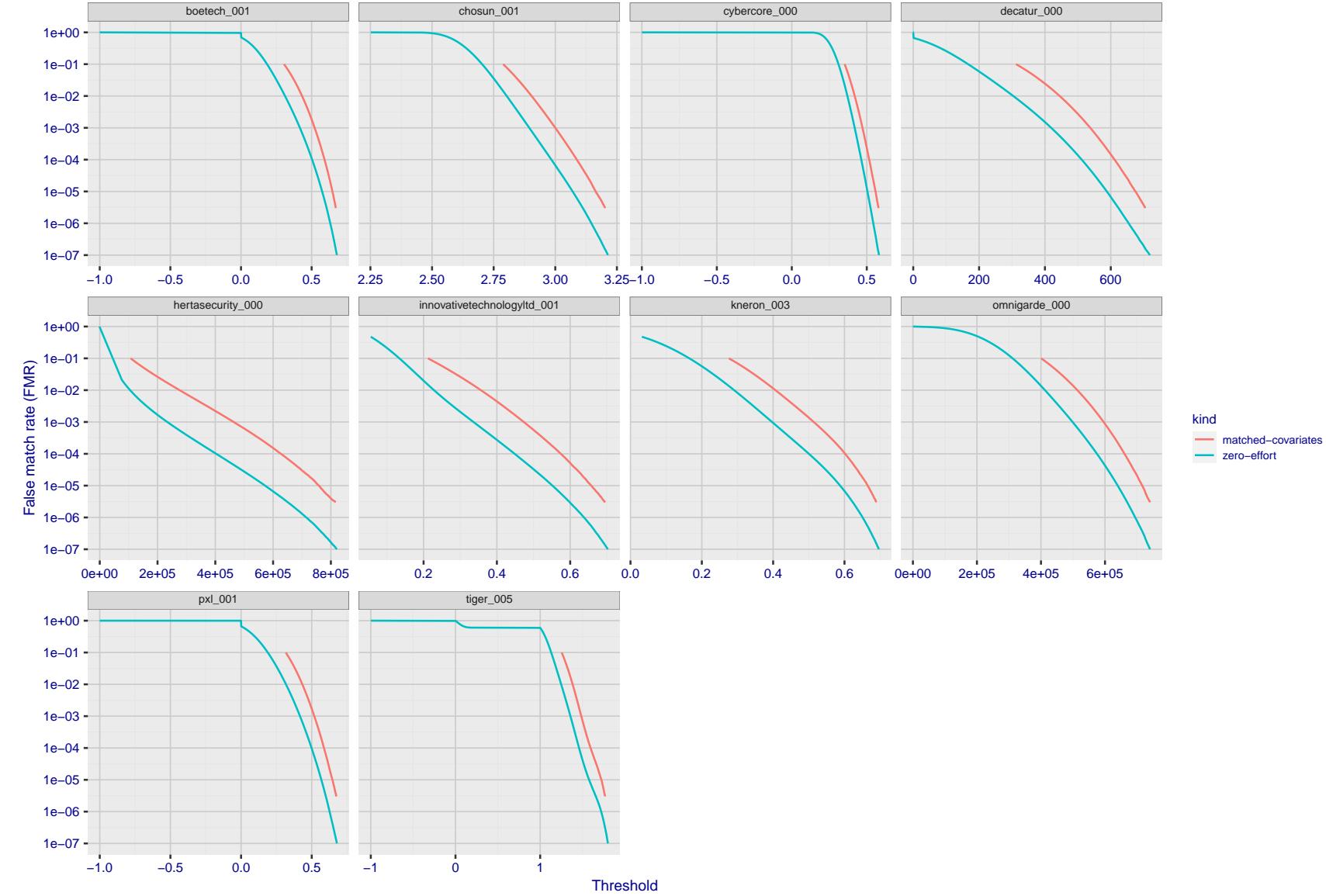


Figure 201: For the visa images, the false match calibration curves show FMR vs. threshold,  $T$ . The blue (lower) curves are for zero-effort impostors (i.e. comparing all images against all). The red (upper) curves are for persons of the same-sex, same-age, and same national-origin. This shows that FMR is underestimated (by a factor of 10 or more) by using a zero-effort impostor calculation to calibrate  $T$ . As shown later (sec. 3.6), FMR is higher for demographic-matched impostors.

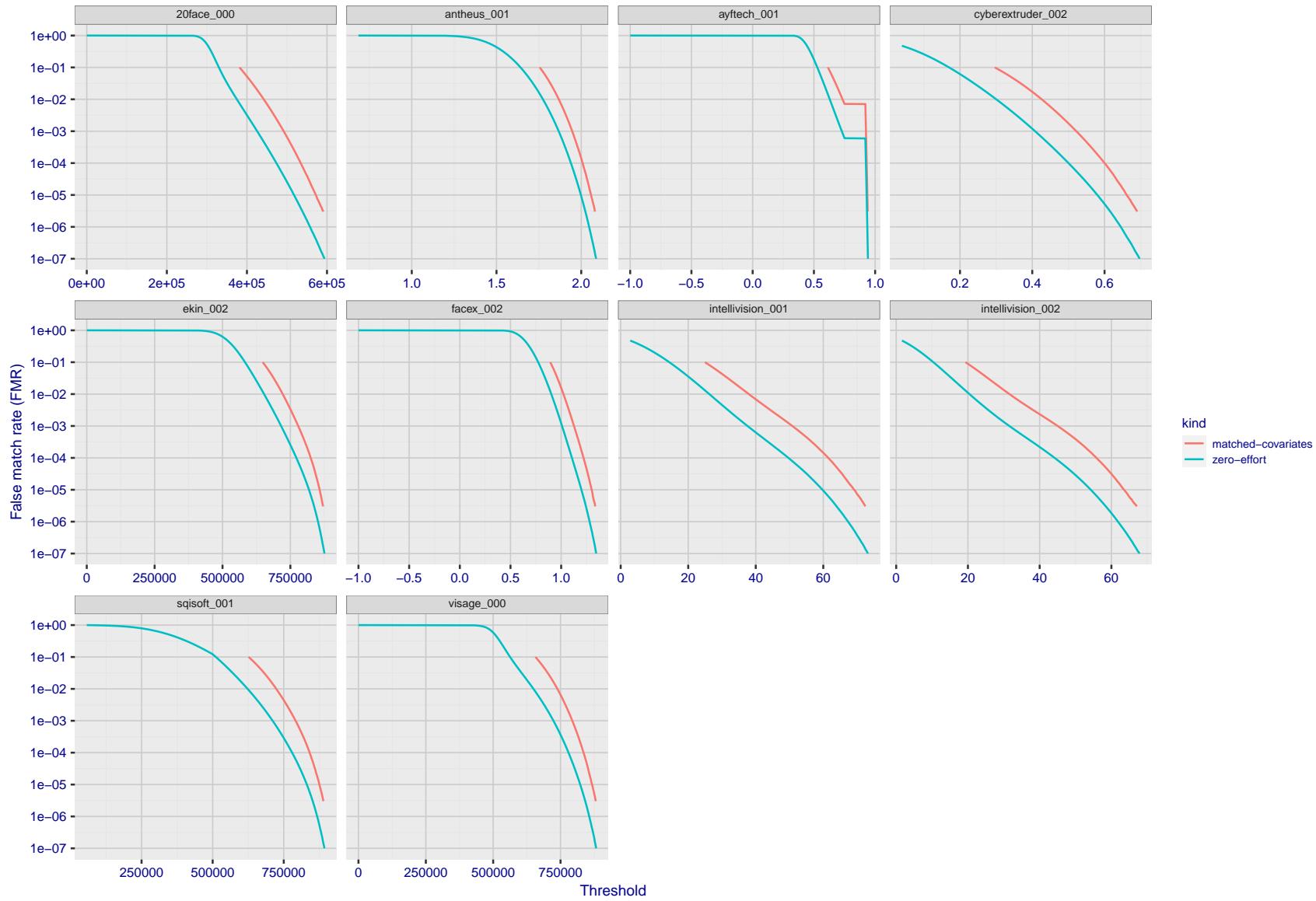


Figure 202: For the visa images, the false match calibration curves show FMR vs. threshold,  $T$ . The blue (lower) curves are for zero-effort impostors (i.e. comparing all images against all). The red (upper) curves are for persons of the same-sex, same-age, and same national-origin. This shows that FMR is underestimated (by a factor of 10 or more) by using a zero-effort impostor calculation to calibrate  $T$ . As shown later (sec. 3.6), FMR is higher for demographic-matched impostors.

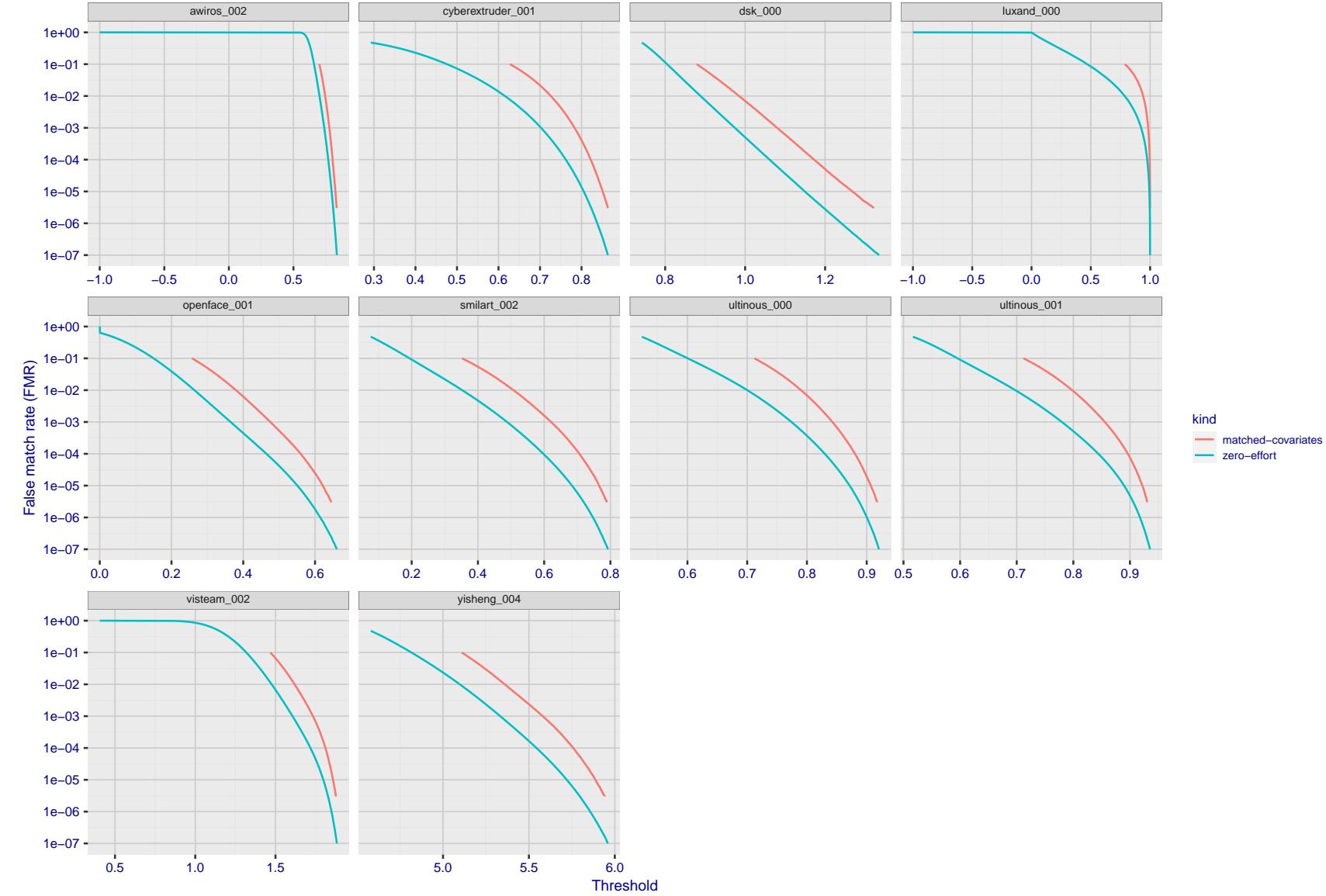


Figure 203: For the visa images, the false match calibration curves show FMR vs. threshold,  $T$ . The blue (lower) curves are for zero-effort impostors (i.e. comparing all images against all). The red (upper) curves are for persons of the same-sex, same-age, and same national-origin. This shows that FMR is underestimated (by a factor of 10 or more) by using a zero-effort impostor calculation to calibrate  $T$ . As shown later (sec. 3.6), FMR is higher for demographic-matched impostors.

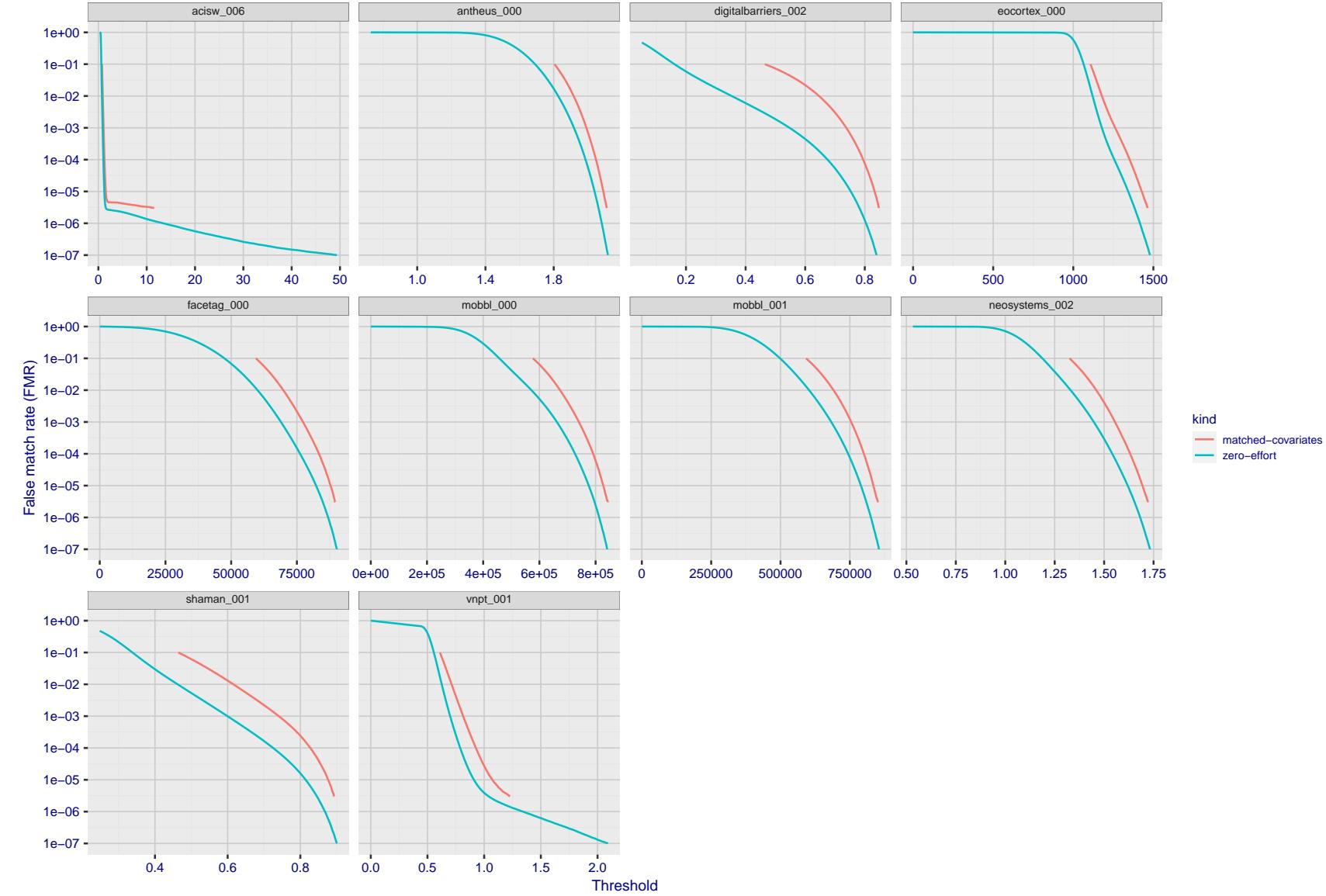


Figure 204: For the visa images, the false match calibration curves show FMR vs. threshold,  $T$ . The blue (lower) curves are for zero-effort impostors (i.e. comparing all images against all). The red (upper) curves are for persons of the same-sex, same-age, and same national-origin. This shows that FMR is underestimated (by a factor of 10 or more) by using a zero-effort impostor calculation to calibrate  $T$ . As shown later (sec. 3.6), FMR is higher for demographic-matched impostors.

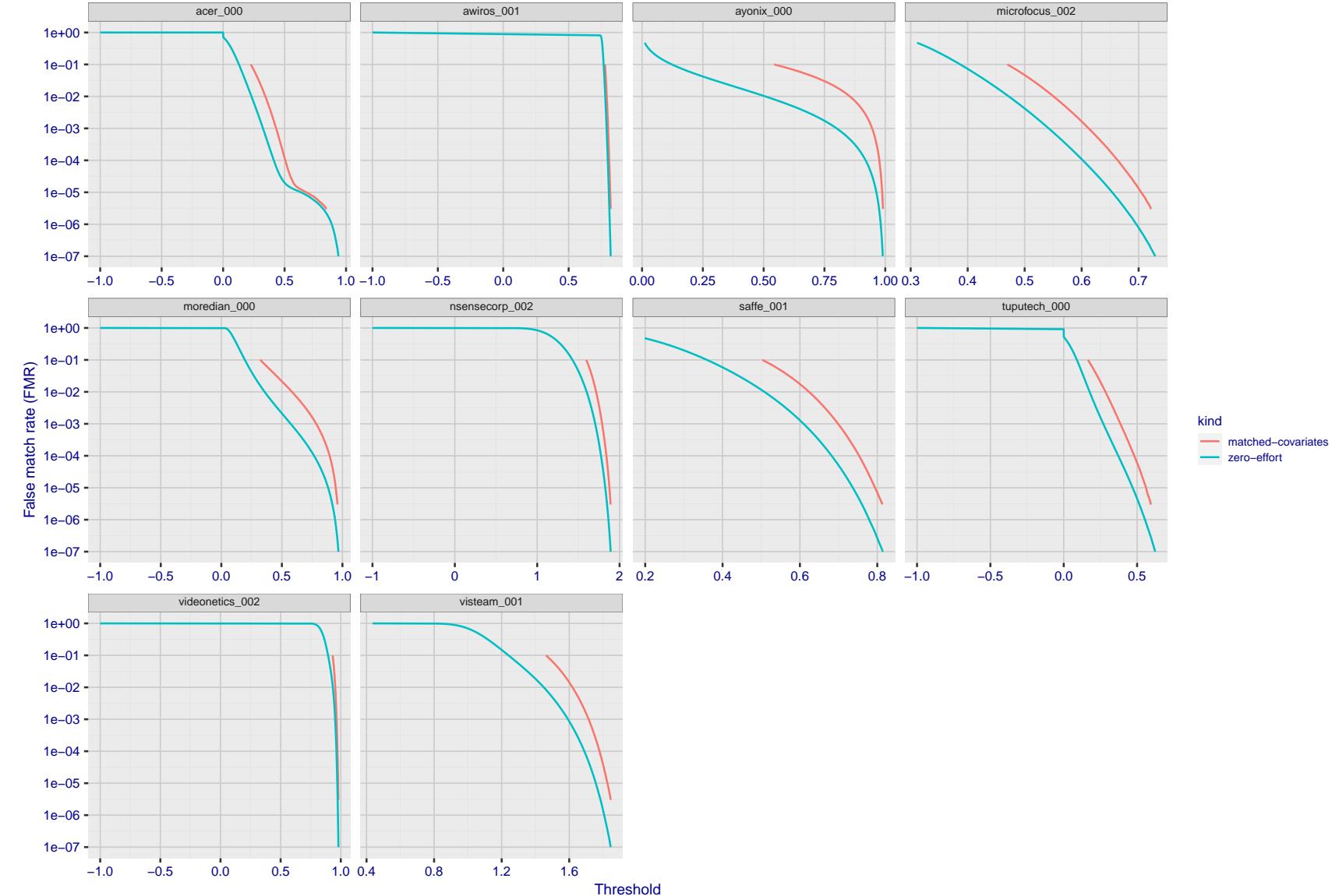


Figure 205: For the visa images, the false match calibration curves show FMR vs. threshold,  $T$ . The blue (lower) curves are for zero-effort impostors (i.e. comparing all images against all). The red (upper) curves are for persons of the same-sex, same-age, and same national-origin. This shows that FMR is underestimated (by a factor of 10 or more) by using a zero-effort impostor calculation to calibrate  $T$ . As shown later (sec. 3.6), FMR is higher for demographic-matched impostors.

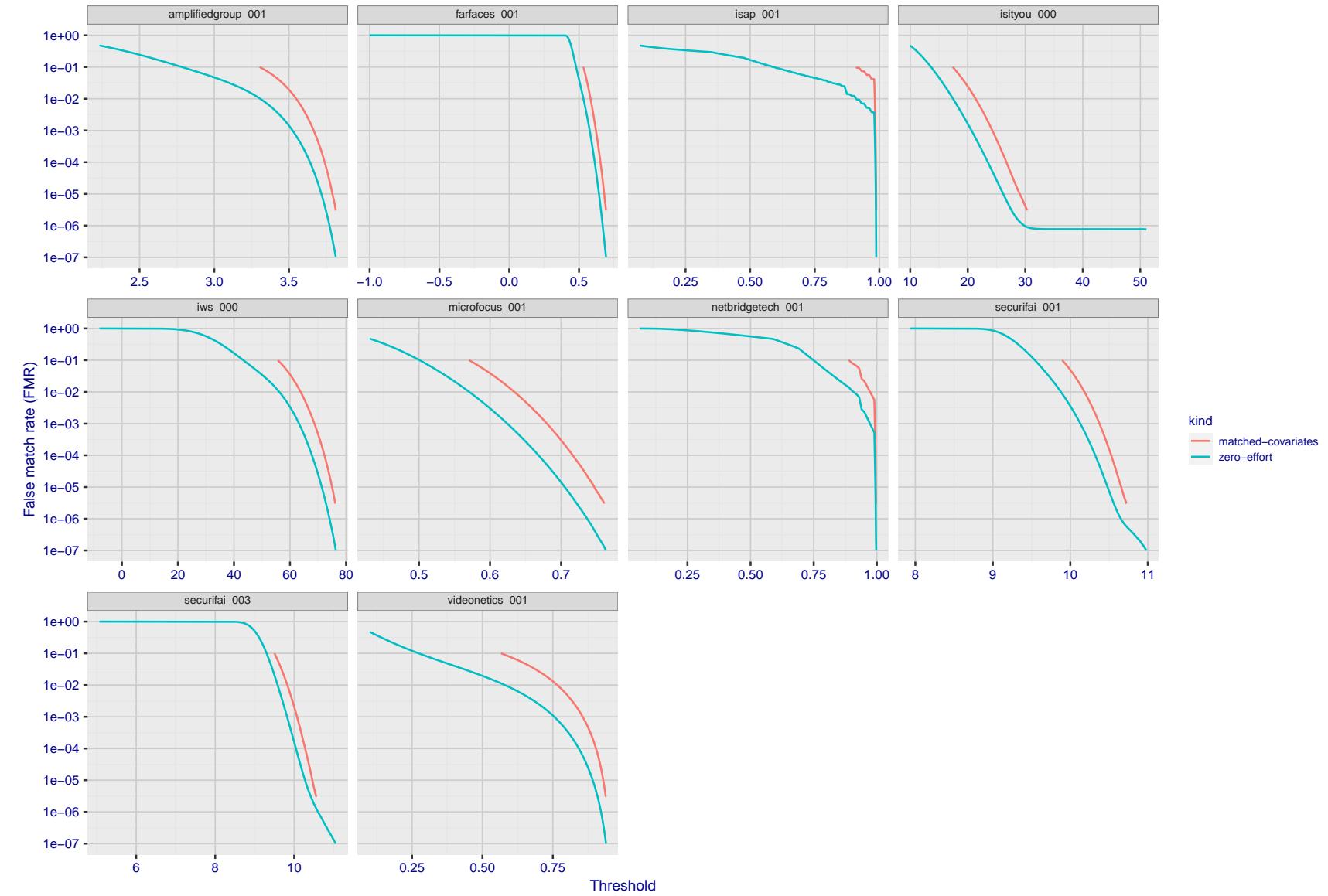


Figure 206: For the visa images, the false match calibration curves show FMR vs. threshold,  $T$ . The blue (lower) curves are for zero-effort impostors (i.e. comparing all images against all). The red (upper) curves are for persons of the same-sex, same-age, and same national-origin. This shows that FMR is underestimated (by a factor of 10 or more) by using a zero-effort impostor calculation to calibrate  $T$ . As shown later (sec. 3.6), FMR is higher for demographic-matched impostors.

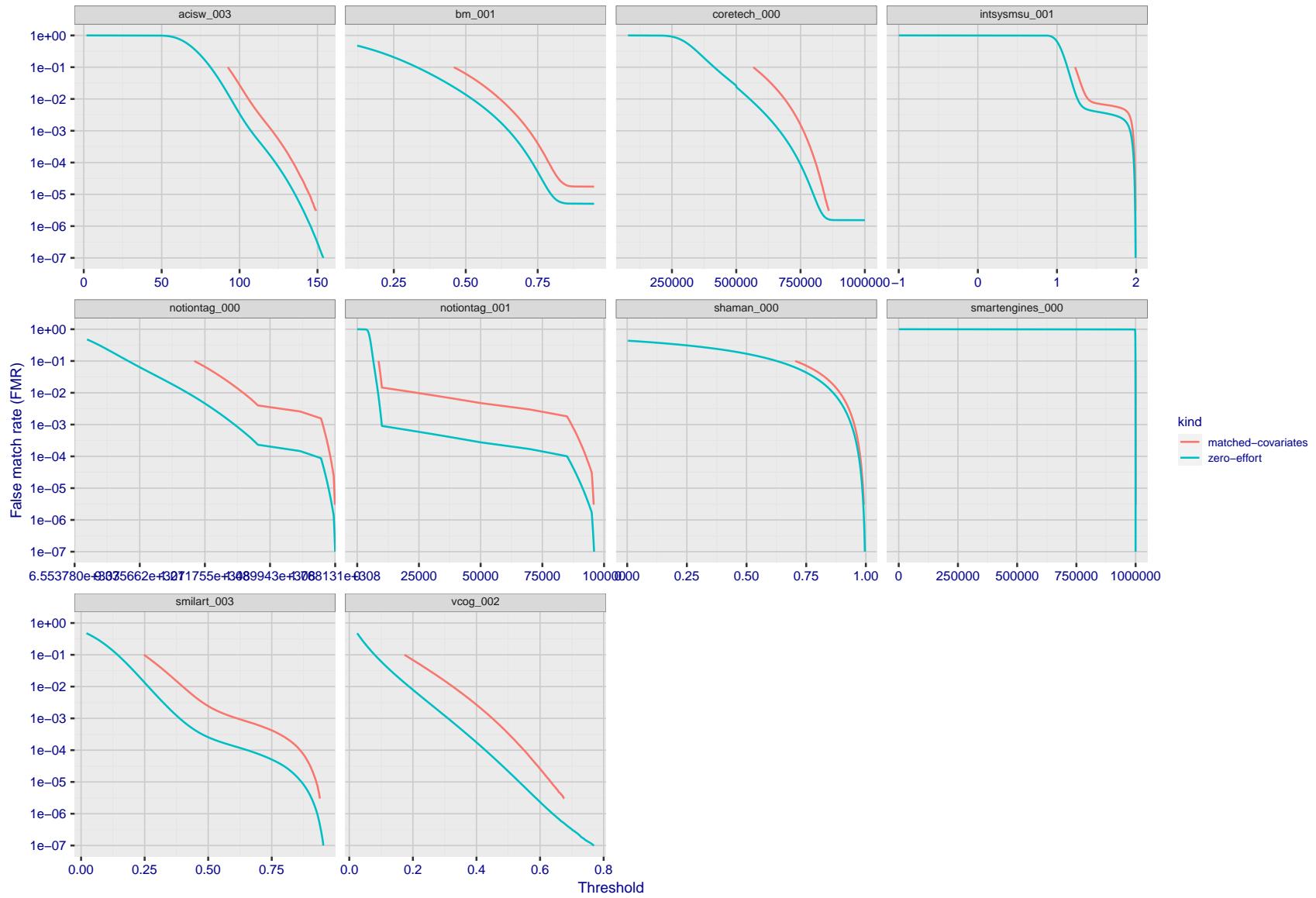


Figure 207: For the visa images, the false match calibration curves show FMR vs. threshold,  $T$ . The blue (lower) curves are for zero-effort impostors (i.e. comparing all images against all). The red (upper) curves are for persons of the same-sex, same-age, and same national-origin. This shows that FMR is underestimated (by a factor of 10 or more) by using a zero-effort impostor calculation to calibrate  $T$ . As shown later (sec. 3.6), FMR is higher for demographic-matched impostors.

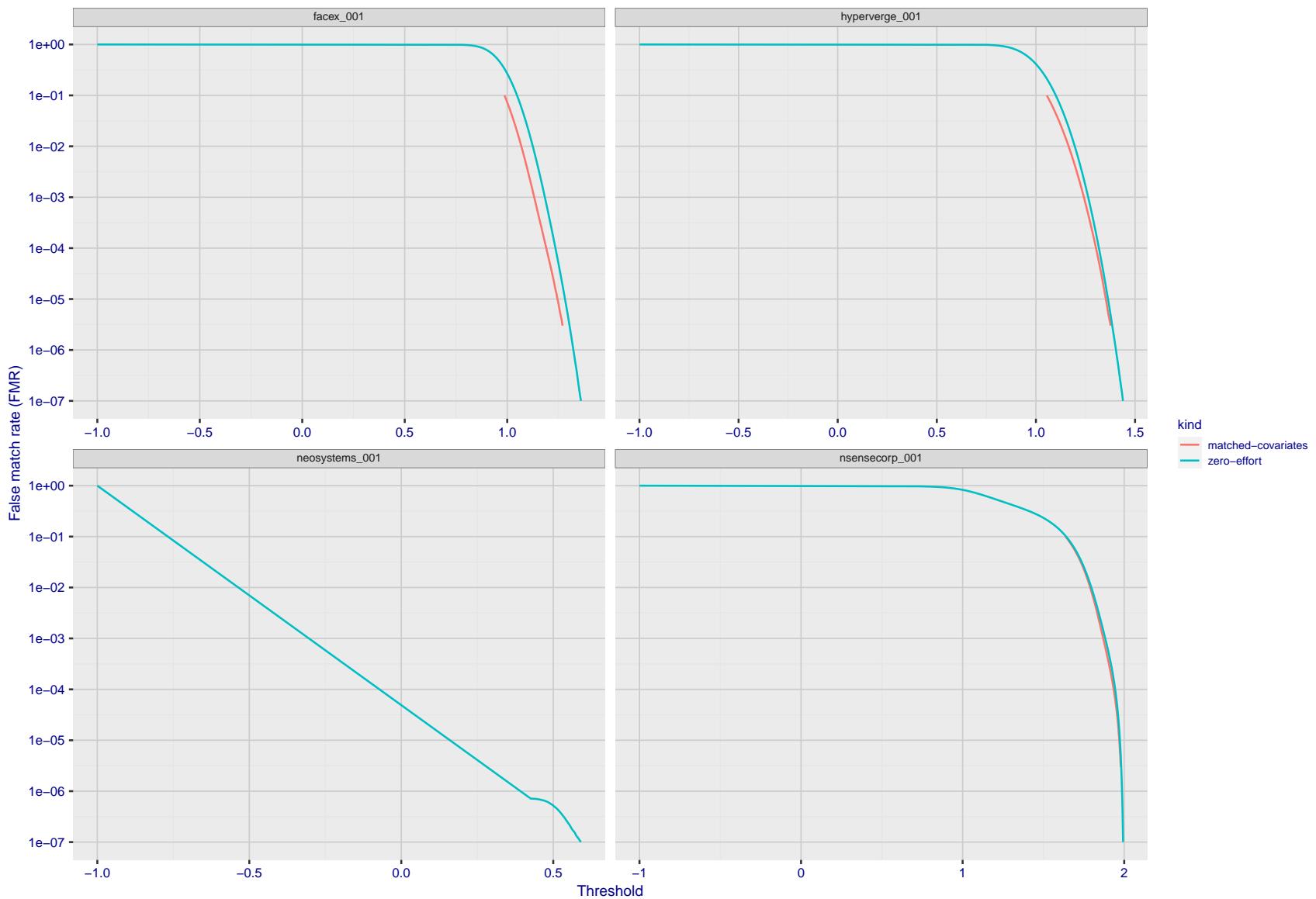


Figure 208: For the visa images, the false match calibration curves show FMR vs. threshold,  $T$ . The blue (lower) curves are for zero-effort impostors (i.e. comparing all images against all). The red (upper) curves are for persons of the same-sex, same-age, and same national-origin. This shows that FMR is underestimated (by a factor of 10 or more) by using a zero-effort impostor calculation to calibrate  $T$ . As shown later (sec. 3.6), FMR is higher for demographic-matched impostors.

## 3.5 Genuine distribution stability

### 3.5.1 Effect of birth place on the genuine distribution

**Background:** Both skin tone and bone structure vary geographically. Prior studies have reported variations in FNMR and FMR.

**Goal:** To measure false non-match rate (FNMR) variation with country of birth.

**Methods:** Thresholds are determined that give  $FMR = \{0.001, 0.0001\}$  over the entire impostor set. Then FNMR is measured over 1000 bootstrap replications of the genuine scores. Only those countries with at least 140 individuals are included in the analysis.

**Results:** Figure 237 shows FNMR by country of birth for the two thresholds.

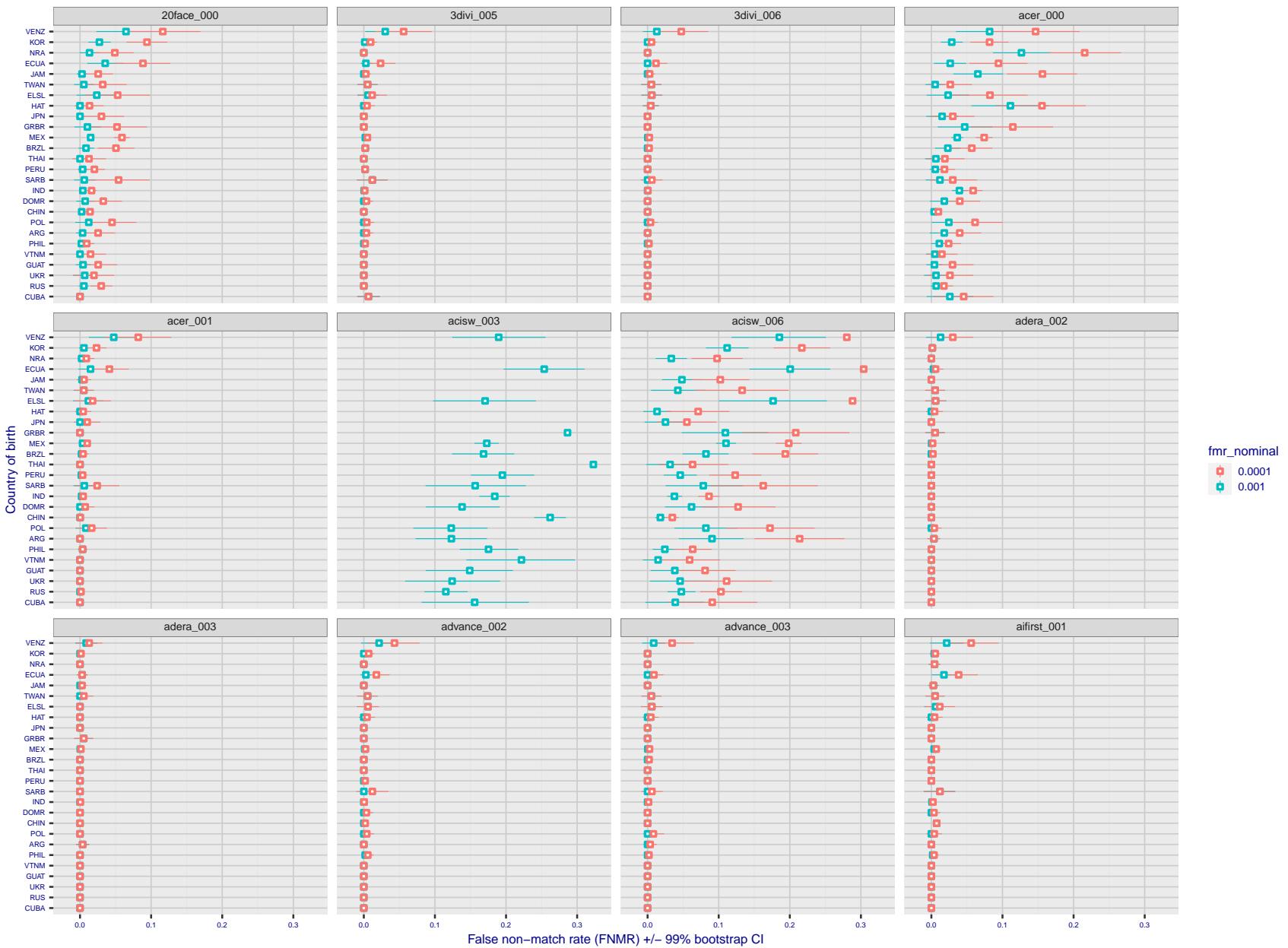


Figure 209: For the visa images, the dots show FNMR by country of birth for two globally set operating thresholds corresponding to  $FMR = \{0.001, 0.0001\}$  computed over all on the order of  $10^{10}$  impostor scores. The FMR in each bin will vary also - see subsequent impostor heatmaps in sec. 3.6.1. The figures shows an order of magnitude variation in FNMR across country of birth; these effects are likely due quality variations, then demographics like age and race. The error rates in some cases are zero, and in others the DET is flat so the error rates at the two thresholds are identical. The lines span 1% and 99% of bootstrap replicated FNMR estimates.

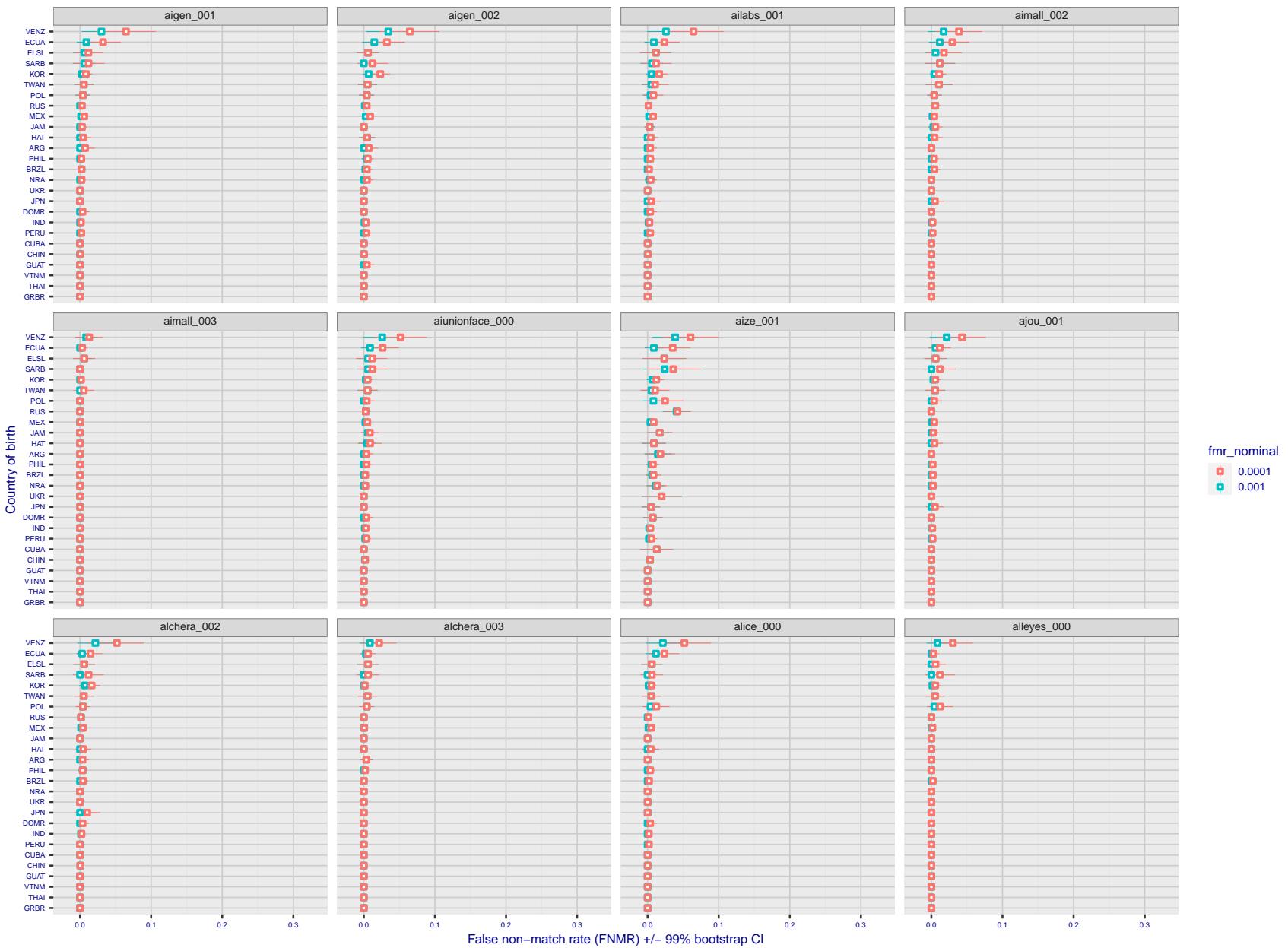


Figure 210: For the visa images, the dots show FNMR by country of birth for two globally set operating thresholds corresponding to  $FMR = \{0.001, 0.0001\}$  computed over all on the order of  $10^{10}$  impostor scores. The FMR in each bin will vary also - see subsequent impostor heatmaps in sec. 3.6.1. The figures shows an order of magnitude variation in FNMR across country of birth; these effects are likely due quality variations, then demographics like age and race. The error rates in some cases are zero, and in others the DET is flat so the error rates at the two thresholds are identical. The lines span 1% and 99% of bootstrap replicated FNMR estimates.

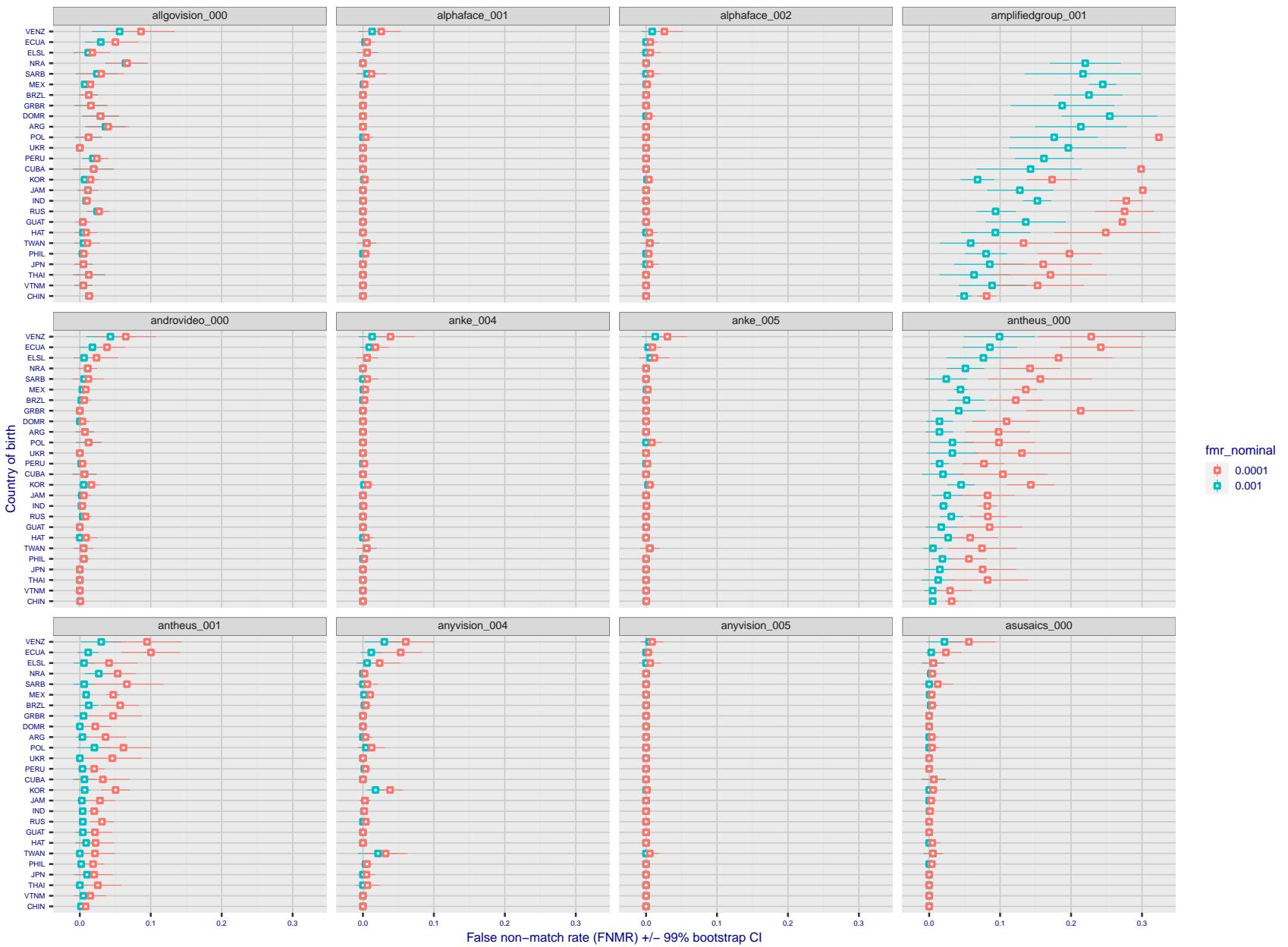


Figure 211: For the visa images, the dots show FNMR by country of birth for two globally set operating thresholds corresponding to  $FMR = \{0.001, 0.0001\}$  computed over all on the order of  $10^{10}$  impostor scores. The FMR in each bin will vary also - see subsequent impostor heatmaps in sec. 3.6.1. The figures shows an order of magnitude variation in FNMR across country of birth; these effects are likely due quality variations, then demographics like age and race. The error rates in some cases are zero, and in others the DET is flat so the error rates at the two thresholds are identical. The lines span 1% and 99% of bootstrap replicated FNMR estimates.

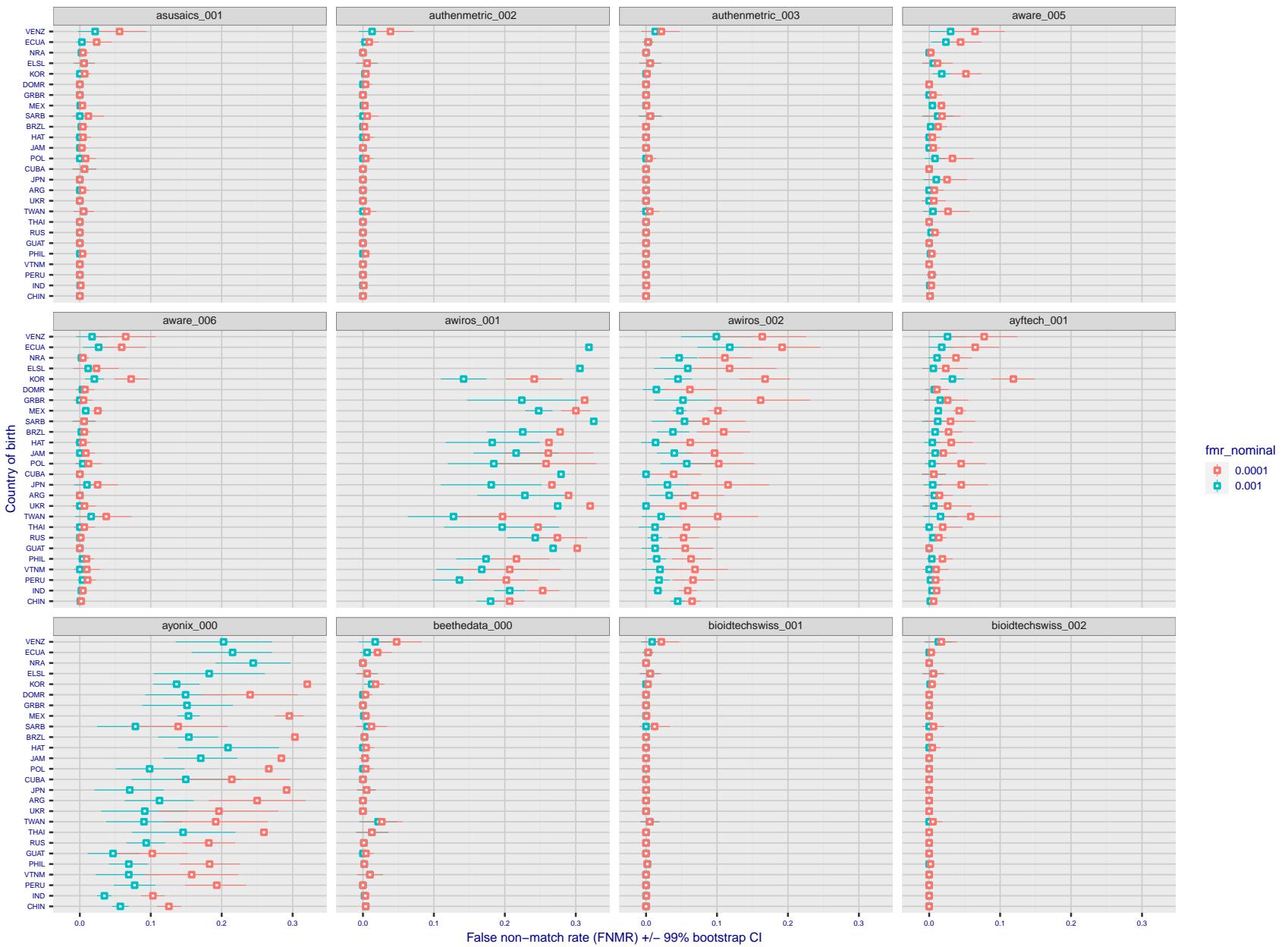


Figure 212: For the visa images, the dots show FNMR by country of birth for two globally set operating thresholds corresponding to  $FMR = \{0.001, 0.0001\}$  computed over all on the order of  $10^{10}$  impostor scores. The FMR in each bin will vary also - see subsequent impostor heatmaps in sec. 3.6.1. The figures shows an order of magnitude variation in FNMR across country of birth; these effects are likely due quality variations, then demographics like age and race. The error rates in some cases are zero, and in others the DET is flat so the error rates at the two thresholds are identical. The lines span 1% and 99% of bootstrap replicated FNMR estimates.

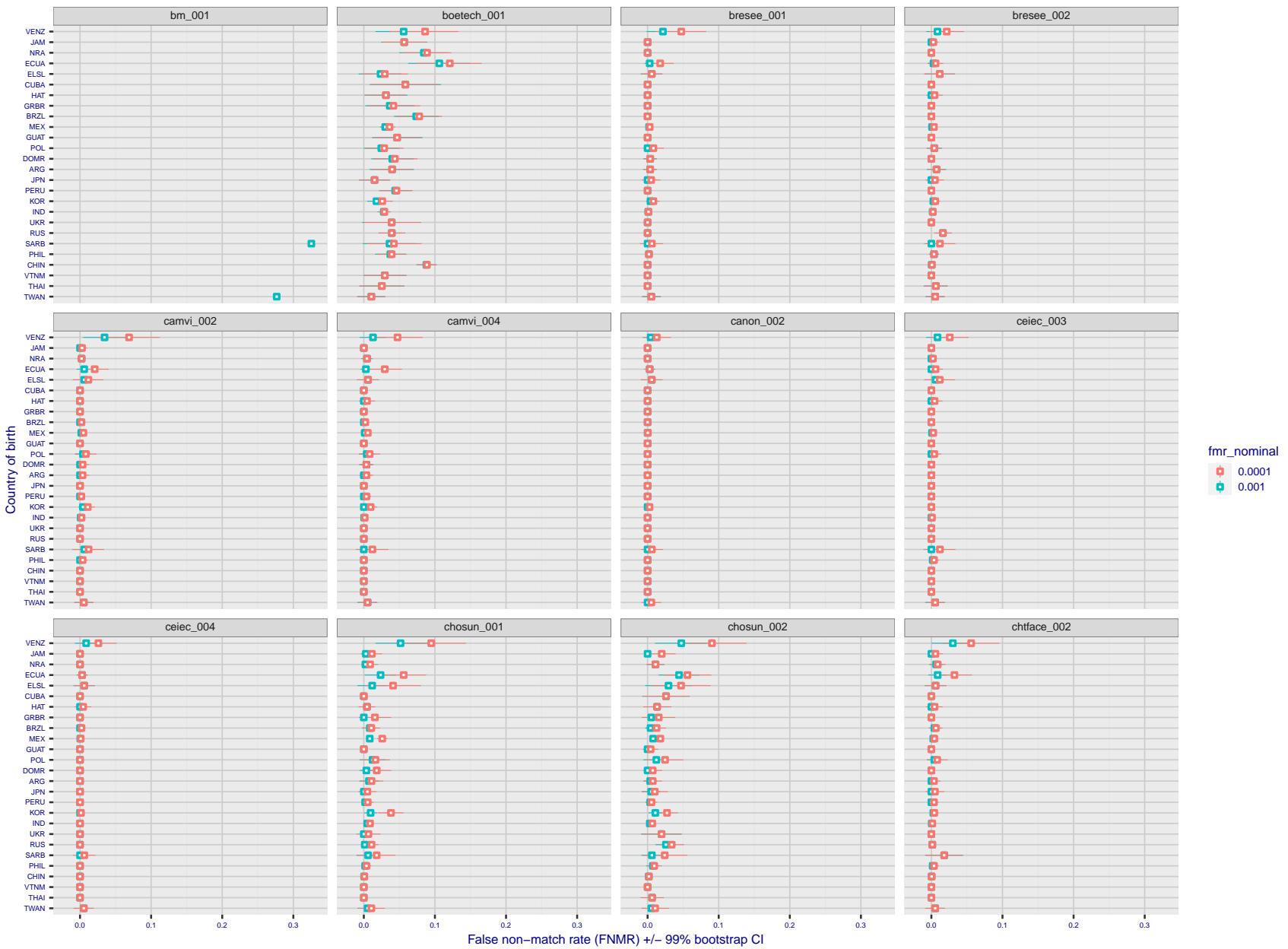


Figure 213: For the visa images, the dots show FNMR by country of birth for two globally set operating thresholds corresponding to  $FMR = \{0.001, 0.0001\}$  computed over all on the order of  $10^{10}$  impostor scores. The FMR in each bin will vary also - see subsequent impostor heatmaps in sec. 3.6.1. The figures shows an order of magnitude variation in FNMR across country of birth; these effects are likely due quality variations, then demographics like age and race. The error rates in some cases are zero, and in others the DET is flat so the error rates at the two thresholds are identical. The lines span 1% and 99% of bootstrap replicated FNMR estimates.

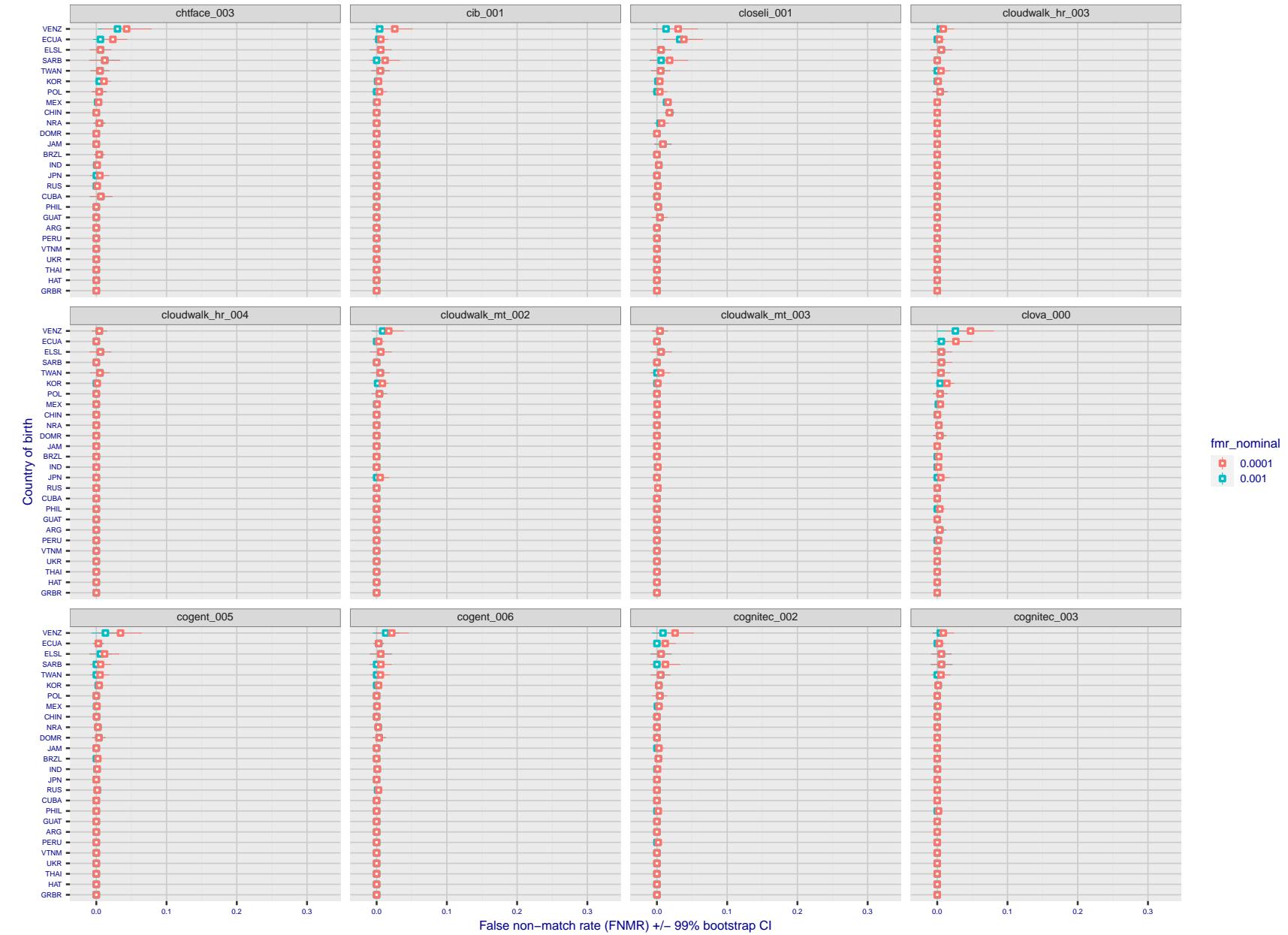


Figure 214: For the visa images, the dots show FNMR by country of birth for two globally set operating thresholds corresponding to  $FMR = \{0.001, 0.0001\}$  computed over all on the order of  $10^{10}$  impostor scores. The FMR in each bin will vary also - see subsequent impostor heatmaps in sec. 3.6.1. The figures shows an order of magnitude variation in FNMR across country of birth; these effects are likely due quality variations, then demographics like age and race. The error rates in some cases are zero, and in others the DET is flat so the error rates at the two thresholds are identical. The lines span 1% and 99% of bootstrap replicated FNMR estimates.

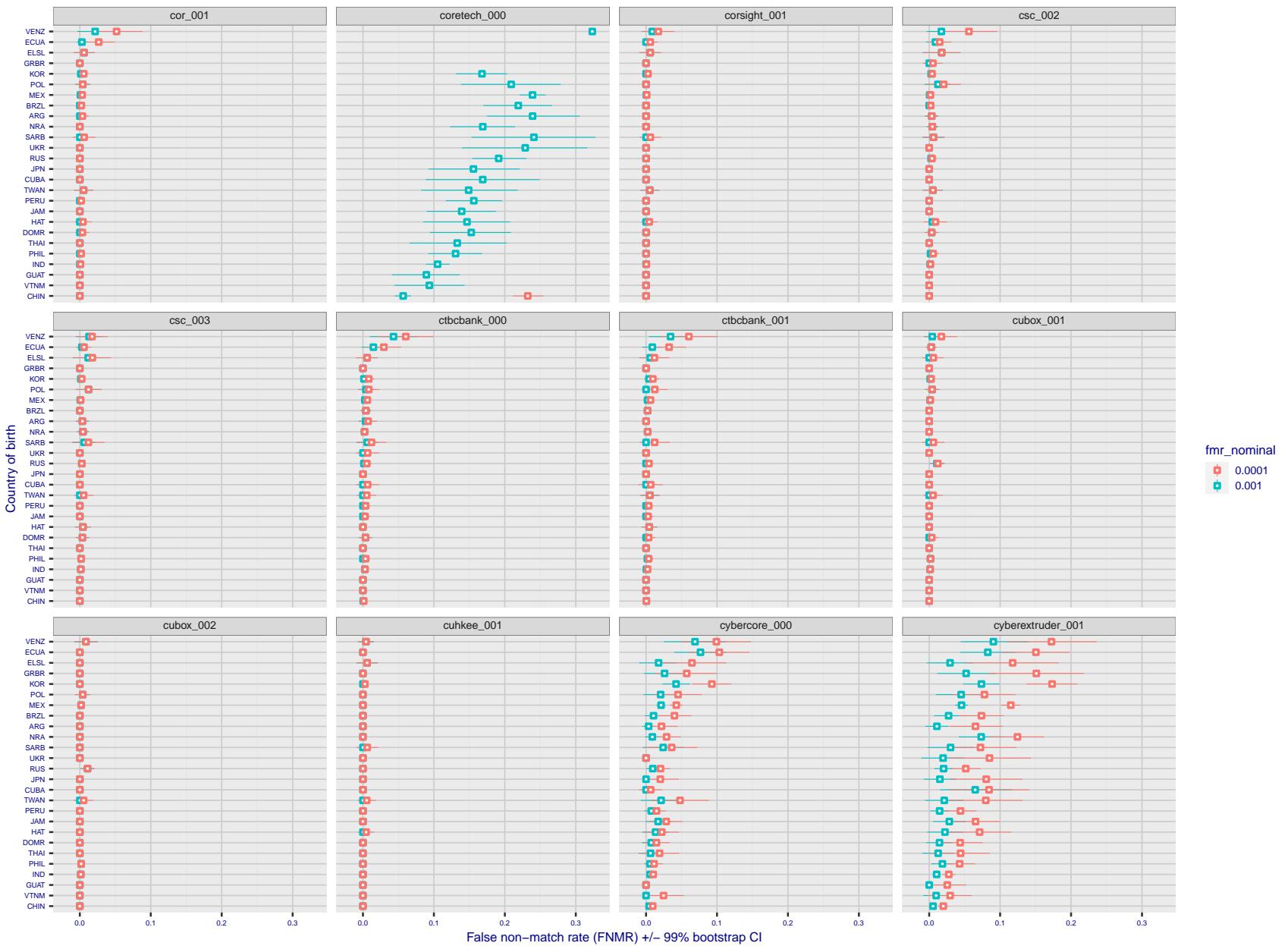


Figure 215: For the visa images, the dots show FNMR by country of birth for two globally set operating thresholds corresponding to  $FMR = \{0.001, 0.0001\}$  computed over all on the order of  $10^{10}$  impostor scores. The FMR in each bin will vary also - see subsequent impostor heatmaps in sec. 3.6.1. The figures shows an order of magnitude variation in FNMR across country of birth; these effects are likely due quality variations, then demographics like age and race. The error rates in some cases are zero, and in others the DET is flat so the error rates at the two thresholds are identical. The lines span 1% and 99% of bootstrap replicated FNMR estimates.

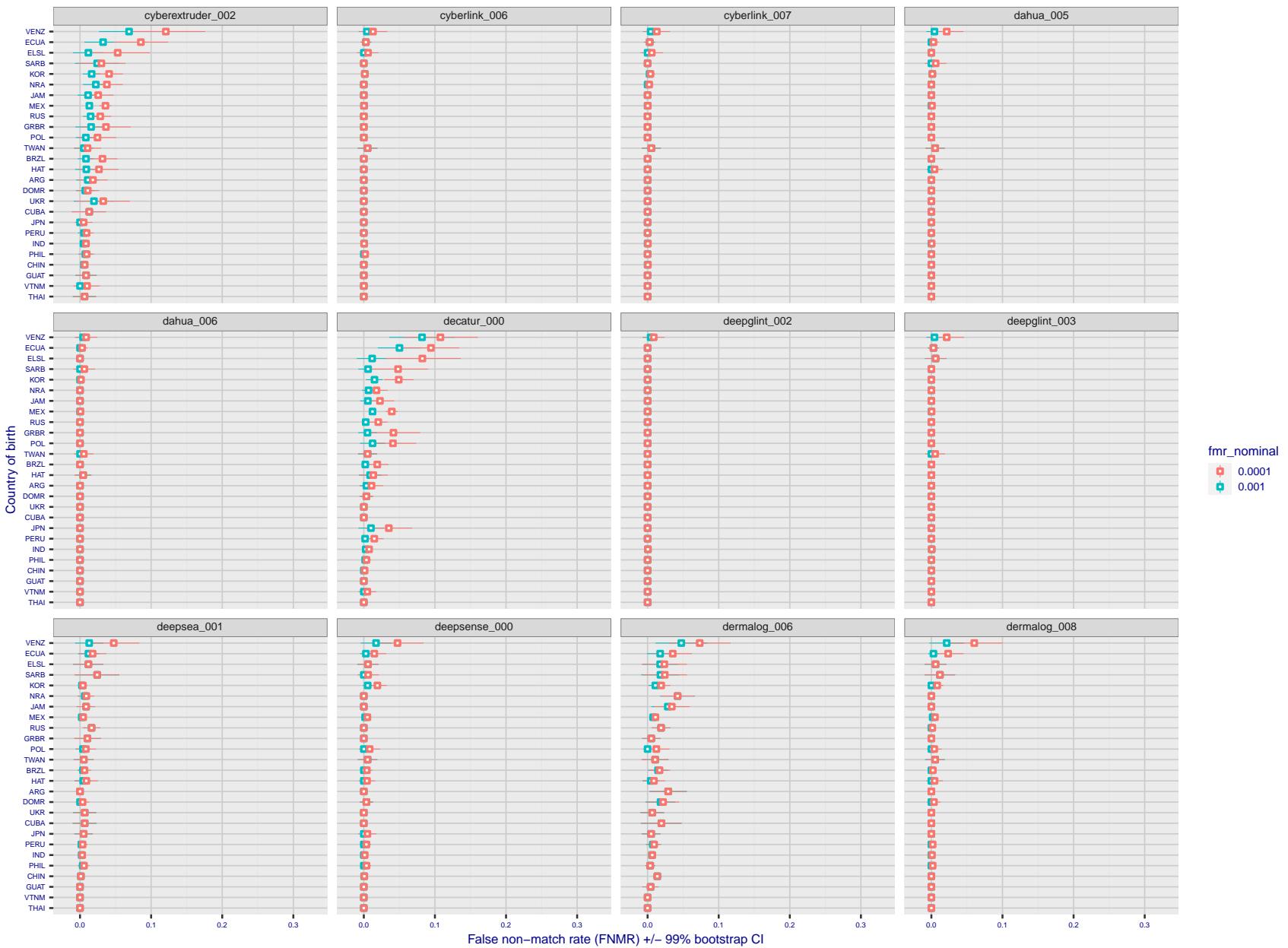


Figure 216: For the visa images, the dots show FNMR by country of birth for two globally set operating thresholds corresponding to  $FMR = \{0.001, 0.0001\}$  computed over all on the order of  $10^{10}$  impostor scores. The FMR in each bin will vary also - see subsequent impostor heatmaps in sec. 3.6.1. The figures shows an order of magnitude variation in FNMR across country of birth; these effects are likely due quality variations, then demographics like age and race. The error rates in some cases are zero, and in others the DET is flat so the error rates at the two thresholds are identical. The lines span 1% and 99% of bootstrap replicated FNMR estimates.

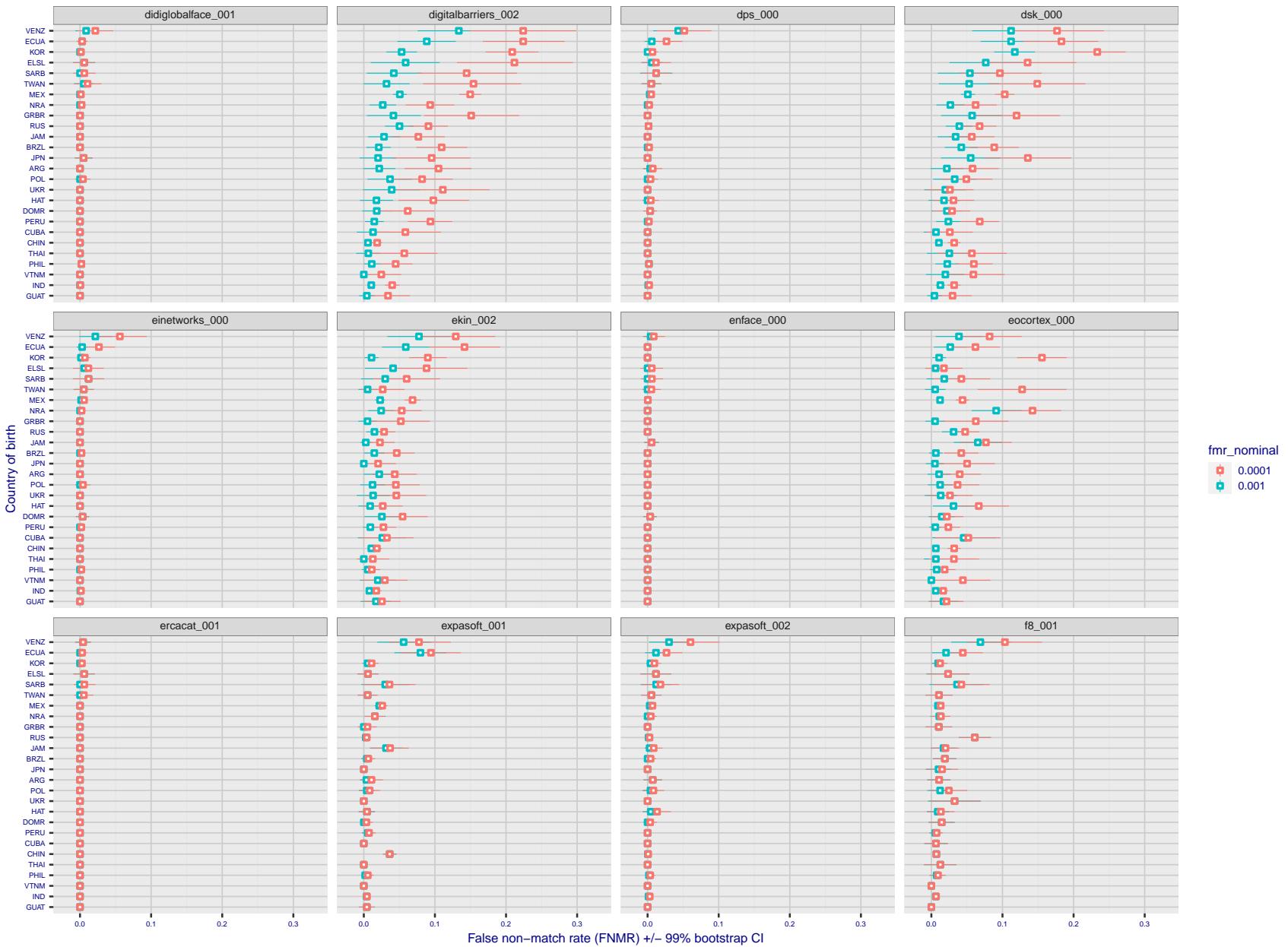


Figure 217: For the visa images, the dots show FNMR by country of birth for two globally set operating thresholds corresponding to  $FMR = \{0.001, 0.0001\}$  computed over all on the order of  $10^{10}$  impostor scores. The FMR in each bin will vary also - see subsequent impostor heatmaps in sec. 3.6.1. The figures shows an order of magnitude variation in FNMR across country of birth; these effects are likely due quality variations, then demographics like age and race. The error rates in some cases are zero, and in others the DET is flat so the error rates at the two thresholds are identical. The lines span 1% and 99% of bootstrap replicated FNMR estimates.

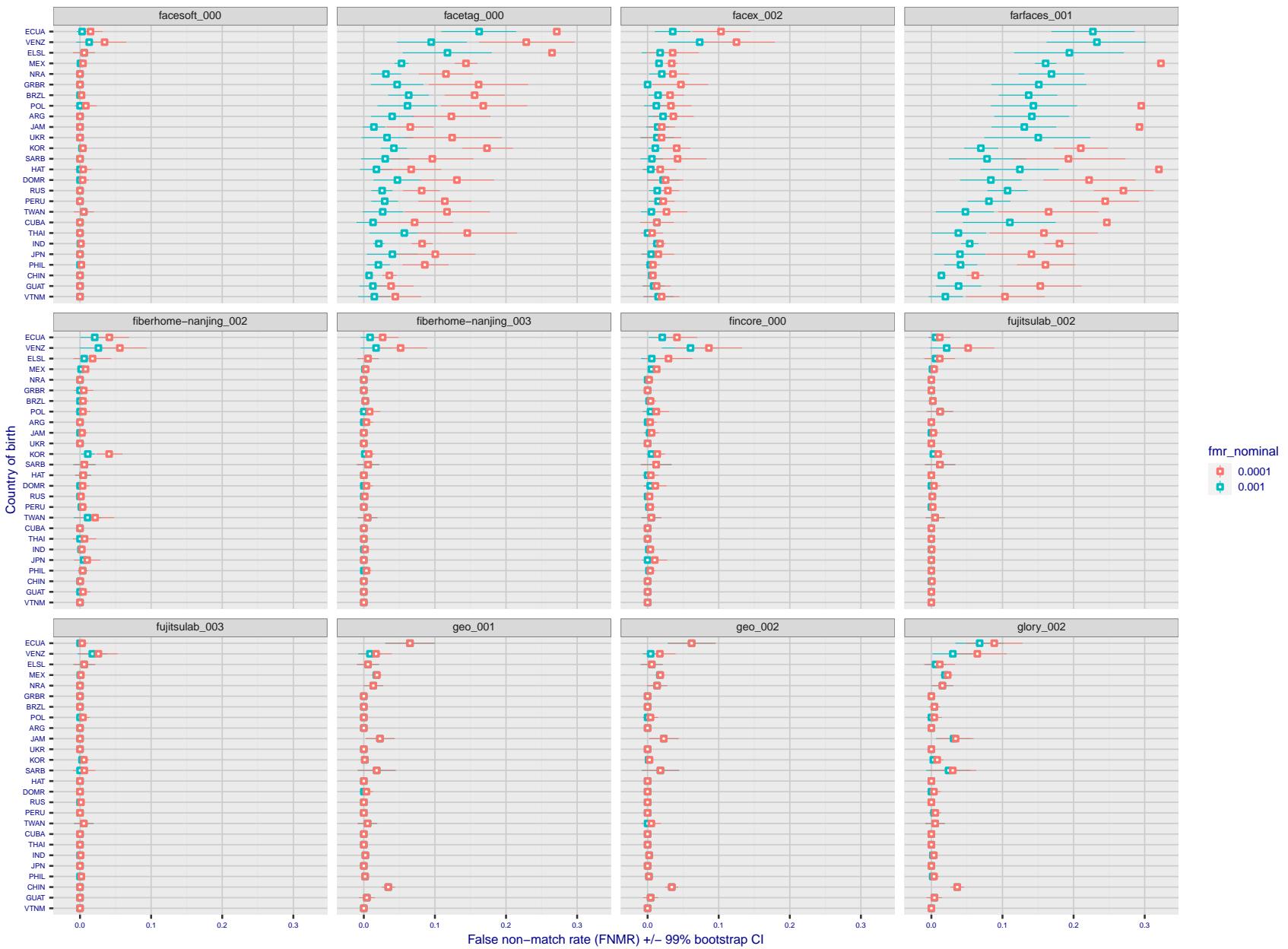


Figure 218: For the visa images, the dots show FNMR by country of birth for two globally set operating thresholds corresponding to  $FMR = \{0.001, 0.0001\}$  computed over all on the order of  $10^{10}$  impostor scores. The FMR in each bin will vary also - see subsequent impostor heatmaps in sec. 3.6.1. The figures shows an order of magnitude variation in FNMR across country of birth; these effects are likely due quality variations, then demographics like age and race. The error rates in some cases are zero, and in others the DET is flat so the error rates at the two thresholds are identical. The lines span 1% and 99% of bootstrap replicated FNMR estimates.

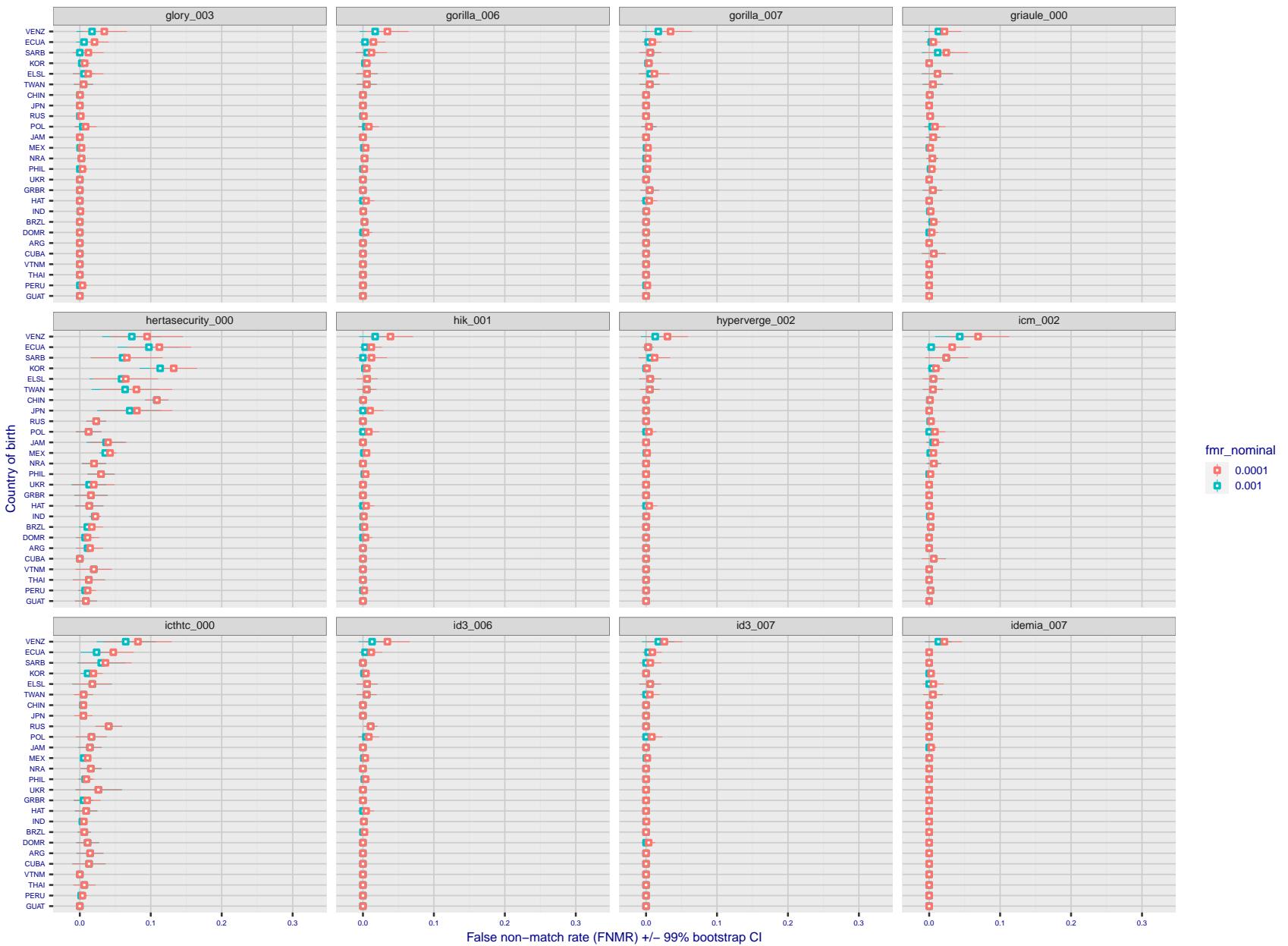


Figure 219: For the visa images, the dots show FNMR by country of birth for two globally set operating thresholds corresponding to  $FMR = \{0.001, 0.0001\}$  computed over all on the order of  $10^{10}$  impostor scores. The FMR in each bin will vary also - see subsequent impostor heatmaps in sec. 3.6.1. The figures shows an order of magnitude variation in FNMR across country of birth; these effects are likely due quality variations, then demographics like age and race. The error rates in some cases are zero, and in others the DET is flat so the error rates at the two thresholds are identical. The lines span 1% and 99% of bootstrap replicated FNMR estimates.

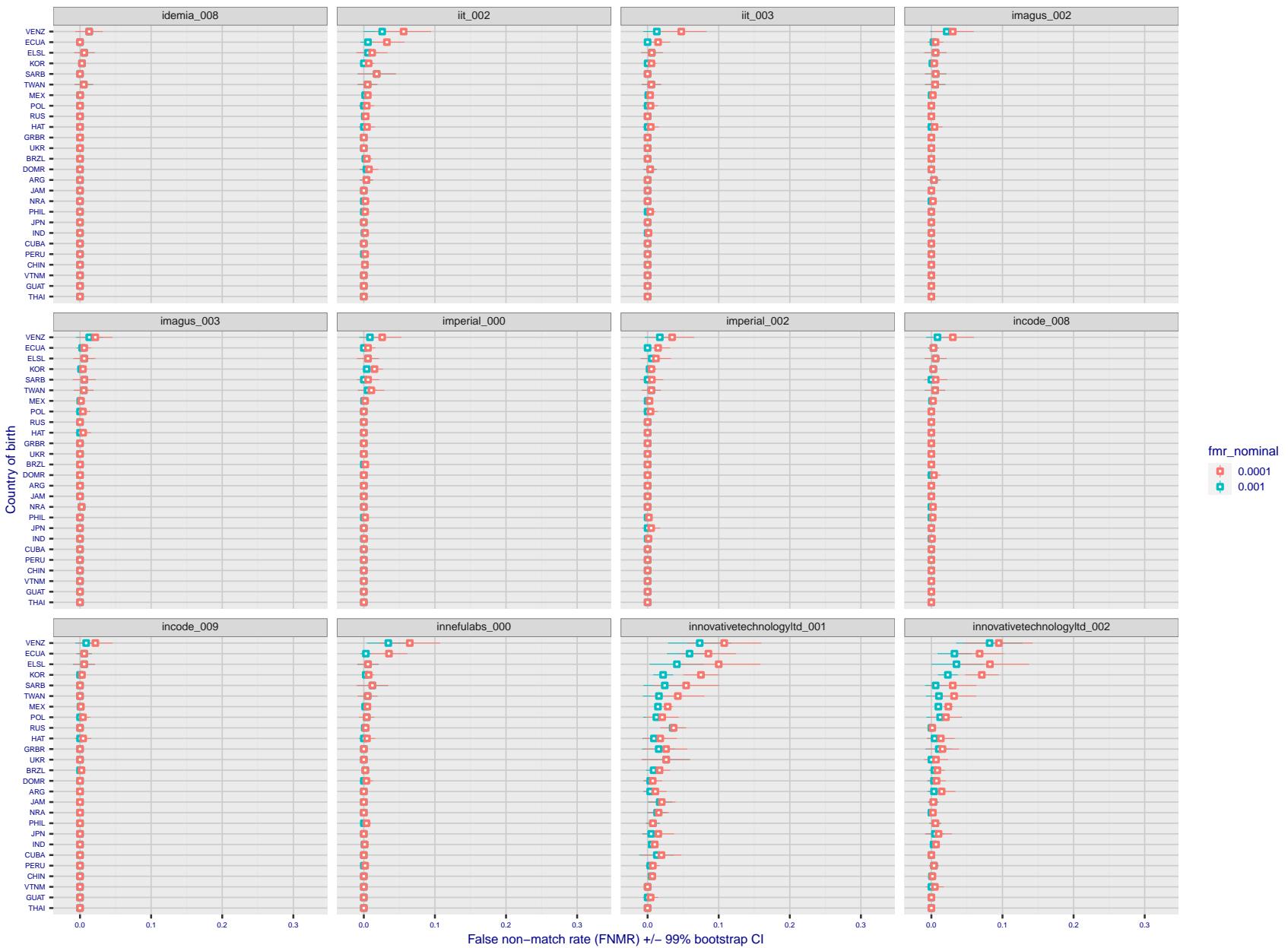


Figure 220: For the visa images, the dots show FNMR by country of birth for two globally set operating thresholds corresponding to  $FMR = \{0.001, 0.0001\}$  computed over all on the order of  $10^{10}$  impostor scores. The FMR in each bin will vary also - see subsequent impostor heatmaps in sec. 3.6.1. The figures shows an order of magnitude variation in FNMR across country of birth; these effects are likely due quality variations, then demographics like age and race. The error rates in some cases are zero, and in others the DET is flat so the error rates at the two thresholds are identical. The lines span 1% and 99% of bootstrap replicated FNMR estimates.

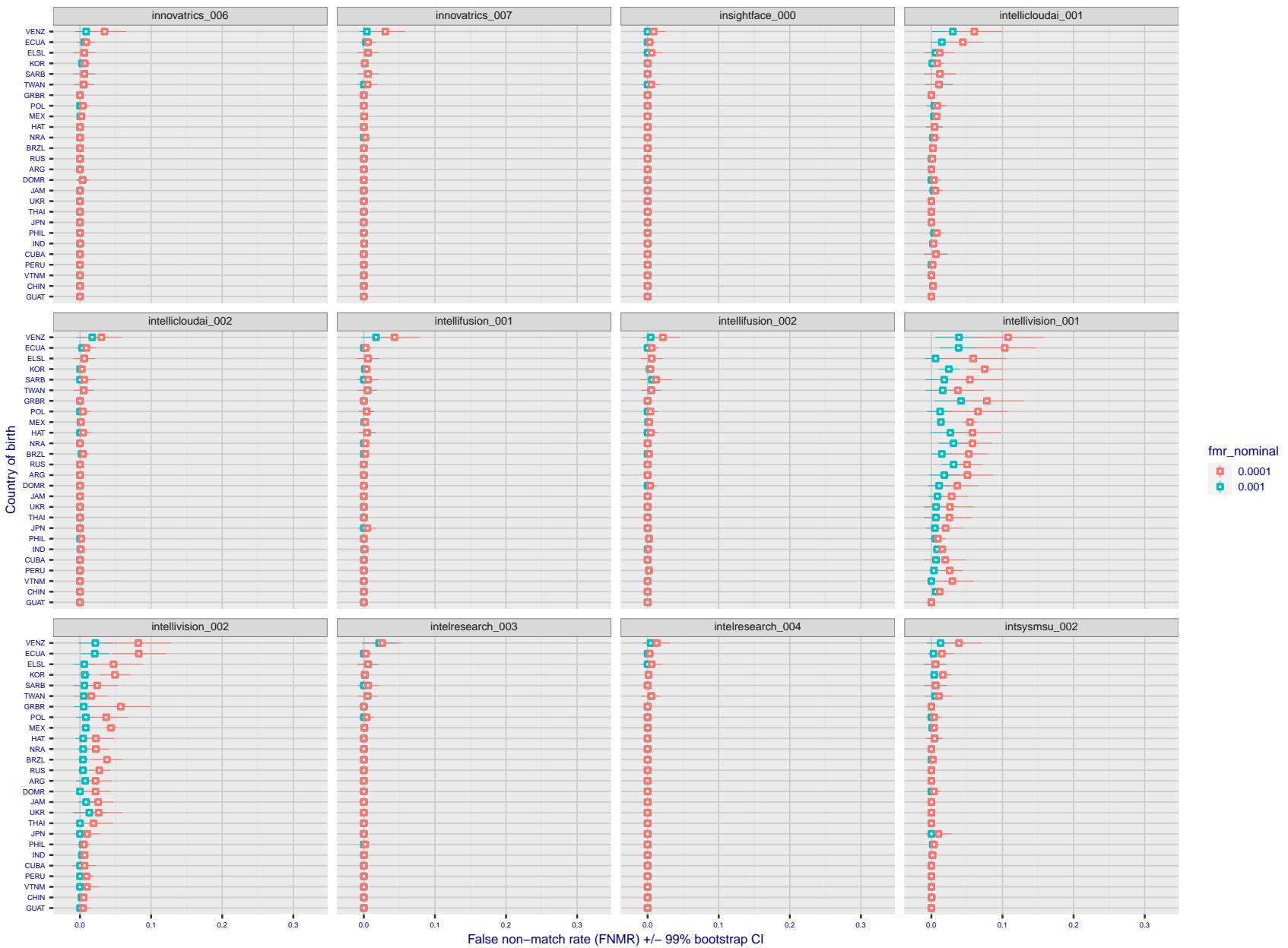


Figure 221: For the visa images, the dots show FNMR by country of birth for two globally set operating thresholds corresponding to  $FMR = \{0.001, 0.0001\}$  computed over all on the order of  $10^{10}$  impostor scores. The FMR in each bin will vary also - see subsequent impostor heatmaps in sec. 3.6.1. The figures shows an order of magnitude variation in FNMR across country of birth; these effects are likely due quality variations, then demographics like age and race. The error rates in some cases are zero, and in others the DET is flat so the error rates at the two thresholds are identical. The lines span 1% and 99% of bootstrap replicated FNMR estimates.

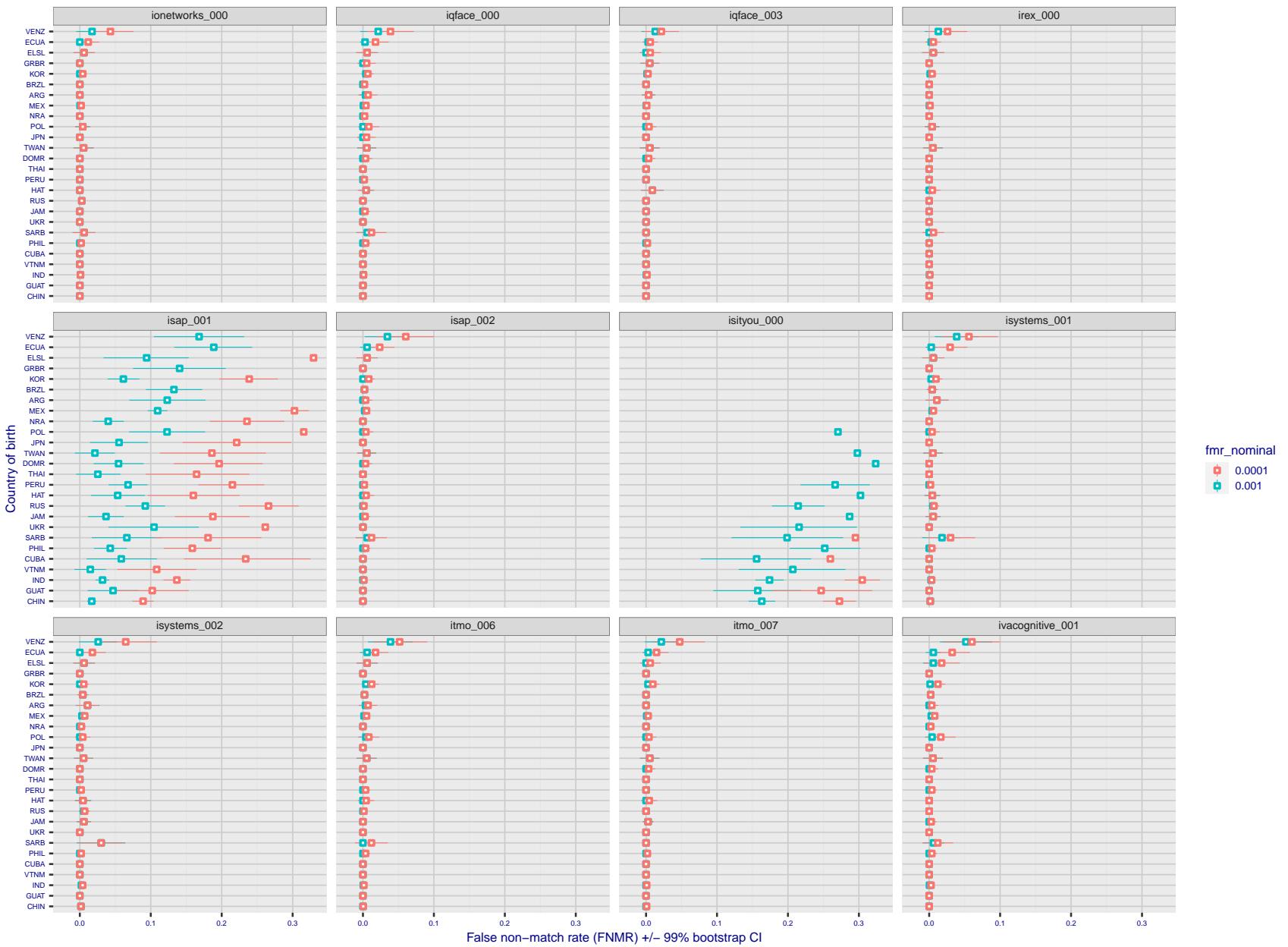


Figure 222: For the visa images, the dots show FNMR by country of birth for two globally set operating thresholds corresponding to  $FMR = \{0.001, 0.0001\}$  computed over all on the order of  $10^{10}$  impostor scores. The FMR in each bin will vary also - see subsequent impostor heatmaps in sec. 3.6.1. The figures shows an order of magnitude variation in FNMR across country of birth; these effects are likely due quality variations, then demographics like age and race. The error rates in some cases are zero, and in others the DET is flat so the error rates at the two thresholds are identical. The lines span 1% and 99% of bootstrap replicated FNMR estimates.

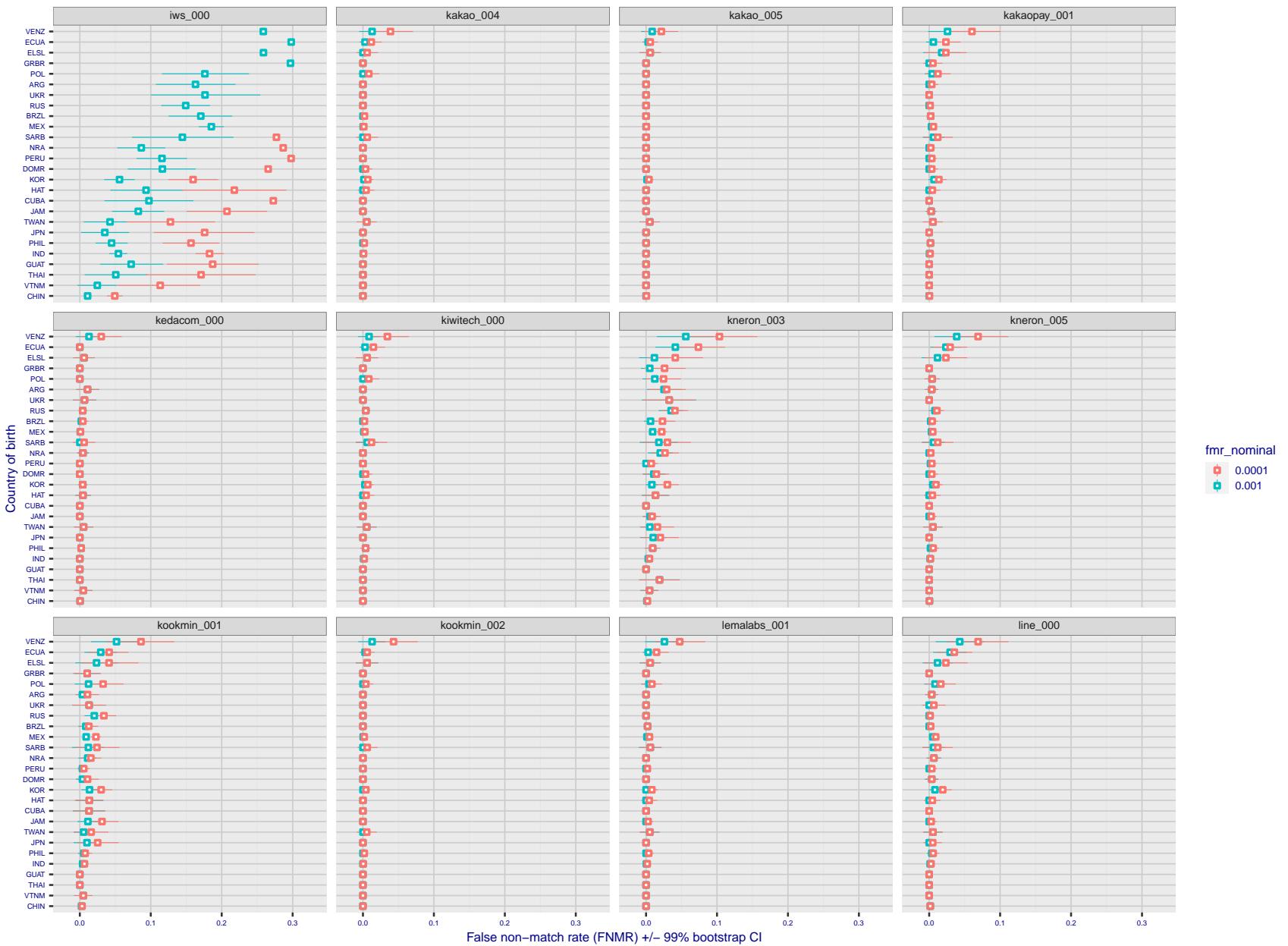


Figure 223: For the visa images, the dots show FNMR by country of birth for two globally set operating thresholds corresponding to  $FMR = \{0.001, 0.0001\}$  computed over all on the order of  $10^{10}$  impostor scores. The FMR in each bin will vary also - see subsequent impostor heatmaps in sec. 3.6.1. The figures shows an order of magnitude variation in FNMR across country of birth; these effects are likely due quality variations, then demographics like age and race. The error rates in some cases are zero, and in others the DET is flat so the error rates at the two thresholds are identical. The lines span 1% and 99% of bootstrap replicated FNMR estimates.

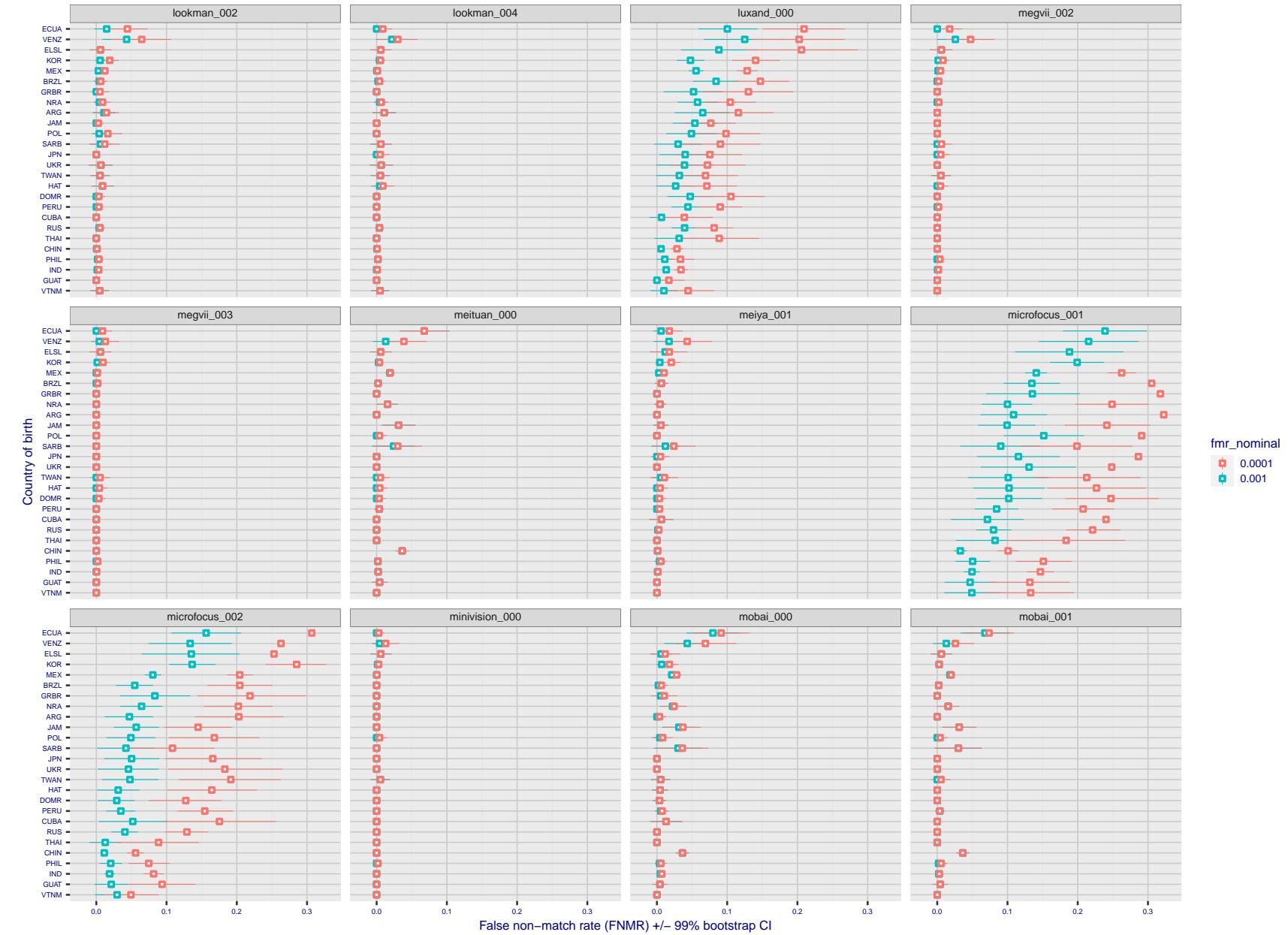


Figure 224: For the visa images, the dots show FNMR by country of birth for two globally set operating thresholds corresponding to  $FMR = \{0.001, 0.0001\}$  computed over all on the order of  $10^{10}$  impostor scores. The FMR in each bin will vary also - see subsequent impostor heatmaps in sec. 3.6.1. The figures shows an order of magnitude variation in FNMR across country of birth; these effects are likely due quality variations, then demographics like age and race. The error rates in some cases are zero, and in others the DET is flat so the error rates at the two thresholds are identical. The lines span 1% and 99% of bootstrap replicated FNMR estimates.

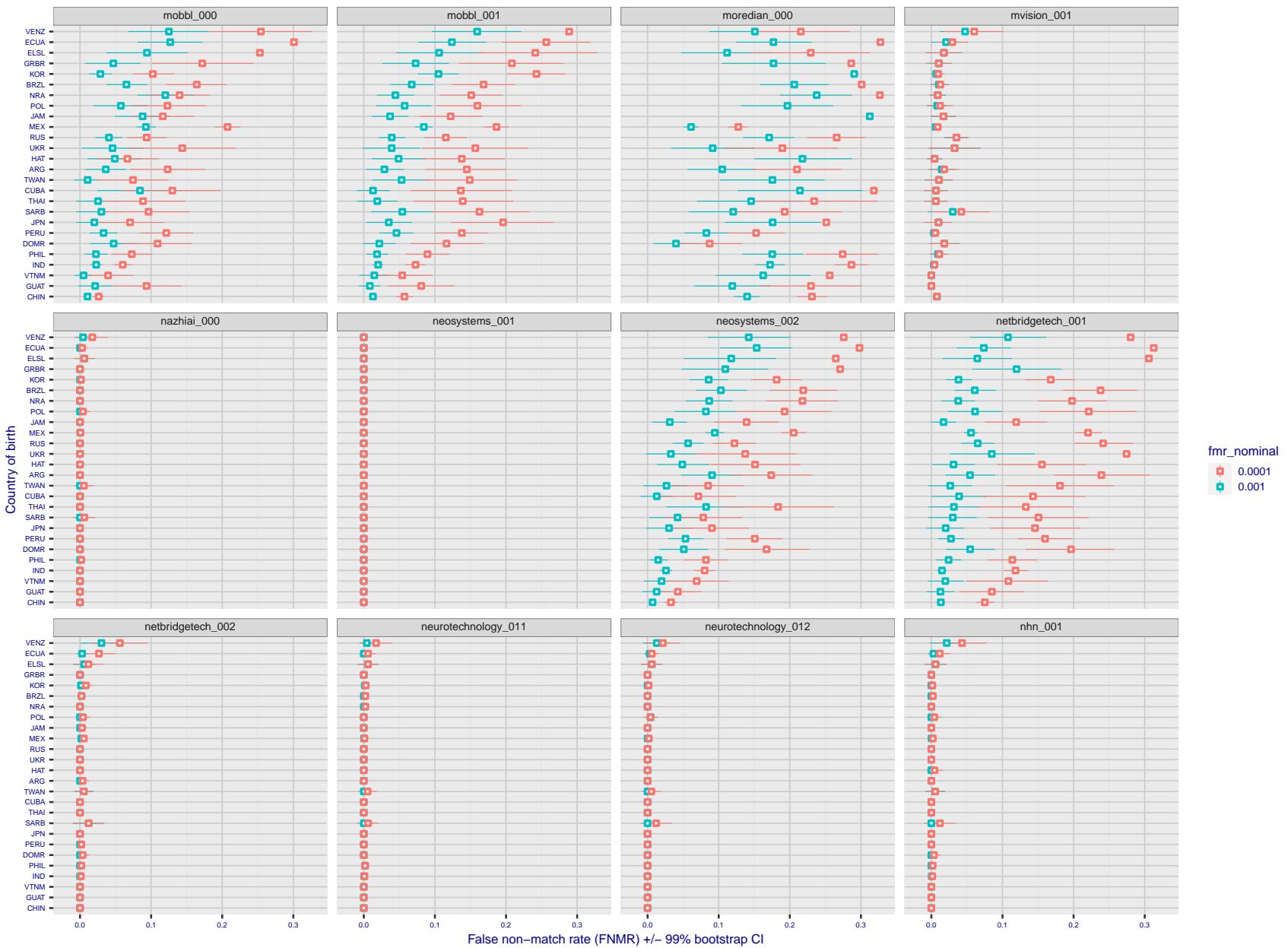


Figure 225: For the visa images, the dots show FNMR by country of birth for two globally set operating thresholds corresponding to  $FMR = \{0.001, 0.0001\}$  computed over all on the order of  $10^{10}$  impostor scores. The FMR in each bin will vary also - see subsequent impostor heatmaps in sec. 3.6.1. The figures shows an order of magnitude variation in FNMR across country of birth; these effects are likely due quality variations, then demographics like age and race. The error rates in some cases are zero, and in others the DET is flat so the error rates at the two thresholds are identical. The lines span 1% and 99% of bootstrap replicated FNMR estimates.

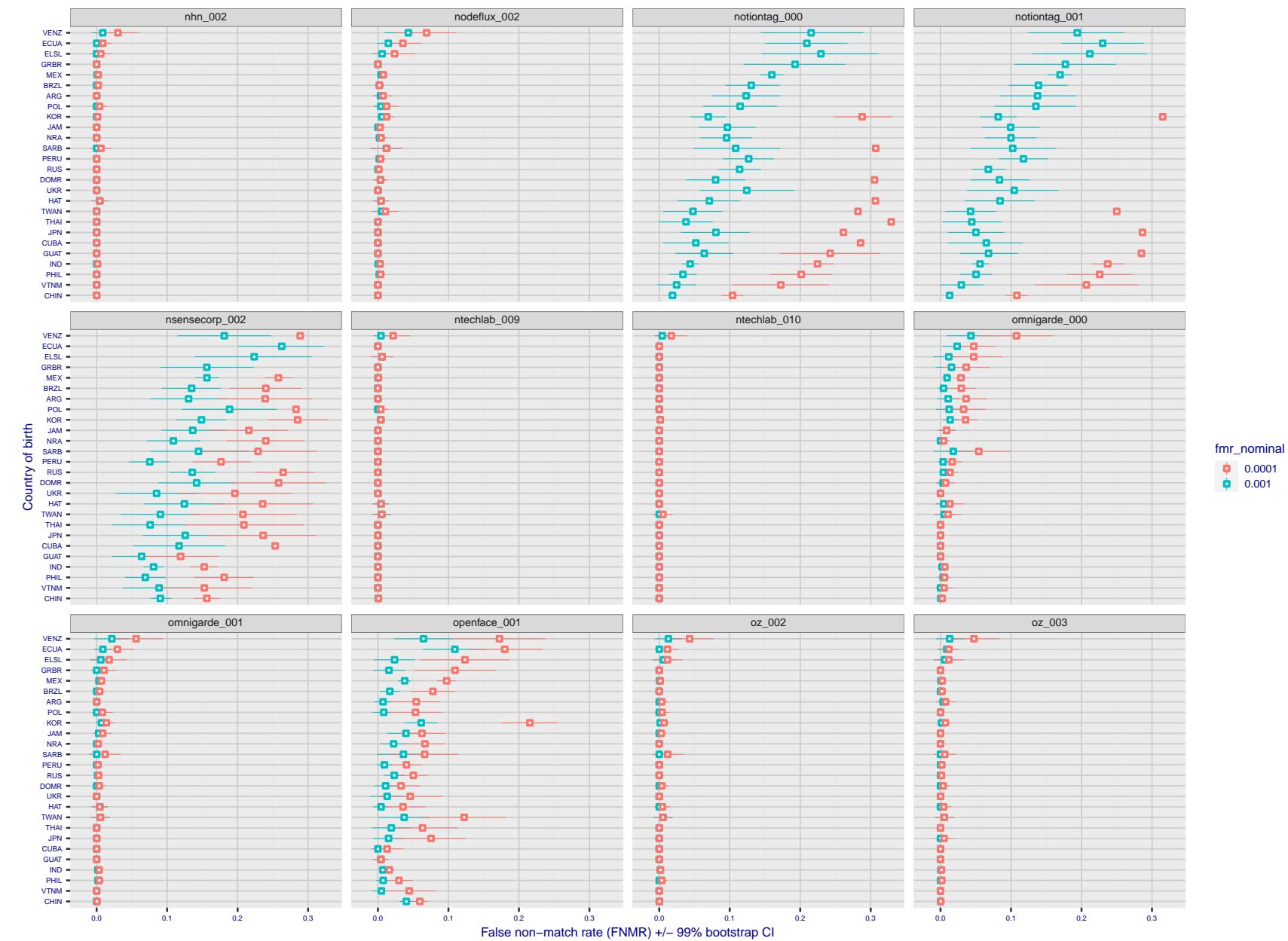


Figure 226: For the visa images, the dots show FNMR by country of birth for two globally set operating thresholds corresponding to  $FMR = \{0.001, 0.0001\}$  computed over all on the order of  $10^{10}$  impostor scores. The FMR in each bin will vary also - see subsequent impostor heatmaps in sec. 3.6.1. The figures shows an order of magnitude variation in FNMR across country of birth; these effects are likely due quality variations, then demographics like age and race. The error rates in some cases are zero, and in others the DET is flat so the error rates at the two thresholds are identical. The lines span 1% and 99% of bootstrap replicated FNMR estimates.

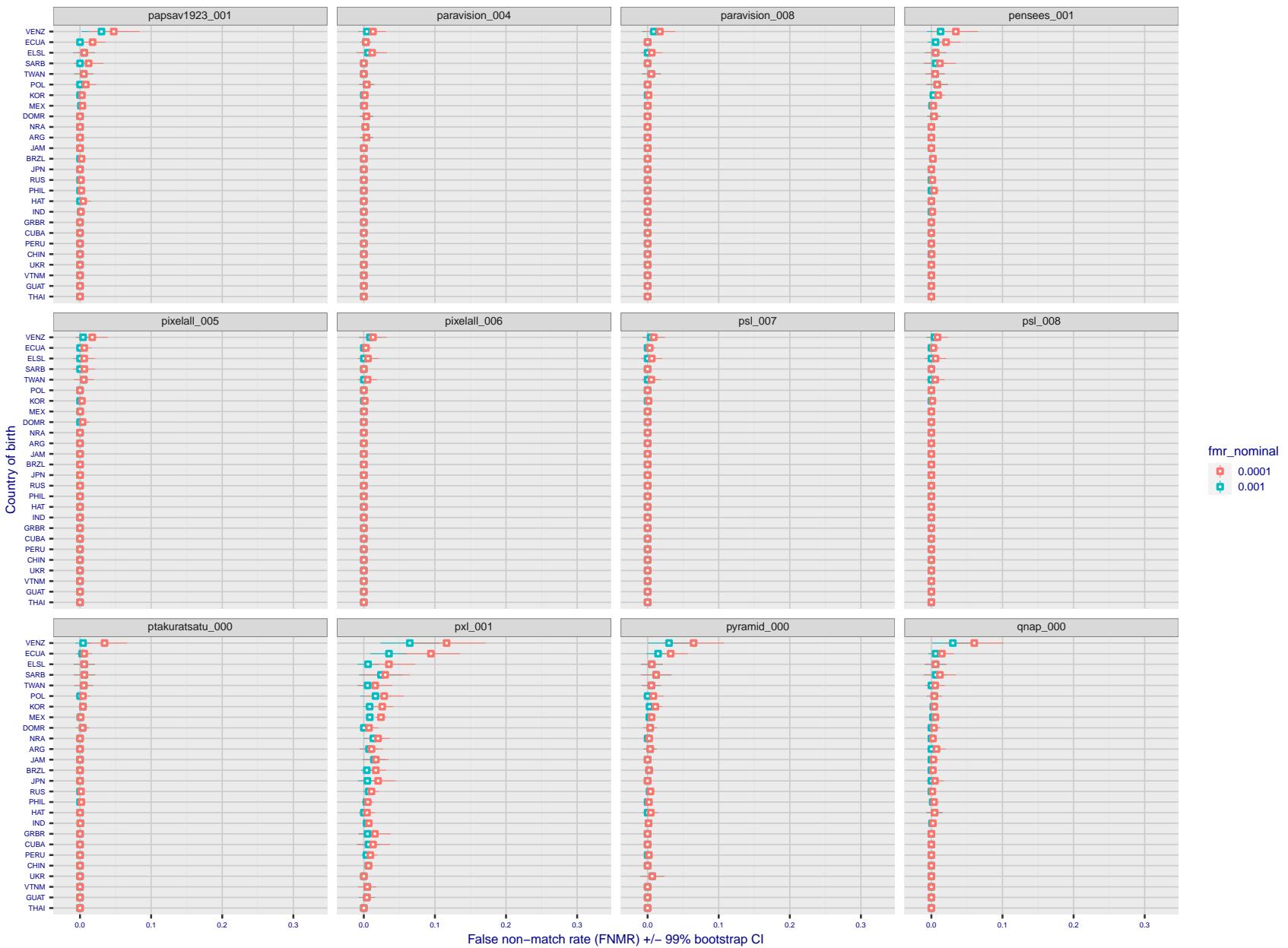


Figure 227: For the visa images, the dots show FNMR by country of birth for two globally set operating thresholds corresponding to  $FMR = \{0.001, 0.0001\}$  computed over all on the order of  $10^{10}$  impostor scores. The FMR in each bin will vary also - see subsequent impostor heatmaps in sec. 3.6.1. The figures shows an order of magnitude variation in FNMR across country of birth; these effects are likely due quality variations, then demographics like age and race. The error rates in some cases are zero, and in others the DET is flat so the error rates at the two thresholds are identical. The lines span 1% and 99% of bootstrap replicated FNMR estimates.

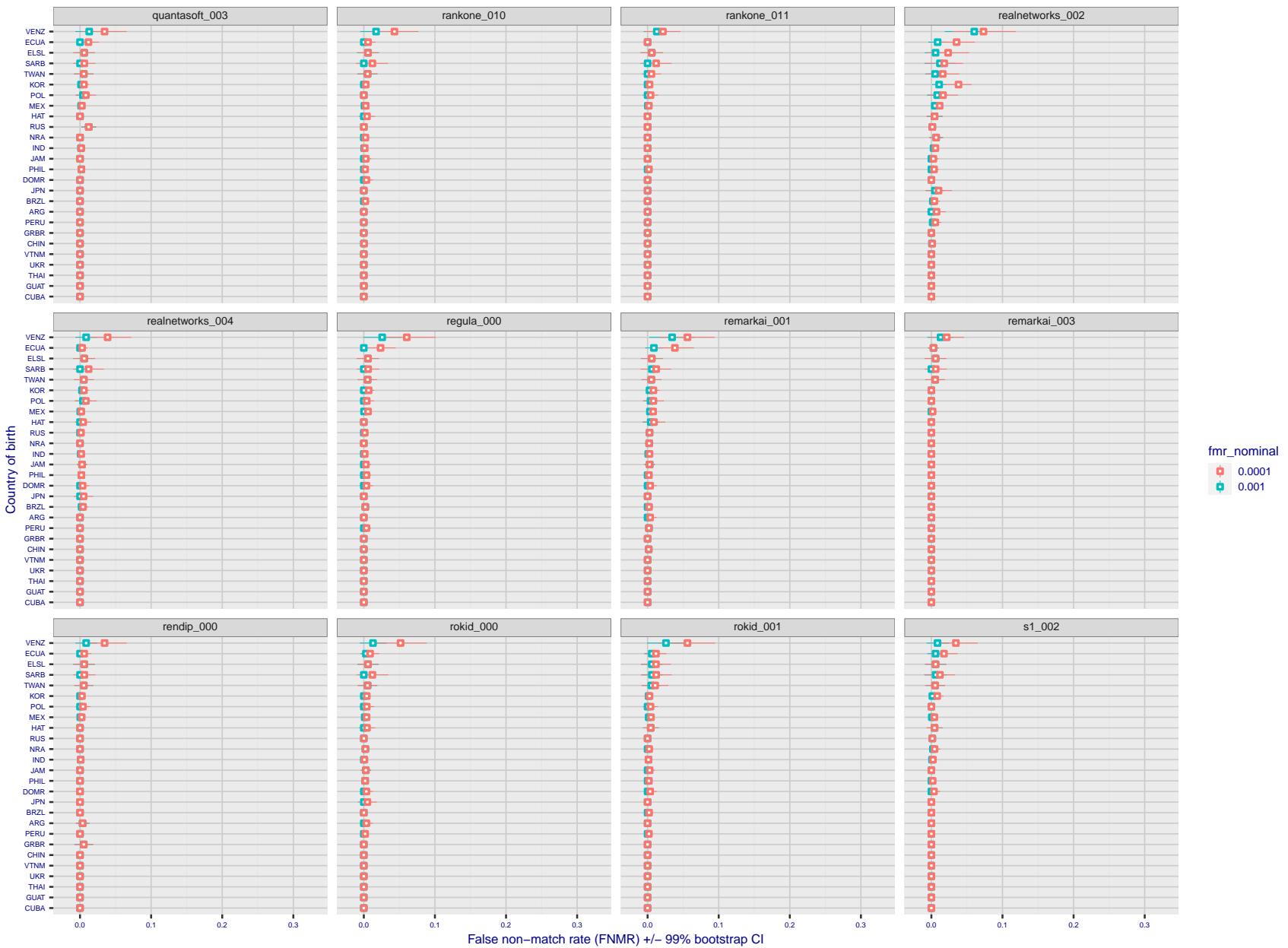


Figure 228: For the visa images, the dots show FNMR by country of birth for two globally set operating thresholds corresponding to  $FMR = \{0.001, 0.0001\}$  computed over all on the order of  $10^{10}$  impostor scores. The FMR in each bin will vary also - see subsequent impostor heatmaps in sec. 3.6.1. The figures shows an order of magnitude variation in FNMR across country of birth; these effects are likely due quality variations, then demographics like age and race. The error rates in some cases are zero, and in others the DET is flat so the error rates at the two thresholds are identical. The lines span 1% and 99% of bootstrap replicated FNMR estimates.

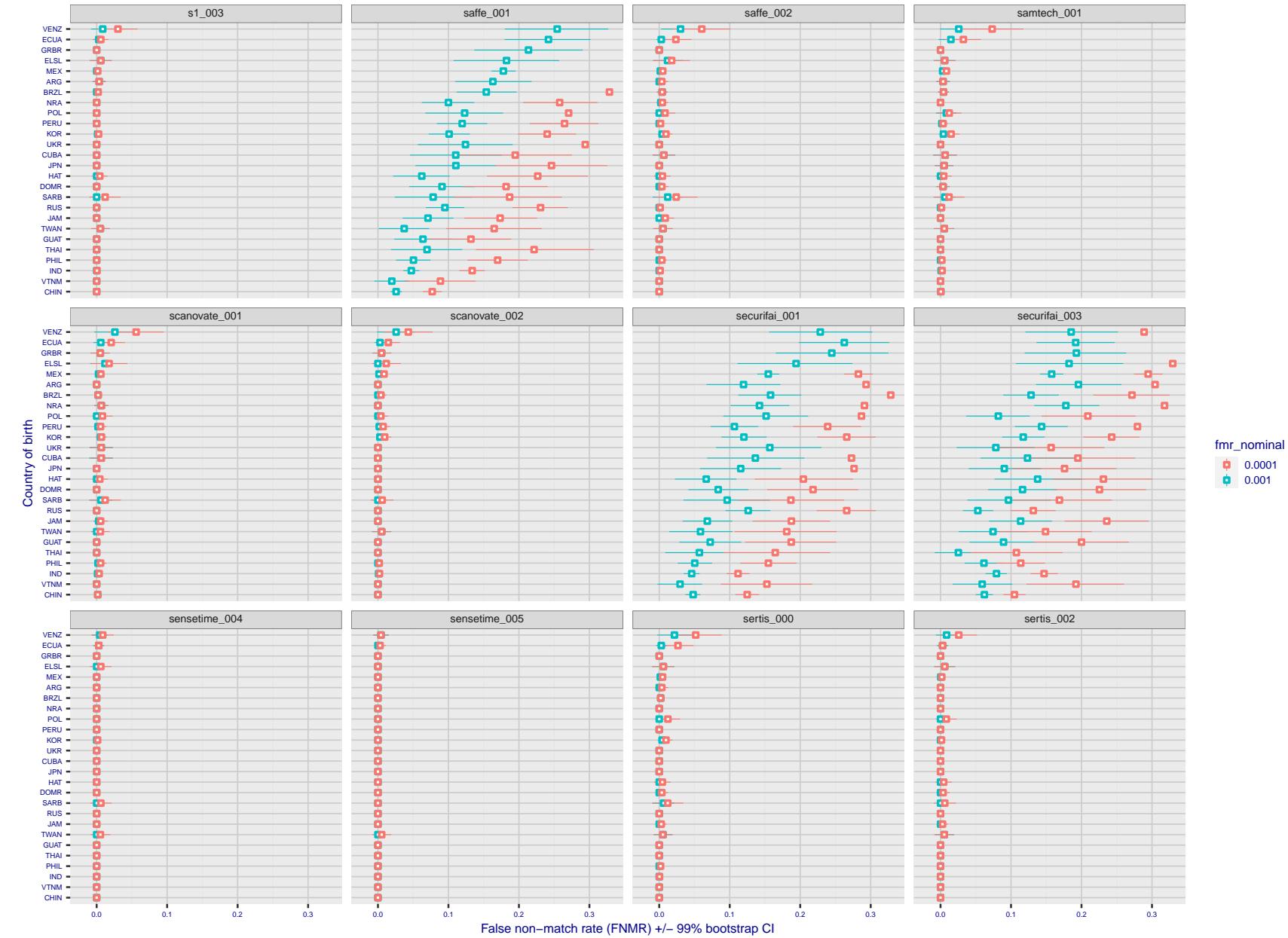


Figure 229: For the visa images, the dots show FNMR by country of birth for two globally set operating thresholds corresponding to  $FMR = \{0.001, 0.0001\}$  computed over all on the order of  $10^{10}$  impostor scores. The FMR in each bin will vary also - see subsequent impostor heatmaps in sec. 3.6.1. The figures shows an order of magnitude variation in FNMR across country of birth; these effects are likely due quality variations, then demographics like age and race. The error rates in some cases are zero, and in others the DET is flat so the error rates at the two thresholds are identical. The lines span 1% and 99% of bootstrap replicated FNMR estimates.

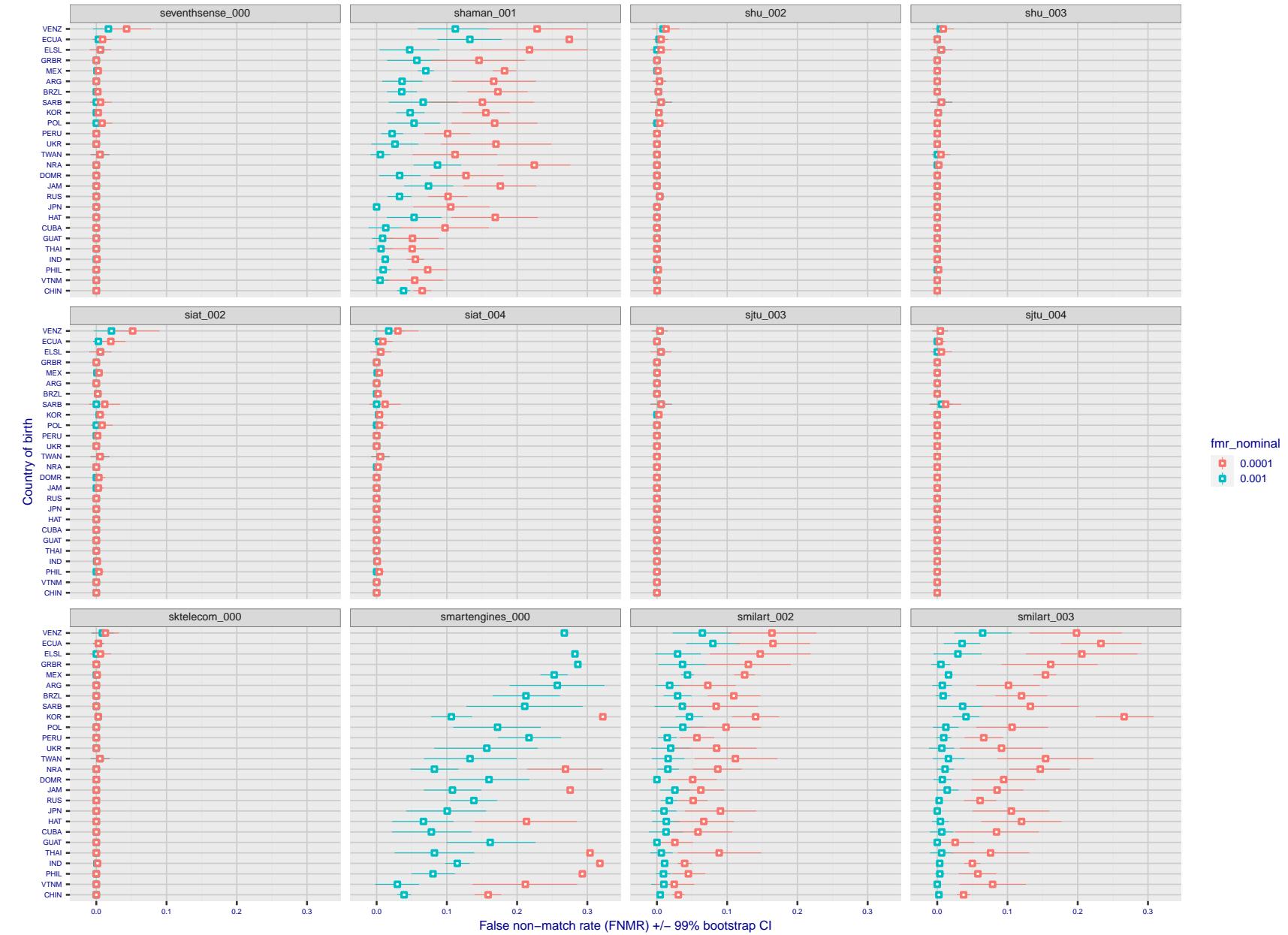


Figure 230: For the visa images, the dots show FNMR by country of birth for two globally set operating thresholds corresponding to  $FMR = \{0.001, 0.0001\}$  computed over all on the order of  $10^{10}$  impostor scores. The FMR in each bin will vary also - see subsequent impostor heatmaps in sec. 3.6.1. The figures shows an order of magnitude variation in FNMR across country of birth; these effects are likely due quality variations, then demographics like age and race. The error rates in some cases are zero, and in others the DET is flat so the error rates at the two thresholds are identical. The lines span 1% and 99% of bootstrap replicated FNMR estimates.

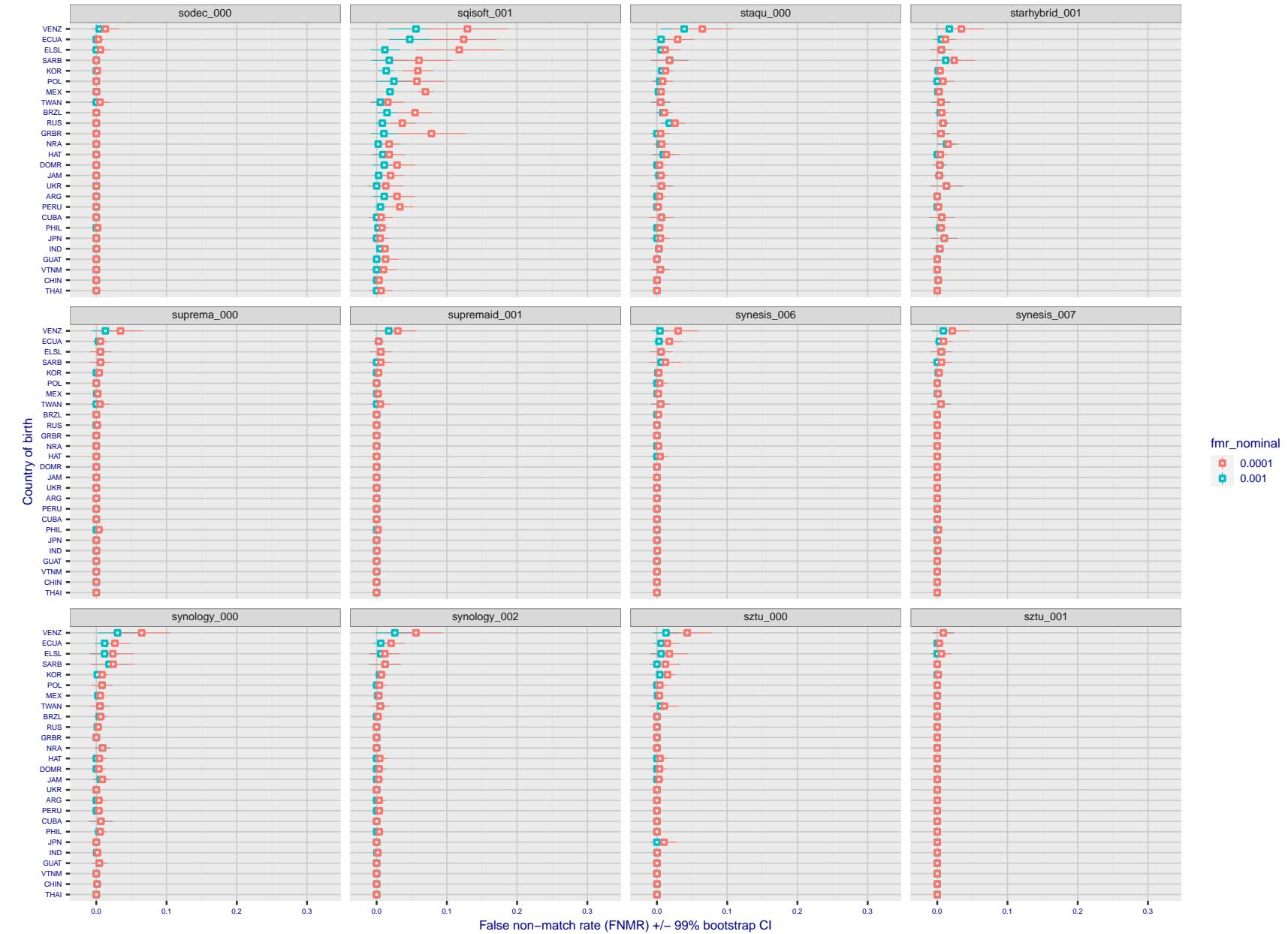


Figure 231: For the visa images, the dots show FNMR by country of birth for two globally set operating thresholds corresponding to  $FMR = \{0.001, 0.0001\}$  computed over all on the order of  $10^{10}$  impostor scores. The FMR in each bin will vary also - see subsequent impostor heatmaps in sec. 3.6.1. The figures shows an order of magnitude variation in FNMR across country of birth; these effects are likely due quality variations, then demographics like age and race. The error rates in some cases are zero, and in others the DET is flat so the error rates at the two thresholds are identical. The lines span 1% and 99% of bootstrap replicated FNMR estimates.

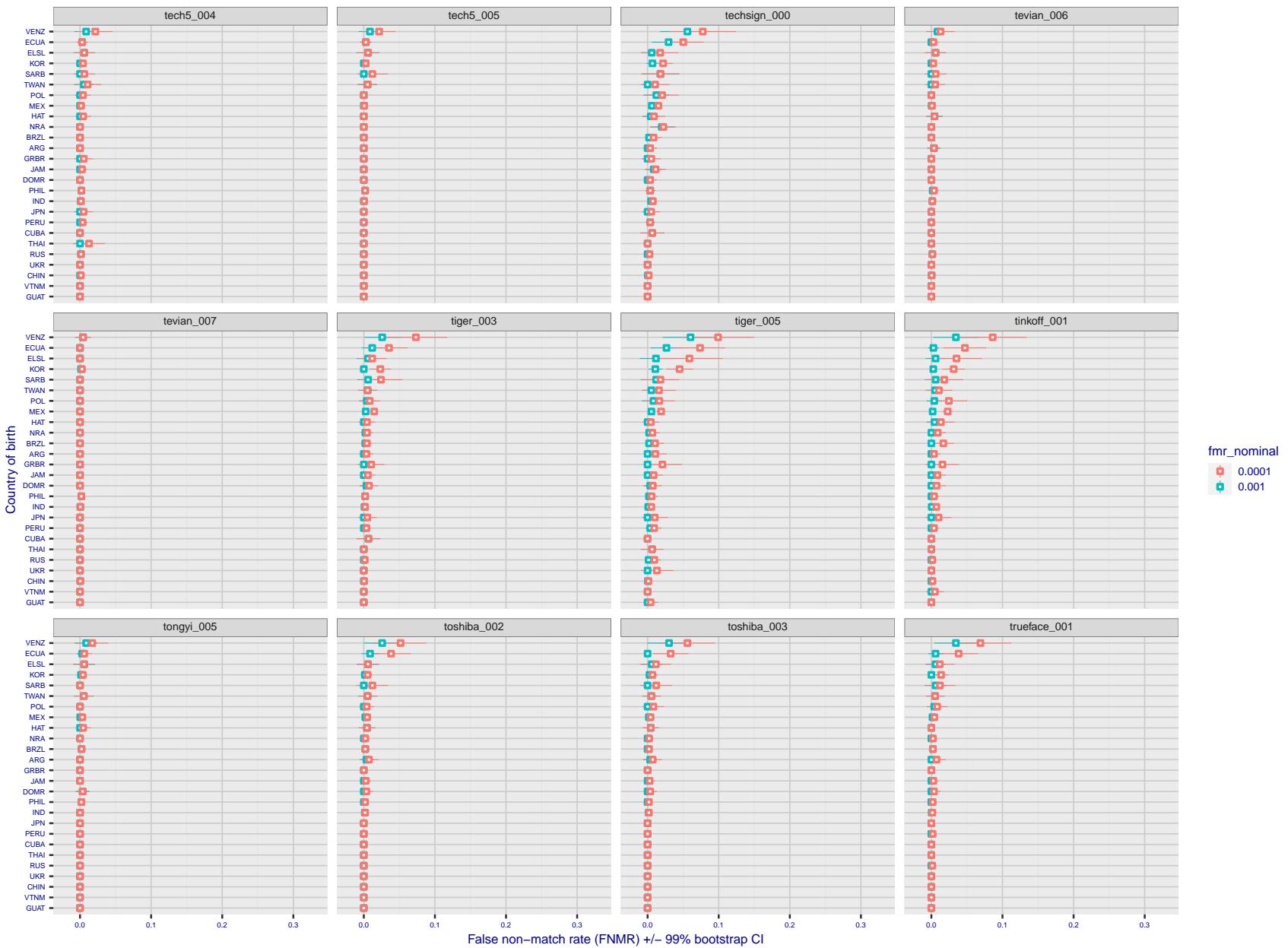


Figure 232: For the visa images, the dots show FNMR by country of birth for two globally set operating thresholds corresponding to  $FMR = \{0.001, 0.0001\}$  computed over all on the order of  $10^{10}$  impostor scores. The FMR in each bin will vary also - see subsequent impostor heatmaps in sec. 3.6.1. The figures shows an order of magnitude variation in FNMR across country of birth; these effects are likely due quality variations, then demographics like age and race. The error rates in some cases are zero, and in others the DET is flat so the error rates at the two thresholds are identical. The lines span 1% and 99% of bootstrap replicated FNMR estimates.

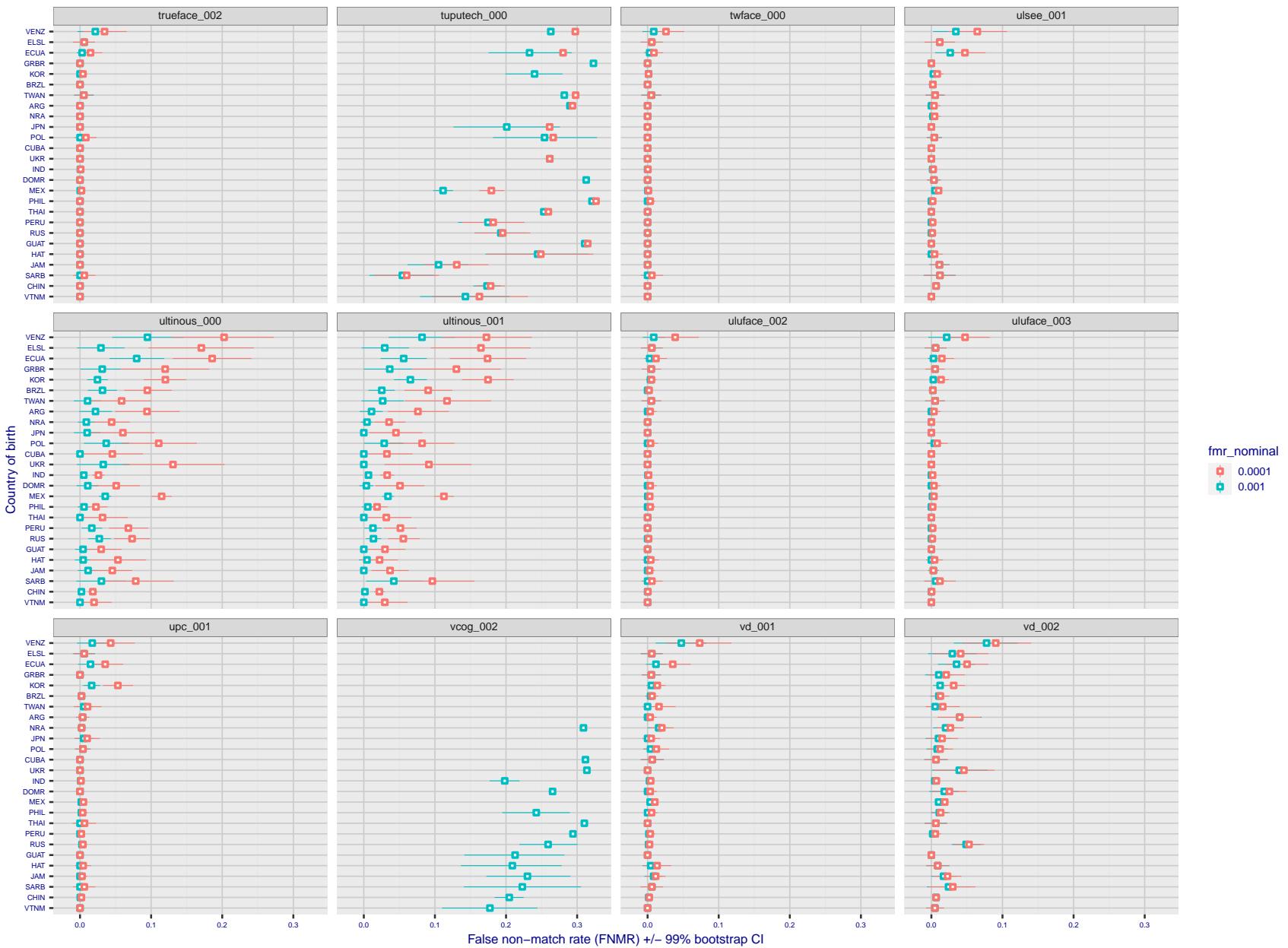


Figure 233: For the visa images, the dots show FNMR by country of birth for two globally set operating thresholds corresponding to  $FMR = \{0.001, 0.0001\}$  computed over all on the order of  $10^{10}$  impostor scores. The FMR in each bin will vary also - see subsequent impostor heatmaps in sec. 3.6.1. The figures shows an order of magnitude variation in FNMR across country of birth; these effects are likely due quality variations, then demographics like age and race. The error rates in some cases are zero, and in others the DET is flat so the error rates at the two thresholds are identical. The lines span 1% and 99% of bootstrap replicated FNMR estimates.

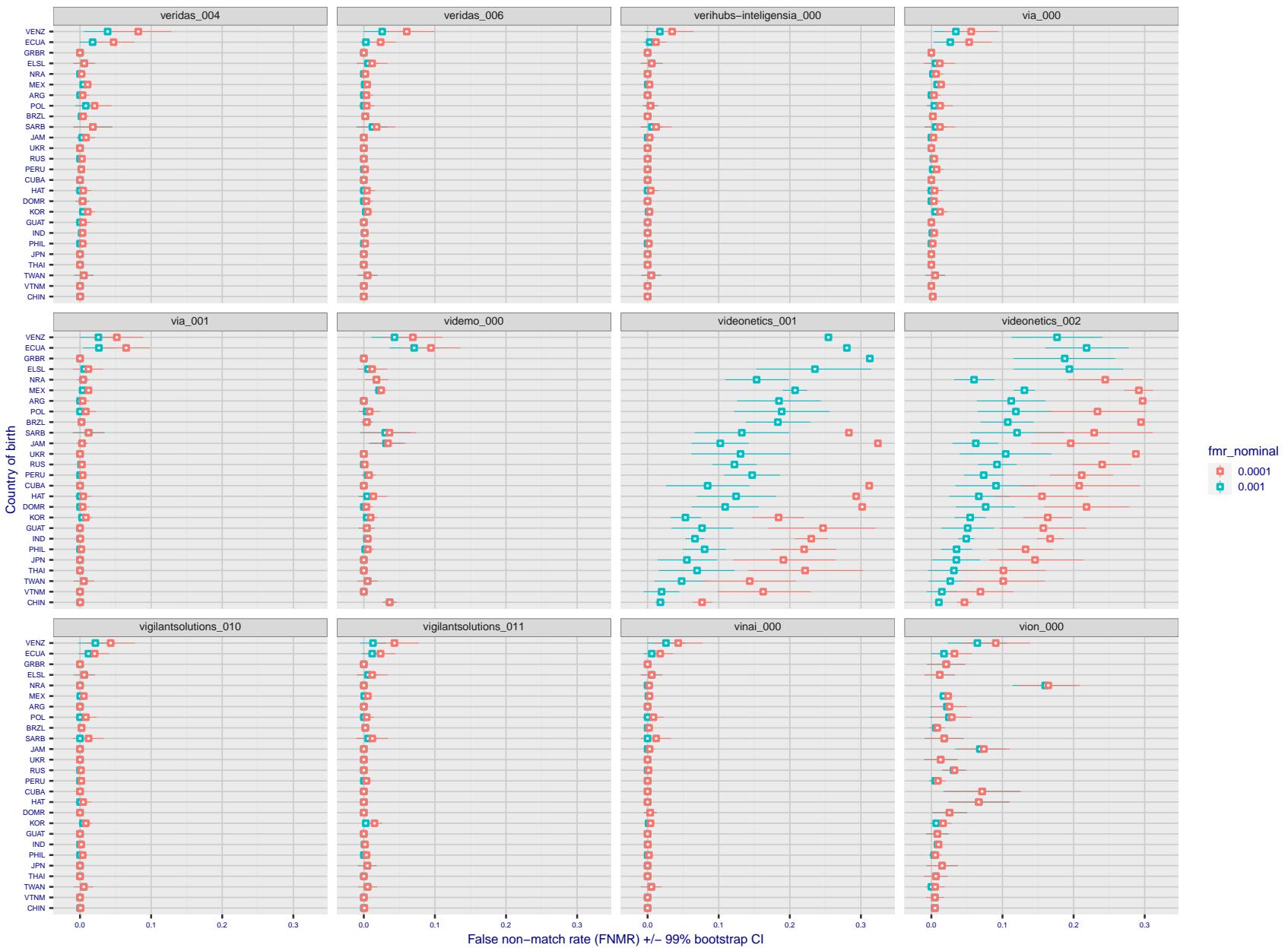


Figure 234: For the visa images, the dots show FNMR by country of birth for two globally set operating thresholds corresponding to  $FMR = \{0.001, 0.0001\}$  computed over all on the order of  $10^{10}$  impostor scores. The FMR in each bin will vary also - see subsequent impostor heatmaps in sec. 3.6.1. The figures shows an order of magnitude variation in FNMR across country of birth; these effects are likely due quality variations, then demographics like age and race. The error rates in some cases are zero, and in others the DET is flat so the error rates at the two thresholds are identical. The lines span 1% and 99% of bootstrap replicated FNMR estimates.

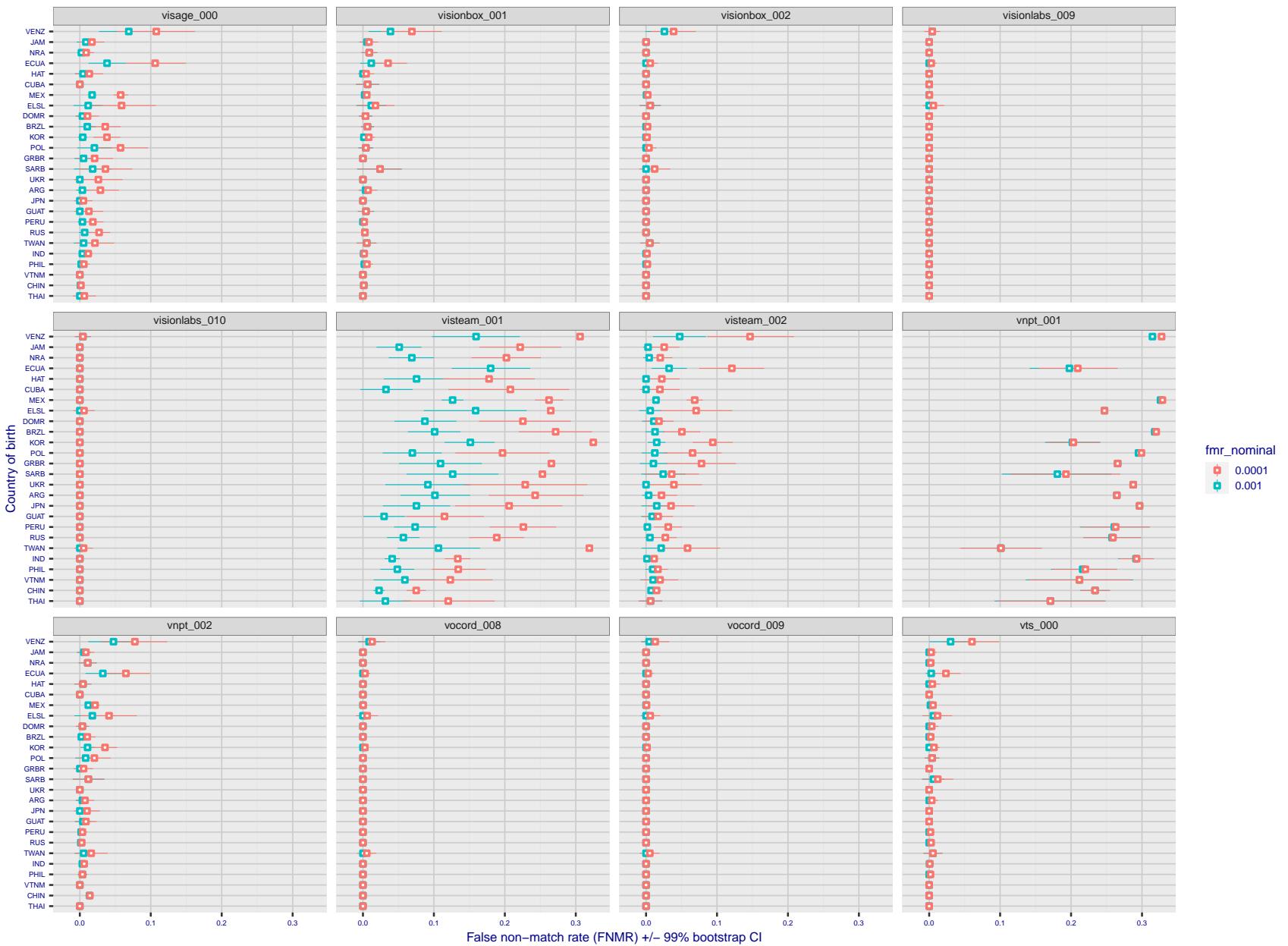


Figure 235: For the visa images, the dots show FNMR by country of birth for two globally set operating thresholds corresponding to  $FMR = \{0.001, 0.0001\}$  computed over all on the order of  $10^{10}$  impostor scores. The FMR in each bin will vary also - see subsequent impostor heatmaps in sec. 3.6.1. The figures shows an order of magnitude variation in FNMR across country of birth; these effects are likely due quality variations, then demographics like age and race. The error rates in some cases are zero, and in others the DET is flat so the error rates at the two thresholds are identical. The lines span 1% and 99% of bootstrap replicated FNMR estimates.

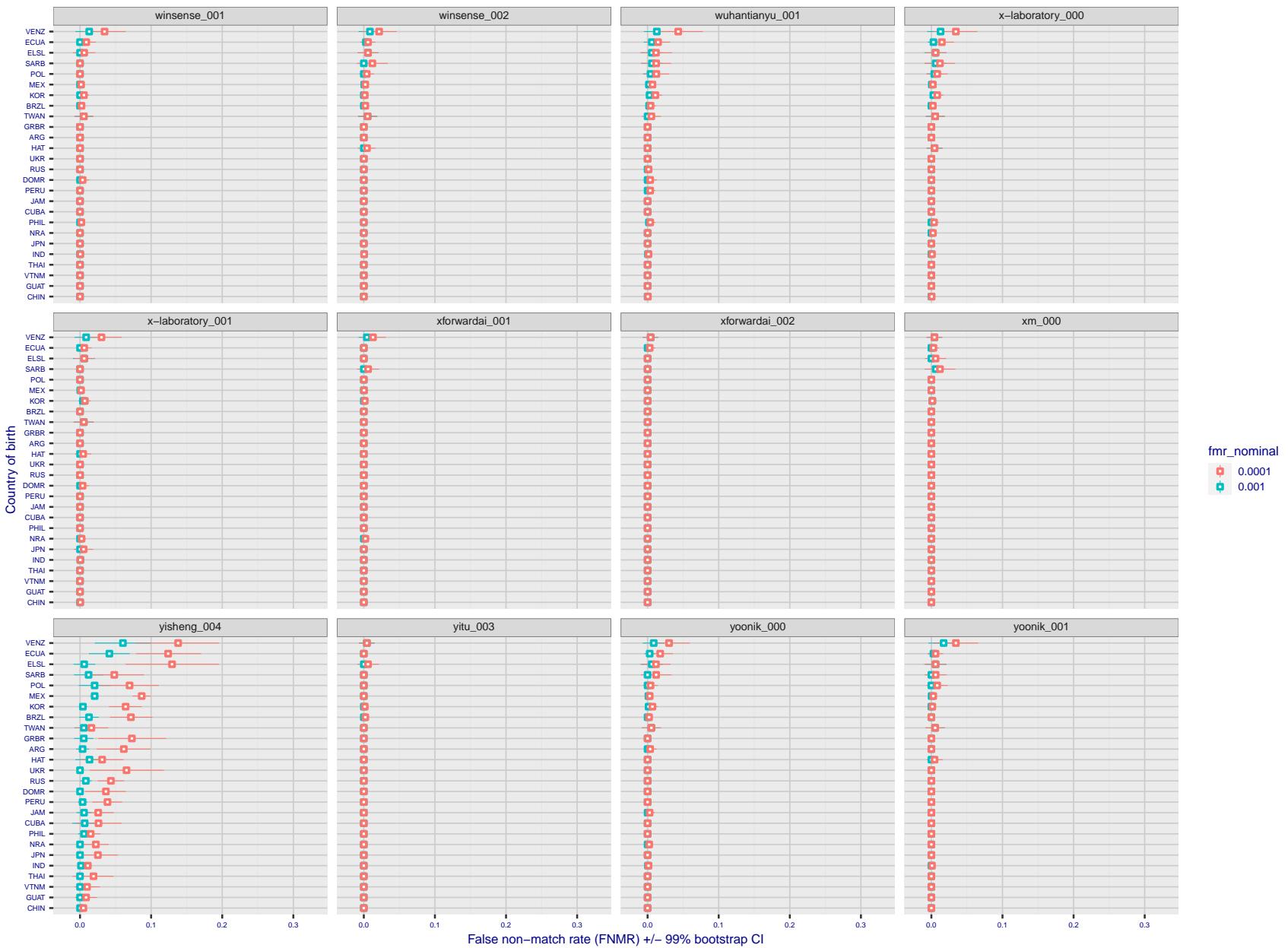


Figure 236: For the visa images, the dots show FNMR by country of birth for two globally set operating thresholds corresponding to  $FMR = \{0.001, 0.0001\}$  computed over all on the order of  $10^{10}$  impostor scores. The FMR in each bin will vary also - see subsequent impostor heatmaps in sec. 3.6.1. The figures shows an order of magnitude variation in FNMR across country of birth; these effects are likely due quality variations, then demographics like age and race. The error rates in some cases are zero, and in others the DET is flat so the error rates at the two thresholds are identical. The lines span 1% and 99% of bootstrap replicated FNMR estimates.

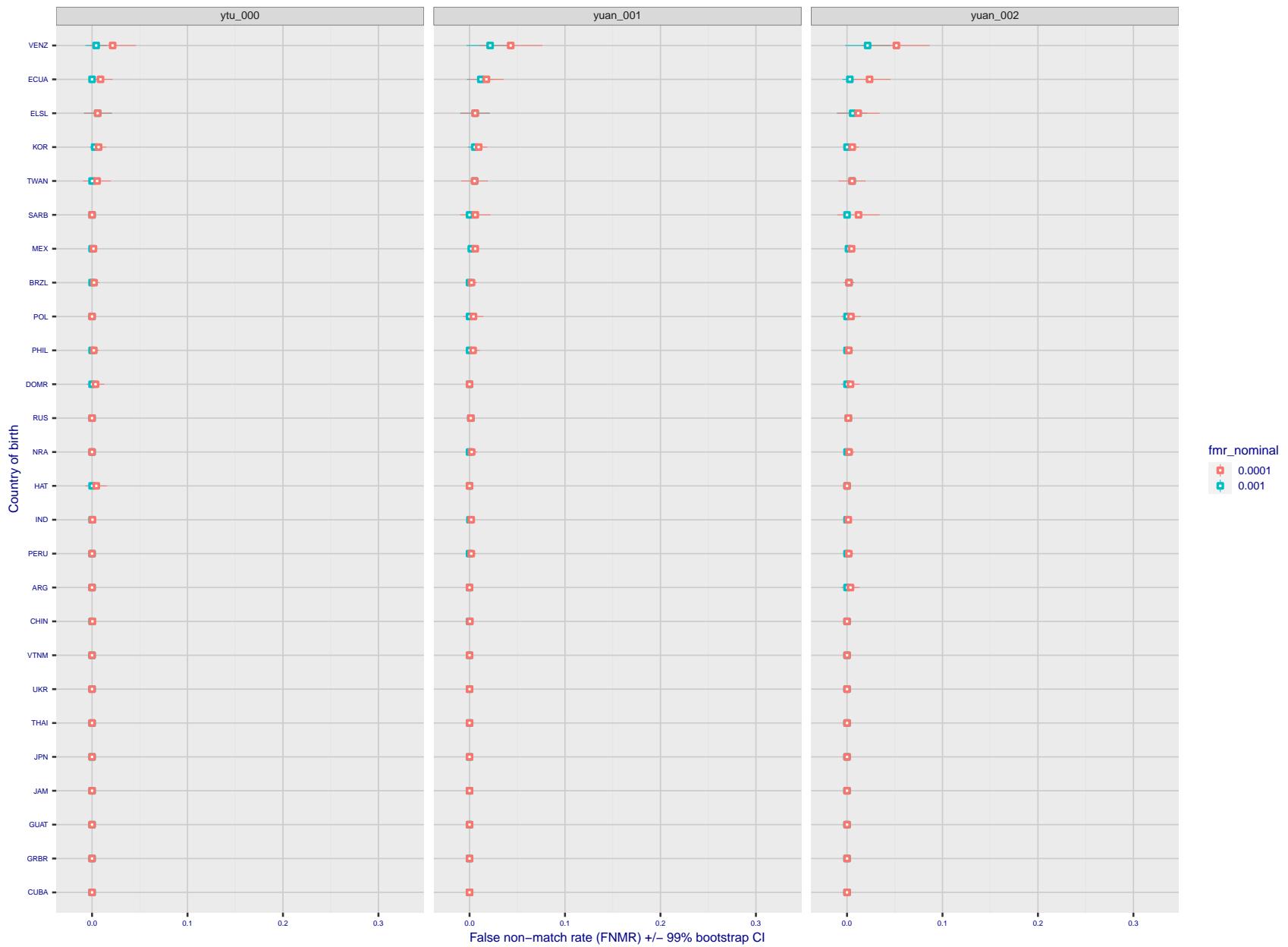


Figure 237: For the visa images, the dots show FNMR by country of birth for two globally set operating thresholds corresponding to  $FMR = \{0.001, 0.0001\}$  computed over all on the order of  $10^{10}$  impostor scores. The FMR in each bin will vary also - see subsequent impostor heatmaps in sec. 3.6.1. The figures shows an order of magnitude variation in FNMR across country of birth; these effects are likely due quality variations, then demographics like age and race. The error rates in some cases are zero, and in others the DET is flat so the error rates at the two thresholds are identical. The lines span 1% and 99% of bootstrap replicated FNMR estimates.

**Caveats:** The results may not relate to subject-specific properties. Instead they could reflect image-specific quality differences, which could occur due to collection protocol or software processing variations.

### 3.5.2 Effect of ageing

**Background:** Faces change appearance throughout life. This change gradually reduces similarity of a new image to an earlier image. Face recognition algorithms give reduced similarity scores and more frequent false rejections.

**Goal:** To quantify false non-match rates (FNMR) as a function of elapsed time in an adult population.

**Methods:** Using the mugshot images, a threshold is set to give FMR = 0.00001 over the entire impostor set. Then FNMR is measured over 1000 bootstrap replications of the genuine scores.

**Results:** For the visa images, Figure 258 shows how false non-match rates for genuine users, as a function of age group.

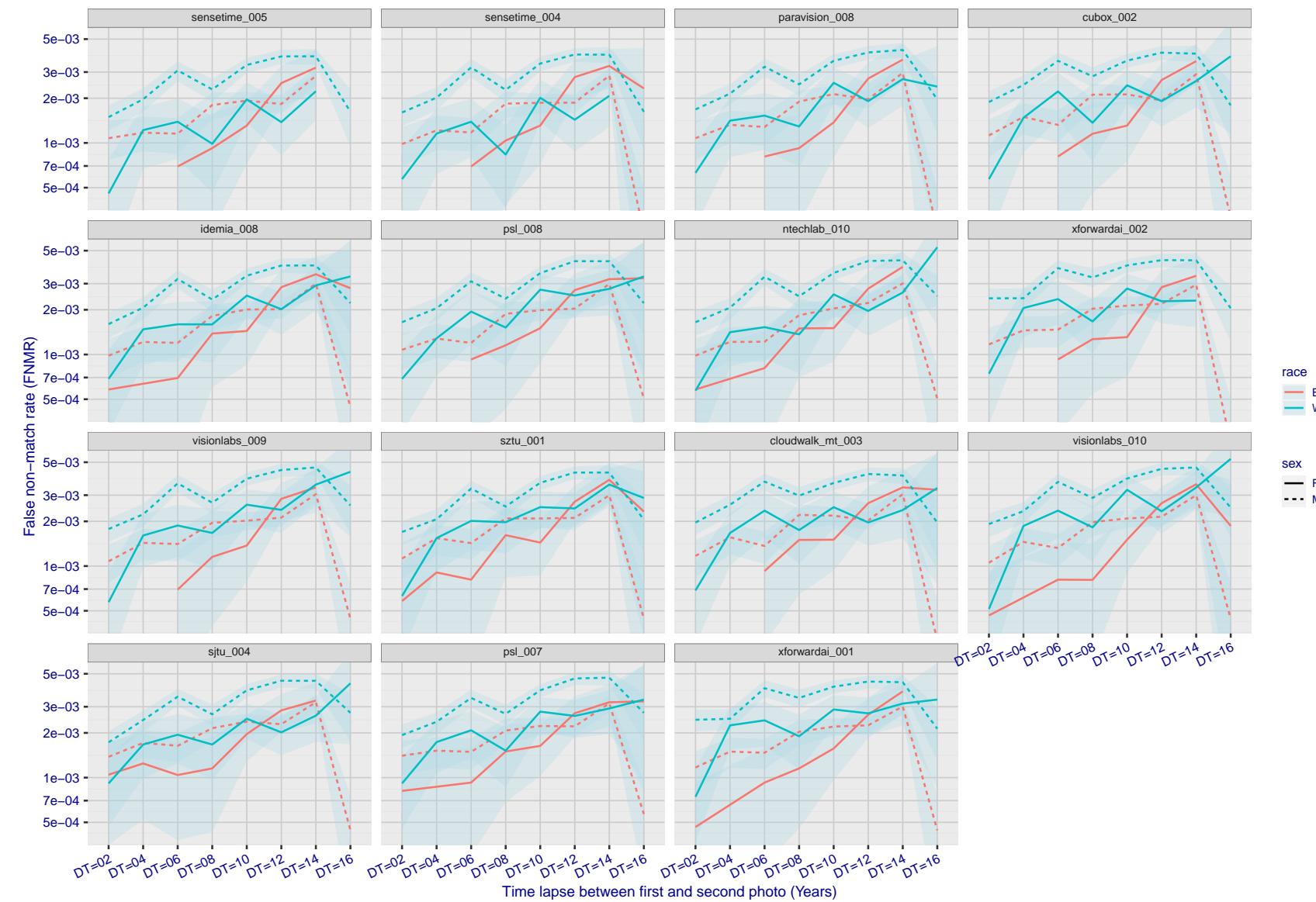


Figure 238: For the mugshot images, FNMR as a function of elapsed time between initial enrollment and second verification images. The panels appear most accurate first, and vertical scale changes on each page. The four traces correspond to images annotated with codes for black female, black male, white female, white male. The threshold is fixed for each algorithm to give FMR = 0.00001 over all ( $10^8$ ) impostor comparisons. For short time-lapses, the most accurate algorithms give very few errors (FNMR < 0.001) so that the uncertainty estimates are high.

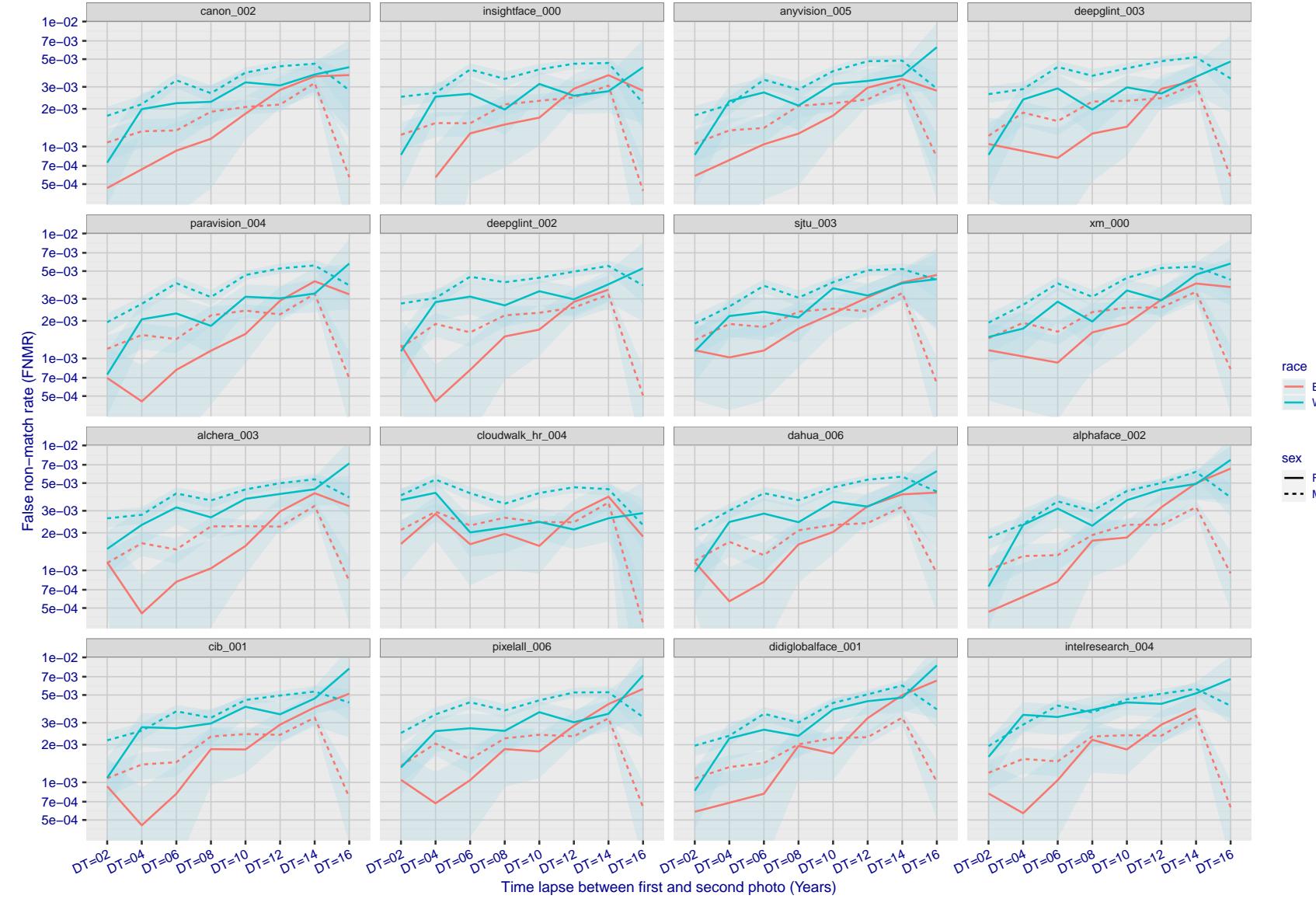


Figure 239: For the mugshot images, FNMR as a function of elapsed time between initial enrollment and second verification images. The panels appear most accurate first, and vertical scale changes on each page. The four traces correspond to images annotated with codes for black female, black male, white female, white male. The threshold is fixed for each algorithm to give  $FMR = 0.00001$  over all ( $10^8$ ) impostor comparisons. For short time-lapses, the most accurate algorithms give very few errors ( $FNMR < 0.001$ ) so that the uncertainty estimates are high.

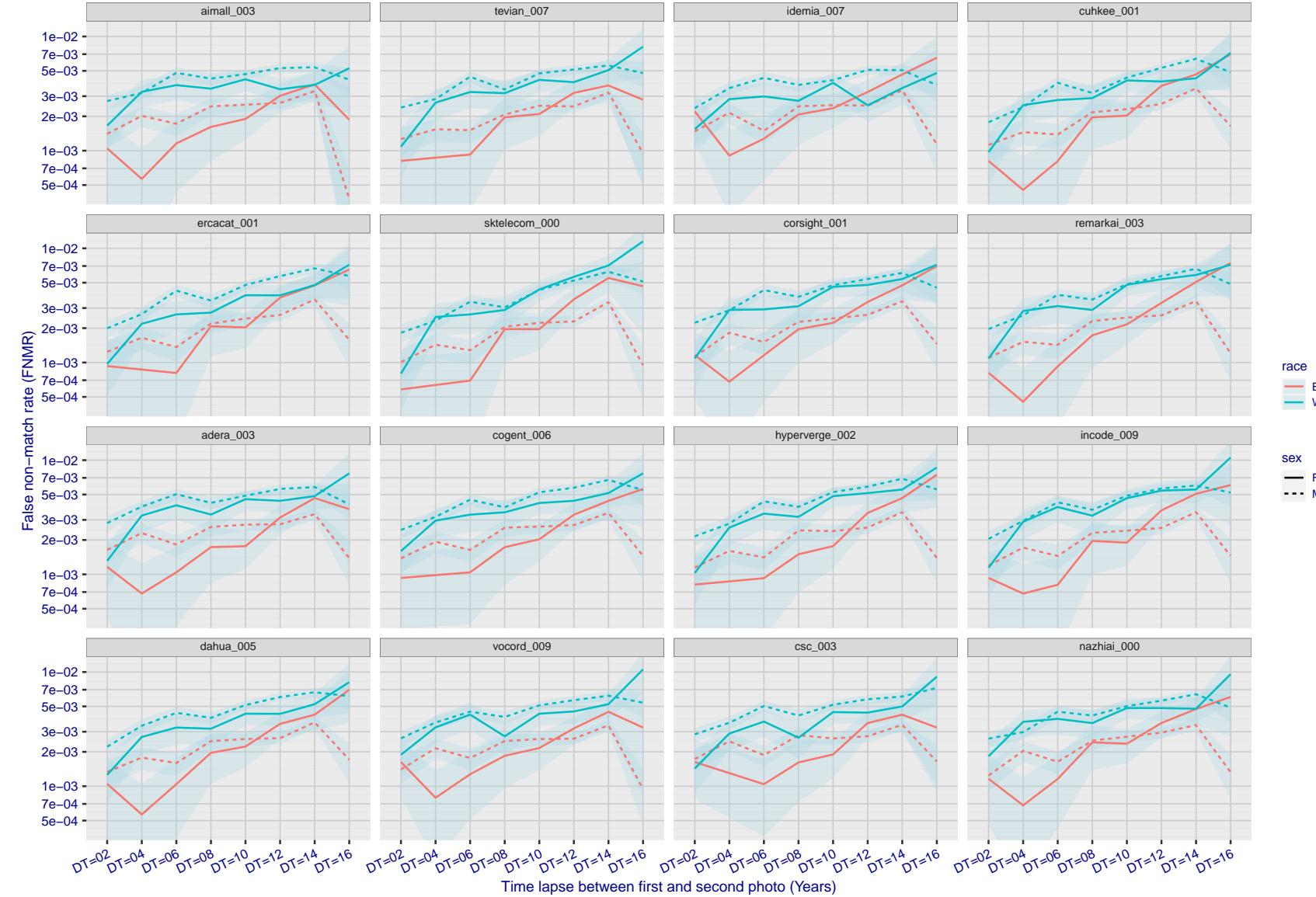


Figure 240: For the mugshot images, FNMR as a function of elapsed time between initial enrollment and second verification images. The panels appear most accurate first, and vertical scale changes on each page. The four traces correspond to images annotated with codes for black female, black male, white female, white male. The threshold is fixed for each algorithm to give  $FMR = 0.00001$  over all ( $10^8$ ) impostor comparisons. For short time-lapses, the most accurate algorithms give very few errors ( $FNMR < 0.001$ ) so that the uncertainty estimates are high.

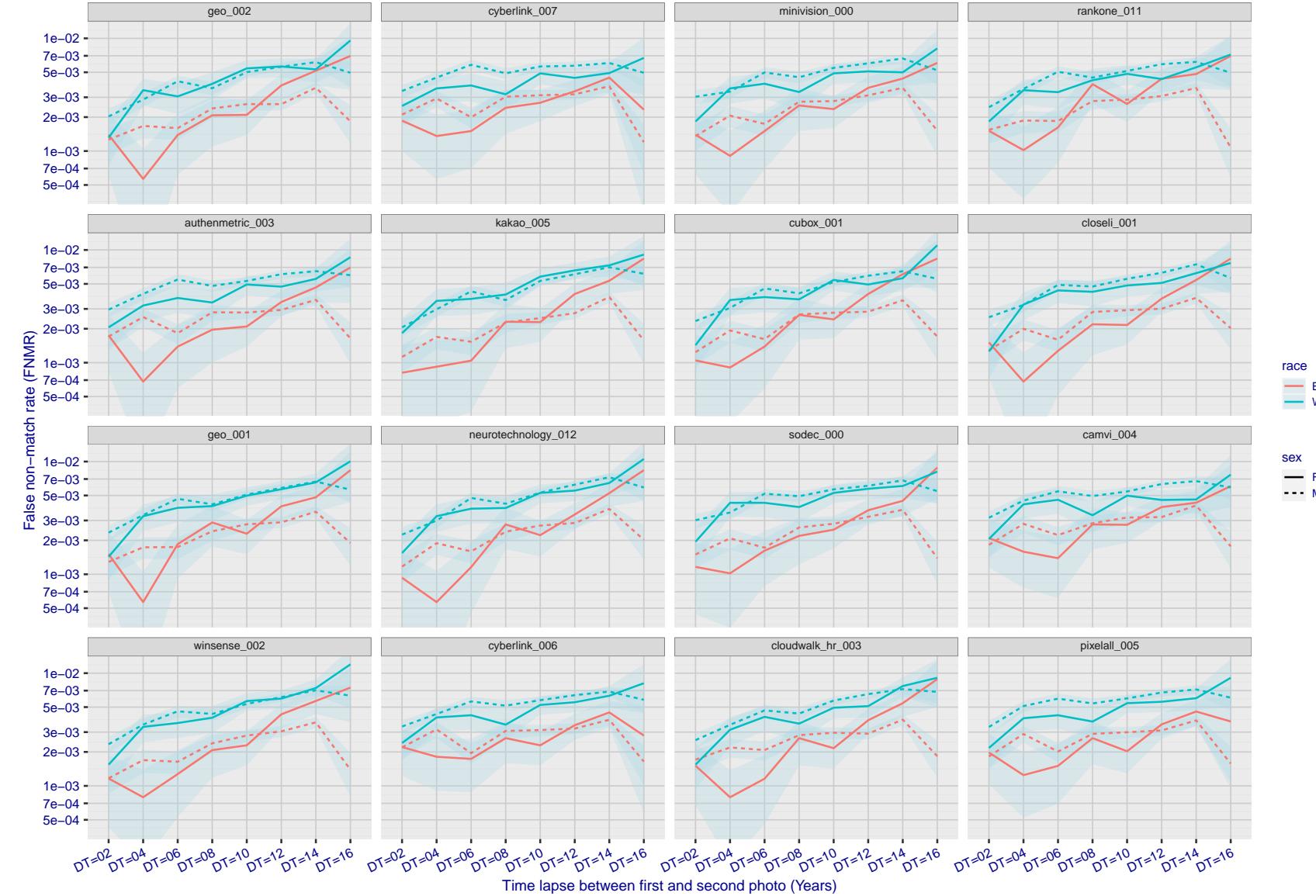


Figure 241: For the mugshot images, FNMR as a function of elapsed time between initial enrollment and second verification images. The panels appear most accurate first, and vertical scale changes on each page. The four traces correspond to images annotated with codes for black female, black male, white female, white male. The threshold is fixed for each algorithm to give  $FMR = 0.00001$  over all ( $10^8$ ) impostor comparisons. For short time-lapses, the most accurate algorithms give very few errors ( $FNMR < 0.001$ ) so that the uncertainty estimates are high.

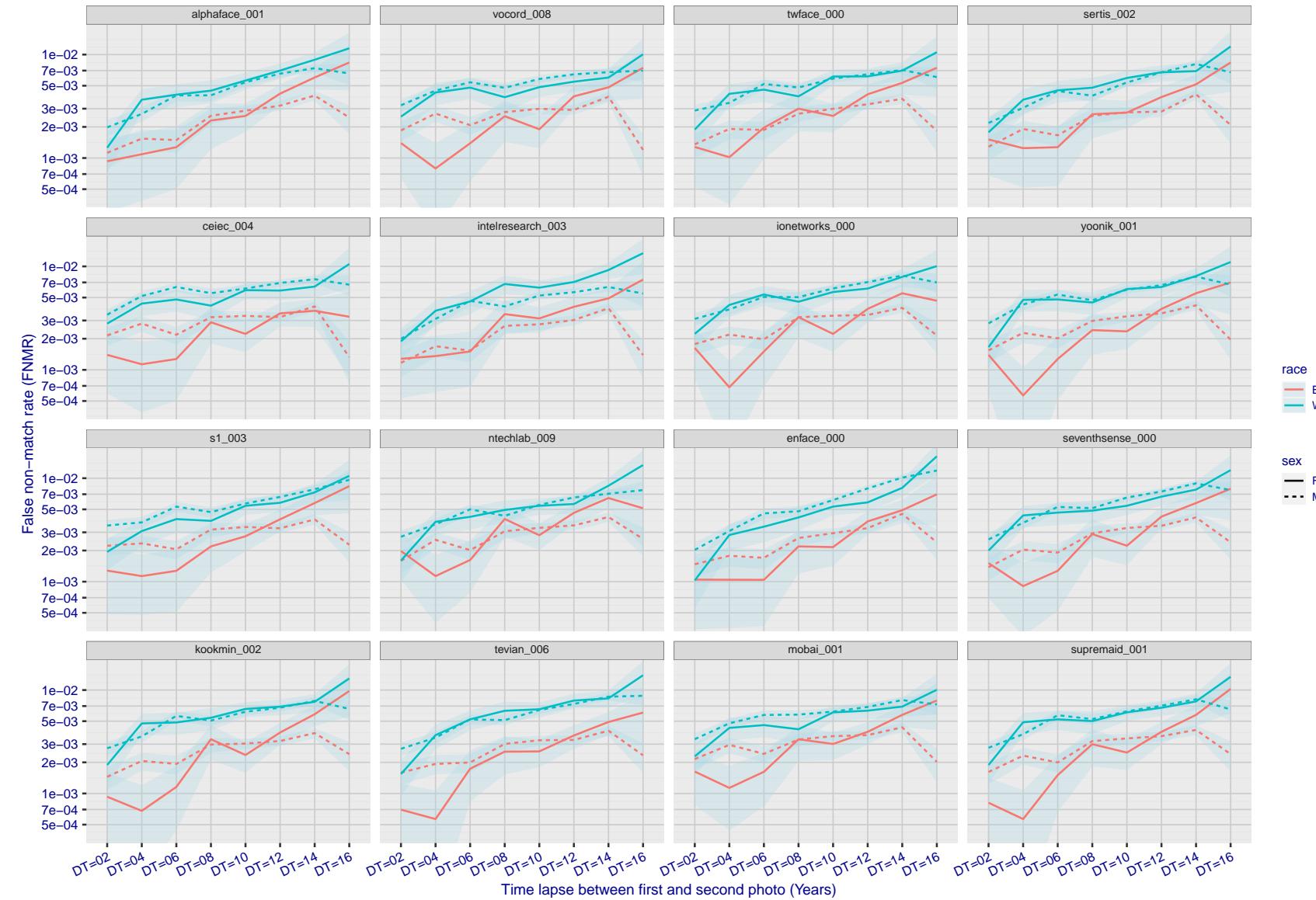


Figure 242: For the mugshot images, FNMR as a function of elapsed time between initial enrollment and second verification images. The panels appear most accurate first, and vertical scale changes on each page. The four traces correspond to images annotated with codes for black female, black male, white female, white male. The threshold is fixed for each algorithm to give  $FMR = 0.00001$  over all ( $10^8$ ) impostor comparisons. For short time-lapses, the most accurate algorithms give very few errors ( $FNMR < 0.001$ ) so that the uncertainty estimates are high.

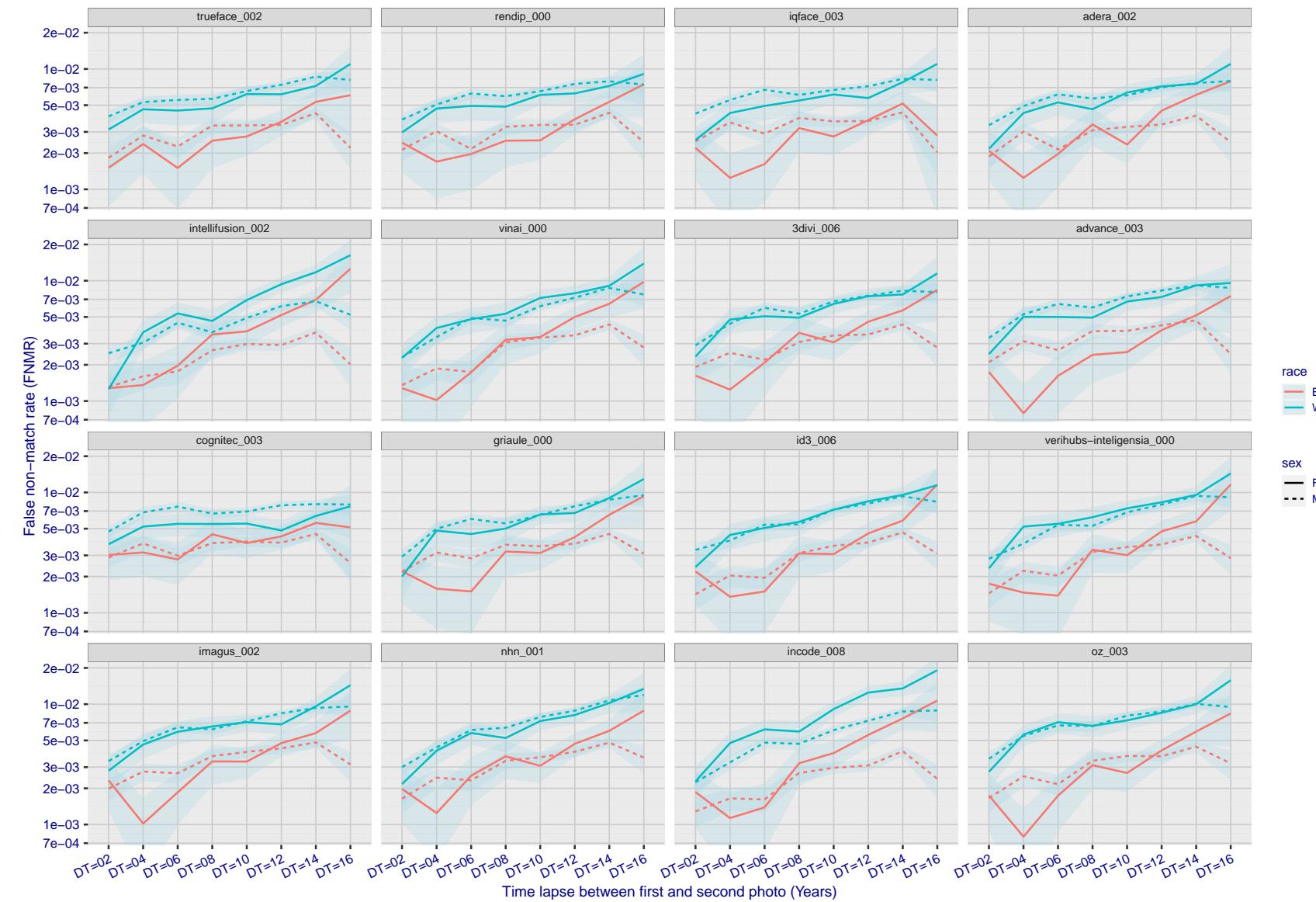


Figure 243: For the mugshot images, FNMR as a function of elapsed time between initial enrollment and second verification images. The panels appear most accurate first, and vertical scale changes on each page. The four traces correspond to images annotated with codes for black female, black male, white female, white male. The threshold is fixed for each algorithm to give  $FMR = 0.00001$  over all ( $10^8$ ) impostor comparisons. For short time-lapses, the most accurate algorithms give very few errors ( $FNMR < 0.001$ ) so that the uncertainty estimates are high.

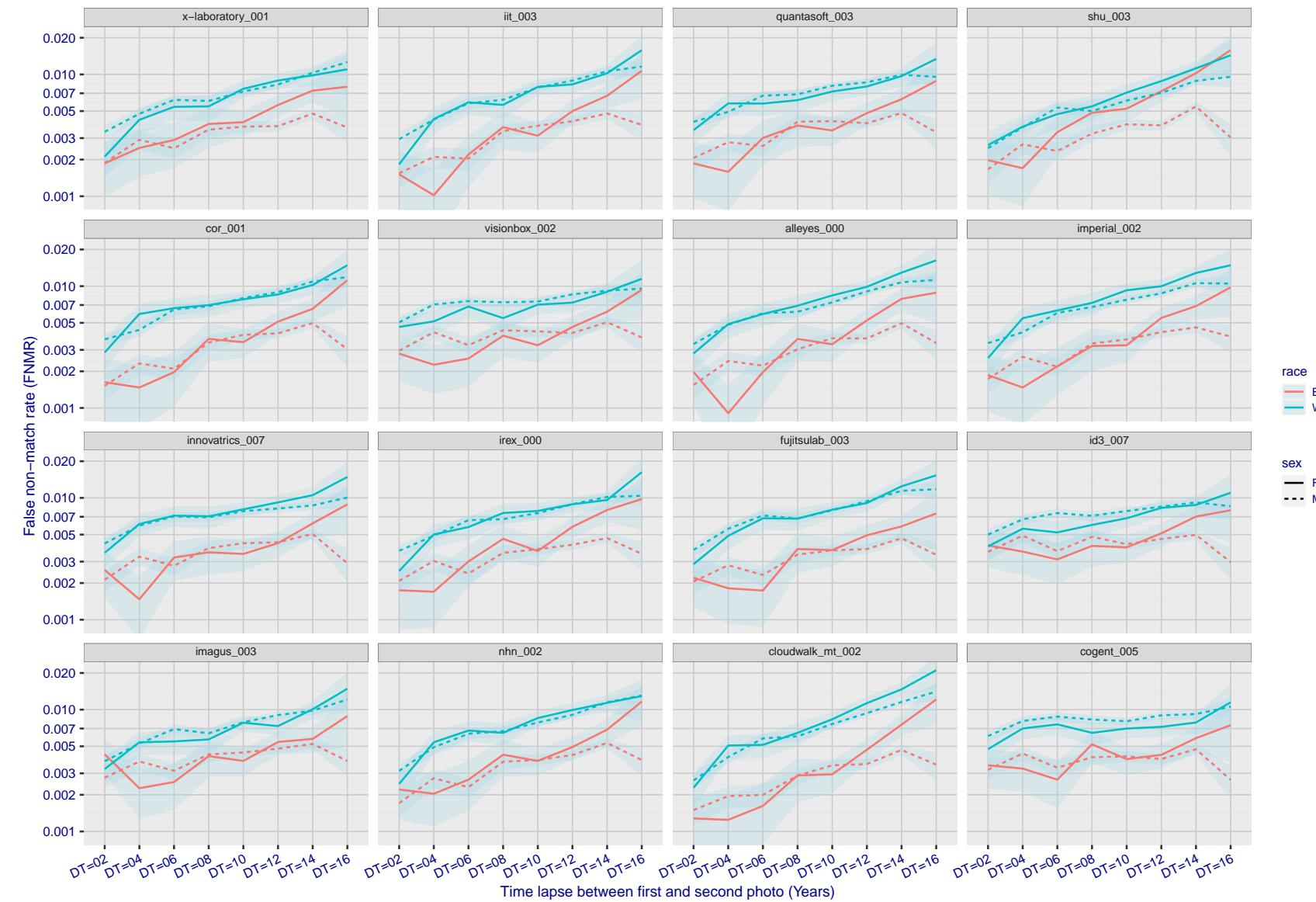


Figure 244: For the mugshot images, FNMR as a function of elapsed time between initial enrollment and second verification images. The panels appear most accurate first, and vertical scale changes on each page. The four traces correspond to images annotated with codes for black female, black male, white female, white male. The threshold is fixed for each algorithm to give  $FMR = 0.00001$  over all ( $10^8$ ) impostor comparisons. For short time-lapses, the most accurate algorithms give very few errors ( $FNMR < 0.001$ ) so that the uncertainty estimates are high.

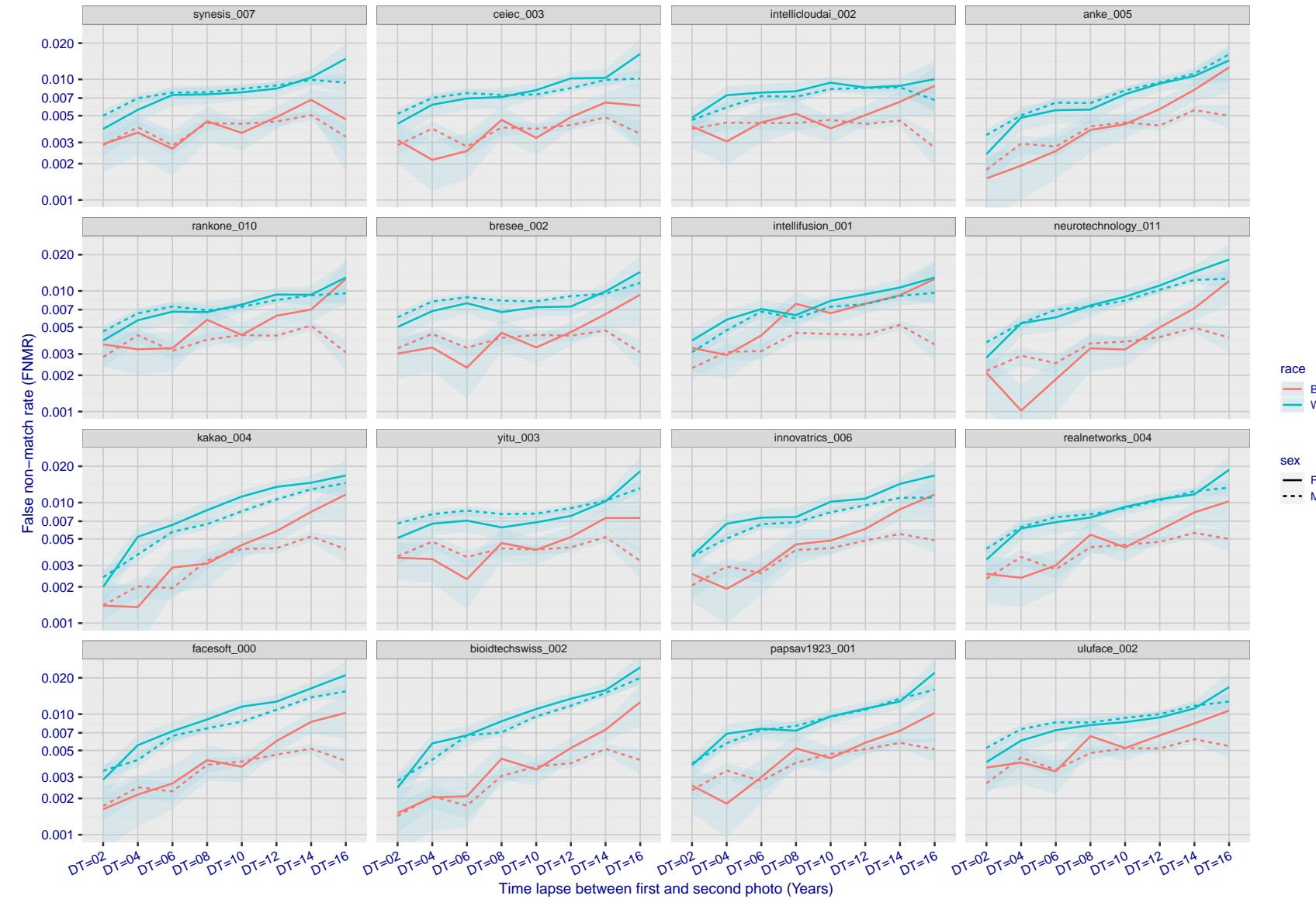


Figure 245: For the mugshot images, FNMR as a function of elapsed time between initial enrollment and second verification images. The panels appear most accurate first, and vertical scale changes on each page. The four traces correspond to images annotated with codes for black female, black male, white female, white male. The threshold is fixed for each algorithm to give FMR = 0.00001 over all ( $10^8$ ) impostor comparisons. For short time-lapses, the most accurate algorithms give very few errors (FNMR < 0.001) so that the uncertainty estimates are high.

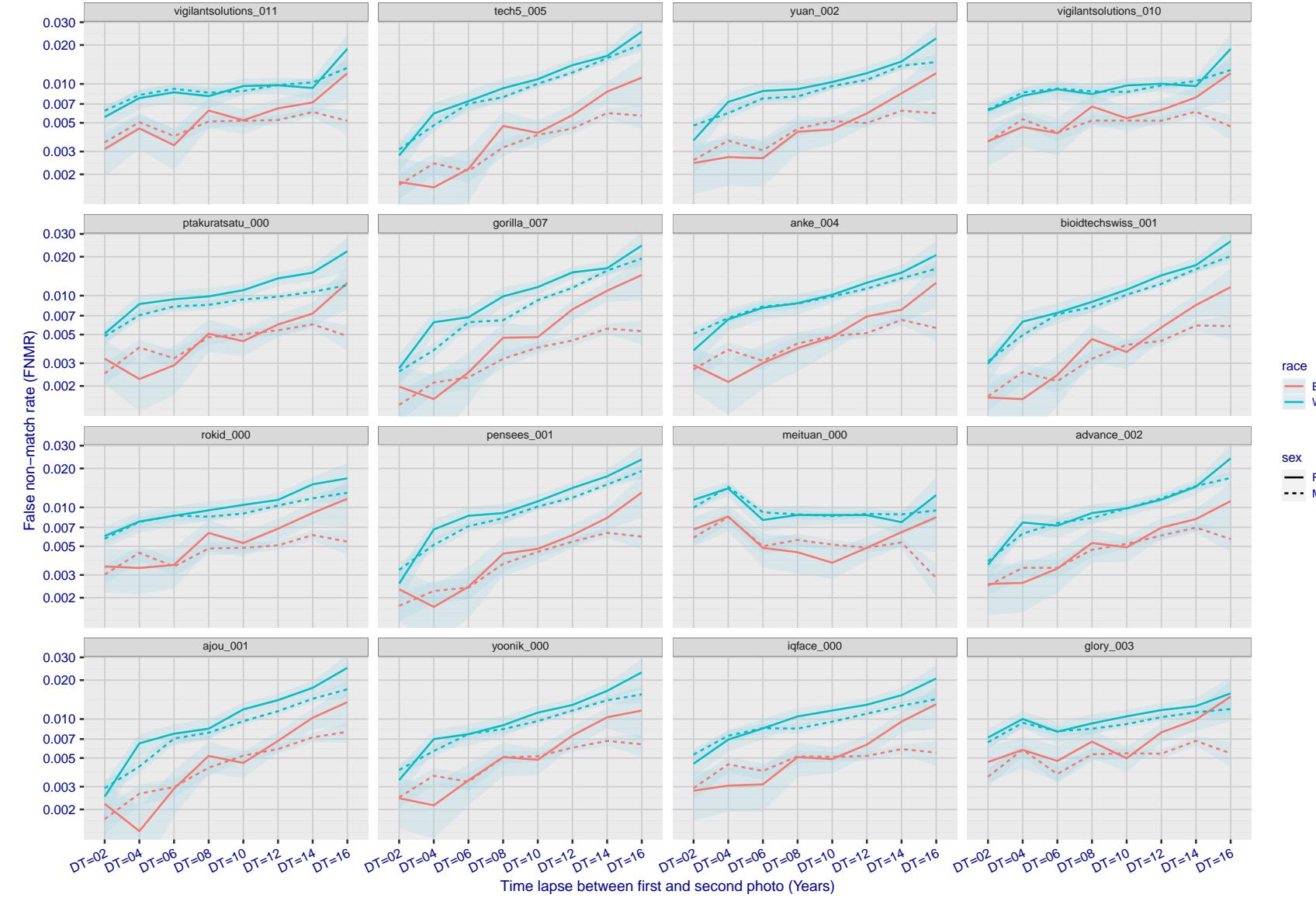


Figure 246: For the mugshot images, FNMR as a function of elapsed time between initial enrollment and second verification images. The panels appear most accurate first, and vertical scale changes on each page. The four traces correspond to images annotated with codes for black female, black male, white female, white male. The threshold is fixed for each algorithm to give  $FMR = 0.00001$  over all ( $10^8$ ) impostor comparisons. For short time-lapses, the most accurate algorithms give very few errors ( $FNMR < 0.001$ ) so that the uncertainty estimates are high.

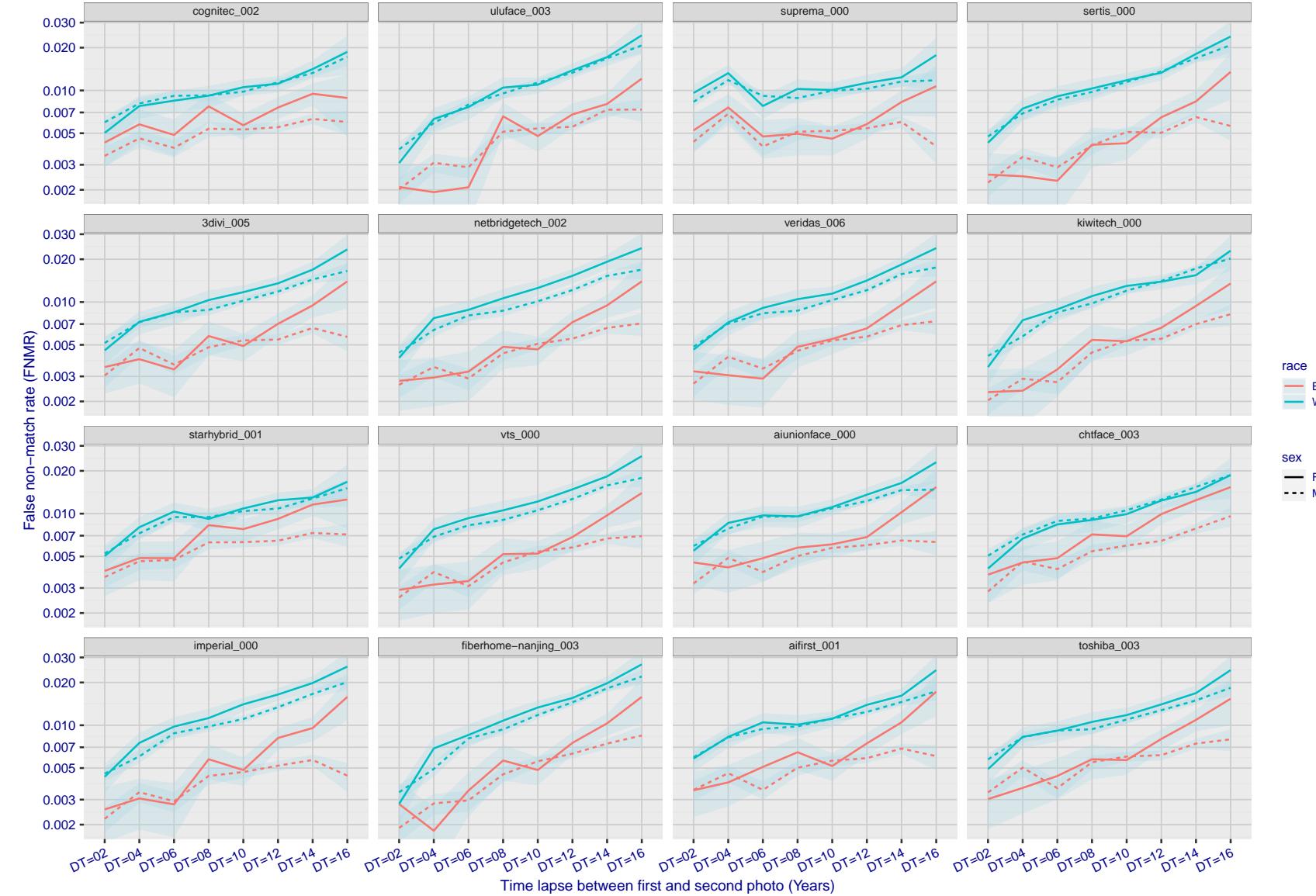


Figure 247: For the mugshot images, FNMR as a function of elapsed time between initial enrollment and second verification images. The panels appear most accurate first, and vertical scale changes on each page. The four traces correspond to images annotated with codes for black female, black male, white female, white male. The threshold is fixed for each algorithm to give FMR = 0.00001 over all ( $10^8$ ) impostor comparisons. For short time-lapses, the most accurate algorithms give very few errors (FNMR < 0.001) so that the uncertainty estimates are high.

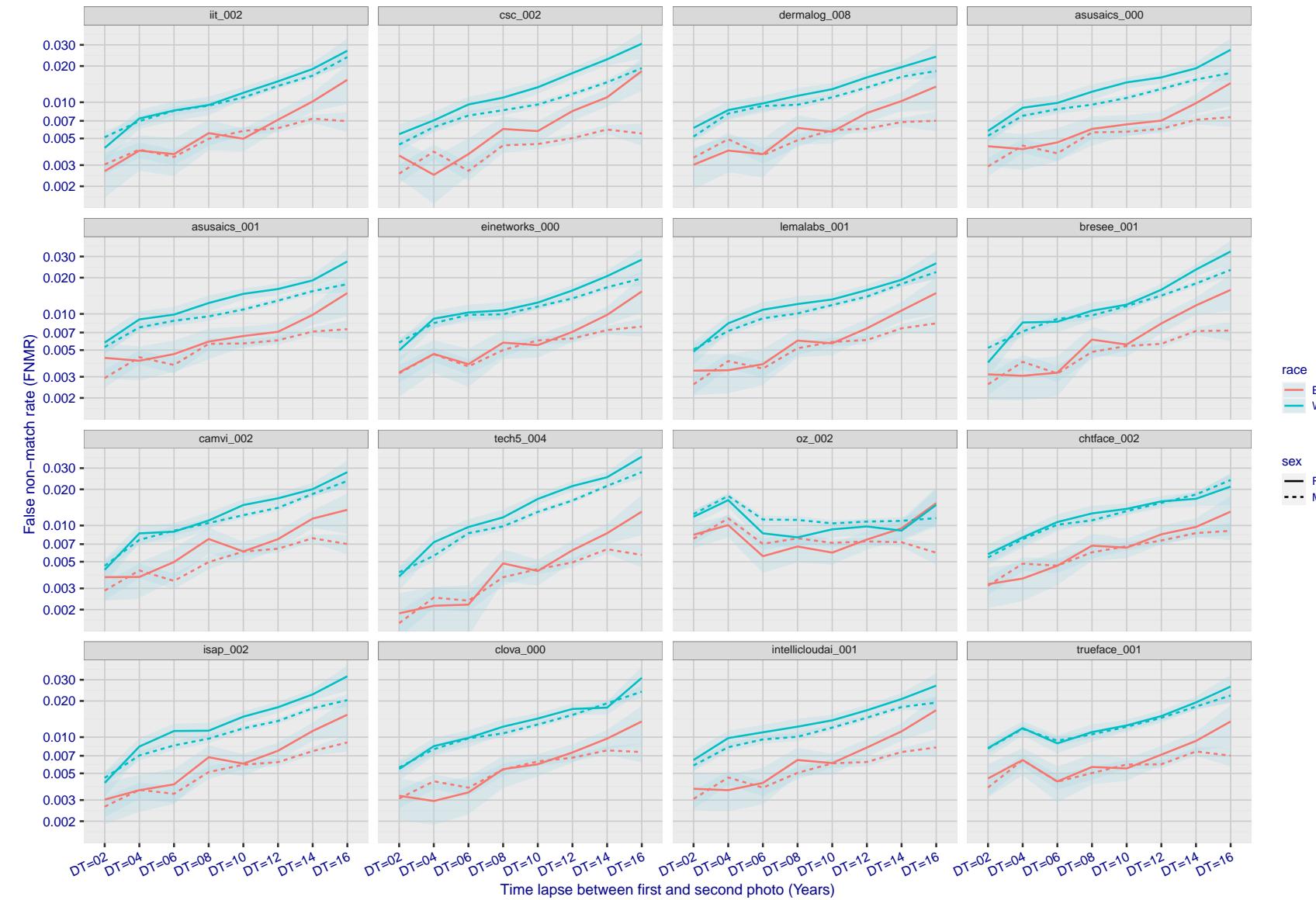


Figure 248: For the mugshot images, FNMR as a function of elapsed time between initial enrollment and second verification images. The panels appear most accurate first, and vertical scale changes on each page. The four traces correspond to images annotated with codes for black female, black male, white female, white male. The threshold is fixed for each algorithm to give  $FMR = 0.00001$  over all ( $10^8$ ) impostor comparisons. For short time-lapses, the most accurate algorithms give very few errors ( $FNMR < 0.001$ ) so that the uncertainty estimates are high.

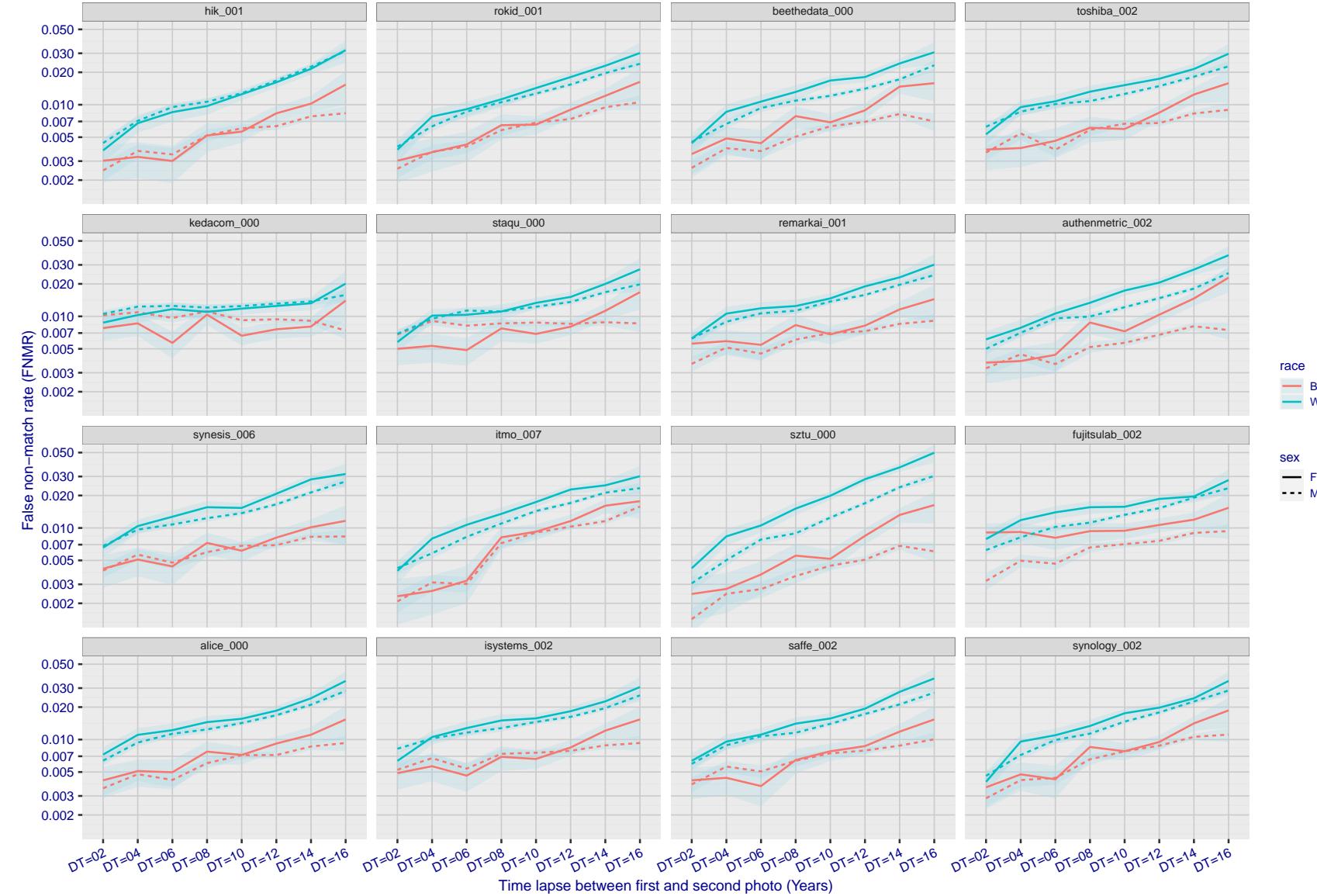


Figure 249: For the mugshot images, FNMR as a function of elapsed time between initial enrollment and second verification images. The panels appear most accurate first, and vertical scale changes on each page. The four traces correspond to images annotated with codes for black female, black male, white female, white male. The threshold is fixed for each algorithm to give  $FMR = 0.00001$  over all ( $10^8$ ) impostor comparisons. For short time-lapses, the most accurate algorithms give very few errors ( $FNMR < 0.001$ ) so that the uncertainty estimates are high.

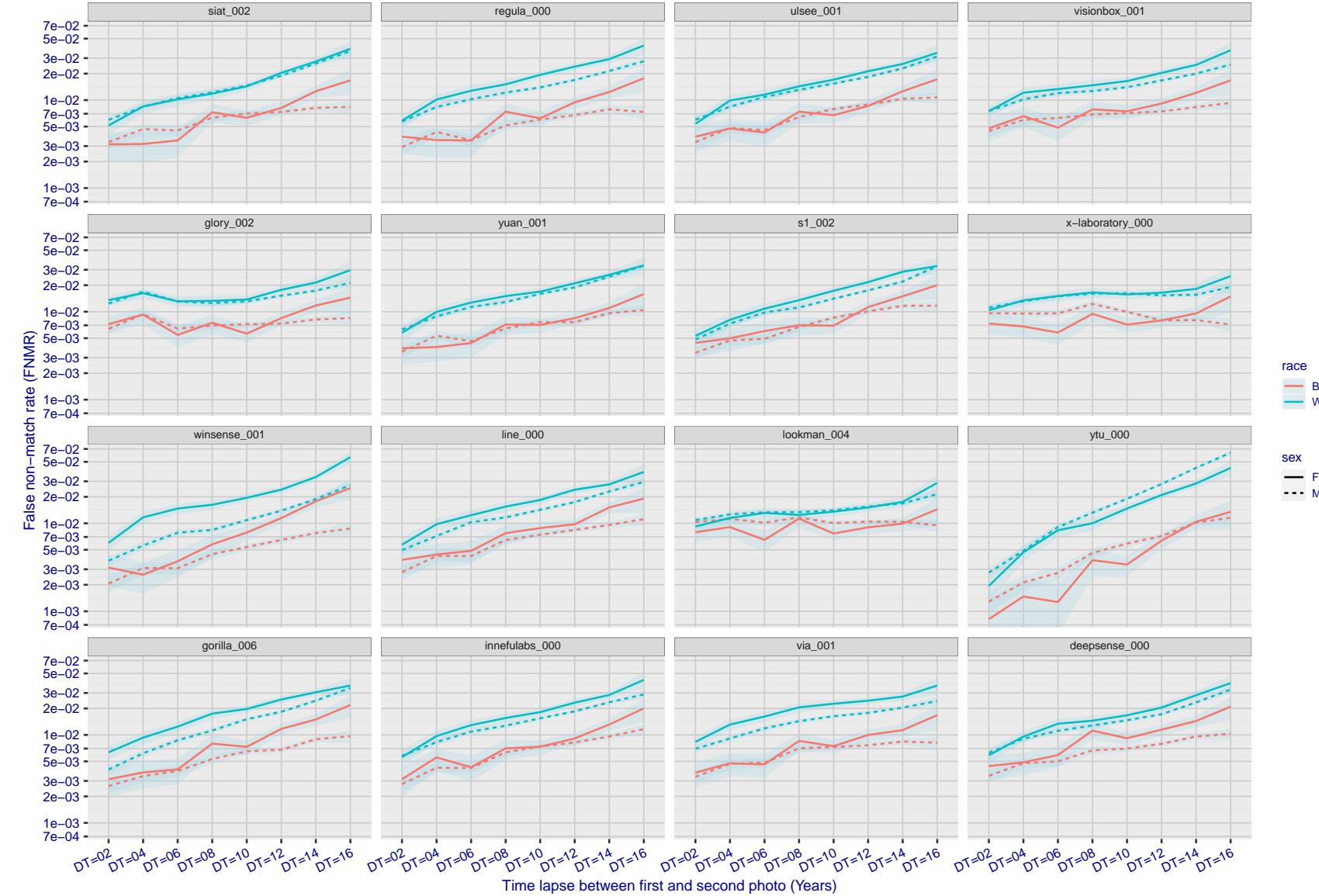


Figure 250: For the mugshot images, FNMR as a function of elapsed time between initial enrollment and second verification images. The panels appear most accurate first, and vertical scale changes on each page. The four traces correspond to images annotated with codes for black female, black male, white female, white male. The threshold is fixed for each algorithm to give  $FMR = 0.00001$  over all ( $10^8$ ) impostor comparisons. For short time-lapses, the most accurate algorithms give very few errors ( $FNMR < 0.001$ ) so that the uncertainty estimates are high.

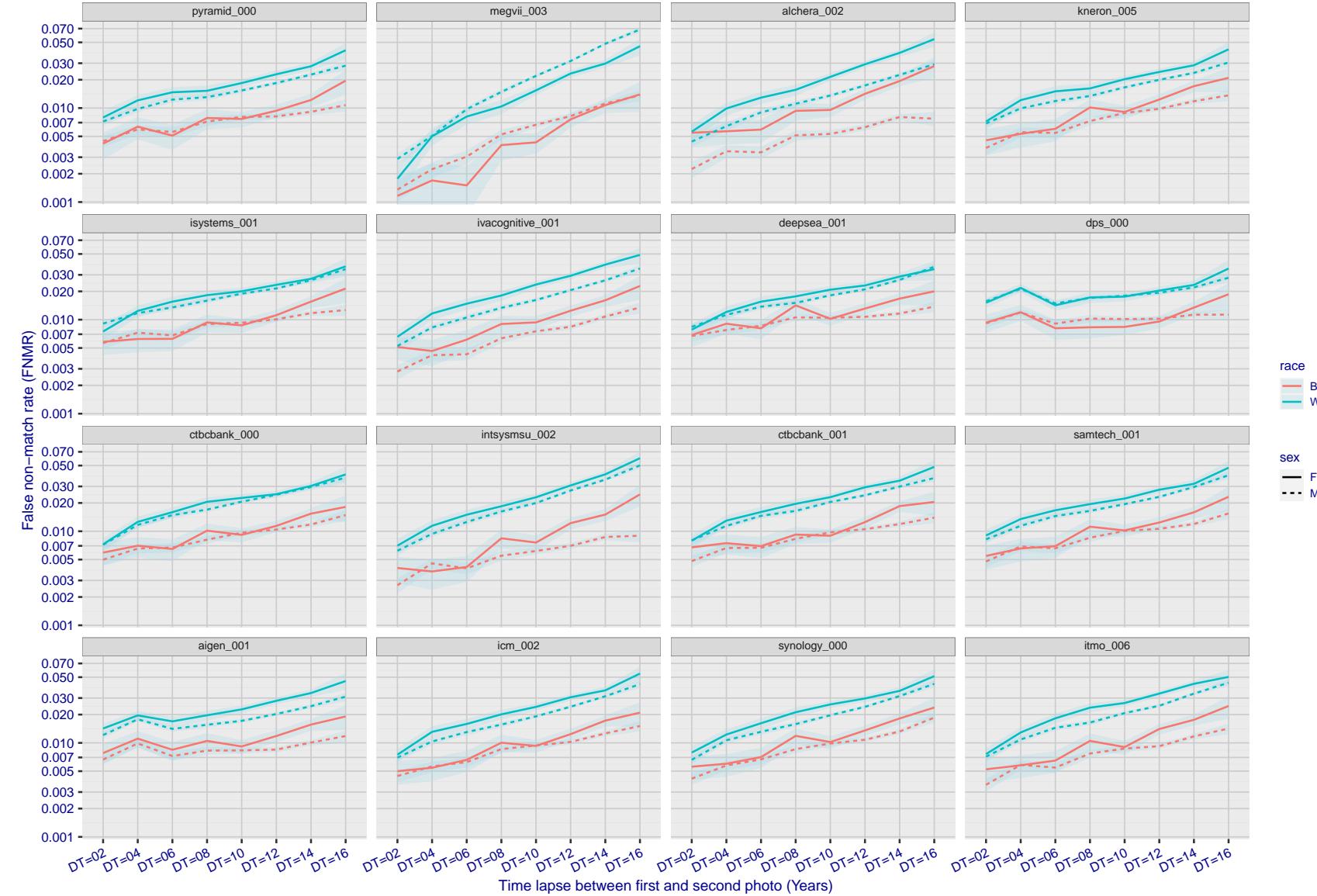


Figure 251: For the mugshot images, FNMR as a function of elapsed time between initial enrollment and second verification images. The panels appear most accurate first, and vertical scale changes on each page. The four traces correspond to images annotated with codes for black female, black male, white female, white male. The threshold is fixed for each algorithm to give FMR = 0.00001 over all ( $10^8$ ) impostor comparisons. For short time-lapses, the most accurate algorithms give very few errors (FNMR < 0.001) so that the uncertainty estimates are high.

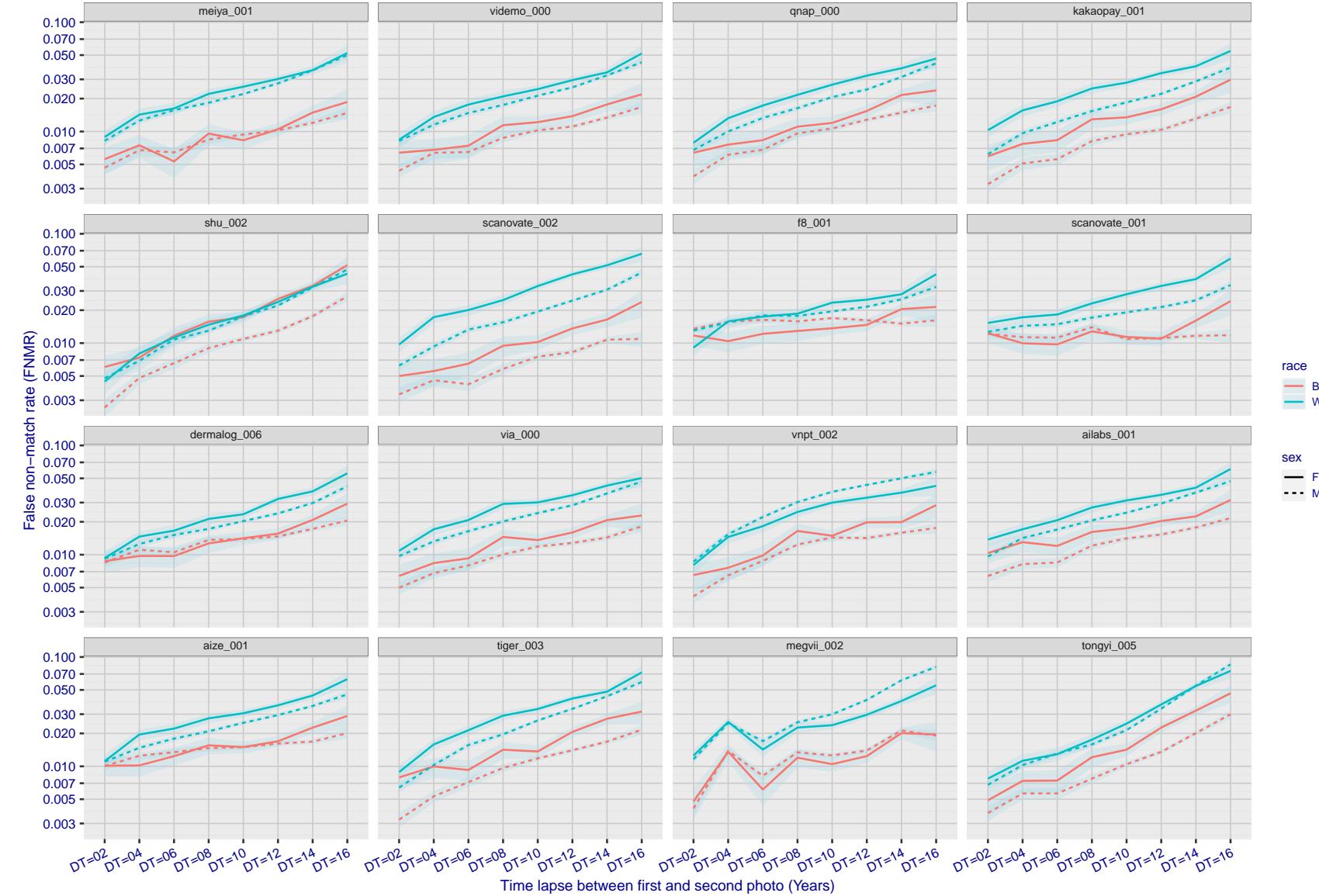
FNMR(T)  
FMR(T)  
"False match rate"

Figure 252: For the mugshot images, FNMR as a function of elapsed time between initial enrollment and second verification images. The panels appear most accurate first, and vertical scale changes on each page. The four traces correspond to images annotated with codes for black female, black male, white female, white male. The threshold is fixed for each algorithm to give FMR = 0.00001 over all ( $10^8$ ) impostor comparisons. For short time-lapses, the most accurate algorithms give very few errors (FNMR < 0.001) so that the uncertainty estimates are high.

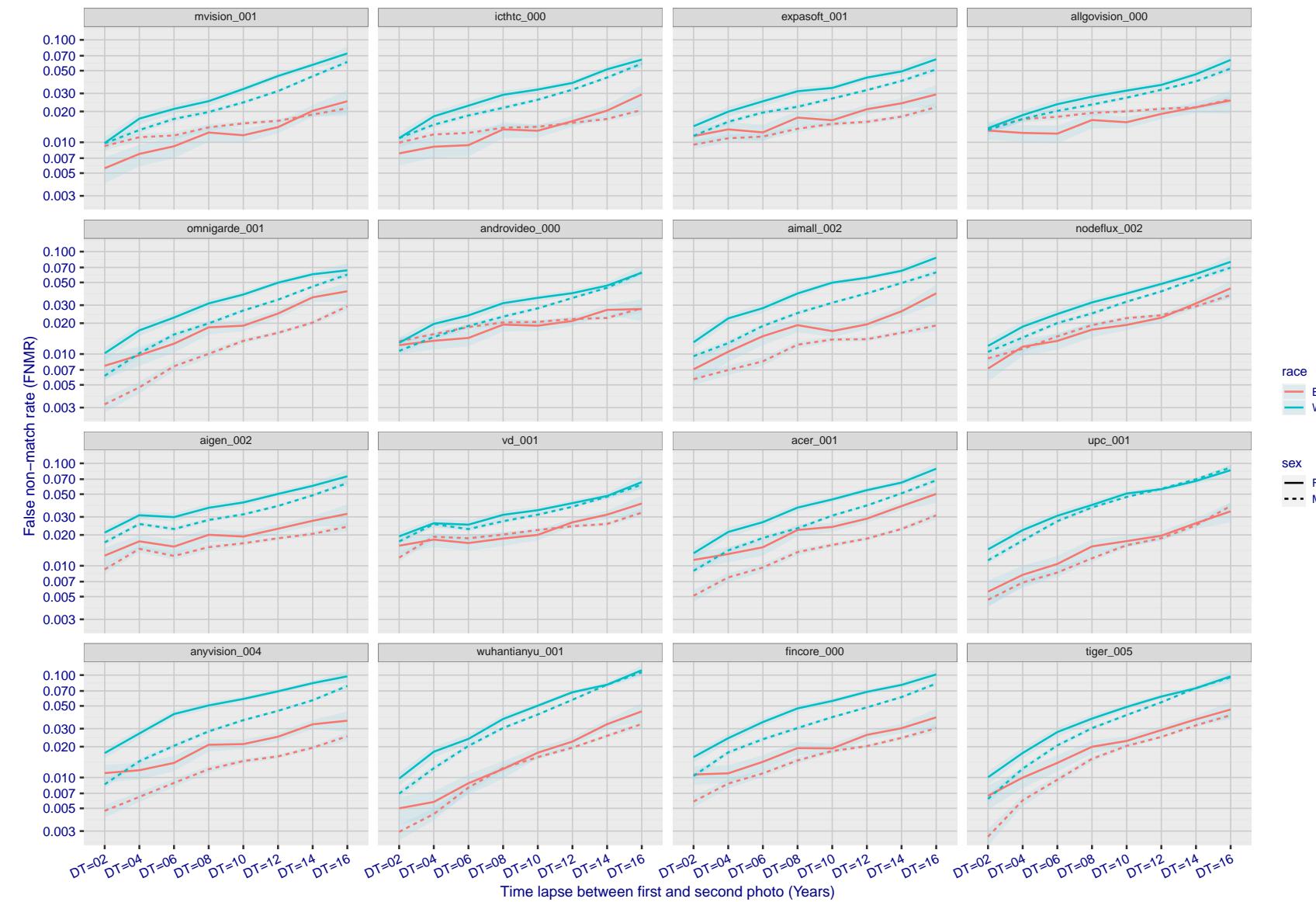


Figure 253: For the mugshot images, FNMR as a function of elapsed time between initial enrollment and second verification images. The panels appear most accurate first, and vertical scale changes on each page. The four traces correspond to images annotated with codes for black female, black male, white female, white male. The threshold is fixed for each algorithm to give  $FMR = 0.00001$  over all ( $10^8$ ) impostor comparisons. For short time-lapses, the most accurate algorithms give very few errors ( $FNMR < 0.001$ ) so that the uncertainty estimates are high.

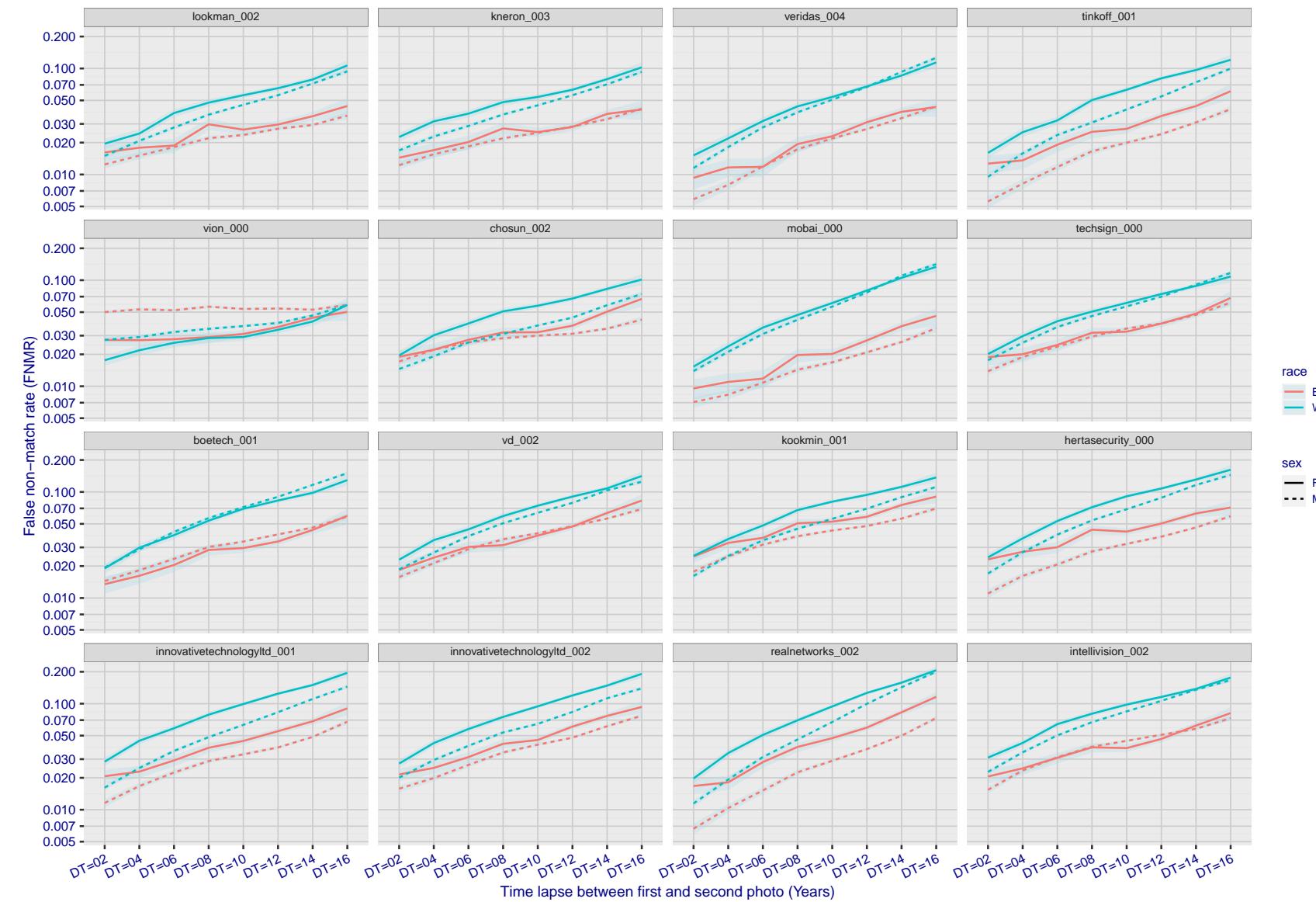


Figure 254: For the mugshot images, FNMR as a function of elapsed time between initial enrollment and second verification images. The panels appear most accurate first, and vertical scale changes on each page. The four traces correspond to images annotated with codes for black female, black male, white female, white male. The threshold is fixed for each algorithm to give FMR = 0.00001 over all ( $10^8$ ) impostor comparisons. For short time-lapses, the most accurate algorithms give very few errors (FNMR < 0.001) so that the uncertainty estimates are high.

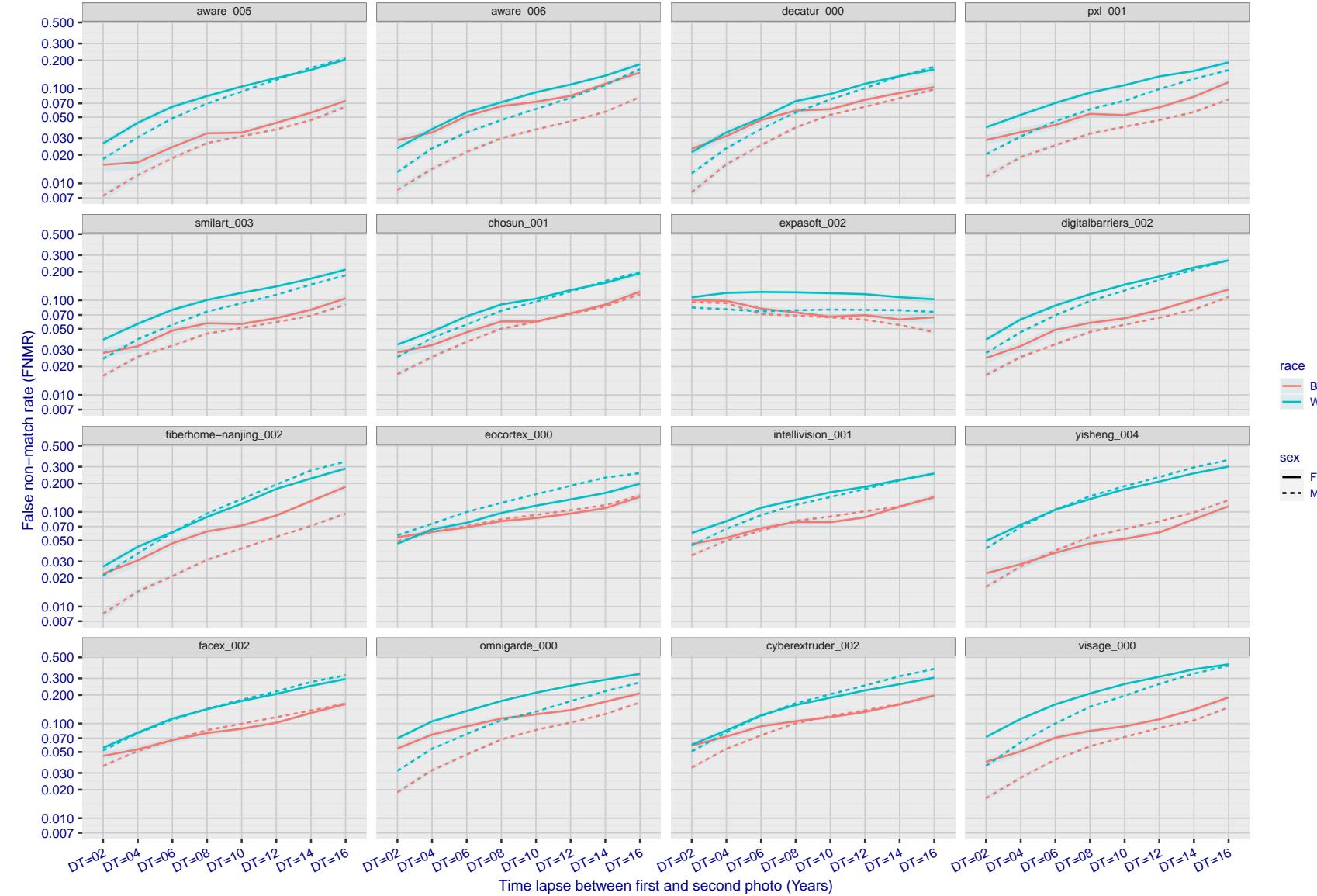
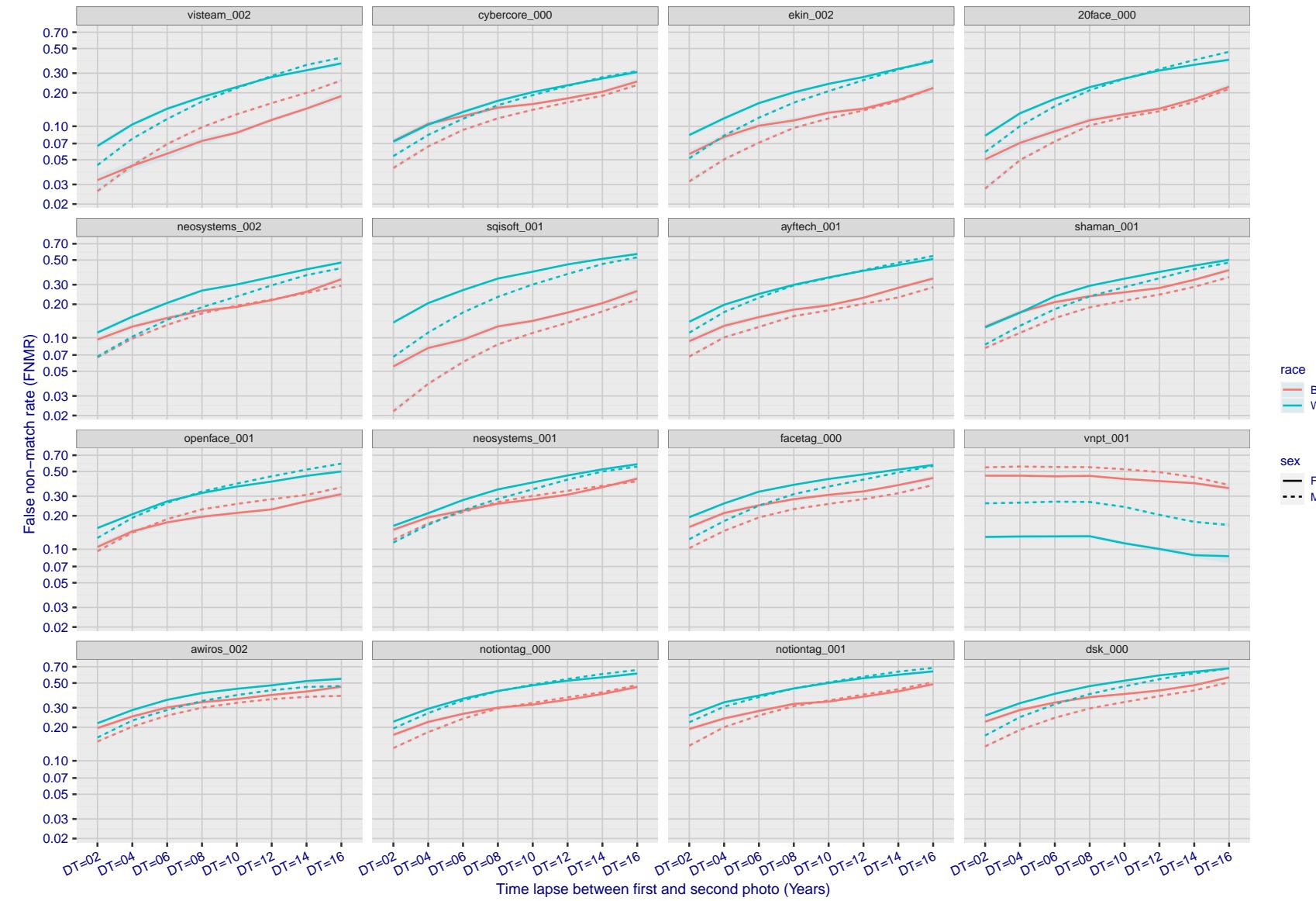


Figure 255: For the mugshot images, FNMR as a function of elapsed time between initial enrollment and second verification images. The panels appear most accurate first, and vertical scale changes on each page. The four traces correspond to images annotated with codes for black female, black male, white female, white male. The threshold is fixed for each algorithm to give  $FMR = 0.00001$  over all ( $10^8$ ) impostor comparisons. For short time-lapses, the most accurate algorithms give very few errors ( $FNMR < 0.001$ ) so that the uncertainty estimates are high.



race  
B (red)  
W (cyan)

sex  
F (solid line)  
M (dashed line)

Figure 256: For the mugshot images, FNMR as a function of elapsed time between initial enrollment and second verification images. The panels appear most accurate first, and vertical scale changes on each page. The four traces correspond to images annotated with codes for black female, black male, white female, white male. The threshold is fixed for each algorithm to give FMR = 0.00001 over all ( $10^8$ ) impostor comparisons. For short time-lapses, the most accurate algorithms give very few errors (FNMR < 0.001) so that the uncertainty estimates are high.

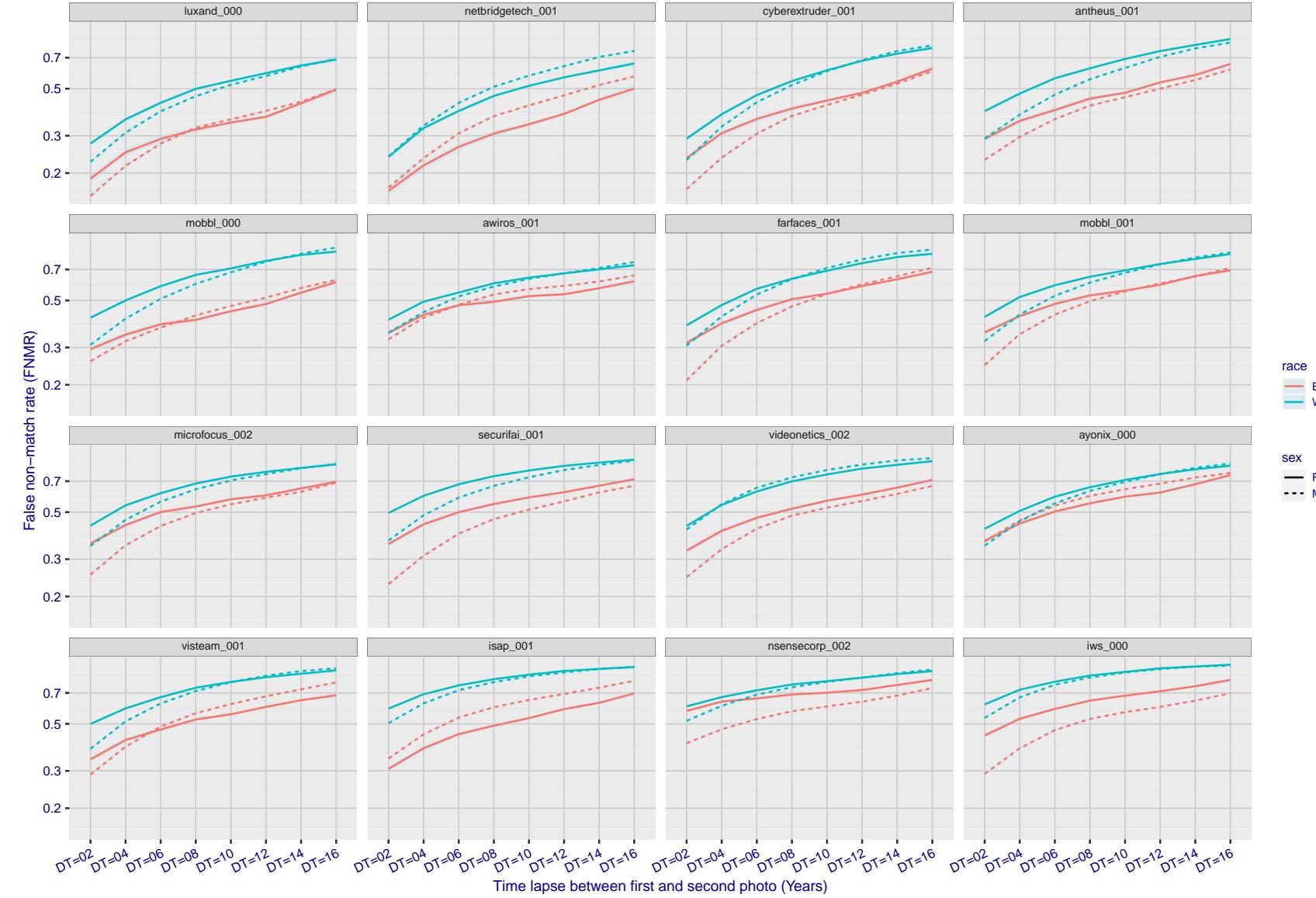


Figure 257: For the mugshot images, FNMR as a function of elapsed time between initial enrollment and second verification images. The panels appear most accurate first, and vertical scale changes on each page. The four traces correspond to images annotated with codes for black female, black male, white female, white male. The threshold is fixed for each algorithm to give FMR = 0.00001 over all ( $10^8$ ) impostor comparisons. For short time-lapses, the most accurate algorithms give very few errors (FNMR < 0.001) so that the uncertainty estimates are high.

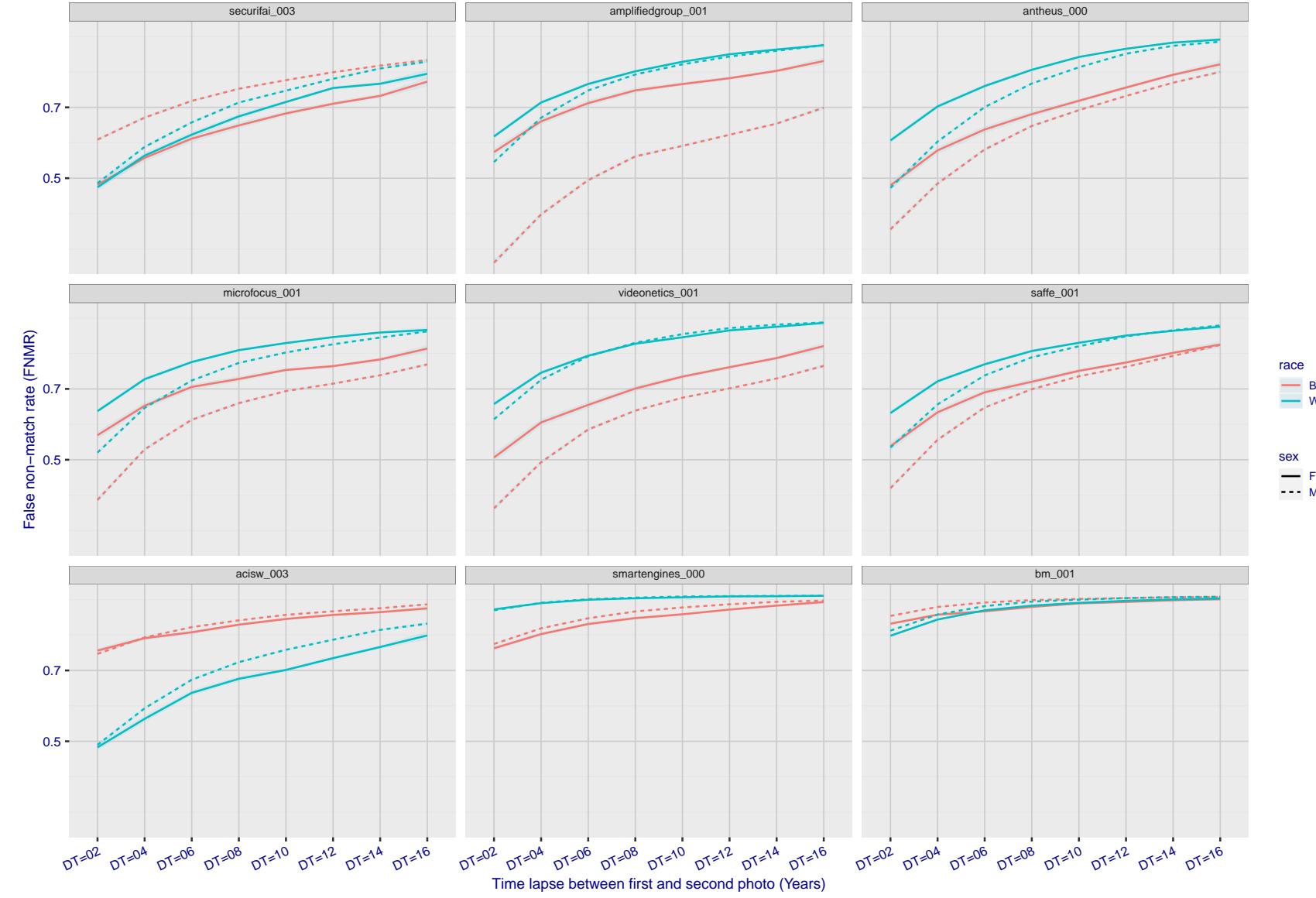


Figure 258: For the mugshot images, FNMR as a function of elapsed time between initial enrollment and second verification images. The panels appear most accurate first, and vertical scale changes on each page. The four traces correspond to images annotated with codes for black female, black male, white female, white male. The threshold is fixed for each algorithm to give  $FMR = 0.00001$  over all ( $10^8$ ) impostor comparisons. For short time-lapses, the most accurate algorithms give very few errors ( $FNMR < 0.001$ ) so that the uncertainty estimates are high.

### 3.5.3 Effect of age on genuine subjects

**Background:** Faces change appearance throughout life. Face recognition algorithms have previously been reported to give better accuracy on older individuals (See NIST IR 8009).

**Goal:** To quantify false non-match rates (FNMR) as a function of age, without an ageing component.

**Methods:** Using the visa images, which span fewer than five years, thresholds are determined that give FMR = 0.001 and 0.0001 over the entire impostor set. Then FNMR is measured over 1000 bootstrap replications of the genuine scores.

**Results:** For the visa images, Figure 287 shows how false non-match rates for genuine users, as a function of age group.

The notable aspects are:

- ▷ Younger subjects give considerably higher FNMR. This is likely due to rapid growth and change in facial appearance.
- ▷ FNMR trends down throughout life. The last bin, AGE > 72, contains fewer than 140 mated pairs, and may be affected by small sample size.

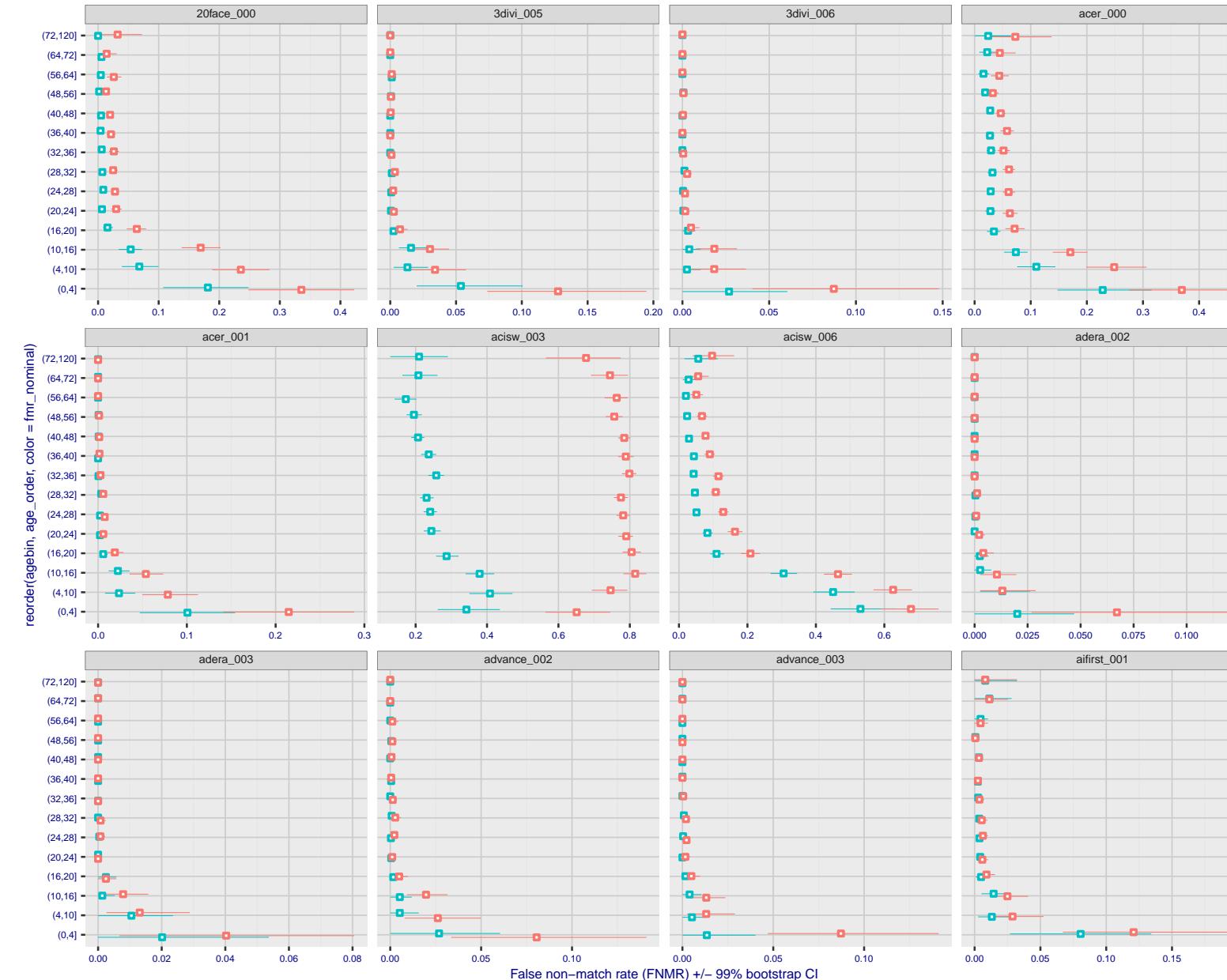


Figure 259: For the visa images, the dots show FNMR by age group for two operating thresholds corresponding to  $FMR = \{0.001, 0.0001\}$  computed over all on the order of  $10^{10}$  impostor scores. The FMR in each bin will vary also - see subsequent impostor heatmaps in sec. 3.6.2. Given a pair of face images taken at different times, we assign the comparison to the bin that is the arithmetic average of the subject's ages. This plot shows only the effect of age, not ageing. The number of comparisons in each bin is generally in the thousands, however the first and last bins are computed over 149 and 124 respectively. The error rates in some (adult) cases are zero, and in others the DET is flat so the error rates at the two thresholds are identical. The lines span 1% and 99% of bootstrap replicated FNMR estimates.



FNMR(T)  
FMR(T)  
"False non-match rate"  
"False match rate"

Figure 260: For the visa images, the dots show FNMR by age group for two operating thresholds corresponding to  $FMR = \{0.001, 0.0001\}$  computed over all on the order of  $10^{10}$  impostor scores. The FMR in each bin will vary also - see subsequent impostor heatmaps in sec. 3.6.2. Given a pair of face images taken at different times, we assign the comparison to the bin that is the arithmetic average of the subject's ages. This plot shows only the effect of age, not ageing. The number of comparisons in each bin is generally in the thousands, however the first and last bins are computed over 149 and 124 respectively. The error rates in some (adult) cases are zero, and in others the DET is flat so the error rates at the two thresholds are identical. The lines span 1% and 99% of bootstrap replicated FNMR estimates.

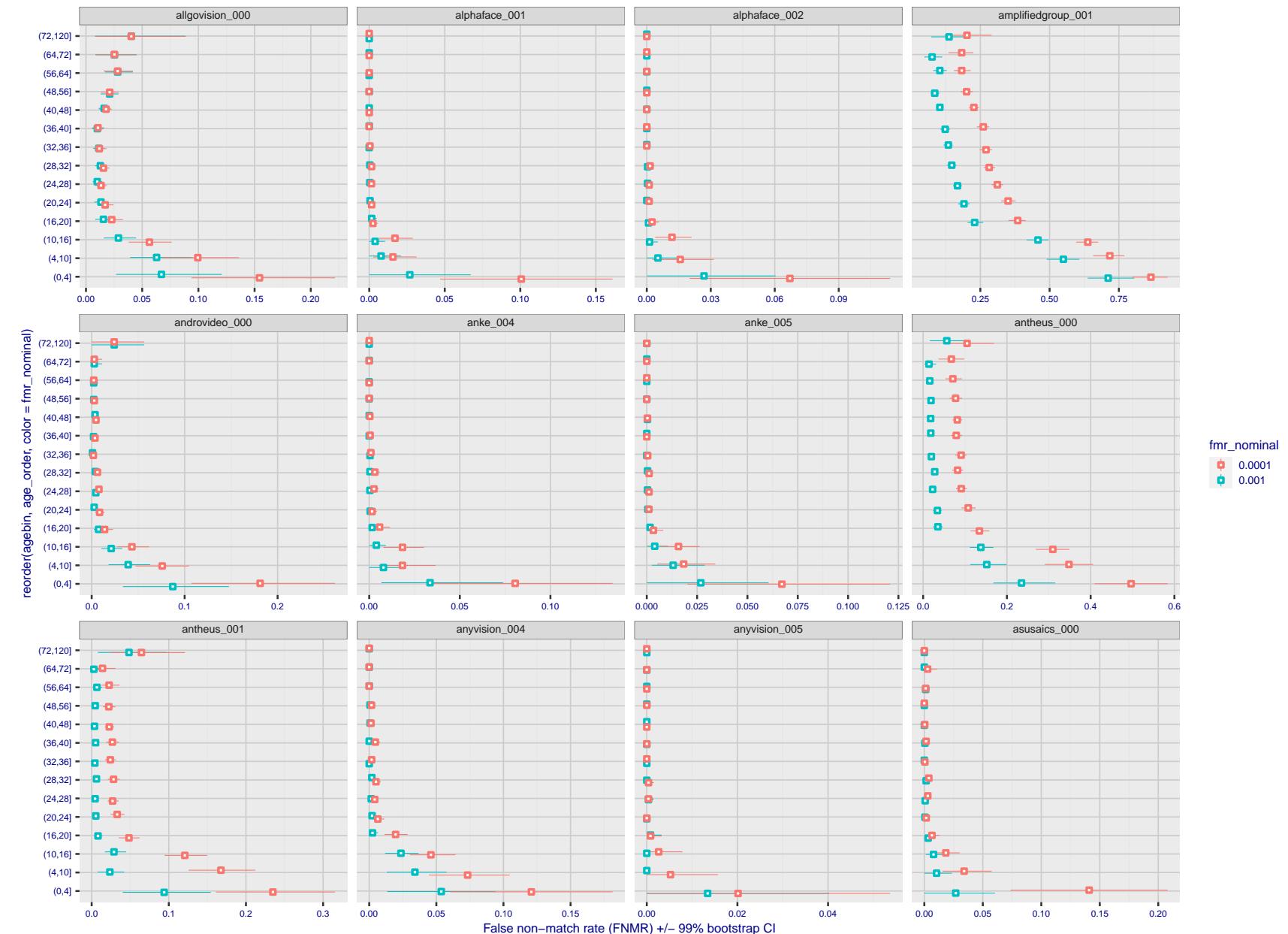


Figure 261: For the visa images, the dots show FNMR by age group for two operating thresholds corresponding to  $FMR = \{0.001, 0.0001\}$  computed over all on the order of  $10^{10}$  impostor scores. The FMR in each bin will vary also - see subsequent impostor heatmaps in sec. 3.6.2. Given a pair of face images taken at different times, we assign the comparison to the bin that is the arithmetic average of the subject's ages. This plot shows only the effect of age, not ageing. The number of comparisons in each bin is generally in the thousands, however the first and last bins are computed over 149 and 124 respectively. The error rates in some (adult) cases are zero, and in others the DET is flat so the error rates at the two thresholds are identical. The lines span 1% and 99% of bootstrap replicated FNMR estimates.



Figure 262: For the visa images, the dots show FNMR by age group for two operating thresholds corresponding to  $FMR = \{0.001, 0.0001\}$  computed over all on the order of  $10^{10}$  impostor scores. The FMR in each bin will vary also - see subsequent impostor heatmaps in sec. 3.6.2. Given a pair of face images taken at different times, we assign the comparison to the bin that is the arithmetic average of the subject's ages. This plot shows only the effect of age, not ageing. The number of comparisons in each bin is generally in the thousands, however the first and last bins are computed over 149 and 124 respectively. The error rates in some (adult) cases are zero, and in others the DET is flat so the error rates at the two thresholds are identical. The lines span 1% and 99% of bootstrap replicated FNMR estimates.



Figure 263: For the visa images, the dots show FNMR by age group for two operating thresholds corresponding to  $FMR = \{0.001, 0.0001\}$  computed over all on the order of  $10^{10}$  impostor scores. The FMR in each bin will vary also - see subsequent impostor heatmaps in sec. 3.6.2. Given a pair of face images taken at different times, we assign the comparison to the bin that is the arithmetic average of the subject's ages. This plot shows only the effect of age, not ageing. The number of comparisons in each bin is generally in the thousands, however the first and last bins are computed over 149 and 124 respectively. The error rates in some (adult) cases are zero, and in others the DET is flat so the error rates at the two thresholds are identical. The lines span 1% and 99% of bootstrap replicated FNMR estimates.



Figure 264: For the visa images, the dots show FNMR by age group for two operating thresholds corresponding to  $FMR = \{0.001, 0.0001\}$  computed over all on the order of  $10^{10}$  impostor scores. The FMR in each bin will vary also - see subsequent impostor heatmaps in sec. 3.6.2. Given a pair of face images taken at different times, we assign the comparison to the bin that is the arithmetic average of the subject's ages. This plot shows only the effect of age, not ageing. The number of comparisons in each bin is generally in the thousands, however the first and last bins are computed over 149 and 124 respectively. The error rates in some (adult) cases are zero, and in others the DET is flat so the error rates at the two thresholds are identical. The lines span 1% and 99% of bootstrap replicated FNMR estimates.

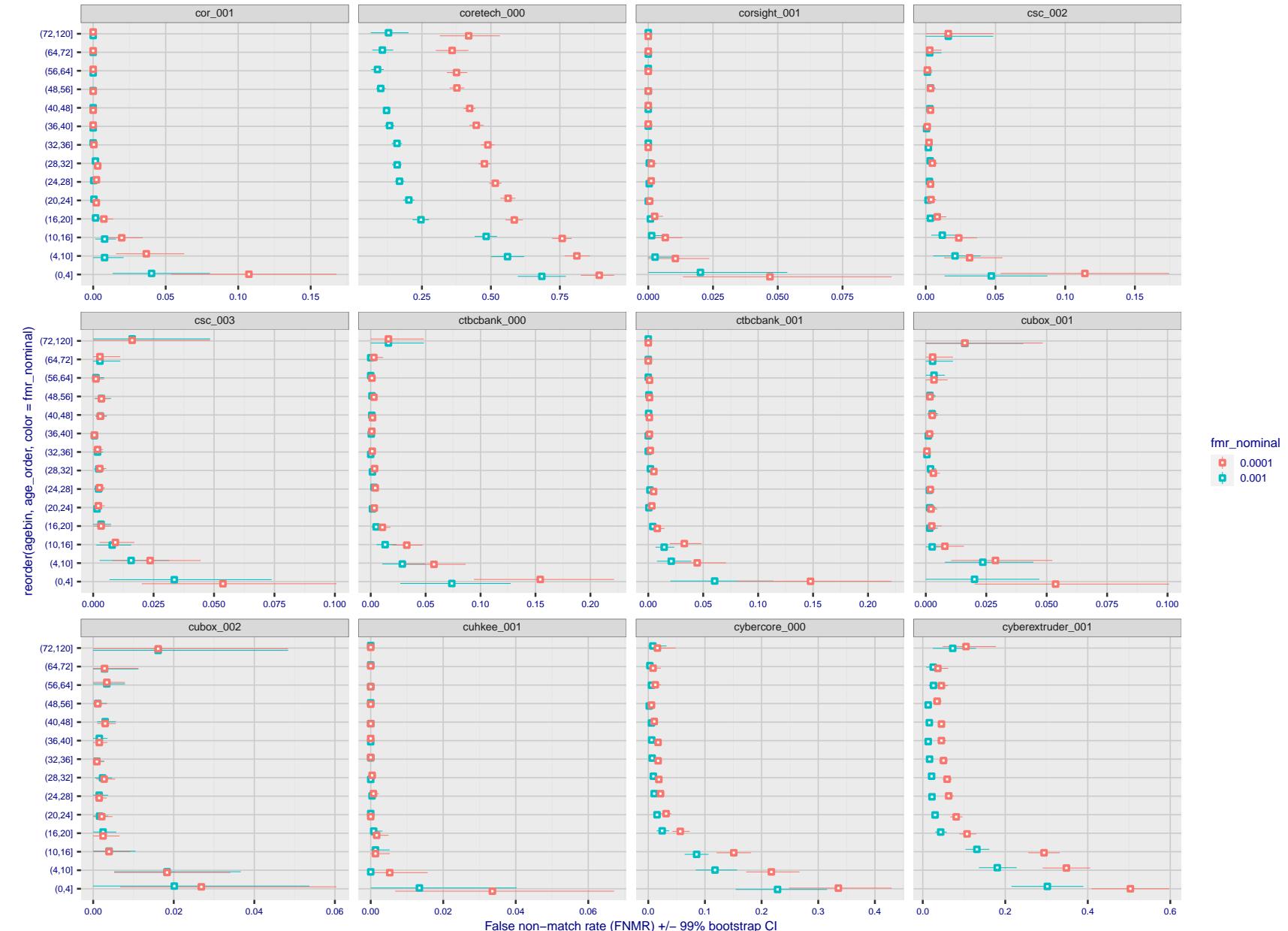


Figure 265: For the visa images, the dots show FNMR by age group for two operating thresholds corresponding to  $FMR = \{0.001, 0.0001\}$  computed over all on the order of  $10^{10}$  impostor scores. The FMR in each bin will vary also - see subsequent impostor heatmaps in sec. 3.6.2. Given a pair of face images taken at different times, we assign the comparison to the bin that is the arithmetic average of the subject's ages. This plot shows only the effect of age, not ageing. The number of comparisons in each bin is generally in the thousands, however the first and last bins are computed over 149 and 124 respectively. The error rates in some (adult) cases are zero, and in others the DET is flat so the error rates at the two thresholds are identical. The lines span 1% and 99% of bootstrap replicated FNMR estimates.



Figure 266: For the visa images, the dots show FNMR by age group for two operating thresholds corresponding to  $FMR = \{0.001, 0.0001\}$  computed over all on the order of  $10^{10}$  impostor scores. The FMR in each bin will vary also - see subsequent impostor heatmaps in sec. 3.6.2. Given a pair of face images taken at different times, we assign the comparison to the bin that is the arithmetic average of the subject's ages. This plot shows only the effect of age, not ageing. The number of comparisons in each bin is generally in the thousands, however the first and last bins are computed over 149 and 124 respectively. The error rates in some (adult) cases are zero, and in others the DET is flat so the error rates at the two thresholds are identical. The lines span 1% and 99% of bootstrap replicated FNMR estimates.

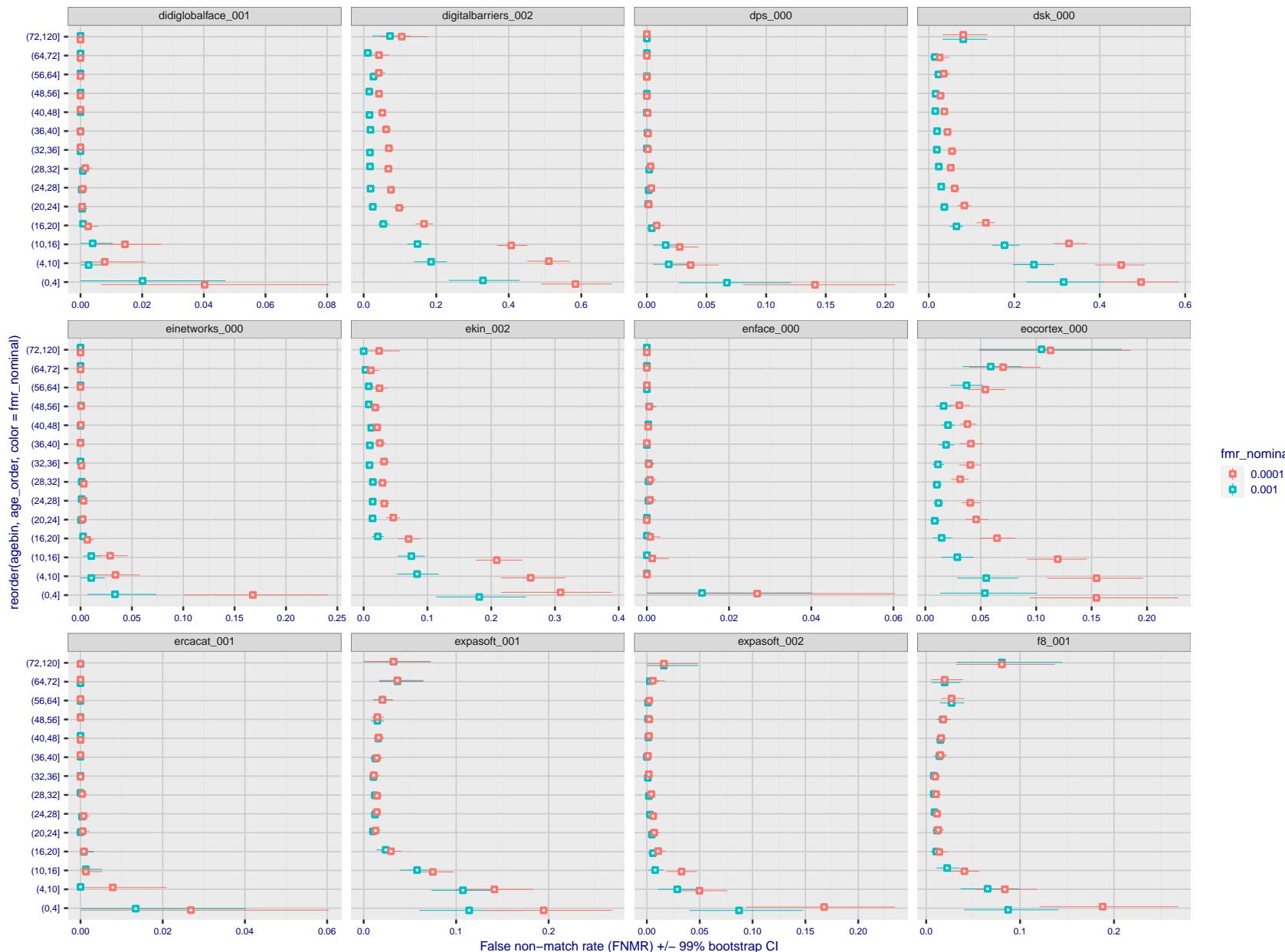


Figure 267: For the visa images, the dots show FNMR by age group for two operating thresholds corresponding to  $FMR = \{0.001, 0.0001\}$  computed over all on the order of  $10^{10}$  impostor scores. The FMR in each bin will vary also - see subsequent impostor heatmaps in sec. 3.6.2. Given a pair of face images taken at different times, we assign the comparison to the bin that is the arithmetic average of the subject's ages. This plot shows only the effect of age, not ageing. The number of comparisons in each bin is generally in the thousands, however the first and last bins are computed over 149 and 124 respectively. The error rates in some (adult) cases are zero, and in others the DET is flat so the error rates at the two thresholds are identical. The lines span 1% and 99% of bootstrap replicated FNMR estimates.

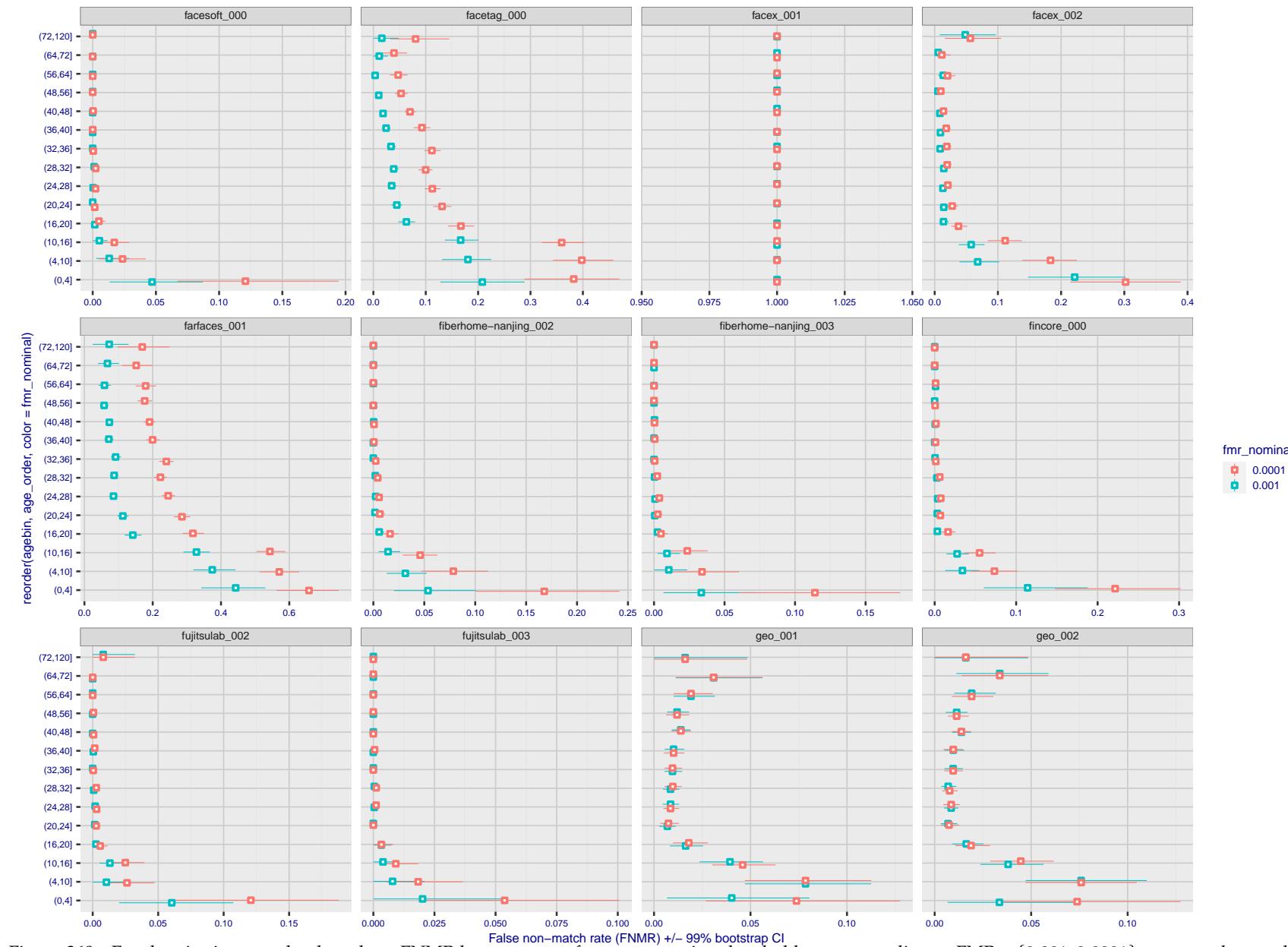


Figure 268: For the visa images, the dots show FNMR by age group for two operating thresholds corresponding to  $FMR = \{0.001, 0.0001\}$  computed over all on the order of  $10^{10}$  impostor scores. The FMR in each bin will vary also - see subsequent impostor heatmaps in sec. 3.6.2. Given a pair of face images taken at different times, we assign the comparison to the bin that is the arithmetic average of the subject's ages. This plot shows only the effect of age, not ageing. The number of comparisons in each bin is generally in the thousands, however the first and last bins are computed over 149 and 124 respectively. The error rates in some (adult) cases are zero, and in others the DET is flat so the error rates at the two thresholds are identical. The lines span 1% and 99% of bootstrap replicated FNMR estimates.



Figure 269: For the visa images, the dots show FNMR by age group for two operating thresholds corresponding to  $FMR = \{0.001, 0.0001\}$  computed over all on the order of  $10^{10}$  impostor scores. The FMR in each bin will vary also - see subsequent impostor heatmaps in sec. 3.6.2. Given a pair of face images taken at different times, we assign the comparison to the bin that is the arithmetic average of the subject's ages. This plot shows only the effect of age, not ageing. The number of comparisons in each bin is generally in the thousands, however the first and last bins are computed over 149 and 124 respectively. The error rates in some (adult) cases are zero, and in others the DET is flat so the error rates at the two thresholds are identical. The lines span 1% and 99% of bootstrap replicated FNMR estimates.



Figure 270: For the visa images, the dots show FNMR by age group for two operating thresholds corresponding to  $FMR = \{0.001, 0.0001\}$  computed over all on the order of  $10^{10}$  impostor scores. The FMR in each bin will vary also - see subsequent impostor heatmaps in sec. 3.6.2. Given a pair of face images taken at different times, we assign the comparison to the bin that is the arithmetic average of the subject's ages. This plot shows only the effect of age, not ageing. The number of comparisons in each bin is generally in the thousands, however the first and last bins are computed over 149 and 124 respectively. The error rates in some (adult) cases are zero, and in others the DET is flat so the error rates at the two thresholds are identical. The lines span 1% and 99% of bootstrap replicated FNMR estimates.

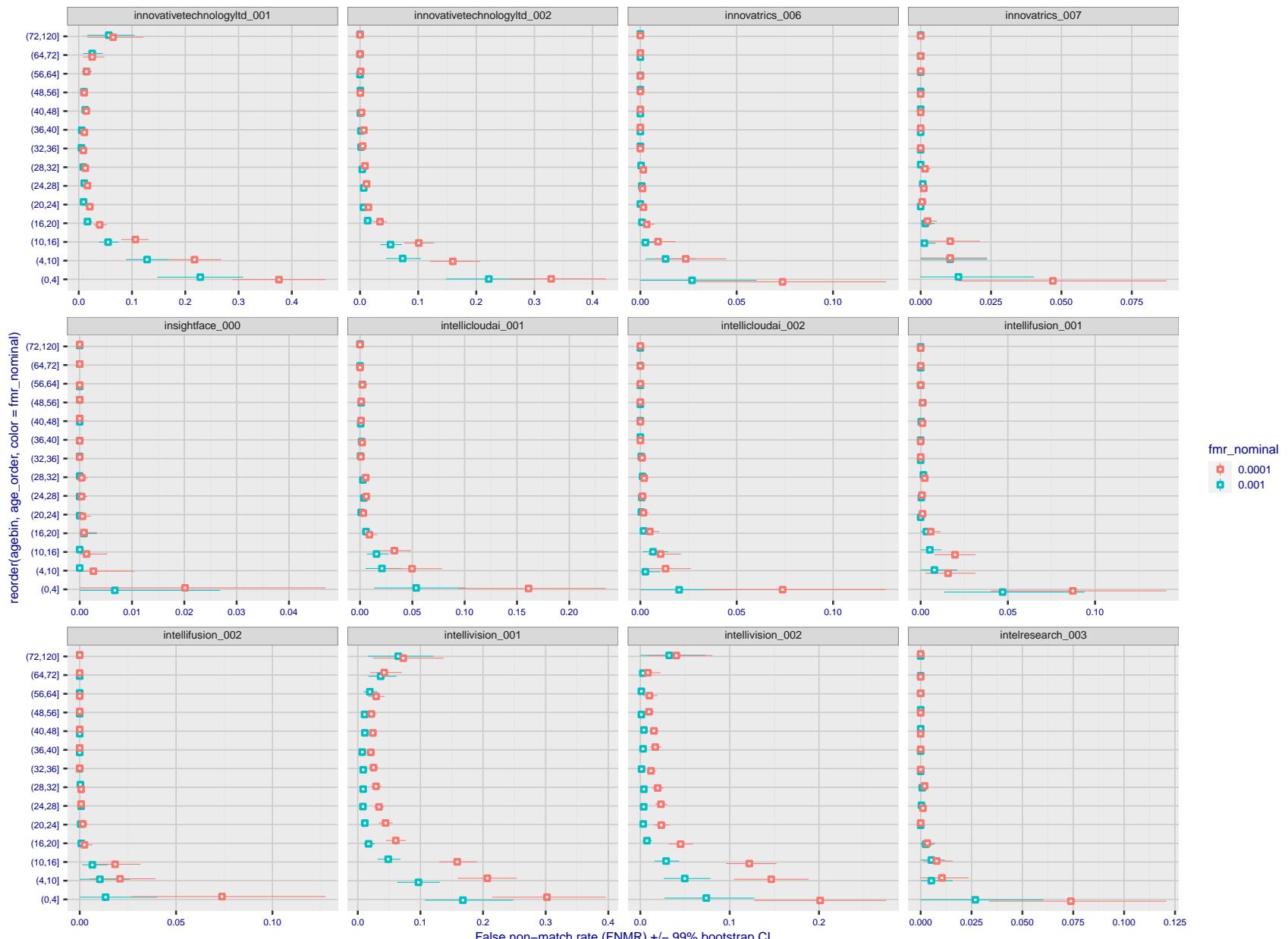


Figure 271: For the visa images, the dots show FNMR by age group for two operating thresholds corresponding to  $FMR = \{0.001, 0.0001\}$  computed over all on the order of  $10^{10}$  impostor scores. The FMR in each bin will vary also - see subsequent impostor heatmaps in sec. 3.6.2. Given a pair of face images taken at different times, we assign the comparison to the bin that is the arithmetic average of the subject's ages. This plot shows only the effect of age, not ageing. The number of comparisons in each bin is generally in the thousands, however the first and last bins are computed over 149 and 124 respectively. The error rates in some (adult) cases are zero, and in others the DET is flat so the error rates at the two thresholds are identical. The lines span 1% and 99% of bootstrap replicated FNMR estimates.

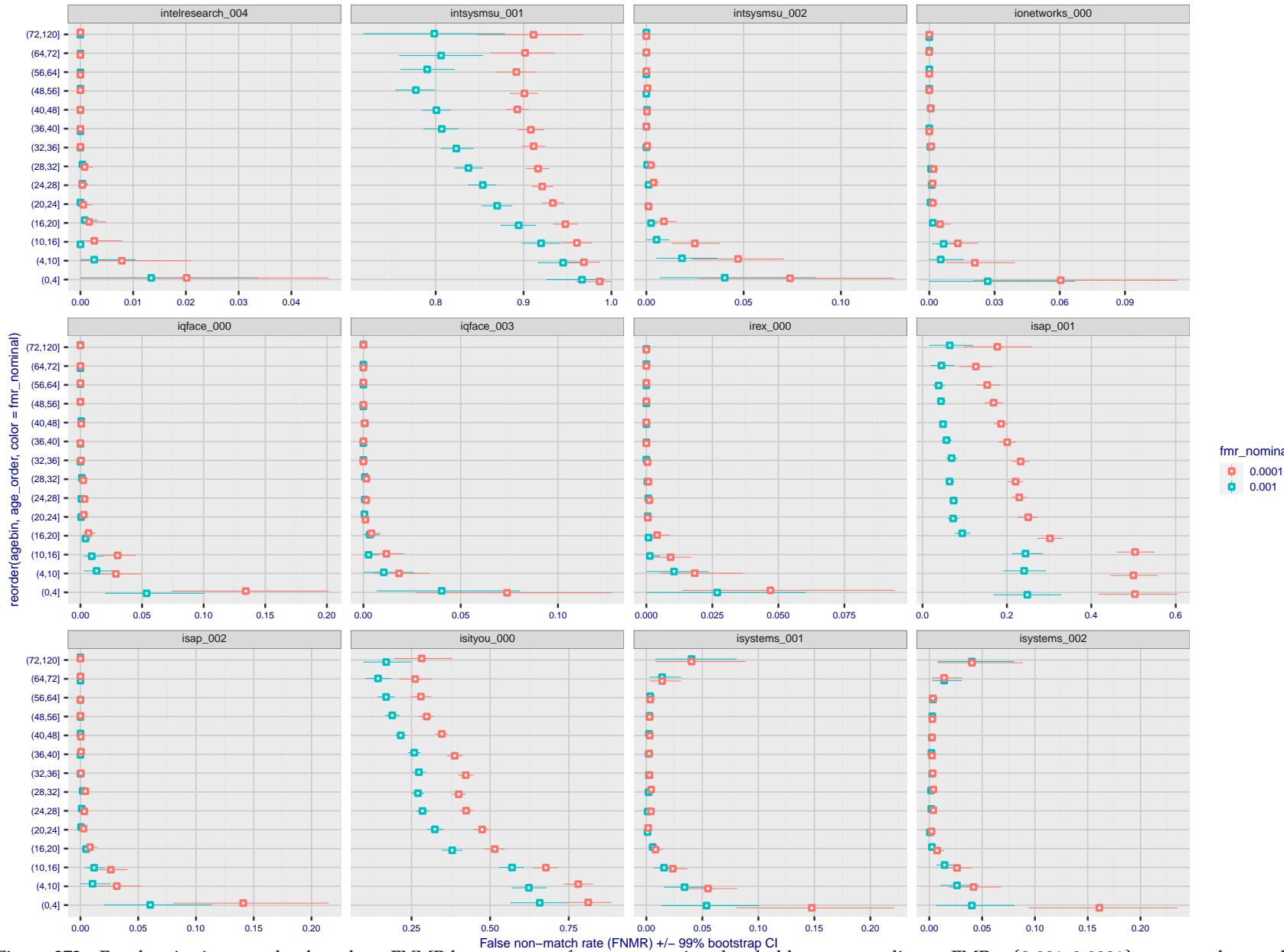


Figure 272: For the visa images, the dots show FNMR by age group for two operating thresholds corresponding to  $FMR = \{0.001, 0.0001\}$  computed over all on the order of  $10^{10}$  impostor scores. The FMR in each bin will vary also - see subsequent impostor heatmaps in sec. 3.6.2. Given a pair of face images taken at different times, we assign the comparison to the bin that is the arithmetic average of the subject's ages. This plot shows only the effect of age, not ageing. The number of comparisons in each bin is generally in the thousands, however the first and last bins are computed over 149 and 124 respectively. The error rates in some (adult) cases are zero, and in others the DET is flat so the error rates at the two thresholds are identical. The lines span 1% and 99% of bootstrap replicated FNMR estimates.



Figure 273: For the visa images, the dots show FNMR by age group for two operating thresholds corresponding to  $FMR = \{0.001, 0.0001\}$  computed over all on the order of  $10^{10}$  impostor scores. The FMR in each bin will vary also - see subsequent impostor heatmaps in sec. 3.6.2. Given a pair of face images taken at different times, we assign the comparison to the bin that is the arithmetic average of the subject's ages. This plot shows only the effect of age, not ageing. The number of comparisons in each bin is generally in the thousands, however the first and last bins are computed over 149 and 124 respectively. The error rates in some (adult) cases are zero, and in others the DET is flat so the error rates at the two thresholds are identical. The lines span 1% and 99% of bootstrap replicated FNMR estimates.

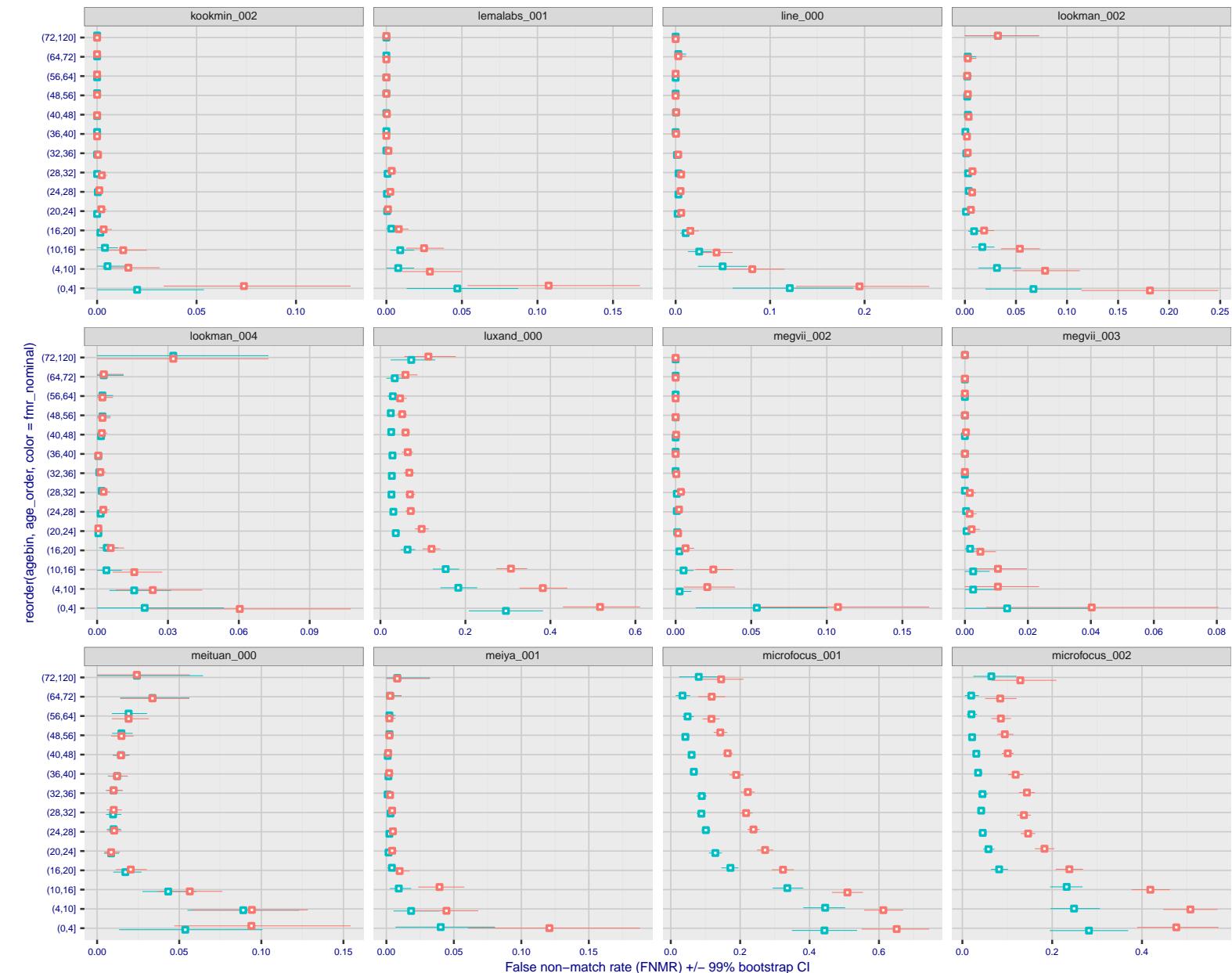
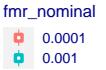


Figure 274: For the visa images, the dots show FNMR by age group for two operating thresholds corresponding to  $FMR = \{0.001, 0.0001\}$  computed over all on the order of  $10^{10}$  impostor scores. The FMR in each bin will vary also - see subsequent impostor heatmaps in sec. 3.6.2. Given a pair of face images taken at different times, we assign the comparison to the bin that is the arithmetic average of the subject's ages. This plot shows only the effect of age, not ageing. The number of comparisons in each bin is generally in the thousands, however the first and last bins are computed over 149 and 124 respectively. The error rates in some (adult) cases are zero, and in others the DET is flat so the error rates at the two thresholds are identical. The lines span 1% and 99% of bootstrap replicated FNMR estimates.

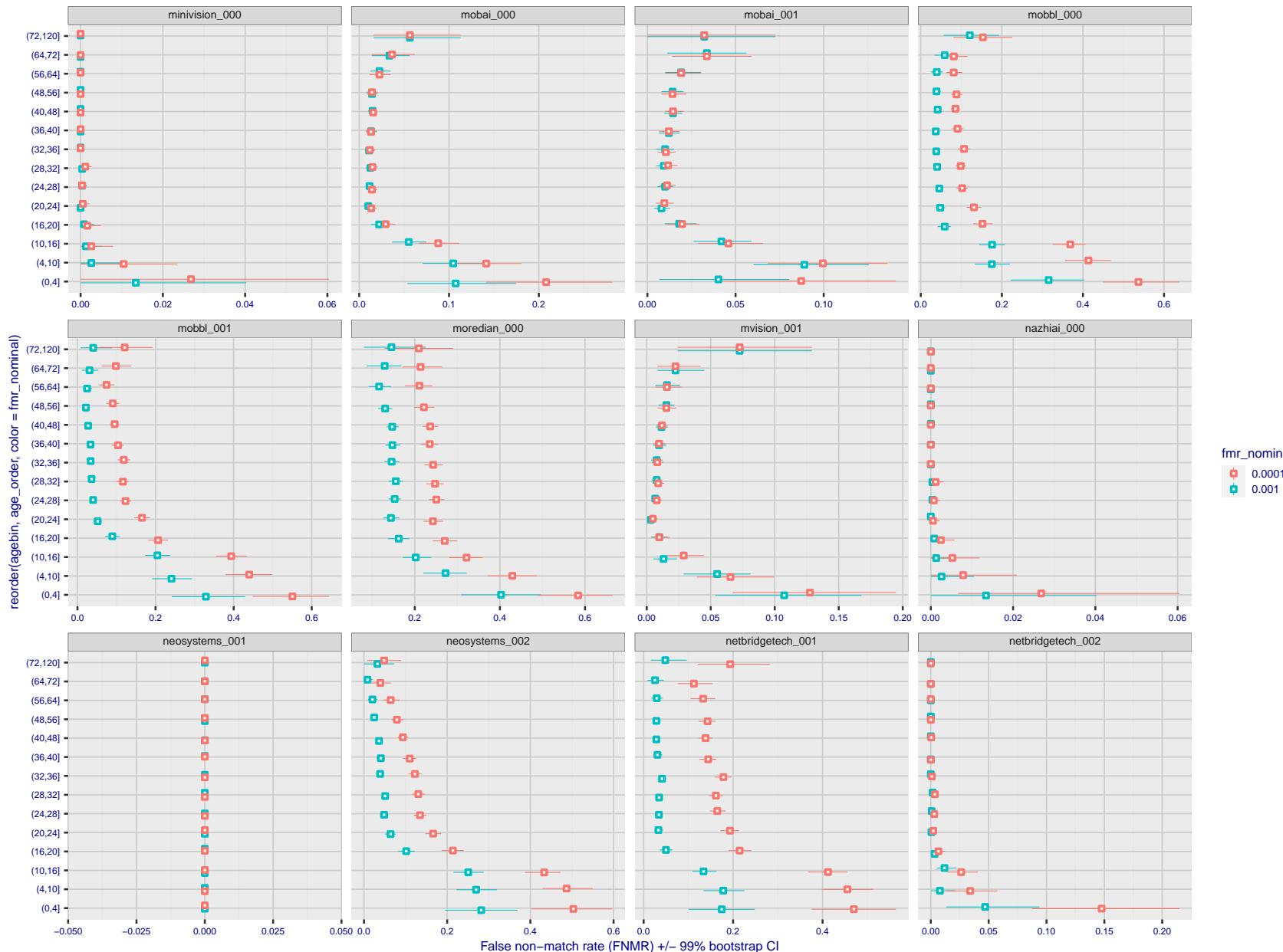


Figure 275: For the visa images, the dots show FNMR by age group for two operating thresholds corresponding to  $FMR = \{0.001, 0.0001\}$  computed over all on the order of  $10^{10}$  impostor scores. The FMR in each bin will vary also - see subsequent impostor heatmaps in sec. 3.6.2. Given a pair of face images taken at different times, we assign the comparison to the bin that is the arithmetic average of the subject's ages. This plot shows only the effect of age, not ageing. The number of comparisons in each bin is generally in the thousands, however the first and last bins are computed over 149 and 124 respectively. The error rates in some (adult) cases are zero, and in others the DET is flat so the error rates at the two thresholds are identical. The lines span 1% and 99% of bootstrap replicated FNMR estimates.

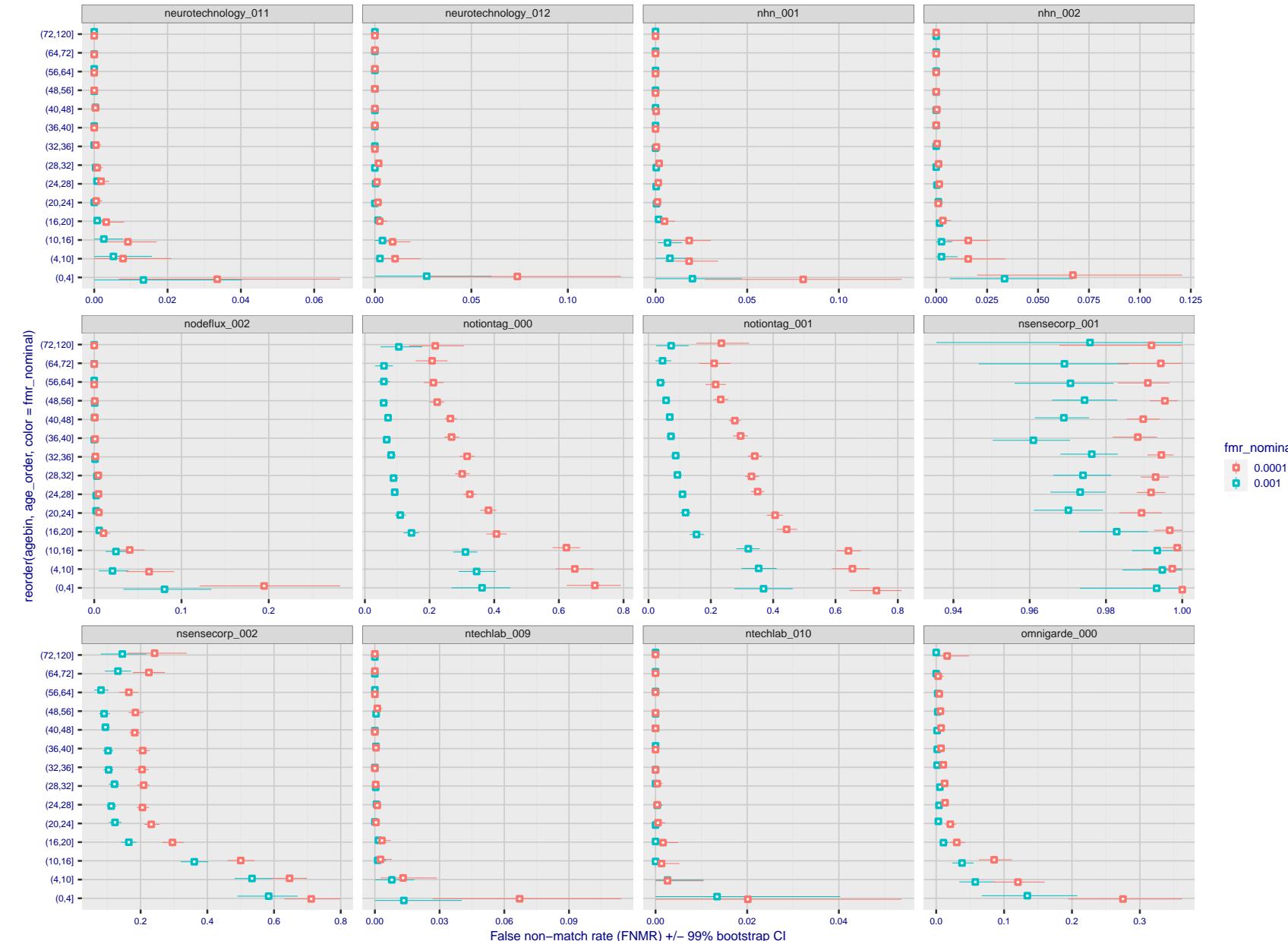


Figure 276: For the visa images, the dots show FNMR by age group for two operating thresholds corresponding to  $FMR = \{0.001, 0.0001\}$  computed over all on the order of  $10^{10}$  impostor scores. The FMR in each bin will vary also - see subsequent impostor heatmaps in sec. 3.6.2. Given a pair of face images taken at different times, we assign the comparison to the bin that is the arithmetic average of the subject's ages. This plot shows only the effect of age, not ageing. The number of comparisons in each bin is generally in the thousands, however the first and last bins are computed over 149 and 124 respectively. The error rates in some (adult) cases are zero, and in others the DET is flat so the error rates at the two thresholds are identical. The lines span 1% and 99% of bootstrap replicated FNMR estimates.

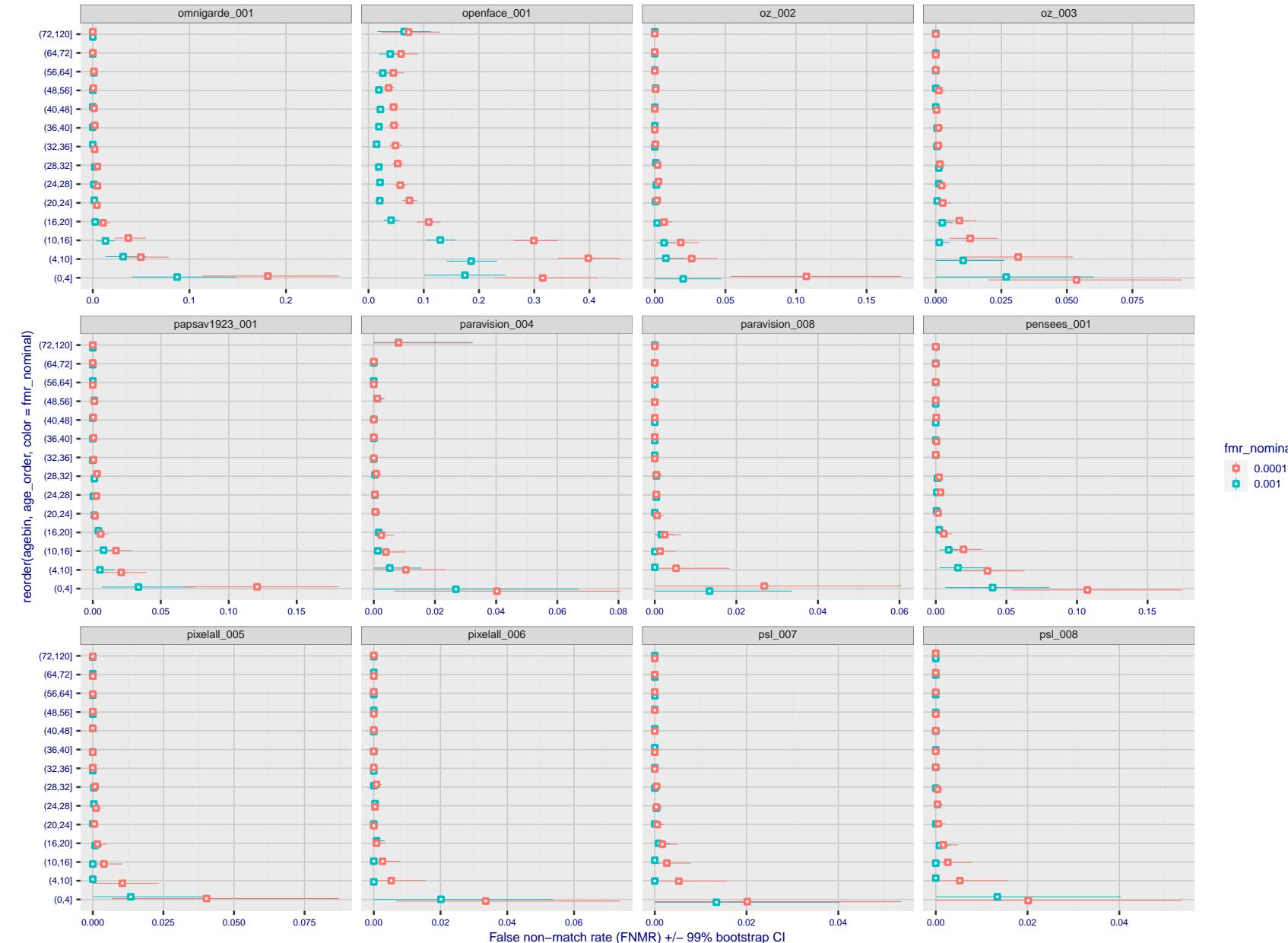


Figure 277: For the visa images, the dots show FNMR by age group for two operating thresholds corresponding to  $FMR = \{0.001, 0.0001\}$  computed over all on the order of  $10^{10}$  impostor scores. The FMR in each bin will vary also - see subsequent impostor heatmaps in sec. 3.6.2. Given a pair of face images taken at different times, we assign the comparison to the bin that is the arithmetic average of the subject's ages. This plot shows only the effect of age, not ageing. The number of comparisons in each bin is generally in the thousands, however the first and last bins are computed over 149 and 124 respectively. The error rates in some (adult) cases are zero, and in others the DET is flat so the error rates at the two thresholds are identical. The lines span 1% and 99% of bootstrap replicated FNMR estimates.



Figure 278: For the visa images, the dots show FNMR by age group for two operating thresholds corresponding to  $FMR = \{0.001, 0.0001\}$  computed over all on the order of  $10^{10}$  impostor scores. The FMR in each bin will vary also - see subsequent impostor heatmaps in sec. 3.6.2. Given a pair of face images taken at different times, we assign the comparison to the bin that is the arithmetic average of the subject's ages. This plot shows only the effect of age, not ageing. The number of comparisons in each bin is generally in the thousands, however the first and last bins are computed over 149 and 124 respectively. The error rates in some (adult) cases are zero, and in others the DET is flat so the error rates at the two thresholds are identical. The lines span 1% and 99% of bootstrap replicated FNMR estimates.

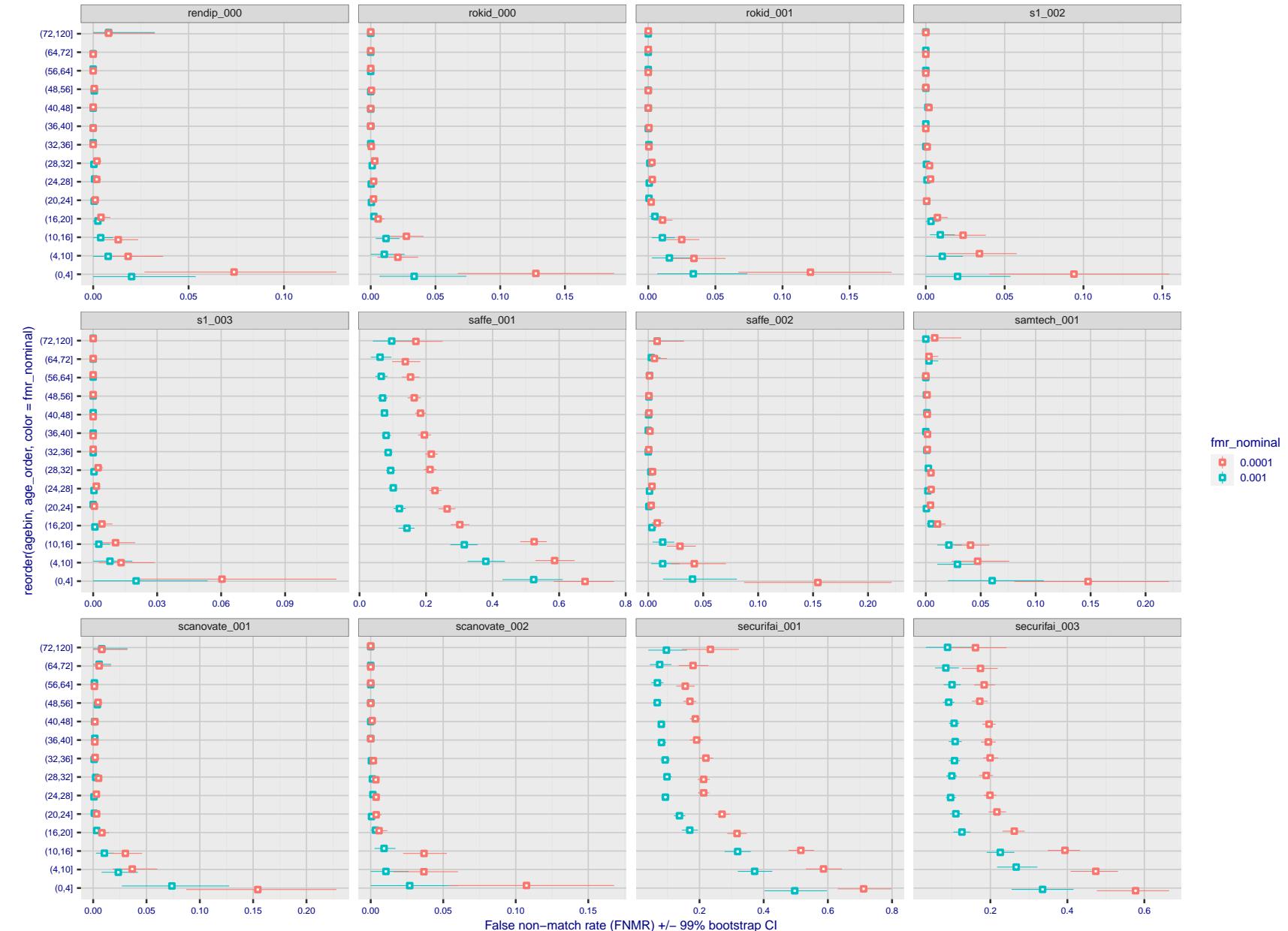


Figure 279: For the visa images, the dots show FNMR by age group for two operating thresholds corresponding to  $FMR = \{0.001, 0.0001\}$  computed over all on the order of  $10^{10}$  impostor scores. The FMR in each bin will vary also - see subsequent impostor heatmaps in sec. 3.6.2. Given a pair of face images taken at different times, we assign the comparison to the bin that is the arithmetic average of the subject's ages. This plot shows only the effect of age, not ageing. The number of comparisons in each bin is generally in the thousands, however the first and last bins are computed over 149 and 124 respectively. The error rates in some (adult) cases are zero, and in others the DET is flat so the error rates at the two thresholds are identical. The lines span 1% and 99% of bootstrap replicated FNMR estimates.

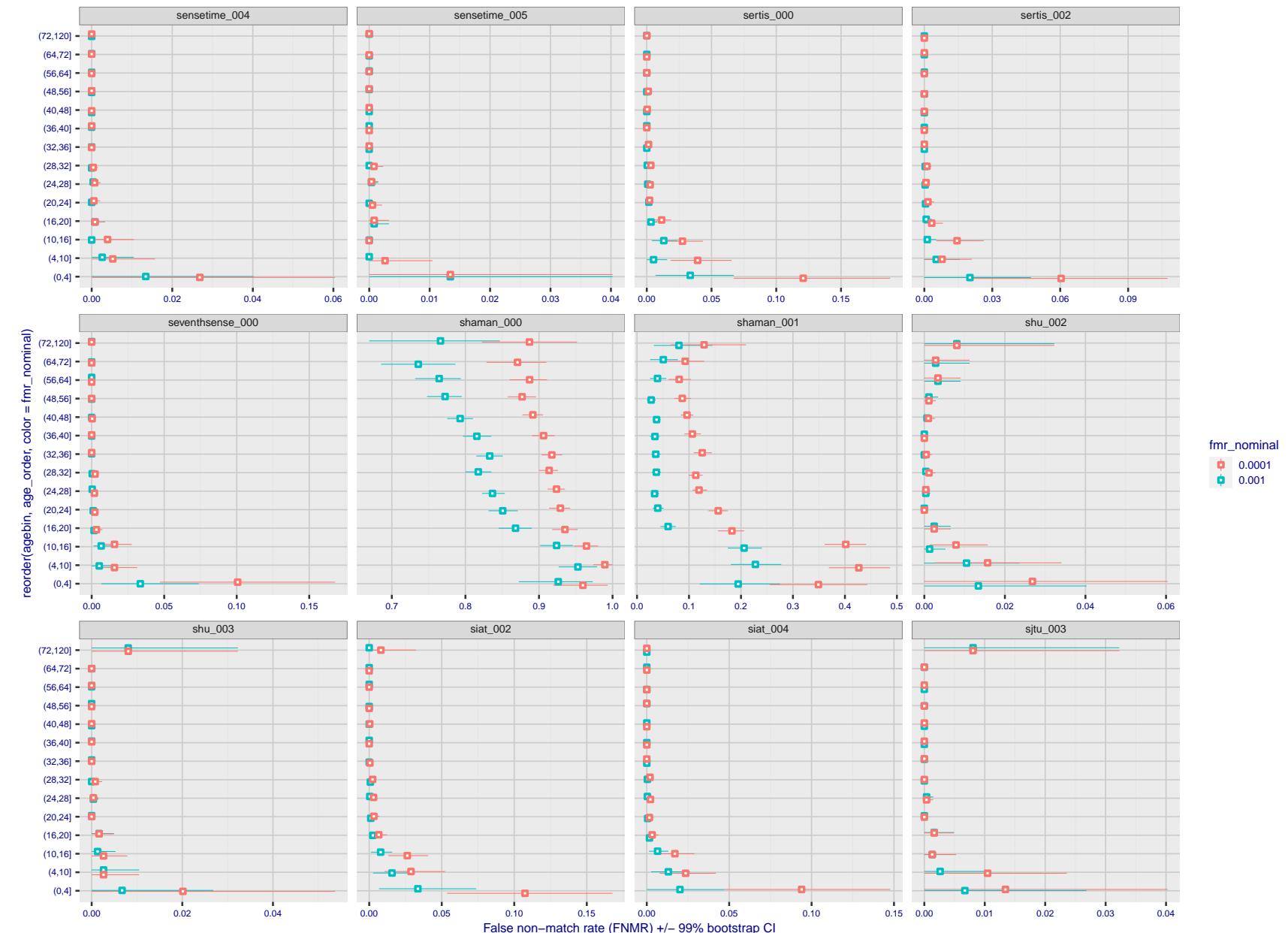
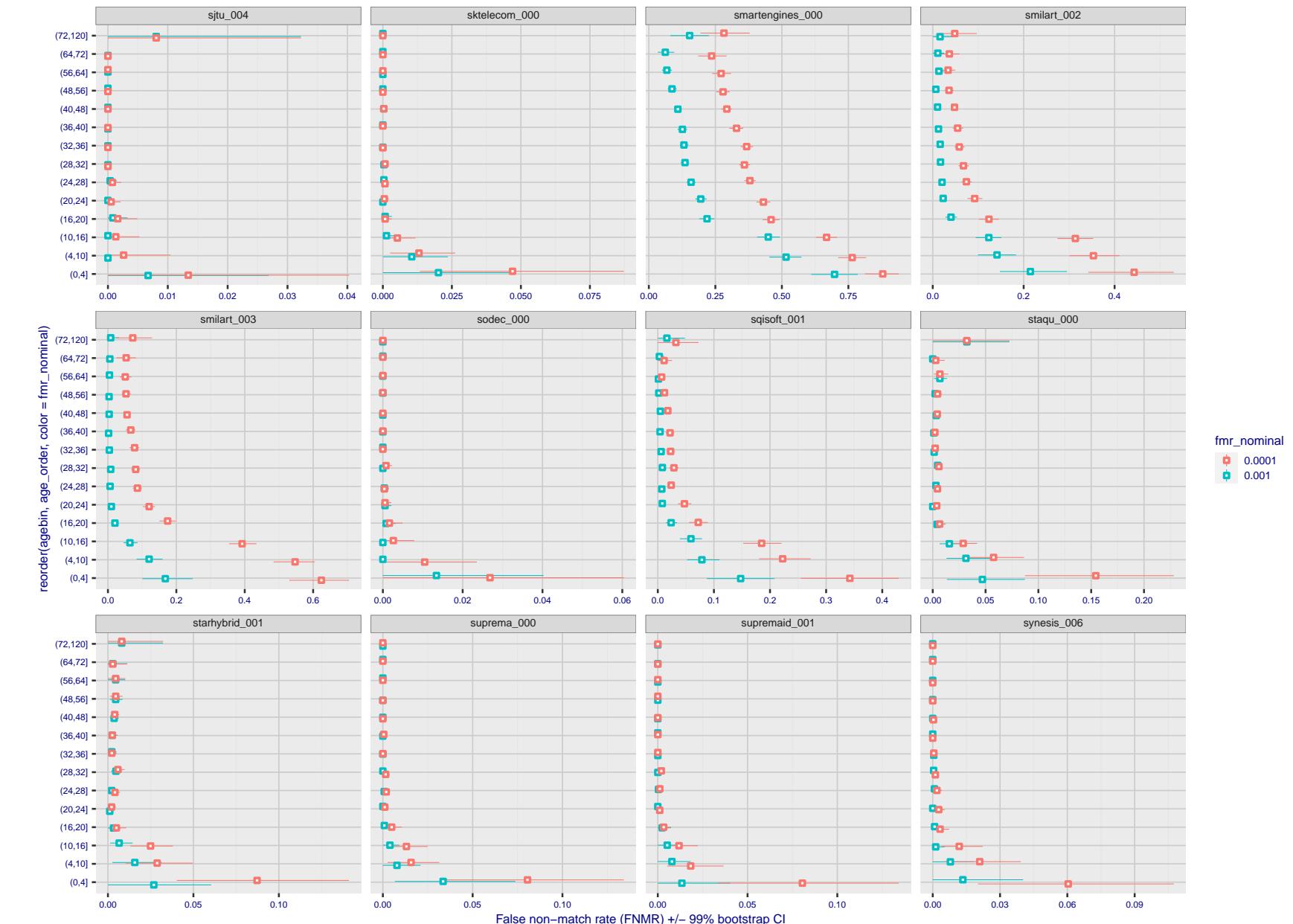


Figure 280: For the visa images, the dots show FNMR by age group for two operating thresholds corresponding to  $FMR = \{0.001, 0.0001\}$  computed over all on the order of  $10^{10}$  impostor scores. The FMR in each bin will vary also - see subsequent impostor heatmaps in sec. 3.6.2. Given a pair of face images taken at different times, we assign the comparison to the bin that is the arithmetic average of the subject's ages. This plot shows only the effect of age, not ageing. The number of comparisons in each bin is generally in the thousands, however the first and last bins are computed over 149 and 124 respectively. The error rates in some (adult) cases are zero, and in others the DET is flat so the error rates at the two thresholds are identical. The lines span 1% and 99% of bootstrap replicated FNMR estimates.



FNMR(T)  
FMR(T)  
"False non-match rate"  
"False match rate"

Figure 281: For the visa images, the dots show FNMR by age group for two operating thresholds corresponding to  $FMR = \{0.001, 0.0001\}$  computed over all on the order of  $10^{10}$  impostor scores. The FMR in each bin will vary also - see subsequent impostor heatmaps in sec. 3.6.2. Given a pair of face images taken at different times, we assign the comparison to the bin that is the arithmetic average of the subject's ages. This plot shows only the effect of age, not ageing. The number of comparisons in each bin is generally in the thousands, however the first and last bins are computed over 149 and 124 respectively. The error rates in some (adult) cases are zero, and in others the DET is flat so the error rates at the two thresholds are identical. The lines span 1% and 99% of bootstrap replicated FNMR estimates.

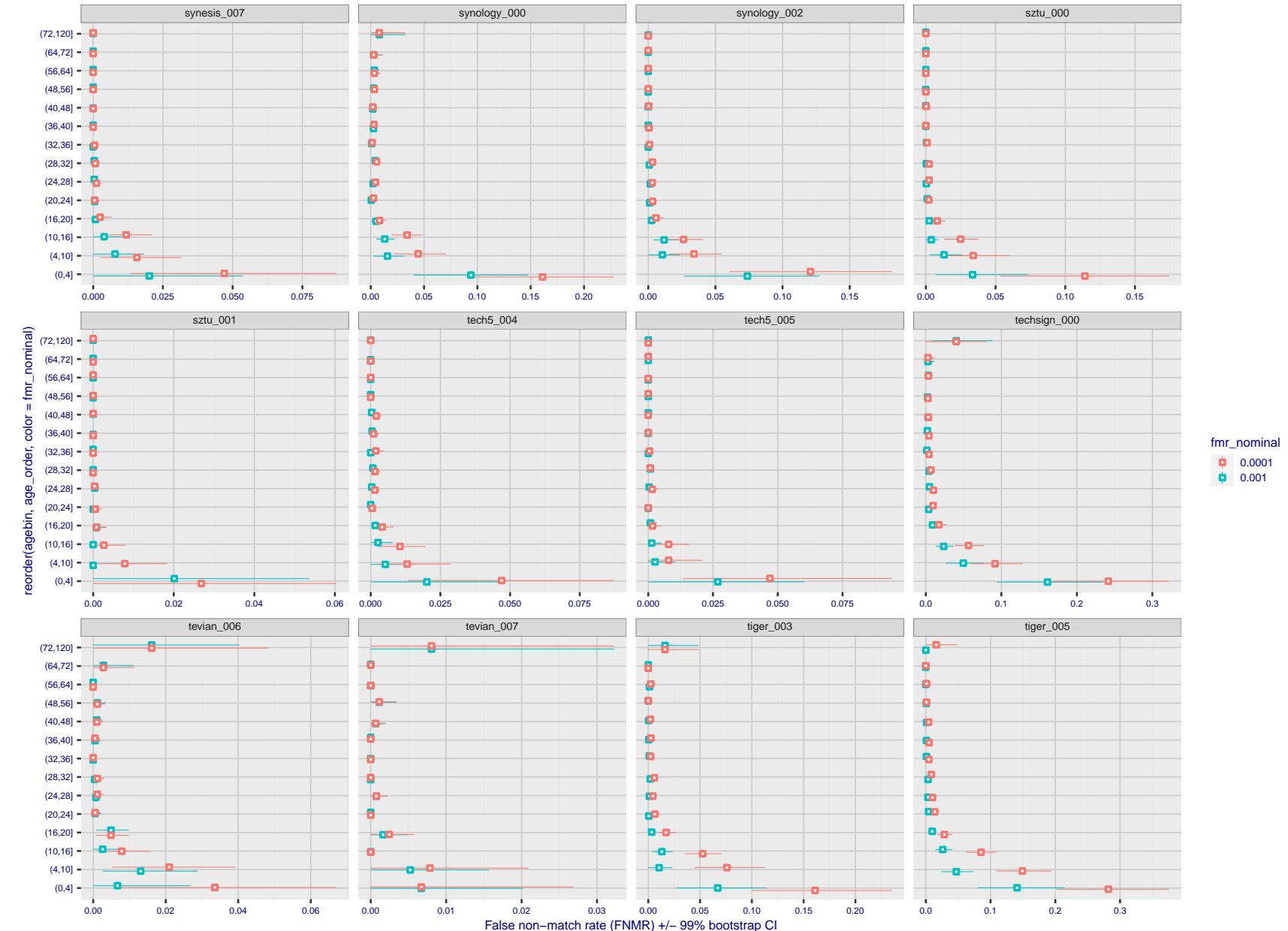


Figure 282: For the visa images, the dots show FNMR by age group for two operating thresholds corresponding to  $FMR = \{0.001, 0.0001\}$  computed over all on the order of  $10^{10}$  impostor scores. The FMR in each bin will vary also - see subsequent impostor heatmaps in sec. 3.6.2. Given a pair of face images taken at different times, we assign the comparison to the bin that is the arithmetic average of the subject's ages. This plot shows only the effect of age, not ageing. The number of comparisons in each bin is generally in the thousands, however the first and last bins are computed over 149 and 124 respectively. The error rates in some (adult) cases are zero, and in others the DET is flat so the error rates at the two thresholds are identical. The lines span 1% and 99% of bootstrap replicated FNMR estimates.



Figure 283: For the visa images, the dots show FNMR by age group for two operating thresholds corresponding to  $FMR = \{0.001, 0.0001\}$  computed over all on the order of  $10^{10}$  impostor scores. The FMR in each bin will vary also - see subsequent impostor heatmaps in sec. 3.6.2. Given a pair of face images taken at different times, we assign the comparison to the bin that is the arithmetic average of the subject's ages. This plot shows only the effect of age, not ageing. The number of comparisons in each bin is generally in the thousands, however the first and last bins are computed over 149 and 124 respectively. The error rates in some (adult) cases are zero, and in others the DET is flat so the error rates at the two thresholds are identical. The lines span 1% and 99% of bootstrap replicated FNMR estimates.

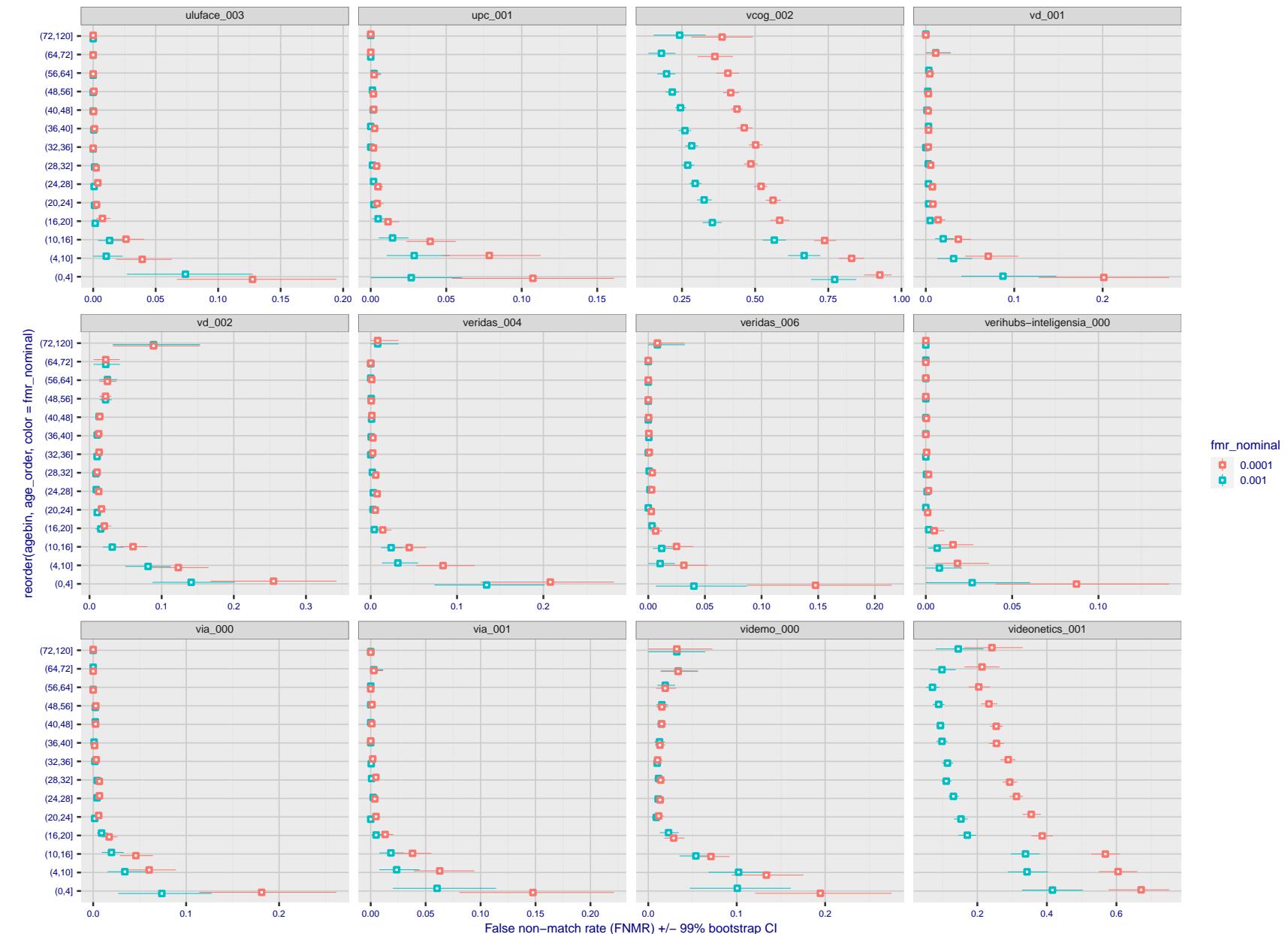


Figure 284: For the visa images, the dots show FNMR by age group for two operating thresholds corresponding to  $FMR = \{0.001, 0.0001\}$  computed over all on the order of  $10^{10}$  impostor scores. The FMR in each bin will vary also - see subsequent impostor heatmaps in sec. 3.6.2. Given a pair of face images taken at different times, we assign the comparison to the bin that is the arithmetic average of the subject's ages. This plot shows only the effect of age, not ageing. The number of comparisons in each bin is generally in the thousands, however the first and last bins are computed over 149 and 124 respectively. The error rates in some (adult) cases are zero, and in others the DET is flat so the error rates at the two thresholds are identical. The lines span 1% and 99% of bootstrap replicated FNMR estimates.



Figure 285: For the visa images, the dots show FNMR by age group for two operating thresholds corresponding to  $FMR = \{0.001, 0.0001\}$  computed over all on the order of  $10^{10}$  impostor scores. The FMR in each bin will vary also - see subsequent impostor heatmaps in sec. 3.6.2. Given a pair of face images taken at different times, we assign the comparison to the bin that is the arithmetic average of the subject's ages. This plot shows only the effect of age, not ageing. The number of comparisons in each bin is generally in the thousands, however the first and last bins are computed over 149 and 124 respectively. The error rates in some (adult) cases are zero, and in others the DET is flat so the error rates at the two thresholds are identical. The lines span 1% and 99% of bootstrap replicated FNMR estimates.

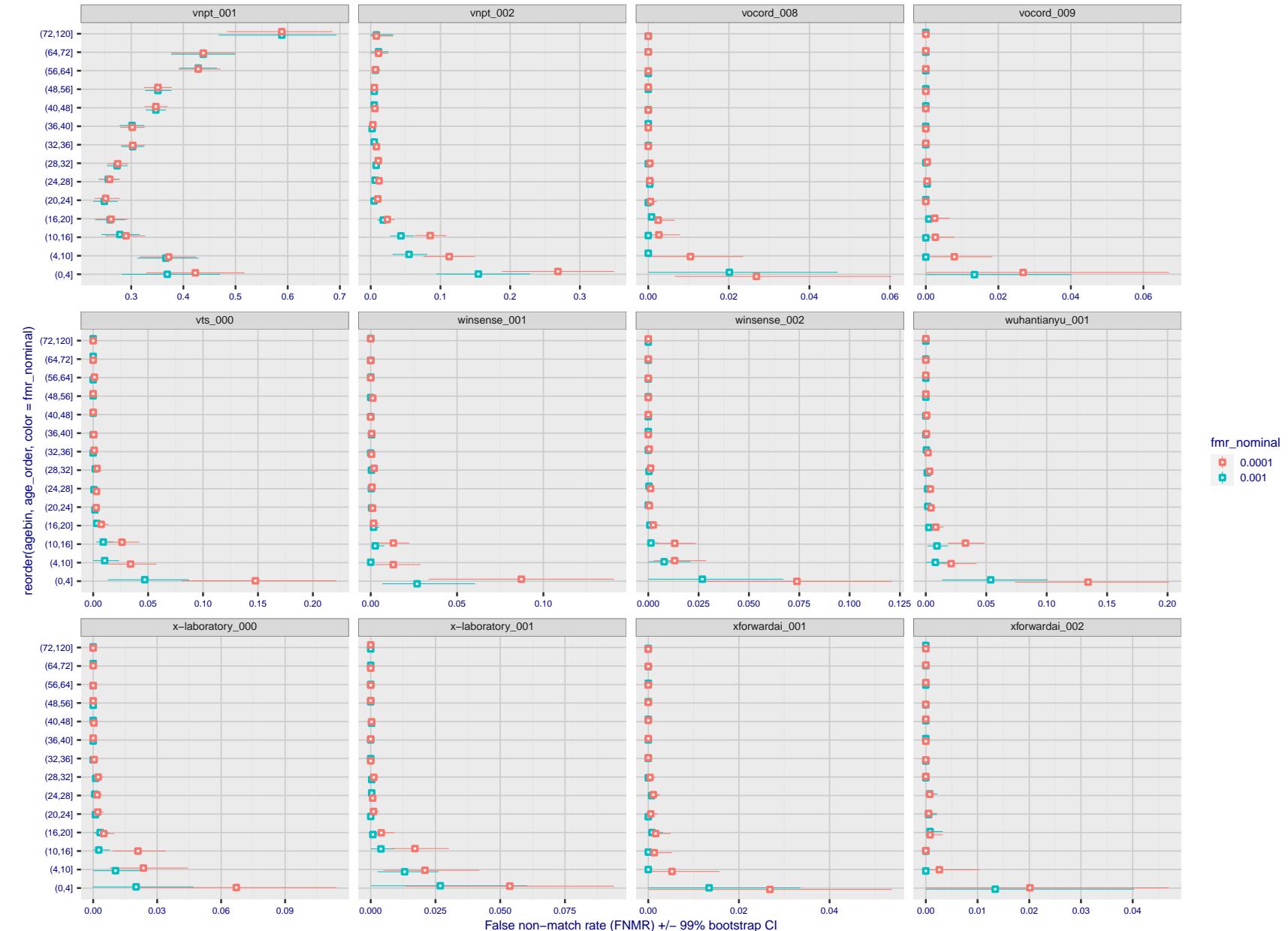


Figure 286: For the visa images, the dots show FNMR by age group for two operating thresholds corresponding to  $FMR = \{0.001, 0.0001\}$  computed over all on the order of  $10^{10}$  impostor scores. The FMR in each bin will vary also - see subsequent impostor heatmaps in sec. 3.6.2. Given a pair of face images taken at different times, we assign the comparison to the bin that is the arithmetic average of the subject's ages. This plot shows only the effect of age, not ageing. The number of comparisons in each bin is generally in the thousands, however the first and last bins are computed over 149 and 124 respectively. The error rates in some (adult) cases are zero, and in others the DET is flat so the error rates at the two thresholds are identical. The lines span 1% and 99% of bootstrap replicated FNMR estimates.



Figure 287: For the visa images, the dots show FNMR by age group for two operating thresholds corresponding to  $FMR = \{0.001, 0.0001\}$  computed over all on the order of  $10^{10}$  impostor scores. The FMR in each bin will vary also - see subsequent impostor heatmaps in sec. 3.6.2. Given a pair of face images taken at different times, we assign the comparison to the bin that is the arithmetic average of the subject's ages. This plot shows only the effect of age, not ageing. The number of comparisons in each bin is generally in the thousands, however the first and last bins are computed over 149 and 124 respectively. The error rates in some (adult) cases are zero, and in others the DET is flat so the error rates at the two thresholds are identical. The lines span 1% and 99% of bootstrap replicated FNMR estimates.

**Caveats:** None.

## 3.6 Impostor distribution stability

### 3.6.1 Effect of birth place on the impostor distribution

**Background:** Facial appearance varies geographically, both in terms of skin tone, cranio-facial structure and size. This section addresses whether false match rates vary intra- and inter-regionally.

**Goals:**

- ▷ To show the effect of birth region of the impostor and enrollee on false match rates.
- ▷ To determine whether some algorithms give better impostor distribution stability.

**Methods:**

- ▷ For the visa images, NIST defined 10 regions: Sub-Saharan Africa, South Asia, Polynesia, North Africa, Middle East, Europe, East Asia, Central and South America, Central Asia, and the Caribbean.
- ▷ For the visa images, NIST mapped each country of birth to a region. There is some arbitrariness to this. For example, Egypt could reasonably be assigned to the Middle East instead of North Africa. An alternative methodology could, for example, assign the Philippines to *both* Polynesia and East Asia.
- ▷ FMR is computed for cases where all face images of impostors born in region  $r_2$  are compared with enrolled face images of persons born in region  $r_1$ .

$$\text{FMR}(r_1, r_2, T) = \frac{\sum_{i=1}^{N_{r_1, r_2}} H(s_i - T)}{N_{r_1, r_2}} \quad (5)$$

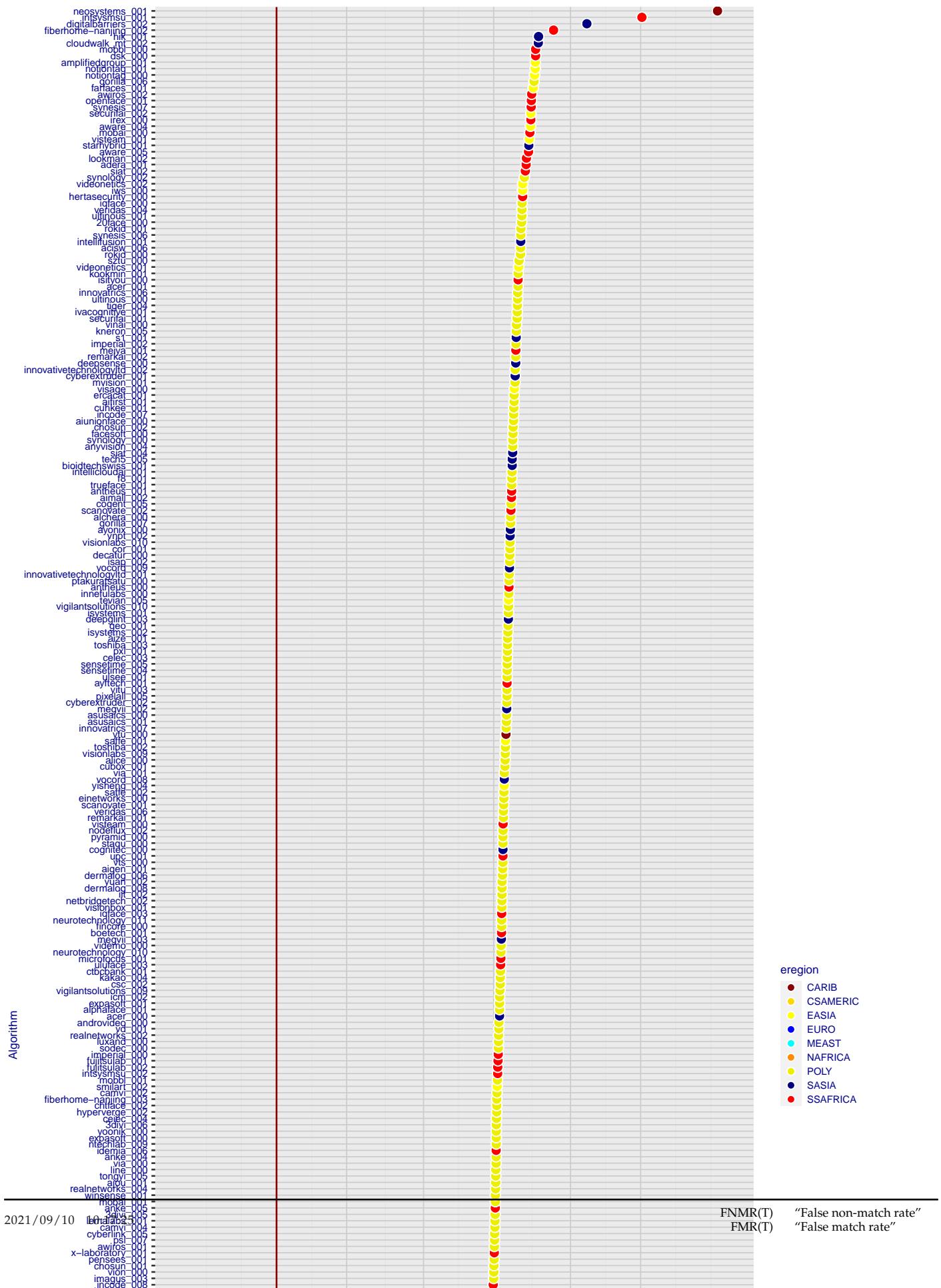
where the same threshold,  $T$ , is used in all cells, and  $H$  is the unit step function. The threshold is set to give  $\text{FMR}(T) = 0.001$  over the entire set of visa image impostor comparisons.

- ▷ This analysis is then repeated by country-pair, but only for those country pairs where both have at least 1000 images available. The countries<sup>1</sup> appear in the axes of graphs that follow.
- ▷ The mean number of impostor scores in any cross-region bin is 33 million. The smallest number of impostor scores in any bin is 135000, for Central Asia - North Africa. While these counts are large enough to support reasonable significance, the number of individual faces is much smaller, on the order of  $N^{0.5}$ .
- ▷ The numbers of impostor scores in any cross-country bin is shown in Figure ??.

**Results:** Subsequent figures show heatmaps that use color to represent the base-10 logarithm of the false match rate. Red colors indicate high (bad) false match rates. Dark colors indicate benign false match rates. There are two series of graphs corresponding to aggregated geographical regions, and to countries. The notable observations are:

- ▷ The on-diagonal elements correspond to within-region impostors. FMR is generally above the nominal value of  $\text{FMR} = 0.001$ . Particularly there is usually higher FMR in, Sub-Saharan Africa, South Asia, and the Caribbean. Europe and Central Asia, on the other hand, usually give FMR closer to the nominal value.
- ▷ The off-diagonal elements correspond to across-region impostors. The highest FMR is produced between the Caribbean and Sub-Saharan Africa.
- ▷ Algorithms vary.

<sup>1</sup>These are Argentina, Australia, Brazil, Chile, China, Costa Rica, Cuba, Czech Republic, Dominican Republic, Ecuador, Egypt, El Salvador, Germany, Ghana, Great Britain, Greece, Guatemala, Haiti, Hong Kong, Honduras, Indonesia, India, Israel, Jamaica, Japan, Kenya, Korea, Lebanon, Mexico, Malaysia, Nepal, Nigeria, Peru, Philippines, Pakistan, Poland, Romania, Russia, South Africa, Saudi Arabia, Thailand, Trinidad, Turkey, Taiwan, Ukraine, Venezuela, and Vietnam.



- ▷ We computed the same quantities for a global FMR = 0.0001. The effects are similar.

**Caveats:**

- ▷ The effects of variable impostor rates on one-to-many identification systems may well differ from what's implied by these one-to-one verification results. Two reasons for this are a) the enrollment galleries are usually imbalanced across countries of birth, age and sex; b) one-to-many identification algorithms often implement techniques aimed at stabilizing the impostor distribution. Further research is necessary.
- ▷ In principle, the effects seen in this subsection could be due to differences in the image capture process. We consider this unlikely since the effects are maintained across geography - e.g. Caribbean vs. Africa, or Japan vs. China.

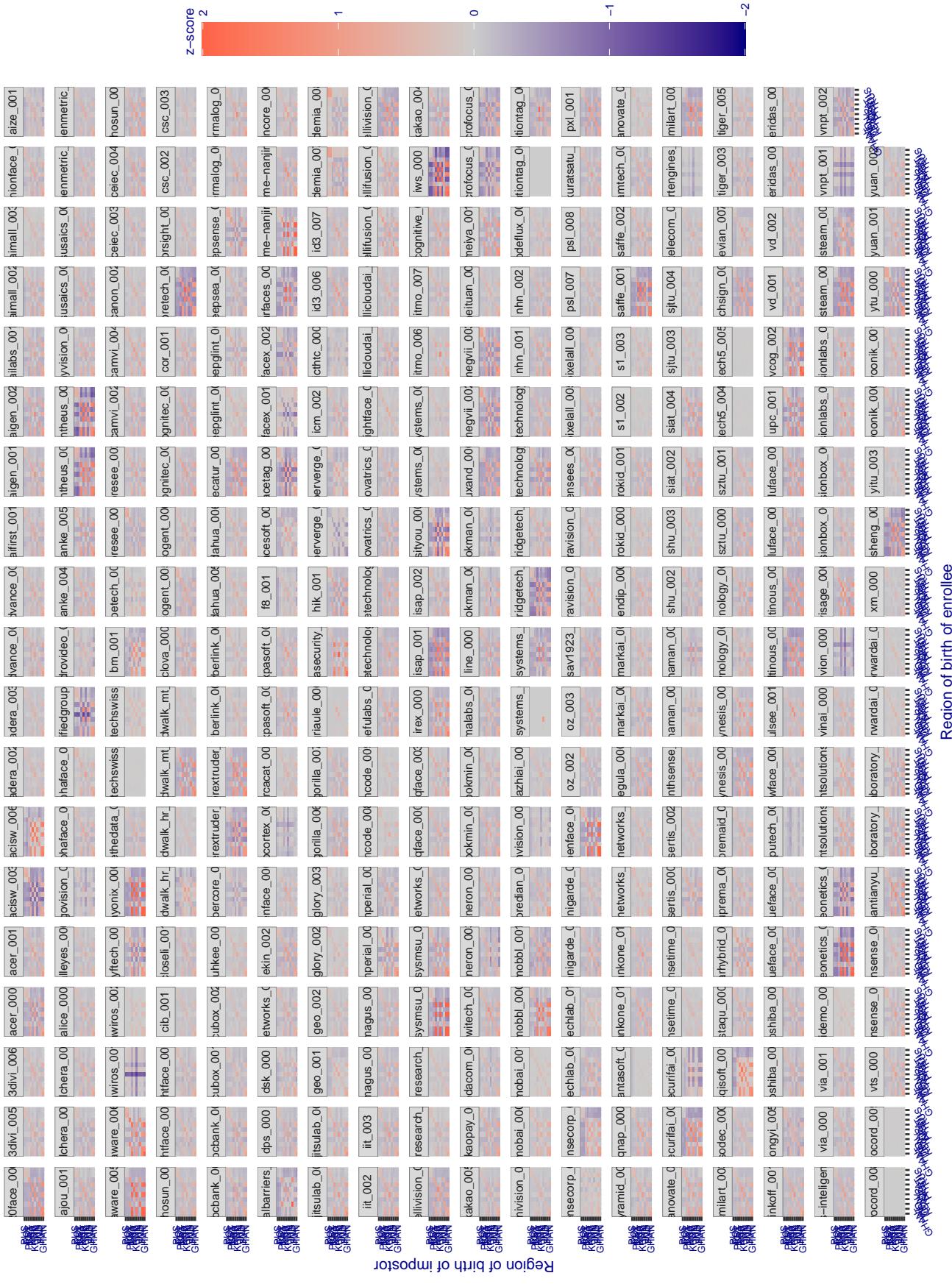


Figure 289: For visa images, the heatmap shows how the mean of the impostor distribution for the country pair (a,b) is shifted relative to the mean of the global impostor distribution, expressed as a number of standard deviations of the global impostor distribution. This statistic is designed to show shifts in the entire impostor distribution, not just tail effects that manifest as the anomalously high (or low) false match rates that appear in the subsequent figures. The countries are chosen to show that skin tone alone does not explain impostor distribution shifts. The reduced shift in Asian populations with the Yitu and Tong YiTrans algorithms, is accompanied by positive shifts in the European populations. This reversal relative to most other algorithms, may derive from use of nationally weighted training sets. The figure is computed from same-sex and same-age impostor pairs.

### 3.6.2 Effect of age on impostors

**Background:** This section shows the effect of age on the impostor distribution. The ideal behaviour is that the age of the enrollee and the impostor would not affect impostor scores. This would support FMR stability over sub-populations.

**Goals:**

- ▷ To show the effect of relative ages of the impostor and enrollee on false match rates.
- ▷ To determine whether some algorithms have better impostor distribution stability.

**Methods:**

- ▷ Define 14 age group bins, spanning 0 to over 100 years old.
- ▷ Compute FMR over all impostor comparisons for which the subjects in the enrollee and impostor images have ages in two bins.
- ▷ Compute FMR over all impostor comparisons for which the subjects are additionally of the same sex, and born in the same geographic region.

**Results:**

The notable aspects are:

- ▷ Diagonal dominance: Impostors are more likely to be matched against their same age group.
- ▷ Same sex and same region impostors are more successful. On the diagonal, an impostor is more likely to succeed by posing as someone of the same sex. If  $\Delta \log_{10} \text{FMR} = 0.2$ , then same-sex same-region FMR exceeds the all-pairs FMR by factor of  $10^{0.2} = 1.6$ .
- ▷ Young children impostors give elevated FMR against young children. Older adult impostor give elevated FMR against older adults. These effects are quite large, for example if  $\Delta \log_{10} \text{FMR} = 1.0$  larger than a 32 year old, then these groups have higher FMR by a factor of  $10^1 = 10$ . This would imply an FMR above 0.01 for a nominal (global) FMR = 0.001.
- ▷ Algorithms vary.
- ▷ We computed the same quantities for a global FMR = 0.0001. The effects are similar.

Note the calculations in this section include impostors paired across all countries of birth.

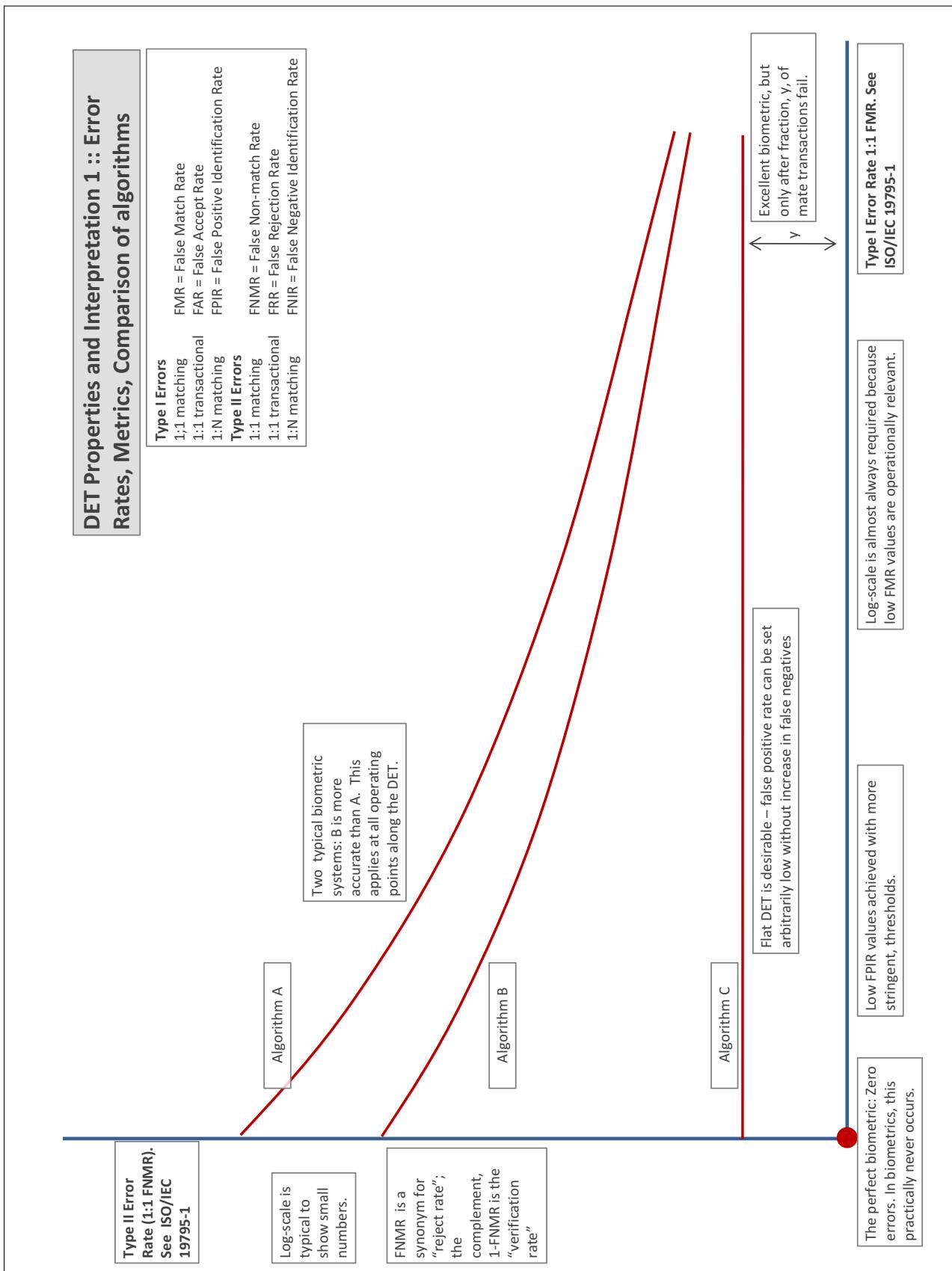
# Accuracy Terms + Definitions

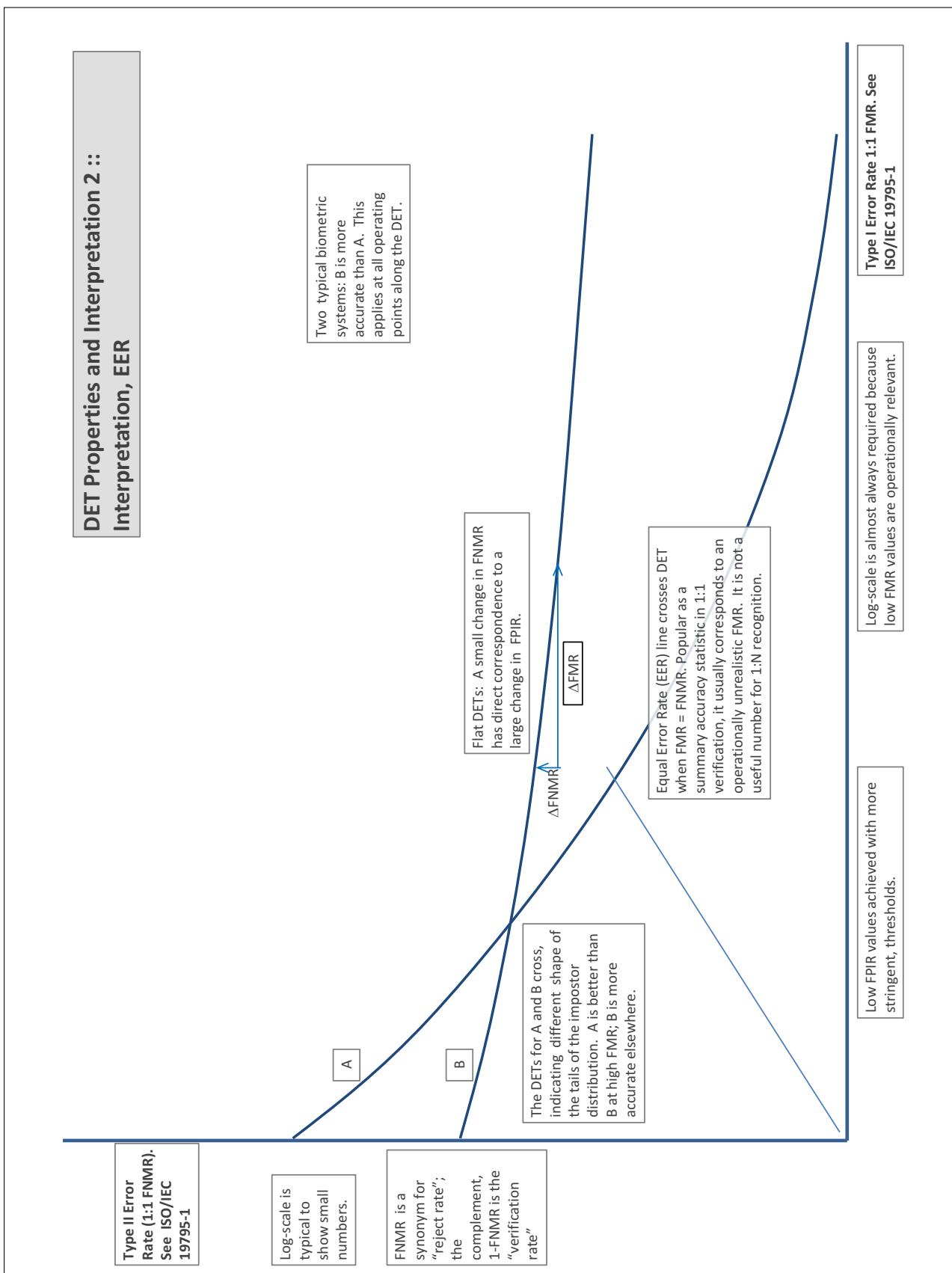
In biometrics, Type II errors occur when two samples of one person do not match – this is called a **false negative**. Correspondingly, Type I errors occur when samples from two persons do match – this is called a **false positive**. Matches are declared by a biometric system when the native comparison score from the recognition algorithm meets some **threshold**. Comparison scores can be either **similarity scores**, in which case higher values indicate that the samples are more likely to come from the same person, or **dissimilarity scores**, in which case higher values indicate different people. Similarity scores are traditionally computed by **fingerprint** and **face** recognition algorithms, while dissimilarities are used in **iris recognition**. In some cases, the dissimilarity score is a distance; this applies only when **metric** properties are obeyed. In any case, scores can be either **mate** scores, coming from a comparison of one person's samples, or **nonmate** scores, coming from comparison of different persons' samples. The words **genuine** or **authentic** are synonyms for mate, and the word **impostor** is used as a synonym for nonmatch. The words mate and nonmatch are traditionally used in identification applications (such as law enforcement search, or background checks) while genuine and impostor are used in verification applications (such as access control).

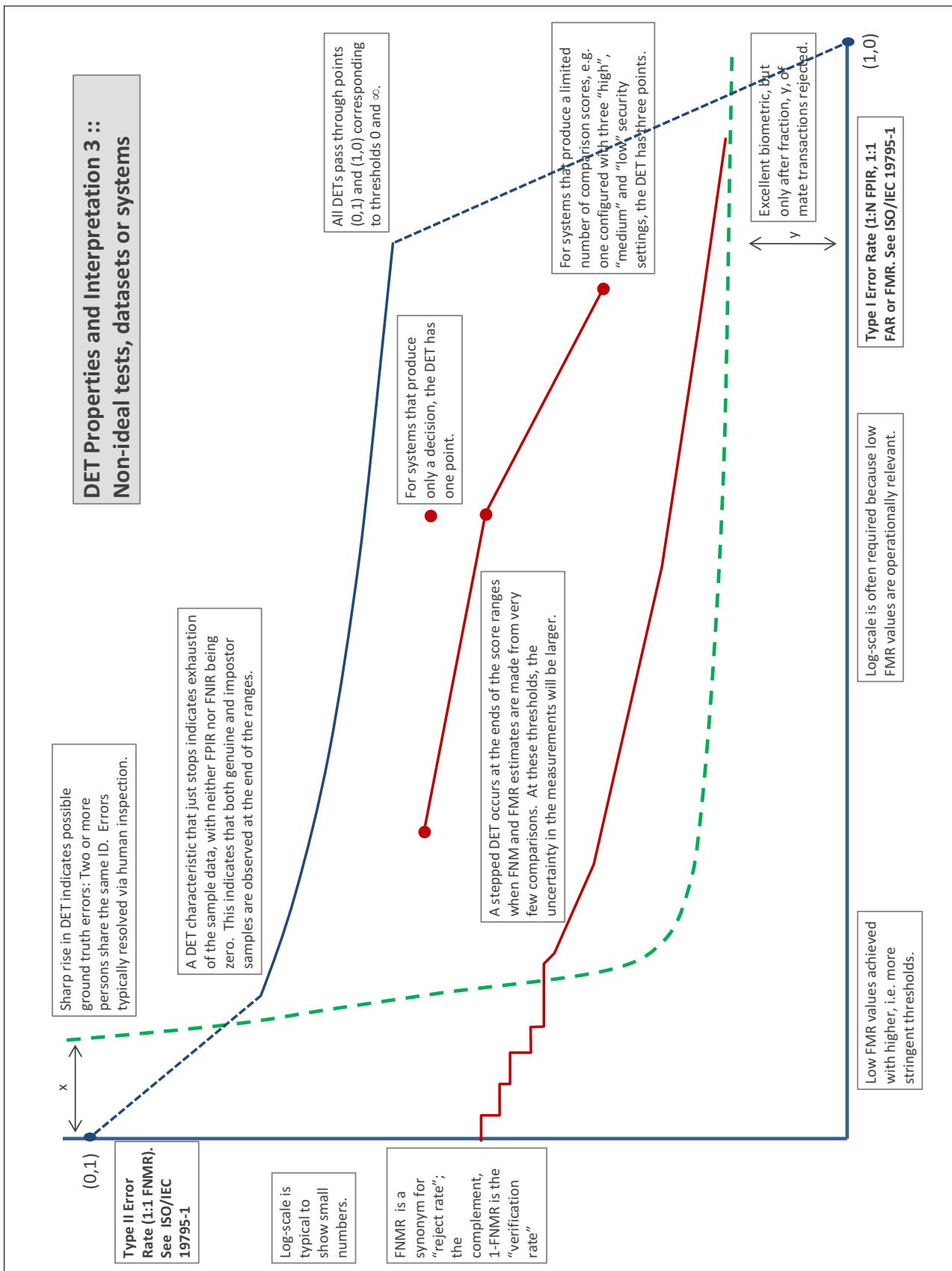
A **error tradeoff** characteristic represents the tradeoff between Type II and Type I classification errors. For verification this plots false non-match rate (FNMR) vs. false match rate (FMR) parametrically with T.

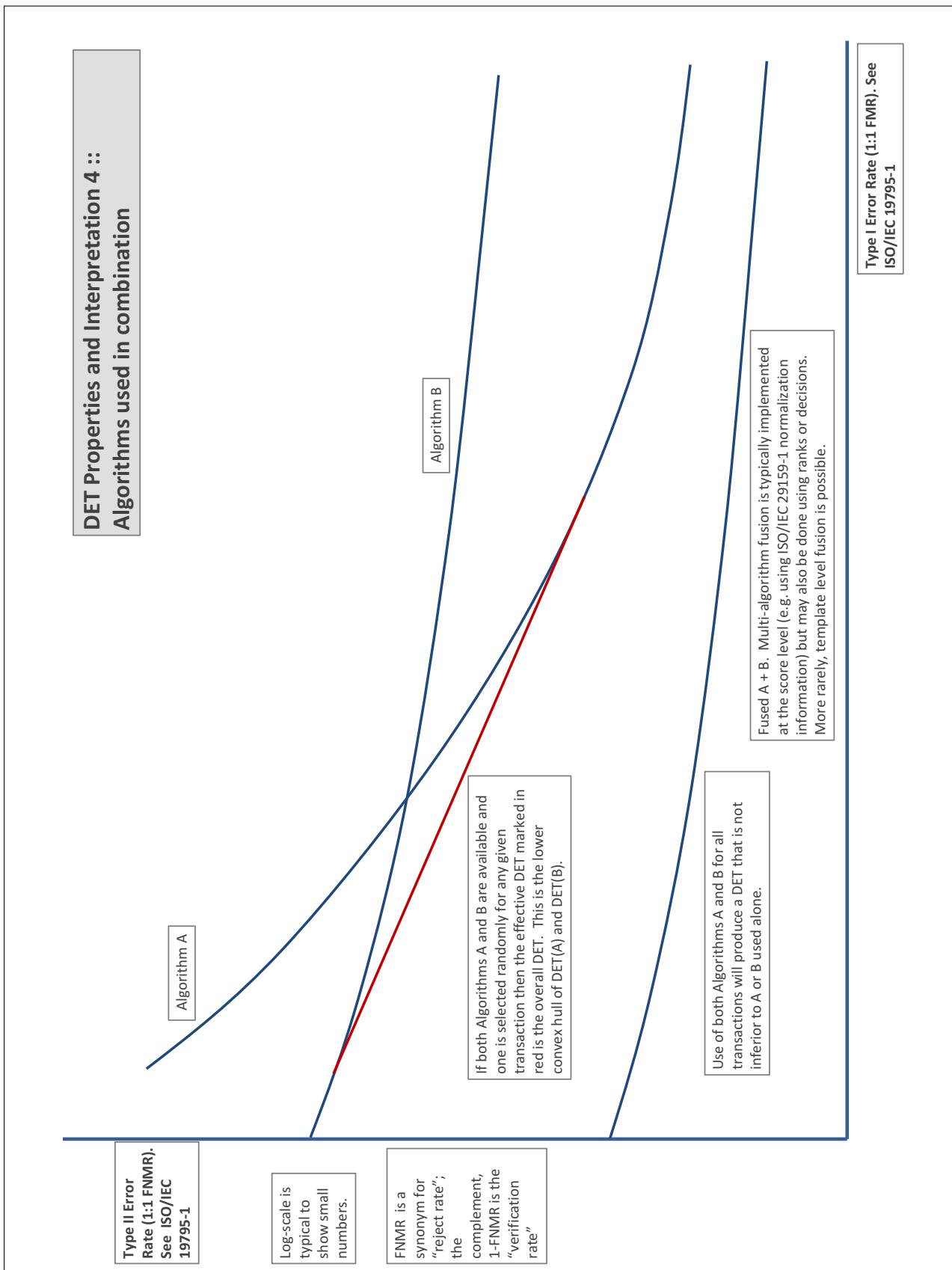
The error tradeoff plots are often called **detection error tradeoff (DET)** characteristics or **receiver operating characteristic (ROC)**. These serve the same function but differ, for example, in plotting the complement of an error rate (e.g.,  $TMR = 1 - FNMR$ ) and in transforming the axes most commonly using logarithms, to show multiple decades of FMR. More rarely, the function might be the inverse Gaussian function.

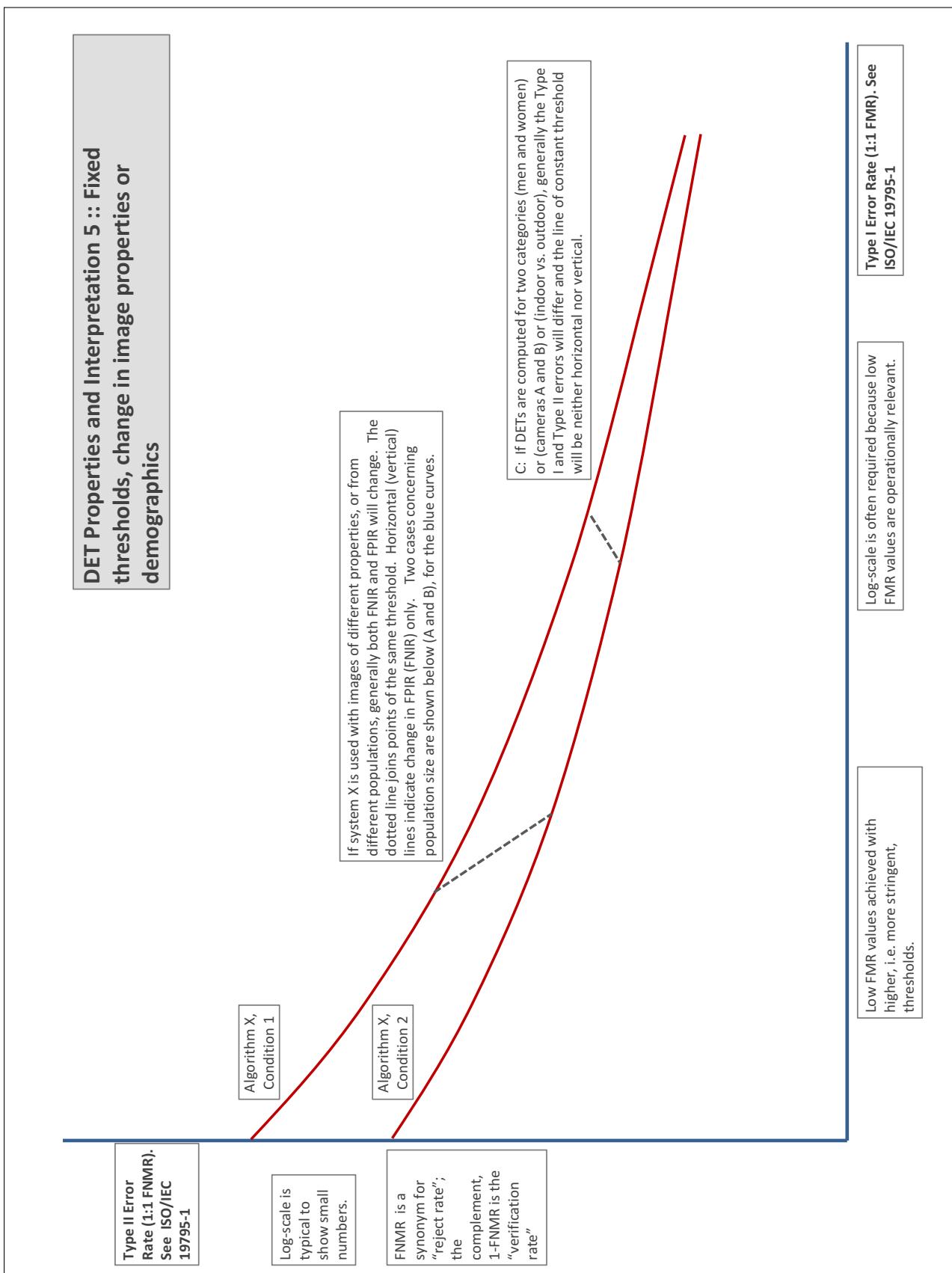
More detail and generality is provided in formal biometrics testing standards, see the various parts of [ISO/IEC 19795 Biometrics Testing and Reporting](#). More terms, including and beyond those to do with accuracy, see [ISO/IEC 2382-37 Information technology -- Vocabulary -- Part 37: Harmonized biometric vocabulary](#)











## References

- [1] P. Jonathon Phillips, Amy N. Yates, Ying Hu, Carina A. Hahn, Eilidh Noyes, Kelsey Jackson, Jacqueline G. Cavazos, Géraldine Jeckeln, Rajeev Ranjan, Swami Sankaranarayanan, Jun-Cheng Chen, Carlos D. Castillo, Rama Chellappa, David White, and Alice J. O'Toole. Face recognition accuracy of forensic examiners, superrecognizers, and face recognition algorithms. *Proceedings of the National Academy of Sciences*, 115(24):6171–6176, 2018.